Springer ThesesRecognizing Outstanding Ph.D. Research

Mattia Walschaers

Statistical Benchmarks for Quantum Transport in Complex Systems

From Characterisation to Design



Springer Theses

Recognizing Outstanding Ph.D. Research

Aims and Scope

The series "Springer Theses" brings together a selection of the very best Ph.D. theses from around the world and across the physical sciences. Nominated and endorsed by two recognized specialists, each published volume has been selected for its scientific excellence and the high impact of its contents for the pertinent field of research. For greater accessibility to non-specialists, the published versions include an extended introduction, as well as a foreword by the student's supervisor explaining the special relevance of the work for the field. As a whole, the series will provide a valuable resource both for newcomers to the research fields described, and for other scientists seeking detailed background information on special questions. Finally, it provides an accredited documentation of the valuable contributions made by today's younger generation of scientists.

Theses are accepted into the series by invited nomination only and must fulfill all of the following criteria

- They must be written in good English.
- The topic should fall within the confines of Chemistry, Physics, Earth Sciences, Engineering and related interdisciplinary fields such as Materials, Nanoscience, Chemical Engineering, Complex Systems and Biophysics.
- The work reported in the thesis must represent a significant scientific advance.
- If the thesis includes previously published material, permission to reproduce this must be gained from the respective copyright holder.
- They must have been examined and passed during the 12 months prior to nomination.
- Each thesis should include a foreword by the supervisor outlining the significance of its content.
- The theses should have a clearly defined structure including an introduction accessible to scientists not expert in that particular field.

More information about this series at http://www.springer.com/series/8790

Mattia Walschaers

Statistical Benchmarks for Quantum Transport in Complex Systems

From Characterisation to Design

Doctoral Thesis accepted by the Albert-Ludwigs-University, Freiburg, Germany and KU Leuven, Leuven, Belgium



Author
Dr. Mattia Walschaers
Laboratoire Kastler Brossel
Sorbonne University, CNRS, École Normale
Supérieure, and Collège de France
Paris, France

Supervisors
Prof. Andreas Buchleitner
Albert-Ludwigs-University
Freiburg, Germany

Prof. Mark Fannes KU Leuven Leuven, Belgium

ISSN 2190-5053 ISSN 2190-5061 (electronic) Springer Theses ISBN 978-3-319-93150-0 ISBN 978-3-319-93151-7 (eBook) https://doi.org/10.1007/978-3-319-93151-7

Library of Congress Control Number: 2018945083

© Springer International Publishing AG, part of Springer Nature 2018

This work is subject to copyright. All rights are reserved by the Publisher, whether the whole or part of the material is concerned, specifically the rights of translation, reprinting, reuse of illustrations, recitation, broadcasting, reproduction on microfilms or in any other physical way, and transmission or information storage and retrieval, electronic adaptation, computer software, or by similar or dissimilar methodology now known or hereafter developed.

The use of general descriptive names, registered names, trademarks, service marks, etc. in this publication does not imply, even in the absence of a specific statement, that such names are exempt from the relevant protective laws and regulations and therefore free for general use.

The publisher, the authors and the editors are safe to assume that the advice and information in this book are believed to be true and accurate at the date of publication. Neither the publisher nor the authors or the editors give a warranty, express or implied, with respect to the material contained herein or for any errors or omissions that may have been made. The publisher remains neutral with regard to jurisdictional claims in published maps and institutional affiliations.

Printed on acid-free paper

This Springer imprint is published by the registered company Springer International Publishing AG part of Springer Nature

The registered company address is: Gewerbestrasse 11, 6330 Cham, Switzerland

Supervisor's Foreword

With an ever-improved understanding and control of elementary building blocks of matter, such as molecules, atoms, and photons, we are today in the position to think anew about the microscopic backbone of the functionality of natural as well as of man-made materials. From the fascinating, highly reliable orchestration of a multitude of degrees of freedom in macromolecular biology, over energy and charge transport mechanisms in photovoltaic devices, to controlled many-particle transport phenomena in cold matter quantum optics or photonic circuitry, and even in quantum computing architectures which do merit this name, we are confronted with the challenging need for novel theoretical approaches able to integrate non-trivial quantum interference phenomena with typical features of complex systems, such as broadly distributed energy, length, and time scales, on the single- and many-particle levels. To fully understand and, ultimately, control observed and/or desired functional properties, potentially aided by quantum interference, we need a suitable blending of—coarse grained—deterministic with robust statistical ingredients, which allows to ponder and exploit the interplay between coherence and statistics. Ouite naturally, though in many ways anti-intuitive for a highly reductionist quantum optical perspective, robust, functionally relevant quantum coherence effects must then manifest on the level of statistics rather than of single, deterministically induced events.

Mattia Walschaers' *first book* provides a comprehensive introduction to the diverse aspects of such a modern quantum theory of complex systems, in the specific, though very versatile setting of quantum transport on finite networks. Combining statistical tools from random matrix, open system, as well as many-particle quantum theories with symmetry considerations, the author demonstrates how robust and efficient statistical quantifiers can be identified, to certify and also to control distinctive features of single- and many-particle transports on—possibly constrained—random networks. The largely analytical theory is applied to diverse scenarios of cutting-edge research—from the potential role of quantum coherence in photosynthetic functional units, over many-particle interferences in photonic quantum computing platforms, to fermionic many-particle currents across multiple connected potential landscapes—what nicely demonstrates the remarkable

adaptability of the here elaborated theoretical framework. The author's plenty original contributions are embedded into a very pedagogical text which collects all necessary ingredients for a thorough justification of the various results and applications, offers some additional thematic excursions for a second reading, and is complemented by a carefully assembled bibliography spanning from the mathematical foundations to experimental implementations. This makes this volume an up-to-date and inspiring reference for experienced researchers specialising on the characterisation and control of complex quantum systems, as well as for freshmen who wish to familiarise with the essential building blocks of the theory.

Freiburg, Germany April 2018 Prof. Andreas Buchleitner

Abstract

We focus on the impact of quantum interference phenomena on transport processes in complex systems. In dynamical problems, complexity typically manifests via the combination of a rapidly growing number of paths which connect initial and final states. We introduce the language of graphs and networks as a useful framework to discuss such scenarios, and explore the rich phenomenology of transport phenomena as induced by quantum interference on such topologies. We ultimately strive to exploit these phenomena to render transport faster and more efficient.

Specifically, we study quantum transport of a single excitation though a disordered network. This means that we consider many realisations of the same type of network (in terms of the number of nodes and of the organisation of bonds), which differ by the specific (random) details of the hardwiring. Generically, in completely disordered network structures, a multitude of pathways interfere in an uncontrolled way, which leads to strong fluctuations of transport timescales and efficiencies. However, there are biomolecular networks in photosynthesis that are claimed to transfer energy in a fast and efficient way by exploiting quantum coherence. To understand the functioning of such a transfer mechanism, we explore possible design principles which allow us to use disorder effects to our advantage.

We uncover centrosymmetry and the presence of a dominant doublet of energy eigenstates as important constraints to be imposed upon the disorder. With these implemented, it is possible to statistically control the transport properties, such that a fine-tuning of specific coarse-grained parameters suffices to characterise the probability distribution of transfer times. We extend these concepts to a scattering scenario and investigate the importance of a finite coupling to leads/scattering channels. We show that, in this case, suitable control of averaged the spectral properties of the (random) ensemble of scattering systems allows to reach a regime of optimal transfer from the input to the output channel. Finally, we present some evidence that these design principles may be of relevance in the Fenna–Matthews–Olson light-harvesting complex.

However, complexity does not solely arise due to topological disorder in single-particle Hamiltonians. In the second part of this work, we add an extra layer of complexity by adding particles to the system. Even in the absence of interactions

viii Abstract

between these particles, a novel, rich phenomenology arises due to the indistinguishability of particles. Indistinguishability forces us to coherently add up many-particle pathways, which implies that, in addition to classical combinatorics, many-particle interference effects kick in. This leads to a hitherto largely unknown phenomenology, which we strive to understand. More specifically, we find statistical signatures of such interferences, which can be handled both theoretically and experimentally. Effectively, this leads to a proposal for a practical certification of boson sampling. On a more fundamental level, these signatures imply that fermions and bosons have fundamentally different dynamical properties, which mathematically follow from the algebraic structures that describe the particles.

We finally present first steps to combine single- and many-particle interference effects in the context of open quantum systems, where particles can be injected from, and scattered into open scattering channels. Here we typically see currents of particles flowing through the system, and our goal is to understand the properties of such particle flows. We, again, study systems where the particles are not interacting with each other and show that, in this case, for both, bosons and fermions, one can derive universal bounds for the current. We find that these bounds are remarkably different for fermions and bosons. We prove that here, too, centrosymmetry is a suitable design principle to force fermionic particle currents to saturate their upper bound, thus achieving efficient quantum transport.

Preface

Besides the study of quantum transport in complex systems, a second goal of this thesis is to build a bridge between the physical models, designed to describe experiments, and more abstract mathematical physics.

Throughout this work, several techniques and perspectives from mathematical physics are applied to concrete experimental problems, such as the certification of many-particle interference in Chap. 8. An understanding of mathematical structures and equivalences can exceed the purpose of mere elegance and is here shown to be of great use to propose both concrete measurement setups and relevant methods for the analysis of experimental data.

On the other hand, we strive to unravel the intricate language of algebraic quantum mechanics (Bratteli and Robinson 1987, 1997; Petz 1990) and translate it into the digestible standard jargon of quantum mechanics (Ballentine 2014; Basdevant and Dalibard 2002). Therefore, Chaps. 2 and 7 provide an essential dictionary of the basics of mathematical quantum physics. They outline several of the reasons why seemingly abstract mathematical structures are useful and even required to describe certain aspects of quantum physics. In particular when dealing with many-particle problems, we extensively use ideas, techniques, and formulations which originate from the algebraic approach to quantum statistical mechanics.

Because the work contained in this dissertation covers topics which are of relevance for several communities, extended background sections have been included, which are identified by the section title set in italic font and garnished with an asterisk. In the beginning of these sections, a short italic text explains the content and indicates specifically relevant elements which are used throughout the remainder of the text.

x Preface

Among these background sections, there are some which can be read together to expand on specific topics of mathematical physics which are relevant in our present context:

- The operational approach to quantum mechanics: Sects. 1.2.2, 2.1, 2.2.2, 2.5, and 8.4.1.
- Quantisation: Sects. 2.2 and 7.7.
- Coherent States and Weyl Systems: Sects. 7.6.2, 7.6.3, 7.7.2, and 8.3.2.
- Quasi-free States: Sects. 7.6.5, 7.7, 8.6, and 9.6.3.

Paris, France

Dr. Mattia Walschaers

References

- L.E. Ballentine, *Quantum Mechanics: A Modern Development* (World Scientific Publishing Company Pte Limited, Singapore, 2014)
- O. Bratteli, D.W. Robinson, Operator Algebras and Quantum Statistical Mechanics 1 (Springer, Berlin, 1987)
- O. Bratteli, D.W. Robinson, Operator Algebras and Quantum Statistical Mechanics Equilibrium States. Models in Quantum Statistical Mechanics (Springer, Berlin, 1997)
- J.-L. Basdevant, J. Dalibard, Quantum Mechanics (Springer, Berlin, 2002)
- D. Petz, An invitation to the algebra of canonical comutation relations, in *Leuven Notes in Mathematical and Theoretical Physics Series* A2 (Leuven University Press, Leuven, 1990)

Publications

The following publications are based on this dissertation:

- M. Walschaers, J. Fernandez-de-Cossio Diaz, R. Mulet, A. Buchleitner, Optimally designed quantum transport across disordered networks. Phys. Rev. Lett. 111, 180601 (2013).
- M. Walschaers, R. Mulet, T. Wellens, A. Buchleitner, Statistical theory of designed quantum transport across disordered networks. Phys. Rev. E 91, 042137 (2015).
- M. Walschaers, F. Schlawin, T. Wellens, A. Buchleitner, Quantum transport on disordered and noisy networks: an interplay of structural complexity and uncertainty. Annu. Rev. Condens. Matter Phys. 7, 223–48 (2016).
- M. Walschaers, J. Kuipers, J.-D. Urbina, K. Mayer, M. C. Tichy, K. Richter, A. Buchleitner, Statistical benchmark for boson sampling. New J. Phys. 18, 032001 (2016).
- M. Walschaers, J. Kuipers, A. Buchleitner, From many-particle interference to correlation spectroscopy. Phys. Rev. A **94**(R), 020104 (2016).
- M. Walschaers, A. Buchleitner, M. Fannes, On optimal currents of indistinguishable particles. New J. Phys. **19**, 023025 (2017).
- M. Walschaers, R. Mulet, A. Buchleitner, Scattering theory of efficient quantum transport across finite networks. J. Phys. B: At. Mol. Opt. Phys. 50, 224003 (2017).

Acknowledgements

To ultimately get to the point of completing this Ph.D. thesis was a hard task, a real endeavour. I realise it would not have been possible without a very important group of people: my teachers. I am truly grateful to each and every one of them, but I feel that some deserve explicit mention:

In de eerste plaats is er Marc Beddegenoodts, mijn gepassioneerde leerkracht fysica. Zonder zijn motiverende lessen had ik de opleiding natuurkunde wellicht niet eens overwogen. Daarenboven zou ik graag mijn leerkracht wiskunde, Ilona Hawrijk, bedanken om mij heel expliciet in mijn keuze voor fysica te steunen.

During my university studies, I enjoyed—and endured—many teachers, ranging from eccentric to superb. However, I cannot think of any teacher who influenced me more than my own master and Ph.D. supervisor, Mark Fannes. If I were to pinpoint one aspect in which Mark excels, it must be his gift to explain the most complicated things in a clear and simple way. Mark, I would like to thank you for your never-ending patience, for all the physics and mathematics you taught me, and, above all, for making me see the beauty quantum mechanics.

When I started looking for a Ph.D. position, I wrote Prof. Dr. Buchleitner, who immediately insisted I should call him Andreas. He was one of the few people who did not merely focus on grades and gave me the chance to come to Freiburg and prove myself. His belief in me and his support have pushed me further than I could have ever imagined. In addition, I enjoyed our—sometimes intense—discussions about politics, culture, art, and life in general. Andreas, thank you for the inspiration and motivation, for helping me see the bigger picture, for believing in me, and most of all for helping me believe in myself.

We, scientists, are passionate people, but even passionate people need to eat, pay their rent, and make the occasional trip to a conference on the other side of the planet. There is, after all, no free lunch (unless it is included in the conference fee). I therefore would like to thank the Studienstiftung des deutschen Volkes for their trust and financial support.

It is enjoyable to do interesting science for several years, but my collaborators certainly made it a more colourful experience. Thank you Juan-Diego, Jack,

xiv Acknowledgements

Klaus R, Klaus M, Malte, Cossio, Thomas, Tobias, Slava, and Frank for the many interesting discussions and for the beautiful work we did together. Additionally, I am very grateful to Roberto Mulet for all the good times and for all the good science. During our work, we encountered many barriers and Roberto taught me that sometimes you just have to use a brute-force approach and break through them. I also thank Roberto for his wise advice on private matters: e.g. "Go home and organise your life." or "You have to find a girlfriend."

Highlights of normal working days are often interesting coffee room discussions: Hans, Eliran, Tarek, Kristof, Ruben, Frederik, Bert, Simi, Winny, Slava, Chahan, Juliane, Manuel, Jochen, Frank, Stefan, Angelika, Fabian, Sebastian, professors of the ITF, and many others; it was a great pleasure to uncover some of the mysteries in physics and in life together with you.

Moreover, I want to explicitly express my gratitude to the people who "run the shop": the great secretaries and the IT guys who are always there to save the day. Anneleen, Gislinde, Susanne, Filip, Gerald, and Stef, thank you for all the help!

I am very grateful to Kristof and Margot (and Jargoth), Slava, Andreas, Tarek and Laura, Michael and Berdien, and Filip and Christine for their hospitality in welcoming me in their homes during some of my scientific trips.

When one makes a four-year-long journey, there are bound to be some bumps along the road. These bumps sometimes cause you to fall flat on your face, luckily, in my case, there were people to help me get back on my feet. I am unbelievably grateful to Chahan, Juliane, Jochen, Slava, Dania, Kathi, Michaël D, Berdien, Michaël M, Christophe, and Thomas for undergoing my signature-style whining. You guys have always been there for me when I needed you most. I could not have wished for any better friends.

Special thanks to Maria, for showing me that not all things in life need to be serious. Also thanks to Maria for making me realise that some things in life do need to be serious.

Daan, Nicki, Leslie, Tjardo, Bieke, en Marc, bij jullie kon ik altijd terecht om even aan alle drukte te ontsnappen. Jullie hebben voor mij het begrip familie nieuw gedefinieerd, wat mij betreft was dat een upgrade. Bedankt voor alle gezelligheid.

Liefste zusje, jou zou ik graag bedanken om me regelmatig met mijn voetjes op de grond te zetten, er zijn weinig dingen geweldiger dan samen met u onnozel doen.

Moemoe, van jou heb ik de laatste jaren geleerd dat het belangrijk is om altijd een doel voor ogen te houden, hoe banaal het ook moge zijn. Bedankt voor de vele levenswijsheden en de ontelbare verhalen over "de goeien ouwen tijd".

Sommige dingen zijn te ingewikkeld om in woorden te gieten. Sara, laat ons het simpel houden, je weet immers wat ik wil zeggen. Bedankt voor alles.

De laatsten zullen de eersten zijn, lieve mama en papa. Op jullie kan ik altijd rekenen voor wat dan ook. Jullie hebben er nooit voor teruggedeinsd om mij te zeggen wat ik moest horen in plaats van wat ik wilde horen. Ik ben jullie oneindig dankbaar voor alle steun, liefde, en vriendschap—en voor de poen om mijn studies te betalen, niet onbelangrijk.

Contents

Part I General Introduction

1	Pers	pective	s and Outline	3
	1.1	Fronti	ers of Quantum Interference	3
	1.2	Quant	um Measurements	8
		1.2.1	Complex Quantum Systems and Statistics	8
		1.2.2	Measurements and Interpretations	9
	1.3	Outlin	e	12
	Refe	erences		15
2	Esse	entials o	of Quantum Theory	21
	2.1		um Mechanics as a Probabilistic Theory*	21
	2.2		isation*	24
		2.2.1	Old and New Quantum Theory*	25
		2.2.2	Quantum Algebra and Quantum Probability*	27
	2.3	Obser	vables and States	29
		2.3.1	Observables	29
		2.3.2	States	33
		2.3.3	The Probabilistic Interpretation	34
	2.4	Dynar	nics of Quantum Systems	35
		2.4.1	The Heisenberg Picture	36
		2.4.2	The Schrödinger Picture	38
	2.5	Quant	um Interference	41
		2.5.1	From Waves to Wave Functions	41
		2.5.2	Projections and Quantum Probability	42
	2.6	Scatte	ring Systems	44
	2.7	Concl	uding Remarks	46
	Refe	rences		47

xvi Contents

3	Con	nplex Quantum Systems and Random Matrix Theory	51
	3.1	Complex Systems	51
		3.1.1 Heuristics	51
		3.1.2 Complexity and Information Theory*	52
		3.1.3 Complexity of Quantum Dynamical Systems	53
	3.2	Complex Networks	54
	3.3	Aspects of Random Matrix Theory	58
		3.3.1 From Atoms and Orbits to Random Matrix Theory*	58
		3.3.2 The Gaussian Ensembles of Random Matrix Theory	60
		3.3.3 Statistical Properties of GOE Eigenvalues	64
		3.3.4 Statistical Properties of GOE Eigenvectors	70
	3.4	Concluding Remarks	71
	Refe	erences	72
Par	t II	Single-Particle Quantum Transport	
4	Effic	cient Transport in Closed Systems	77
	4.1	Introduction	77
	4.2	Measuring Transfer Efficiency	81
	4.3	Influence of Network Structures	83
		4.3.1 Regular Networks	83
		4.3.2 Random Networks	89
	4.4	Design Principles	92
		4.4.1 Centrosymmetry	92
		4.4.2 The Dominant Doublet	99
	4.5		106
			106
			114
		8 1	122
			127
	4.6	· · · · · · · · · · · · · · · · · ·	137
	Refe	erences	140
5	Scat	ttering Approach to Efficient Transport	145
	5.1	Introduction	145
	5.2	Transfer Probability and Dwell Time	146
	5.3	The Two Level System*	149
			149
			150
	5.4	· · · · · · · · · · · · · · · · · · ·	154
	5.5		159
			159
			162
		5.5.3 Numerical Results	164

Contents xvii

	5.6 Refe	Summary and Outlook	167 168
6	Quantum Effects in Biological Systems		
	6.1	From Schrödinger to "Quantum Biology"	171
	6.2	Photosynthesis: Disorder Versus Noise	175
	6.3	Design Principles in Photosynthesis	179
	6.4	Outlook	187
	Refe	rences	190
Par	t III	Many-Particle Quantum Transport	
7	Desc	ribing Many-Particle Quantum Systems	199
	7.1	Introduction	199
	7.2	Postulates for Bosons and Fermions	201
		7.2.1 The Two-Particle System	201
		7.2.2 The N-Particle System	204
		7.2.3 Permanents and (Slater) Determinants	207
	7.3	Fock Space	208
		7.3.1 Constructing Fock Space	208
		7.3.2 Structuring Fock Space	211
		7.3.3 Exponential Vectors	215
	7.4	Commutation Relations	216
	7.5	Second Quantisation	218
	7.6	Many-Particle Quantum States	222
		7.6.1 Number States	223
		7.6.2 Bosonic Coherent States*	227
		7.6.3 Bosonic Squeezed States*	231
		7.6.4 Representing Bosonic States*	235
		7.6.5 Thermal States for Non-interacting Particles	239
	7.7	Abstract Algebraic Description	241
		7.7.1 The CAR Algebra	242
		7.7.2 The CCR Algebra*	249
	7.8	Concluding Remarks	258
	Refe	rences	259
8	Man	y-Particle Interference	265
	8.1	Introduction	265
	8.2	Dynamics of Non-interacting Particles	267
		8.2.1 Unitary Dynamics	268
		8.2.2 Beamsplitters*	271
	8.3	Many-Particle Interference: The Wave Function Approach	276
		8.3.1 From Single-Particle to Many-Particle Interference	276
		8.3.2 Many-Boson Interference	

xviii Contents

		8.3.3 Many-Fermion Interference	283
		8.3.4 Distinguishability and the Hong-Ou-Mandel Effect	286
		8.3.5 Boson Sampling	294
	8.4	J 11	298
			299
			305
	8.5	1 &	318
		\mathcal{C}	320
		•	323
		8.5.3 Partial Distinguishability and Correlation	
	0.6	1 17	345
	8.6	•	363
	Refe	erences	366
9	Cur	rents of Indistinguishable Particles	375
	9.1		375
	9.2	1	378
	9.3	, e	381
			381
		1	382
			383
			384
	9.4		387
	9.5		393
	9.6	1 0	398
			399
			403
	0.7		406
	9.7 9.8		407
			414
	KCIC	ichees	410
Par	t IV	General Conclusions and Prospects	
10	Con	clusions and Outlook	423
	Refe	erences	429
Арр	endi	x A: Basic Definitions of Mathematical Algebras	433
Арр	endi	x B: Averaging over Random Unitary Matrices	439
App	endi	x C: Higher-Order Many-Particle Interference	445
Appendix D: Fermionic Correlation Functions			447
Clossary			110

Symbols

\overline{z}	The <i>complex conjugate</i> of $z \in \mathbb{C}$
${\cal H}$	The (single-particle) <i>Hilbert space</i>
$\mathcal{B}(\mathcal{H})$	The bounded operators on (single-particle) Hilbert space—defined
	p. 30
A^{\dagger}	The adjoint of $A \in \mathcal{B}(\mathcal{H})$
$\Gamma^b(\mathcal{H})$	The bosonic Fock space, constructed on \mathcal{H} —defined p. 209
$\Gamma^f(\mathcal{H})$	The fermionic Fock space, constructed on \mathcal{H} —defined p. 209
$\mathcal{B}(\Gamma^{b/f}(\mathcal{H}))$	The bounded operators on Fock space
Ω	The vacuum state vector, describing the system without particles,
	$\Omega \in \Gamma^{b,f}(\mathcal{H})$ —defined p. 209
$a^{\dagger}(\psi)$	The creation operator, creating a particle with single-particle state
	vector $\psi \in \mathcal{H}$ in (bosonic or fermionic) Fock space—defined p. 210
$a(\psi)$	The annihilation operator, annihilating a particle with
	single-particle state vector $\psi \in \mathcal{H}$ for (bosonic or fermionic) Fock
	space—defined p. 216
W(lpha)	The Weyl (or displacement) operator, creating a coherent state in
	$\Gamma^b(\mathcal{H})$, characterised by a vector $\alpha \in \mathcal{H}$ (which need not be
	normalised)—defined p. 217
$\Gamma(A)$	The second quantisation of $A \in \mathcal{B}(\mathcal{H})$, an additive embedding (7.87)
	of operator A in $\mathcal{B}(\Gamma^{b/f}(\mathcal{H}))$ —defined p. 218
E(A)	The exponential element of $A \in \mathcal{B}(\mathcal{H})$, a multiplicative embedding
	$(7.106-7.107)$ of operator A in $\mathcal{B}(\Gamma^{b/f}(\mathcal{H}))$ —defined p. 222
$\exp(\psi)$	The <i>exponential vector</i> constructed from $\psi \in \mathcal{H}$,
	$\exp(\psi) \in \Gamma^b(\mathcal{H})$ —defined p. 215
$\mathcal{A}^{\mathrm{CAR}}$	The abstract C^* -algebra generated by the canonical anticommuta-
	tion relations—defined p. 242
$\overline{\Delta(\mathcal{S},\sigma)}$	The abstract C*-algebra generated by the Weyl elements on a
_(-,-)	symplectic space (S, σ) —defined p. 250

xx Symbols

$c(\psi)$	An abstract generator of the CAR algebra on \mathcal{H} , with $\psi \in \mathcal{H}$ —defined p. 242
$q_\pi(\psi)$	An <i>abstract quadrature</i> or <i>field</i> in the representation π of C^* -algebra on \mathcal{H} , with $\psi \in \mathcal{H}$ —defined p. 251
w(f)	An abstract Weyl element in $\overline{\Delta(S, \sigma)}$ on S , with $f \in S$ —defined p. 250
χ^*	An abstract *-operation on an element $x \in A$ of a *-algebra—defined on p. 435
.	The <i>norm</i> of any normed space
⟨.⟩	A <i>state</i> (an expectation value) on a <i>Hilbert space</i> (which may also be a Fock space)—defined p. 33
ω	A state (an expectation value) on a C*-algebra—defined p. 243

Part I General Introduction

Chapter 1 Perspectives and Outline



To measure what is measurable and to try to render measurable what is not so as yet

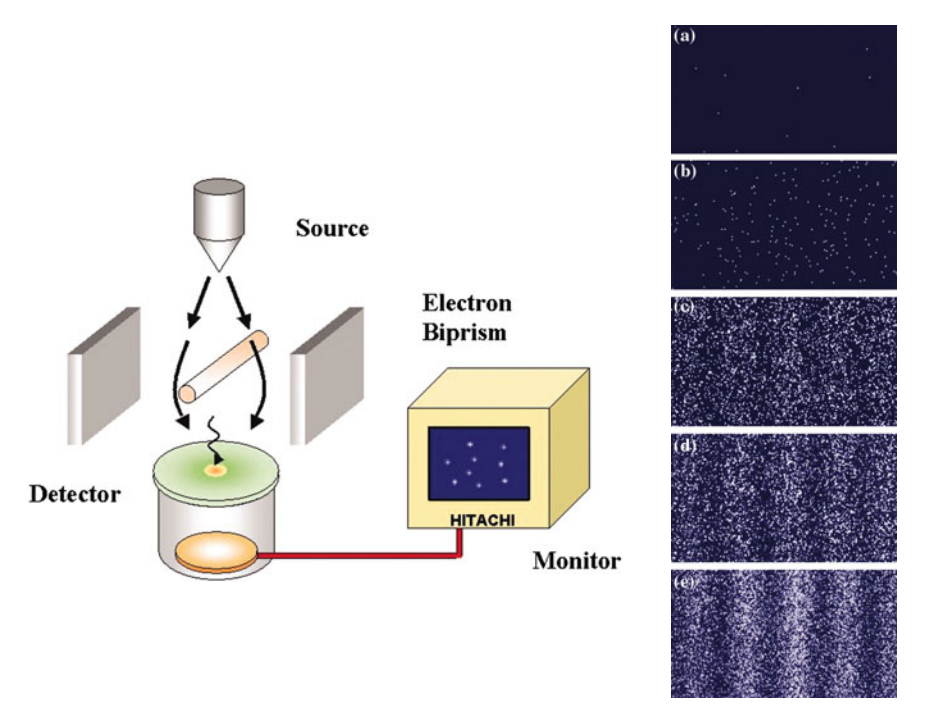
Galileo Galilei, as quoted by Hermann Weyl (Weyl 1949)

1.1 Frontiers of Quantum Interference

To Galileo and his contemporaries, pioneers on the matter of experimentation, *measurement* was the cornerstone of natural science. Centuries later, measurement would also drive the development of quantum mechanics. The formalism of quantum theory, though highly counter-intuitive, was ultimately accepted by the scientific community based on its ability to both describe and predict measurable phenomena. It were the experiments in the early twentieth century, which gradually explored a wide range of phenomena that challenged classical physics and paved the road for the "quantum revolution".

Among these experiments were those describing the photoelectric- (Einstein 1905; Lenard 1902) and Compton (Compton 1923) effects, which imply that light behaves as a particle. However, the development of Maxwell's theory of electromagnetism and the pioneering experiment by Young (Young 1804) had conclusively established the wave nature of light, thus causing a paradox. This paradox is famously solved by the wave-particle duality in quantum mechanics, which, as de Broglie conjectured, is valid for all matter (de Broglie 1924). Again, this theoretical result survived due the extensive amount of experimental validation (Gerlich et al. 2011; Hornberger et al. 2012; Jönsson 1961; Marton 1952; Tonomura 2005) (see also Fig. 1.1).

The wave-particle duality is one of the oldest cornerstones of quantum mechanics, later to be replaced by the more general notion of complementarity (Bohr 1935). The wave-like dynamics directly implies the applicability of the superposition principle, which in a dynamical system leads to interference phenomena, e.g. Young's experiment. Such quantum mechanical interference phenomena lie at the heart of this dissertation.



Akira Tonomura PNAS 2005;102:14952-14959

Fig. 1.1 Sketch (left) of an experimental way to implement an electron interference experiment, equipped with a sensitive detector with single-electron resolution. With this setup, one can see how, gradually, an interference pattern forms (right). Numbers of electrons are 10 **a**, 200 **b**, 6000 **c**, 40,000 **d**, and 140,000 **e**. Figures taken from (Tonomura 2005)

On the microscopic level, quantum mechanics predicts that even a single particle (e.g. photon, electron, exciton, atom, *et cetera*) can experience these interference effects when it passes through a Young interferometer. In a simplified description of this setup, there are two pathways for the particle to progress to the detector. Each pathway corresponds to passing through a specific slit. Classical logic would dictate that an individual particle goes through one of the two slits, and therefore a repeated experiment with millions of particles should result in two spots on the detector, one spot for each slit. However, when the particles have a well-characterised momentum, the millions of particles collide with the detection screen in a very different way: Interference fringes arise, as is shown in the experimental results of Fig. 1.1.

These interference fringes show regions with many particles and regions with very few particles. When we compare this phenomenology to the classical expectation,

¹ In Young's double slit the detector is usually a screen that detects the position at which the particles hit it.

²The particles must be described by a plane wave in position space (at least up to good approximation)

we find regions where quantum mechanics enhances the probability for a particle to arrive there, whereas there are other regions where quantum mechanics suppresses the presence of particles. This observation implies that quantum interference has an influence on transport properties, an idea which lies at the basis of *quantum transport theory* (Dittrich 1998; Rammer 1998).

In simple terms, the field of quantum transport deals with transport of physical quantities, e.g. charge, energy, particles, from one state to another. In principle, the transport can occur either in real space—as is the case for the double slit—, in momentum space, or simply in state space. In a context of open systems, one considers transport from one channel³ to another. Such a framework is well-suited for connections to mesoscopic physics and thermodynamics. The field of quantum transport is rather rich in the specific phenomena it considers, and also in tools it applies. In the open system setting we can isolate two large sets of formalisms, both of which will be encountered throughout this dissertation: approaches which use propagators, on the one side (see Chaps. 5 and 8), and dynamical maps, on the other side (see Chap. 9). Although these approaches differ from the technical point of view, ultimately they all study the impact of quantum interference, coherence, and decoherence on transport phenomena.

In quantum transport theory, the setting is usually more complicated than the paradigmatic double slit interferometer. In the field of mesoscopic physics, for example, one often studies systems which classically manifest chaotic dynamics (or chaotic scattering) (Brouwer 1997; Imry 2009). Upon quantisation, quantum interference effects become intractable, but provably lead to universal statistical features (Bohigas et al. 1984, 1993; Jalabert et al. 1994). Also, when studying scattering in disordered media, one is confronted with a multitude of interfering pathways which are typically studied via diagrammatic techniques (Vollhardt and Wölfle 1980). It can be shown that in such disordered media the influence of interference can even leave signatures upon averaging over disorder realisations (Wolf and Maret 1985).

Building on these earlier insights and partially expanding them, the central themes of the present work are single- and many-particle interference phenomena in different scenarios of quantum transport on network-like structures. Even though we often treat systems that are finite—they allow an effective description in terms of a finite dimensional Hilbert space—, increasing the size quickly prevents us from fully controlling them. This leads us into a regime where an exact, analytical treatment is unfeasible, while continuum approximations⁴ are not yet applicable.

Even though this regime is not straightforwardly analytically tractable, it is highly relevant both for natural and engineered systems. Specifically its relevance to (bio)molecular physics, e.g. in the recent debates on quantum effects in photosynthesis (see Chap. 6), is a main motivation for our present work. Molecular complexes are

³We will show in Chap. 9 that for many-particle systems there is a natural connection between a "channel" in mesoscopic physics and a "reservoir"—or "bath", or "environment"—in the theory of open quantum systems. Moreover, we note that these channels should not be confused with the single-particle unitary channels in Chap. 8.

⁴Techniques which are often used in for example statistical mechanics to simplify computations.

often set in a harsh environment, where fluctuations and molecular reconfigurations are ubiquitous. The number of basic building blocks that make up such networks of molecules can vary strongly (Blankenship 2002), and transfer processes can depend on the system's size (Boon and Barton 2002; Hall et al. 1996; Jortner et al. 1998; Klotsa et al. 2005; Schuster 2000). The transport of charge (Beratan and Skourtis 1998) and energy (i.e. excitons Amerongen et al. (2000)) is fundamental for a large variety of biological processes, ranging from photosynthesis (Scholes et al. 2011), over respiration (Walker 1992), to DNA repair mechanisms (Boon et al. 2003) and more.

In the context of quantum engineering, similar problems are encountered when one tries to scale up the system size while maintaining the possible "quantum advantages". Thinks, for example, of the universal quantum computer, where one realises that the *full control* of hundreds of qubits⁵ is an unreachable goal. This implies that disorder effects and network structures are highly relevant for the construction of a robust quantum computer (Bunyk et al. 2014; Lanting et al. 2014).

However, our present work is not merely intended as a toolbox to study existing systems and treat expected problems in "quantum technologies". We strive to uncover the potential of quantum interference in complex networks, by proactively constructing *design principles*. Since Anderson (Anderson 1958) it is known that in infinitely large systems, disorder has a disastrous effect on quantum transport, due to localisation effects (Abrahams et al. 1979; Albada and Lagendijk 1985; Bergmann 1984; Billy et al. 2008; Casati et al. 1990; Hu et al. 2008; Kramer and MacKinnon 1993; Modugno 2010; Roati et al. 2008; Schelle et al. 2009; Vollhardt and Wölfle 1980; Wolf and Maret 1985). When these effects are studied using diagrammatic techniques, which literally consider different pathways that can interfere, one observes that they are a consequence of destructive quantum interference. However, these studies of localisation effects focus on systems in the thermodynamic limit, whereas—as mentioned above—we consider systems which are finite. Moreover, we strive to use the *richness in network topologies and energy scales* to our advantage, i.e. to enhance the transfer of particles.

With recent developments of quantum metamaterials (Barends et al. 2013, 2014; Macha et al. 2014; Rakhmanov et al. 2008), multimode quantum optics (Armstrong et al. 2012), integrated photonic circuits (Carolan et al. 2015; Metcalf et al. 2013), and ultra-cold atoms (Ahlbrecht et al. 2012; Genske et al. 2013; Reetz-Lamour et al. 2008), very clean testing grounds for transport models are becoming available. This may soon lead to experimental probes and tests of several phenomena which are described in this dissertation.

The scenario depicted in sketch (b) of Fig. 1.2 indicates an additional source of complexity: *multiple particles which jointly pass the interferometer*. When this happens, many-particle effects come into play, i.e. we see a difference between bosons and fermions. In the case where two bosons or two fermions are sent through

⁵A qubit is the quantum analog of a bit (Nielsen and Chuang 2010). In a more physical context, it can be thought of as a system with two distinct energy levels.

⁶This implies that the length scales of the system are much larger than a typical localisation length.

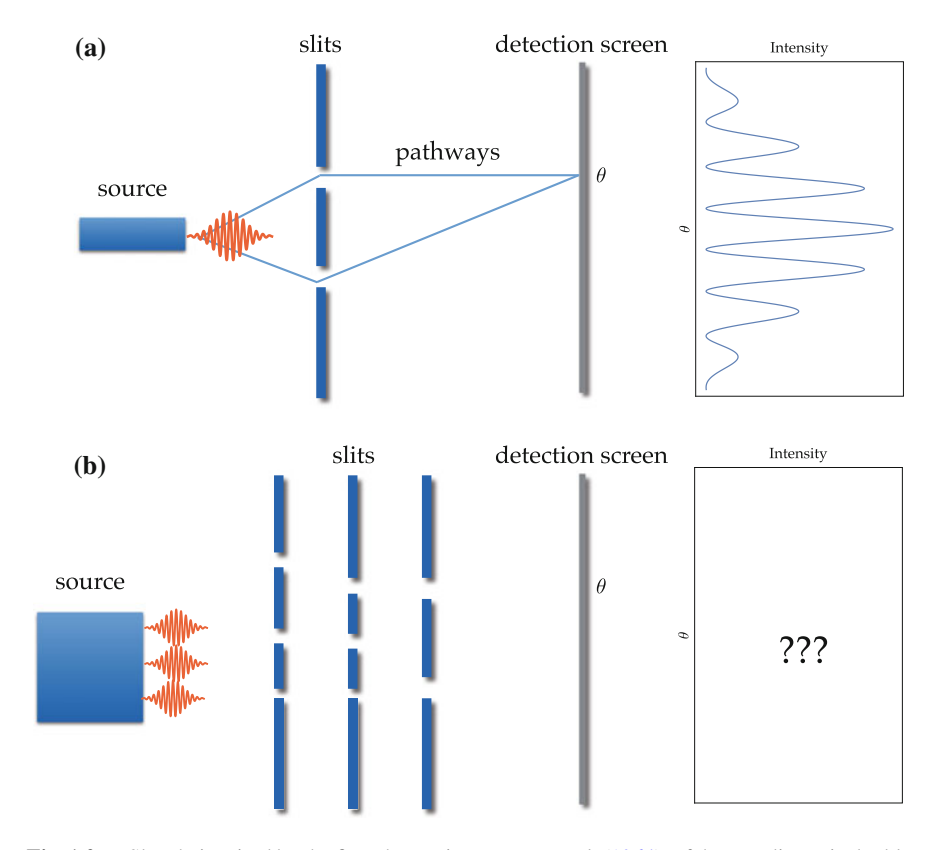


Fig. 1.2 a Sketch, inspired by the first chapter in Feynman et al. (1964), of the paradigmatic double slit setup. **b** Possible extension of Feynman's scenario to more complex many-particle interference devices: Increasing the number of *identical* particles that pass the slit system *simultaneously*, and increasing the number of interfering path alternatives by increasing the number of slits per grating, and by inserting several grating patterns of enormous complexity (see main text)

two slits, the observed phenomenology is well-understood in terms of Hong-Ou-Mandel interference (Hong et al. 1987) and Pauli's exclusion principle (Pauli 1925, 1940), respectively. However, when we consider a complex network of slits and a larger number of particles, the interference pattern rapidly acquires a much more complicated structure.

Recently, the topic of boson sampling (Aaronson and Arkhipov 2013) attracted interest from both quantum information and quantum optics communities (Bentivegna et al. 2015; Broome et al. 2013; Crespi et al. 2013; Gogolin et al. 2013; Spagnolo et al. 2014; Spring et al. 2013; Tillmann et al. 2013). In the language of quantum transport theory, one may translate the boson sampling results of Aaronson and Arkhipov (2013) as a mathematical proof that it is hard to completely understand the fine structure of the interference pattern which arises when many particles travel through a complex network of slits at the same time. Because the boson sampling setup in many respects resembles a complex system, this result is also in line with physical intuition.

Initially we argued that one may send particle after particle through the double slit, to ultimately accumulate a pattern of interference fringes when all the dots on the screen are shown. The boson sampling result proves that even simulating the sampling of such dots—for n particles, n dots will simultaneously appear on the detector screen of the interferometer is computationally hard. From a pure physics point of view, this implies that it is not only hard to analytically obtain and understand the full structure of the many-particle interference pattern, it is even unfeasible to simulate it using Monte Carlo techniques of standard computational physics (Landau and Binder 2009). Therefore, in Chap. 8 we will devise methods which reliably characterise the statistical fingerprints of many-particle interference in such complex many-particle interference patterns. With the development of such statistical benchmarks, we provide tools for future investigations on whether manyparticle interference can be used as a resource to enhance quantum transport, in analogy to our single-particle design principles. We provide the first steps in this direction by studying currents of indistinguishable particles in the non-equilibrium steady state in Chap. 9.

1.2 Quantum Measurements

1.2.1 Complex Quantum Systems and Statistics

When we measure quantum systems, there is no escape from their fundamental probabilistic properties. Any measurement which is done in quantum mechanics requires statistical treatment of the measurement data. This probabilistic nature is implied by the very existence of \hbar , which implies that there is a minimal uncertainty in any physical system. Ergo, in contrast to its classical counterpart, quantum mechanics does not allow the description of a single point in phase space. We are always forced to consider a given amount of fluctuations in quantum mechanics, and, therefore, must always resort to probability theory. However, when we describe a generic quantum system in a generic state, even the usual probabilistic description on phase space, which is commonplace in classical statistical mechanics, is inappropriate. A phase space representation of a quantum state is in general not a well-defined probability distribution, as we discuss in Sect. 7.6.4. This is the reason for the development of a whole field in mathematical physics, baptised *quantum probability theory* (Holevo 2001; Maassen 2010). We present a more formal introduction to the probabilistic and algebraic structure of quantum physics in Chap. 2.

Because we study complex systems, we are confronted with an additional layer of uncertainty: The the intricate structure of the system which we describe. As mentioned in the previous section, the complex nature of the system forbids full control of all parameters, which leads to a lack of knowledge that needs to be accounted for. To overcome these problems, we employ a framework that was originally advocated by Bohr (Bohr 1936) and Wigner (Wigner 1955, 1958), and base our study on the char-

acterisation of statistical features of ensembles of such complex systems. Chap. 3 provides an introduction to these techniques in the context of complex quantum systems.

The use of probability theory to understand, characterise and control systems is a recurring theme throughout all chapters in this dissertation. Both, the probabilistic nature of quantum mechanics in our analysis of quantum interference phenomena, as well as the statistical properties of complex systems, offer a rich variety of statistical signatures, which we study by analysing moments, correlations functions, and full probability distributions.

In Chaps. 4 and 5, we base a mechanism of efficient and fast transport of excitations through complex systems on the appropriate design and control of the probability distribution of the transfer times. This sets a new paradigm of quantum control and quantum transport: We do not require optimal control of a large set of parameters, but rather manage to describe an enhancement of transport in terms of ensemble averaged properties. The ensemble is designed such that a (statistically) controllable fraction of realisations exhibit a speed-up of excitation transfer times.

The statistical signatures obtained via those *design principles for statistical control* can also be used in a reverse fashion: When one analyses transport phenomena in complex systems, the statistical properties of the transfer times sampled for an ensemble of systems may offer insight in the specific transport mechanism. The possibility to conduct such analyses is gradually moving into reach (Hildner et al. 2013; Krüger et al. 2012). In a very similar fashion, many-particle systems offer us the possibility to study spatial correlations⁷ between different particles, and the statistics of such correlations is a vital tool for the understanding of many-particle interference in complex systems, as pointed out in Chap. 8.

1.2.2 Measurements and Interpretations

This section briefly discusses the interpretation of measurements, a conceptual "problem" in quantum mechanics. Although this Dissertation does not contribute to this debate, the operational approach to quantum mechanics (Kraus 1983b) has inspired several of our results, most notably those described in Sects. 8.4 and 8.5.

There are few scientific theories that are as thoroughly tested and verified as quantum mechanics. However successful the formalism of quantum mechanics may be, there has been extensive debate about its interpretation. Although there are many aspects of quantum mechanics that defy the common sense of classical mechanics, the interpretation of the measurement process is certainly the most contested issue of all.

This discussion is often centred around the so-called *measurement problem*. The alleged problem arises due to the probabilistic nature of measurement results in quantum mechanics. As discussed in Sect. 1.1, the early quantum theory was confronted

⁷Or, more generally, correlations between different degrees of freedom.

with the duality between particles and waves, which was initially startling. The first experiments (Compton 1923; Lenard 1902) established that the behaviour of a quantum system is intricately connected to the measurements performed on it. Again, the double slit sets a paradigmatic example: When only the intensity distribution on the final detection screen is observed, we obtain the previously discussed interference fringes. However, when in addition a device is in place to register through which slit a particle passes, the interference pattern on the final screen vanishes to make place for two spots—as would be dictated by classical physics. *Ergo*, the measurement setup can dramatically affect the measurement result.

Von Neumann introduced the concept of projective measurements to account for this effect (von Neumann 1932a). His mathematical model selects a set of possible measurement outcomes $\mathcal{O} = \{o_1, \ldots, o_n\}$, such that outcomes o_j is observed with probability p_j . The operator theory which is used to describe these probabilities naturally associates a specific quantum state (see Chap. 2 for a formal definition) to each measurement outcome. It is postulated that immediately after measuring a given outcome o_j , a repetition of the same measurement deterministically leads to the same result. It is commonly said that therefore the quantum state changes in a discontinuous way because of the measurement. This measurement procedure and its intrinsically probabilistic nature have been subject of discussion for many decades, and lie at the heart of most interpretations of quantum mechanics.

Throughout the twentieth century, the dominant interpretation of quantum mechanics was the *Copenhagen interpretation*. This interpretation refers to a collection of ideas that were formulated mainly by Bohr, Heisenberg, and Born during the early developments of quantum mechanics: *The correspondence principle* (Bohr 1913, 1920; Ehrenfest 1927), *the uncertainty relation* (Heisenberg 1927; Kennard 1927; Robertson 1929; Weyl 1928), the *statistical interpretation* of the wave function (Born 1926), and the *complementarity principle* (Bohr 1935)—a more general formulation of the particle-wave duality. Although the actual stance of Bohr and Heisenberg with respect to several elements of what is now considered the Copenhagen interpretation is still subject of debate, ¹⁰ the collapse of the wave function upon measurement is presently considered a fundamental part of the framework.

Many prominent scientists and philosophers, e.g. Einstein et al. (1935), Popper (1967), have been troubled by both the probabilistic nature of quantum mechanics and by the proposed collapse of the wave function. Therefore, several alternative interpretations have been introduced. Einstein always assumed that the probabilistic nature of quantum mechanics merely indicated that the theory was incomplete and that some relevant variables remained hidden (Einstein et al. 1935). Bell's theorem (Bell 1964) and the development of entanglement theory (Horodecki et al. 2009), together with decades of experimental work (Aspect 1976; Aspect et al. 1982;

⁸In principle there can be several quantum states that lead to the same outcome for the measurement of an observable.

⁹It is often said to "collapse".

¹⁰An overview is provided in Katsumori (2011).

Freedman and Clauser 1972; Hensen et al. 2015) have excluded such local hidden variable theories.

Additional mathematical and conceptual attempts have been made to circumvent the fundamentally probabilistic nature of quantum measurement. One of the more well-known alternative formulations of quantum mechanics was provided by Bohm (1952a, b), and has the benefit to avoid the collapse of the wave function. On a mathematical level, the theory is considerably less practical than the standard formulation of quantum mechanics, which is based on functional analysis and operator algebra. On the conceptual level, one of the more "popular" interpretations of quantum mechanics is that based on Everett's "relative state formulation" (Everett 1957), which was later reformulated by DeWitt (1970) as the "many-worlds interpretation". The starting point of the interpretation is the assumption that not only the system which is measured, but also the measurement apparatus is quantum mechanical. Although it has been argued that a collapse model is a reasonable consequence of a quantum mechanical measurement apparatus in combination with decoherence (Schlosshauer 2005), the most radical formulation of the many-worlds interpretation avoids the probabilistic nature of measurement by assuming a multitude of different universes, one for each possible measurement outcome. An common criticism for the many-worlds interpretation is that the solution to the alleged measurement problem is conceptually just as radical as the idea of quantum state collapse.

All interpretations of quantum mechanics reproduce the same physical phenomena and therefore this dissertation can be read starting from each of these different points of view. The author, however, would like to emphasise one particular interpretation which in many ways served as an inspiration for this work. This interpretation is traced back to works by Ludwig (1964, 1967, 1968), Kraus (1983b) and Davies and Lewis (1970), and is often called "the operational approach". Although there are considerable similarities to the Copenhagen interpretation in terms of an underlying probability theory, the status of measurement is considerably different.

The operational approach originated from attempts to formalise physical theories by introducing an axiomatic system to construct them (Ludwig 1964, 1967, 1968; Mackey 1963). However, it is mainly the heuristic derivation of these fundamental principles which is of interest in the debate of interpretations. Kraus steps away from the more mathematical reasoning and provides a very digestible introduction to this approach to quantum theory (Kraus 1983b). Essentially, the operational approach is built to describe mathematical models of physical experiments. The probabilistic nature of quantum mechanics is an experimental observation that goes into the initial heuristics, rather than a consequence of the theory. Moreover, the quantum state is generally considered to be a summary of the initial preparation procedure of the experiment. Measurement is treated as a connection between microscopic and macroscopic systems. The starting point of the operational approach is not the microscopic world of the systems, but the macroscopic world in which the measurement instruments are described. The "objective reality" is associated with the measurement apparatus rather than with the quantum system itself. This is one of the most

¹¹This does not imply that the measurement apparatus is completely described by classical physics.

distinctive features of the operational interpretation and clearly separates it from the Copenhagen interpretation: The operational treatment considers quantum mechanics as a theory of the measurement of physical systems, i.e. a theory of how the detectors "click". In the operational approach, one may even refuse to extrapolate the theory to a non-laboratory setting. ¹² The "realist" approaches interpret the theory on the level of the system, and consider measurement as an invasive action within this reality. In such interpretational frameworks, the theory is valid independent of the setting and quantum states are real physical objects.

In the operational language, the statistical nature of quantum theory and quantum measurement is central. The collapses of quantum states are no longer problematic when one formulates everything in terms of probability theory and statistical methods. Kraus explains that, indeed, a measurement can be interpreted as an operation on the system (Kraus 1983a), but this operation is a mere consequence of a post-selection procedure which is conditioned on a given measurement outcome. The measurement problem is therefore only a problem when one refuses to accept fundamentally probabilistic theories as complete descriptions of nature.

Throughout this thesis, we follow the treatment of quantum mechanics as a *fundamentally probabilistic theory*. It is our goal, starting from Chap. 2, to both make the connection between probability theory and the formalism of operator algebras plausible, based on Davies and Lewis (1970), Holevo (2001), Maassen (2010), Kraus (1983b). Moreover, the acceptance of the intrinsically probabilistic nature of measurement is sufficient to describe many of the fundamental features of quantum physics. This philosophy beautifully connects to our central methodology as described in Sect. 1.2.1: To exploit the statistical features of quantum mechanics to the fullest, in order to gain a deeper understanding of physical phenomena. Most profoundly, this reasoning is fundamental for the results obtained in Chap. 8.

1.3 Outline

This dissertation is divided in four parts: The first part seeks to provide a general introduction into the context of the presented work, we introduce the theme an situate it in the broader context of *quantum transport theory*. Furthermore, we discuss the mathematical framework upon which this dissertation is built and describe the operational perspective in which the author prefers to situate the work. ¹³ In the second part, we focus on single-particle transport processes in complex quantum systems, to understand the ways in which we can exploit quantum coherence to enhance

¹²A concrete example: one may insist that quantum mechanics only manifests itself upon repeated measurement, e.g. a single dot on the detection screen in Fig. 1.1 is insufficient to discuss any quantum phenomena, quantum effects only become apparent when we accumulate point as shown in Fig. 1.1. Hence, the "operationalist" may decide not to apply her theory outside of a context where statistics can be accumulated.

¹³ The work of course allows any interpretation of quantum mechanics, but several results are specifically inspired by operational reasoning.

1.3 Outline

energy transfer. The third part treats many-particle phenomena, most notably those which are dynamical in nature. We emphasise the role of indistinguishability in the manifestation of intricate interference phenomena and we also provide new insights in particle currents which emerge in the non-equilibrium steady states of complex systems. Finally, the last part of the dissertation summarises the main results and provides an outlook in which open questions are addressed.

In concreto, the first part is structured in three chapters. Chapter 1 sets the stage for the specific contributions presented in this dissertation. We describe how this work studies quantum interference phenomena in the context of quantum transport in complex systems. Additionally, we strive to never loose sight of what is actually measurable and therefore we provide a brief introduction to quantum measurement and what we consider to be a vital element in it: Its probabilistic nature.

Chapter 2 sketches a more technical introduction to quantum mechanical systems and more notably to the dynamics thereof. The theory is introduced in a rather operational fashion; we start out from phenomenological considerations that require the quantum mechanical formalism. From the (of course greatly simplified) experimental setting, we build up the theory and explain the equivalence of several descriptions by determining the mathematical objects which are (in principle) accessible in experiments. Our goal is to introduce a deep and abstract mathematical framework from the perspective of physics, explaining the meaning and need for these mathematical structures.

Subsequently, in Chap 3, we enlarge the provided toolbox to the more specific setting of this dissertation: complex quantum system. At first we focus on attempts to formally define what a complex system is. Because these systems require specialised tools that allow us to deal with statistical properties and disorder, we introduce the mathematical framework of Random Matrix Theory in the second part of the chapter.

Part II considers a single-particle problem where a quantum of energy is given the task to travel rapidly and efficiently through such a complex system. This part is inspired by the debate on quantum effects in biological systems and is—again—divided in three chapters, the first of which represents the lion's share. Chapter 4 deals with the quest to design complex quantum systems such that they can transfer energy from one specific initial state to another specific target state. The aim is to provide minimalistic *design principles*, which allow a considerable amount of additional disorder, for these network-like structures. The main workhorse of this section is random matrix theory implemented on the level of Hamiltonians, which are additionally constrained according to these design principles. We develop a mechanism where *centrosymmetry* of the Hamiltonian and a *dominant doublet* of eigenstates manage to exploit the statistical properties of the disorder. This leads us towards a mechanism of *statistical control*, where we shape statistical transfer properties of the full ensemble, which by construction are robust against statistical fluctuations.

Chapter 5 changes the setting to a scattering problem, in which the excitation must enter and leave. In order to describe the transport, we need to consider additional parameters, which are mainly related to the coupling between the system and the channels. We show that there are no significant problems when we implement the

design principles from Chap.4 in this setting, and we manage to derive several analytical results by using the scattering matrix formalism.

To conclude this part of the dissertation, we take a closer look at quantum effects in biology in Chap. 6. This chapter strives to situate the whole discussion on what is by some called "quantum biology" and provides a range of critical remarks about the field. We specifically zoom in on the debate about quantum effects in photosynthesis and present indications that the model of the previous two chapters may be relevant in this context. There are, however, several issues that oppose the direct applicability of our model and these are extensively discussed. The field still presents many open questions, several of which are discussed in detail. We ultimately identify those issues that provide the biggest and most important challenges for the future in order to "render measurable what is not so as yet."

In Part III we focus on systems which contain many identical, potentially indistinguishable particles. To begin with, Chap. 7 introduces the formal mathematical description of many-particle systems. It offers no new results, but should be seen as a compendium of relevant mathematical tools from functional analysis and operator algebra. We connect these mathematical methods to concepts from solid-state physics and quantum optics. Much of this chapter is based on books and lecture notes (Alicki and Fannes 2001; Bratteli and Robinson 1997; Verbeure 2011), which we present in a digestible way by focusing on the direct physical relevance.

Chapter 8 uses several of the presented concepts and techniques from Chap. 7 to study many-particle interference, which arises as a mere consequence of the indistinguishability of particles. We first present many known result from this field using the mathematical physics toolbox. We later shift to a measurement-based paradigm which not only provides technical advantages, but also brings the discussion closer to experimental setups. In this framework we can use the techniques of mathematical quantum statistical mechanics, combined with random matrix theory in order to study relevant statistical properties of boson sampling.

In Chap. 9, we consider systems where the number of particles is not conserved, but particles can freely move in and out of the system. This chapter mainly focusses on fermions, for which we derive an expression for the particle current and study the behaviour thereof in the long-time limit, where it reaches a non-equilibrium steady state. In this stationary state, we prove the existence of a universal upper bound for the current, which can be reached by carefully engineering the system. We explain how yet again centrosymmetry appears to be an important design principle to reach the optimal current regime. Additionally, we show how dephasing noise can significantly enhance the current in the system, but the dephasing model also imposes interesting open questions. The chapter is concluded with analogous results for bosons, where the upper bound for the current can be replaced by a lower bound. Yet again, we see that minor changes in algebraic structure can lead to enormous differences in physical phenomenology.

Ultimately Part IV (and the there contained Chap. 10) wraps up the conclusions from the different chapters, situating these results in the broad context of the quantum theory of complex systems, and takes a look in the direction of future research.

References 15

References

S. Aaronson, A. Arkhipov, The computational complexity of linear optics. Theory Comput. 9, 143–252 (2013)

- E. Abrahams, P.W. Anderson, D.C. Licciardello, T.V. Ramakrishnan, Scaling theory of localization: absence of quantum diffusion in two dimensions. Phys. Rev. Lett. **42**, 673–676 (1979)
- A. Ahlbrecht, A. Alberti, D. Meschede, V.B. Scholz, A.H. Werner, R.F. Werner, Molecular binding in interacting quantum walks. New J. Phys. 14, 073050 (2012)
- M.P.V. Albada, A. Lagendijk, Observation of weak localization of light in a random medium. Phys. Rev. Lett. 55, 2692–2695 (1985)
- R. Alicki, M. Fannes, *Quantum Dynamical Systems* (Oxford University Press, Oxford, 2001)
- P.W. Anderson, Absence of diffusion in certain random lattices. Phys. Rev. 109, 1492–1505 (1958)
- S. Armstrong, J.-F. Morizur, J. Janousek, B. Hage, N. Treps, P.K. Lam, H.-A. Bachor, Programmable multimode quantum networks. Nat. Commun. 3, 1026 (2012)
- A. Aspect, Proposed experiment to test the nonseparability of quantum mechanics. Phys. Rev. D 14, 1944–1951 (1976)
- A. Aspect, P. Grangier, G. Roger, Experimental realization of Einstein–Podolsky–Rosen–Bohm Gedanken experiment: a new violation of Bell's inequalities. Phys. Rev. Lett. 49, 91–94 (1982)
- R. Barends, J. Kelly, A. Megrant, D. Sank, E. Jeffrey, Y. Chen, Y. Yin, B. Chiaro, J. Mutus, C. Neill, P. O'Malley, P. Roushan, J. Wenner, T.C. White, A.N. Cleland, J.M. Martinis, Coherent Josephson Qubit suitable for scalable quantum integrated circuits. Phys. Rev. Lett. 111, 080502 (2013)
- R. Barends, J. Kelly, A. Megrant, A. Veitia, D. Sank, E. Jeffrey, T.C. White, J. Mutus, A.G. Fowler, B. Campbell, Y. Chen, Z. Chen, B. Chiaro, A. Dunsworth, C. Neill, P. O'Malley, P. Roushan, A. Vainsencher, J. Wenner, A.N. Korotkov, A.N. Cleland, J.M. Martinis, Superconducting quantum circuits at the surface code threshold for fault tolerance. Nature 508, 500–503 (2014)
- J.S. Bell, On the Einstein–Podolsky–Rosen paradox. Physics 1, 195–200 (1964)
- M. Bentivegna, N. Spagnolo, C. Vitelli, F. Flamini, N. Viggianiello, L. Latmiral, P. Mataloni, D.J. Brod, E.F. Galvao, A. Crespi, R. Ramponi, R. Osellame, F. Sciarrino, Experimental scattershot boson sampling. Sci. Adv. 1, e1400255–e1400255 (2015)
- D. Beratan, S. Skourtis, Electron transfer mechanisms. Curr. Opin. Chem. Biol. 2, 235–243 (1998)
- G. Bergmann, Weak localization in thin films: a time-of-flight experiment with conduction electrons. Phys. Rep. **107**, 1–58 (1984)
- J. Billy, V. Josse, Z. Zuo, A. Bernard, B. Hambrecht, P. Lugan, D. Clément, L. Sanchez-Palencia, P. Bouyer, A. Aspect, Direct observation of Anderson localization of matter waves in a controlled disorder. Nature 453, 891–894 (2008)
- R.E. Blankenship, *Molecular Mechanisms of Photosynthesis* (Blackwell Science, Oxford, 2002)
- O. Bohigas, M.J. Giannoni, C. Schmit, Characterization of chaotic quantum spectra and universality of level fluctuation laws. Phys. Rev. Lett. **52**, 1–4 (1984)
- O. Bohigas, S. Tomsovic, D. Ullmo, Manifestations of classical phase space structures in quantum mechanics. Phys. Rep. **223**, 43–133 (1993)
- D. Bohm, A suggested interpretation of the quantum theory in terms of "Hidden" variables. I. Phys. Rev. **85**, 166–179 (1952a)
- D. Bohm, A suggested interpretation of the quantum theory in terms of "Hidden" variables. II. Phys. Rev. **85**, 180–193 (1952b)
- N. Bohr, I. On the constitution of atoms and molecules. Philos. Mag. 26, 1–25 (1913)
- N. Bohr, Über die Serienspektra der Elemente. Z. Phys. 2, 423–469 (1920)
- N. Bohr, Can quantum-mechanical description of physical reality be considered complete? Phys. Rev. **48**, 696–702 (1935)
- N. Bohr, Neutron capture and nuclear constitution. Nature 137, 344–348 (1936)
- E.M. Boon, J.K. Barton, Charge transport in DNA. Curr. Opin. Struct. Biol. 12, 320–329 (2002)
- E.M. Boon, A.L. Livingston, N.H. Chmiel, S.S. David, J.K. Barton, DNA-mediated charge transport for DNA repair. PNAS 100, 12543–12547 (2003)

- M. Born, Quantenmechanik der Stoßvorgänge. Z. Phys. 38, 803–827 (1926)
- O. Bratteli, D.W. Robinson, *Operator Algebras and Quantum Statistical Mechanics Equilibrium States*. Models in Quantum Statistical Mechanics (Springer, Berlin, 1997)
- M.A. Broome, A. Fedrizzi, S. Rahimi-Keshari, J. Dove, S. Aaronson, T.C. Ralph, A.G. White, Photonic boson sampling in a tunable circuit. Science 339, 794–798 (2013)
- P.W. Brouwer, On the random-matrix theory of quantum transport, Ph.D. thesis, Leiden University, Leiden, 1997
- P. Bunyk, E. Hoskinson, M. Johnson, E. Tolkacheva, F. Altomare, A. Berkley, R. Harris, J. Hilton, T. Lanting, A. Przybysz, J. Whittaker, Architectural considerations in the design of a superconducting quantum annealing processor. IEEE Trans. Appl. Supercond. 24, 1–10 (2014)
- J. Carolan, C. Harrold, C. Sparrow, E. Martín-López, N.J. Russell, J.W. Silverstone, P.J. Shadbolt, N. Matsuda, M. Oguma, M. Itoh, G.D. Marshall, M.G. Thompson, J.C.F. Matthews, T. Hashimoto, J.L. O'Brien, A. Laing, Universal linear optics. Science 349, 711–716 (2015)
- G. Casati, I. Guarneri, F. Izrailev, R. Scharf, Scaling behavior of localization in quantum chaos. Phys. Rev. Lett. 64, 5–8 (1990)
- A.H. Compton, A quantum theory of the scattering of X-rays by light elements. Phys. Rev. 21, 483–502 (1923)
- A. Crespi, R. Osellame, R. Ramponi, D.J. Brod, E.F. Galvão, N. Spagnolo, C. Vitelli, E. Maiorino, P. Mataloni, F. Sciarrino, Integrated multimode interferometers with arbitrary designs for photonic boson sampling. Nat. Photon. 7, 545–549 (2013)
- E.B. Davies, J.T. Lewis, An operational approach to quantum probability. Commun. Math. Phys. 17, 239–260 (1970)
- L. de Broglie, Recherches sur la théorie des quanta, Ph.D. thesis, Migration-université en cours d'affectation, Paris, 1924
- B.S. DeWitt, Quantum mechanics and reality. Phys. Today 23, 30–35 (1970)
- T. Dittrich (ed.), Quantum Transport and Dissipation (Wiley-VCH, Weinheim, New York, 1998)
- P. Ehrenfest, Bemerkung über die angenäherte Gültigkeit der klassischen Mechanik innerhalb der Quantenmechanik. Z. Phys. 45, 455–457 (1927)
- A. Einstein, Über einen die Erzeugung und Verwandlung des Lichtes betreffenden heuristischen Gesichtspunkt. Ann. Phys. 322, 132–148 (1905)
- A. Einstein, B. Podolsky, N. Rosen, Can quantum-mechanical description of physical reality be considered complete? Phys. Rev. 47, 777–780 (1935)
- H. Everett, "Relative state" formulation of quantum mechanics. Rev. Mod. Phys. 29, 454-462 (1957)
- R.P. Feynman, R.B. Leighton, M.L. Sands, R.P. Feynman, in *Quantum mechanics*, vol. 3, ed. by R.P. Feynman, R.B. Leighton, M. Sands. The Feynman Lectures on Physics (Addison-Wesley, Reading/Mass., 1964), nachdr. edn
- S.J. Freedman, J.F. Clauser, Experimental test of local hidden-variable theories. Phys. Rev. Lett. **28**, 938–941 (1972)
- M. Genske, W. Alt, A. Steffen, A.H. Werner, R.F. Werner, D. Meschede, A. Alberti, Electric quantum walks with individual atoms. Phys. Rev. Lett. 110, 190601 (2013)
- S. Gerlich, S. Eibenberger, M. Tomandl, S. Nimmrichter, K. Hornberger, P.J. Fagan, J. Tüxen, M. Mayor, M. Arndt, Quantum interference of large organic molecules. Nat. Commun. 2, 263 (2011)
- C. Gogolin, M. Kliesch, L. Aolita, J. Eisert, Boson-Sampling in the light of sample complexity (2013). arXiv:1306.3995 [quant-ph]
- D.B. Hall, R.E. Holmlin, J.K. Barton, Oxidative DNA damage through long-range electron transfer. Nature **382**, 731–735 (1996)
- W. Heisenberg, Über den anschaulichen Inhalt der quantentheoretischen Kinematik und Mechanik.Z. Phys. 43, 172–198 (1927)
- B. Hensen, H. Bernien, A.E. Dréau, A. Reiserer, N. Kalb, M.S. Blok, J. Ruitenberg, R.F.L. Vermeulen, R.N. Schouten, C. Abellán, W. Amaya, V. Pruneri, M.W. Mitchell, M. Markham, D.J. Twitchen, D. Elkouss, S. Wehner, T.H. Taminiau, R. Hanson, Loophole-free Bell inequality violation using electron spins separated by 1.3 kilometres. Nature 526, 682–686 (2015)

References 17

R. Hildner, D. Brinks, J.B. Nieder, R.J. Cogdell, N.F. von Hulst, Quantum coherent energy transfer over varying pathways in single light-harvesting complexes, Science **340**, 1448–1451 (2013)

- A.S. Holevo, Statistical Structure of Quantum Theory (Springer Science & Business Media, Berlin, 2001)
- C.K. Hong, Z.Y. Ou, L. Mandel, Measurement of subpicosecond time intervals between two photons by interference. Phys. Rev. Lett. **59**, 2044–2046 (1987)
- K. Hornberger, S. Gerlich, P. Haslinger, S. Nimmrichter, M. Arndt, Colloquium: quantum interference of clusters and molecules. Rev. Mod. Phys. **84**, 157–173 (2012)
- R. Horodecki, P. Horodecki, M. Horodecki, K. Horodecki, Quantum entanglement. Rev. Mod. Phys. 81, 865–942 (2009)
- H. Hu, A. Strybulevych, J.H. Page, S.E. Skipetrov, B.A. van Tiggelen, Localization of ultrasound in a three-dimensional elastic network. Nat. Phys. **4**, 945–948 (2008)
- Y. Imry, Introduction to Mesoscopic Physics (Oxford University Press, Oxford, 2009)
- R.A. Jalabert, J.-L. Pichard, C.W.J. Beenakker, Universal quantum signatures of chaos in ballistic transport. EPL **27**, 255 (1994)
- C. Jönsson, Elektroneninterferenzen an mehreren künstlich hergestellten Feinspalten. Z. Phys. 161, 454–474 (1961)
- J. Jortner, M. Bixon, T. Langenbacher, M.E. Michel-Beyerle, Charge transfer and transport in DNA. PNAS 95, 12759–12765 (1998)
- M. Katsumori, *Niels Bohr's complementarity: its structure, history, and intersections with hermeneutics and deconstruction.* Boston Studies in the Philosophy of Science, vol. 286 (Springer, Dordrecht [Netherlands], New York, 2011)
- E.H. Kennard, Zur Quantenmechanik einfacher Bewegungstypen. Z. Phys. 44, 326–352 (1927)
- D. Klotsa, R.A. Römer, M.S. Turner, Electronic transport in DNA. Biophys. J. 89, 2187–2198 (2005)
- B. Kramer, A. MacKinnon, Localization: theory and experiment. Rep. Prog. Phys. 56, 1469 (1993)
- K. Kraus, Operations, in States, Effects, and Operations Fundamental Notions of Quantum Theory, ed. by A. Böhm, J.D. Dollard, W.H. Wootters. Lecture Notes in Physics, vol. 190 (Springer, Berlin, 1983a), pp. 13–41
- K. Kraus, States, Effects, and Operations Fundamental Notions of Quantum Theory: Lectures in Mathematical Physics at the University of Texas at Austin (Springer, Berlin, 1983b)
- T.P. Krüger, C. Ilioaia, M.P. Johnson, A.V. Ruban, E. Papagiannakis, P. Horton, R. van Grondelle, Controlled disorder in plant light-harvesting complex II explains its photoprotective role. Biophys. J. 102, 2669–2676 (2012)
- D.P. Landau, K. Binder, A Guide to Monte Carlo Simulations in Statistical Physics (Cambridge University Press, Cambridge, New York, 2009)
- T. Lanting, A.J. Przybysz, A.Y. Smirnov, F.M. Spedalieri, M.H. Amin, A.J. Berkley, R. Harris, F. Altomare, S. Boixo, P. Bunyk, N. Dickson, C. Enderud, J.P. Hilton, E. Hoskinson, M.W. Johnson, E. Ladizinsky, N. Ladizinsky, R. Neufeld, T. Oh, I. Perminov, C. Rich, M.C. Thom, E. Tolkacheva, S. Uchaikin, A.B. Wilson, G. Rose, Entanglement in a quantum annealing processor. Phys. Rev. X 4, 021041 (2014)
- P. Lenard, Ueber die lichtelektrische Wirkung. Ann. Phys. 313, 149–198 (1902)
- G. Ludwig, Versuch einer axiomatischen Grundlegung der Quantenmechanik und allgemeinerer physikalischer Theorien. Z. Phys. 181, 233–260 (1964)
- G. Ludwig, Attempt of an axiomatic foundation of quantum mechanics and more general theories II. Commun. Math. Phys. **4**, 331–348 (1967)
- G. Ludwig, Attempt of an axiomatic foundation of quantum mechanics and more general theories III. Commun. Math. Phys. **9**, 1–12 (1968)
- H. Maassen, Quantum Probability and Quantum Information Theory, in *Quantum Information*, *Computation and Cryptography* ed. by F. Benatti, M. Fannes, R. Floreanini, D. Petritis). Lecture Notes in Physics, vol. 808 (Springer, Berlin, 2010), pp. 65–108. https://doi.org/10.1007/978-3-642-11914-9_3

- P. Macha, G. Oelsner, J.-M. Reiner, M. Marthaler, S. André, G. Schön, U. Hübner, H.-G. Meyer, E. Il'ichev, A.V. Ustino, Implementation of a quantum metamaterial using superconducting qubits, Nat. Commun. 5, 5146 (2014)
- G.W. Mackey, *Mathematical Foundations of Quantum Mechanics*. Mathematical Physics Monograph Series (W.A. Benjamin, New York, 1963)
- L. Marton, Electron interferometer. Phys. Rev. 85, 1057–1058 (1952)
- B.J. Metcalf, N. Thomas-Peter, J.B. Spring, D. Kundys, M.A. Broome, P.C. Humphreys, X.-M. Jin, M. Barbieri, W. Steven Kolthammer, J.C. Gates, B.J. Smith, N.K. Langford, P.G.R. Smith, I.A. Walmsley, Multiphoton quantum interference in a multiport integrated photonic device. Nat. Commun. 4, 1356 (2013)
- G. Modugno, Anderson localization in Bose–Einstein condensates. Rep. Prog. Phys. **73**, 102401 (2010)
- M.A. Nielsen, I.L. Chuang, *Quantum Computation and Quantum Information*, 10th edn. (Cambridge University Press, Cambridge, New York, 2010)
- W. Pauli, Über den Zusammenhang des Abschlusses der Elektronengruppen im Atom mit der Komplexstruktur der Spektren. Z. Phys. 31, 765–783 (1925)
- W. Pauli, The connection between spin and statistics. Phys. Rev. 58, 716–722 (1940)
- K.R. Popper, Quantum mechanics without "The observer", in *Quantum Theory and Reality*, ed. by M. Bunge. Studies in the Foundations Methodology and Philosophy of Science, vol. 2 (Springer, Berlin, 1967), pp. 7–44
- A.L. Rakhmanov, A.M. Zagoskin, S. Savel'ev, F. Nori, Quantum metamaterials: electromagnetic waves in a Josephson qubit line. Phys. Rev. B 77, 144507 (2008)
- J. Rammer, Quantum Transport Theory. Frontiers in Physics, vol. 99 (Perseus Books, Reading, MA, 1998)
- M. Reetz-Lamour, T. Amthor, J. Deiglmayr, M. Weidemüller, Rabi oscillations and excitation trapping in the coherent excitation of a mesoscopic Frozen Rydberg Gas. Phys. Rev. Lett. 100, 253001 (2008)
- G. Roati, C.D. "Errico, L. Fallani, M. Fattori, C. Fort, M. Zaccanti, G. Modugno, M. Modugno, M. Inguscio, Anderson localization of a non-interacting Bose–Einstein condensate. Nature 453, 895–898 (2008)
- H.P. Robertson, The uncertainty principle. Phys. Rev. **34**, 163–164 (1929)
- A. Schelle, D. Delande, A. Buchleitner, Microwave-driven atoms: from Anderson localization to Einstein's photoeffect. Phys. Rev. Lett. **102**, 183001 (2009)
- M. Schlosshauer, Decoherence, the measurement problem, and interpretations of quantum mechanics. Rev. Mod. Phys. **76**, 1267–1305 (2005)
- G.D. Scholes, G.R. Fleming, A. Olaya-Castro, R. van Grondelle, Lessons from nature about solar light harvesting. Nat. Chem. 3, 763–774 (2011)
- G.B. Schuster, Long-range charge transfer in DNA: transient structural distortions control the distance dependence. Acc. Chem. Res. 33, 253–260 (2000)
- N. Spagnolo, C. Vitelli, M. Bentivegna, D.J. Brod, A. Crespi, F. Flamini, S. Giacomini, G. Milani, R. Ramponi, P. Mataloni, R. Osellame, E.F. Galvão, F. Sciarrino, Experimental validation of photonic boson sampling. Nat. Photon. 8, 615–620 (2014)
- J.B. Spring, B.J. Metcalf, P.C. Humphreys, W.S. Kolthammer, X.-M. Jin, M. Barbieri, A. Datta, N. Thomas-Peter, N.K. Langford, D. Kundys, J.C. Gates, B.J. Smith, P.G.R. Smith, I.A. Walmsley, Boson Sampling on a photonic chip. Science 339, 798–801 (2013)
- M. Tillmann, B. Dakić, R. Heilmann, S. Nolte, A. Szameit, P. Walther, Experimental boson sampling. Nat. Photon. **7**, 540–544 (2013)
- A. Tonomura, Direct observation of thitherto unobservable quantum phenomena by using electrons. PNAS **102**, 14952–14959 (2005)
- H. van Amerongen, L. Valkunas, R. van Grondelle, *Photosynthetic Excitons* (World Scientific, Singapore, 2000)
- A. Verbeure, *Many-body Boson Systems: Half a Century Later*. Theoretical and Mathematical Physics (Springer, London; New York, 2011)

References 19

D. Vollhardt, P. Wölfle, Diagrammatic, self-consistent treatment of the Anderson localization problem in d <= 2 dimensions. Phys. Rev. B 22, 4666–4679 (1980)

- J. von Neumann, Mathematische Grundlagen der Quantenmechanik (Springer, Berlin, 1932a)
- J.E. Walker, The NADH:ubiquinone oxidoreductase (complex I) of respiratory chains. Q. Rev. Biophys. **25**, 253–324 (1992)
- H. Weyl, Gruppentheorie und Quantenmechanik (Hirzel, Leipzig, 1928)
- H. Weyl, *Philosophy of Mathematics and Natural Science* (Princeton University Press, Princeton, 1949)
- E.P. Wigner, Characteristic vectors of bordered matrices with infinite dimensions. Ann. Math. **62**, 548–564 (1955)
- E.P. Wigner, On the distribution of the roots of certain symmetric matrices. Ann. Math. **67**, 325–327 (1958)
- P.-E. Wolf, G. Maret, Weak localization and coherent backscattering of photons in disordered media. Phys. Rev. Lett. **55**, 2696–2699 (1985)
- T. Young, The Bakerian lecture: experiments and calculations relative to physical optics. Phil. Trans. R. Soc. Lond. **94**, 1–16 (1804)

Chapter 2 Essentials of Quantum Theory



There is a theory which states that if ever anyone discovers exactly what the Universe is for and why it is here, it will instantly disappear and be replaced by something even more bizarre and inexplicable. There is another theory which states that this has already happened

Douglas Adams in (Adams 1995)

The goal of this section is to refresh the physical concepts underlying quantum physics and specifically quantum dynamical system. For more details, the reader is referred to several excellent books and lecture notes, on which this chapter is loosely based (Alicki 1987; Alicki and Fannes 2001; Benatti et al. 2010; Bratteli and Robinson 1987, 1997; Holevo 2001; Peres 1995).

2.1 Quantum Mechanics as a Probabilistic Theory*

We present an introduction to the operational approach of quantum mechanics. This introduction is heuristic and focusses on quantum mechanics as a fundamentally probabilistic theory.

From classical physics, we know a dynamical system as a system where the observables change in time. This evolution is typically governed by basic physical laws. For example, think of position x(t) and linear momentum p(t), the dynamics of which is determined by the canonical Hamiltonian equations of motion

$$\frac{\partial H}{\partial x} = -\dot{p} \tag{2.1}$$

$$\frac{\partial H}{\partial p} = \dot{x}.\tag{2.2}$$

Here we introduce the classical Hamiltonian H, which serves as a generator for the dynamics. Note that a well-defined position and momentum are assumed to exist at each point in time. In quantum mechanics, however, this assumption is invalid as a consequence of the uncertainty relation.

Performing a measurement in physics typically leads to a dataset of measurement outcomes. Assuming that the experimenter lives in an idealised classical world, where his devices can work as precisely as he wants, he should obtain the same value over and over again upon repeating the same experiment. However, lived he in a quantum world, he would be confronted with an intrinsic notion of statistics in his data. If we assume that he measures some observable O, he would acquire a whole set of possible outcomes $o_1, \ldots, o_N \in \mathbb{R}$. Moreover, with enough statistics, he would see that some outcomes are more probable than others, allowing him to construct couples of the form (p_i, o_i) , where p_i is the relative frequency with which o_i is measured. From the underlying theory, the set of possible outcomes could be continuous, such that instead of p_i one rather describes $\mathrm{d}\mu(o)$, a probability density on the set of possible outcomes.

Quantities which are of particular interest are the statistical moments of such a distribution, e.g. the expectation value, the variance, et cetera. These can be obtained from standard statistics as

$$\langle O^n \rangle = \int_{\mathcal{O} \subset \mathbb{R}} d\mu(o) \, o^n \text{ (theoretical)}$$
 (2.3)

$$\langle O^n \rangle = \frac{1}{N} \sum_{j=1}^N o_j^n$$
 (experimental estimate after N measurements). (2.4)

The important aspect of such quantities is that they are both experimentally and theoretically accessible. The demand that $d\mu(o)$ be a probability distribution straightforwardly implies that $\langle \mathbb{1} \rangle = 1$, where $\mathbb{1}$ is the observable that under any measurement returns "1" as measurement outcome. Although this seems completely obvious, it has has important consequences on the level of dynamics, since it imposes additional constraints (see Sect. 2.4). Another statistical fact is that $\langle O^{2k} \rangle \geqslant 0$.

Let us now divert our attention to dynamics in such a statistical theory. In principle, all we need is a set $\mathcal{O} \subset \mathbb{R}$ of all possible outcomes on top of which we define a probability distribution. The quantities in such a theory which can be observed are $\langle O^n \rangle (t)$, implying that measuring the observable at time t_1 can lead to a different statistics than measuring at t_2 . We assume that the set \mathcal{O}^2 of all possible measurement

¹In quantum mechanics, measurement outcomes are always assumed to be real numbers.

²Upon doing measurements, the experimenter samples measurement outcomes from the set \mathcal{O} . This implies that \mathcal{O} can be estimated by $\{o_1, \ldots, o_j, \ldots\}$. When measuring for example spin, the

outcomes for a given observable O is fixed, however the probability density may vanish for some possible outcomes (at some points in time). That leaves us with the idea that the dynamics is actually described by a time dependence in the probability distribution, $\mathrm{d}\mu_t(o)$. We must require our theory to be probabilistic at all times t, which implies that $\mathrm{d}\mu_t(o)$ is a probability distribution for all times t, and therefore $\langle \mathbb{1} \rangle(t) = 1$ for any time t.

By pure reasoning, we obtain that a dynamical quantum system is essentially described by mapping probability distributions on other probability distributions. Arguably this would hold for any statistical theory, and from this argumentation it is not completely clear where "quantum" pops up. In Sect. 2.2, we will consider specific properties of quantum probability theory, but first we must introduce the idea of a fundamentally probabilistic theory in contrast to a theory which is probabilistic due to a lack of knowledge of the experimental preparation procedure. To build such intuition, we elaborate on the elements which determine the probability measure $\mathrm{d}\mu_t(o)$ which describes the measurement outcomes.

Let us start from a dynamical setup and consider the initial probability distribution $\mathrm{d}\mu_0(o)$. We assume that at least this distribution is under some degree of control. Now, one may ask how such a probability distribution is physically determined. The most obvious dependency is that on the measured observable, O, e.g. we expect a different probability distribution when measuring angular momentum than when measuring the position. A comparison of the set of measurement outcomes for angular momentum \mathcal{O}_L with that for position \mathcal{O}_x clarifies this point, because $\mathcal{O}_L \neq \mathcal{O}_x$. However, even if we measure the same observable multiple times, it is not hard to imagine that we can still prepare the system in a different initial state. When measuring position, one may, for example, prepare the system in a distribution with expectation value $\langle x \rangle = x_1$, but just as well in one with $\langle x \rangle = x_2$. This can only mean that the distributions are different, although the abstract observable is the same. This freedom can be captured by the abstract concept of "state" ϕ .³

In short, we have reasoned that the distribution $d\mu_0(o)$ depends both on what we are measuring (the observable) and on how we prepare the system (the state). There is, however, more. We assume that one is able to prepare the system in two possible states ϕ and ψ , which lead to two probability distributions $d\mu_0^{\phi}(o)$ and $d\mu_0^{\psi}(o)$, respectively. Therefore, one will also be able to, alternatively, flip a coin each time one prepares the initial state and repeats the experiment. If the coins gives heads, one prepares the system in ϕ , otherwise one prepares ψ . If we assume that the preparation and the measurement are done by different people, the experimenter who does the measurement will not have the information on whether the coin flip was heads or tails; he generally just sees a set of measurement outcomes on which

spectrum is discrete and one may hope to recover the full set \mathcal{O} upon measurement. However, when for example linear momentum is measured, the set of possible measurement outcomes is in general continuous.

³Notice that we do not even define a set in which ϕ is contained. At this stage of our heuristic treatment, it is not yet described by a functional on an algebra of observables, nor a vector in a Hilbert space. At this stage, it is just an abstract way of summarising the preparation procedure in an experiment.

he can do statistics. More generally, we wish to allow for this type of uncertainty in the state that was prepared. This leads to the idea that

$$p_{\text{heads}} d\mu_0^{\phi}(o) + (1 - p_{\text{heads}}) d\mu_0^{\psi}(o) = d\mu_0^{p\phi + (1-p)\psi}(o),$$
 (2.5)

which can be generalised to the idea that convex combinations (Gudder 1973; Rockafellar 1997) of these physical probability measures, related to different states, lead to a new physical probability measure given by a new state. Alternatively one can also say that the space of all states is a convex set. More specifically, we can thus decompose every state ρ in a convex combination of states. When the only convex decomposition of a state is the state itself, it is said to be an extreme point, or in physics language a "pure state". To understand the terminology, we stress that operations which generate convex combinations, like flipping a coin, are always associated with classical randomness. The degree of uncertainty which is introduced into the state by such operation is governed by classical probability theory. A pure state, one which cannot be decomposed, has no coin flipping or other classical randomness in it, and all uncertainty is therefore purely of quantum mechanical origin. Notice that in classical mechanics these pure states would always be delta functions.

In summary, we have seen that a statistical physical theory is determined by a set of possible measurement outcomes ($\mathcal{O} \subset \mathbb{R}$, which depends on the specific observable), equipped with a probability distribution. Additionally, there is also the freedom in preparation of the initial state of the system, which again influences the probability distribution for the possible measurement outcomes. Convex combinations of states lead to new states and therefore also convex combinations of physical probability measures lead to new physical probability measures. Finally, we deduced that dynamics should take place on the level of such distributions in the sense that the dynamics should map the physical probability distributions on new physical probability distributions. However, our complete discussion was based on the measurement of a single observable and, as it turns out, genuine quantum effect only become apparent in the relations between different observables.

2.2 Quantisation*

Quantum mechanics is fundamentally different from classical probability theory. This difference becomes explicitly clear as a consequence of quantisation. Canonical quantisation lies at the basis of the algebraic approach to quantum mechanics and it as such also stimulated the development of quantum logic and quantum probability theory. Since these fields set the context in which the here presented research was done, we provide a short overview.

In the previous section, we introduced quantum mechanics as a fundamentally probabilistic theory and we heuristically derived several of its properties. However, the above discussion does not highlight those features of the theory which are specific 2.2 Quantisation* 25

to *quantum* theory. Indeed, quantum theory is more than a theory which is fundamentally probabilistic, it also requires a new framework of probability theory, which is exactly what is studied by the field of *quantum probability theory*. At its foundation, this can be seen as a probability theory formulated using the quantum logic of Birkhoff and von Neumann (1936). In this section, we highlight those aspects which give quantum mechanics its counter-intuitive nature. To do so, we first provide a brief overview of its historical development.

2.2.1 Old and New Quantum Theory*

One of the most fundamental structures in classical mechanics is *phase space*, which describes the coordinates (x_1, \ldots, x_N) and their associated generalised momenta (p_1, \ldots, p_N) in one huge space constructed by points of the form $(x_1, x_2, \ldots, x_N, p_1, p_2, \ldots, p_N) := (\mathbf{x}, \mathbf{p})$. Centuries of developing classical mechanics ultimately led to a mathematical description of phase space in terms of *canonical* (or symplectic) structures, on which the Hamiltonian dynamics describes a symplectic flow (Arnold 1989). The standard study of classical mechanics is based on the description of points in phase space and their orbits.

In the early twentieth century, such descriptions were confronted with both experimental and theoretical problems (see e.g. Sect. 1.1), which ultimately led to the development of quantum mechanics. Just as the introduction of the speed of light c as fundamental constant led to a new type of mechanics at high energies, quantum mechanics imposed constraints on low-energy physics. The introduction of Planck's constant h was initially just a computational trick, but quickly became a fundamental part of physics. The *old quantum theory*, which was formalised by Bohr (1913) and Sommerfeld (1916) to describe the hydrogen atom, focusses strongly on putting limits upon the allowed orbits in phase space. Fundamentally, the theory postulated that volume elements in phase space (thus describing an action) could not be made arbitrarily small, but had a minimum size, given exactly by h. This led to the Bohr-Sommerfeld quantisation rule for every $i \in \{1, \ldots, N\}$

$$\oint_{H(\mathbf{x},\mathbf{p})=E} p_i dx_i = n_i h, \text{ with } n_i \in \mathbb{N}.$$
(2.6)

The condition is clearly related to the symplectic structure, because it connects coordinates to their associated generalised momenta. The quantity $H(\mathbf{x}, \mathbf{p})$ describes the Hamiltonian of the system, which is known from classical mechanics. Since $H(\mathbf{x}, \mathbf{p}) = E$ characterises an orbit in phase space, the quantisation condition (2.6) can be read as a prescription for the allowed orbits and thus the allowed energies of the system. In other words, the only allowed energies are those which lead to orbits with an action given by an integer multiple of the fundamental quantum of action h. Notice that this quantisation procedure does *not* require a specific statistical interpretation, it merely constrains the allowed orbits in phase space.

This first quantisation method was very successful in describing the hydrogen atom and predicting the position of spectral emission and absorption lines. However, the formalism had its limitation, the most profound of which was the lack of a description for the process of the absorption and emission of electromagnetic radiation. This specifically made it impossible to theoretically predict the intensity of the observed spectral lines. Nevertheless, Kramers managed to heuristically describe a "law of dispersion" for the theory of atomic spectra (Kramers 1924). Kramers' idea to introduce a transition matrix to describe the transitions between energy levels later became the basis for Heisenberg's formulation of matrix mechanics (Heisenberg 1925). This new perspective turned quantum theory into a fundamentally probabilistic theory. Jordan and Born (1925) realised that Heisenberg's matrix mechanics required a formulation of "position" *Q* and "momentum" *P* in terms of *matrices* and they derived the quantum condition ("Quantenbedingung")

$$PQ - QP = \frac{h}{2\pi i} \mathbb{1}. (2.7)$$

With this formulation they provide an explicit connection between the canonical phase space structure and Heisenberg's matrix mechanics. This identity is the foundation of the mathematical structure of the quantum mechanics we know today, with its basics described in Born et al. (1926).

Independently of Born and Jordan, also Dirac formulated Eq. (2.7) (Dirac 1925). Although Dirac's work is very similar to that of Born and Jordan (1925), the provided perspective is slightly different: Born and Jordan start from the framework of matrices, whereas Dirac provides a more algebraic perspective. Dirac realised that the fundamental insight of Heisenberg was not the exact formulation in terms of matrices, but rather the introduction of a new type of non-commutative algebra.

Furthermore, Dirac realised that this different type of algebra explicitly used information which was already hidden in the structure of classical mechanics. Literally, he states

In a recent paper Heisenberg puts forward a new theory, which suggests that it is not the equations of classical mechanics that are in any way at fault, but that the mathematical operations by which physical results are deduced from them require modification. All the information supplied by the classical theory can thus be made use of in the new theory.

Paul Dirac in (Dirac 1925)

Dirac's starting point in developing these new mathematical operations was the structure of phase space and more notably the relation between observables determined by the *Poisson bracket*. In classical mechanics, observables are functions on the phase space. The Poisson bracket $\{.,.\}_P$ (Arnold 1989) relates two such observables $O_1(\mathbf{x}, \mathbf{p})$ and $O_2(\mathbf{x}, \mathbf{p})$ according to the following procedure

$$\{O_1, O_2\}_P := \sum_i \frac{\partial O_1}{\partial x_i} \frac{\partial O_2}{\partial p_i} - \frac{\partial O_2}{\partial x_i} \frac{\partial O_1}{\partial p_i}.$$
 (2.8)

2.2 Quantisation* 27

The Poisson bracket describes how observables are related to each other with respect to the canonical form that lies upon the phase space. The most profound example of such a relation is given by $\{x_i, p_j\}_P = \delta_{ij}$, a relation which at least seems similar to (2.7). Dirac realised that Heisenberg's formulation of quantum theory as matrix mechanics could be generalised in a more abstract way via the demand that

$$\hat{O}_1 \cdot \hat{O}_2 - \hat{O}_2 \cdot \hat{O}_1 = i\hbar \{O_1, O_2\}_P. \tag{2.9}$$

On the lefthand side we depict the quantised versions of the observables O_1 and O_2 . The "·" defines the modified mathematical operation that Dirac refers to. With (2.9), Dirac provides the mechanism for constructing the algebra that describes quantum mechanics and at the same time respects the classical phase space's structure. This process of *canonical quantisation* lies at the basis of the later development of algebraic quantum mechanics by von Neumann and the construction of quantum probability theory.

We finally note that, indeed, (2.9) leads to $\hat{q}_i \hat{p}_j - \hat{p}_j \hat{q}_i = i\hbar \delta_{ij}$, which lies at the basis of the algebra of *canonical commutation relations* (CCR), and will discussed extensively in Sect. 7.7.2. It ultimately turns out that this algebra describes bosonic systems and therefore it is possible to provide phase space interpretations for many-boson systems. These mathematical structures will reappear in Part III of this dissertation.

2.2.2 Quantum Algebra and Quantum Probability*

The heuristics of Sect. 2.1 made it feasible to interpret quantum mechanics as a probabilistic theory, based on the observation that the measurement outcomes show specific statistical features. Still, the phenomena that lead to the development of quantum mechanics require more than mere probability theory; they also impose a need for "quantisation". The first decades of theoretical research on quantum theory were largely dominated by the search for a correct quantisation postulate and Dirac's procedure, as expressed in (2.9), became one of the most widely spread quantisation protocols. Although there have been other notable proposals, such as Feynman's path integrals (Feynman 1948) and Moyal's quantisation by means of phase space deformation (Moyal 1949), it is Dirac's work that inspired von Neumann to develop the framework of quantum probability theory (von Neumann 1932a), based on the functional analysis of Hilbert spaces. Later this work would develop further into more abstract algebraic formulations, which occur throughout several chapters of this dissertation, mainly in Part III. In Sect. 2.3 we provide an introduction to the foundations of the algebraic quantum theory that is generated starting from the algebraic reasoning that led Dirac to Eq. (2.9). However, before we enter the technical realm of spectral theory and operator algebras, let us discuss the very fundamental probabilistic consequences of the quantisation procedure (2.9).

Quantum mechanical experiments, ranging from Stern–Gerlach (1922a, b) to electron beam interferometry (Marton 1952), empirically confront us with an intrinsic notion of probability theory. This observation led us to the operational introduction of Sect. 2.1. However, in Sect. 2.2.1, we saw that quantum physics ultimately requires a new type of non-commutative algebra, which is not contained within classical probability. Von Neumann realised that Dirac's idea, pushed to the extreme, imposed a completely new type of logic and a new type of probability theory (Birkhoff and von Neumann 1936; von Neumann 1932a).

From the discussion in Sect. 2.2.1, we clearly see that the new algebraic properties and the new theory, induced by the existence of \hbar , only become apparent when *multiple* observables are considered. In other words, when we measure a single observable we recover classical probability theory, but once several observables are jointly investigated we require quantum probability, which is a consequence of noncommutative algebra. The earliest example where quantum probability manifests itself is provided by Heisenberg's (preparation) uncertainty relation (Heisenberg 1927; Kennard 1927; Robertson 1929; Weyl 1928)

$$\Delta x \, \Delta p \geqslant \frac{\hbar}{2},\tag{2.10}$$

with Δx and Δp the standard deviations of position and momentum, respectively. The presented standard deviations are not related to the measurement process, but rather to the statistics determined by the *state*, *i.e.* the preparation procedure (for a detailed discussion, see Holevo (2001)). In a purely probabilistic language, we see that the finite \hbar forbids us to prepare the statistics of the position with influencing the statistics of the momentum. Recently there has been research on determining similar uncertainty relations on the "joint measurement" of quantum observables (Busch et al. 2013; Kraus 1987; Martens and Muynck 1990; Ozawa 2003).

The derivation of (2.10) can be generalised to other observables O_1 and O_2 (Robertson 1929), where we find that

$$\Delta O_1 \Delta O_2 \geqslant \frac{1}{2} \left| \langle [O_1, O_2] \rangle \right|, \tag{2.11}$$

where [A, B] = AB - BA is the *commutator*. However, this relation has the unpleasant feature that the lower bound on the standard deviations is state dependent. It can nevertheless be noted that these quantities are narrowly related to Bohr's complementarity principle (Bohr 1935).

Other manifestations specific to quantum probability are quantum correlations, which are able to violate Bell's inequalities (Bell 1964). These inequalities are derived for classical probability theory, and set constraints on the correlation between two classical observables. It has only very recently been shown experimentally, in a loophole-free way (Hensen et al. 2015; Giustina et al. 2015; Shalm et al. 2015), that these bounds are broken by quantum systems, in accordance with the prediction of quantum probability theory (Holevo 2001; Maassen 2010).

2.2 Quantisation*

In the remainder of this chapter, we elaborate on the mathematical structure of quantum systems and of their dynamics. Because we always work in the limit where quantum effects are relevant, we choose to work in natural units, where \hbar is the unit of action, i.e. $\hbar=1$.

2.3 Observables and States

In this section, we present the formalism of quantum mechanics, which historically evolved from the new type of algebra that results from (2.7, 2.9). The development of this framework led to the mathematics of operator algebras (Birkhoff and von Neumann 1936; von Neumann 1932a), which later was interpreted (Holevo 2001; Ludwig 1983; Mackey 1963) in a framework comparable to Kolmogorov's treatment of classical probability theory. It is our goal here to gradually build up the algebra required to describe non-relativitic quantum mechanics in a general form. We start from linear algebra with matrices, which can be thought of as Heisenberg's initial matrix mechanics, and ultimately proceed to the theory of abstract C^* -algebras (Bratteli and Robinson 1987, 1997; Evans and Kawahigashi 1998; Sakai 1998). Again, this section is loosely based on Holevo (2001).

2.3.1 Observables

As a starting point, we consider observables as modelled by matrices with complex entries. This is common practice in finite dimensional quantum mechanics and examples are ubiquitous. Even though an observable can be described by a matrix O, a priori these matrices are of course not measurable in experiments, because measurement outcomes are just real numbers. Matrices are interesting because their eigenvalues can be associated with measurement outcomes in a natural way. The central idea is that these eigenvalues are exactly the quantities which are accessible in a measurement and therefore physics implies they must be real. This leads us to demand that $O^{\dagger} = O$. Now we can use the eigenvalue decomposition to write

$$O^k = \sum_i o_i^{\ k} P_i, \tag{2.12}$$

and P_i a projector (meaning that $P_i^2 = P_i$) on the eigenspace associated to the eigenvalue (and thus potential measurement outcome) o_i . An interesting aspect of

projectors is that their eigenvalues are either 0 or 1 and, therefore, we find that, for any normalised vector \vec{v} , $\langle \vec{v}, P_i \vec{v} \rangle \in [0, 1]$. Hence, we find that, for any \vec{v} ,

$$\langle \vec{v}, O^k \vec{v} \rangle = \sum_i o_i^k \langle \vec{v}, P_i \vec{v} \rangle, \quad \text{and} \quad \sum_i \langle \vec{v}, P_i \vec{v} \rangle = 1.$$
 (2.13)

This clearly suggests a nice notion of moments for the distribution of measurement outcomes, and a clear notion of probabilities. One can say that the P_i are a natural way to associate matrices with probabilities. However, one should realise that this framework is very limited as concerns the type of systems that it can describe.

Let us generalise the concept of matrices and vector spaces to that of Hilbert spaces and operators that act on them. This allows us to also capture systems where the dimensions are infinite and where we may even have to consider spectra (the generalisation to the set of eigenvalues) which are continuous. The demand for such an operator O to be an observable is only that its spectrum $\sigma(O) \subset \mathbb{R}$, a straightforward way of saying that, again, we want physical measurement outcomes to be real numbers.

The set of *all* self-adjoint operators on the Hilbert space \mathcal{H} is usually somewhat hard to handle and therefore we tend to focus on the set of bounded operators $\mathcal{B}(\mathcal{H})$. An operator X on \mathcal{H} is said to be bounded if there exists a $\lambda \in \mathbb{R}$, such that for all $\phi \in \mathcal{H}$

$$||X\phi|| \leqslant \lambda ||\phi|| \tag{2.14}$$

Bounded operators have many nice properties; if we assume that $A, B \in \mathcal{B}(\mathcal{H})$, we find that

$$A + B \in \mathcal{B}(\mathcal{H}), \tag{2.15}$$

$$AB \in \mathcal{B}(\mathcal{H}),$$
 (2.16)

$$A^{\dagger} \in \mathcal{B}(\mathcal{H}), \tag{2.17}$$

$$1 \in \mathcal{B}(\mathcal{H}). \tag{2.18}$$

These properties together imply that these operators form an algebra (see Appendix A). If we now also include the fact that they are closed under the norm topology (Conway 1997), we can call $\mathcal{B}(\mathcal{H})$ a C^* -algebra (see Sect. A.4 of Appendix A). One may even say that this type of operator algebra lies at the historical basis of C^* -algebras.

In this algebra of bounded operators, we find elements with the property $O^{\dagger} = O$. Such operators are now again the observables. However, we must emphasise that they themselves do not form a *-algebra. The notion of bounded operators is natural, in the sense of keeping quantities (for example energy) finite, but obviously one may

⁴Notice that the spectrum $\sigma(O)$ of the linear operator O on \mathcal{H} takes over the role of the set of possible measurement outcomes, which was referred to as \mathcal{O} in Sect. 2.1.

find many physically relevant objects (such as position and momentum operators) that are unbounded.

The self-adjoint operators in $\mathcal{B}(\mathcal{H})$ have one very beautiful property, which lies at the core of the mathematical fields of spectral analysis and of the study of operator algebras: One can construct a spectral decomposition for them, this result is called the *spectral theorem* (Conway 1997). In general, this theorem tells us that we can correctly define a *projector-valued measure* E(do), which is a *spectral measure* on $\sigma(O) \subset \mathbb{R}$, such that for any analytic function $f: \sigma(O) \to \mathbb{R}$, we find that

$$f(O) = \int_{\sigma(O)} f(o)E(do). \tag{2.19}$$

In addition, such a spectral measure is a resolution of the identity

$$\int_{\sigma(O)} E(\mathsf{d}o) = 1. \tag{2.20}$$

This implies that this is a generalisation of the eigen-decomposition on finite dimensional spaces. Notice that demanding that these $E(\mathrm{d}o)$ are "projector-valued" really means that they behave as projectors and therefore also manifest a sense of orthogonality.

To make these statements more rigorous, one must begin by considering the set of interest, X, and equip it with a measure. This set is denoted by (X, \mathfrak{M}) and is a measurable space. Here \mathfrak{M} is a so-called *Borel* σ -algebra on X. To define a *spectral measure*, we also require a Hilbert space \mathcal{H} , such that we can construct a mapping $E: \mathfrak{M} \to \mathcal{B}(\mathcal{H})$. Note that it connects the elements of the Borel σ -algebra \mathfrak{M} to bounded operators on the Hilbert space.

To obtain a well-defined projector-valued spectral measure, E must fulfil several properties:

- $E(\Delta)$ is a projector for all $\Delta \in \mathfrak{M}$.
- $E(\emptyset) = 0$ and E(X) = 1.
- $E(\Delta_1 \cap \Delta_2) = E(\Delta_1)E(\Delta_2)$ for all $\Delta_1, \Delta_2 \in \mathfrak{M}$.
- E is σ additive: for all disjoint sequences $(\Delta_n)_{n\in\mathbb{N}}\in\mathfrak{M}$ and all $\phi\in\mathcal{H}$ on has

$$E(\cup_n \Delta_n) \phi = \sum_n E(\Delta_n) \phi. \tag{2.21}$$

- $X \in \mathfrak{M}$.
- When $A \subset X \in \mathfrak{M}$, also $X \setminus A \in \mathfrak{M}$.
- When $A_1, \ldots A_n \in \mathfrak{M}$, also $\bigcup_{i=1}^n A_i \in \mathfrak{M}$, for any $n \in \mathbb{N}_0$.

⁵To define a Borel σ -algebra on X (Billingsley 2012; Doob 1994; Pedersen 1989), we must start by defining the *power set* which is commonly denoted 2^X . The elements of a power set are sets themselves, more specifically 2^X is the set of all subsets of X. A *Borel* σ -algebra $\mathfrak{M} \subset 2^X$ is a subset of this power set, with the following properties:

Just as in other branches of analysis, we can use measure theory to connect these measures to the concept of integrals. Therefore we now can make sense of $\int_X f(x)E(\mathrm{d}x)$. A useful fact to do so is that for all $\phi, \psi \in \mathcal{H}$, $E_{\phi,\psi}: \mathfrak{M} \to \mathbb{C}: \Delta \mapsto \langle \phi, E(\Delta)\psi \rangle$ defines a complex measure on (X,\mathfrak{M}) . To connect these results to what we did earlier, we can now consider $X = \sigma(O)$ and therefore we recover $E(\mathrm{d}o)$ as spectral measure.

These notions of operator theory are interesting, but one can think of more general constructions that lead to well-defined probability measures. Notably, one can construct *positive operator-valued measures*, which form a (non-orthogonal) *resolution of the identity*. This essentially means that in the above definition of the spectral measure, we drop the demand that our measure be formed by projectors. In the finite dimensional case, this is what one often finds in textbooks as POVM's (Benatti et al. 2010), but one can also generalise this concept to the generic Hilbert space. Such objects can be used to construct a type of *generalised observables* (Holevo 2001).

A particularly interesting result is that one can actually orthogonalise any such resolutions of the identity, although one must typically embed the system in a larger Hilbert space in order to do so. In other words, a positive operator-valued measure originates from a projector valued-measure on a larger space, and therefore such generalised observables can be connected to standard observables in a larger Hilbert space.

A final level of abstraction which can be added is to forget about the Hilbert space all together and focus on the basic properties of the algebra of observables. Typically this algebra is a C^* -algebra⁶: The fact that it is an algebra essentially means that it is closed under operations that act as addition and multiplication. The demand that it is a *-algebra reflects that we can additionally define a "*-operation", which fundamentally has the same properties as the adjoint operation on $\mathcal{B}(\mathcal{H})$. A C^* -algebra also sets demands on the topology, more specifically, the algebra should be closed under the norm topology. This means that, if the algebra \mathcal{A} contains a sequence $x_n \in \mathcal{A}$, that any limit x reached by making $\|x_n - x\|$ small, should also be contained in the algebra \mathcal{A} . An additional—and crucial—requirement is the so-called C^* -property, which demands that $\|x^*x\| = \|x\|^2$, and this gives us a notion of a positivity, which is fundamental for describing quantum systems in a probabilistic framework. Although this generalisation to C^* -algebras appears overly abstract, it is the required language to formulate the theory of many-body quantum physics, as we will see in Part III.

Remarkably, we can also generalise the machinery of the spectral decomposition to these more general C^* -algebras. However, abstract algebras are usually not the most pleasant mathematical structures to use for doing computations. Luckily, there is a beautiful theoretical framework that allows us to represent any such abstract algebra as a sub-algebra of $\mathcal{B}(\mathcal{H})$, for a suitably chosen \mathcal{H} . The price we pay is that

⁶We briefly note that this need not be the case. For example, in quantum statistical mechanics one also considers von Neumann algebras (Bratteli and Robinson 1987, 1997).

⁷See also Appendix A.

this \mathcal{H} is not uniquely determined, but depends on the other fundamental ingredient of quantum theory: *the quantum state*.

2.3.2 **States**

At the moment, we lack something to connect the observables, elements of some C^* -algebra \mathcal{A} , to actual numbers. These objects are called functionals (Bratteli and Robinson 1987; Conway 1997),⁸

$$\langle . \rangle_{\phi} : \mathcal{A} \to \mathbb{C},$$
 (2.22)

which have the additional properties that

$$\langle \mathbb{1} \rangle_{\phi} = 1, \tag{2.23}$$

$$\langle x^* x \rangle_{\phi} \geqslant 0 \text{ for all } x \in \mathcal{A}.$$
 (2.24)

With these properties, we can interpret the functionals as objects that map observables onto their expectation values. Even though the mathematics is elegant, it again is rather unpractical for the purpose of calculations. Therefore, we will introduce the "GNS" construction (Gelfand and Neumark 1943; Segal 1947), a way of associating states and elements of the algebra to a Hilbert space \mathcal{H}_{ϕ} and the bounded operators thereon. The key idea is that the duo $(\mathcal{A}, \langle . \rangle_{\phi})$ naturally gives rise to the *GNS triplet* $(\mathcal{H}_{\phi}, \Omega_{\phi}, \pi_{\phi})$. \mathcal{H}_{ϕ} is the Hilbert space and $\Omega_{\phi} \in \mathcal{H}$. Finally, $\pi_{\phi} : \mathcal{A} \to \mathcal{B}(\mathcal{H})$ is a representation of the C^* -algebra (see Appendix A). These objects fulfil the following properties:

$$\pi_{\phi}(x^*) = \pi_{\phi}(x)^{\dagger}, x \in \mathcal{A}, \tag{2.25}$$

$$\langle x \rangle_{\phi} = \langle \Omega_{\phi}, \pi_{\phi}(x) \Omega_{\phi} \rangle, \tag{2.26}$$

$$\pi_{\phi}(\mathcal{A})\Omega_{\phi}$$
 is dense in \mathcal{H}_{ϕ} , (2.27)

implying that any state on a given algebra naturally determines a Hilbert space, in a way that connects the state to a vector in that Hilbert space. From this vector, we can then generate the rest of the Hilbert space by acting on it with elements of the algebra, such that Ω_{ϕ} is a *cyclic vector* (see Appendix A). We must stress, however, that this Hilbert space \mathcal{H}_{ϕ} depends on the specific state of the system.

We now consider the case where the C^* -algebra is given by $\mathcal{B}(\mathcal{H})$ for some Hilbert space \mathcal{H} and discuss the structure of states on such an algebra. To do so, we must introduce another space of interesting operators on \mathcal{H} : the *trace-class operators*

⁸In Part III we change notation for functionals on abstract C^* -algebras to " ω " to stress contrast between abstract algebras and algebras of the form $\mathcal{B}(\mathcal{H})$ for a specific Hilbert space.

 $\mathcal{T}(\mathcal{H})$. This is the space of operators on \mathcal{H} , for which the trace is well-defined, in the sense that for $X \in \mathcal{T}(\mathcal{H})$ we obtain that $\operatorname{tr}(X) < \infty$. Now it actually turns out that $\mathcal{B}(\mathcal{H})$ is isomorphic to the *dual space* of $\mathcal{T}(\mathcal{H})$. Without going into too much of the functional analysis, we conclude that generally *not* every state $\langle . \rangle_{\phi}$ can be associated to an element of $\mathcal{T}(\mathcal{H})$. Still, there is a given set of states where it is possible, these are called *normal states*. Such normal states have the beautiful property that *for all* $B \in \mathcal{B}(\mathcal{H})$,

$$\langle B \rangle_{\rho} = \operatorname{tr}(\rho B), \ \rho \in \mathcal{T}(\mathcal{H}) \text{ if and only if } \langle . \rangle_{\rho} \text{ is normal}$$

with $\rho \geqslant 0$ and $\operatorname{tr}\rho = 1$.

This trace-class operator used to describe the state is of course the well-known density operator. From this brief discussion one should remember that in all generality the common belief that any state is representable by a density matrix, is actually false. Density operators which are of rank one describe the pure states, and can be associated with state vectors (elements of \mathcal{H}).

Notice that only the pure states are captured by the GNS construction. If one were to provide a non-pure normal state $\langle . \rangle_{\rho}$ on the algebra $\mathcal{B}(\mathcal{H})$, the GNS construction would actually give rise to another Hilbert space \mathcal{K}_{ρ} , such that $\langle . \rangle_{\rho}$ can be associated with a state vector $\Omega_{\rho} \in \mathcal{K}_{\rho}$. This means that, in this case, the GNS construction actually leads to a purification of a mixed state.

Furthermore, we may consider \mathcal{H}_{ϕ} of the GNS triplet of a state $\langle . \rangle_{\phi}$ as the Hilbert space on which a different state $\langle . \rangle_{\rho}$ can be represented by a density operator $\rho \in \mathcal{T}(\mathcal{H}_{\phi})$. In such a situation, $\langle . \rangle_{\rho}$ is said to be *normal with respect to the representation* of $\langle . \rangle_{\phi}$. This formulation will reoccur in Sect. 9.3.3.

2.3.3 The Probabilistic Interpretation

Now that we have some formal understanding of states on algebras of observables, we can make the connection to probability theory. A fundamental class of objects in quantum probability theory is given by the moments of an observable: $\langle O^k \rangle_{\phi}$. In the most general case, where $O \in \mathcal{A}$, we can of course use the GNS construction to write that

$$\langle O^k \rangle_{\phi} = \langle \Phi, \pi(O)^k \Phi \rangle.$$
 (2.29)

Since we know that the GNS construction naturally provides us with a Hilbert space \mathcal{H} and $\pi(O) \in \mathcal{B}(\mathcal{H})$, we can use the spectral theorem and write

$$\pi(O) = \int_{\sigma(\pi(O))} o E(do), \qquad (2.30)$$

⁹However in finite dimensional systems, it clearly holds.

and therefore we straightforwardly obtain that

$$\langle O^k \rangle_{\phi} = \int_{\sigma(\pi(O))} o^k \langle \Phi, E(do) \Phi \rangle.$$
 (2.31)

It can be shown that $\langle \Phi, E(do)\Phi \rangle$ indeed forms of good measure on $\sigma(\pi(O))$ (Conway 1997). Thus this gives us a generally applicable way of connecting statistical theory to the theory of operator algebras. It moreover leads to a very general formulation of quantum theory.

When we take one step down on the ladder of abstraction, consider that $O \in \mathcal{B}(\mathcal{H})$, and assume that the states are normal, we obtain

$$\langle O^k \rangle_{\rho} = \operatorname{tr}(\rho \, O^k) \tag{2.32}$$

$$\langle O^k \rangle_{\rho} = \int_{\sigma(O)} o^k \operatorname{tr}(\rho E(\operatorname{d}o)).$$
 (2.33)

This, indeed, provides a clean generalisation of the finite dimensional case.

2.4 Dynamics of Quantum Systems

Now that we have provided the mathematical structure of quantum theory, by identifying observables with elements of a C^* -algebra, and states with the functionals thereupon, we can start to consider dynamics. In order to do so, there are two logical approaches; either we propagate the states, or we propagate the observables. ¹⁰ The former is known as the *Schrödinger picture*, the latter as the *Heisenberg picture*.

Whichever picture we employ, the key issue is that the physics which is described must always be the same. This means that the probability distribution remains a well-defined probability distribution for all times and for any observable which we measure. A different way of formulating this requirement is to demand that moments are mapped into moments of a new probability distribution. These demands summarise to

$$\langle X^*X\rangle_{\phi}(t)\geqslant 0\quad \text{for all }X\in\mathcal{A} \text{ and all states }\langle .\rangle_{\phi}, \tag{2.34}$$

$$\langle \mathbb{1} \rangle_{\phi}(t) = 1. \tag{2.35}$$

The former demand is called *positivity*, the latter *normalisation*. Here we did not consider the time dependence in any specific picture, but one can make things more specific by for example deciding to focus on the Heisenberg picture.

¹⁰Note, however, that hybrid descriptions such as the interaction picture are also possible and can in some cases be fruitful.

2.4.1 The Heisenberg Picture

In the Heisenberg picture, we consider a single fixed state $\langle . \rangle_{\phi}$ which remains unchanged over time. The dynamics is hence described by means of an automorphism

$$\Lambda_{t t_0}: \mathcal{A} \to \mathcal{A},$$
 (2.36)

where t_0 denotes the starting point of the dynamics and t is the final time. As we see, elements of the C^* -algebra of observables are mapped onto other elements of the same algebra. Requirements (2.34) and (2.35) now need to be expressed by conditions on Λ_{t,t_0} , which leads to

$$\|\Lambda_{t,t_0}(X^*X)\| \geqslant 0$$
 for all $X \in \mathcal{A}$ (positive map), (2.37)

$$\Lambda_{t,t_0}(\mathbb{1}) = \mathbb{1} \quad \text{(unital map)}, \tag{2.38}$$

for any possible t_0 and t. These are the most straightforward demands on the dynamics, arising by simply demanding that our theory remains a well-defined statistical theory throughout time. Another natural demand is that

$$\lim_{t \to t_0} \Lambda_{t,t_0}(X) = X. \tag{2.39}$$

Now one can make additional assumptions on the dynamics, for example by demanding that it be continuous in the norm topology that lies upon the algebra \mathcal{A} , which makes the dynamics "smooth". Typically, however, there is a wide range of other constraints which are imposed to make the dynamics tractable.

It is common to assume that the dynamics is not only positive (as demanded by 2.37), but even *completely positive*. The problem with positive, unital maps as the ones defined here above, is that they are in general no longer well-defined positive maps upon a trivial embedding in a larger system. Such embeddings can have very different origins, an important one being the inclusion of internal degrees of freedom. This is important because the majority of actual systems which are described by quantum mechanics are effective models, where we ignore several degrees of freedom. If the dynamics is not completely positive, the model cannot be well-defined, since these additional internal degrees of freedom oppose the existence of a probabilistic interpretation of the theory.

Formally, we embed a map Λ_{t,t_0} on \mathcal{A} in a larger space $\mathcal{A} \otimes \mathcal{M}_n$ (where \mathcal{M}_n are the $n \times n$ complex matrices) by simply defining $\Lambda_{t,t_0} \otimes \mathbb{I}_n$ as

$$(\Lambda_{t,t_0} \otimes \mathbb{I}_n)(O \otimes \mathbb{I}_n) = \Lambda_{t,t_0}(O) \otimes \mathbb{I}_n \quad \text{and} \quad (\Lambda_{t,t_0} \otimes \mathbb{I}_n)(\mathbb{1} \otimes M) = \mathbb{1} \otimes M.$$
(2.40)

For the dynamics to be physically sensible, we demand that just extending the space by including an "ancilla" does keep the probabilistic structure of our theory intact. In other words, we demand that $\Lambda_{t,t_0} \otimes \mathbb{I}_n$ be a positive map *for all n*. Such maps are called *completely positive maps* (CP maps).

Considering algebras of the type $\mathcal{B}(\mathcal{H})$, a CP map always allows a Kraus representation (Kraus 1971), given in the following way: Choose $O \in \mathcal{B}(\mathcal{H})$ and consider a unital CP map Λ_{t,t_0} . In that case, Kraus showed that, for all t and t_0 , there exists a set of operators $V_{i:t,t_0} \in \mathcal{B}(\mathcal{H})$ such that

$$\Lambda_{t,t_0}(O) = \sum_{i} V_{i;t,t_0}^{\dagger} O V_{i;t,t_0}. \tag{2.41}$$

Therefore, when the state is normal, we can write

$$\langle O \rangle_{\rho}(t) = \operatorname{tr}(\rho \, \Lambda_{t,t_0}(O)) = \operatorname{tr}\left(\rho \sum_{i} V_{i;t,t_0}^{\dagger} O \, V_{i;t,t_0}\right). \tag{2.42}$$

An important additional condition, which boils down to demanding normalisation, is that $\sum_{i} V_{i;t,t_0}^{\dagger} V_{i;t,t_0} = \mathbb{1}$. This result is actually a special case of Stinespring's characterisation of CP maps of C^* -algebras (Stinespring 1955).

An additional assumption which is regularly encountered is called *divisibility*, meaning that the dynamics can be arbitrarily stopped at any point and thereafter may just be continued again. Mathematically, this reads

$$\Lambda_{t,t_0} = \Lambda_{t,s} \circ \Lambda_{s,t_0} \quad \text{for all } s \in [t_0, t]$$
 (2.43)

and of course, it must hold for all possible choices for t_0 and t. An important consequence of this choice is that

$$\frac{d}{dt}\Lambda_{t,t_0} = \lim_{\epsilon \to 0} \frac{\Lambda_{t+\epsilon,t_0} - \Lambda_{t,t_0}}{\epsilon} = \left(\lim_{\epsilon \to 0} \frac{\Lambda_{t+\epsilon,t} - \mathrm{id}}{\epsilon}\right) \circ \Lambda_{t,t_0} := \mathcal{L}_t \circ \Lambda_{t,t_0}, \quad (2.44)$$

thereby defining the generator \mathcal{L}_t of the dynamical map.

One can again go one step further and demand that the dynamics is a *one-parameter semi-group*, which essentially implies that our divisible map of (2.43) is independent of the starting time t_0 , and only depends on the elapsed time $t - t_0$. In other words, we can set $t_0 = 0$ without any loss of generality. A simple calculation now shows that

$$\frac{d}{dt}\Lambda_t := \mathcal{L} \circ \Lambda_t. \tag{2.45}$$

Thus, the dynamics is determined by a specific, time-independent, generator.

A famous result by Lindblad (1976) states that Λ_t forms a one-parameter semi-group of completely positive maps on $\mathcal{B}(\mathcal{H})$ if and only if the generator can be written as

$$\mathcal{L}(X) = i[H, X] + \sum_{j} L_{j}^{\dagger} X L_{j} - \frac{1}{2} \{ L_{j}^{\dagger} L_{j}, X \}, \quad \text{for all } X \in \mathcal{B}(\mathcal{H}). \tag{2.46}$$

The conditions on L_j are surprisingly general, demanding only that $L_j \in \mathcal{B}(\mathcal{H})$ and $\sum_i L_i^{\dagger} L_j \in \mathcal{B}(\mathcal{H})$.

A more general result for any C^* -algebra \mathcal{A} is also provided by Lindblad (1976), and will be used throughout Chap. 9. It states that Λ_t is completely positive if

$$\mathcal{L}(X) = \Psi(X) + KX + XK^*, \quad \text{for all } X \in \mathcal{A}, \tag{2.47}$$

whenever $K \in \mathcal{A}$ and $\Psi : \mathcal{A} \to \mathcal{A}$ a CP map. Notice that we can, in principle, always use the GNS construction to cast the dynamics in the form (2.46), given a specific state of the system.

Similar results were independently obtained by Gorini et al. (1976), but they limited themselves to the case where the algebra of observables is $\mathcal{B}(\mathcal{H})$ and \mathcal{H} is finite dimensional. In this case, the proof is rather easy to obtain via Choi's criterion for complete positivity (Choi 1972).

One can now make an even stronger demand on the dynamics, namely that it is a one-parameter *group*. This means that the dynamics is also reversible and that for any map Λ_t , there is also a map Λ_{-t} , such that $\Lambda_{-t} \circ \Lambda_t = \text{id}$. Using representation theory for groups, it follows that $\Lambda_t := \mathcal{U}_t$ is a unitary map. Limiting ourselves to $\mathcal{B}(\mathcal{H})$, this means that

$$X(t) := \mathcal{U}_t(X) = U_t^{\dagger} X U_t \quad \text{for all } X \in \mathcal{B}(\mathcal{H}),$$
 (2.48)

$$U_t^{\dagger} U_t = U_t U_t^{\dagger} = \mathbb{1}, \tag{2.49}$$

which is actually the Kraus representation of the map. It also is straightforward to deduce the Heisenberg equation of motion (assuming no explicit time dependence of X) by using for example Stone's theorem (Stone 1930, 1932; von Neumann 1932b),

$$\frac{\mathrm{d}}{\mathrm{d}}tX(t) = i[H, X(t)]. \tag{2.50}$$

One can now understand this as a special case of the Lindblad generator for $\mathcal{B}(\mathcal{H})$. Equivalently, we also obtain that

$$U_t = e^{-itH}. (2.51)$$

Of course, in the Schrödinger picture, this will lead us to Schrödinger's and von Neumann's equations, which are generating the dynamics studied in Chap. 4.

2.4.2 The Schrödinger Picture

In the Schrödinger picture, the dynamics is assumed to happen on the level of the quantum states, rather than of the observables. This implies that the Schrödinger

picture is actually the (pre)dual picture of the Heisenberg picture. Here we will briefly explain this duality, starting from a system described by observables on a fixed Hilbert space \mathcal{H} , such that the algebra is given by $\mathcal{B}(\mathcal{H})$. If we assume that the initial state is normal and determined by a density operator $\rho \in \mathcal{T}(\mathcal{H})$, we can write the evolution of the moments as

$$\langle O^k \rangle_{\rho}(t) = \operatorname{tr}(\rho \Lambda_{t,t_0}(O^k))$$
 (Heisenberg) (2.52)

=:
$$\operatorname{tr}(\Lambda'_{t,t_0}(\rho)O^k)$$
 (Schrödinger), (2.53)

where we already use the 2assumption that the dynamics is continuous. In the Schrödinger picture this continuity must be with respect to the so-called *ultraweak* topology, ¹¹ a technicality that serves to make sure that the state remains normal and can therefore be represented by a density operator at each moment in time.

Let us consider some typical dynamics, such as the simple unitary case. If the dynamics is unitary and given by a map U_t and we can determine (2.53) as

$$\langle O^k \rangle_{\rho}(t) = \operatorname{tr}(\rho \mathcal{U}_t(O^k)) = \operatorname{tr}(\rho U_t^{\dagger} O^k U_t) = \operatorname{tr}(U_t \rho U_t^{\dagger} O^k),$$
 (2.54)

then the dynamics on the density matrices is given by

$$\mathcal{U}_t'(\rho) := U_t \rho U_t^{\dagger}. \tag{2.55}$$

It can be shown von Neumann (1932a, b) that this dynamics is generated by von Neumann's equation

$$\frac{\partial}{\partial t}\rho(t) = -i[H, \rho(t)]. \tag{2.56}$$

Of course, the most fundamental property of unitary dynamics is that it does not change the pureness of the state. Most notably, state vectors (the vectors in Hilbert space that can be associated with pure states) are mapped onto other state vectors. This means, in familiar notation, that one may write

$$\langle O^k \rangle_{\phi}(t) = \langle \psi, U_t^{\dagger} O^k U_t \psi \rangle = \langle \psi(t), O^k \psi(t) \rangle, \tag{2.57}$$

where the equation of motion for $\psi(t) \in \mathcal{H}$ is probably one of the most famous equations in physics,

$$\frac{\partial}{\partial t}\psi(t) = -iH\psi(t). \tag{2.58}$$

Notice that this is all equivalent to considering the density matrix approach for $\rho = |\psi\rangle \, \langle \psi|$.

¹¹The ultraweak or weak* topology is defined on the space X^* , which is the dual space of a Banach space X. First consider the seminorm $p_x: X^* \to \mathbb{C}$ with $p_x(\phi) = |\phi(x)|$. The topology generated by these seminorms is the ultraweak topology (Conway 1997).

It is straightforward to generalise the result for unitary dynamics to a general dynamics that forms a completely positive map. We already mentioned that such maps allow for a Kraus representation for the operator algebra $\mathcal{B}(\mathcal{H})$. When we translate this type of dynamics into the Schrödinger picture, and, again, assume normal states, we can simply use the properties of the trace to obtain

$$\operatorname{tr}\left(\rho \sum_{i} V_{i;t,t_0}^{\dagger} O V_{i;t,t_0}\right) = \operatorname{tr}\left(\sum_{i} V_{i;t,t_0} \rho V_{i;t,t_0}^{\dagger} O\right). \tag{2.59}$$

and therefore we identify

$$\Lambda'_{t,t_0}(\rho) := \sum_{i} V_{i;t,t_0} \rho V_{i;t,t_0}^{\dagger}.$$
 (2.60)

Usually, for dynamical systems, such a Kraus representation is not given in any natural way. Just as in the unitary case, it is more convenient to consider the problem on the level of generators. For general CP maps, the structure of the generators is not known. On the other hand, we can again additionally assume a *one-parameter semigroup*, and for this class Lindblad provided us with a general expression for the dynamics of the density operators (Lindblad 1976). It can be shown that the generator of the predual Lindblad dynamics is given by

$$\mathcal{L}'(\rho) = -i[H, \rho] + \frac{1}{2} \sum_{j} \left([L_j, \rho L_j^{\dagger}] + [L_j \rho, L_j^{\dagger}] \right), \tag{2.61}$$

where the L_j are the same Lindblad operators as those found in the Heisenberg picture. Notice that, in general, $\mathcal{L}'(\mathbb{1}) \neq 0$, but that $\operatorname{tr}(\mathcal{L}'(\rho)) = 0$. This nicely shows that a unital map in the Heisenberg picture translates to a trace-preserving map in the Schrödinger picture.

Let us now conclude this section by giving some formal remarks on the Schrödinger picture for more general C^* -algebras. If we consider an algebra \mathcal{A} and a dynamics $\Lambda_{t,t_0}: \mathcal{A} \to \mathcal{A}$, then we can again write that, for any $X \in \mathcal{A}$,

$$\langle X \rangle_{\phi}(t) = \langle \Lambda_{t,t_0}(X) \rangle_{\phi} = \langle . \rangle_{\phi} \circ \Lambda_{t,t_0}(X), \tag{2.62}$$

where the last step is just a formal rewriting. We take an observable from the algebra, we first propagate it in time, and then we map it on its expectation value. Given that Λ_{t,t_0} is a well-defined Heisenberg dynamics, it is not difficult to see that the combined object $\langle . \rangle_{\phi} \circ \Lambda_{t,t_0}$ has all the properties of a well-defined state. Therefore, we can define a new state, for any t and t_0 :

$$\langle . \rangle_{\phi(t)} := \langle . \rangle_{\phi} \circ \Lambda_{t,t_0}. \tag{2.63}$$

Thereby we thus describe the dynamics on the level of states. Formally we can define the dynamical map in the Schrödinger picture as

$$\Lambda'_{t,t_0}(\langle . \rangle_{\phi}) := \langle . \rangle_{\phi} \circ \Lambda_{t,t_0}. \tag{2.64}$$

We will see in Chap. 9 that even this formal version of the Schrödinger picture has its benefits when we discuss non-equilibrium steady states.

Although a lot of formalism was introduced above, general semigroup dynamics will only be explicitly considered in Chap. 9, and most of this dissertation will focus on unitary dynamics. Hence, in Sect. 2.6, we introduce an additional formalism to describe dynamics on asymptotic time scales, in the context of scattering theory. First, however, we focus on a particular consequence of the unitary dynamics: The appearance of quantum interference effects, which are a key element of most of this work.

2.5 Quantum Interference

Among the most striking properties of quantum mechanics we find the particle-wave duality, through which we discover wave-like phenomena in the dynamics of quantum systems. The most well-known of these effects—and the central theme of this dissertation—is quantum interference. This phenomenon is intuitive when one studies quantum wave functions in the Schrödinger picture, however, the more abstract view in terms of quantum probability is rarely spelled out. Here, we elaborate on the meaning of quantum interference in general quantum models.

2.5.1 From Waves to Wave Functions

The notion of interference is much older than quantum physics, see e.g. Young (1804), and was originally developed as a characteristic property of waves. When waves are superposed, their phases play an important role in the superposition. The wave which results from such superposition generically has a different amplitude than its constituents. In Young's experiment (Young 1804), these amplitudes are enhanced in some directions and strongly suppressed in other directions, building the famous interference fringes.

In quantum mechanics, this terminology was adopted to describe continuous-variable system, e.g. a particle propagating in a potential landscape. In these setups, pure quantum states can be represented as complex valued functions $\psi(x)$, defined on position space (generally \mathbb{R}^3). This description was ultimately formalised by Schrödinger (1926). To connect these wave functions, which are formally denoted $\psi \in \mathcal{L}^2(\mathbb{R}^3)$ and describe a *single* particle, to experimental measurements such as those shown in Fig. 1.1, we require Born's rule (Born 1926). Applied to this specific

continuous-variable setting, this rule tells us that $|\psi(x)|^2$ describes the probability to find the particle at a given position x. Hence, repeating an experiment many times, measuring the position of the particle, results in a histogram which approximates $|\psi(x)|^2$.

A very coarse-grained and effective way of describing the paradigmatic double slit experiment uses two wave functions ψ_u and ψ_l , which describe the wave function propagating through the upper and the lower slit, respectively (see Fig. 1.2). To describe the detection on the final screen, we must superpose these two wave functions which leads to

$$\psi_{\text{total}}(x) = \frac{1}{\sqrt{2}}(\psi_u(x) + \psi_l(x)), \qquad (2.65)$$

where we add the normalisation to make sure that $\|\psi_{\text{total}}\|^2 = 1$, otherwise we cannot interpret the resulting wave function as a probability distribution. The probability to find the particle at position x is now given by

$$|\psi_{\text{total}}(x)|^2 = \frac{1}{2} |\psi_u(x)|^2 + \frac{1}{2} |\psi_l(x)|^2 + \text{Re}\left(\overline{\psi_u(x)}\psi_l(x)\right).$$
 (2.66)

Here we clearly see the incoherent mixture of the probability distribution given by the wave functions related to the upper and lower slits in the first two terms, and the additional contribution Re $(\psi_u(x)\psi_l(x))$, which is due to the interference between the two waves.

Even though the experiments are typically performed by sending many particles through the double slit interferometer, it remains a single particle description. This implies that the particles can be distinguished from one another during the whole experiment and any effects due to indistinguishability of identical particles can safely be ignored. Chapter 8 is fully devoted to the regime where such instances of indistinguishability cannot be ignored.

Although this discussion focussed on interference in position space, the final result (2.66) can be generalised to a more abstract framework.

2.5.2 Projections and Quantum Probability

The phenomenon of quantum interference takes a slightly different shape in more abstract quantum probability theory. In this section, we provide a generalisation of (2.66) to such a more general framework.

Let us start by recalling Sect. 2.3.3, where we discussed the connection between states and observables on the one side and projectors and probability distributions on the other side. If we consider a general Hilbert space \mathcal{H} , we can consider the couples (a, P_a) , where $a \in \mathbb{R}$ is a possible measurement outcome and $P_a \in \mathcal{B}(\mathcal{H})$

is a projector, *i.e.* $P_a^2 = P_a$. If we prepare the system in a given state $\langle . \rangle$, we may denote the probability of measuring a as

$$p(a) = \langle P_a \rangle. \tag{2.67}$$

Now, we can also define a quantum equivalent of joint probability, using Kraus's notion of selective channels (Kraus 1983a), ¹²

$$p(b \text{ and } a) = \langle P_b P_a P_b \rangle,$$
 (2.69)

where we first measure b and then a. To this expression to quantum interference, let us select a set of measurement outcomes $\{b_j\}$, such that

$$\sum_{i} P_{b_j} = 1. (2.70)$$

Notice that, in *classical* probability theory, we find

$$\sum_{b_j} p(b_j \text{ and } a) = p(a).$$
 (2.71)

However, in quantum probability theory, this is no longer valid

$$\sum_{j} \langle P_{b_j} P_a P_{b_j} \rangle \neq \langle P_a \rangle. \tag{2.72}$$

This is a direct consequence of the fact that in general $[P_a, P_b] \neq 0$ (which in turn follows from the fact that quantum observables generally do not commute). What we do find is that

$$\langle P_a \rangle = \left\langle \sum_j P_{b_j}^2 P_a \right\rangle = \sum_j \langle P_{b_j} P_a P_{b_j} \rangle + \sum_{b_j} \langle P_{b_j} [P_{b_j}, P_a] \rangle. \tag{2.73}$$

The first term on the right hand side of (2.73) clearly corresponds to the first two terms in (2.66), which denote the incoherent mixture of probabilities. The latter becomes apparent from (2.69), where p(b and a) is obtained from a sequential measurement of b and then a. The last term in (2.73) generalises the quantum interference.

$$p(a \mid b) = \frac{p(b \text{ and } a)}{p(b)} = \frac{\langle P_b P_a P_b \rangle}{\langle P_b \rangle}.$$
 (2.68)

Indeed, this may be seen as the probability to get a measurement outcome a, given that we previously "collapsed" the wave function on measurement outcome b.

¹²Notice that this allows us to reformulate "collapse of the wave function" as a conditional probability:

Example 2.5.1 We explicitly connect (2.73) to (2.66), by choosing a general initial wave function $\psi_0 \in \mathcal{L}^2(\mathbb{R}^3)$, the set of projectors $\{P_{b_j}\} = \{P_u, P_l\}$, which project on the upper and lower slits, respectively. Therefore, we can set $\frac{1}{\sqrt{2}}\psi_u = P_u\psi_0$ and $\frac{1}{\sqrt{2}}\psi_l = P_l\psi_0$. Ultimately, we measure the position on the measurement screen, which implies the choice $P_a = |x\rangle \langle x|$ (which projects onto a single point on the screen). Inserting this choices in (2.73) leads to

$$\begin{split} p(x) &= \frac{1}{2} |\psi_{u}(x)|^{2} + \frac{1}{2} |\psi_{l}(x)|^{2} + \left(\frac{1}{\sqrt{2}} (\overline{\psi_{u}(x)} + \overline{\psi_{l}(x)}) \psi_{0}(x) - \frac{1}{2} |\psi_{u}(x)|^{2} - \frac{1}{2} |\psi_{l}(x)|^{2}\right) \\ &= \frac{1}{2} |\psi_{u}(x)|^{2} + \frac{1}{2} |\psi_{l}(x)|^{2} + \left(\frac{1}{2} (\overline{\psi_{u}(x)} + \overline{\psi_{l}(x)}) (\psi_{u}(x) + \psi_{l}(x)) - \frac{1}{2} |\psi_{u}(x)|^{2} - \frac{1}{2} |\psi_{l}(x)|^{2}\right) \\ &= \frac{1}{2} |\psi_{u}(x)|^{2} + \frac{1}{2} |\psi_{l}(x)|^{2} + \text{Re}\left(\overline{\psi_{u}(x)} \psi_{l}(x)\right). \end{split} \tag{2.74}$$

Hence we have shown that quantum interference can be cast in a much more general framework of general Hilbert spaces, and it can be shown (Holevo 2001) that an additional abstraction to the language of C^* -algebras is possible.

2.6 Scattering Systems

In this section, we consider a more specific type of unitary dynamics, namely scattering. We assume that the states which we consider are given by state vectors. Therefore, the demand that the probabilistic structure of our theory be conserved under dynamics automatically leads to unitary dynamics. In scattering theory, we uphold this constraint, but we typically are not interested in the details at each time t, but rather in the asymptotic behaviour ($t \to \pm \infty$). This is also the framework which is considered in Chap. 5 and to some extent in Chap. 8 (see specifically Sect. 8.2.2).

In general, a scattering system is *open* in the sense that the dynamics cannot be confined to any finite volume in configuration space. Scattering only makes sense when we are dealing with systems that are continuous (or a continuum coupled to a set of discrete levels). Around 1960, the works of Fano (1961) and Feshbach (1958, 1962, 1967) cast the theory in a form with is still widely used today.

Surprisingly, it is rather difficult to find a straightforward, general approach to scattering theory and therefore this brief introduction is based on the more extended introduction in a diploma thesis (Zimmermann 2011) which, in turn, was based on a composition of different parts of Cohen-Tannoudji et al. (1998).

Our goal is to find a universal description of the scattering matrix. As this is essentially a representation of unitary dynamics, it must depend on the unitary evolution operator that is obtained from Schrödinger's equation. We assume the Hamiltonian that generates the dynamics to be time-independent and given by $H = H_0 + V$. V acts locally in space, which leads to the assumption that after asymptotically long time the system is just evolving with dynamics determined by H_0 . Ultimately, we want the scattering matrix to tell us how eigenvectors $|\phi_i\rangle = |c; E\rangle$ and $|\phi_f\rangle = |c'; E'\rangle$

of H_0 , where c, c' label the "channel", are connected by the dynamics. We define the scattering matrix S via

$$\langle \phi_f | S | \phi_i \rangle := \lim_{t \to \infty} \exp\left(i \frac{t}{2} (E_i + E_f)\right) \langle \phi_f | U\left(\frac{t}{2}, -\frac{t}{2}\right) | \phi_i \rangle,$$
 (2.75)

where one can motivate the additional phase factor via the interaction picture, as we are actually interested in $\lim_{t\to\infty}|\phi_i\rangle_I$ and $\lim_{t\to\infty}|\phi_f\rangle_I$ and how they are mapped on each other by the unitary dynamics. In the end, this avoids convergence problems in the limit $t\to\pm\infty$ due to the evolution of the phase generated by H_0 .¹³

In order to calculate S we thus have to calculate U(t/2, -t/2) in a convenient way, such that we can later on take the limit $t \to \infty$. This is usually done by considering the resolvent G, which is related to U via

$$U(t, t_0) = \int_{C_+} \frac{e^{-iz(t-t_0)}}{2i\pi} G(z), \qquad (2.76)$$

and one readily obtains $G(z) = (z - H)^{-1}$. We can now also define $G_0(z) = (z - H_0)^{-1}$, and we then obtain that

$$G(z) = G_0(z) + G_0(z)VG(z),$$
 (2.77)

$$G(z) = G_0(z) + G(z)VG_0(z), (2.78)$$

what can be used to obtain

$$G(z) = G_0(z) + G_0(z)VG_0(z) + G_0(z)VGVG_0(z),$$
(2.79)

and one can go on like that, constructing a perturbation series. However, one can also approach the problem in a different fashion. We start by

$$\langle \phi_f | G(z) | \phi_i \rangle = \frac{\delta_{i,f}}{z - E_i} + \frac{\langle \phi_f | V + VG(z)V | \phi_i \rangle}{(z - E_i)(z - E_f)}, \tag{2.80}$$

and after some calculus one obtains

$$\langle \phi_f | S | \phi_i \rangle = \delta_{i,j} - 2\pi i \langle \phi_f | V + VG(E_i + i\eta)V | \phi_i \rangle \delta(E_i - E_f),$$
 (2.81)

where the additional $i\eta$ appears in order to avoid divergences, and we assume that $\eta \to 0$, which implies that it is much smaller than all other relevant energy scales. One directly sees that the result is reasonable, in the sense that $S \to 1$ when $V \to 0$.

An explicit calculation of $\langle \phi_f | V + VG(E_i + i\eta)V | \phi_i \rangle$ is often tedious and therefore one tends to fall back on perturbative techniques. However, when H_0 and V have some particular structures, there are some strong methods that can be used. One of

¹³One may think of a reference frame moving along with H_0 .

such instances is the one where we have a continuum and a set of bounded states in the system, which leads to an unperturbed Hamiltonian of the form

$$H_0 = \sum_c \int \mathrm{d}E \, E \, |c;E\rangle \, \langle c;E| + \sum_b E_b \, |b\rangle \, \langle b| \,, \text{ and } V = \sum_{b,E,c} (V_{c,b}(E) \, |c;E\rangle \, \langle b| + \mathrm{h.c.}). \tag{2.82}$$

a technique introduced by Feshbach (1958, 1962, 1967) now uses projectors of the form $P = \sum_{b} |b\rangle \langle b|$ and $Q = \mathbb{1} - P$, to rewrite the scattering matrix in a form

$$\langle \phi_f | S | \phi_i \rangle \approx \delta_{i,j} - 2\pi i \langle \phi_f | W^{\dagger} \frac{1}{E - H_b - i\pi W W^{\dagger}} W | \phi_i \rangle,$$
 (2.83)

where W = QVP, encrypting the couplings between the channels and the bounded system. The scattering matrix described in (2.83) will be the main work horse of Chap. 5.

2.7 Concluding Remarks

Throughout this chapter we recollected the foundations of dynamical quantum systems, which makes it the backbone of our study of quantum transport theory. The illustrated techniques will be applied extensively throughout the subsequent chapters. In Chap. 4, the mathematical tool of choice to describe the dynamics is the Schrödinger equation (2.58), which is suited for the context of single-particle transport on finite networks. When we couple these networks to external channels in Chap. 5, we extensively use the scattering formalism of (2.83).

When we describe dynamical many-particle systems in Chap. 8, we explore both the Schrödinger picture (2.58) and the Heisenberg picture (2.48). In Sect. 8 we present the Heisenberg picture as the more natural framework to describe the study of correlation functions, which we later use extensively for the certification of boson sampling in Sect. 8.5. Continuing in the many-particle setting, we explore particle currents in open, many-particle quantum systems throughout Chap. 9, extensively using Lindblad's equations (2.46) and (2.47).

However, before we can present our results on quantum transport phenomena in complex systems, we must introduce the notion of complex systems in more detail in Chap. 3. Indeed, the stochastic nature of the Hamiltonians and Lindbladians in complex systems significantly influence the phenomenology of the dynamics. More specifically, throughout the thesis, Hamiltonians are often represented using network structures (as introduced in Sect. 3.2) or random matrix theory (see Sect. 3.3).

References 47

References

- D. Adams, The Restaurant at the End of the Universe (Ballantine, New York, 1995)
- R. Alicki, in *Quantum Dynamical Semigroups and Applications*, 2nd edn. (Springer Science & Business Media, Berlin, 1987)
- R. Alicki, M. Fannes, in Quantum Dynamical Systems (Oxford University Press, Oxford, 2001)
- V.I. Arnold, in Mathematical Methods of Classical Mechanics (Springer, New York, 1989)
- J.S. Bell, On the einstein-podolsky-rosen paradox. Physics 1, 195–200 (1964)
- F. Benatti, M. Fannes, R. Floreanini, D. Petritis, in *Quantum Information, Computation and Cryptography: An Introductory Survey of Theory, Technology and Experiments* (Springer Science & Business Media, Berlin, 2010)
- P. Billingsley, in *Probability and Measure*. Wiley Series in Probability and Statistics (Wiley, Hoboken, N.J, 2012), anniversary ed edition
- G. Birkhoff, J. von Neumann, The logic of quantum mechanics. Ann. Math. 37, 823–843 (1936)
- N. Bohr, I. On the constitution of atoms and molecules. Philos. Mag. 26, 1–25 (1913)
- N. Bohr, Can quantum-mechanical description of physical reality be considered complete? Phys. Rev. **48**, 696–702 (1935)
- M. Born, Quantenmechanik der Stoßvorgänge. Z. Physik 38, 803–827 (1926)
- M. Born, P. Jordan, Zur Quantenmechanik. Z. Physik 34, 858–888 (1925)
- M. Born, W. Heisenberg, P. Jordan, Zur Quantenmechanik. II. Z. Physik 35, 557–615 (1926)
- O. Bratteli, D.W. Robinson, in *Operator Algebras and Quantum Statistical Mechanics 1* (Springer, Berlin, 1987)
- O. Bratteli, D.W. Robinson, in *Operator Algebras and Quantum Statistical Mechanics Equilibrium States. Models in Quantum Statistical Mechanics* (Springer, Berlin, 1997)
- P. Busch, P. Lahti, R.F. Werner, Proof of Heisenberg's error-disturbance relation. Phys. Rev. Lett. 111, 160405 (2013)
- M.D. Choi, Positive linear maps on C*-algebras. Canad. J. Math. **24**, 520–529 (1972)
- C. Cohen-Tannoudji, J. Dupont-Roc, G. Grynberg, in Atom-Photon Interactions: Basic Processes and Applications (Wiley, New York, 1998)
- J.B. Conway, in A Course in Functional Analysis. Graduate Texts in Mathematics, vol. 96, 2nd edn. (Springer, New York, 1997)
- P.A.M. Dirac, The fundamental equations of quantum mechanics. Proc. R. Soc. A **109**, 642–653 (1925)
- J.L. Doob, Measure Theory. Graduate Texts in Mathematics, vol. 143 (Springer, New York, 1994)
- D.E. Evans, Y. Kawahigashi, in *Quantum Symmetries on Operator Algebras*. Oxford Mathematical Monographs (Clarendon Press, Oxford, 1998)
- U. Fano, Effects of configuration interaction on intensities and phase shifts. Phys. Rev. 124, 1866–1878 (1961)
- H. Feshbach, Unified theory of nuclear reactions. Ann. Phys. 5, 357–390 (1958)
- H. Feshbach, A unified theory of nuclear reactions: II. Ann. Phys. 19, 287–313 (1962)
- H. Feshbach, The unified theory of nuclear reactions: III. overlapping resonances. Ann. Phys. 43, 410–420 (1967)
- R.P. Feynman, Space-time approach to non-relativistic quantum mechanics. Rev. Mod. Phys. 20, 367–387 (1948)
- I. Gelfand, Neumark, On the imbedding of normed rings into the ring of operators in Hilbert space. Rec. Math. [Mat. Sbornik] N.S. 12, 197–217 (1943)
- W. Gerlach, O. Stern, Das magnetische moment des silberatoms. Z. Physik 9, 353–355 (1922a)
- W. Gerlach, O. Stern, Der experimentelle Nachweis der Richtungsquantelung im Magnetfeld. Z. Physik 9, 349–352 (1922b)
- M. Giustina, M.A.M. Versteegh, S. Wengerowsky, J. Handsteiner, A. Hochrainer, K. Phelan, F. Steinlechner, J. Kofler, J.-Å. Larsson, C. Abellán, W. Amaya, V. Pruneri, M.W. Mitchell, J. Beyer, T. Gerrits, A.E. Lita, L.K. Shalm, S.W. Nam, T. Scheidl, R. Ursin, B. Wittmann, A. Zeilinger,

- Significant-loophole-free test of Bell's theorem with entangled photons. Phys. Rev. Lett. 115, (2015)
- V. Gorini, A. Kossakowski, E.C.G. Sudarshan, Completely positive dynamical semigroups of N-level systems. J. Math. Phys. 17, 821–825 (1976)
- S. Gudder, Convex structures and operational quantum mechanics. Commun. Math. Phys. 29, 249–264 (1973)
- W. Heisenberg, Über quantentheoretische Umdeutung kinematischer und mechanischer Beziehungen. Z. Physik 33, 879–893 (1925)
- W. Heisenberg, Über den anschaulichen Inhalt der quantentheoretischen Kinematik und Mechanik.
 Z. Physik 43, 172–198 (1927)
- B. Hensen, H. Bernien, A.E. Dréau, A. Reiserer, N. Kalb, M.S. Blok, J. Ruitenberg, R.F.L. Vermeulen, R.N. Schouten, C. Abellán, W. Amaya, V. Pruneri, M.W. Mitchell, M. Markham, D.J. Twitchen, D. Elkouss, S. Wehner, T.H. Taminiau, R. Hanson, Loophole-free Bell inequality violation using electron spins separated by 1.3 kilometres. Nature 526, 682–686 (2015)
- A.S. Holevo, in *Statistical Structure of Quantum Theory* (Springer Science & Business Media, Berlin, 2001)
- E.H. Kennard, Zur Quantenmechanik einfacher Bewegungstypen. Z. Physik 44, 326–352 (1927)
- H.A. Kramers, The law of dispersion and Bohr's theory of spectra. Nature 113, 673–674 (1924)
- K. Kraus, General state changes in quantum theory. Ann. Phys. **64**, 311–335 (1971)
- K. Kraus, Operations, in *States, Effects, and Operations Fundamental Notions of Quantum Theory*, ed. by A. Böhm, J. D. Dollard, W. H. Wootters. Lecture Notes in Physics, vol. 190 (Springer, Berlin, 1983), pp. 13–41
- K. Kraus, Complementary observables and uncertainty relations. Phys. Rev. D 35, 3070–3075 (1987)
- G. Lindblad, On the generators of quantum dynamical semigroups. Commun. Math. Phys. 48, 119–130 (1976)
- G. Ludwig, in Foundations of Quantum Mechanics I (Springer, Berlin, 1983)
- H. Maassen, Quantum probability and quantum information theory, in *Quantum Information, Computation and Cryptography*, ed. by F. Benatti, M. Fannes, R. Floreanini, D. Petritis. Lecture Notes in Physics, vol. 808 (Springer, Berlin, 2010), pp. 65–108. https://doi.org/10.1007/978-3-642-11914-9_3
- G.W. Mackey, in *Mathematical Foundations of Quantum Mechanics*. Mathematical Physics Monograph Series (W.A. Benjamin, New York, 1963)
- H. Martens, W.M.d. Muynck, The inaccuracy principle. Found. Phys. 20, 357–380 (1990)
- L. Marton, Electron interferometer. Phys. Rev. 85, 1057–1058 (1952)
- J.E. Moyal, Quantum mechanics as a statistical theory. Math. Proc. Camb. 45, 99–124 (1949)
- M. Ozawa, Universally valid reformulation of the Heisenberg uncertainty principle on noise and disturbance in measurement. Phys. Rev. A 67, 042105 (2003)
- G.K. Pedersen, Analysis Now (Springer, New York, 1989)
- A. Peres, in *Quantum Theory: Concepts and Methods* (Springer Science & Business Media, Berlin, 1995)
- H.P. Robertson, The uncertainty principle. Phys. Rev. **34**, 163–164 (1929)
- R.T. Rockafellar, in *Convex analysis, Princeton landmarks in mathematics and physics* (Princeton Univ. Press, Princeton, NJ, 1997)
- S. Sakai, in C*-algebras and W*-algebras. Classics in Mathematics (Springer, Berlin, 1998)
- E. Schrödinger, Quantisierung als Eigenwertproblem. Ann. Phys. 385, 437–490 (1926)
- I.E. Segal, Irreducible representations of operator algebras. Bull. Amer. Math. Soc. 53, 73–88 (1947)
- L.K. Shalm, E. Meyer-Scott, B.G. Christensen, P. Bierhorst, M.A. Wayne, M.J. Stevens, T. Gerrits,
 - S. Glancy, D.R. Hamel, M.S. Allman, K.J. Coakley, S.D. Dyer, C. Hodge, A.E. Lita, V.B. Verma, C. Lambrocco, E. Tortorici, A.L. Migdall, Y. Zhang, D.R. Kumor, W.H. Farr, F. Marsili, M.D.
 - Shaw, J.A. Stern, C. Abellán, W. Amaya, V. Pruneri, T. Jennewein, M.W. Mitchell, P.G. Kwiat, J.C. Bienfang, R.P. Mirin, E. Knill, S.W. Nam, Strong loophole-free test of local realism*. Phys. Rev. Lett. 115, 250402 (2015)

References 49

- A. Sommerfeld, Zur Quantentheorie der Spektrallinien. Ann. Phys. 356, 1–94 (1916)
- W. Stinespring, Positive functions on C*-algebras. Proc. Amer. Math. Soc. 6, 211 (1955)
- M.H. Stone, Linear transformations in Hilbert space: III. operational methods and group theory. PNAS 16, 172–175 (1930)
- M.H. Stone, On one-parameter unitary groups in Hilbert space. Ann. Math. 33, 643 (1932)
- J. von Neumann, in Mathematische Grundlagen der Quantenmechanik (Springer, Berlin, 1932a)
- J. von Neumann, Über Einen Satz Von Herrn M. H. Stone. Ann. Math. 33, 567 (1932b)
- H. Weyl, Gruppentheorie und Quantenmechanik (Hirzel, Leipzig, 1928)
- T. Young, The bakerian lecture: experiments and calculations relative to physical optics. Phil. Trans. R. Soc. Lond. **94**, 1–16 (1804)
- J. Zimmermann, Anderson localization and non-linear scattering in a disordered 1D quantum system. Diploma thesis, Albert-Ludwigs Universität Freiburg, Freiburg (2011)

Chapter 3 Complex Quantum Systems and Random Matrix Theory



What... what are these words? Explain! Explain! Dalek in "Doctor Who" (Hurran 2013)

3.1 Complex Systems

3.1.1 Heuristics

Complex systems are ubiquitous in a wide variety of scientific disciplines. The terminology is profoundly present in fields ranging from social sciences (Sawyer 2005), over economics (Arthur 1999) and neuroscience (Hopfield 1982), to engineering (Ottino 2004), biology (Odum and Barrett 2005) and physics (Richter and Rost 2004). Given the multitude of different themes considered in these different fields, it is legitimate to wonder whether there are general properties that unify the "complex systems" of these different disciplines. In other words, what is a complex system?

Exactly this question has been addressed in many fields, often leading to different answers. Let us begin by listing several concepts which are commonly related to complex system:

- *Nonlinear dynamics*, typically connected to chaos and bifurcation theory (Atlee Jackson 1991; Nicolis and Gaspard 1994; Richter and Rost 2004).
- Patterns and manifestation of hierarchical structures (Albert and Barabási 2002).
- *Irreversibility* and out-of-equilibility behaviour (Prigogine 1987).
- Emergent phenomena and self-organisation (Ottino 2004).
- Error tolerance (Albert and Barabási 2002)

There is a wide consensus in literature, see e.g. Albert and Barabási (2002), Prigogine (1987), that systems which are efficiently described in terms of Newtonian physics,

ideal gas models or chemical reactions are "simple". Also on the level of system topologies, there is a general consensus that lattices and other "simple graphs" (Biggs 1993; Bollobás (1998a) cannot be considered complex. On the other hand, a more debatable topic is whether a fully random or fully chaotic system (Schuster 1989) can be considered a complex system.

The problem of both randomness as chaos lies in their behaviour which is strictly intractable and unpredictable, but allows statistical treatments with universal properties describable by few parameters. It is clear that fully chaotic systems do not display the patterns and hierarchical structures which are often associated with complex systems. In this sense, a complex system is usually said to be a mixture of both chaotic and regular behaviour (Richter and Rost 2004).

A long standing debate in theoretical physics and mathematics considers the question whether one can go beyond such heuristic descriptions of complex systems. This has led to several attempts to find a quantitative measure of complexity.

3.1.2 Complexity and Information Theory*

We present a brief overview and criticism to the use of information theoretical tools to characterise complex systems.

Not long after Shannon formulated his mathematical theory of information (Shannon 1948), it became clear that there is a fundamental connection between information and statistical physics, which is by now standard textbook knowledge (Kardar 2007). This connection is naturally forged via mathematical probability theory. Because physical complex systems are situated within the statistical mechanics framework (Prigogine 1987), various attempts have been undertaken to quantify the complexity of a system, using techniques of information theory.

Usually these attempts treat the system as a string of data, from which the information content is analysed. In such an approach, the system is represented as a source of information and the string of data can be interpreted as a series of measurement outcomes. Several methods which where developed throughout the early days of information theory can serve as a first attempt for measuring complexity: The Shannon (joint) entropy (Shannon 1948) and Kolmogorov's algorithmic complexity (Kolmogorov 1983).

The methods which use Shannon's techniques from Shannon (1948) describe the *compressibility of the data*, in the sense that one characterises the simplest signal which is required to encode the string of data and transmit it. In a similar way, it can be viewed as the minimal amount of memory required to store the data. Kolmogorov's method counts the minimal amount of code required to write an algorithm that *exactly reproduces* the data. Both methods quantify a highly regular set of data (e.g. a sequence of zeroes) with a very low complexity. However, they also appoint a high complexity to a fully random set of data, because they strive to characterise the *exact* string of data, rather than its statistical properties. Indeed, there is no easy

algorithm to *reproduce* a long string of random numbers, but one can easily produce a second string which manifests the same statistical properties.

A proposed method to go beyond such mere reproduction is based on finding patterns in the data. One such scheme uses so-called epsilon-machines (Crutchfield and Young 1989; Shalizi and Crutchfield 2001), i.e. Markov processes that are inferred from the data and can predict future data (i.e. future measurement outcomes) after analysing a string of sufficient length. One of the most profound problems is that the epsilon-machine approach assumes that the stochastic processes which generate the string of data are stationary. In a physics language, this implies that the method cannot be used to treat dynamical quantum systems or out-of-equilibrium physics. This renders it impossible to make the connection to nonlinear, emergent, and non-equilibrium phenomena—phenomena which were all commonly related to complex systems (recall Sect. 3.1.1).

A second problem lies exactly in the connection between a system and a string of data. The framework highly depends on what exactly is measured to create such a string of data. When one uses this method to characterise the complexity of the system, one may obtain different "complexities" for the measurement of different observables. Therefore, it is inaccurate to refer to the complexity of the *system*, since one actually characterises the complexity of the *measurement process* for a given observable in the system. In this sense, epsilon-machines and the methods driven by information theory and data analysis are arguably most relevant in the study of metrology, e.g. in the problem of parameter estimation.

3.1.3 Complexity of Quantum Dynamical Systems

We propose a different perspective to describe complex systems, which focusses more on the system itself. Indeed, it is only natural that the properties of the *system* are used to classify it. Because this dissertation focusses on dynamical properties of quantum systems, we start from that specific framework. By virtue of Chap. 2, we define a dynamical quantum system in terms of $(\langle . \rangle, A, \Lambda_t)$ (Alicki and Fannes 2001; Verbeure 2011): An algebra of observables A with both a state $\langle . \rangle$ and a dynamical map Λ_t defined upon it. We now explore whether the heuristics of complex systems can be connected to this specific context.

In this dissertation, both open and closed systems are considered. However, when we refer to a complex *system*, we consider it independent of the environment in which it is embedded and therefore the complexity should already be present in a closed system setup. When the system is closed, it implies that the dynamics is reversible and that $\{\Lambda_t \mid t \in \mathbb{R}\}$ is a one-parameter *group*. In addition to the dynamical system $(\langle ... \rangle, \mathcal{A}, \Lambda_t)$, we obtain the GNS construction $(\pi, \mathcal{H}, \Omega)$ (see Sect. 2.3.2).

¹Since patterns can occur over long ranges of data, it is difficult to practically estimate the required measurement time. In the literature, one often assumes that the available string of data is infinitely long (Crutchfield and Young 1989).

When the state $\langle . \rangle$, which is the foundation of the description, is a stationary state for the dynamics, which means that

$$\langle \Lambda_t(O) \rangle = \langle O \rangle, \quad \forall O \in \mathcal{A},$$
 (3.1)

we can always find a self-adjoint operator h in the Hilbert space \mathcal{H} (Alicki and Fannes 2001; Verbeure 2011), for which

$$\pi(\Lambda_t(O)) = e^{ith}\pi(O)e^{-ith} \quad \text{with } h\Omega = 0.$$
 (3.2)

We must note that in general this Hamiltonian h is a linear operator on \mathcal{H} , but it is typically not contained in $\pi(\mathcal{A})$ and it cannot even be *approximated* by represented elements of the algebra \mathcal{A} . This implies that every closed dynamical system $(\langle . \rangle, \mathcal{A}, \Lambda_t)$ in a stationary state leads to a natural notion of a Hamiltonian. This Hamiltonian representation of the dynamics on the Hilbert space \mathcal{H} is generically *state dependent*. A fundamental consequence of this result is that any definition a complex dynamical quantum system must depend on this Hamiltonian h.

Of course, for dynamical quantum systems which are closed, bounded, and contain one or few particles, we can often avoid the complicated language of C^* -algebras. These systems allow for an effective description in terms of a unique Hilbert space \mathcal{H} and the reversible dynamics is naturally described by a unique Hamiltonian on that space. However, in the context of quantum statistical mechanics, which we touch upon in Sect. 7.7 and Chap. 9, this uniqueness is no longer guaranteed.

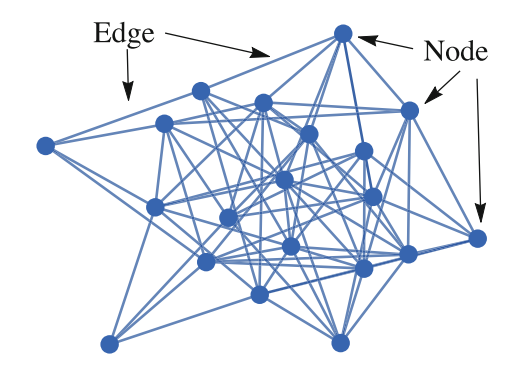
The properties of the Hamiltonian h are crucial for the description of the system: Its spectral properties determine the relevant time scales of the coherent dynamics. Therefore, if we "define" what a complex dynamical quantum system is, it is naturally to do so based on properties of the spectrum of the Hamiltonian h. Because time scales are directly related to spectral properties, these complex systems also have specific signatures in the relevant time scales that govern their quantum dynamics.

Spectral theory leads us to a natural connection with several well-studied types of systems, such as billiards and—most notably—graphs (Chung 1997). It is spectral graph theory which provides a natural connection to a specific type of complex systems, namely those which can be represented by network structures. In order to describe complex quantum systems, we start by studying the spectral theory of complex networks.

3.2 Complex Networks

Complex networks (Albert and Barabási 2002) are almost as widely studied as complex systems themselves. Popular examples of complex networks include Facebook and the internet (Hooyberghs 2013), but also power grids and road networks. Closer to statistical quantum physics is the fact that complex networks can even be connected

Fig. 3.1 Random Erdös and Rényi graph (see text) with 20 nodes and 75 edges. Edges and nodes are indicated. Generated using Graph toolbox in Mathematica 10



to Bose-Einstein condensation (Bianconi and Barabási 2001). The underlying mathematical toolbox which is generally used to describe complex networks is *graph theory* (Albert and Barabási 2002; Biggs 1993; Chung 1997).

A graph is described by a set $\{P, E\}$, where $P = \{p_1, \dots p_N\}$ are *nodes* and E is a set of *edges* which connect the different nodes—see Fig. 3.1 for an example. Graphs can be directed (such that an edge can be thought of as an arrow which goes from one node to another) and they can be weighted (implying that each edge is given a specific weight). We focus on graphs without such extra features, such that we have a set of nodes which are either connected or not. A final quantity of interest is the *degree* k_j of node p_j : The degree of a node denotes the number of edges that are connected to it. A graph is called a *simple graph* when there are no loops (i.e. nodes are not connected to themselves), nor double edges (i.e. there can be at most one edge between any two nodes).

Graphs are connected to linear algebra and spectral theory in a natural way, via the adjacency and Laplacian matrices. The *adjacency* (or connectivity) matrix A (see Fig. 3.2 for an example) is an $N \times N$ matrix, given that we consider N nodes, with

$$A_{ij} \equiv \#$$
 number of edges between p_i and p_j . (3.3)

The Laplacian matrix L is given by L = D - A (see Fig. 3.2 for an example), where A is the adjacency matrix and D is a diagonal matrix, where the jth diagonal element is the degree k_j . This implies that $\sum_{j=1}^{N} L_{ij} = \sum_{i=1}^{N} L_{ij} = 0$. It can be shown that L is a positive semi-definite matrix and that its smallest eigenvalue is always zero. When this smallest eigenvalue is degenerate, there are several connected components in the system (Chung 1997).

The field of spectral graph theory focusses on the study of the eigenvalues of both adjacency and Laplacian matrices. Until the late 1950's, graph theory mainly studied systems which were highly regular (e.g. lattices, lines, circles, fully-connected, *et cetera*), but this changed when Erdös and Rényi developed the theory of random graphs (Bollobás 1998b; Erdös and Rényi 1961) (see Figs. 3.1 and 3.2 for examples). Their model fixes the number of modes *N* and the number of edges *n* and samples a simple graph that fulfils these constraints. The distribution is uniform in the sense

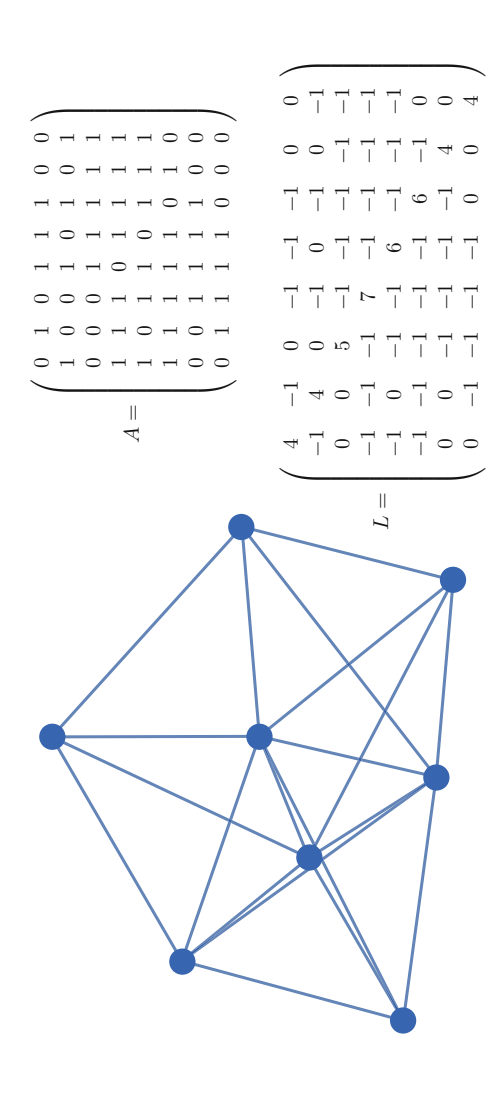


Fig. 3.2 Random Erdös and Rényi graph (see text) with 8 nodes and 20 edges with its associated adjacency matrix A and Laplacian matrix L. Generated using Graph toolbox in Mathematica 10

that every such graph with N nodes and n edges is equally probable. A closely related way of generating the random graphs is the binomial method, here edges are sampled according to a fixed probability c. Due to the law of large numbers both methods are equivalent when n = cN with $N \to \infty$ and c constant.

Although these random graphs are conceptually relevant in the study of complex networks, they can themselves hardly be considered complex systems because they can be characterised by a single quantity, the average degree $\langle k \rangle = cN$. Barabási and Albert argue that the networks behind realistic complex systems are not completely random, but also manifest some degree of structure (Albert and Barabási 2002). The quest for descriptions of such complex networks has led to the development of *small world-* and *scale-fee networks*.² It has been argues that in particular the latter type of networks are ubiquitous in real-world complex systems (Barabási 2009), even though this idea is still subject to debate (Clauset et al. 2009; Broido and Clauset 2018).

A scale-free network is commonly "grown" using the Barabási-Albert algorithm (Barabási and Albert 1999), which starts from a small random network and adds additional nodes. Whenever a node is added, it connects to node p_j with probability $k_j / \sum_j k_j$. This implies that nodes with a high connectivity have a higher probability of being connected to. In this type of networks, one generically forms "hubs", i.e. nodes with very high connectivity. A small-world network focusses on limiting the distance l between pairs of nodes such that $l \sim \log N$. In graph theory, the resulting graphs are described by the Watts–Strogatz model (Watts and Strogatz 1998).

Our goal is to find specific criteria for complexity of a system based on spectral properties and we explained that there is a clear connection between the theory of graphs and spectral theory. Moreover, complex networks are naturally connected to random graphs, thus we must investigate the spectral properties of random graphs. Since the graphs under consideration are random, the adjacency matrices describing them are also random objects. This makes a natural connection to Random Matrix Theory (RMT) and it was even shown that the spectral density of the random graphs described by Erdös and Rényi is given by Wigner's semicircular distribution (Füredi and Komlós 1981). However, the adjacency matrix of a graph grown by the Barabási-Albert algorithm does not manifest such spectral statistics. It was shown that for graphs related to scale-free networks, the adjacency matrix typically manifests a power-law distribution in the normalised density of states (Chung et al. 2003). These spectral properties are direct manifestations of the degrees, which can vary greatly between nodes and one can even say that such a power-law distribution is a manifestation of hierarchy within the topology of the system.

To ultimately connect the theory of the topological structures as they appear in graph and network theory to quantum mechanics and Hamiltonians, we must make the transition from random graphs to RMT. Inspired by the spectral properties that

²One may also consider other types of complex networks, but these are the most well-known examples.

became apparent in graph theory, we propose to use the manifestation of power-law behaviour in the Hamiltonian's spectral density as a hallmark for complex dynamical quantum system.

3.3 Aspects of Random Matrix Theory

3.3.1 From Atoms and Orbits to Random Matrix Theory*

Random matrix theory was introduced with the specific purpose of studying statistical properties of disordered and/or complex systems. It does not necessarily attempt to provide a complete microscopic picture of the investigated system. This Section introduces the historical context in which this framework was developed and applied.

The physicist's first reflex to tackle a problem is usually to break it down into its fundamental building blocks and use them as ingredients for the solution. In mechanics, this typically implies finding all relevant degrees of freedom, writing down the equations of motion for each one of them and solving a system of equations. Such methods work fine, as long as the degrees of freedom are not too many and the equations of motion can be integrated. Essentially the latter boils down to finding as many constants of motion as degrees of freedom. Of course, by now it is well-known, also from our previous discussion on complex systems, that often we cannot resort to such straightforward methods.

Letting go of such well-controlled, deterministic, solution methods historically proves to be hard. Remarkable in the context of their time were the ideas, pioneered by Maxwell, Boltzmann and Gibbs, that the laws of thermodynamics are governed by the probability theory of an enormous underlying number of degrees of freedom (Boltzmann 1878; Gibbs 1878; Maxwell 1867). The idea that the underlying *microscopic* degrees of freedom are so abundant that statistics obtains near exact predictive power, was thoroughly shocking at the time. It was only when Einstein presented undeniable evidence via his work on Brownian motion (Einstein 1905) that the broad community embraced the ideas of statistical physics.

A similar story occurred during the early developments of quantum mechanics, when Bohr quantised the hydrogen atom (Bohr 1913). Bohr's atomic theory, based on the model by Rutherford, was enormously successful in explaining several mysteries underlying the field at that time, most notably the spectral lines of hydrogen. However, as can be read in Heisenberg (1975), several of Bohr's colleagues had their doubts about the completeness of the model. Einstein pointed out that the Bohr–Sommerfeld quantisation only works for integrable systems (Einstein 1917) and also Pauli explicitly made mention of such problems (Pauli 1922). These problems were soon forgotten as Heisenberg, together with Born and Jordan, introduced a much more general form of quantum mechanics (Heisenberg 1925; Born and Jordan 1925; Born et al. 1926), soon after which Dirac introduced the canonical quantisation method (Dirac 1925).

Even though somewhat forgotten, it was a fact that early quantum mechanics did not provide many possibilities in case of classically chaotic systems. It was at some point even believed that such systems could not be quantised. However, a new milestone came when Gutzwiller proved that in any system, knowledge of the periodic orbits is sufficient for quantisation (Gutzwiller 1967, 1969, 1970, 1971), and similar results were obtained in Balian and Bloch (1970, 1971, 1972, 1974). His work revitalised the field studying the transition between classical and quantum mechanics, known as (now, modern) semiclassics, and contributed to the birth of quantum chaos.³ Even though Gutzwiller's trace formula is highly successful, it is not always practical in usage: Not only is it far from trivial to actually find all the periodic orbits (due to their exponential proliferation), there are also more intricate mathematical problems of convergence (Eckhardt and Aurell 1989; Miller 1975; Voros 1988).

A complementary approach, much in the spirit of what the founding fathers of statistical mechanics did, is to drop the urge to exactly calculate everything and to focus on an alternative, stochastic treatment of the such systems. By means of such method, Bohigas, Giannoni and Schmit (Bohigas et al. 1984) managed to formulate a conjecture for universality in the fluctuations of the eigenvalues of "chaotic" quantum systems, connecting quantum chaos to random matrix theory (RMT). Recently, new developments have attempted to formally prove such connection (Müller et al. 2004).

The study of RMT in physics dates back to nuclear physics, another branch that grew out of quantum theory. In the thirties, decades after the first quantum endeavours in atomic physics, many physicists started digging deeper and explored the nucleus itself. It was again Bohr who proposed a very interesting model with his *compound nucleus* (Bohr 1936). Somehow it seems that Bohr realised that the generic nucleus lacks the necessary features to allow for a simple description, since he explicitly points towards our lack of knowledge of the exact structure inside of the nucleus. It was Wigner who later suggested not to strive for knowledge, but rather use a statistical model to describe our lack of microscopic control (Wigner 1955).

Many excellent textbooks have been written about this topic, from very accessible introductions which mainly focus on applications in quantum chaos (Haake 2010; Stöckmann 2007), to very extended technical works (Mehta 2004; Akemann et al. 2011). In the remainder of this section, we will base ourselves on these textbooks, and review some of the most fundamental results in RMT.

We start by focusing on Wigner's idea, which originated from his studies in nuclear physics (Lane et al. 1955), where they realised that even when the compound structure of the nucleus is exploited, some statistics is required to solve the problem. This triggered Wigner to explore the potential of RMT in this system (Wigner 1955). He starts his introduction with an important statement:

The present problem arose from the consideration of the properties of the wave functions of quantum mechanical systems which are assumed to be so complicated that statistical considerations can be applied to them. [...] Actually, the model which underlies the present calculations shows only a limited similarity to the model which is believed to be correct.

³For an more complete introduction to the genesis of quantum chaos, see (Gutzwiller 2007).

Nevertheless, the calculation which follows may have some independent interest; it certainly provided the encouragement for a detailed investigation of the model which may reproduce some features of the actual behavior of atomic nuclei.

Eugene P. Wigner (Wigner 1955)

In this work, Wigner works in a basis in which all the symmetries in the system have been exploited, meaning that the Hamiltonian is block diagonal. He now focusses on one of such blocks and decides not to attempt to describe its exact structure, but rather some statistical features it manifests. In the quote he clearly states the assumption that the system is so complicated that statistical considerations are required. Additionally, and very importantly, he stresses that the random matrix model is not supposed to reproduce the Hamiltonian, but rather it should reproduce some essential features. Not much later, Wigner realised that his ideas applied to a much broader set of matrices (Wigner 1958).

3.3.2 The Gaussian Ensembles of Random Matrix Theory

Following Wigner's logic of replacing the Hamiltonian (or at least the blocks in their block-diagonal representation) by a stochastic object, we start by taking into account the most fundamental property of the Hamiltonian H: It is a Hermitian matrix, which implies that $H^{\dagger} = H$ or, in other words,

$$H_{ii} \in \mathbb{R}$$
, and $H_{ij} = \overline{H_{ji}}$, (3.4)

thus already limiting the maximal number of independent components. The Hermitian structure of the matrix is preserved under unitary transformations, since indeed

$$(U^{-1}HU)^{\dagger} = (U^{\dagger}HU)^{\dagger} = U^{\dagger}H^{\dagger}U = U^{-1}HU. \tag{3.5}$$

The classical (or Gaussian) ensembles of random matrix theory are defined by the type of transformations that keep their basic structure intact. One may after all say that $U^\dagger H U$ is just the Hamiltonian H, viewed in a different basis, meaning that at least from a physics perspective they are one and the same object. With this intuition in mind, we demand that the probability density for sampling H and $U^\dagger H U$ is the same for all unitary matrices U. Introducing the notation P for a probability density, we may therefore write that

$$P(H) = P(U^{\dagger}HU). \tag{3.6}$$

This will ultimately lead us to the *Gaussian Unitary Ensemble* (GUE), which owes its name exactly to identity (3.6).

We started our excursion into RMT by assuming that we treated a block in the block diagonal representation of the Hamiltonian in such a way that symmetries where already exploited. These are, however, only those symmetries that allow for a unitary representation, meaning that, on the Hilbert space \mathcal{H} , angles, and thus inner products $\langle \phi, \psi \rangle$ of wave functions, are left invariant. It was reasoned by, again, Wigner (Ballentine 2014; Wigner 1931; Bargmann 1964) that the relevant quantity to be preserved in quantum mechanics is rather $|\langle \phi, \psi \rangle|$, which also allows for antiunitary operations to represent symmetries. These symmetries are not yet exploited by going to a block diagonal structure and need to be dealt with differently. Here we will focus on the most prominent member of this class of symmetries: *time-reversal*.

We define a time-reversal operator T on a Hilbert space $\mathcal H$ as an operator with the properties

$$\langle T\phi, T\psi \rangle = \langle \psi, \phi \rangle = \overline{\langle \phi, \psi \rangle}, \text{ for } \psi, \phi \in \mathcal{H}$$
 (3.7)

$$T^2 = \alpha \mathbb{1} \quad \text{with} \quad |\alpha|^2 = 1. \tag{3.8}$$

The first of these guarantees consistency with Schrödinger's equation. The second demand accounts for the fact that we do not allow a measurable effect of a double time-reversal. This is verified by the observation that, for any observable $A \in \mathcal{B}(\mathcal{H})$, any moment $\langle \psi, A^k \psi \rangle$ (for all $k \in \mathbb{N}$ and thus the full measurement statistics) remains unchanged under T^2 .

Interestingly, time-reversal operations are far from unique. More specifically, we can take any time-reversal operator T and any unitary operation U and define a new time reversal operation T' = UT. Haake (2010) argues that any T can be written in a so-called standard form T = UK, where K acts on any operator A as $KAK^{-1} = \overline{A}$. This operator K is *conjugate linear*, giving it the properties (for ψ , $\phi \in \mathcal{H}$)

$$K^2 = 1, (3.9)$$

$$\langle K\phi, K\psi \rangle = \langle \psi, \phi \rangle, \tag{3.10}$$

$$\langle \psi, K^{\dagger} \phi \rangle = \langle \phi, K \psi \rangle = \langle K^2 \psi, K \phi \rangle = \langle \psi, K \phi \rangle.$$
 (3.11)

With these properties and (3.8), one can now show that

$$\alpha \mathbb{1} = T^2 = UKUK = U\overline{U}, \tag{3.12}$$

where it should be stressed that \overline{U} is now the *complex conjugate* and not the conjugate transpose. Rewriting the identity gives⁵

$$U\overline{U} = \alpha \mathbb{1} = \alpha U U^{\dagger} \implies \overline{U} = \alpha U^{\dagger} = \alpha \left(\overline{U}\right)^{t} \implies \overline{U} = \alpha^{2} \overline{U}, \tag{3.13}$$

⁴The notation \overline{A} represents the component-wise *complex conjugate*, rather than the complex transpose. Notice also that $K^2 = 1$ implies that $KAK = \overline{A}$.

⁵The last step is obtained by a very short "iterative expansion".

which can only be true if $\alpha = \pm 1$ and therefore, (3.8) implies that

$$T^2 = \pm 1. (3.14)$$

In other words, the defining properties (3.7, 3.8) directly lead to stronger constraints on T, which are ultimately contained in (3.14). This implies physically that a double reversal either returns the original state vector, or it adds a minus sign.

A system is called *time reversal invariant* if there exists a time reversal operator T, with properties (3.7, 3.8), which leaves the Hamiltonian invariant, i.e. the Hamiltonian commutes with T. However, we know that every time reversal operator has the property (3.14). The behaviour upon double time reversal (whether (3.14) leads to the "+1" or "-1") depends on the system Hamiltonian. This gives three natural classes of Hamiltonians H with respect to the time reversal operation:

- Those where [H, T] = 0 and $T^2 = 1$, these lead to the *Gaussian Orthogonal Ensemble* (GOE).
- Those where [H, T] = 0 and $T^2 = -1$, these lead to the *Gaussian Symplectic Ensemble* (GSE).⁶
- Those where $[H, T] \neq 0$, these lead to the Gaussian Unitary Ensemble (GUE).

As one may expect, each of these ensembles have different statistical properties.

As most of the RMT applications in Part II explicitly use the GOE, we from now on focus mainly on its properties. Its first important property is $T^{-1}HT = H$, which implies that for a basis where $T |e_i\rangle = |e_i\rangle$ and $\langle e_i, e_j\rangle = \delta_{ij}$,

$$H_{ij} = \langle e_i, He_j \rangle = \overline{\langle Te_i, THe_j \rangle} = \overline{\langle e_i, THe_j \rangle} = \overline{\langle e_i, HTe_j \rangle} = \overline{H_{ij}}.$$
 (3.15)

Since this implies that there is a basis in which H is not diagonal, but still contains only real elements, it is typically assumed that the GOE is essentially built from real symmetric matrices, rather than hermitian ones. As this is a fundamental, but non-unitary, symmetry of our system, the statistics should express this fact. The group that leaves this property intact is SO(N), the $N \times N$ (N being the dimension of the Hilbert space H on which the Hamiltonian H acts) orthogonal matrices. The key property of these matrices is that $O^tO = OO^t = 1$ and they form the natural symmetry group of the GOE, which is expressed by the demand that the probability density to sample a matrix H from this ensemble is the same as that to sample OHO^t for all $O \in SO(N)$. In other words,

$$P(H) = P(O^t H O), \tag{3.16}$$

where P is the probability density on the GOE.

⁶This ensemble will not be considered in our subsequent work and thus we refer the reader to (Mehta 2004) for further details.

At the foundation of the GOE lies the identity (3.16), but how exactly should one interpret such probabilities on the set of matrices? *A priori*, one can think of *P* as a function which connects these real matrices in the GOE to a number,

$$P: \mathbb{R}^{N \times N} \to [0, \infty). \tag{3.17}$$

This function must fulfil the additional constraint (3.16) and can therefore be expressed as (Mehta 2004)

$$P(H) = f[tr(H), tr(H^2), \dots, tr(H^N)]$$
 (3.18)

Now notice that each matrix in the ensemble is characterised by a set of N(N+1)/2 different components $H_{11}, H_{12}, \dots H_{NN} \in \mathbb{R}$. These elements completely determine H, allowing the interpretation

$$P(H) = P(H_{11}, \dots, H_{NN}).$$
 (3.19)

This leads to the interpretation of the probability to sample a given matrix as a joint probability distribution on its components. In completely the same way we can define $H'_{11}, \ldots H'_{NN}$ as the components of $O^t H O$, which allows us to understand Eq. (3.16) as

$$P(H_{11}, \dots, H_{NN}) = P(H'_{11}, \dots, H'_{NN}). \tag{3.20}$$

This notation now leads us to another constraint which is *imposed* on the GOE: The different components are all uncorrelated. Consequently,

$$P(H_{11}, \dots, H_{NN}) = P(H_{11})P(H_{12}) \dots, P(H_{NN}). \tag{3.21}$$

The only way to fulfil both constraints (3.18) and (3.21) is by giving P the following form (Stöckmann 2007)

$$P(H_{11}, \dots, H_{NN}) = c \exp[-b \operatorname{tr}(H) - a \operatorname{tr}(H^2)],$$
 (3.22)

and without loss of generality we can set b=0, since this boils down to just shifting the overall average energy. The constant c can also be further specified by demanding that

$$\int P(H)dH = \int P(H_{11}, \dots, H_{NN})dH_{11} \dots, dH_{NN} = 1,$$
(3.23)

and a quick calculation of some Gaussian integrals (Mehta 2004) tells us that

$$c = \left(\frac{a}{\pi}\right)^{N/2} \left(\frac{2a}{\pi}\right)^{N(N-1)/2}.$$
 (3.24)

One can verify⁷ that, with this normalisation taken into account, we obtain

$$\mathbb{E}(H_{ij}^2) = \frac{1 + \delta_{ij}}{4a} =: (1 + \delta_{ij})v^2.$$
 (3.25)

The choice of v is a priori arbitrary and is often motivated by physical or mathematical demands. For example, one may want the spectral radius to be independent of the matrix dimension N, or one may want the completely opposite situation, where the mean level spacing Δ is independent of N.

Generically stated, it naturally follows from the *invariance under orthogonal* transformations and the statistical independence of matrix components that the components of the Hamiltonian are distributed by a normal distribution

$$H_{ij} \sim \text{Normal}\left(0, (1 + \delta_{ij})v^2\right),$$
 (3.26)

where v is the only free parameter left to determine. Now that we fully know what GOE matrices are and how they can be sampled, it is time to review some useful properties.

3.3.3 Statistical Properties of GOE Eigenvalues

Wigner's original motivation to introduce random Hamiltonians was motivated by the study of nuclear spectra. Such spectroscopic data are dictated by the energy levels and by the energy eigenvectors of the system.⁸ From this perspective, one can clearly conclude that the statistical properties of the eigenvalues (and eigenvectors) of the random Hamiltonians are the goal of such studies.

Joint Probability Distribution*

Probabilistic properties of eigenvalue distributions are naturally within reach. Assuming that H is a real $N \times N$ matrix with $H^t = H$, there exists an orthogonal matrix O such that $H = O^t DO$, where D is a diagonal matrix and the entries on its diagonal are the eigenvalues of H. By virtue of the first fundamental property (3.16) of the GOE the probability density for sampling any random GOE Hamiltonian H is the same as that for sampling the specific set of eigenvalues. In other words, the set of N eigenvalues fully determines the GOE matrix, implying that, somehow,

$$P(H_{11}, \dots, H_{NN}) dH_{11} \dots dH_{NN} \leftrightarrow P(E_1, \dots, E_N) dE_1 \dots dE_N.$$
 (3.27)

⁷Starting from Eq. (3.22), with b=0, we first note that ${\rm tr} H^2=\sum_{i,j}H_{ij}H_{ji}$. Because we consider the GOE $H_{ij}=H_{ji}$, thus we find that ${\rm tr} H^2=\sum_i H_{ii}^2+2\sum_{i>j}H_{ij}^2$. Inserting this in (3.22) leads to $P(H_{11},\ldots,H_{NN})=c\prod_i \exp\left(-aH_{ii}^2\right)\prod_{i>j} \exp\left(-2aH_{ij}^2\right)$. The results (3.25) and (3.26) follow immediately from straightforward integration.

⁸This dependence appears via factors $|\langle \eta_i, \phi \rangle|^2$, where ϕ is the state vector of the system and η_i is an eigenvector of the Hamiltonian.

There is, however, a profound difference between the two expressions, which lies in the number of variables, N(N+1)/2 on the lefthand side, and N on the right. Therefore, quite some care is required when we derive the quantity $P(E_1, \ldots, E_N) dE_1 \ldots dE_N$.

When one begins to derive $P(E_1, \ldots, E_N)$ from $P(H_{11}, \ldots, H_{NN})$, one must correctly take the different dimensions of the function P's domains into account. To do so, one first realises that E_1, \ldots, E_N cannot be the only parameters in play, and thus introduces L = N(N+1)/2 - N additional parameters p_1, \ldots, p_L . Now, one may state that

$$P(H_{11}, ..., H_{NN}) \sim P(E_1, ..., E_N; p_1, ..., p_L).$$
 (3.28)

To turn this into an equality, the coordinate transformation mediated by O must be correctly taken into account by means of a Jacobian J,

$$P(H_{11}, \dots, H_{NN}) = \det(J)P(E_1, \dots, E_N; p_1, \dots, p_L),$$
 (3.29)

where J is a matrix given by

$$J_{mn,kl} = \frac{\partial H_{mn}}{\partial E_k \partial p_l}. (3.30)$$

Since we want to obtain the probability density function for the eigenvalues, we integrate out all the additional parameters, which formally means that

$$P(E_1, ..., E_N) = \int \det J P(E_1, ..., E_N; p_1, ..., p_L) dp_1 ... dp_L.$$
 (3.31)

After evaluation of det J in (Mehta 2004), it follows:

$$P_{\text{GOE}}(E_1, \dots, E_N) = C_{\text{GOE}} \exp\left[-\frac{1}{2v^2} \sum_{k=1}^N E_k\right] \prod_{m < n} |E_n - E_m|.$$
 (3.32)

The constant prefactor C_{GOE} depends on the chosen ensemble and on the Hilbert space dimension N, and is obtained by integrating over the relevant symmetry group SO(N) (Mehta 2004; Stöckmann 2007). Before giving an explicit expression, we divert the attention to one of the most fundamental properties of these random matrix ensembles: The appearance of $\prod_{m < n} |E_n - E_m|$ in the joint probability distribution (3.32) of eigenvalues. This quantity reads zero whenever two eigenvalues coincide and, therefore, these matrices never show degeneracies. This really drives the eigenvalues away from each other. On the other hand, the factor $\exp\left[-\frac{1}{2v^2}\sum_{k=1}^N E_k\right]$ makes sure that no eigenvalues dwell too far away from the central value (here set

 $^{^9}$ This does imply that the notation using the same "P" is somewhat unfortunate, since we are really talking about different functions. Still, to avoid notational overhead, we stick to the P wherever a probability density is treated.

to zero). In other words, the eigenvalues are confined to some finite region because of the Gaussian, but there is also a strong *eigenvalue repulsion* present.

By similar calculations one finds the following results for the other two ensembles (Mehta 2004; Stöckmann 2007)

$$P_{\text{GUE}}(E_1, \dots, E_N) = C_{\text{GUE}} \exp\left[-\frac{1}{v^2} \sum_{k=1}^N E_k\right] \prod_{m < n} |E_n - E_m|^2$$
 (3.33)

$$P_{\text{GSE}}(E_1, \dots, E_N) = C_{\text{GSE}} \exp\left[-\frac{2}{v^2} \sum_{k=1}^N E_k\right] \prod_{m < n} |E_n - E_m|^4.$$
 (3.34)

Note that the level repulsion in the GUE is stronger than that in the GOE, and the GSE has again stronger repulsion than the GUE. There is a type of systematics in these results and we can summarise them as

$$P_{\beta}(E_1, \dots, E_N) = C_{\beta} \exp\left[-\frac{\beta}{2v^2} \sum_{k=1}^N E_k\right] \prod_{m \le n} |E_n - E_m|^{\beta}.$$
 (3.35)

The parameter $\beta = 1, 2, 4$ now serves to identify the different ensembles. $\beta = 1$ results in the GOE, $\beta = 2$ gives the GUE and $\beta = 4$ reproduces the GSE result. These values nicely *characterise the strength of the level repulsion* and we can thus see these typical level repulsion strengths as a defining property of the ensemble. Using β , we can now also write down a general result for the C_{β} ,

$$\frac{1}{C_{\beta}} = (2\pi)^{N/2} \beta^{-N/2 - \beta N(N-1)/4} [\Gamma(1+\beta/2)]^{-N} \prod_{j=1}^{N} \Gamma(1+\beta j/2), \qquad (3.36)$$

where Γ is the *Gamma function* as defined in Abramowitz and Stegan (1965).

Hence, we have explained the fundamental steps in the derivations of the *joint probability density function* for the eigenvalues of a GOE and presented the analogous results for the GUE and GSE. However, often one is not really interested in the full joint probability distribution and, specially for higher dimensions N, these distributions are far from practical to handle. Because they characterise the probability to sample a complete spectrum of the system we cannot use (3.35) to infer information about the ensemble in which the system is contained if we only have a single system at our disposal. However, we should not forget that RMT is in essence a type of multivariate analysis and when we have an energy spectrum at our disposal, we can extract coarse grained information from it, which *can* be used to infer information about the RMT ensemble in which the system may be contained. This implies asking questions of the type "What is the probability to find an energy eigenvalue at energy

¹⁰This would be similar to sampling the value 0.12345 for a stochastic quantity and trying to use that value to identify the probability distribution from which that value was sampled.

E?" or "What is the probability, upon ordering the energy eigenvalues in increasing order, of finding a spacing s between a level and its nearest neighbour?". The answer to the former question is given by the density of states, whereas the latter query is answered via the nearest-level spacing distribution. RMT allows us to analytically compute these averages over the ensemble. However, we can numerically obtain estimates for these distributions from a single energy spectrum. We now briefly describe these coarse grained probability distributions in the context of Gaussian ensembles.

Density of States

A first quantity of potential interest is a global one, *the density of states* (DOS). The DOS does not provide us with information on the set of eigenvalues, but rather describes the behaviour of one typical eigenvalue. It is most commonly defined as

$$D(E) \equiv \sum_{i=1}^{N} \delta(E - E_i)$$
 (3.37)

and therefore is closely related to the counting function which counts all the energy levels from the ground state up to a certain level ϵ :

$$N(\epsilon) \equiv \sum_{i=1}^{N} \theta(\epsilon - E_i), \tag{3.38}$$

where θ is the Heaviside step function. It is easy to verify that

$$\frac{\mathrm{d}}{\mathrm{d}\epsilon}N(\epsilon)\bigg|_{\epsilon=E} = D(E).$$
 (3.39)

The density of states is for example of vital importance in solid-state physics, where it is often used to treat continuous spectra rather than the discrete ones we encounter here. In the context of RMT, where statistics is central, it is more logical to deal with the quantity

$$\rho(E) = \frac{1}{N}D(E),\tag{3.40}$$

which has the property

$$\int \rho(E) dE \equiv \frac{1}{N} \sum_{i=1}^{N} \int \delta(E - E_i) dE = 1.$$
 (3.41)

¹¹Note that this is exactly what is done in (Bohigas et al. 1984), where one considers the local properties the spectra of three different systems to acquire the data presented in this publication's Fig. 3.1. Another example is (Walschaers 2011), where the density of states of a single, large (5000×5000) random matrix is sufficient to accurately estimate the Marchenko-Pastur statistics (Marčenko and Pastur 1967).

Notice, however, that, due to (3.37), the definition of $\rho(E)$ treats $E_1, \ldots E_N$ as known quantities, which contrasts the logic of RMT, where these are supposed to be stochastic quantities. Thus the most natural quantity to treat in the framework of RMT is actually $\langle \rho(E) \rangle$, which is the normalised density of states, averaged over the RMT ensemble. This quantity allows an interpretation as the probability density functions for a single eigenvalue

$$\langle \rho(E) \rangle = \int P_{\text{GOE}}(E_1, \dots, E_N) dE_2 \dots dE_N,$$
 (3.42)

where we integrate over all but one variable of the joint probability density.

The calculation of $\langle \rho(E) \rangle$ can be done in many different ways: An appealing and accessible method relies on the calculation of moments m_q^N (for the qth moment). These moments are formally defined by

$$m_q^N = \int E^q \langle \rho(E) \rangle dE \tag{3.43}$$

and with little effort, involving only the property that $\int_{\mathbb{R}} \delta(x - x_0) f(x) dx = f(x_0)$, we find that

$$m_q^N = \frac{1}{N} \langle \operatorname{tr}(H^q) \rangle. \tag{3.44}$$

The central idea to the moment method is that the full set of moments uniquely defines the distribution (3.42).¹² This method is extensively applied in Stöckmann (2007) for the GOE, and in Walschaers (2011) for the Wishart ensemble (Marčenko and Pastur 1967; Wishart 1928).

Another, related, method relies on calculating resolvents, which makes sense because one can prove that

$$\rho(E) = -\frac{1}{\pi N} \lim_{\epsilon \to 0} \operatorname{Im} \operatorname{tr} \left(\frac{1}{E\mathbb{1} - H - i\epsilon} \right). \tag{3.45}$$

This method, too, is treated in Stöckmann (2007), where the combination of this method and the moment method provides the final *explicit* expression for $\langle \rho(E) \rangle$.

The problem with methods exploiting moments is that they usually require an expression for all the moments, which can be hard to obtain (Walschaers 2011). Therefore, one often resorts to different methods, a very powerful one being the *replica trick* and its mathematically more satisfying brother: the *supersymmetry method*. Since these methods require quite some technical skills in complex analysis and Grassman calculus, we restrict ourselves to providing some references. An extensive and accessible paper on the replica trick is found in Edwards and Jones

¹²Even though the moments contain all the information about the probability distribution, that does not imply that it is straightforward to find an explicit expression for the probability density function based on the moments.

(1976), but this method later received a lot of criticism, mainly due to its lack of mathematical rigour. It was even pointed out that it may provide false results (Verbaarschot and Zirnbauer 1985). A way to circumvent the criticism and fix the method is to introduce anticommuting variables and apply methods known from supersymmetry. These methods are treated in Chap. 10 of Haake (2010) and in Chaps. 7 and 8 of Akemann et al. (2011).

Whichever method is applied, in the limit $N \to \infty$ one will always recover Wigner's celebrated result for the Gaussian ensembles: the *semicircle law*. When the variance v of (3.26) is chosen such that $v = \xi/\sqrt{N}$, where ξ is a constant which is independent of N, the semicircle law is elegantly written as

$$\lim_{N \to \infty} \langle \rho(E) \rangle = \begin{cases} \frac{1}{\pi \xi} \sqrt{1 - \frac{E^2}{4\xi^2}} & \text{if } -2\xi \leqslant E \leqslant 2\xi \\ 0 & \text{otherwise.} \end{cases}$$
 (3.46)

This result implies that ξ is naturally interpreted as half the spectral radius (Conway 1997). Although this result as such is interesting and powerful, one will rarely encounter such a global density of states in a real physical system. When we recall Wigner's original motivation, we also realise that RMT is not necessarily intended to investage such global behaviour; it is often the case that global spectral properties of real physical systems are not well captured by RMT models. The statistical properties of spectra on which RMT is, however, typically *triumphant* are the *local spectral properties*.

Nearest-Level Spacing*

Of all *local spectral properties*, the nearest-level spacing is arguably the most significant of all. To calculate this quantity, one orders the levels by increasing energy and calculates the distance between two subsequent levels: $s = |E_{i+1} - E_i|$. It is an intriguing endeavour to extract the statistics P(s): The first proposal was again formulated by Wigner and became known as the *Wigner surmise*, obtained by exactly collocating P(s) for a 2×2 random matrix, sampled from one of the Gaussian ensembles:

$$P(s/\Delta) = \begin{cases} \frac{\pi s}{2\Delta} \exp\left[-\frac{\pi s^2}{4\Delta^2}\right], & \text{GOE} \\ \frac{32s^2}{\pi^2 \Delta^2} \exp\left[-\frac{4s^2}{\pi \Delta^2}\right], & \text{GUE} \end{cases}$$
(3.47)

where Δ is the mean level-spacing, such that the distribution is centred around $s/\Delta=1$. Striking about the Wigner surmise is its elegance and the insight which it provides. Surprisingly, the result is also a *very* good estimate for the spacing distributions of $N\times N$ Gaussian matrices. These distributions were derived exactly by Mehta and Des Cloizeaux (1972), but the final expressions are highly non-transparent and therefore one often resorts to the Wigner surmise for practical purposes. We specifically also make mention of the GUE result, since comparing both allows us to see that, as $s/\Delta \to 0$, $P(s/\Delta)$ scales as

$$P(s/\Delta) \sim \frac{s}{\Lambda}$$
 (GOE), (3.48)

$$P(s/\Delta) \sim \left(\frac{s}{\Delta}\right)^2$$
 (GUE), (3.49)

thus nicely showing again the level repulsion, already discussed with (3.32), and, more specifically, a different scaling of level repulsion for different ensembles.

3.3.4 Statistical Properties of GOE Eigenvectors

Another type of statistics which is important in our work is the statistics of eigenvectors. The eigenvectors can be obtain via $H = O^t DO$, as columns of the orthogonal transformation O. When we combine this with the fundamental symmetry (3.16) for the GOE, it can directly be understood that in principle the eigenvectors are distributed in a uniform way: Because $P(O^t DO) = P(D)$ for all $O \in SO(N)$ by virtue of (3.16), any column of any $O \in SO(N)$ is equally likely to be sampled (Haake and Życzkowski 1990).

The probability distribution to get a given eigenvector boils down to the joint probability distribution for a set of eigenvector components c_1, \ldots, c_N . Given that all eigenvectors are equally probable, we find that (Haake 2010; Haake and Życzkowski 1990)

$$P_{\text{GOE}}(c_1, \dots, c_N) = \pi^{-N/2} \Gamma\left(\frac{N}{2}\right) \delta\left(1 - \sum_{i=1}^{N} c_i^2\right),$$
 (3.50)

where the choice for the GOE is important since we can therefore assume that the vectors are real. This implies that this distribution is nothing more than the uniform distribution on the unit sphere of \mathbb{R}^N . Often our interest does not lie in the full distribution, but rather in the statistical properties of a single vector component, i.e. the probability distribution of $y = c_1^2$. Again, we obtain this via (Haake and Życzkowski 1990; Haake 2010)

$$P_{\text{GOE}}(y) = \pi^{-N/2} \Gamma\left(\frac{N}{2}\right) \int dc_1 \dots dc_N \delta(y - c_1^2) \delta\left(1 - \sum_{i=1}^N c_i^2\right)$$

$$= \frac{1}{\sqrt{\pi}} \frac{\Gamma(N/2)}{\Gamma[(N-1)/2]} \frac{(1-y)^{(N-3)/2}}{\sqrt{y}}.$$
(3.51)

What is not explicitly found in literature, but follows directly (Walschaers et al. 2015) from rewriting this equation, is that this is actually a special type of *Beta distribution* (Gupta 2011):

$$P_{\text{GOE}}(y) = \frac{1}{\sqrt{\pi}} \frac{\Gamma(N/2)}{\Gamma[(N-1)/2]} \frac{(1-y)^{(N-3)/2}}{\sqrt{y}},$$

$$= \frac{1}{B(1/2, N/2 - 1/2)} y^{1/2-1} (1-y)^{N/2-1/2-1},$$
(3.52)

where B(1/2, N/2 - 1/2) is the *beta function* (Abramowitz and Stegan 1965) with parameters 1/2 and N/2 - 1/2. This implies that y's statistics is governed by a *Beta distribution* (Gupta 2011) with parameters 1/2 and (N - 1)/2, in other words

$$y \sim \text{Beta}\left(\frac{1}{2}, \frac{N-1}{2}\right). \tag{3.53}$$

Although this result does not provide much new practical information compared to Eq. (3.51), it does provide a somewhat broader statistical context.

Let us conclude with a useful approximation to (3.51, 3.52) in the thermodynamic limit $N \to \infty$. With the substitution $\eta = Ny$, and subsequent evaluation of the limit $N \to \infty$, one finds (Haake 2010) that

$$P_{\text{GOE}}(\eta) = \frac{1}{\sqrt{2\pi\eta}} e^{-\eta/2},$$
 (3.54)

which is commonly known as the Porter-Thomas distribution (Porter and Thomas 1956), and is usually preferred as an approximation over the exact Eq. (3.51).

3.4 Concluding Remarks

Now that we reviewed the heuristic properties of complex systems as they are often presented throughout a wide range of fields of research, and studied the specific case of dynamical quantum systems in Sect. 3.1.3, we can combine the results of Chaps. 2 and 3 in our study of quantum transport problems. In Chaps. 4 and 5 we extensively use the results of Sect. 3.3. Specifically the GOE matrices (3.26) and associated semicircle distribution (3.46) are crucial in Sects. 4.5 and 5.5. Furthermore, the GUE ensemble (3.6) is used throughout Chap. 9 for most numerical examples.

In Sect. 8.5, we combine the complexity which arises when we insert many particles in the system, with topological disorder which is there represented by random unitary channels defined in (8.5). The treatment of random unitary operators will given by the *circular* ensembles of RMT, a framework which is complementary to the Gaussian ensembles discussed in Sect. 3.3. We leave the introduction of these RMT techniques for Appendix B.

In the following chapter we present results on single-particle transport through complex network structures, introduce design principles which constrain the disorder in these systems, and thereby achieve near optimal excitation transfer. This model heavily relies on RMT, and was specifically inspired by the physical intuition which underlies the mechanism of chaos assisted tunnelling (Tomsovic and Ullmo 1994).

References

- M. Abramowitz, I. Stegan, in Handbook of Mathematical Functions (Dover Publications, NY, 1965)
- G. Akemann, J. Baik, P.D. Francesco (eds.) *The Oxford Handbook of Random Matrix Theory* (Oxford Handbooks in Mathematics, Oxford, 2011)
- R. Albert, A.-L. Barabási, Statistical mechanics of complex networks. Rev. Mod. Phys. 74, 47–97 (2002)
- R. Alicki, M. Fannes, Quantum Dynamical Systems (Oxford University Press, Oxford, 2001)
- W.B. Arthur, Complexity and the economy. Science 284, 107–109 (1999)
- E. Atlee Jackson, On the control of complex dynamic systems. Phys. D 50, 341–366 (1991)
- R. Balian, C. Bloch, Distribution of eigenfrequencies for the wave equation in a finite domain. Ann. Phys. **60**, 401–447 (1970)
- R. Balian, C. Bloch, Distribution of eigenfrequencies for the wave equation in a finite domain. II. Electromagnetic field. Riemannian spaces. Ann. Phys. **64**, 271–307 (1971)
- R. Balian, C. Bloch, Distribution of eigenfrequencies for the wave equation in a finite domain: III. Eigenfrequency density oscillations. Ann. Phys. **69**, 76–160 (1972)
- R. Balian, C. Bloch, Solution of the Schrödinger equation in terms of classical paths. Ann. Phys. 85, 514–545 (1974)
- L.E. Ballentine, *Quantum Mechanics: A Modern Development* (World Scientific Publishing Company Pte Limited, Singapore, 2014)
- A.-L. Barabási, Scale-free networks: a decade and beyond. Science 325, 412–413 (2009)
- A.-L. Barabási, R. Albert, Emergence of scaling in random networks. Science 286, 509-512 (1999)
- V. Bargmann, Note on Wigner's theorem on symmetry operations. J. Math. Phys. 5, 862–868 (1964)
- G. Bianconi, A.-L. Barabási, Bose–Einstein condensation in complex networks. Phys. Rev. Lett. 86, 5632–5635 (2001)
- N. Biggs, *Algebraic Graph Theory*. Cambridge Mathematical Library (Cambridge University Press, Cambridge, 1993)
- O. Bohigas, M.J. Giannoni, C. Schmit, Characterization of chaotic quantum spectra and universality of level fluctuation laws. Phys. Rev. Lett. **52**, 1–4 (1984)
- N. Bohr, I. On the constitution of atoms and molecules. Philos. Mag. 26, 1–25 (1913)
- N. Bohr, Neutron capture and nuclear constitution. Nature 137, 344–348 (1936)
- B. Bollobás, Graphs, groups and matrices, in Modern Graph Theory. Graduate Texts in Mathematics, vol. 184 (Springer, New York, 1998a), pp. 253–293. https://doi.org/10.1007/978-1-4612-0619-4-8
- B. Bollobás, Random graphs, in *Modern Graph Theory*. Graduate Texts in Mathematics, vol. 184 (Springer, New York, 1998b), pp. 215–252. https://doi.org/10.1007/978-1-4612-0619-4_7
- L. Boltzmann, Zur Theorie der elastischen Nachwirkung. Ann. Phys. 241, 430–432 (1878)
- M. Born, P. Jordan, Zur Quantenmechanik. Z. Physik 34, 858–888 (1925)
- M. Born, W. Heisenberg, P. Jordan, Zur Quantenmechanik. II. Z. Phys. 35, 557–615 (1926)
- A.D. Broido, A. Clauset, Scale-free networks are rare (2018). arXiv:1801.03400
- F.R.K. Chung, *Spectral Graph Theory*. Regional Conference Series in Mathematics, vol. 92 (Published for the Conference Board of the Mathematical Sciences by the American Mathematical Society, Providence, 1997)
- F. Chung, L. Lu, V. Vu, Spectra of random graphs with given expected degrees. PNAS **100**, 6313–6318 (2003)
- A. Clauset, C.R. Shalizi, M.E.J. Newman, Power-law distributions in empirical data. SIAM Rev. 51, 661–703 (2009)
- J.B. Conway, *A Course in Functional Analysis*. Graduate Texts in Mathematics, vol. 96, 2nd edn. (Springer, New York, 1997)
- J.P. Crutchfield, K. Young, Inferring statistical complexity. Phys. Rev. Lett. 63, 105–108 (1989)
- P.A.M. Dirac, The fundamental equations of quantum mechanics. Proc. R. Soc. A **109**, 642–653 (1925)

References 73

B. Eckhardt, E. Aurell, Convergence of the semi-classical periodic orbit expansion. EPL 9, 509 (1989)

- S.F. Edwards, R.C. Jones, The eigenvalue spectrum of a large symmetric random matrix. J. Phys. A Math. Gen. **9**, 1595 (1976)
- A. Einstein, Über die von der molekularkinetischen Theorie der Wärme geforderte Bewegung von in ruhenden Flüssigkeiten suspendierten Teilchen. Ann. Phys. **322**, 549–560 (1905)
- A. Einstein, Zum Quantensatz von Sommerfeld und Epstein. Verhandlungen der Deutschen Physikalischen Gesellschaft 19, 82–92 (1917)
- P. Erdös, A. Rényi, On the strength of connectedness of a random graph. Acta Math. Hung. 12, 261–267 (1961)
- Z. Füredi, J. Komlós, The eigenvalues of random symmetric matrices. Combinatorica 1, 233–241 (1981)
- J.W. Gibbs, On the equilibrium of heterogeneous substances. AJS 96, 441–458 (1878)
- A.K. Gupta, Beta distribution, in *International Encyclopedia of Statistical Science*, ed. by M. Lovric (Springer, Berlin, 2011), pp. 144–145
- M.C. Gutzwiller, Phase-integral approximation in momentum space and the bound states of an atom. J. Math. Phys. 8, 1979–2000 (1967)
- M.C. Gutzwiller, Phase-integral approximation in momentum space and the bound states of an atom II. J. Math. Phys. **10**, 1004–1020 (1969)
- M.C. Gutzwiller, Energy spectrum according to classical mechanics. J. Math. Phys. 11, 1791–1806 (1970)
- M.C. Gutzwiller, Periodic orbits and classical quantization conditions. J. Math. Phys. **12**, 343–358 (1971)
- M. Gutzwiller, Quantum chaos. Scholarpedia 2, 3146 (2007)
- F. Haake, *Quantum Signatures of Chaos*, vol. 54 (Springer Science & Business Media, New York, 2010)
- F. Haake, K. Życzkowski, Random-matrix theory and eigenmodes of dynamical systems. Phys. Rev. A 42, 1013–1016 (1990)
- W. Heisenberg, Über quantentheoretische Umdeutung kinematischer und mechanischer Beziehungen. Z. Phys. 33, 879–893 (1925)
- W. Heisenberg, Development of concepts in the history of quantum theory. Am. J. Phys. 43, 389–394 (1975)
- H. Hooyberghs, Statistical physics of cooperative phenomena on complex networks. Ph.D thesis, KU Leuven, Leuven, 2013
- J.J. Hopfield, Neural networks and physical systems with emergent collective computational abilities. PNAS 79, 2554–2558 (1982)
- N. Hurran, The Day of the Doctor, 2013
- M. Kardar, Statistical Physics of Particles (Cambridge University Press, Cambridge, 2007)
- A.N. Kolmogorov, Combinatorial foundations of information theory and the calculus of probabilities. Russ. Math. Surv. 38, 29 (1983)
- A.M. Lane, R.G. Thomas, E.P. Wigner, Giant resonance interpretation of the nucleon-nucleus interaction. Phys. Rev. **98**, 693–701 (1955)
- V.A. Marčenko, L.A. Pastur, Distribution of eigenvalues for some sets of random matrices. Mat. Sb. 1, 457–483 (1967)
- J.C. Maxwell, On the dynamical theory of gases. Phil. Trans. R. Soc. Lond. 157, 49–88 (1867)
- M. Mehta, J. Des Cloizeaux, The probabilities for several consecutive eigenvalues of a random matrix. Indian J. Pure Appl. Math. 3, 329–351 (1972)
- M.L. Mehta, Random Matrices (Elsevier/Academic Press, Amsterdam, 2004)
- W.H. Miller, Semiclassical quantization of nonseparable systems: a new look at periodic orbit theory. J. Chem. Phys. 63, 996–999 (1975)
- S. Müller, S. Heusler, P. Braun, F. Haake, A. Altland, Semiclassical foundation of universality in quantum chaos. Phys. Rev. Lett. **93**, 014103 (2004)

- G. Nicolis, P. Gaspard, Toward a probabilistic approach to complex systems. Chaos, Solitons Fractals 4, 41–57 (1994)
- E.P. Odum, G.W. Barrett, *Fundamentals of Ecology*, 5th edn. (Thomson Brooks/Cole, Belmont, 2005)
- J.M. Ottino, Engineering complex systems. Nature **427**, 399 (2004)
- W. Pauli, Über das Modell des Wasserstoffmolekülions. Ann. Phys. 373, 177–240 (1922)
- $C.E.\ Porter, R.G.\ Thomas, Fluctuations\ of\ nuclear\ reaction\ widths.\ Phys.\ Rev.\ \textbf{104}, 483-491\ (1956)$
- I. Prigogine, Exploring complexity. Eur. J. Oper. Res. 30, 97–103 (1987)
- K. Richter, J.-M. Rost, *Komplexe Systeme*, vol. 15550. [Fischer] Fischer kompakt, orig.-ausg., 2. aufl edn. (Fischer-Taschenbuch-Verl, Frankfurt am Main, 2004)
- R.K. Sawyer, Social Emergence: Societies as Complex Systems (Cambridge University Press, Cambridge, 2005)
- H.G. Schuster, Deterministic Chaos: An Introduction, 1st edn. (VCH, Weinheim, 1989)
- C.R. Shalizi, J.P. Crutchfield, Computational mechanics: pattern and prediction, structure simplicity. J. Stat. Phys. 104, 817–879 (2001)
- C.E. Shannon, A mathematical theory of communication. Bell Syst. Tech. J. **27**(379–423), 623–656 (1948)
- H.-J. Stöckmann, Quantum Chaos: An Introduction (Cambridge University Press, Cambridge, 2007)
- S. Tomsovic, D. Ullmo, Chaos-assisted tunneling. Phys. Rev. E 50, 145–162 (1994)
- J.J.M. Verbaarschot, M.R. Zirnbauer, Critique of the replica trick. J. Phys. A Math. Gen. 18, 1093 (1985)
- A. Verbeure, *Many-Body Boson Systems: Half a Century Later*, Theoretical and Mathematical Physics (Springer, New York, 2011)
- A. Voros, Unstable periodic orbits and semiclassical quantisation. J. Phys. A Math. Gen. 21, 685 (1988)
- M. Walschaers, Counting messages of quantum sources. Master thesis, KU Leuven, 2011
- M. Walschaers, R. Mulet, T. Wellens, A. Buchleitner, Statistical theory of designed quantum transport across disordered networks. Phys. Rev. E 91, 042137 (2015)
- D.J. Watts, S.H. Strogatz, Collective dynamics of small-world networks. Nature 393, 440–442 (1998)
- E.P. Wigner, Gruppentheorie und ihre Anwendung auf die Quantenmechanik der Atomspektren (Vieweg+Teubner Verlag, Wiesbaden, 1931)
- E.P. Wigner, Characteristic vectors of bordered matrices with infinite dimensions. Ann. Math. 62, 548–564 (1955)
- E.P. Wigner, On the distribution of the roots of certain symmetric matrices. Ann. Math. 67, 325–327 (1958)
- J. Wishart, The generalised product moment distribution in samples from a normal multivariate population. Biometrika **20A**, 32–52 (1928)

Part II Single-Particle Quantum Transport

Chapter 4 Efficient Transport in Closed Systems



Chaos isn't a pit. Chaos is a ladder

Lord Petyr Baelish, played by Aidan Gillen in "Game of Thrones" (Sakharov 2013)

4.1 Introduction

In Sect. 1.1, we introduced the field of quantum transport theory and more specifically discussed the influence of quantum interference effects on transport phenomena. The present chapter, based on Walschaers et al. (2013, 2015), presents the first results of this dissertation, which fit into that framework.

In Chap. 1, we noted that there are several possible ways to generalise quantum interference beyond the paradigmatic double slit experiment, i.e. a two-pathway setup, as indicated in Fig. 1.2. This sketches the perspective of the dissertation: We can induce more intricate inference effects by

- introducing additional, disordered pathways which may all interfere,
- simultaneous injection of several indistinguishable particles,
- addition of an environment.

In this chapter, we focus solely on the first point, which in general implies that we enter the realm of complex systems. Indeed, Panel (a) of Fig. 4.1, shows a sketch which depicts a multi-slit experiment as a complex network. We study the potential of such a disordered network of interference pathways to achieve *fast and efficient excitation transfer*. In particular, we consider the network as closed quantum system and investigate the single excitation quantum evolution on such structure.

Closed systems are systems where energy and particles are conserved and when they are bounded, the related Hamiltonian gives rise to a discrete spectrum. A closed system must be governed by unitary dynamics, described by a time-independent Hamiltonian H (see Sects. 2.4 and 3.1.3). Note that, in this formulation, a scattering system is also considered a closed (unbounded) system, in contrast to the term "open system" as used in mesoscopic physics (Gaspard 2014; Rotter 2009). However, when

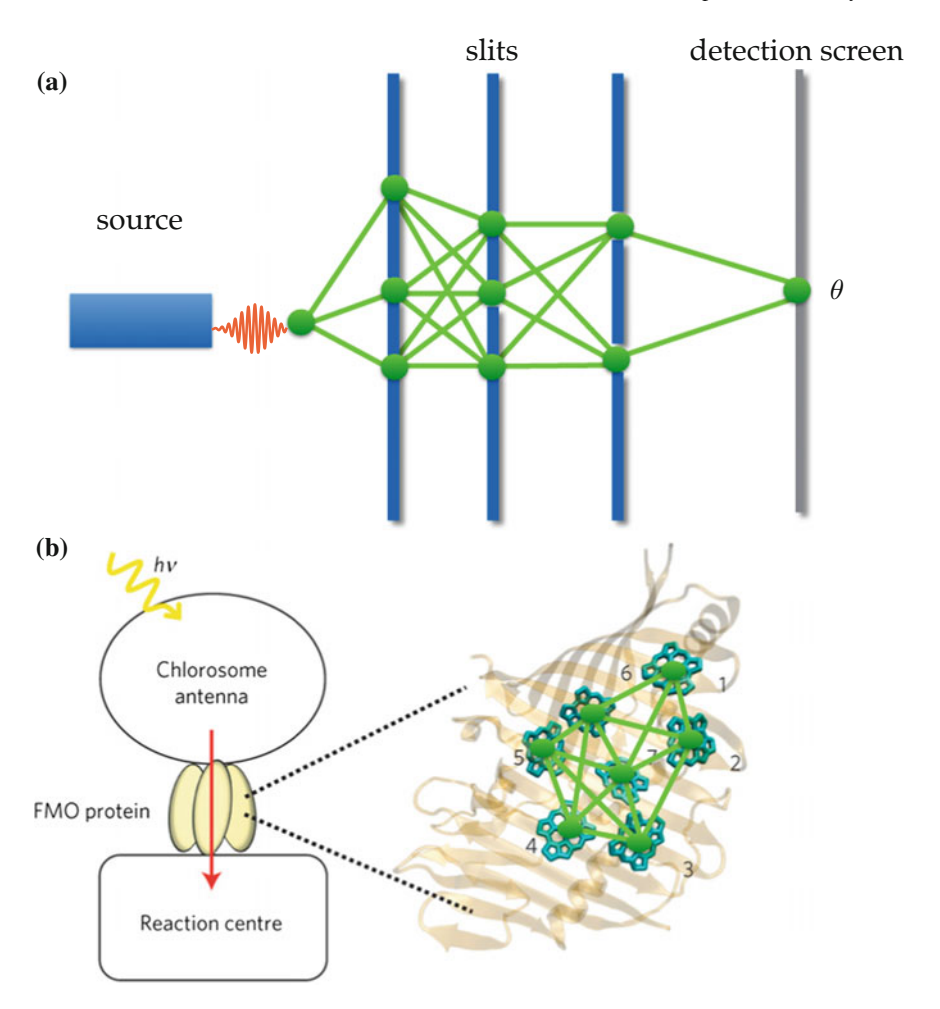


Fig. 4.1 Many-slit extension of Young's setup (**a**) and chlorophyll molecules of the FMO photosynthetic complex (**b**). Both systems can be related to a network structure of interferring pathways, as indicated in green. These networks can be understood as representations of the systems' Hamiltonians. Panel **b** was taken from Sarovar et al. (2010), the network was drawn on top

one projects the scattering dynamics to a subsystem of finite volume, one will also observe dissipative effects, which brings both terminologies closer together. The extension of the model for efficient transport, deduced in this chapter, to such a scattering formalism is left for Chap. 5. In Chap. 9, we then connect this scattering approach to the many-particle framework, where we deal with open systems in the context of dynamical semigroups. This will lead us to conclude in Sect. 9.1 that the "open systems" in mesoscopic physics (Gaspard 2014; Imry 2009; Rotter 2009) can be related to the "open systems" in quantum statistical mechanics and quantum optics (Alicki 1987; Breuer and Petruccione 2007; Loudon 2000).

4.1 Introduction 79

Our predominant motivation to investigate such a setup is shown in Panel (b) of Fig. 4.1 and is connected to the discussion on "quantum biology" in Chap. 6: Throughout the past decade, evidence has piled up that in light harvesting complexes quantum interference effects survive on time scales which are similar to the typical energy transfer time. This energy transport is mediated via quasi-particles, known as excitons, which naturally appear in semi-conductor physics (Kittel 2005): When valence and conduction band are sufficiently close to allow for interaction between electrons and the holes they leave behind, the electron-hole pair travels as one quasiparticle, an exciton. In molecular systems, there is a similar construct, although we must now consider discrete molecular orbitals rather than bands (Amerongen et al. 2000; Bardeen 2014). In photosynthesis, such *molecular excitons* are created upon photo-excitation of a chlorophyll molecule, and dipole-dipole interaction between such molecules allows the exciton to travel from one chlorophyll molecule to the other. Because the system is of a quantum mechanical nature, this transport process is governed by Schrödinger's equation and quantum interference arises between different pathways through the complex.

Situations as sketched in Fig. 4.1 can be modelled in an abstract and quite general fashion with the help of Random Matrix Theory (RMT), introduced in Chap. 3. Therefore, we assume that the system Hamiltonian can effectively be described by means of a matrix-like structure, which implies that there is a natural basis of single-particle state vectors $\{|e_1\rangle, |e_2\rangle, \dots\}$, such that the Hamiltonian is given by

$$H = \sum_{i,j} H_{ij} |e_i\rangle \langle e_j|. \tag{4.1}$$

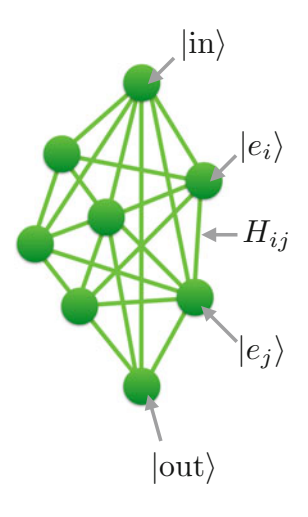
Figure 4.2 shows how we can represent such Hamiltonians by network structures (remember Sect. 3.2), where the nodes represent the state vectors $|e_i\rangle$ and the edges depict the couplings H_{ij} between $|e_i\rangle$ and $|e_j\rangle$ (Scholak 2011). The fact that we are dealing with a Hamiltonian tells us that $H_{ij} = H_{ji}^*$, and when we assume *time-reversal invariance* (as discussed in Sect. 3.3.2), we find that $H_{ij} = H_{ji}$.

In the typical literature on this topic, the state vectors $|e_i\rangle$ are given a specific meaning: They form the fundamental building blocks of a more complicated structure, and are here referred to as *sites*. These sites may themselves exhibit internal degrees of freedom, but these are initially considered unimportant for the description of the problem. As an example, one may imagine that the state vectors represent electronic excitations which are localised on (bacterio)chlorophyll molecules (Scholak et al. 2010, 2011a) or (Rydberg) atoms (Scholak et al. 2014), but also on different minima of an a-periodic lattice, such that $|e_i\rangle$ are given by the Wannier functions (Wannier 1937). In this sense, the network structure gets and additional interpretation as it explicitly represents a spatial structure.

¹ Although there is literature on several of such light harvesting complexes, the clearest results were obtained for the FMO complex, e.g. in Engel et al. (2007). It is, however, not obvious that these results can be extrapolated to all types of light harvesting complexes, as we discuss in Chap. 6.

Complex Network

Benchmark Network



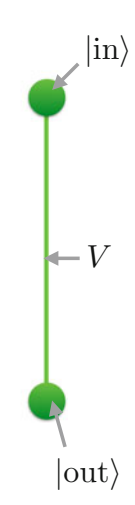


Fig. 4.2 Complex networks represent dynamical quantum systems by associating state vectors $|e_j|$ with their nodes and coupling strengths H_{ij} with their edges, thus justifying the model (4.1). Input and output sites are identified, respectively, as initial condition and target of the transport process. The aim is to make transport on complex networks (left) faster and more efficient (see Sect. 4.2) than on the associated benchmark system (right), where all sites but input and output are stripped away

This "geometric" treatment of the problem is useful, since it allows us to directly visualise topological effects and symmetries. On the other hand, it can also be deceiving, because some symmetries are not apparent from the spatial structure of the natural constituents and will remain hidden in such visualisation (Zech 2013; Zech et al. 2013, 2014).

In a quantum transport setting, one usually is interested in the transport of the population of one state vector $|\psi_i\rangle \in \mathcal{H}$ to another state vector $|\psi_f\rangle \in \mathcal{H}$. The probability for this transport to occur at time t is given by

$$p_{i\to f}(t) = \left| \left\langle \psi_f, e^{-itH} \psi_i \right\rangle \right|^2. \tag{4.2}$$

A useful way to look at this problem is by using the spectral decomposition $H = \sum_j E_j |\eta_j\rangle\langle\eta_j|$, where E_j are the energy levels of H, with $|\eta_j\rangle$ their respective eigenvectors. We use this identity to rewrite

$$p_{i \to f}(t) = \left| \sum_{j} e^{-itE_{j}} \langle \psi_{f}, \eta_{j} \rangle \langle \eta_{j}, \psi_{i} \rangle \right|^{2}. \tag{4.3}$$

4.1 Introduction 81

This expression indicates that in order to have transport from $|\psi_i\rangle$ to $|\psi_f\rangle$, there must be at least one eigenvector for which $\langle \psi_f, \eta_i \rangle \langle \eta_i, \psi_i \rangle \neq 0$.

These results can be made less abstract by assuming that we want to transport energy from one fundamental building block (site) to another. If we choose for example $|e_1\rangle$ as initial and $|e_n\rangle$ as final state (i.e. some exciton initially localised at site 1, and to be delivered at site n), we obtain

$$p_n(t) = \left| \sum_{j} e^{-itE_j} \left\langle e_n, \eta_j \right\rangle \left\langle \eta_j, e_1 \right\rangle \right|^2. \tag{4.4}$$

By varying n, we can use this expression to study how energy spreads over the different sites of the system. From the contributions $\langle e_n, \eta_j \rangle \langle \eta_j, e_1 \rangle$ it can be seen that the localisation properties of the eigenvectors over these different constituents are crucial in determining how the initial excitation spatially spreads out over the network.

4.2 Measuring Transfer Efficiency

Before we can identify design principles to optimise the transport efficiency on the above random networks, we need a precise definition of our figure of merit, i.e. we need to give a quantifier of transport efficiency and speed.

The concept of efficiency is actually not unproblematic to define, since it goes hand in hand with the functionality of the system. When we think about devices, a simple example is found in the field of photovoltaics, where one often deals with the *quantum efficiency* (Nelson 2003). In the present context, the name may cause confusion, because it does not deal with a coherent quantum processes, rather the "quantum" refers to a fundamental quantum of light, being a photon (much as for photodetectors). Specifically, the quantum efficiency is defined by

$$QE := \frac{\text{# outgoing electrons}}{\text{# incoming photons}}.$$
 (4.5)

This definition is much more subtle than one expects at first glance, since it is not a priori clear where one should measure these outgoing electrons. Therefore, it is common practice in the photovoltaics community to both talk about *internal* and *external* quantum efficiency, where the internal efficiency refers to the number of successful charge separations and the external one only considers the amount of electrons that ultimately contribute to a measurable current (i.e. all types of losses occurring within the device are also taken into account by the external QE).

The example of quantum efficiency will not only be important later-on when we discuss quantum effects in photosynthesis, it is also a good example to indicate a fundamental point related to efficiency: *Efficiency is always defined with respect to a*

given functionality. To come up with a definition of any type of efficiency, one must first have a good understanding of the exact functionality which the efficiency is to describe. It is for example quite clear that to the consumer, the external quantum efficiency of solar panels is the relevant quantity, whereas the constructor of the semi-conductor material requires the internal quantum efficiency.

We focus on quantum transport devices, and thus need a *transfer efficiency* that quantifies how well the system performs its task of delivering the excitation to a specific output site. Since we deal with quantum mechanics, we must formulate the problem in terms of measurements and probabilities. Therefore we assume that there is some form of detector connected to the output site, which should detect the excitation with a high probability. Of course, from (4.4) it can be seen that this probability, $p_{\text{out}}(t)$, depends on time and, therefore, the time component must also enter the definition of efficiency. The way to include time is not completely obvious, because there are two competing notions of what is efficient: On the one side, one may deem it most important that there exists a point in time where $p_{\text{out}}(t)$ is close to one. On the other side, one may consider it more important that the time-average of $p_{\text{out}}(t)$ is high, implying that the excitation spends a lot of time on the output site.

Another aspect in our required notion of efficiency is that we are interested in *fast* transfer of the excitation, thus requiring some form of benchmark time scale T_B . With the introduction of such a benchmark comes the possibility to formulate two potential definitions of efficiency (Scholak 2011). We refer to the first one as the *localisation efficiency*:

$$\mathcal{P}_H = \max_{t \in [0, T_R]} p_{\text{out}}(t). \tag{4.6}$$

The alternative can be denoted as the occupation efficiency:

$$\mathcal{P}_H = \frac{1}{T_B} \int_0^{T_B} p_{\text{out}}(t) \, \mathrm{d}t. \tag{4.7}$$

Most results in this thesis have been obtained by using a benchmark time T_B determined by the direct coupling between the input and output sites. We compare a system with an intermediate, complex network of sites to a systems consisting only of input and output, as shown in Fig. 4.2. It is straightforward to treat the benchmark system, since we must only consider the Hamiltonian

$$H_0 = \begin{pmatrix} H_{\text{in,in}} & H_{\text{in,out}} \\ H_{\text{out,in}} & H_{\text{out,out}} \end{pmatrix}. \tag{4.8}$$

We assume that there is time-reversal symmetry which implies that $H_{\text{in,out}} = H_{\text{out,in}}$, and a quick calculation teaches us that for H_0

$$p_{\text{out}}(t) = \frac{1}{4 + \frac{(H_{\text{in,in}} - H_{\text{out,out}})^2}{H_{\text{in,out}}^2}} \left| 1 - e^{-it\sqrt{(H_{\text{in,in}} - H_{\text{out,out}})^2 + 4H_{\text{in,out}}^2}} \right|^2. \tag{4.9}$$

It then follows that

$$p_{\text{out}}(t) \leqslant \frac{1}{1 + \frac{(H_{\text{in,in}} - H_{\text{out,out}})^2}{4H - \frac{2}{2}}},$$
 (4.10)

where the equability is obtained for

$$T_B := \frac{\pi}{\sqrt{(H_{\text{in,in}} - H_{\text{out,out}})^2 + 4H_{\text{in,out}}^2}},$$
 (4.11)

which we define as our *benchmark time*. The philosophy of this choice is that we wish to outperform the isolated input – output system by the addition of extra sites or by strongly coupling to additional degrees of freedom (Bohigas et al. 1993).

Whenever, by virtue of (4.10), $H_{\rm in,in} \neq H_{\rm out,out}$, the excitation cannot localise in the output site with probability 1. This is fundamentally impossible because unitary dynamics, generated by a time-independent Hamiltonian, conserves energy, in the sense that, for any state vector $|\phi(t)\rangle$, $\langle\phi(t), H\phi(t)\rangle = \langle\phi(0), H\phi(0)\rangle$. Unitary, reversible dynamics only allows us to reach states with the same energy expectation value as the initial state. For this reason, we choose to consider only systems where $H_{\rm in,in} = H_{\rm out,out} := E$ and we refer to $H_{\rm in,out} = H_{\rm out,in} := V$. With these choices, the final benchmark time scale reads

$$T_B = \frac{\pi}{2|V|}. (4.12)$$

4.3 Influence of Network Structures

In the previous sections we set the stage to investigate transport of a single excitation throughout a generic, network-like system. Of course, the actual structures of the networks are of crucial importance for the resulting transport properties. In general, there are several numerical results known for a quite wide range of network types, often in the context of (continuous-time) quantum walks (Mülken and Blumen 2011). We note, however, that this community strongly focusses attention to the graph-like topological structures of the networks—which means that sites all talk to each other in the same way or not at all—rather than on disorder in the coupling strengths. In the following sections, we briefly discuss some specific types of networks in order to emphasise how structure influences transport.

4.3.1 Regular Networks

Regular networks come in very different forms, what they have in common is that we know all couplings between the different nodes exactly. This allows the explicit

construction of the Hamiltonian H, which can than be diagonalised, at least given that the system is not too large. To gain deeper understanding, we focus on *analytically solvable* types of networks, characterised by a high degree of *symmetry*. In such structures we can find clear connections between spatial and spectral properties of the networks, and understand how these properties influence the transport.

A very common and fundamental structure in the literature on quantum transport is the *chain* of finite length N (Ashcroft and Mermin 1976; Haken 1976; Kittel 2005; Kittel and Fong 1987). In its most fundamental form, a chain is a 1D network of nodes that are connected to their nearest neighbours, and the adjacency matrix A (Biggs 1993) for the graph can be written as

$$A = \sum_{\substack{i,j=1\\|i-j|=1}}^{N} |e_i\rangle \langle e_j|, \qquad (4.13)$$

such that the bulk sites have two nearest neighbours, and the first and last site are only connected to a single neighbour. To convert this matrix to a Hamiltonian, one can simply multiply it with an overall energy scale v, such that

$$H = vA. (4.14)$$

It is easy to see that H is represented in the site basis as a specifically structured type of tridiagonal Toeplitz matrices (Barnett 1990), and therefore the structure of the eigenvalues $\{E_j\}$ and eigenvectors $\{|\eta_j\rangle\}$ of H is well-known:

$$E_j = 2v\cos\left(\frac{j\pi}{N+1}\right),\tag{4.15}$$

$$\langle e_k, \eta_j \rangle = \sqrt{\frac{2}{N+1}} \sin\left(\frac{jk\pi}{N+1}\right).$$
 (4.16)

Most remarkable is the structure of the eigenvectors, where we do not only see an oscillatory behaviour over the sites, given by $\sin\left(\frac{jk\pi}{N+1}\right)$, but also an overall factors

 $\sqrt{\frac{2}{N+1}}$. Since the sine factor is contained within [-1, 1], normalisation implies that none of the eigenvectors localise on a limited number of sites. To understand the dynamics in such as system we must calculate $p_{\text{out}}(t)$. Let us assume that we transport an excitation from one side of the chain to the other,

$$p_{\text{out}}(t) = \left| \left\langle e_N, e^{-itH} e_1 \right\rangle \right|^2 \tag{4.17}$$

$$= \sum_{j,k=1}^{N} e^{-it\omega_{kj}} \langle e_1, \eta_j \rangle \langle \eta_j, e_N \rangle \langle e_N, \eta_k \rangle \langle \eta_k, e_1 \rangle, \qquad (4.18)$$

$$=\frac{4}{(N+1)^2}\sum_{j,k=1}^N e^{-it\omega_{kj}}\sin\left(\frac{j\pi}{N+1}\right)\sin\left(\frac{jN\pi}{N+1}\right)\sin\left(\frac{k\pi}{N+1}\right)\sin\left(\frac{kN\pi}{N+1}\right)$$
(4.19)

where $\omega_{kj} = E_k - E_j$. As such, this expression does not allow further simplification, implying that it is difficult to obtain a straightforward understanding of \mathcal{P}_H for this system. However, it is interesting to consider \mathcal{P}_H , although in this case there is no obvious benchmark time scale, since (4.13), (4.14) directly imply that $\langle e_N, He_1 \rangle = 0$. For that reason, we rather choose to consider the asymptotic case where

$$\mathcal{P}_{H} = \lim_{T \to \infty} \frac{1}{T} \int_{0}^{T} p_{\text{out}}(t) dt$$
 (4.20)

$$= \frac{4}{(N+1)^2} \sum_{i=1}^{N} \left\{ \sin\left(\frac{j\pi}{N+1}\right) \right\}^4$$
 (4.21)

$$\leq \frac{4N}{(N+1)^2}. (4.22)$$

The scaling with N is rather pessimistic and indicates that long chains are actually unfit for efficient excitation transfer as quantified by \mathcal{P}_H . However, there might be specific moments in time where $p_{\text{out}}(t)$ is high. Rather than going into an in depth study, in Fig. 4.3 we simply show the behaviour of $p_{\text{out}}(t)$ as generated by Mathematica. Figure 4.3 clearly shows how the excitation quickly leaves the initial site and travels to the other side of the chain. We initially see alternating peaks at input and output site, and we can interpret this as a wave packet travelling back and forth several of times. Since the peaks decrease, it is also clear that the wave packet is becoming ever more delocalised. Ultimately this systematic behaviour breaks up and p(t) is dominated by fluctuations, as can be seen on the righthand side of Fig. 4.3.

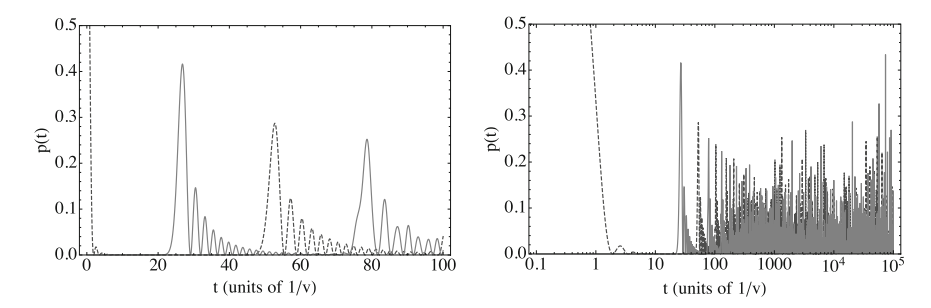


Fig. 4.3 $p_{\rm in}(t)$ (dashed) and $p_{\rm out}(t)$ (solid) as obtained for a chain Hamiltonian (4.13), (4.14) of N = 50 sites. The lefthand image focusses on the short time dynamics, whereas the righthand side shows a logarithmic depiction stretching towards the long time scales

Looking at the maximal occupations of the output site, we observe relatively high peaks (\sim 0.4), at least compared to the value for \mathcal{P}_H . On the other hand, even when monitoring long time scales, the excitation never fully localises on the output site as we may have hoped. In conclusion we can say that the chain does manage to transfer the excitation to the output site with a non-vanishing probability, but to achieve our goal of fast and efficient transfer this system is suboptimal.

Before we proceed to random networks, we treat yet another system, a chain bent to a *circle*. Remarkable for the circle is its extreme symmetry, especially because it is a completely translationally invariant structure. The Hamiltonian of such a circular network is very similar to that of a chain-like network, with the exception that we also connect the first and the last site, which implies that

$$A = |e_1\rangle \langle e_N| + |e_N\rangle \langle e_1| + \sum_{\substack{i,j=1\\|i-j|=1}}^{N} |e_i\rangle \langle e_j|, \qquad (4.23)$$

$$H = vA, (4.24)$$

where v again sets a typical energy scale. In this case, the Hamiltonian is translation invariant and therefore can be treated using discrete Fourier transformations (Davis 1979; Reed and Simon 1975). The resulting eigenvalues and eigenvectors are given by

$$E_j = 2v\cos\left(\frac{2\pi}{N}(j-1)\right),\tag{4.25}$$

$$\langle e_k, \eta_j \rangle = \frac{1}{\sqrt{N}} e^{-\frac{2\pi i}{N}(k-1)(j-1)}.$$
 (4.26)

We can again see that the eigenstates are fully delocalised over the whole network, but have a very different structure than those of the chain: The chain, having fixed boundary conditions, leads to a form of standing waves (4.16), whereas the circular system, with periodic boundary conditions, produces running waves. A more profound difference between both structures is hidden in the seemingly simple eigenvalues E_j ; the circular network gives rise to a multitude of two-fold degeneracies, since $E_k = E_{N-k+2}$. The calculation of $p_n(t)$ according to (4.4) results in²

$$p_{n}(t) = \sum_{k} |\langle e_{n}, \eta_{k} \rangle \langle \eta_{k}, e_{1} \rangle|^{2} + 2 \sum_{l}^{\lceil N/2 - 1 \rceil} \operatorname{Re}(\langle e_{1}, \eta_{l} \rangle \langle \eta_{l}, e_{n} \rangle \langle e_{n}, \eta_{N-l+2} \rangle \langle \eta_{N-l+2}, e_{1} \rangle)$$

$$+ \sum_{k,l,\omega_{k,l} \neq 0} \langle e_{1}, \eta_{l} \rangle \langle \eta_{l}, e_{n} \rangle \langle e_{n}, \eta_{k} \rangle \langle \eta_{k}, e_{1} \rangle e^{-it\omega_{k,l}}.$$

$$(4.27)$$

²We introduce the standard mathematics notation $\lceil . \rceil$ for rounding up and $\lfloor . \rfloor$ for rounding down. For example $\lceil 1.1 \rceil = 2$ and $\lceil 1.9 \rceil = 1$

The second term on the right hand side of (4.27) arises solely because of the degeneracies, which imply $\omega_{k,N-k+2} = 0$. Substituting this with the actual expression for the eigenvalues and eigenvectors, we obtain

$$p_{n}(t) = \frac{1}{N} + \frac{2}{N^{2}} \sum_{l=2}^{\lceil N/2 \rceil} \cos\left(\frac{2\pi}{N}(n-1)(N-2l+2)\right) + \frac{2}{N^{2}} \sum_{k>l,\omega_{k,l}\neq 0} \cos\left(\omega_{k,l}t - \frac{2\pi}{N}(n-1)(k-l)\right).$$
(4.28)

For this quantity, too, it is hard to get solid analytical insight in the maxima of $p_n(t)$. On the other hand, we can again compute \mathcal{P}_H for infinite time scales. We now obtain

$$\mathcal{P}_{H} = \frac{1}{N} + \frac{2}{N^{2}} \sum_{l=2}^{\lceil N/2 \rceil} \cos\left(\frac{2\pi}{N}(n-1)(N-2l+2)\right). \tag{4.29}$$

Something special happens for even N either when n=1 or when n=N/2+1; in both cases we find that $\cos\left(\frac{2\pi}{N}(n-1)(N-2l+2)\right)=1$. In other words, here we obtain that

$$\mathcal{P}_{H} = \lim_{T \to \infty} \frac{1}{T} \int_{0}^{T} p(t) = \frac{2}{N} \left(1 - \frac{1}{N} \right). \tag{4.30}$$

On the other hand, for all other values of n we rewrite

$$\sum_{l=2}^{\lceil N/2 \rceil} \cos \left(\frac{2\pi}{N} (n-1)(N-2l+2) \right) = \frac{1}{2} \left(\exp \left(-\frac{2\pi i}{N} (n-1)(N+2) \right) \sum_{l=2}^{\lceil N/2 \rceil} \left(\exp \left(\frac{4\pi i}{N} (n-1) \right) \right)^{l} + \exp \left(\frac{2\pi i}{N} (n-1)(N+2) \right) \sum_{l=2}^{\lceil N/2 \rceil} \left(\exp \left(-\frac{4\pi i}{N} (n-1) \right) \right)^{l} \right)$$
(4.31)

Now we use that $\sum_{i=0}^{n} a^i = \frac{1-a^{n+1}}{1-a}$, to ultimately find for $n \neq 1$ and $n \neq \lfloor \frac{N}{2} \rfloor + 1$:

$$\sum_{l=2}^{\lceil N/2 \rceil} \cos \left(\frac{2\pi}{N} (n-1)(N-2l+2) \right)$$

$$= \csc \left(\frac{2\pi(n-1)}{N} \right) \sin \left(\frac{2\pi(n-1)\left(\left\lceil \frac{N}{2} \right\rceil - 1 \right)}{N} \right) \cos \left(\frac{2\pi(n-1)\left\lfloor \frac{N}{2} \right\rfloor}{N} \right) = -1$$
(4.32)

and thus that

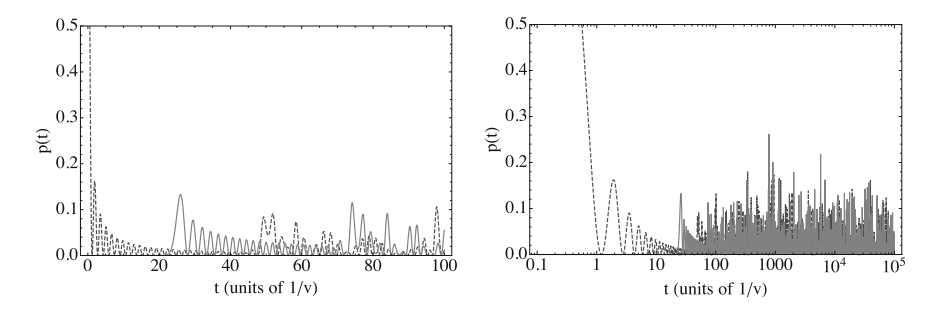


Fig. 4.4 $p_{\rm in}(t)$ (dashed) and $p_{\rm out}(t)$ (solid) as obtained for a circle Hamiltonian (4.23), (4.24) with N=98 sites, with the output site chosen to be the one with label n=50. The lefthand image focusses on the short time dynamics, whereas the righthand side shows the long-time dynamics on a logarithmic time scale

$$\mathcal{P}_H = \frac{1}{N} \left(1 - \frac{2}{N} \right). \tag{4.33}$$

Moreover, it can be seen that for large values of N,

$$\mathfrak{P}_H \approx \begin{cases} \frac{2}{N} & \text{if } n = 1 \text{ or } n = N/2 + 1, \\ \frac{1}{N} & \text{else.} \end{cases}$$
(4.34)

Just as for the the chain, we see that \mathfrak{P}_H decreases with increasing N. However, we observe an interesting interference effect, which is purely related to symmetry: One may interpret a circular system as two pathways connecting the input and output site. It now becomes clear that whenever these pathways have the same length, there is a constructive interference which enhances the time averaged occupation probability in the output site by a factor two. We notice that this process seems similar to coherent backscattering (Wolf and Maret 1985). However, the coherent enhancement now happens in the forward direction because the exploited symmetry is not time reversal, but a spatial symmetry that matches the length of the two pathways from site 1 to N/2+1.

A numerical assessment of $p_{out}(t)$, as depicted in Fig. 4.4, is specifically interesting to compare with the chain (see Fig. 4.3). We choose N=98 sites, to be able to interpret this as an input and output site connected by two chains rather than one. The figure clearly shows that the dynamics is initially very similar for chain and circle, in the sense that the first peak in $p_{out}(t)$ shoots up at exactly the same point in time for both structures. On the other hand, there are also clear differences, most profoundly in the height of these localisation peaks. We note that the dynamics on the circle is governed by fluctuations much earlier than on the chain. One can connect this to

³The factor two enhancement, as compared to the typical 1/N, obtained for n=1 is more closely related to coherent backscattering, since it is a manifestation of weak localisation.

the fact that the initial excitation splits into two wave packets, each moving along a different pathway.

The study of these two highly structured systems pinpoints several structural properties that are vital for quantum transport:

- Interference
- Symmetries
- Structure of the eigenstates

4.3.2 Random Networks

Although the highly symmetric and controlled structures in the previous discussion express many interesting features, they also have a problem: In reality, they are almost impossible to recreate, since ultimately one would have to control too many parameters. Realistic systems always manifest some degree of disorder and, for that reason, we now study the completely opposite limit of a completely random system, in the hope to gain additional insight.

Rather than focussing on a network structure, determined by an adjacency matrix, we just assume that all sites are coupled to one another and that each coupling is randomly sampled from a probability distribution. As a matter of fact, the relevant Hamiltonians were already discussed in detail in Sect. 3.3. We consider systems which are invariant under time-reversal and therefore yield GOE statistics. Assuming that the Hamiltonian is sampled in a site basis $\{e_1, \ldots, e_N\}$, we fix input and output sites as those that are coupled weakest in absolute value. In other words, in and out are those sites for which $|H_{ij}|$, with $i \neq j$, is minimal. We can now define $V = \min_{i \neq j} |H_{ij}|$, such that

$$T_B = \frac{\pi}{2V}. (4.35)$$

As both the eigenvectors and eigenvalues of H are stochastic objects, the only way to obtain significant insight in the transport properties is by doing statistics. Although the statistical origin forbids exact control of individual systems, its statistics as such is characterised by a surprisingly small amount of relevant parameters due to our choice of the GOE. We sample the couplings such that

$$H_{ij} \sim \text{Normal}\left(0, (1+\delta_{ij})\frac{\xi^2}{N}\right),$$
 (4.36)

which implies that the full statistics can be determined from ξ , which is half the radius of Wigner's semi-circle, and from N, the size of the system. This specific choice of variance makes sure that the width of the normalised density of states is independent of N at leading order.⁴ Although this is an interesting description,

⁴One retrieves the semicircle, but should incorporate finite size corrections for small *N*.

where the Hamiltonian of the systems remains bounded in the limit $N \to \infty$, the typical time scales in the system are determined by the mean-level spacing between consecutive energy levels, which is not independent of the system size. This also implies that the typical time scales of the dynamics depend on N.

A brief glance at p(t) for several random realisations of the Hamiltonian in Fig. 4.5 shows us that there is a similarity in the sense that each pattern is extremely unstructured to the eye. On the other hand, we do see that there is also diversity; the height of the peak in p(t) or the typical time scales tend to differ. One profound feature,

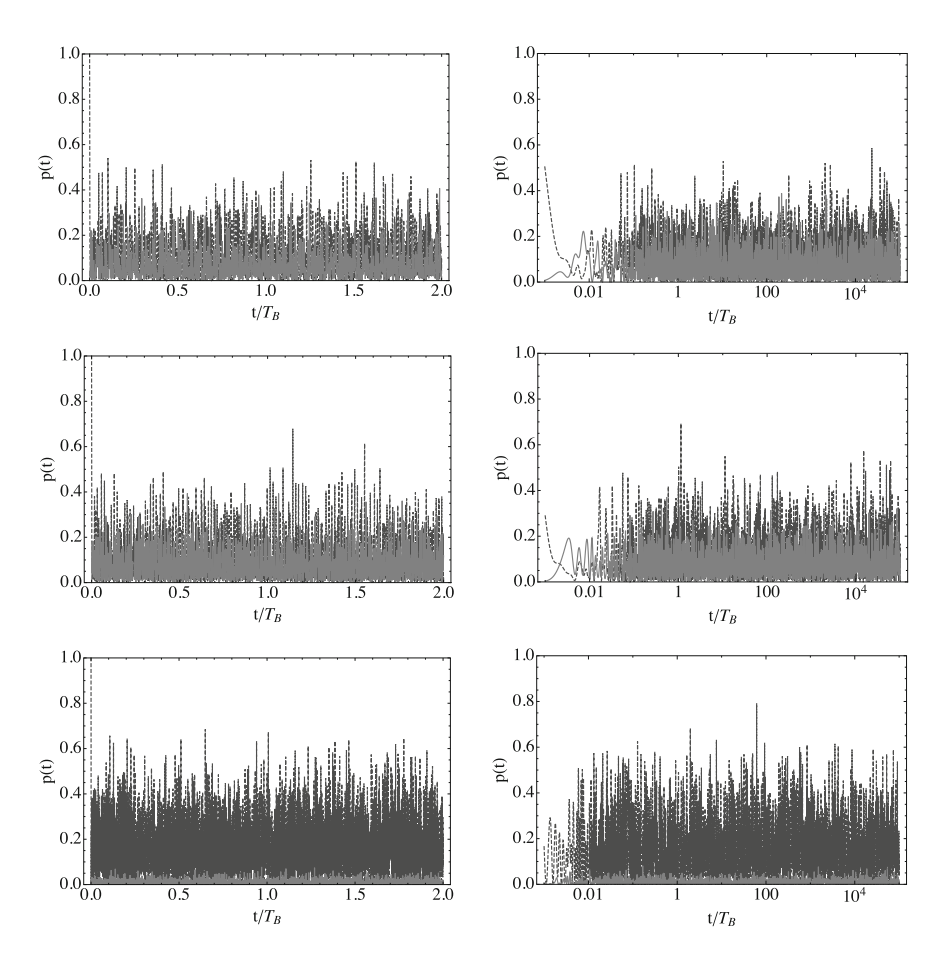


Fig. 4.5 $p_{\rm in}(t)$ (black, dashed) and $p_{\rm out}(t)$ (gray, solid) as obtained for three (from top to bottom) randomly sampled GOE Hamiltonians with N=20 sites and root-mean-squared (RMS) coupling between the sites $\sqrt{H_{ij}^2}=\xi/\sqrt{N}$, with $\xi=2$. The output sites are chosen to be those with weakest direct coupling in absolute value to the input site. The lefthand image focusses on the short time dynamics, whereas the righthand side shows the population dynamics on a logarithmic time scale

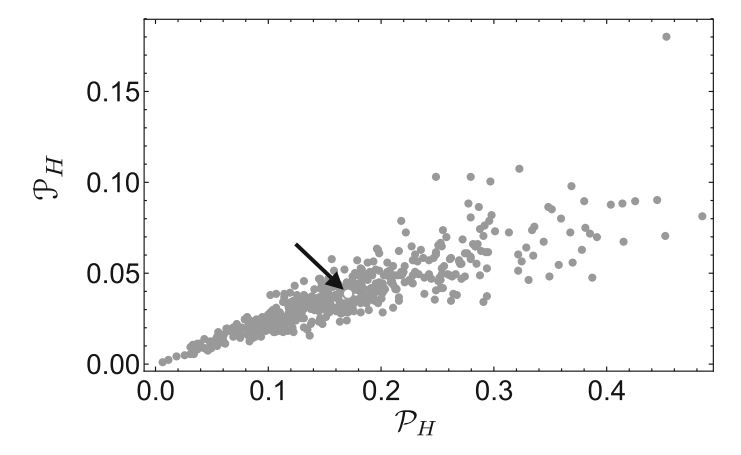


Fig. 4.6 Localisation efficiencies \mathcal{P}_H and occupation efficiencies \mathcal{P}_H as defined by (4.6), (4.7), respectively, for 500 realisations (grey dots) of random GOE Hamiltonians with RMS coupling ξ/\sqrt{N} between the sites, where $\xi=2$, and N=20 sites. The average value of \mathcal{P}_H and \mathcal{P}_H over all the realisations are represented by the white dot (indicated by an arrow)

noted in comparison to the regular networks, is the absence of a structured phase in the dynamics; the fluctuation-dominated regime commences immediately.

Although these randomly selected samples provide some intuitive insights in the dynamics, we cannot draw actual conclusions from it. A more appropriate way would be to do actual statistics. Here we will limit ourselves mainly to numerical results, obtained by generating many random Hamiltonians. The resulting data for \mathcal{P}_H and \mathcal{P}_H are depicted in Fig. 4.6. Interestingly, there is clearly a correlation between both quantities, but, on the other hand, from the 500 realisations of H considered, there are none that manifest remarkably good transport. The central point (marked by the arrow) has the mean values of \mathcal{P}_H and \mathcal{P}_H as coordinates and therefore indicates that random networks typically perform poorly.

On the matter of transfer efficiency the structured, regular networks of the last section generally perform slightly better than the random networks considered here. On the other hand, the random networks require far less control and are therefore also more reasonable candidates for realistic transfer devices. However, these random networks are not designed to perform a specific task, thus their poor performance is no surprise. The random networks are simply too simplistic and too generic to live up to the task. In the following section, we explore potential design principles that allow for as much disorder as possible, but still force the system to manifest near-optimal excitation transfer from input to output site.

4.4 Design Principles

For systems to manifest near optimal excitation transfer between two preselected sites, it appears important that the system is correctly designed, as was concluded in the previous section. In order for a system to be realistic, one must also allow for some degree of disorder. Therefore our goal is to develop minimalistic design principles that allow for efficient and *robust* transfer of the excitations in the system.

The simplest well-designed system to accomplish such task was already treated in Sect. 4.2: The two-level system. In our context, these systems are described by

$$H_0 = \begin{pmatrix} E & V \\ V & E + \Delta \end{pmatrix}. \tag{4.37}$$

The necessary and sufficient condition to achieve $\mathcal{P}_H = 1$ is $\Delta = 0$, i.e. the input and output site are in resonance. Indeed, a straightforward calculation shows that $p_{\text{out}}(t) = 1$ for $t = T_B = \pi/2V$. One can therefore say that this resonance condition is a *design principle*. However, our goal is to achieve near-optimal transfer of the excitation in a larger and more disordered system, on a faster time scale. Therefore, we strive to generalise this design principle.

4.4.1 Centrosymmetry

Obviously, we can simply consider the random networks given by GOE Hamiltonians, and impose the condition that $H_{\text{in,in}} = H_{\text{out,out}}$. Figure 4.7 shows us that such a naive implementation of the design principle is insufficient to achieve the desired transport properties, at most does it slightly enhance the probability to find good realisations when compared to Fig. 4.6, where input and output energies could also differ.

A second glimpse at H_0 (4.37) shows us that the matrix as such is highly symmetric and when the regular networks of Sect. 4.3 were studied, it became apparent that symmetries can have profound influence on the dynamics. The most obvious symmetry present in the two-site network (essentially an effective model for the double-well potential), is a reflection symmetry.

Such reflection symmetries have been studied rather extensively in the literature on "perfect state transfer" (Christandl et al. 2004, 2005; Kay 2006). In these works one typically optimises a quantity which in our notation would read

$$f(t) = |\langle \text{out}, \phi(t) \rangle|, \tag{4.38}$$

where $|\phi(t)\rangle$ is the state vector of the system at time t. Perfect state transfer implies the existence of a time $t_0 \in (0, \infty)$ such that $f(t_0) = 1$. It now follows from the Schrödinger equation (2.58), and $f(t_0) = 1$, that

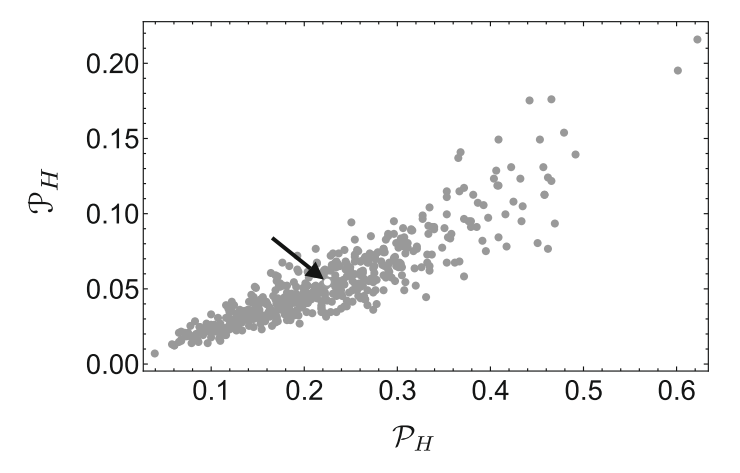


Fig. 4.7 Localisation efficiencies \mathcal{P}_H and occupation efficiencies \mathcal{P}_H as defined by (4.6), (4.7), respectively, for 500 realisations (grey dots) of random GOE Hamiltonians, where $H_{\text{in,in}} = H_{\text{out,out}}$ was imposed as design principle. Parameters were chosen to be $\xi = 2$ and N = 20. The average value of \mathcal{P}_H and \mathcal{P}_H over all the realisations is represented by the white dot (indicated by an arrow)

$$|\phi(t_0)\rangle = e^{-it_0H} |\text{in}\rangle = e^{i\theta} |\text{out}\rangle,$$
 (4.39)

for some phase θ . As stressed in Christandl et al. (2005), the condition of reflection symmetry, which ultimately states that the network looks exactly the same from the perspective of the input site and the output site, implies that the dynamics must be periodic to allow for perfect state transfer.⁵ Indeed, the symmetry implies that

$$e^{-i2t_0H} |\text{in}\rangle = e^{-it_0H} e^{i\theta} |\text{out}\rangle = e^{2i\theta} |\text{in}\rangle,$$
 (4.40)

where the last equality holds because the system (and thus its Hamiltonian) looks identical when going from output to input compared to going vice versa.⁶ This directly leads to

$$\left| \langle \text{in}, e^{-i2t_0 H} \text{in} \rangle \right| = 1 \tag{4.41}$$

and therefore the period of the state transfer is $2t_0$. Since it must hold that

$$\sum_{j} \langle \eta_{j}, \operatorname{in} \rangle e^{-i2t_{0}E_{j}} | \eta_{j} \rangle = e^{2i\theta} \sum_{j} \langle \eta_{j}, \operatorname{in} \rangle | \eta_{j} \rangle, \tag{4.42}$$

⁵The quantum recurrence theorem (Bocchieri and Loinger 1957) implies that for any state vector $\psi \in \mathcal{H}$, any one-parameter group $\{U_t \mid t \in \mathbb{R}\}$ and any $\epsilon > 0$, there is a time $t_0 > 0$ such that $\|(\mathbb{1} - U_{t_0}) \mid \psi \rangle\| < \epsilon$. However, note that this does *not* imply periodicity.

⁶Using the exchange operator which is later defined in (4.46), we can make this reasoning more rigorous by noting that $e^{-it_0H}e^{i\theta}$ |out $\rangle = e^{-it_0H}e^{i\theta}J$ |in $\rangle = Je^{-it_0H}e^{i\theta}$ |in $\rangle = e^{2i\theta}J$ |out $\rangle = e^{2i\theta}J$ |in \rangle .

for any possible choice of input state, one must impose conditions on the eigenvalues and finds

$$2E_{i}t_{0} - 2\theta = 2k_{i}\pi \tag{4.43}$$

where k_j is an integer. Such equation is obtained for every index j, allowing to eliminate θ from the set of equations, which results in

$$(E_i - E_i)t_0 = \pi(k_i - k_i). \tag{4.44}$$

The last step consists of eliminating t_0 from the equations, which sets the condition

$$\frac{E_i - E_j}{E_{i'} - E_{j'}} \in \mathbb{Q}, \quad \text{for all } i \neq j \text{ and } i' \neq j'. \tag{4.45}$$

In summary, any network-like system with a reflection symmetry and spectral properties fulfilling constraint (4.45) manifests perfect state transfer for some time scale t_0 .

Notice however, that the result does not make any mention of what this time scale t_0 is. The works (Christandl et al. 2004, 2005; Kay 2006) typically focus on several more specific systems for which these time scales can be calculated, but in principle speed is not a primary goal. Moreover, one can immediately see that the condition (4.45) is extremely restrictive, in the sense that it does not only demand perfect control over the symmetry in the system, but it also requires *fine-tuning of all level spacings*.

Although these results are crucial landmarks on the road towards fast and efficient excitation transfer, they require too much control. Moreover, the demand that there is good transfer from any input state to its symmetric counterpart is much stronger than our demand to achieve transport between two well-chosen sites.

Nevertheless, numerical studies conducted in Freiburg (Zech 2013; Zech et al. 2014) have clearly shown that also in random networks, where the constituents couple via dipole-dipole coupling, one can clearly see a correlation between the tendency towards centrosymmetry (Cantoni and Butler 1976) (a form of reflection symmetry, explicitly visible in the Hamiltonian structure) and fast and efficient excitation transfer.

Motivated by these results, we also impose centrosymmetry as a first design principle for our systems. Formally, this implies that the Hamiltonians which describe the networks under consideration, commute with the exchange operator J,

$$[H, J] = 0$$
, with $J_{i,j} = \delta_{i,N-j+1}$ (represented in the site basis). (4.46)

This demand significantly influences the structure of the Hamiltonians, since it imposes that $H_{ij} = H_{iN-j+1} = H_{N-i+1j} = H_{N-i+1N-j+1j}$. However, inspired by the literature (Christandl et al. 2004, 2005; Kay 2006), we also demand that this symmetry connects the input site to the output site, which implies

$$J|\text{in}\rangle = |\text{out}\rangle. \tag{4.47}$$

This symmetry constraint on the input and output state vector implies that the choice of input site automatically fixes the output site. More specifically, for any choice $|\text{in}\rangle = |e_i\rangle$, it must hold that $|\text{out}\rangle = |e_{N-i+1}\rangle$. The input and output site must therefore be selected respecting this constraint. Additionally, we require them to be the sites which couple weakest and therefore consider

$$V = \min_{i} |H_{i N - i + 1}| \tag{4.48}$$

defining the input site as the one for which the minimum is achieved.

Note that centrosymmetry implies that $H_{\text{in,in}} = H_{\text{out,out}}$ and thus centrosymmetry is compatible with the constraint imposed by the conservation of energy. Considering the structure of the Hamiltonian, centrosymmetry is a reasonably strong demand. Still, it allows for a considerable amount of disorder in the system.

To genuinely understand the way in which the presence of centrosymmetry influences the system, we again have to consider its impact on $p_{\text{out}}(t)$. To reach such an understanding, we first dig deeper into the implications of this symmetry on the Hamiltonian. In what follows, we consider an *even* number of sites N in the network, which simplifies notation considerably.

The only constraints resting upon H are that it is a real, symmetric and centrosymmetric matrix. To understand how the centrosymmetry affects the dynamics, the spectral properties of the Hamiltonian can be studied. All influence of the centrosymmetry on the Hamiltonian is contained within the demand that [H, J] = 0. Whenever two operators commute, one can find a mutual set of eigenvectors, but one must take degeneracies into account. The structure of J is remarkably simple and therefore we can easily derive its eigenvalues. There are only two possible eigenvalues: +1 and -1, 7 which is obvious because J is a representation of the group \mathbb{Z}_2 and therefore $J^2 = \mathbb{1}$. Because we limit ourselves to even N, we find that both eigenvalues have multiplicity N/2, implying that the N dimensional Hilbert space \mathcal{H} , in which the problem is described, falls apart into two N/2-dimensional eigen-subspaces of J, \mathcal{H}^+ and \mathcal{H}^- .

Let us start by providing a very simple recipe for the construction of \mathcal{H}^+ and \mathcal{H}^- . When we choose any vector $|\phi\rangle \in \mathcal{H}$, we can simply construct two states

$$\left|\phi^{\pm}\right\rangle := \frac{1}{\sqrt{2}} \left(\left|\phi\right\rangle \pm J\left|\phi\right\rangle\right).$$
 (4.49)

When we now apply J to these states, we directly obtain that

$$J \left| \phi^{\pm} \right\rangle = \frac{1}{\sqrt{2}} \left(J \left| \phi \right\rangle \pm \left| \phi \right\rangle \right) = \pm \left| \phi^{\pm} \right\rangle. \tag{4.50}$$

⁷Which fixes a state's *parity*.

Therefore, we obtain that

$$\mathcal{H}^{+} = \operatorname{span} \left\{ \left| \phi^{+} \right\rangle \mid \phi \in \mathcal{H} \right\}, \tag{4.51}$$

$$\mathcal{H}^{-} = \operatorname{span} \left\{ |\phi^{-}\rangle \mid \phi \in \mathcal{H} \right\}. \tag{4.52}$$

A specific consequence of $|\mathrm{in}\rangle = J |\mathrm{out}\rangle$ is that this demand naturally defines two states

$$|\pm\rangle := \frac{1}{\sqrt{2}} (|\text{in}\rangle \pm |\text{out}\rangle),$$
 (4.53)

where, clearly, $|\pm\rangle \in \mathcal{H}^{\pm}$.

We divert attention to the spectral properties of the Hamiltonian, as dictated by [H, J] = 0, and write that

$$JH \left| \phi^{\pm} \right\rangle = HJ \left| \phi^{\pm} \right\rangle = \pm H \left| \phi^{\pm} \right\rangle, \tag{4.54}$$

thus H preserves the blocked structure of the Hilbert space \mathcal{H} in the sense that

$$|\psi\rangle \in \mathcal{H}^{\pm} \implies H |\psi\rangle \in \mathcal{H}^{\pm}.$$
 (4.55)

This property implies that in the basis where the decomposition $\mathcal{H}=\mathcal{H}^+\oplus\mathcal{H}^-$ is explicit, hence in any possible eigenbasis representation of J, the Hamiltonian H has a block-diagonal structure

$$H = \begin{pmatrix} H^+ & 0\\ 0 & H^- \end{pmatrix},\tag{4.56}$$

such that $H^+ \in \mathcal{B}(\mathcal{H}^+)$ and $H^- \in \mathcal{B}(\mathcal{H}^-)$, implying they are both $N/2 \times N/2$ matrices. This also has consequences for the spectral properties of the system: The structure is transferred to the eigenvectors such that any eigenvector $|\eta_j\rangle$ of H is an eigenvector of J and therefore

$$J | \eta_j \rangle = \pm | \eta_j \rangle. \tag{4.57}$$

An interesting corollary of this property and (4.47) is that

$$\langle \text{in}, \eta_j \rangle \langle \eta_j, \text{out} \rangle = \langle \text{in}, \eta_j \rangle \langle J \eta_j, \text{in} \rangle = \pm |\langle \eta_j, \text{in} \rangle|^2.$$
 (4.58)

With this result, and explicitly denoting E_j^{\pm} and $\left|\eta_j^{\pm}\right|$ as the eigenvalues and associated eigenvectors of the Hamiltonian blocks H^{\pm} , we can write

$$p_{\text{out}}(t) = \left| \sum_{j=1}^{N/2} e^{-itE_i^+} \left| \left\langle \eta_j^+, \text{in} \right\rangle \right|^2 - \sum_{j=1}^{N/2} e^{-itE_i^-} \left| \left\langle \eta_j^-, \text{in} \right\rangle \right|^2 \right|^2.$$
 (4.59)

It is possible to alternatively use (4.53) and (4.57) to obtain $\left\langle \eta_j^{\mp}, \pm \right\rangle = 0$, and rewrite that

$$p_{\text{out}}(t) = \frac{1}{4} \left| \sum_{j=1}^{N/2} e^{-itE_i^+} \left| \left\langle \eta_j^+, + \right\rangle \right|^2 - \sum_{j=1}^{N/2} e^{-itE_i^-} \left| \left\langle \eta_j^-, - \right\rangle \right|^2 \right|^2, \tag{4.60}$$

such that the first term is fully determined by the H^+ block and the second term fully by the H^- block in (4.56). The most profound influence of the centrosymmetry is that it directly implies that one should only focus on a single component of each eigenvector, rather than the product of two of them. Indeed, considering $|\langle \eta_j, \text{in} \rangle|^2$ rather than a generic overlap $\langle \text{in}, \eta_j \rangle \langle \eta_j, \text{out} \rangle$ is a huge simplification. Nevertheless, a glance at Eqs. (4.59) and (4.60) makes clear that these are still long coherent sums of many oscillating terms, which are generically hard to handle.

Our study of centrosymmetry up to now neglected the fact that H is assumed to be a random GOE Hamiltonian, controlled by some additional constraints. The most natural way to impose this randomness under the centrosymmetry constraint (4.46) is by immediate use of the eigenbasis of J together with the demand that H^+ and H^- be each GOE matrices. This implies that centrosymmetry also offers a huge technical advantage, in the sense that both terms in Eq. (4.60) are statistically independent.

It is natural to wonder how centrosymmetry influences \mathcal{P}_H and \mathcal{P}_H , which is shown in Fig. 4.8. It can be seen that the realisations are spread over a wide range of \mathcal{P}_H and \mathcal{P}_H values, and still clearly show a correlation between the two quantities. We observe that even on average there is a clear enhancement in the transfer efficiency measures compared to the fully random networks. More specifically, comparison to Figs. 4.6 and 4.7 suggests an average enhancement of roughly a factor two.

From weak localisation, we know that even in weakly disordered systems there is an enhancement of the return probability to the initial state which survives the disorder average (Akkermans 2011). The effect of the centrosymmetry, as stressed in the previous paragraphs, is exactly to connect transfer from in to out to the return probability to the initial input state. This relation is made explicit by Eq. (4.58). Even though there is a parallel between $p_{\rm in}(t)$ and $p_{\rm out}(t)$, the presence of the minus sign for half of the terms in Eq. (4.59) imposes a difference. Nevertheless, going to the other extreme regime of asymptotically long time scales, we may calculate

$$H_{ij} \sim \begin{cases} \text{Normal}\left(0, \frac{2\xi^2}{N}\right) & \text{if } i = j, \text{ or } i = N - j + 1, \\ \text{Normal}\left(0, \frac{\xi^2}{N}\right) & \text{else,} \end{cases}$$
(4.61)

while explicitly fixing $H_{ij} = H_{iN-j+1} = H_{N-i+1j} = H_{N-i+1N-j+1j}$.

⁸This is equivalent to sampling the Hamiltonian in the site basis, with

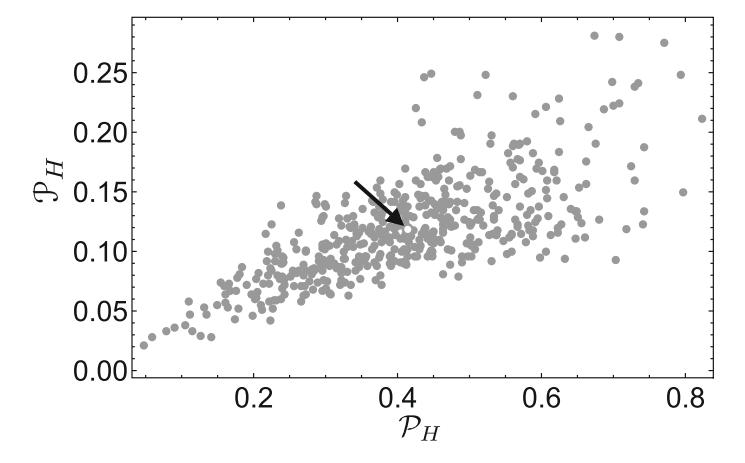


Fig. 4.8 Localisation efficiencies \mathcal{P}_H and occupation efficiencies \mathcal{P}_H as defined by (4.6), (4.7), respectively, for 500 realisations (grey dots) of random GOE Hamiltonians with centrosymmetry (4.46) imposed on them. RMS coupling ξ/\sqrt{N} between the intermediate sites, with $\xi=2$, and N=20 sites. The average values of \mathcal{P}_H and \mathcal{P}_H over all the realisations is again represented by the white dot (indicated by an arrow). A clear enhancement compared to Figs. 4.6 and 4.7 is evident

$$\lim_{T \to \infty} \frac{1}{T} \int_0^T dt \ p_{\text{out}}(t) = \sum_{j=1}^N \left| \left\langle \text{out}, \eta_j \right\rangle \left\langle \eta_j, \text{in} \right\rangle \right|^2$$
 (4.62)

$$= \sum_{j=1}^{N} \left| \left\langle \eta_{j}, \text{in} \right\rangle \right|^{4} \tag{4.63}$$

$$= \lim_{T \to \infty} \frac{1}{T} \int_0^T dt \ p_{\text{in}}(t). \tag{4.64}$$

This unambiguously shows that centrosymmetry makes sure that the input and output site occupation are the same, when fluctuations in time are averaged out and the considered time scales are sufficiently long. *This statement is in general false in the absence of centrosymmetry*. Using that the ensemble is a GOE, one can even evaluate the disorder average occupation using the results in Haake and Życzkowski (1990)

$$\left\langle \lim_{T \to \infty} \frac{1}{T} \int_0^T dt \ p_{\text{out}}(t) \right\rangle_{\text{realisations}} = \frac{3}{2+N}. \tag{4.65}$$

This also implies an interesting interpretation of $\sum_{j=1}^{N} |\langle \eta_j, \text{in} \rangle|^4$ in (4.63), which is closely related to the *inverse participation ratio* (Haake 2010): The inverse of $\sum_{j=1}^{N} |\langle \eta_j, \text{in} \rangle|^4$ counts how many eigenvectors are on average contributing to the transport. On average (see (4.65)) it is clear that even in the centrosymmetric case, there are still at least N/3 eigenvectors that actively contribute to the transport. They can typically give rise to large fluctuations, both on shorter and longer time

scales, which may be beneficial for transport. On the other hand, they forbid us from controlling \mathcal{P}_H in a satisfactory way.

In summary, the centrosymmetry is certainly a beneficial ingredient to enforce fast and efficient transfer, but on its own it is insufficient. Therefore we must include a second *design principle* as final constituent of our theory.

4.4.2 The Dominant Doublet

As emphasised in previous sections, the long-time dynamics is typically dominated by the structure of the eigenvectors of the Hamiltonian. On shorter time scales, interference effects which are driven by the structure of the energy eigenvalues can have profound effects. However, we have seen that these are extremely hard to control. In the works of Christandl et al. (2004, 2005), Kay (2006), one requires a perfect tuning of all level spacings, which in disordered systems is unrealistic and certainly not a robust solution. From Eqs. (4.59) and (4.60) it becomes apparent that there are still a total of N terms that need to be considered. Even though the centrosymmetry drastically influences the structure of the eigenvectors of the Hamiltonian, a stronger demand is required to achieve near-optimal excitation transfer.

Inspiration for this additional design principle can be obtained from many fronts, a profound one being optimised realisations. In earlier work (Manzano 2013; Scholak 2011; Scholak et al. 2010, 2011a, b, c, 2014; Zech 2013; Zech et al. 2013, 2014) there was extensive study of networks of coupled dipoles, which were randomly positioned and oriented. The quantum dynamics that manifests in such a system is governed by a Hamiltonian of the form

$$H = E \sum_{i=1}^{N} |e_i\rangle \langle e_i| + \sum_{i\neq i}^{N} V_{i,j} |e_i\rangle \langle e_j|, \qquad (4.66)$$

where i and j label dipoles, which now form the sites of our network. The actual dipolar behaviour is encrypted in $V_{i,j}$, which are dependent on both the positions and orientations of the dipoles. The exact expression for this coupling is given by

$$V_{i,j} = \frac{1}{\|\vec{r}_i - \vec{r}_j\|^3} \frac{\vec{\alpha}_i \cdot \vec{\alpha}_j - 3\vec{\alpha}_i \cdot (\vec{r}_i - \vec{r}_j)\vec{\alpha}_j \cdot (\vec{r}_i - \vec{r}_j)}{\|\vec{r}_i - \vec{r}_j\|^2},$$
 (4.67)

where \vec{r}_i is the position of the *i*th dipole and $\vec{\alpha}_i$ is its dipole moment. The strategy of Scholak et al. (2010, 2011a, b, c), Scholak (2011) consists in placing the input and output site on the north- and south pole of a sphere, respectively, with the additional dipoles placed randomly inside that sphere. These initial random configurations are then used as seeds in a *genetic algorithm* to optimise the positions and orientations to obtain $\mathcal{P}_H \approx 1$ (using a benchmark time $T_B = 0.1\pi/2 |V|$). One hardly learns anything significant from the spatial structures of such systems, the true interest lies

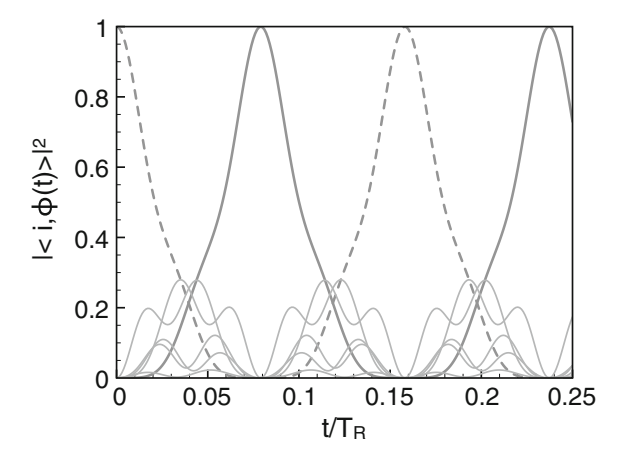


Fig. 4.9 Population dynamics of a near-to-optimal network conformation of coupled dipoles, from Scholak et al. (2011a). Mainly input (dashed) and output (solid) sites are populated during the dynamics, contrary to the bulk sites (thin, grey), which exhibit weak populations never larger than approximately 30%. Exactly this feature lies at the fundament of the dominant doublet design principle

in the structure of the dynamics of the excitations, as can be seen in Fig. 4.9, which is taken from Scholak et al. (2011a).

Note the analogy with optimal (quantum) control theory (Krotov 1993; Shapiro and Brumer 2003; Wiseman and Milburn 2010), where one drives systems with carefully optimised pulse shapes to perform a given task. One typically does not gain any insight from studying the pulse shape alone (Kuprov 2013); it is only when one studies it's influence on the system, that the properties of the pulse shape become clear (Kuprov 2013). In our context, it is also only from combining the dynamics of excitations with the optimised Hamiltonians, that we can ultimately identity the final, useful design principle.

Studying Fig. 4.9, we observe the tendency towards centrosymmetry, which, together with the condition of near-perfect state transfer, induces a symmetry on the time axis. More striking, however, is that the excitation mainly dwells on the input and output sites and only weakly spreads over the intermediate (bulk) sites. This behaviour is to be expected from a system which is essentially a two-level system. The fact, however, that we observe both, a much higher speed of transport, and a small, though appreciable population of the intermediate sites, does imply that

⁹This symmetric behaviour on the time axis is quantified by $|\langle e_i, e^{-itH} \text{in} \rangle|^2 = |\langle e_i, e^{-itH} J^2 \text{in} \rangle|^2 = |\langle J e_i, e^{-itH} \text{out} \rangle|^2 \approx |\langle J e_i, e^{-i(t+t_0)H} \text{in} \rangle|^2$, where we explicitly use that there is a time t_0 for which $e^{-it_0H} |\text{in} \rangle \approx e^{i\theta} |\text{out} \rangle$. Moreover, an additional symmetry around $t_0/2$ is implied, which follows from $|\langle \text{out}, e^{-itH} \text{in} \rangle|^2 \approx |\langle e^{-it_0H} \text{in}, e^{-itH} \text{in} \rangle|^2 = |\langle e^{-i(t_0-t)H} \text{in}, \text{in} \rangle|^2 = |\langle \text{in}, e^{-i(t_0-t)H} \text{in} \rangle|^2$.

¹⁰Or, rather, the paradigmatic double-well potential.

the system is not merely a two-level system, but rather one which is considerably perturbed by coupling to additional degrees of freedom.

Using a mathematical line of argument, the perturbed two-level system implies that the relevant transfer probability $p_{\text{out}}(t)$, as given by Eq. (4.59) or (4.60), is dominated by a small number of terms. Furthermore, there must be two dominating energy eigenvectors $|\eta^+\rangle$ and $|\eta^-\rangle$ which are baptised the *dominant doublet*. If we consider the isolated two-level system, i.e. do zeroth order perturbation theory, we obtain a system where $|\text{in}\rangle$ and $|\text{out}\rangle$ are interacting with one another, whereas the bulk of intermediate sites only couple to each other and not with the input and output sites. The relevant transport in the pure two-level system was already discussed in Sect. 4.2 and we know that $|+\rangle$ and $|-\rangle$ are exactly these relevant energy eigenvectors, with E+V and E-V as respectively associated energy levels.

When we proceed to higher orders in perturbation theory, and assume the system is perturbed such that Eq. (4.60) is dominated by two terms, we obtain the demand that there be *actual eigenvectors* of the system, i.e. the dominant doublet $|\eta^{\pm}\rangle$, which obey the condition

$$\left|\left\langle \eta^{\pm},\pm\right\rangle \right|^{2}\approx1.$$
 (4.68)

The energy levels associated with $|\eta^{\pm}\rangle$ are denoted E^{\pm} . From the assumption that such dominant eigenstates exist, we can estimate the dynamics by simply ignoring all other contributions in Eq. (4.60), and find

$$p_{\text{out}}(t) \approx \frac{1}{4} \left| \left| \left| \left| \eta^+, + \right| \right|^2 e^{-itE^+} - \left| \left| \eta^-, - \right| \right|^2 e^{-itE^-} \right|^2.$$
 (4.69)

Both, the time scales, governed by the energy eigenvalues E^{\pm} , and the weights $|\langle \eta^{\pm}, \pm \rangle|^2$, are strictly different from those described earlier for the two-level system (4.9). However, from Eq. (4.68) it is clear that the weights cannot vary strongly. This constraint can be formalised in various manners: One may demand that

$$\left|\left\langle \eta^{\pm}, \pm \right\rangle\right|^2 \geqslant \alpha \approx 1,$$
 (4.70)

for *all* realisations of the random system, under the assumption that α is controlled. Because here we have an additional constraint imposed on spectral properties, which can only be verified after construction of the Hamiltonian, we refer to Eq. (4.70) as the *post-selected dominant doublet*. Alternatively, one can design the Hamiltonian appropriately, such that

$$\langle \left| \left\langle \eta^{\pm}, \pm \right\rangle \right|^2 \rangle_{\text{realisations}} = \alpha' \approx 1,$$
 (4.71)

which, for obvious reasons, carries the name averaged dominant doublet.

Both Eqs. (4.70) and (4.71) are variations of the *dominant doublet design principle* and one can clearly feel that the essential physics is the same. However, the strong

requirement imposed by Eq. (4.70) offers the benefit that we can formally construct a lower bound for \mathcal{P}_H by exploiting the accurate estimate (4.69),

$$\mathcal{P}_{H} \geqslant \frac{2\alpha - 1}{4} \max_{t \in [0, T_{B})} \left| 1 - e^{-it(E^{-} - E^{+})} \right|^{2} = \frac{2\alpha - 1}{2} \max_{t \in [0, T_{B})} \left(1 - \cos\left(t(E^{-} - E^{+})\right)\right). \tag{4.72}$$

Impressively, this bound must hold for all realisations and therefore we can find a condition for near-optimal excitation transfer. Indeed, whenever

$$t^* = \frac{\pi}{|E^- - E^+|} \leqslant T_B,\tag{4.73}$$

Equation (4.72) automatically implies that

$$\mathcal{P}_H \geqslant 2\alpha - 1 \approx 1. \tag{4.74}$$

More generally, we can refer to t^* as the *first passage time*¹¹: The dynamics in a perturbed two-level system will be quasi-periodic (exactly the feature which we used to arrive at the dominant doublet design principle), and the period at which the dominant oscillatory behaviour is observed is given by t^* . Therefore, the excitation strongly localises on the output site for all time which are integer multiples of t^* , hence the first of this series of localisations is t^* itself.

With the alternative dominant doublet design principle as specified by Eq. (4.71), one may use a rather handwaving argumentation, replacing $\left|\left\langle \eta^{\pm},\pm\right\rangle \right|^2$ by its expectation value over all realisations, which is usually called an *annealed approximation* (Derrida and Pomeau 1986; Seung et al. 1992), to state that one expects

$$\mathcal{P}_{H} \approx \frac{\alpha'^{2}}{4} \max_{t \in [0, T_{B})} \left| 1 - e^{-it(E^{-} - E^{+})} \right|^{2} = \frac{\alpha'^{2}}{2} \max_{t \in [0, T_{B})} \left(1 - \cos\left(t(E^{-} - E^{+})\right)\right). \tag{4.75}$$

Since also $\alpha'^2 \approx 1$, the same logic as for the design principle Eq. (4.70) holds. However, as concerns their statistical treatment, the two options (4.70) and (4.71) differ strongly. If one can replace $|\langle \eta^\pm, \pm \rangle|^2$ by their expectation values, the statistical treatment (see Sect. 4.5) is by far the easiest. From an engineering perspective, one might also argue that controlling properties (4.71) of the ensemble of random Hamiltonians is potentially more feasible than imposing a hard constraint (4.70) on eigenvector properties.

The dominant doublet assumptions formulated in Eqs. (4.70) and (4.71) also allow us to gain insight in \mathcal{P}_H , since the constraint essentially allows for a serious simplification of the expression (4.60) for $p_{\text{out}}(t)$. Indeed, we find that

¹¹Throughout the remainder of this chapter, the terms "first passage time" and "transfer time" are therefore used interchangeably.

$$p_{\text{out}}(t) \geqslant \frac{2\alpha - 1}{2} \left(1 - \cos\left(t(E^{-} - E^{+})\right) \right)$$
 (post-selected doublet), (4.76)

$$p_{\text{out}}(t) \approx \frac{\alpha'^2}{2} \left(1 - \cos\left(t(E^- - E^+)\right) \right)$$
 (averaged doublet), (4.77)

which can now be used to calculate \mathcal{P}_H . After integration we obtain that

$$\mathcal{P}_H \geqslant \frac{2\alpha - 1}{2} \left(1 - \operatorname{sinc} \left(T_B(E^- - E^+) \right) \right) \quad \text{(post-selected doublet)}, \quad (4.78)$$

$$\mathcal{P}_H \approx \frac{{\alpha'}^2}{2} \left(1 - \text{sinc} \left(T_B (E^- - E^+) \right) \right)$$
 (averaged doublet). (4.79)

The relevant parameter in this case is given by $T_B(E^--E^+)$. Using graphical methods in combination with Newton-Raphson (Hildebrand 1987), we obtain the estimate that \mathcal{P}_H reaches it's maximal value (≈ 0.608617) for $T_B(E^--E^+) \approx 4.49341$. Therefore, choosing $T_B = \pi/2V$, optimal transfer, with respect to the efficiency measure \mathcal{P}_H , is achieved when

$$|E^- - E^+| \approx 2.86059V.$$
 (4.80)

Notice that the coupling between the input and output site V (4.48) is a *stochastic* quantity, and, as we will show in Eq. (4.130), this implies a dependence on the number of sites N and on the spectral radius. However, if one controls V, the condition for an optimal occupation efficiency \mathcal{P}_H is fixed. For $|E^- - E^+| \gg 2V$ the value for \mathcal{P}_H saturates around 0.5, which is also obtained for the isolated input—output system, i.e. the system with all intermediate sites removed. Because $|E^- - E^+|/2V = T_B/t^*$, this result actually implies that a *high localisation efficiency* \mathcal{P}_H , due to a short first-passage time t^* , automatically implies an occupation efficiency close to that of the two-level system. Because the focus of this chapter is fast and efficient transport, we from now on pursue the objective $\mathcal{P}_H \approx 1$ and $t^* \ll T_B$, as it will automatically guarantee a high (though not optimal) occupation efficiency $\mathcal{P}_H \approx 0.5$.

To gain insight in the dominant doublet and its structure, we can use perturbation theory on both the energy levels and eigenvectors. In order to do so, it is convenient to start from the structure of Eq. (4.56). Since we showed that $|\pm\rangle \in \mathcal{H}^{\pm}$, we can explicitly write out the rows and columns related to these vectors:

$$H = \begin{pmatrix} E + V \langle \mathcal{V}^{+} | \\ | \mathcal{V}^{+} \rangle & H_{sub}^{+} \\ & E - V \langle \mathcal{V}^{-} | \\ & | \mathcal{V}^{-} \rangle & H_{sub}^{-} \end{pmatrix}, \tag{4.81}$$

where $|\mathcal{V}^{\pm}\rangle$ describes how $|\pm\rangle$ are coupled to the bulk sites, which in turn have their internal interactions grasped by H^{\pm}_{sub} . Standard application of perturbation theory leads to

$$1 - \left| \left\langle \tilde{\pm}, \pm \right\rangle \right|^2 \approx \sum_{i=1}^{N/2-1} \frac{\left| \left\langle \mathcal{V}^{\pm}, \psi_i^{\pm} \right\rangle \right|^2}{(E \pm V - e_i^{\pm})^2}, \tag{4.82}$$

where $|\psi_i^{\pm}\rangle$ are the eigenvectors of H^{\pm}_{sub} and e^{\pm}_i their associated eigenvalues. The two components "+" and "–" can be treated fully independently, as a consequence of centrosymmetry. This result will later be exploited to understand the dominant doublet constraint in a statistical framework.

First, however, we can further exploit the perturbative approach, to gain an explicit understanding of the time scales $t^* = \pi/\left|E^- - E^+\right|$. Indeed, according to the perturbative logic, the relevant eigenvalues are the eigenvalues of the two-level system up to an energy shift s^\pm , induced by the coupling to the additional sites. These energy shifts are given by

$$s^{\pm} = \sum_{i} \frac{\left| \left\langle \mathcal{V}^{\pm}, \psi_{i}^{\pm} \right\rangle \right|^{2}}{E \pm V - e_{i}^{\pm}}, \tag{4.83}$$

such that

$$E^{\pm} \approx E \pm V + s^{\pm}.\tag{4.84}$$

Therefore, the time scale of the energy transfer can be expressed in terms of the resulting relative energy shift $\Delta s = s^- - s^+$, and we find

$$t^* = \frac{\pi}{|2V + \Delta s|}.\tag{4.85}$$

To understand the transfer time scales boils down to an understanding of the energy shifts Δs . A crucial observation in both, Eqs. (4.82) and (4.83), is that the energy level structure of the complex constituted by the intermediate sites (as represented by H_{sub}^{\pm}) can strongly affect these perturbations: When one of the bulk energy levels e_i^{\pm} dwells too closely in the vicinity of $E \pm V$, the perturbative corrections described by (4.83) seem to blow up. This is a manifestation of the general notion of avoided crossings, and although such crossings can have a drastic effect they never cause divergences. The solution lies in degenerate perturbation theory: In non-degenerate perturbation theory, one assumes that eigenvectors are uniquely defined, which in case of degeneracies is no longer the case. When a degeneracy manifests, and hence a symmetry is present in the system, one must consider eigenspaces rather than eigenvectors. The perturbation breaks this symmetry and selects a natural set of eigenvectors, but this effect as such is non-perturbative. It can be incorporated in a more general form of perturbation theory, where one fixes the correct eigenvectors in a non-perturbative way and uses them as basis for a perturbative treatment. The relevant adjustment is given by

$$1 - \left| \left\langle \tilde{\pm}, \pm \right\rangle \right|^2 \approx \frac{1}{2} \sum_{i=1}^{N/2 - 1} \left(1 - \left[1 + 4 \frac{\left| \left\langle \mathcal{V}^{\pm}, \psi_i^{\pm} \right\rangle \right|^2}{(E \pm V - e_i^{\pm})^2} \right]^{-1/2} \right), \tag{4.86}$$

$$s^{\pm} = \frac{1}{2} \sum_{i=1}^{N/2-1} (E \pm V - e_i^{\pm}) \left(1 - \left[1 + 4 \frac{\left| \left\langle \mathcal{V}^{\pm}, \psi_i^{\pm} \right\rangle \right|^2}{(E \pm V - e_i^{\pm})^2} \right]^{-1/2} \right). \tag{4.87}$$

To exploit the dominant doublet to the fullest, one strives to make (4.87) as large as possible, while (4.86) remains small. This is an intricate task, but it can be accomplished, as can for example be seen in the theory of *Chaos Assisted Tunnelling* (CAT) (Dembowski et al. 2000; Leyvraz and Ullmo 1996; Steck et al. 2001; Tomsovic and Ullmo 1994; Zakrzewski et al. 1998).

Finally, we show that the constraint of a dominant doublet in either form (4.70), (4.71) does strongly enhance the efficiency of the quantum transport as compared to both random and merely centrosymmetric networks. By construction we expect that $\mathcal{P}_H \geqslant 2\alpha - 1$ for many realisations. Again studying the numerically realised random networks in Fig. 4.10, with dominant doublet and centrosymmetry design principles imposed upon them, we find a pleasingly high density of realisations where $\mathcal{P}_H \geqslant 2\alpha - 1$ (for Fig. 4.10 this implies $\mathcal{P}_H \geqslant 0.9$).

In the following section, we introduce analytical and numerical results to gain a deeper understanding of the transport properties arising from the dominant doublet structure. We present the statistical constraints implied by the different dominant doublet requirements. Furthermore, we derive the statistics of transfer time scales, from which, ultimately, Fig. 4.10 can be—to some extent—quantitatively understood.

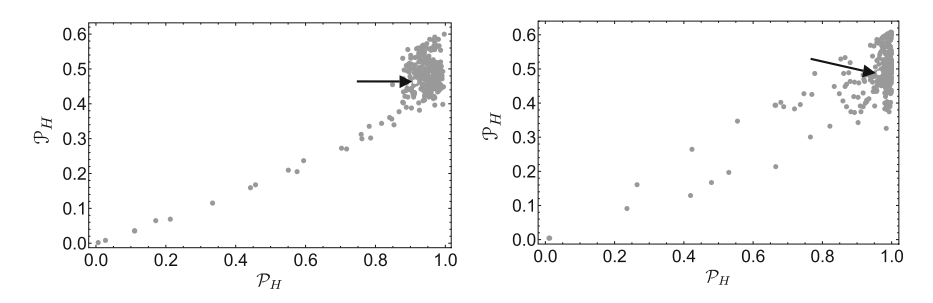


Fig. 4.10 Localisation efficiencies \mathcal{P}_H and occupation efficiencies \mathcal{P}_H as defined by (4.6), (4.7), respectively, for 500 realisations (grey dots) of random GOE Hamiltonians with centrosymmetry (4.46) and the dominant doublet constraint (4.68) imposed on them. The left panel shows the dominant doublet realisations as obtained from post-selection (as proposed in Eq. (4.70)), whereas the right panel depicts realisations where the doublet is engineered by controlling $|\mathcal{V}^{\pm}\rangle$ and ξ separately, to realise a dominant doublet structure on average (following Eq. (4.71)). The RMS coupling ξ/\sqrt{N} between the intermediate sites, is fixed by $\xi=2$, for N=8 sites, and the new dominant doublet constraints are set to $\alpha=0.95$ (left) and $\alpha'=0.95$ (right). The average value of \mathcal{P}_H and \mathcal{P}_H over all the realisations is again represented by the white dot that is indicated by an arrow (which shows a clear enhancement compared to Figs. 4.6, 4.7 and 4.8)

Imposing the design principles of the previous section comes with a shift in paradigm: The construction of efficient devices is often seen as a deterministic process, where a lot of control is involved. We now focus on a very different approach, where we control the *statistics* of an *ensemble* of systems (or devices). In this section, we study the statistical implications of the design principles derived above, and explain how they affect transport time scales and efficiencies.

We first treat the statistical properties of the dominant doublet (4.70), (4.71) in Sect. 4.5.1. This design principle controls the statistics of the energy eigenvectors in the Hamiltonians and does so in a very different way for the *averaged* than for the *post-selected* doublet. The difference already appears directly in the construction of the Hamiltonian, which in the former case is assumed to be controlled in the form (4.81), such that the statistics of $|\mathcal{V}^{\pm}\rangle$ is governed by a distribution independent from H^{\pm}_{sub} . In contrast, the post-selected doublet is a criterion on the Hamiltonian structure (4.56), where we impose a spectral condition on H^{\pm} , making $|\mathcal{V}^{\pm}\rangle$ and H^{\pm}_{sub} far from independent of each other.

The influence of the different dominant doublet construction methods reaches beyond statistical properties of the dominant doublet itself: it also impacts the statistics of other transport properties (such as, e.g., the transfer time t^* and the efficiency \mathcal{P}_H). In Sect. 4.5.2, where we discuss the transfer time scales, we find an important difference in statistics between both types of doublets. We analytically derive the probability distribution of transfer time scales and we show that the weights of the distributions' tails are very different for the different doublet constructions. The tail relates to realisations which are extraordinarily fast and therefore such change in weight is highly relevant (for our purpose as described in Chap. 1 and in Sect. 4.1 above). These effects are studied more closely in Sect. 4.5.3, where we study the scaling of the density of efficient realisations based on the tail of the transfer time distribution.

This long discussion on statistical control is finalised in Sect. 4.5.4 by studying numerical realisations of random matrix ensembles, to verify the validity of all the results which were derived before. Due to all approximations that were made, this numerical verification is a crucial final step.

4.5.1 Statistics of the Dominant Doublet

Averaged Dominant Doublet

Let us start by investigating the statistics that is hidden in Eq. (4.71), which ultimately is the most straightforward one of the two dominant doublet constraints. It is clear from the very definition that an average over all realisations is required. It follows directly from Eq. (4.86) that

$$\langle \left| \langle \tilde{\pm}, \pm \rangle \right|^2 \rangle_{\text{realisations}} \approx 1 - \frac{1}{2} \langle \sum_{i=1}^{N/2-1} \left(1 - \left[1 + 4 \frac{\left| \langle \mathcal{V}^{\pm}, \psi_i^{\pm} \rangle \right|^2}{(E \pm V - e_i^{\pm})^2} \right]^{-1/2} \right) \rangle_{\text{realisations}}, \tag{4.88}$$

which implies that we include the possibility of (near-) degeneracies in the spectrum of H^{\pm}_{sub} with the energies $E \pm V$. With this expression, one can perform a straightforward averaging. Crucial is that these eigenvalues are by construction behaving according to GOE statistics, because H^{\pm}_{sub} are independently controlled. The statistical independence of \mathcal{V}^{\pm} allows us to independently perform an integration over its components, the statistics of which are Gaussian:

$$\langle \mathcal{V}^{\pm}, \psi_i^{\pm} \rangle \sim \text{Normal}\left(0, \frac{\chi^2}{N/2 - 1}\right).$$
 (4.89)

 χ is here introduced to control the variance of the coupling between input (or output) site and the bulk sites, as an independent parameter. Therefore, the average over realisations in Eq. (4.88) must contain an integral over this distribution. Moreover, one must also consider the influence of the energy levels of H^{\pm}_{sub} , which are again governed by GOE statistics. One way to deal with these is introduced by Bohigas et al. (1993) and explicitly takes the two-point correlations between eigenvalues into account, resulting in

$$1 - \langle \left| \left\langle \tilde{\pm}, \pm \right\rangle \right|^2 \rangle_{\text{realisations}} \approx \frac{1}{2\sqrt{2\pi}} \int_{\mathbb{R}} dv \, de \, e^{-\frac{v^2}{2}} \left(1 - \frac{|e|}{\sqrt{e^2 + \frac{\chi^2}{(N/2 - 1)\Delta^2} v^2}} \right)$$

$$= 2\sqrt{\frac{2}{\pi (N/2 - 1)}} \frac{\chi}{\Delta}, \tag{4.91}$$

where we introduced Δ , the mean level spacing of the energy levels of H^{\pm}_{sub} in the vicinity of $E \pm V$. If we assume that $E \pm V$ lies in the centre of the spectrum, we may estimate that Δ is the mean level spacing around 0.

Because we numerically generate the Hamiltonians by controlling the root-meansquared (RMS) value of the interaction between intermediate sites ξ (4.61), it is desirable to express this result in terms of ξ rather than Δ . Therefore, one may use an approximation for the mean level spacing, given the density of states $\langle \rho(E) \rangle$ and the dimension n_{levels} of H_{sub}^{\pm} :

$$\Delta = \frac{1}{n_{\text{levels}} \langle \rho(E=0) \rangle} = \pi \frac{\xi}{n_{\text{levels}}}.$$
 (4.92)

In the present case, we consider H_{sub}^{\pm} and therefore, by (4.81), $n_{levels} = N/2 - 1$, such that

$$\alpha' = \langle \left| \left\langle \tilde{\pm}, \pm \right\rangle \right|^2 \rangle_{\text{realisations}} \approx 1 - \left(\frac{2}{\pi}\right)^{3/2} \sqrt{\frac{N}{2} - 1} \frac{\chi}{\xi}. \tag{4.93}$$

This estimate becomes more accurate as N grows larger, since is was derived in the limit $N \to \infty$ (Bohigas et al. 1993).

From Eq. (4.93) we deduce that control

- of the total system size N
- of the typical interaction strength χ/\sqrt{N} of coupling between the input/output site and the bulk system
- of the typical interaction strength ξ/\sqrt{N} between the sites in the bulk system

allows us to tune the dominant doublet condition. ¹² These *control knobs* have been employed to generate the data which underlie the right panel of Fig. 4.10.

Post-selected Dominant Doublet

The second possible dominant doublet constraint (4.70) is more subtle and was extensively discussed in Walschaers et al. (2015). The main source of difficulties is that we post-select the dominant doublets which fulfil condition (4.70) on the eigenvectors of H^{\pm} , and therefore one *cannot* treat H^{\pm}_{sub} and $|\mathcal{V}^{\pm}\rangle$ in (4.81) as independent statistical objects. In the following paragraphs, we strive to derive a relation between α , ξ and N, the coarse grained parameters which we can reasonably control, and $\|\mathcal{V}^{\pm}\|$, a parameter which we extract from numerical simulations. The derivation is somewhat subtle and certainly rather unorthodox.

First, we consider the implications of post-selection on Eq. (4.86). The sole demand which derives from the dominant doublet condition is cast upon the complete sum on the right hand side of Eq. (4.86), and implies that one should treat

$$\frac{\left|\left\langle \mathcal{V}^{\pm}, \psi_{i}^{\pm} \right\rangle\right|^{2}}{(E \pm V - e_{i}^{\pm})^{2}}$$

as one statistical quantity. This quantity must be sufficiently small in order to satisfy the dominant doublet condition. This implies, on the one hand, that very small values of $\left|\left\langle \mathcal{V}^{\pm},\psi_{i}^{\pm}\right\rangle\right|^{2}$ also allow $(E\pm V-e_{i}^{\pm})^{2}$ to be small, as long as the ratio between the two terms satisfies the dominant doublet condition. On the other hand, realisations of H^{\pm} where $\left|\left\langle \mathcal{V}^{\pm},\psi_{i}^{\pm}\right\rangle\right|^{2}$ is large can still fulfil the dominant doublet constraint, provided that also $(E\pm V-e_{i}^{\pm})^{2}$ is sufficiently large. Since matters are complicated by the sum over the index i, it appears reasonable to require that

$$D := \min_{i} \left| E \pm V - e_{i}^{\pm} \right| \tag{4.94}$$

 $^{^{12}}$ We do notice that finite size effects slightly alter the prediction of Eq. (4.93), resulting for example in an actual $\alpha' \approx 0.93$, obtained by numerics, instead of the analytically predicted $\alpha' = 0.95$ both for N = 20, $\xi = 2$ and $\chi = 0.0656234$.

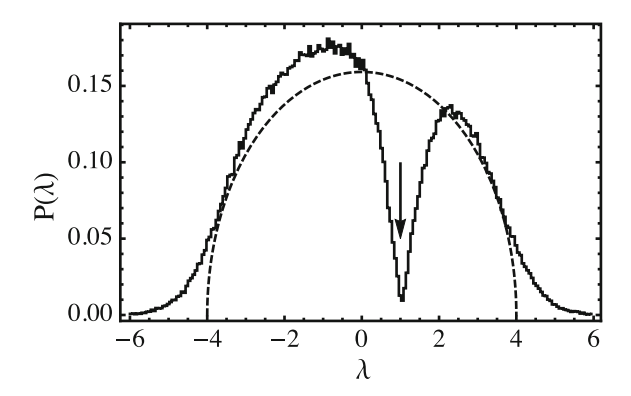


Fig. 4.11 Density of states of H_{sub}^+ , where λ probes possible values of the energy levels, for N=10 sites, RMS coupling between intermediate sites ξ/\sqrt{N} , with $\xi=2$, and fixed E+V=1 (arrow), to highlight the effect of a dominant doublet in the vicinity of this energy level. In contrast to the Wigner semicircle (dashed line, see Eq. (3.46)), valid for the GOE ensemble with $N\to\infty$, the density of states exhibits a cusp at $\lambda=E+V$. This figure is taken from Walschaers et al. (2015)

be sufficiently large. Notice that the post-selection procedure thereby imposes additional constraints on the eigenvalue statistics for the resulting post-selected H^{\pm}_{sub} . There is no reason to assume that the normal Wigner-Dyson statistics is still obeyed by these matrices. Indeed, Fig. 4.11 shows a seriously scarred distribution with a cusp exactly at the value $E \pm V$.

A crucial corollary of the cusp in the density of states is that one can no longer use (4.92) to relate the level spacing Δ_{loc} in the vicinity of $E\pm V$, to the quantities ξ and N, since the derivation of (4.92) explicitly relied on Wigner's semicircle distribution (3.46). To study the relation between ξ , α , N and $\|V^{\pm}\|^2$, we therefore assume two limiting regimes, which *both occur in the post-selected ensemble*, to obtain an estimate for Δ_{loc} . ¹³

The first limiting case is the one where all eigenvalues of H^{\pm}_{sub} remain sufficiently far away from $E \pm V$ and therefore contribute roughly equally to the sum Eq. (4.86). This also implies that we can assume that all eigenvalues are far from degeneracy with $E \pm V$ and therefore we can safely use Eq. (4.82). Now we need to make a series of assumptions in order to proceed: First of all, based on numerics, we assume that the distribution of the statistical objects $|\langle \tilde{\pm}, \pm \rangle|^2$ is, in the post-selected ensemble, strongly peaked around α , leading to the estimate that

$$\langle \frac{\left| \left\langle \mathcal{V}^{\pm}, \psi_{i}^{\pm} \right\rangle \right|^{2}}{(E \pm V - e_{i}^{\pm})^{2}} \rangle_{\text{realisations}} \approx \frac{1 - \alpha}{N/2 - 1}.$$
 (4.95)

¹³Due to the subtlety of the argument, the phrasing is delicate, hence the wording here is similar to that of Walschaers et al. (2015).

To evaluate the average on the left hand side, we assume that the statistics of e_i^\pm is governed by the Wigner-semicircle. This can be done since the eigenvalues are, by definition of this limiting case, far away from $E\pm V$ and therefore do not feel its repulsion. On the level of the couplings, we assume, loosely based on the central limit theorem, that the statistics of $v=\left\langle \mathcal{V}^\pm,\psi_i^\pm\right\rangle$ is Gaussian, where the variance $\overline{\|\mathcal{V}\|^2}/(N/2-1)$ is the very parameter which is to be determined. This allows to calculate

$$\langle \frac{\left| \left\langle \mathcal{V}^{\pm}, \psi_{i}^{\pm} \right\rangle \right|^{2}}{(E \pm V - e_{i}^{\pm})^{2}} \rangle_{\text{Realisations}} \approx \sqrt{\frac{N/2 - 1}{2\pi \|\mathcal{V}\|^{2}}} \int_{\mathbb{R}} dv \, e^{-\frac{(N/2 - 1)v^{2}}{2\|\mathcal{V}^{\pm}\|}} |v|^{2}$$

$$\times \frac{1}{\pi \xi} \int_{-2\xi}^{2\xi} de \, \frac{1}{(E \pm V - e)^{2}} \sqrt{1 - \frac{e^{2}}{4\xi^{2}}}$$

$$= \frac{2\|\mathcal{V}\|^{2}}{\pi \xi^{2} (N/2 - 1)},$$

$$(4.96)$$

which can be inserted into expression (4.95) to obtain

$$1 - \alpha \approx \frac{2\overline{\|\mathcal{V}\|^2}}{\pi\xi^2}.\tag{4.97}$$

This is of course a rough estimate at first sight, given all the assumptions that were made. Notice for example that we also integrate over the whole spectral range for the intermediate energy level, from -2ξ to 2ξ , which implies to ignore the cusp in Fig. 4.11.

To verify the above assumptions, one can numerically generate random Hamiltonians and actually perform the <u>post-selection</u> procedure, with the purpose to extract the relation between ξ , α and $\|V\|^2$, to ultimately verify the proposed relation in Eq. (4.97) with the approximation

$$\alpha \approx 1 - C \frac{\|\overline{\mathcal{V}}\|^2}{\xi^2},\tag{4.98}$$

where C is a fit parameter. We scan α from 0.99 to 0.8, for fixed $\xi=2$ and N=14. For each value of α we extract $\|\mathcal{V}\|^2$ from the numerics. Inspecting data with $\alpha \in [0.94, 0.99]$, $\xi=20$, and N=10, suggests that indeed there is no significant dependence on N, as is expected from Eq. (4.97). Figure 4.12 suggests a linear dependence as in (4.98). However, since the ansatz (4.98) results from perturbation theory, it appears reasonable to add a term quadratic in $\|\mathcal{V}\|^2/\xi^2$ for $\alpha\approx0.8$. We therefore fit the data to the form

$$\alpha \approx 1 - C \frac{\|\overline{\mathcal{V}}\|^2}{\xi^2} - b \left(\frac{\|\overline{\mathcal{V}}\|^2}{\xi^2} \right)^2, \tag{4.99}$$

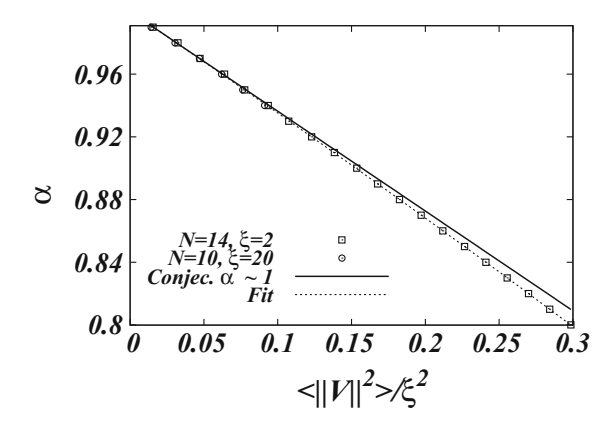


Fig. 4.12 Dependence of α on $\overline{||\mathcal{V}||^2}/\xi^2$, for different network realisations. In order to extract the constant C in (4.98), (4.99), a fit is performed. The dependence as conjectured by Eq. (4.97) for $\alpha \approx 1$, where $C = 2/\pi$, is given by the solid line. This figure is taken from Walschaers et al. (2015)

Table 4.1 Estimated parameters C and b for Eq. (4.99) and their respective standard errors. The fit was obtained with the Fit routine in Mathematica 10

	Estimate	Standard error
С	0.636789	0.00218418
b	0.111501	0.00933118

and obtain the results shown in Table 4.1.

Since, however, the dominant doublet is obtained in the regime where $\alpha \approx 1$, the term $\sim \left(\overline{\|\mathcal{V}\|^2}/\xi^2 \right)^2$ should become negligible, such that we numerically estimate Eq. (4.97) as

$$1 - \alpha \approx 0.636(\pm 0.002) \frac{\|\mathcal{V}\|^2}{\xi^2}.$$
 (4.100)

Indeed, this implies that the analytical prediction $C = 2/\pi$ falls nicely within the error margin and that Eq. (4.97) holds.

Remarkably, via (4.71), expression (4.93), which was derived from the alternative method for imposing the dominant doublet, leads to a very different outcome than Eq. (4.97). Thus, although the dynamical quantities $p_{\text{out}}(t)$, \mathcal{P}_H and \mathcal{P}_H (see (4.6), (4.7)) seemed very similar for both possible definitions of the dominant doublet, they lead to very different statistics.

The difference between (4.93) and (4.97) arises because the averaged ensemble does not allow for correlations between the statistical quantities $|\langle \mathcal{V}^{\pm}, \psi_i^{\pm} \rangle|^2$ and $(E \pm V - e_i^{\pm})^2$. This implies that a cusp such as shown in Fig. 4.11 cannot be formed in an ensemble where the dominant doublet is imposed by an averaging condition (4.71). The presence such a cusp implies the possibility of separating local statis-

tics in the vicinity of $E\pm V$ from global effects such as the density of states far away from $E\pm V$. It is exactly there, when $(E\pm V-e_i^\pm)^2\to 0$, that constraints upon the parameter χ , which governs the coupling between input/output and the intermediate sites, arise in the averaged dominant doublet ensemble. Because, in addition, $|\langle \mathcal{V}^\pm, \psi_i^\pm \rangle|^2$ and $(E\pm V-e_i^\pm)^2$ are independently controlled throughout the averaged doublet ensemble, these constraints are felt everywhere. They are at the origin of the difference (4.93) and (4.97). For realisations with $(E\pm V-e_i^\pm)^2\to 0$ similar problems would arise in the post-selected ensemble, but because the post-selection does not make any assumptions on the specific statistics of the spectrum of the intermediate sites $\{e_i^\pm\}$, these constraints can be avoided by locally adjusting the mean-level spacing. In other words, the post-selected ensemble gives the system the freedom to effectively push energy levels away from $E\pm V$, as we discuss in the second limiting case. It is this effective repulsion between levels in the bulk and the energies $E\pm V$ that allows assumption (4.95), which is key to obtaining the exact expression (4.97).

The second limiting case focusses on understanding the cusp in Fig. 4.11 by assuming that one deals with the completely opposite regime. We consider the situation where one *single* eigenvalue e_i^{\pm} approaches as closely as possible to $E \pm V$, in a way such that the contributions of the additional eigenvalues can safely be neglected. Therefore, we are interested in the quantity D_{\min} , which is the minimal value that the quantity D (4.94) can have within the ensemble. To study the statistics of a single term in (4.86)

$$\tau = 1 - \left[1 + 4 \frac{\left| \left\langle \mathcal{V}^{\pm}, \psi_i^{\pm} \right\rangle \right|^2}{(E \pm V - e_i^{\pm})^2} \right]^{-1/2}, \tag{4.101}$$

assumptions must again be made. ¹⁴ In our present case we also assume that $v = \langle \mathcal{V}^{\pm}, \psi_i^{\pm} \rangle$ is governed by Gaussian statistics, though we make no assumptions at all on D, and just leave it as a parameter. Rather than averaging, as was done in the first limiting case above, we consider de probability distribution of τ , given by

$$P_D(\tau) = \sqrt{\frac{N/2 - 1}{2\pi \|V\|^2}} \int_{\mathbb{R}} dv \, e^{-\frac{(N/2 - 1)v^2}{2\|V^{\pm}\|}} \delta\left(\tau - \frac{1}{2} \left[1 - \left(1 + 4\frac{v^2}{D^2}\right)^{-1/2}\right]\right). \tag{4.102}$$

We use probability distributions because the dominant doublet of Eq. (4.70) is a hard constraint, implying that we fulfil the inequality with probability one in the post-selected ensemble. Due to $1-\alpha\approx 0$, it is necessary that also $\tau\approx 0$, allowing us to only consider the leading order scaling behaviour in the limit where $\tau\to 0$. This leads to

$$P_D(\tau) \approx \frac{D\sqrt{N-2}}{4\sqrt{\pi \overline{\|\mathcal{V}\|^2}\tau}},$$
 (4.103)

¹⁴We warn the reader that throughout the text τ is used as a *stochastic quantity*, which may make definition (4.101) somewhat misleading.

which can now be used to impose the hard dominant doublet constraint (4.70):

$$\operatorname{Prob}(\tau \leqslant 1 - \alpha) = \int_0^{(1 - \alpha)} d\tau \, P_D(\tau) = 1. \tag{4.104}$$

This identity defines an equation which can be solved to obtain the smallest possible value for D, denoted D_{\min} :

$$D_{\min} \approx \frac{\sqrt{2\pi \|\overline{\mathcal{V}}\|^2}}{\sqrt{(1-\alpha)(N/2-1)}}.$$
(4.105)

This concludes our study on the statistical implications of the dominant doublet conditions.

To summarise, we investigated two possible methods of imposing the dominant doublet condition, one based on a disorder average (4.71), the other one on post-selection (4.70). We concluded that both choices have a pronounced effect on the statistics of $|\langle \tilde{\pm}, \pm \rangle|^2$, but that these effects are very different. For the averaged dominant doublet, the effect is expressed by Eq. (4.93), whereas the result for the post-selection procedure is summarised by Eq. (4.97). The scaling behaviour with respect to the parameters ξ , N and χ (or $\sqrt{\|\mathcal{V}\|^2}$) is remarkably different in both cases

Moreover, we pointed out that the post-selected ensemble has a scarred density of states, with a cusp around $E \pm V$, as shown in Fig. 4.11. We have shown that this cusp results from a type of level repulsion, which is caused by the unperturbed levels of H^{\pm}_{sub} interacting with the level $E \pm V$. We found that the dominant doublet constraint leads to a typical, minimally allowed distance D_{\min} between e^{\pm}_i and $E \pm V$ as given by Eq. (4.105). This effect is of crucial importance in the derivation of the statistics of transfer time scales.

In conclusion, the more straightforward way of constructing the averaged dominant doublet by manually controlling the ratio between energy scales χ/ξ is effective. However, introducing the dominant doublet via random sampling and post-selecting the realisations where (4.70) is fulfilled teaches us that there are more ingenious ways to reach the doublet structure. The altered density of states in Fig. 4.11 indicates a highly non-trivial energy level statistics for the intermediate sites, characterised by H_{sub}^{\pm} . This serves as a clear example that there can be more non-trivial ways of introducing a dominant doublet structure than merely via an overall separation of energy scales. Moreover, in the following section we explain that these post-selected dominant doublet structures lead to different statistics of transfer times as compared to the averaged dominant doublet.

4.5.2 Statistics of the Transfer Time

As we learned in the previous section, imposing the dominant doublet constraint on the level of eigenvectors puts constraints on the statistics of the random Hamiltonian ensembles by governing the statistics of the different building blocks of (4.81). However, once these constraints are in place, all the pieces are set for achieving near-optimal excitation transfer. Again, we start by considering the averaged dominant doublet condition as given by (4.71) since this case was already studied in the literature of CAT (Leyvraz and Ullmo 1996; Tomsovic and Ullmo 1994; Zakrzewski et al. 1998). The definition of the transfer time scale, given by Eq. (4.85), tells us that the relevant statistical objects to consider are the dominant doublet level shifts Δs .

The Cauchy Distribution for T_B/t^*

We start by highlighting the key ideas of the derivation conducted by Leyvraz and Ullmo (1996), assuming E = V = 0. The authors start from the assumption that s^{\pm} can be faithfully approximated by Eq. (4.83), after which they rescale variables to

$$x = \frac{s^{\pm} \Delta (N/2 - 1)}{\chi^2}$$
, and $E_i = \frac{e_i^{\pm}}{D}$, (4.106)

and thus it remains to calculate

$$P(x) = \int \delta\left(x - \sum_{i=1}^{N/2-1} \frac{1}{E_i}\right) P(E_1, \dots, E_{N/2-1}) dE_1 \dots dE_{N/2-1}.$$
 (4.107)

An exact calculation of the distribution for GOE statistics is unfeasible, therefore they choose to rather focus on two regimes which are easier to handle: the case where all the E_i are uncorrelated, such that P factorises, or the case where the eigenvalues are maximally correlated. The first case is treated by assuming that E_i is governed by a Poisson distribution p_0 and this leads to

$$P(x) = \int \prod_{i} dy_{i} p_{0}(y_{i}) \delta\left(x - \frac{1}{N/2 - 1} \sum_{i} y_{i}\right), \tag{4.108}$$

where again a change in variable was conducted, using $y_i = [(N/2 - 1)E_i]^{-1}$. It is then argued in Leyvraz and Ullmo (1996) that the Fourier transform of P(x) is given by

$$\hat{P}(q) = \lim_{N \to \infty} \left(1 - \frac{\pi |q|}{N/2 - 1} \right)^{N/2 - 1} = e^{-\pi |q|}, \tag{4.109}$$

from which is directly follows that

$$P(x) = \frac{1}{x^2 + \pi^2}. (4.110)$$

Notice here that this result is only valid for $N \to \infty$, whereas we will use it as an estimate for system sizes which are much smaller.

The opposite regime of maximally correlated eigenvalues assumes that these are all equally spaced, leading to the following expression as an estimate for Eq. (4.107):

$$P(x) = \int_{-1/2}^{1/2} dE \, \delta \left(x - \sum_{n = -\infty}^{\infty} \frac{-1}{n + E} \right), \tag{4.111}$$

which after some calculations also results in

$$P(x) = \frac{1}{x^2 + \pi^2}.$$

The authors reason that, since these two extremes lead to the same result, the GOE result, which is somewhere in between, must also lead to the same statistics. Ultimately they thus reach the result that

$$P(s^{\pm}) = \frac{1}{\pi} \frac{\sigma^{\pm}}{(\sigma^{\pm})^{2} + (s^{\pm} - s_{0}^{\pm})^{2}} = \text{Cauchy}(s_{0}^{\pm}, \sigma^{\pm}),$$
with $\sigma^{\pm} = \pi \frac{\chi^{2}}{(N/2 - 1)\Delta}$, $s_{0}^{\pm} = 0$,
$$(4.112)$$

a distribution which is well-known as the Cauchy (or Lorentzian) distribution, in this case with parameters s_0^\pm and σ^\pm . A much more advanced method, using supersymmetry methods, was used in Ergün and Fyodorov (2003) in order to exactly calculate the distribution. They obtain the result both in a more rigorous and a more general way. The biggest advantage of these methods, which we will not discuss in detail, is that they allow for an additional consideration of general $E \pm V$. The result is again the Cauchy distribution, but with $s_0^\pm = \pm V \frac{\chi^2}{2\xi^2}$. The main difference with respect to our present study is that in Ergün and Fyodorov (2003) V is still assumed to be fixed, rather than a stochastic variable.

Note that the probability distribution (4.112) describes the fluctuations in dominant doublet energy levels throughout the ensemble. If we assume that the disorder is generated by configuration changes in the network, which occur on time scales much longer than the transfer time, we can also interpret (4.112) as the distribution of the energy fluctuations generated by these configurational changes over time. In the philosophy of Chap. 3 this is clearly a complex system, since we observe a power-law distribution in the spectrum.

The next step in the derivation of the transfer time distribution for our centrosymmetric ensemble is to find the distribution for $\Delta s = s^+ - s^-$. This is a straightforward task, due to the nice properties of the Cauchy distribution: The Cauchy distribution is a stable distribution (Fama and Roll 1968), meaning that for two independent variables A, B which are distributed according to

$$A \sim \text{Cauchy}(a_0, \sigma_a)$$
 and $B \sim \text{Cauchy}(b_0, \sigma_b)$,

we find that

$$A + cB + d \sim \text{Cauchy}\left(a_0 + cb_0 + d, \sigma_a + |c|\sigma_b\right), \quad \text{for any } c, d \in \mathbb{R}.$$

$$(4.113)$$

Because of the centrosymmetry s^+ and s^- are statistically independent, each described by a distribution (4.112). Thus, (4.113) leads us to

$$P(\Delta s) = \frac{1}{\pi} \frac{\sigma}{\sigma^2 + (\Delta s - s_0)^2},$$
with $s_0 = s_0^+ - s_0^- = V \frac{\chi^2}{\xi^2},$
and $\sigma = \sigma^+ + \sigma^- = 2\pi \frac{\chi^2}{(N/2 - 1)\Delta}.$

Diverting attention to Eq. (4.85), we can now apply (4.113) to obtain that

$$\frac{T_B}{t^*} = 1 - \frac{\Delta s}{2V} \sim \text{Cauchy}\left(1 - \frac{s_0}{2V}, \frac{\sigma}{2V}\right). \tag{4.115}$$

The distribution of the absolute value $\left|1 - \frac{\Delta s}{2V}\right|$ thus reads:

$$P\left(\left|1 - \frac{\Delta s}{2V}\right| = x\right) = \frac{1}{\pi} \left(\frac{\gamma}{\gamma^2 + (1 + x_0 + x)^2} + \frac{\gamma}{\gamma^2 + (1 + x_0 - x)^2}\right),$$
with $x_0 = \frac{\chi^2}{2\xi^2},$
and $\gamma = \frac{1}{V} \frac{\pi \chi^2}{(N/2 - 1)\Delta}.$
(4.116)

There is, however, still the issue of V, which for the above needs to be considered a fixed quantity, and we now devote some words to tackling this matter.

Statistics of the Direct Input-Output Coupling*

This discussion on the approximation for the average coupling between the input and the output site is rather technical. The essential result which is used in the remainder of the text is contained in Eq. (4.130).

We define V to be the coupling between the input and output site, and these sites are assumed to be those that couple the weakest (in absolute value), as given by (4.48). Therefore, we must assume that V itself is also a stochastic quantity. Since it is the minimum absolute value of a set of N/2-1 normally distributed variables, we must go through a minor derivation to uncover its statistics, which in principle is

a type of *extreme value statistics*. We first start by elucidating the general method to treat such problems.

Method 1 Let $X_1, ..., X_n$ be a sample of n independent, identically distributed stochastic variables, and denote $m = \min_{k \in \{1,...n\}} X_k$. We are now interested in the probability density P(m). To obtain this function, we consider the cumulative distribution function (CDF) of m, $F_m(x) = \text{Prob}(m \le x)$. Since m is the minimum, we have that

$$F_m(x) = \text{Prob}(m \le x) = 1 - \prod_{k=1}^n \text{Prob}(X_k > x)$$

$$= 1 - \prod_{k=1}^n (1 - \text{Prob}(X_k \le x))$$

$$= 1 - (1 - F(x))^n$$
(4.117)

where $F(x) := \text{Prob}(X_k \leq x)$ is the CDF of X_k . Because X_1, \ldots, X_n are identically distributed, they all lead to the same CDF. What we explicitly show in (4.117), by the very definition of the sample minimum, is that m does not follow the same statistics as X_1, \ldots, X_n . The probability density P(m) can be obtained as

$$P(m) = \frac{dF_m(x)}{dx}\Big|_{x=m} = \frac{d}{dx} (1 - F(x))^n \Big|_{x=m},$$
 (4.118)

which is seen to strongly depend on the sample size n.

Here we must consider $X_k = |H_{k,N-k+1}|$ and $H_{k,N-k+1} \sim \text{Normal}\left(0, \frac{2\xi^2}{N}\right)$, what implies that $|H_{k,N-k+1}|$ is a half-normal distribution, ¹⁵ therefore the CDF is given by Leone et al. (1961)

$$F_{\left|H_{k,N-k+1}\right|}(x) = \frac{2}{\sqrt{\pi}} \int_{0}^{x} d\left|H_{k,N-k+1}\right| e^{-\left(\frac{\sqrt{N}\left|H_{k,N-k+1}\right|}{2\xi}\right)^{2}}$$

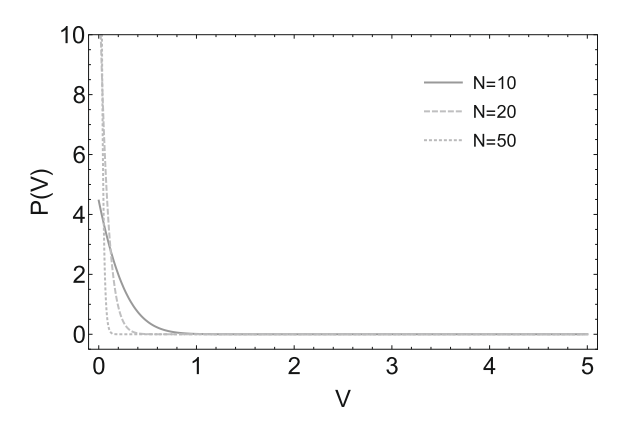
$$= \operatorname{erf}\left(\frac{\sqrt{N}x}{2\xi}\right), \tag{4.119}$$

where erf (x) denotes the error function (Abramowitz and Stegan 1965). By virtue of this result and n = N/2 in (4.117) and (4.118), we obtain that the probability density of V is given by

$$P(V) = \frac{e^{-\frac{NV^2}{4\xi^2}} N^{3/2} \left(\operatorname{erfc}\left(\frac{\sqrt{N}V}{2\xi}\right)\right)^{\frac{N}{2}-1}}{2\sqrt{\pi}\xi},$$
(4.120)

¹⁵Given that a stochastic variable X is normally distributed, the distribution of |X| is called a *half-normal* (if $\mathbb{E}(X) = 0$) or *folded normal* distribution (Leone et al. 1961). The terminology refers to the fact that the negative part of the probability distribution is literally folded to the positive side.

Fig. 4.13 Probability distribution P(V) of the direct input to output coupling V, in an N-site random network, for variable N=10, N=20 and N=50. The parameter describing the RMS coupling strength between the intermediate sites was set to $\xi=2$. Clearly, the distribution is strongly peaked near its mean value $\langle V \rangle$ (see (4.130))



with $\operatorname{erfc}(x) = 1 - \operatorname{erf}(x)$, the complementary error function (Abramowitz and Stegan 1965).

Although the probability distribution is now obtained and we can *in principle* average $P(T_B/t_*)$ as given in Eq. (4.116), by integrating over the measure P(V) dV, such an integration is extremely cumbersome due to the presence of the (complementary) error function. ¹⁶ Therefore, we make an *annealed approximation* (Derrida and Pomeau 1986; Seung et al. 1992): When averaging a function f of a stochastic variable V, one approximates $\langle f(V) \rangle \approx f(\langle V \rangle)$. This assumption is usually valid in the regime where the probability distribution of V is strongly peaked near its mean (at least in comparison to the other relevant variables). Figure 4.13 shows that, indeed, the distribution is strongly peaked around its mean value $\langle V \rangle$, which we now set out to calculate.

We start from Eq. (4.120), since by definition

$$\langle V \rangle = \int_0^\infty dV P(V) V$$

$$= \int_0^\infty dV \frac{e^{-\frac{NV^2}{4\xi^2}} N^{3/2} \left(\operatorname{erfc} \left(\frac{\sqrt{N}V}{2\xi} \right) \right)^{\frac{N}{2} - 1}}{2\sqrt{\pi}\xi} V. \tag{4.121}$$

With the change of variable

$$V' = \frac{\sqrt{N}V}{2\xi},\tag{4.122}$$

the right hand side of (4.121) turns into

$$\frac{2\xi\sqrt{N}}{\sqrt{\pi}}\int_0^\infty dV' e^{-V'^2} \left(\operatorname{erfc}\left(V'\right)\right)^{\frac{N}{2}-1} V'. \tag{4.123}$$

¹⁶All our attempts resulted in page-long expressions which were neither useful nor insightful.

Assuming that we are in the regime of large N, as we did to obtain (4.112), we have $N/2 - 1 \approx N/2$. We now apply Laplace's method (Laplace 1986), and thus need to define a function f such that

$$\int_{0}^{\infty} dV' e^{-V'^{2}} \left(\text{erfc} \left(V' \right) \right)^{\frac{N}{2} - 1} V' = \int_{0}^{\infty} dV' \exp \left(N f(V') \right). \tag{4.124}$$

It is straightforward¹⁷ to check that

$$f(V') = -\frac{{V'}^2}{N} + \left(\frac{1}{2} - \frac{1}{N}\right) \log\left(\text{erfc}\left(V'\right)\right) + \frac{1}{N}\log V'$$
 (4.125)

is a suitable choice. In order to apply Laplace's method, we need to find that V_0 for which f is extremal, hence $f'(V_0) = 0$. We straightforwardly calculate the derivative of (4.125) and find

$$f'(V') = \frac{1}{NV'} - \frac{2V'}{N} - \left(1 - \frac{2}{N}\right) \frac{e^{-V'^2}}{\sqrt{\pi}\operatorname{erfc}(V')},\tag{4.126}$$

what only allows for an implicit expression for V_0 . We can however get an explicit result by the following approximation: Since the maximum of f(V') is achieved for $V_0 \ll 1$, we can expand $e^{-V'^2}$ and erfc(V') around $V' \approx 0$, and obtain a tractable approximation for f(V'), leading to

$$\frac{e^{-V'^2}}{\sqrt{\pi}\operatorname{erfc}(V')} = \frac{1 - V'^2 + \frac{1}{2}V'^4 - \dots}{\sqrt{\pi}(1 - 2V' + \frac{2}{3}V'^3 + \dots)} \approx \frac{1}{\sqrt{\pi}}.$$
 (4.127)

Even though this is a rough approximation, the corrections due to higher orders are negligible for large N. Numerical evaluation of (4.121) shows that, even for N = 10, the exact results are very well approximated by (4.127).

With the low order approximation (4.127), $f'(V_0) = 0$ is satisfied for

$$V_0 \approx \frac{\sqrt{N^2 + 8\pi} - N}{4\sqrt{\pi}} \approx \frac{\sqrt{\pi}}{N} \left(1 + \frac{2}{N} \right),\tag{4.128}$$

and Laplace's method now tells us that

$$\int_{0}^{\infty} dV' \exp(Nf(V')) \approx e^{Nf(V_0)} \sqrt{\frac{2\pi}{N |f''(V_0)|}},$$
 (4.129)

¹⁷We use the property that $x = e^{\log x}$, which implies that $f(V') = \frac{1}{N} \log \left(e^{-V'^2} \left(\operatorname{erfc} \left(V' \right) \right)^{\frac{N}{2} - 1} V' \right)$.

resulting in

$$\langle V \rangle \approx \frac{2\pi\xi}{eN\sqrt{N/2-1}}.$$
 (4.130)

Transfer Times for the Averaged Dominant Doublet

With the results of the previous sections, all the pieces are collected to obtain the probability distribution for the transfer times across centrosymmetric, finite, random networks with the averaged dominant doublet. Turning back to Eq. (4.116), we can now substitute $V \to \langle V \rangle$ as dictated by the annealed approximation. Moreover, we already know an expression (4.92) for Δ in terms of ξ and N: We assume, as is supported by numerical data, that the mean level-spacing in the bulk of the semicircle is similar everywhere. Therefore, we estimate Δ , which is the mean level-spacing in the vicinity of $E \pm V$, by the mean level-spacing around energy E = 0. This result can be applied for the averaged doublet without any problems. With these previously obtained results (4.92), (4.116), and (4.130) we find the final distribution

$$P\left(\frac{T_B}{t^*} = x\right) = \frac{1}{\pi} \left(\frac{\gamma}{\gamma^2 + (1 + x_0 + x)^2} + \frac{\gamma}{\gamma^2 + (1 + x_0 - x)^2}\right),$$
with $x_0 = \frac{\chi^2}{2\xi^2}$,
and $\gamma = \frac{eN\sqrt{N/2 - 1}}{2\pi} \frac{\chi^2}{\xi^2}$.
$$(4.131)$$

The parameter γ seems to scale strongly with the system size $\gamma \sim N^{3/2}$, which is inherited from our above expression (4.130) for the average coupling $\langle V \rangle$.

Although expression (4.131) is formally correct, it does hide part of the story; we still have to take the dominant doublet condition (4.71) into account: Upon *designing* a system, we can control the localisation efficiency \mathcal{P}_H by requiring an ensemble averaged dominant doublet (4.71), the strength α' of which depends on the specific value of \mathcal{P}_H in (4.75) which we wish to achieve. By virtue of (4.93), the required doublet strength α' , and thus the *desired transport properties*, constrains the allowed values for N, ξ and χ by imposing an N-dependence on the ratio χ/ξ of typical coupling strengths.¹⁸ More specifically, Eq. (4.93) allows to rewrite

$$\gamma \approx \frac{e\sqrt{N}\pi^2(1-\alpha')^2}{16}.\tag{4.132}$$

Hence, constraints on the transfer efficiency translate to a "different" scaling behaviour of γ with the number of sites N, i.e. $\gamma \sim N^{1/2}$. The reason for the discrepancy compared to (4.131) is that the scaling $\gamma \sim N^{3/2}$ is only valid when we assume that the ratio χ/ξ is independent of N. However, such independence implies,

¹⁸Where χ/\sqrt{N} is the typical (RMS) coupling between the input/output and the intermediate sites, and ξ/\sqrt{N} denotes the typical (RMS) coupling strength between the intermediate sites.

through (4.93), that α' , and therefore the lower bound on \mathcal{P}_H , *decrease* with N up to the point where the dominant doublet breaks down.

In summary, the relevant scaling of the weight γ of the tail of the Cauchy distribution with the number N of sites is determined by the desired (localisation) efficiency of the transfer process. The resulting, actual scaling with the system size is $\gamma \sim N^{1/2}$.

As for a Cauchy distribution, the weight in the heavy, algebraic tail is determined by this parameter γ . We can see that in larger systems, the tail is expected to grow fatter. We may interpret $x=T_B/t^*$ as the speedup of excitation transfer by adding the intermediate sites. When the distribution becomes broader, there are more realisations strongly enhancing the transfer. On the other hand, the direct coupling between input and output sites, and thus the direct tunnelling, strongly decreases when the system size is increased as seen from $\langle V \rangle$ (4.130). Therefore the indirect (or chaos-assisted) tunnelling will get the upper hand. ¹⁹

Transfer Times for the Post-selected Dominant Doublet

As already discussed in Sect. 4.5.1, the post-selected dominant doublet is more subtle, but all the required pieces of the puzzle are already on the table. Most fundamental is the behaviour shown in Fig. 4.11, which implies that we can no longer simply use the GOE assumption for Δ , the mean-level spacing *in the vicinity of* $E \pm V$. This is a fundamental consequence of the post-selection procedure, which leads to the repulsion grasped by Eq. (4.105), and this repulsion is responsible for the locally altered mean-level spacing.

To correctly estimate the value of Δ , we need to consider one additional subtle aspect: Δ is the mean-level spacing between the *levels of* H^{\pm}_{sub} in the vicinity of $E \pm V$. The result for D_{\min} in Eq. (4.105), however, describes the distance from one such energy level to the value $E \pm V$, as given by Eq. (4.94). Focusing on the cusp in Fig. 4.11, this roughly implies that an energy level can approach this closely, both from the left and from the right. Hence, we reach the rough estimate that

$$\Delta \approx 2D_{\min}.\tag{4.133}$$

In order to express this result in terms of ξ , the parameter governing the RMS coupling between the intermediate sites, we can combine the constraints imposed by both limiting cases (4.97) and (4.105). Since both cases occur in the same post-selected ensemble, both constraints imposed by them have to be fulfilled. This leads us to the final result that

$$\Delta \approx \frac{2\pi\xi}{\sqrt{N/2 - 1}}.\tag{4.134}$$

¹⁹This is also consistent with the physical idea behind the CAT mechanism: The coupling to a second *chaotic* (hence modelled by the GOE Bohigas et al. 1993) degree of freedom (here the randomly interacting intermediate sites, where the randomness comes from conformational changes in the macromolecular arrangement, in particular mimicking vibrational background degrees of freedom) enhances the tunnelling rate in a donor-acceptor system with *vanishing* direct coupling (Tomsovic and Ullmo 1994).

For the ultimate distribution of T_B/t^* , this implies

$$P\left(\frac{T_B}{t^*} = x\right) = \frac{1}{\pi} \left(\frac{\gamma}{\gamma^2 + (1 + x_0 + x)^2} + \frac{\gamma}{\gamma^2 + (1 + x_0 - x)^2}\right),$$
with $x_0 = \frac{\|\mathcal{V}\|^2}{2\xi^2},$
and $\gamma = \frac{\|\mathcal{V}\|^2 Ne}{4\pi\xi^2}.$

$$(4.135)$$

We write " $\|\mathcal{V}\|^2$ " to stress that this quantity is not controlled, but obtained from numerics, since the controllable parameters are the number N of sites, the RMS coupling ξ/\sqrt{N} between the intermediate sites, and the dominant doublet strength α (4.70).

For the post-selected doublet we thus find that $\gamma \sim N$, which is in contrast to (4.132) as derived for the averaged doublet. The doublet strength α (4.70) can be explicitly taken into account by virtue of (4.97) to obtain

$$\gamma \approx \frac{eN(1-\alpha)}{8},\tag{4.136}$$

which eliminates the need for the numerical extraction of $\overline{\|\mathcal{V}\|^2}$. We still find a scaling $\gamma \sim N$ for a given α (and hence for a given desired localisation efficiency \mathcal{P}_H), which is a manifestation of the fact that the doublet strength α controls $\overline{\|\mathcal{V}\|^2}/\xi^2$ independently of N (as shown in Fig. 4.12). Equations (4.135), (4.136) imply that the tail for the post-selected doublet ensemble grows heavier with N than the tail of the averaged doublet, which is governed by Eq. (4.132). In the following section, we will further explore this scaling behaviour.

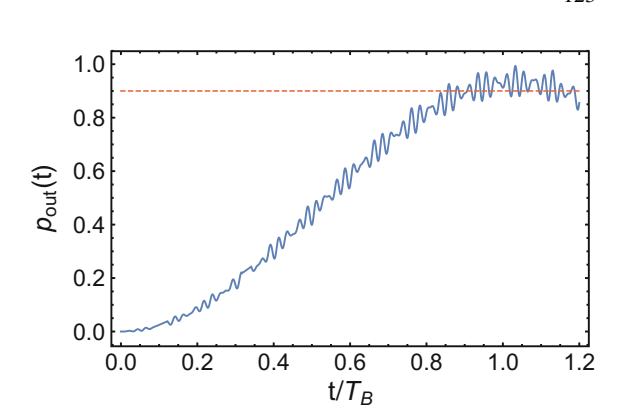
4.5.3 Scaling Properties

Although we now understand the statistics of the time scales for different dominant doublet ensembles, we still lack thorough insight in the statistics of the localisation efficiency \mathcal{P}_H . Because this efficiency requires a maximisation over a time interval (recall Sect. 4.4.2), it is completely unfeasible to obtain its distribution in either of the different dominant doublet ensembles. On the other hand, we show in this section that one can obtain implicit information about the localisation efficiency via the time scale statistics.

Scaling for the Post-Selected Dominant Doublet

As was already remarked by Eq. (4.73), whenever the transfer time $t^* < T_B$, we can be sure that $\mathcal{P}_H \geqslant 2\alpha - 1$. Therefore, in order to acquire information on the density of realisations that manifest efficient transfer, we must evaluate

Fig. 4.14 Probability $p_{\text{out}}(t)$ to find the excitation at the output site, for a single realisation of the system Hamiltonian (4.81). The value $2\alpha - 1$ is indicated by a dashed line. Even though the transfer time $t = 1.03T_B$ for this realisation, the efficiency condition $\mathcal{P}_H > 2\alpha - 1$, (4.74), is fulfilled. This figure was taken from Walschaers et al. (2015)



 $P(T_B/t^* > 1)$. However, this is a *lower bound* for the density of realisations for which $\mathcal{P}_H \geqslant 2\alpha - 1$: Whenever $t^* < T_B$ we can be sure that the the condition on the efficiency holds, but the opposite statement is not true. It is possible to find realisations where $\mathcal{P}_H \geqslant 2\alpha - 1$ and still $t^* > T_B$. This is typically the case when the maximum of $p_{\text{out}}(t)$, obtained at t^* , is somewhat larger than $2\alpha - 1$. In this case, $p_{\text{out}}(t)$ may already cross $2\alpha - 1$ before T_B , although the maximum is only reached at $t^* > T_B$. One such realisation is shown in Fig. 4.14.

To comprehend the scaling behaviour (when increasing the system size N) of the density of realisations with $\mathcal{P}_H \geqslant 2\alpha - 1$, we can use our above result for the probability density $P(T_B/t^*)$, since

$$P(\mathcal{P}_H > 2\alpha - 1) \geqslant P\left(\frac{T_B}{t^*} > 1\right) = \int_1^\infty \mathrm{d}x \ P\left(\frac{T_B}{t^*} = x\right). \tag{4.137}$$

The calculation of this quantity is straightforward and leads to interesting insights. Specifically, different types of questions will lead to different choices of modelling on which we can now shed light. The matter of scaling automatically relates to questions such as: Is there an optimal system size? Are there trade-offs between different parameters? These questions are particularly relevant in the biological context of Chap. 6, where evolution can optimise structures which offer an advantage, i.e. more efficient light harvesting in photosynthetic organisms. 20 We focus our attention on the scaling with the system size N. In the previous section we already indicated that, due to the many relations between different parameters, among which the system size, the apparent scaling properties can sometimes be misleading. One point of interest is that $\langle V \rangle$ depends strongly on the system size N. This is of course the case by construction, but one can equally well ask what happens when we fix a specific direct coupling V^* and try to enhance the transport.

²⁰Whether more efficient light harvesting is (or has ever been) evolutionarily beneficial (and to what extent) remains an open question. There is a chance that the answer to this question depends on the organism and even on its ecosystem.

Assuming that V is a stochastic variable chosen as described in Sect. 4.5.2, we can use the result from Eq. (4.135) and insert it into Eq. (4.137), to obtain

$$P(\mathcal{P}_H > 2\alpha - 1) \geqslant 1 - \frac{1}{\pi} \arctan\left(\frac{4\pi\xi^2}{\|\mathcal{V}\|^2 Ne} \left(1 - \frac{\|\mathcal{V}\|^2}{2\xi^2}\right)\right). \tag{4.138}$$

As we are interested in the scaling behaviour of the density of efficient (quantified by the condition $\mathcal{P}_H > 2\alpha - 1$) realisations in our ensemble, we can study this quantity in the limit where the number of sites N grows large (and the dominant doublet strength α is kept constant) to obtain:

$$P(\mathcal{P}_H > 2\alpha - 1) \geqslant P\left(\frac{T_B}{t^*} > 1\right) \approx 1 - \frac{4\xi^2}{\|\mathcal{V}\|^2 Ne} = 1 - \frac{8}{\pi e N(1 - \alpha)}.$$
 (4.139)

These larger systems sizes lead to a larger density of efficient realisations. This tempting conclusion should however be nuanced, since we consider T_B/t^* in a setup where both T_B and t^* are stochastic variables. The correct statement is therefore that large system sizes lead to a situation where fast tunnelling, mediated by the intermediate sites (the mechanism described by CAT Tomsovic and Ullmo 1994) is typically dominant over direct tunnelling. This implies a broad distribution with a very fat tail. However, this does not imply that necessarily t^* becomes very small, since we know from Sect. 4.5.2 that also V typically decreases rapidly for increasing N. In other words, the reason that T_B/t^* becomes large is not just that the transfer time t^* is typically short, but just as much that the reference time scale T_B becomes very large. In this sense one can say that the scaling behaviour is mainly due to the vanishing of the direct tunnelling from in to out, rather than the positive impact of the system size on the CAT-like process. To verify this argument, we must explicitly consider the scaling of the density of efficient realisations in the ensemble for fixed $V = V^*$.

Assuming that $V = V^*$ **is kept fixed** we thus expect a very different scaling behaviour with N, which can be derived from Eq. (4.116), with $V = V^*$. We find that, indeed, the scaling is given by

$$P(\mathcal{P}_{H} > 2\alpha - 1) \geqslant P\left(\frac{T_{B}}{t^{*}} > 1\right) = 1 - \frac{1}{\pi}\arctan\left(\frac{2V^{*}\xi\sqrt{N/2 - 1}}{\|\mathcal{V}\|^{2}}\left(1 - \frac{\|\mathcal{V}\|^{2}}{2\xi^{2}}\right)\right). \tag{4.140}$$

To study this expression, we again focus on the large N regime, which now results in

$$P\left(\frac{T_B}{t^*} > 1\right) \approx \frac{1}{2} + \frac{\|\overline{\mathcal{V}}\|^2}{\pi V^* \xi \sqrt{2N}} = \frac{1}{2} + \frac{(1-\alpha)\xi}{2V^* \sqrt{2N}}.$$
 (4.141)

This is clearly very different from the N-dependence obtained above, when V was considered a stochastic variable, chosen to be the weakest coupling in the system, respecting the in-out symmetry (4.47). In this case, V^* remains fixed and therefore we

find statistics of T_B/t^* which really reflects the behaviour of t^* , since $T_B = \pi/2V^*$ is completely independent of N. Noteworthy is that, whenever dominant doublet strength α and the parameter governing the typical coupling between intermediate sites ξ remain constant, an increase of N reduces the density of efficient realisations. In the limit $N \to \infty$, only $\sim 50\%$ of the realisations are efficient. This implies that a choice of V^* , ξ and α imposes an optimal system size N, encrypted in Eq. (4.140). A simple analysis shows that the optimal number of constituents in such a system is small ($N^{\rm opt} \approx 4$). However, in this regime simulations show deviations from our analytic prediction; remember that the Cauchy distribution was in principle obtained for $N \to \infty$.

Note that Eq. (4.141) does not only depend on the dominant doublet strength α , but also explicitly on ξ , which determines the RMS coupling between intermediate sites. We see that large values of ξ/V^* have a positive effect on the density of enhanced realisations. This implicitly tells us that the intermediate sites must be strongly coupled to each other the get efficient transfer. Notice that whenever ξ is large, $\|V\|^2$ will become larger too, since both quantities are bound to satisfy the constraint (4.97). Thus this result must be interpreted as follows:

For a given direct coupling between input and output, stronger couplings among intermediate sites and stronger couplings between bulk sites and the input/output lead to a higher density of efficient realisations.

Scaling for the Averaged Dominant Doublet

As shown in Eq. (4.75), no lower bound can be derived for \mathcal{P}_H as in the above case of the post-selected doublet. However, Eq. (4.75) also indicates that when $T_B/t^* > 1$, we find that $\mathcal{P}_H \approx {\alpha'}^2$. Even though this statement should rather be interpreted as \mathcal{P}_H contained in a small interval around ${\alpha'}^2$, we can still use T_B/t^* and its probability distribution $P(T_B/t^*)$ as an estimator for efficient excitation transfer.

V a stochastic variable allows to straightforwardly compute

$$P\left(\frac{T_B}{t^*} > 1\right) = \int_1^\infty \mathrm{d}x \, P\left(\frac{T_B}{t^*} = x\right). \tag{4.142}$$

When using (4.131), we find

$$P(\mathcal{P}_H \approx {\alpha'}^2) \geqslant P\left(\frac{T_B}{t^*} > 1\right) \approx 1 - \frac{1}{\pi} \arctan\left(\frac{2\pi\xi^2}{e\sqrt{N/2 - 1}N\chi^2}\left(1 - \frac{\chi^2}{2\xi^2}\right)\right).$$
(4.143)

A series expansion for large N yields the dominant scaling behaviour:

$$P(\mathcal{P}_H \approx {\alpha'}^2) \geqslant P\left(\frac{T_B}{t^*} > 1\right) \approx 1 - \frac{2\sqrt{2}\xi^2}{eN^{3/2}\chi^2} = 1 - \frac{16}{e\sqrt{N}\pi^3(1-{\alpha'})^2},$$
(4.144)

²¹Due to the centrosymmetry we only consider even numbers of sites N. Moreover, N=2 implies there are *no intermediate sites* and thus we obtain the benchmark system.

which is different from that obtained in (4.139), although it has similar characteristics. Also in this case the density of efficient realisations increases for growing N. The reasons are the same as for the post-selected doublet treated above, but the scaling with $\sim 1/\sqrt{N}$ results from a different scaling of the spectral shift statistics which determines t^* (as seen upon comparison of (4.132) with (4.136)).

When $V = V^*$ is kept fixed we can again evaluate (4.142) as an estimate for the density of efficient realisation, i.e. those with $\mathcal{P}_H \geqslant \alpha'^2$. Straightforward integration using Eq. (4.116) in combination with (4.92) and (4.93) leads to

$$P(\mathcal{P}_{H} \approx {\alpha'}^{2}) \geqslant 1 - \frac{1}{\pi} \arctan\left(\frac{V^{*}}{\xi(1 - \alpha')^{2}} \left(\frac{2}{\pi}\right)^{3} \left(\frac{N}{2} - 1\right) \left(1 - \frac{\pi^{3}}{8} \frac{(1 - \alpha')^{2}}{N - 2}\right)\right). \tag{4.145}$$

The limiting behaviour of this estimate for $P(\mathcal{P}_H \approx {\alpha'}^2)$ as $N \to \infty$ can be found via a series expansion:

$$P(\mathcal{P}_H \approx \alpha'^2) \geqslant P\left(\frac{T_B}{t^*} > 1\right) \approx \frac{1}{2} + \frac{\xi(1 - \alpha')^2 \pi^2}{4NV^*}.$$
 (4.146)

This implies, again, a behaviour which is qualitatively similar to the post-selected doublet ensemble, in the sense that increasing N has a negative impact on the density of efficient realisations. Indeed, we see that in the limit $N \to \infty$, $P(T_B/t^* > 1) \to 1/2$. On the other hand, we here notice the scaling $\sim 1/N$, i.e. a more drastic dependence on N as compared to (4.141).

Summary and Discussion

Ultimately we must conclude that both types (4.70) and (4.71) of dominant doublets lead to results which are intuitively similar, although the detailed scaling behaviour of the density of efficient realisations as N grows is very different. Indeed, we obtain that this density, which we always infer from $P(T_B/t^* > 1)$, is governed by the following scaling with the system size N: Assuming that V is stochastic we find²²

$$P\left(\frac{T_B}{t^*} > 1\right) \sim 1 - \text{cte}\frac{1}{N}$$
 (post-selected doublet), (4.147)

$$P\left(\frac{T_B}{t^*} > 1\right) \sim 1 - \text{cte}\frac{1}{\sqrt{N}}$$
 (averaged doublet), (4.148)

whereas for the fixed input-output coupling $V = V^*$, we obtain

$$P\left(\frac{T_B}{t^*} > 1\right) \sim \frac{1}{2} + \text{cte}\frac{1}{\sqrt{N}}$$
 (post-selected doublet), (4.149)

$$P\left(\frac{T_B}{t^*} > 1\right) \sim \frac{1}{2} + \text{cte}\frac{1}{N}$$
 (averaged doublet). (4.150)

²²Note that we use "cte" to indicate an unspecified constant.

Remember that our goal is to statistically control fast and efficient quantum transport in the centrosymmetric networks we study. Since expressions (4.147)–(4.150) all function as estimates for the density of efficient realisations in an ensemble of centrosymmetric networks, subject to specific constraints, this goal translates to $P(T_B/t^* > 1) \approx 1$. Even though, in this sense, we always observe a positive influence of the system size for stochastic V, and always observe a negative impact of growing network size with fixed $V = V^*$, we can now clearly conclude that the post-selected doublet is the better design principle: When $N \to \infty$, the density of efficient realisations in ensembles with a post-selected doublet increases faster for stochastic V (comparing (4.147) and (4.148)), and it decreases slower when $V = V^*$ is kept fixed (comparing (4.149) and (4.150)).

We close this discussion with a more physical interpretation for the different types of scaling which we derived: Where V is a stochastic variable, scaling with N boils down to considering a system with increasing number of constituents in a way such that the density remains constant and thus the volume changes. In the case where $V = V^*$ is fixed, we keep the volume of the system constant, but add additional sites, thus increasing the density. Thus, there is also a clear physical difference between the two types of assumptions on V, which immediately helps us understand why there is such a grave difference between the scaling properties in both regimes: For a given density of sites in the system, increasing the volume—and hence the distance between input and output sites—leads to a larger fraction of the transport being mediated through the intermediate sites. In the opposite regime, where the volume of the system—and therefore also the distance between input and output sites—is constant, it is favourable to have very low density of sites to guarantee a high density of realisations where the transport is mediated by the intermediate sites. The latter result may seem counter-intuitive, but it relates to the fact that we need to make (4.86) sufficiently small to fulfil the dominant doublet condition, and (4.87) as large as possible to achieve enhancement in transfer time. Ultimately, these are competing demands. Specifically when $V = V^*$ (and therefore also the benchmark time T_R) is fixed, large densities of sites make it harder to fulfil both demands (as we ultimately rigorously showed in this section).²³

4.5.4 Numerics

In this section, we present numerical material to validate the model developed above, as well as the quantitative predictions which we derived from it. Although our above results were obtained analytically, they are subject to many approximations and one of the main questions is whether the RMT results, which are in principle derived for the thermodynamic limit $N \to \infty$, hold in situations where $N \sim 10^{.24}$ Of course,

²³Note that large densities of sites translate in many contributing energy levels in the perturbative series.

²⁴Relevant network sizes in photosynthesis are of the order $N \sim 10$ (Blankenship 2002).

the fact that the CAT mechanism as described in Sect. 4.5 essentially depends on local spectral properties, such as on the mean-level spacing Δ at a specific point in the spectrum (the vicinity of $E \pm V$), does suggest that the system size is ultimately not of great importance, at least not at leading order.

Additionally, several of the derivations in Sect. 4.5.1 were slightly unorthodox and the results obtained from them must be numerically verified.

Structure of the Simulations

At the core of the numerical calculations lies the ensemble of random matrices as described by the GOE, with different design principles imposed. To construct such matrices, a set of independent components of the matrix is sampled according to the basic rule (3.26) $H_{ij} \sim \text{Normal}\left(0, \frac{(1+\delta_{ij})\xi^2}{N}\right)$, with $H_{ij} = H_{ji}$. In case we demand *centrosymmetry*, this rule is extended to (4.61):

$$H_{ij} \sim \begin{cases} \text{Normal}\left(0, \frac{2\xi^2}{N}\right) & \text{if } i = j \text{ or } i = N - j + 1 \\ \text{Normal}\left(0, \frac{\xi^2}{N}\right) & \text{else,} \end{cases}$$

$$(4.61)$$

while explicitly fixing $H_{i,j} = H_{i,N-j+1} = H_{N-i+1,j} = H_{N-i+1,N-j+1}$.

For the averaged dominant doublet, there is again an additional rule (assuming that for simplicity $|\text{in}\rangle = |e_1\rangle$):

$$H_{ij} \sim \begin{cases} \text{Normal}\left(0, \frac{2\xi^2}{N}\right) & \text{if } i = j, \text{ or } i = N - j + 1, \\ \text{Normal}\left(0, \frac{\chi^2}{N}\right) & \text{if } i = 1 \text{ and } j \neq 1, \\ \text{Normal}\left(0, \frac{\xi^2}{N}\right) & \text{else,} \end{cases}$$

$$(4.151)$$

while again making sure that $H_{i,j} = H_{i,N-j+1} = H_{N-i+1,j} = H_{N-i+1,N-j+1}$. The structures of these different possible choices of sampled Hamiltonians are visualised in Fig. 4.15, to get an accurate idea of which components are sampled independently. The triangular structures in Fig. 4.15 can subsequently be mirrored along the relevant symmetry axes to acquire a matrix with the correct symmetry properties.

The post-selected dominant doublet cannot be grasped as easily as the averaged dominant doublet. More specifically, it generates a type of correlations within the centro-symmetric triangle. As the name suggests, we cannot generate these structures, but we have to post-select them after sampling centrosymmetric matrices. This post-selection procedure is straightforward, but highly inefficient: Each realisation of a centrosymmetric H must be diagonalised and its eigenvectors $|\eta_i\rangle$ checked for the presence of a dominant doublet. We do this by constructing $|+\rangle$ and $|-\rangle$ as prescribed by Eq. (4.53), and subsequently calculate $|\langle \eta_i, + \rangle|^2$ and $|\langle \eta_i, - \rangle|^2$. In the case of a dominant doublet, we must find an eigenvector $|\eta^+\rangle$ for $|+\rangle$ and another one, $|\eta^-\rangle$, for $|-\rangle$, such that both these overlaps are larger than α . The larger we make the system size N or the doublet strength α , the more unlikely to find such a match. As

4.5 Statistical Control 129

$$H = \left(\begin{array}{c} \\ \\ \end{array}\right) H = \left(\begin{array}{c} \\ \\ \end{array}\right)$$

Fig. 4.15 The structures of the random Hamiltonians subject to different constraints. A highlighted area indicates a set of independent, identically distributed random variables. On the leftmost panel, the structure of the unconstrained GOE is shown, where half of the elements are sampled from a normal distribution. In the middle, the structure for a centrosymmetric Hamiltonian is shown, which is clearly different from the right panel, showing the structure for the averaged dominant doublet, where the separated rectangle indicates that the components in this area are governed by different statistics (also given by a Gaussian distribution, but with a different variance). The other components of the matrix are obtained from imposing symmetry and—if applicable—centrosymmetry conditions

the method to identify the dominant doublet already provides us with $|\eta^{\pm}\rangle$, we can also straightforwardly obtain E^{\pm} .

Once the correct sampling procedure of Hamiltonians is implemented, we calculate $p_{\text{out}}(t)$, with the help of the spectral decomposition of the Hamiltonian and Eq. (4.4). Because $p_{\text{out}}(t)$ is formally defined as a function of t, we can calculate \mathcal{P}_H by means of a maximisation algorithm, 25 and \mathcal{P}_H is obtained via numerical integration. This may provide us with statistics of the efficiencies, but it does not allow us to directly study the statistics of the transfer times.

The latter can be understood in various ways: The most direct route to obtain them is by extraction from the maximisation algorithm, where we assume that t^* is also the time t' at which $p_{\text{out}}(t=t')=\mathcal{P}_H$. One issue is that such a procedure will not allow to acquire information on transfer times which are slower than T_B . Therefore t' is actually obtained by propagation of the excitation over a longer time, here $1.7\,T_B$. Therefore, it is more precise to identify t' with the time for which $p_{\text{out}}(t=t')=\mathcal{P}'_H$, where \mathcal{P}'_H is the efficiency obtained for times $t\in[0,1.7\,T_B)$.

For the dominant doublet systems, an alternative method, closer to the analytical derivation, is to extract the statistics directly from the spectral properties of the system. We noted above that our method of finding the dominant doublet states also allows us to obtain E^{\pm} , and, therefore, we can directly extract T_B/t^* as described in Eq. (4.73). Of course, following the analytical derivation, the transfer time estimate t' appears to be equivalent to estimates obtained from E^{\pm} . As explained in the next section, and indicated in Fig. 4.17, this intuition is false.

Numerical Result for Transfer Time Scales

We now compare the analytical predictions for the different types of dominant doublets, as described in Sect. 4.5.2, to numerical simulations.

²⁵We here employ either the algorithm which was also used in Scholak et al. (2011a), Scholak (2011) or the NMaximize routine in Mathematica.

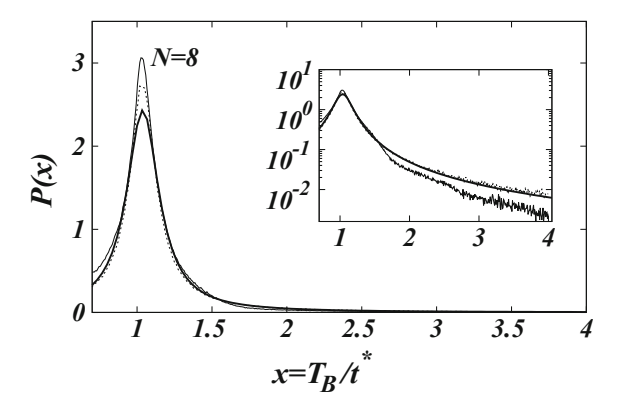


Fig. 4.16 Probability density of the transfer times T_B/t^* for the post-selected dominant doublet, as predicted by Eq. (4.135) (thick solid line), together with the numerical estimate obtained from t' (thin solid line, see main text) or from E^{\pm} (thin dashed line), according to Eq. (4.73). The results are for doublet strength $\alpha = 0.95$, RMS coupling ξ/\sqrt{N} between intermediate sites characterised by $\xi = 2$ and network size N = 8. This figure was taken from Walschaers et al. (2015)

Let us start by considering whether the t', for which $p_{\text{out}}(t=t') = \mathcal{P}'_H$, is really the correct estimate for t^* . For the *post-selected dominant doublet*, we show both numerical results in Fig. 4.16, together with the analytics of Eq. (4.135). We observe that there is no perfect agreement between analytics and numerics, but we clearly see from the inset that the distribution of time scales as obtained from E^\pm , using Eq. (4.73), is closer to the analytical predictions than the results obtained from t'. More specifically, it seems that the t' method systematically overestimates realisations with $T_B/t^* \approx 1$ and underestimates the weight of the tail, which is formed by realisations where $T_B/t^* \gg 1$.

It is essential that we now understand whether such a mismatch implies that there is a flaw in our analytics, or whether this simply implies that t' is not a good estimate for the first passage time. It turns out that the latter is the correct conclusion. This can be seen when we zoom in on a randomly sampled realisation where Eq. (4.73) gives a very different estimate than t', as for example is the case in Fig. 4.17. We notice that the dominant oscillatory behaviour is the one which is expected from a dominant doublet structure. The garnish by oscillations of much higher frequency is generated by the coupling to the intermediate sites. Their influence is indeed small, and therefore their explicit contribution was ignored in our analytical calculations above. Nevertheless, these high frequency oscillations do imply that the dynamics is not exactly periodic, but rather quasi-periodic. Although the theoretical prediction for the first passage time t^* indeed points towards the first maximum of the dominant oscillation, as clearly pointed out in Fig. 4.17, the actual maximum within the relevant time window $[0, 1.7 T_B)$ may be shifted to a later point in time. Indeed, we see that here t' predicts that the maximum is reached after T_B . Although, by all reasonable quantifiers, this is a very efficient realisation, it is not recognised as such by the quantity t'. Exactly this potential recurrence of the desired population localisation at

4.5 Statistical Control 131

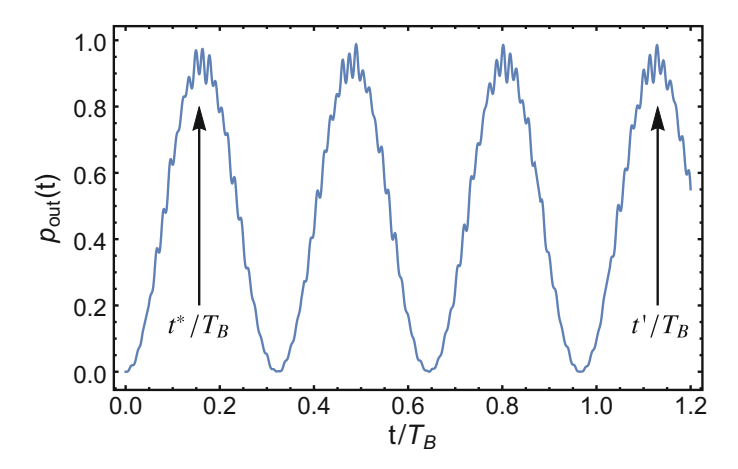


Fig. 4.17 Output site population probability $p_{\text{out}}(t)$ for a single realisation of the Hamiltonian (4.81). Spectral estimate (4.73) for the first-passage time t^* is compared to t', for which $p_{\text{out}}(t=t')=\mathcal{P}_H'$ obtained over $[0,1.7\,T_B)$ (see main text p. 129). There are multiple strong population recurrences at the output site within $[0,T_R)$. High frequency oscillations show that the dynamics is quasi periodic rather than periodic. This figure was taken from Walschaers et al. (2015)

the output site, within the time window on which \mathcal{D}'_H is defined, leads t' to strongly misjudge the actual first passage time t^* , especially when t^* is very small and thus when $T_B/t^*\gg 1$. Therefore, we conclude that the spectral estimate, which uses E^\pm and Eq. (4.73), is the most accurate numerical method to extract the transfer time distribution. Indeed, the spectral estimate also produces the agreement with the numerically exact result.

Although it is hard to generate systems with dominant doublet via post-selection, this procedure is feasible up to system sizes N=14, given several thousands of CPU hours (on an Octa-core Intel Xeon processors E5-2670 (Sandy Bridge) architecture²⁶) worth of sampling. Due to the difficult sampling, it is hard to verify whether the good agreement, as presented in Fig. 4.16, between theoretical prediction of in Eq. (4.135) and numerics, holds for larger systems. In Fig. 4.18 we scan over the system sizes which are within reach and show that, indeed, theory and simulations match well, independently of N. The failure to correctly capture the tail, when using t' as an estimate for t^* , is observed for all four choices of N. We already see a considerable difference between the different system sizes when considering the peak of the curve around $T_B = t^*$. A well pronounced decrease thereof while increasing N is a consequence of the linear scaling of γ , as given in Eq. (4.135), with the system size.

Once we have established the good agreement between our theory, Eq. (4.135), and the numerical results for T_B/t^* , on the basis of the spectral estimate for t^* as given by Eq. (4.73), we can move on to study the *averaged dominant doublet*. We note that

²⁶Clock speed of 2.6 GHz, 8x256 KB of level 2 cache and 20 MB level 3 cache. All demanding computations, i.e. those that cannot be done on a normal laptop, were done on the bwGRiD.

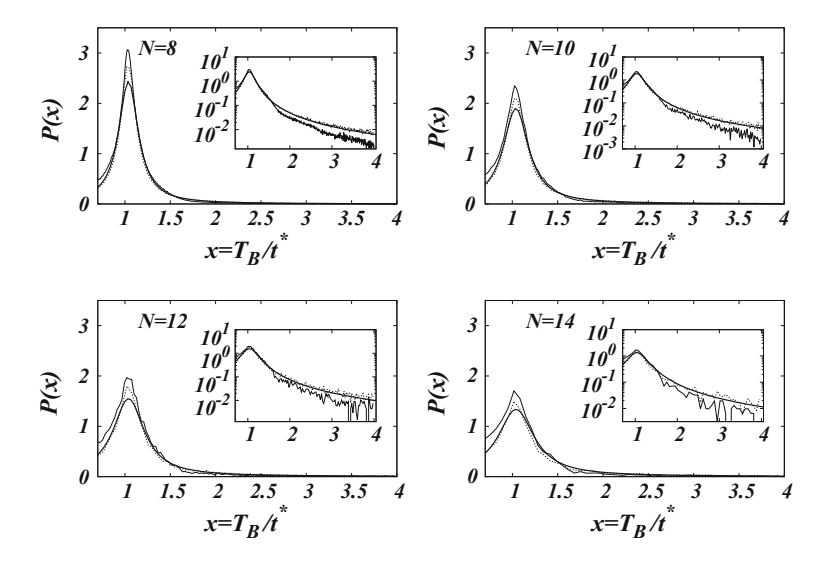


Fig. 4.18 Histograms of the simulated inverse transfer times T_B/t^* (thin solid lines) across fully connected random networks of variable size N, and of $|E^+ - E^-|/2V$ (dashed lines), together with the theoretical distribution (4.135) (thick solid line). The parameters $\xi = 2$, characterising the RMS coupling ξ/\sqrt{N} between intermediate sites and dominant doublet strength $\alpha = 0.95$ are kept fixed for all realisations. The variance of the coupling between input/output site and the intermediate sites is given by $||V||^2/N$, where, for each value of N, $||V||^2 \approx 0.31$ is extracted from the simulations (which is to be expected from (4.97)). The numerical simulations only consider a time window $[0, 1.7 \, T_B)$. Therefore the minimum value of the inverse transfer time is given by $T_B/t^* = (1.7)^{-1}$. The inset stresses the agreement between the theoretically predicted algebraic tail (thick solid line) and the $|E^+ - E^-|/2V$ histogram (dashed line). The histogram for T_B/t^* (thin solid line) slightly deviates from the other two curves because the quasi-periodicity of the dynamics suppresses the tail of the distribution (see text and Fig. 4.17). This figure was taken from Walschaers et al. (2015)

here we generate systems using Eq. (4.151), where χ is chosen such that Eq. (4.93) should lead to $\alpha'=0.95$. This predicted value for α' is typically not the value which is extracted from numerics; we usually obtain $\langle \min_{\pm} | \langle \eta^{\pm}, \pm \rangle |^2 \rangle_{\text{realisations}} \approx 0.92$. Although this difference seems small, inserting it in Eq. (4.132) leads to a significantly different result. In what follows, we choose to insert the numerically obtained α' , rather than the theoretically predicted one in Eq. (4.132), to get the analytical curves given by Eq. (4.131).

To begin with, Eqs. (4.132) and (4.136) predict not only different scaling laws with N, but also a different weight of the tail of the distribution. Most notably, the post-selected dominant doublet ensemble is expected to produce considerably more realisations with enhanced transport than the averaged dominant doublet ensemble. This prediction is indeed verified conclusively by Fig. 4.19, where we consider rather small systems with N=8. The difference is expected to become only more pronounced for increasing N. The histogram in Fig. 4.19 is cut off at $T_B/t^*=5$ since

4.5 Statistical Control 133

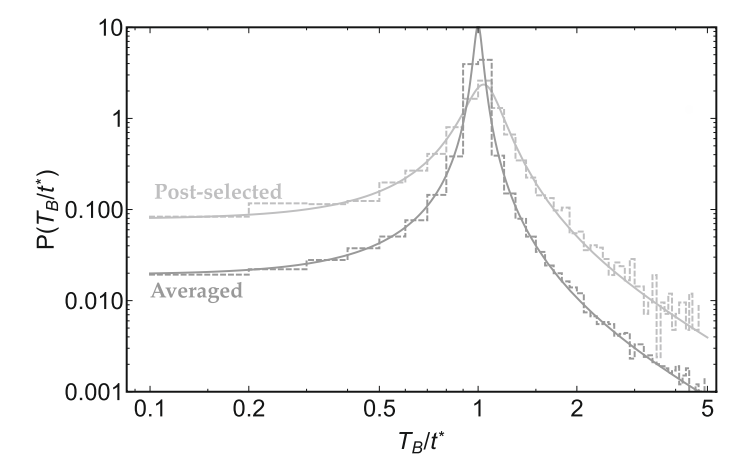


Fig. 4.19 Histograms (dashed) and their theoretical predictions (solid) for the statistics of T_B/t^* . The averaged dominant doublet ensemble (darker grey) is compared to the post-selected ensemble (lighter grey) for a system size of N=8. The other control parameters are the RMS interaction between intermediate sites ξ/\sqrt{N} , with $\xi=2$, and the dominant doublet strengths $\alpha=0.95$ (post-selected) and $\alpha'=0.95$ (averaged). The analytical curve, Eq. (4.131), (4.132), for the averaged dominant doublet ensemble is obtained by inserting $\langle \min_{\pm} \left| \left\langle \eta^{\pm}, \pm \right\rangle \right|^2 \rangle_{\text{realisations}} \approx 0.92$ rather than the control parameter α' itself

there is not enough statistics to go beyond; as commonly the case for a power-law distribution, the accumulation of statistics in the tails is a challenging task.

Finally, the averaged dominant doublet does provide the possibility to probe larger system sizes, results of which are shown in Fig. 4.20. Although there are 30 sites more in the one system than in the other, the statistics is remarkably similar. This turns out to be a consequence of Eq. (4.132) which predicts a scaling $\gamma \sim \sqrt{N}$, and this behaviour is nicely visualised by Fig. 4.20. Even for N=50, the weight of the tail for the averaged dominant doublet ensemble is still smaller than that of the tail of the post-selected dominant doublet ensemble in Fig. 4.19, which is obtained for only N=8 sites. This again strengthens the conclusion that the post-selected dominant doublet ensemble is far superior to the averaged dominant doublet ensemble: For network ensembles with a post-selected dominant doublet structure the density of realisations where the transport is enhanced, i.e. where $T_B/t^* > 1$, is significantly higher than in networks with an averaged dominant doublet structure contain five times more sites.

Numerical Results for the Efficiencies

Even though we have presented simulation results that indicate very satisfactory agreement between analytical derivations of transfer times statistics and their numerical counterparts, the main goal of this chapter is to understand *efficient* transport; therefore a study of efficiency statistics is required. We note that Figs. 4.6, 4.7, 4.8 and 4.10 were already produced using the simulation techniques described earlier in

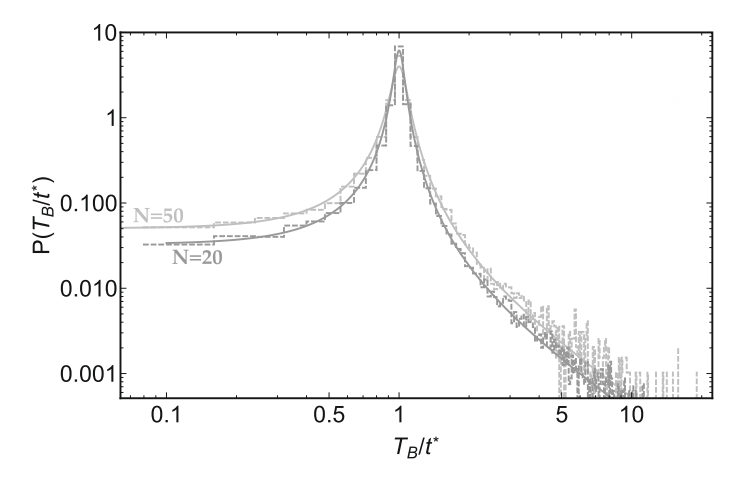


Fig. 4.20 Histograms (dashed) and their theoretical predictions (solid lines) for the statistics of T_B/t^* . Different system sizes, N=20 (darker grey) and N=50 (lighter grey), are compared for the averaged dominant doublet ensemble. The analytical curve for the averaged dominant doublet ensemble, Eq. (4.131), (4.132), is obtained by inserting $\langle \min_{\pm} | \langle \eta^{\pm}, \pm \rangle |^2 \rangle_{\text{realisations}} \approx 0.92$ rather than the control parameter α' itself

this section. Such scatterplots are, however, not very enlightening when one wishes to understand the density of realisations, for which histograms are more feasible. We choose to focus our attention on \mathcal{P}_H .

At first instance, we compare the efficiency distribution of the plain random GOE ensemble to ensembles with design principles built in: GOE with centrosymmetry, and centrosymmetric GOE with post-selection of the dominant doublet. Figure 4.21 shows the dramatic impact of imposing these design principles. We notice, first of all, that the centrosymmetry is indeed beneficial for excitation transfer, since it broadens the distribution and pushes it towards higher efficiencies. On the other hand, the centrosymmetry alone clearly is insufficient, as was also noted in Sect. 4.4. It becomes impressively clear in Fig. 4.21 that, as was predicted in Sects. 4.4 and 4.5.3, the presence of a dominant doublet pushes and concentrates the entire distribution to the range of high efficiencies where $\mathcal{P}_H > 2\alpha - 1$. We notice that this effect is seen for all numerically tractable system sizes N in Fig. 4.21. Although the distributions without dominant doublet are subject to scaling effects, the results with dominant doublet remain remarkably similar.

In addition, it is natural to wonder whether there is a detectable difference between the dominant doublet as obtained from post-selection and the averaged dominant doublet. Such a comparison is made in Fig. 4.22 and leads to a surprisingly counterintuitive result: Although we have clearly verified that, on the matter of time scales, the dominant doublet as obtained by post-selection is superior to the averaged dominant doublet, for the latter the distribution of transfer efficiencies is peaked more strongly around $\mathcal{P}_H \approx 1$. A potential explanation is that the time scale statistics only allows conclusions such as the ones presented in Sect. 4.5.3, which are, as was stressed by

4.5 Statistical Control 135

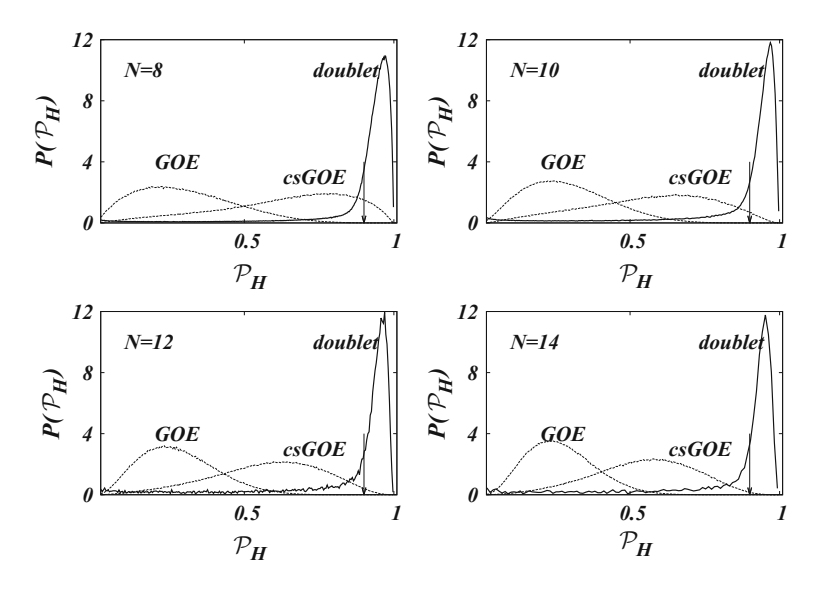


Fig. 4.21 Distribution of the transfer efficiency \mathcal{P}_H , Eq. (4.6), for variable network sizes N and three Hamiltonian ensembles: GOE, GOE with centrosymmetry, and GOE with centrosymmetry and post-selected dominant doublet. The transfer efficiency $\mathcal{P}_H = 2\alpha - 1$ is indicated by the arrow. The control parameters in (4.61), (4.70) are set to $\xi = 2$, thus characterising the RMS coupling strength between the intermediate sites ξ/\sqrt{N} , and dominant doublet strength $\alpha = 0.95$. This figure was taken from Walschaers et al. (2015)

Fig. 4.14, only lower bounds on the density of realisations with $\mathcal{P}_H > 2\alpha - 1$. Or, more plastically, the time scale statistics provides us only with a lower bound on the integral of the distribution between the point indicated by the arrow in Fig. 4.21 and the maximal value of \mathcal{P}_H . Neither of both distributions in Fig. 4.22 is in violation with these results. The reason for this unexpectedly strong peak in the efficiency distribution of the averaged doublet remains unclear, but we do observe that there seems to be a trade-of between the density of extremely fast realisations and the density of extremely efficient realisations. A similar result is also found in the scattering approach to similar systems in Sect. 5.4.

A final test that remains to be conducted is an explicit study of the scaling behaviour of the density of efficient realisations for increasing N, as derived in Sect. 4.5.3. Focussing on the post-selected dominant doublet, we can easily obtain an estimate for the density of efficient realisations: One simply counts the number of realisations with $\mathcal{P}_H > 2\alpha - 1$. Figure 4.23 shows clearly that, indeed, the prediction of Sect. 4.5.3, based on time scale statistics, provides a lower bound to the actual density of efficient realisations. Therefore, we acquired some analytical, predictive power for the efficiency statistics, deduced from the time scale statistics. We

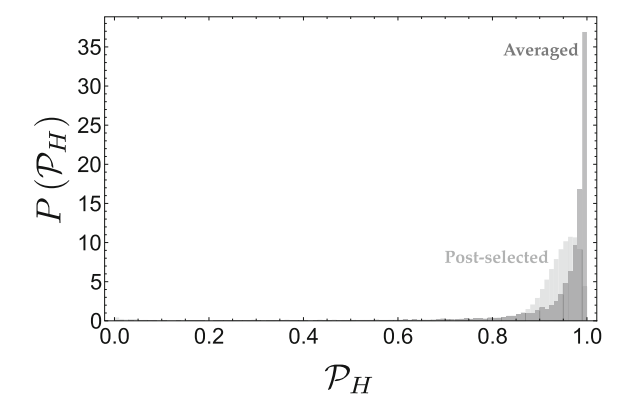


Fig. 4.22 Distribution of the transfer efficiency \mathcal{P}_H , Eq. (4.6), for two Hamiltonian ensembles: the averaged dominant doublet ensemble (darker grey) and the post-selected dominant doublet ensemble (lighter grey). The control parameters in (4.61), (4.70), (4.71) are the dominant doublet strengths $\alpha = 0.95$, $\alpha' = 0.95$, the system size N = 8 and the energy scale $\xi = 2$, which together determine the RMS coupling ξ/\sqrt{N} between intermediate sites

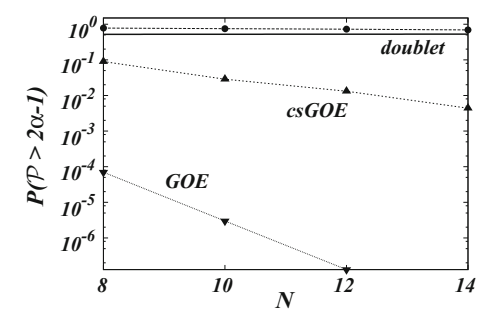


Fig. 4.23 Density $P(\mathcal{P}_H > 2\alpha - 1)$ of efficient network realisations, as a function of the network size N, for three different ensembles (GOE, GOE with centrosymmetry, GOE with centrosymmetry and post-selected dominant doublet). The theoretical curve for $P(T_B/t^* > 1)$ (solid line), Eq. (4.138), defines a lower bound to the dominant doublet ensemble, as expected (see text). The GOE curve is cut off at N=12, since it takes too long to sample a sufficient amount of data for larger values of N. The control parameters in (4.61), (4.70) are the dominant doublet strength $\alpha=0.95$ and energy scale $\xi=2$, which determines the RMS coupling ξ/\sqrt{N} between intermediate sites. This figure was taken from Walschaers et al. (2015)

also depict the rather dramatic scaling of this density for the ensembles lacking the dominant doublet all together: The GOE and the GOE with centrosymmetry imposed on it. This figure clearly shows the enormous advantage provided by the dominant doublet constraint, and concludes our set of numerical checks.

4.6 Summary and Outlook

In this chapter we treated quantum transport in closed finite systems with constraints, which were modelled by adopting network terminology. Our main goal throughout this chapter was to transfer a single excitation from an input site to an output site (a setting which chemists would refer to as donor and acceptor May and Kühn 2000). We aim for the process to be both fast, compared to a relevant benchmark time scale, and efficient, in the sense that the excitation is transferred with high probability to the output site. By studying highly symmetric, analytically solvable network structures, we explored the fundamental role played by symmetry. However, such well-controlled, perfectly engineered systems are not the systems we are ultimately interested in, since they lack any sense of robustness and do not manifest any disorder —which any realistic system would do. Hence we diverted attention to random networks, using random matrix theory.

It quickly becomes clear that fully random networks, as modelled by the Gaussian orthogonal ensemble, perform sub-optimally. Although the transport times can be made fast, we completely lack the efficiency which we strive for, as shown in Figs. 4.6 and 4.21. To exploit the robustness of random systems and some of the engineering advantages of regular networks, we introduced the concept of *design principles*: Preferentially minimalistic and coarse grained constraints imposed upon the systems under consideration to enhance their ability to transfer excitations from a given input site to a given output site. This leads us really into the realm of complex systems, since these structures are on the intersection between order and chaos, neither regular, nor fully disordered.

The first design principle which we introduced was *centrosymmery*, a type of reflection symmetry which is manifested on the structure of the Hamiltonian. Crucial is that this symmetry also connects the input and output state vectors to one another. It seems that this system leads to an effect which is very similar to coherent backscattering (Wolf and Maret 1985), but which occurs in forward direction, see (4.64). The exact reason for the positive influence of the centrosymmetry is not fully known, although it is clear from Fig. 4.21 that it is a beneficial design principle.

Potentially the centrosymmetry mainly serves to facilitate²⁷ the manifestation of the next design principle: the presence of a *dominant doublet*. The key idea of this requirement is that the transport is dominated by two eigenstates, but that these are effectively assisted by the presence of the other energy levels, i.e. those describing the energetics of the intermediate sites. We introduced two different ways of imposing this constraint on the system, post-selection and a separation of energy scales. The former method generates the *post-selected dominant doublet ensemble*, whereas the latter can only impose a constraint on the average over all realisations, hence it is baptised the *averaged dominant doublet ensemble*. The idea of the dominant doublet is based on the theory of chaos assisted tunnelling, where one implicitly considers the

 $^{^{27}}$ There is a much higher density of dominant doublet realisations in the centrosymmetric GOE than in the standard GOE.

averaged dominant doublet ensemble (Dembowski et al. 2000; Leyvraz and Ullmo 1996; Steck et al. 2001; Tomsovic 1998; Tomsovic and Ullmo 1994; Zakrzewski et al. 1998).

Once the network structures are designed, we arrive at the central philosophy of our work, which relies on letting go the notion of deterministic enhancement of the transport. Rather than perfectly controlling—or engineering—systems, we introduce a mechanism based on statistical control. Instead of manipulating the expectation value of a physical observable, we control its statistical fluctuations. We elaborated extensively on the analytically obtained statistics of the transfer times for both dominant doublet ensembles, contained in Eq. (4.131) for the averaged ensemble, and in Eq. (4.135) for the post-selected ensemble. The obtained distribution is a Cauchy (or Lorenzian) distribution, its parameters depend on the doublet strength α (4.70) or α' (4.71), or can equivalently be controlled by the density of states for the bulk sites and the average coupling between the bulk and the input/output site. Crucial is that this distribution has an algebraic tail—which thus does not decay exponentially. This implies that realisations which are *much* faster than the benchmark time scales are abundant.

Moreover, in Sect. 4.5.3 we carefully study the scaling of the density of these efficient realisations with the system size, where we conclude that increasing the system size such that the density is kept constant leads to a stronger enhancement by the proposed mechanism. When the system size is increased such that also the density of sites increases, and thus the total volume of the system remains constant, we tend to find a negative influence on excitation transfer. Remarkably, there is a clear difference between the averaged and the post-selected ensemble: The latter exhibits a clearly heavier tail, which also shows a different scaling with the system size. The post-selected dominant doublet ensemble therefore give rise to a much higher density of very fast realisations.

We verified all these findings by comparison to numerics, which was extensively analysed. Analytically we only have indirect predictions for the statistics of the efficiencies themselves, but we manage to extract their histograms from numerics. This provides a striking proof, see Fig. 4.21, that the introduction of the dominant doublet design principle has a dramatic impact on the efficiency distribution. A surprising result is shown in Fig. 4.22, where it becomes clear that the averaged dominant doublet ensemble leads to higher efficiencies than the post-selected ensemble. This difference falls outside of what can be explained by the presented analytical results, but it suggests a trade-off between efficiency and speed-up of the excitation transfer.

The results presented in this chapter were mainly built on previous works on quantum transport in disordered systems (Scholak 2011; Scholak et al. 2010, 2011a, b, c; Zech 2013; Zech et al. 2013, 2014), and on results from the field of quantum chaos, more specifically chaos assisted tunnelling (Dembowski et al. 2000; Leyvraz and Ullmo 1996; Steck et al. 2001; Tomsovic and Ullmo 1994; Zakrzewski et al. 1998). Even though this is a rather extensive legacy to serve as a foundation, this work is in many ways rather minimalistic; one might consider our model as the simplest mechanism which consists of an active backbone structure and a rather passive assisting structure. In chaos assisted tunnelling, one would coin these two parts the *regu*-

lar islands and the *chaotic sea*. However, our abstract statistical model allows for applications outside of the realm of standard quantum chaology.

The idea of backbone structures carrying the excitation (or, in chemistry and in AMO²⁸ terminology, "population"), while additional constituents drastically impact the spectral properties of the system, without actually hosting the excitation at any relevant point in time, pops up in several recent works. However, one often encounters network structures which have more complicated backbone structures (Mostarda et al. 2013) than our dominant doublet, which with its two sites can be considered as the most simplistic model of its kind. We suspect that these structures describe a natural extension of our statistical model, much in the same way as resonance assisted tunnelling extends the framework of chaos assisted tunnelling (Brodier et al. 2002).

Although both crucial and powerful, the dominant doublet is a somewhat straightforward design principle to impose, in the sense that its presence clearly leads to a well understood enhancement of transport. Far less clear is why centrosymmetry (or even only the tendency to centrosymmetry Zech 2013, Zech et al. 2013, 2014) is beneficial for the transfer efficiency. What makes it more intriguing is that such a symmetry is encountered so often in various contexts of enhanced transport, going from driven quantum walks (Hamilton et al. 2014), over embedded ensembles (Ortega et al. 2015),²⁹ to currents in the non-equilibrium steady state as discussed in Chap. 9 of this dissertation. A possible line of thought to explain the fruitfulness of such builtin reflection symmetries in the context of excitation transfer, is to make a connection to time reversal. Currently, a very exciting field of research in wave dynamics (both linear and non-linear) rests upon the idea that time reversal can be used for focusing (Chabchoub and Fink 2014; Frazier et al. 2013; Lerosey et al. 2007). Essentially the phenomenon which is observed in the centrosymmetric networks is exactly such a focussing effect, and, although there is clearly no equivalence in the mathematical sense, the underlying physical intuition behind the focussing by means of "spatial reflection" may be very similar to the essence of focussing exploiting "temporal reflection".

A final, but important prospect lies in the concept of statistical control and disorder enhanced transport. As will become clear in Chap. 6, we mainly develop this mechanism for its potential relevance to describe quantum effects in biology. Nevertheless, the notion of a complex network of connected quantum states, on which an excitation roams around, is from a structural point of view one of the most generic settings which one can describe in quantum transport theory. One way or the other, the language and model exploited here can be adjusted to facilitate almost any type of system.³⁰ In principle, one might therefore suggest that our modelling could also find applications in quantum computing. Given the extremely clean and controlled setting in which quantum information theory is usually treated, this may sound coun-

²⁸Common acronym to denote the community studying atomic, molecular, and optical physics.

²⁹This provides a natural connection to the random matrix theory of many-particle systems.

 $^{^{30}}$ Whether the proposed mechanism can also be implemented in such systems is of course a very different question.

terintuitive. However, a complex systems approach will be inevitable when quantum information processors or quantum communication networks are scaled up. Disorder- and noise induced effects are ubiquitous in large systems, hence their understanding is indispensable.

Although quantum transport and quantum information seem two extremes, the former tending more towards condensed matter physics or physical chemistry, the latter affiliated to mathematics and informatics, they actually are intertwined at some points. Quantum-walk based algorithms make the connection explicit (Childs 2009; Farhi and Gutmann 1998; Hein and Tanner 2010; Roland and Cerf 2005). Tools such as random matrix theory have already been imported in this field (Roland and Cerf 2005), however much of the knowledge present in the disorder physics community has not yet been incorporated in quantum computing. As developments currently progress, driven by machines such as the *D-Wave two* (Bunyk et al. 2014; Lanting et al. 2014), one must learn how to deal with unavoidable disorder effects. A confirmation of this suspicion was recently provided by the numerical prediction of power-law statistics for the time-to-solution in quantum annealing algorithms (Steiger et al. 2015). The results presented in this chapter indicate that disorder is not guaranteed to have a negative impact, and can even be exploited and controlled by a suitable design of the system.

Throughout this chapter we have not considered the influence of inserting and extracting the excitation. Given our motivation to describe quantum transport in photosynthetic light harvesting complexes, this issue is, nevertheless, highly relevant. In the next chapter, we introduce coupling to external channels and implement the design principles of the present chapter into a context of scattering theory. Via the presented design principle, we can also achieve enhanced excitation transfer in the scattering framework. However, there is also a significant interplay between the system and the the external channels, as will be discussed extensively.

References

- M. Abramowitz, I. Stegan, *Handbook of Mathematical Functions* (Dover Publications, Mineola, 1965)
- E. Akkermans, *Mesoscopic Physics of Electrons and Photons* (Cambridge University Press, Cambridge, 2011)
- R. Alicki, *Quantum Dynamical Semigroups and Applications*, 2nd edn. (Springer Science & Business Media, Berlin, 1987)
- H.V. Amerongen, L. Valkunas, R.V. Grondelle, *Photosynthetic Excitons* (World Scientific, Singapore, 2000)
- N.W. Ashcroft, N.D. Mermin, *Solid State Physics* (Holt, Rinehart and Winston, New York, 1976)
- C.J. Bardeen, The structure and dynamics of molecular excitons. Annu. Rev. Phys. Chem. 65, 127–148 (2014)
- S. Barnett, *Matrices: Methods and Applications*, Oxford Applied Mathematics and Computing Science Series (Clarendon Press, Oxford University Press, Oxford [England], New York, 1990)
- N. Biggs, *Algebraic Graph Theory*, 2nd edn. Cambridge Mathematical Library (Cambridge University Press, Cambridge, 1993)

References 141

- R.E. Blankenship, Molecular Mechanisms of Photosynthesis (Blackwell Science, Oxford, 2002)
- P. Bocchieri, A. Loinger, Quantum recurrence theorem. Phys. Rev. 107, 337–338 (1957)
- O. Bohigas, S. Tomsovic, D. Ullmo, Manifestations of classical phase space structures in quantum mechanics. Phys. Rep. **223**, 43–133 (1993)
- H.-P. Breuer, F. Petruccione, *The Theory of Open Quantum Systems* (Oxford University Press, Oxford, 2007)
- O. Brodier, P. Schlagheck, D. Ullmo, Resonance-assisted tunneling. Ann. Phys. 300, 88–136 (2002)
- P. Bunyk, E. Hoskinson, M. Johnson, E. Tolkacheva, F. Altomare, A. Berkley, R. Harris, J. Hilton, T. Lanting, A. Przybysz, J. Whittaker, Architectural considerations in the design of a superconducting quantum annealing processor. IEEE Trans. Appl. Supercond. 24, 1–10 (2014)
- A. Cantoni, P. Butler, Eigenvalues and eigenvectors of symmetric centrosymmetric matrices. Linear Algebra Appl. 13, 275–288 (1976)
- A. Chabchoub, M. Fink, Time-reversal generation of rogue waves. Phys. Rev. Lett. **112**, 124101 (2014)
- A.M. Childs, Universal computation by quantum walk. Phys. Rev. Lett. 102, 180501 (2009)
- M. Christandl, N. Datta, A. Ekert, A.J. Landahl, Perfect state transfer in quantum spin networks. Phys. Rev. Lett. 92, 187902 (2004)
- M. Christandl, N. Datta, T.C. Dorlas, A. Ekert, A. Kay, A.J. Landahl, Perfect transfer of arbitrary states in quantum spin networks. Phys. Rev. A 71, 032312 (2005)
- P.J. Davis, Circulant Matrices. Pure and Applied Mathematics (Wiley, New York, 1979)
- C. Dembowski, H.-D. Gräf, A. Heine, R. Hofferbert, H. Rehfeld, A. Richter, First experimental evidence for chaos-assisted tunneling in a microwave annular billiard. Phys. Rev. Lett. 84, 867– 870 (2000)
- B. Derrida, Y. Pomeau, Random networks of automata: a simple annealed approximation. EPL 1, 45 (1986)
- G.S. Engel, T.R. Calhoun, E.L. Read, T.-K. Ahn, T. Mančal, Y.-C. Cheng, R.E. Blankenship, G.R. Fleming, Evidence for wavelike energy transfer through quantum coherence in photosynthetic systems. Nature **446**, 782–786 (2007)
- G. Ergün, Y.V. Fyodorov, Level curvature distribution in a model of two uncoupled chaotic subsystems. Phys. Rev. E 68, 046124 (2003)
- E.F. Fama, R. Roll, Some properties of symmetric stable distributions. JASA 63, 817–836 (1968)
- E. Farhi, S. Gutmann, Quantum computation and decision trees. Phys. Rev. A 58, 915–928 (1998)
- M. Frazier, B. Taddese, T. Antonsen, S.M. Anlage, Nonlinear time reversal in a wave chaotic system. Phys. Rev. Lett. **110**, 063902 (2013)
- P. Gaspard, Quantum chaotic scattering. Scholarpedia 9, 9806 (2014)
- F. Haake, QuantumSignatures of Chaos, vol. 54 (Springer Science & Business Media, Berlin, 2010)
- F. Haake, K. Życzkowski, Random-matrix theory and eigenmodes of dynamical systems. Phys. Rev. A 42, 1013–1016 (1990)
- H. Haken, *Quantum Field Theory of Solids: An Introduction* (North-Holland Pub. Co, Amsterdam, New York, 1976)
- C.S. Hamilton, R. Kruse, L. Sansoni, C. Silberhorn, I. Jex, Driven quantum walks. Phys. Rev. Lett. 113, 083602 (2014)
- B. Hein, G. Tanner, Quantum search algorithms on a regular lattice. Phys. Rev. A **82**, 012326 (2010)
- F.B. Hildebrand, *Introduction to Numerical Analysis*, 2nd edn. (Dover Publications, New York, 1987)
- Y. Imry, *Introduction to Mesoscopic Physics* (Oxford University Press, Oxford, 2009)
- A. Kay, Perfect state transfer: Beyond nearest-neighbor couplings. Phys. Rev. A 73, 032306 (2006)
- C. Kittel, Introduction to Solid State Physics, 8th edn. (Wiley, Hoboken, NJ, 2005)
- C. Kittel, C.Y. Fong, *Quantum Theory of Solids*, 2nd edn. (Wiley, New York, 1987)
- V.F. Krotov, Global methods in optimal control theory, in *Advances in Nonlinear Dynamics and Control: A Report from Russia*, ed. by A.B. Kurzhanski. Progress in Systems and Control Theory, vol. 17 (Birkhäuser, Boston, 1993), pp. 74–121. https://doi.org/10.1007/978-1-4612-0349-0_3

- I. Kuprov, Spin system trajectory analysis under optimal control pulses. J. Mag. Reson. 233, 107–112 (2013)
- T. Lanting, A.J. Przybysz, A.Y. Smirnov, F.M. Spedalieri, M.H. Amin, A.J. Berkley, R. Harris, F. Altomare, S. Boixo, P. Bunyk, N. Dickson, C. Enderud, J.P. Hilton, E. Hoskinson, M.W. Johnson, E. Ladizinsky, N. Ladizinsky, R. Neufeld, T. Oh, I. Perminov, C. Rich, M.C. Thom, E. Tolkacheva, S. Uchaikin, A.B. Wilson, G. Rose, Entanglement in a quantum annealing processor. Phys. Rev. X 4, 021041 (2014)
- P.S. Laplace, Memoir on the probability of the causes of events. Stat. Sci. 1, 364–378 (1986)
- F.C. Leone, L.S. Nelson, R.B. Nottingham, The folded normal distribution. Technometrics 3, 543–550 (1961)
- G. Lerosey, J.D. Rosny, A. Tourin, M. Fink, Focusing beyond the diffraction limit with far-field time reversal. Science 315, 1120–1122 (2007)
- F. Leyvraz, D. Ullmo, The level splitting distribution in chaos-assisted tunnelling. J. Phys. A: Math. Gen. 29, 2529 (1996)
- R. Loudon, *The Quantum Theory of Light*, 3rd edn. (Oxford science publications, Oxford University Press, Oxford, New York, 2000)
- D. Manzano, Quantum transport in networks and photosynthetic complexes at the steady state. PLoS ONE 8, e57041 (2013)
- V. May, O. Kühn, Charge and Energy Transfer dynamics in Molecular Systems: A Theoretical Introduction, 1st edn. (Wiley-VCH, Berlin, New York, 2000)
- S. Mostarda, F. Levi, D. Prada-Gracia, F. Mintert, F. Rao, Structure–dynamics relationship in coherent transport through disordered systems. Nat. Commun. 4 (2013)
- O. Mülken, A. Blumen, Continuous-time quantum walks: Models for coherent transport on complex networks. Phys. Rep. **502**, 37–87 (2011)
- J. Nelson, The Physics of Solar Cells (Imperial College Press, Distributed by World Scientific Publication, River Edge, London, 2003)
- A. Ortega, M. Vyas, L. Benet, Quantum efficiencies in finite disordered networks connected by many-body interactions: Quantum efficiencies in finite disordered networks. Ann. Phys. 527, 748–756 (2015)
- M. Reed, B. Simon, Fourier Analysis, Self-Adjointness, 1st edn. (Academic Press, New York, 1975)
- J. Roland, N.J. Cerf, Noise resistance of adiabatic quantum computation using random matrix theory. Phys. Rev. A 71, 032330 (2005)
- I. Rotter, A non-Hermitian Hamilton operator and the physics of open quantum systems. J. Phys. A: Math. Theor. **42**, 153001 (2009)
- A. Sakharov, The Climb (2013)
- M. Sarovar, A. Ishizaki, G.R. Fleming, K.B. Whaley, Quantum entanglement in photosynthetic light-harvesting complexes. Nat. Phys. 6, 462–467 (2010)
- T. Scholak, Transport and coherence in disordered networks. Ph.D. thesis, Albert-Ludwigs Universität Freiburg, Freiburg, 2011
- T. Scholak, F. Mintert, T. Wellens, A. Buchleitner, Transport and entanglement, in *Biomolecular Systems*, ed. by E.R. Weber, M. Thorwart, U. Würfel. Quantum Efficiency in Complex Systems, 1st edn. (Elsevier, Oxford, 2010)
- T. Scholak, F. de Melo, T. Wellens, F. Mintert, A. Buchleitner, Efficient and coherent excitation transfer across disordered molecular networks. Phys. Rev. E 83, 021912 (2011a)
- T. Scholak, T. Wellens, A. Buchleitner, Optimal networks for excitonic energy transport. J. Phys. B: At. Mol. Opt. Phys. **44**, 184012 (2011b)
- T. Scholak, T. Wellens, A. Buchleitner, The optimization topography of exciton transport. EPL **96**, 10001 (2011c)
- T. Scholak, T. Wellens, A. Buchleitner, Spectral backbone of excitation transport in ultracold Rydberg gases. Phys. Rev. A 90, 063415 (2014)
- H.S. Seung, H. Sompolinsky, N. Tishby, Statistical mechanics of learning from examples. Phys. Rev. A 45, 6056–6091 (1992)

References 143

M. Shapiro, P. Brumer, *Principles of the Quantum Control of Molecular Processes* (Wiley-Interscience, Hoboken, 2003)

- D.A. Steck, W.H. Oskay, M.G. Raizen, Observation of chaos-assisted tunneling between islands of stability. Science 293, 274–278 (2001)
- D.S. Steiger, T.F. Rønnow, M. Troyer, Heavy tails in the distribution of time to solution for classical and quantum annealing. Phys. Rev. Lett. **115**, 230501 (2015)
- S. Tomsovic, Chaos-assisted tunnelling in the absence of reflexion symmetry. J. Phys. A: Math. Gen. **31**, 9469 (1998)
- S. Tomsovic, D. Ullmo, Chaos-assisted tunneling. Phys. Rev. E **50**, 145–162 (1994)
- M. Walschaers, J.F.-d.-C. Diaz, R. Mulet, A. Buchleitner, Optimally designed quantum transport across disordered networks. Phys. Rev. Lett. 111, 180601 (2013)
- M. Walschaers, R. Mulet, T. Wellens, A. Buchleitner, Statistical theory of designed quantum transport across disordered networks. Phys. Rev. E 91, 042137 (2015)
- G.H. Wannier, The structure of electronic excitation levels in insulating crystals. Phys. Rev. **52**, 191–197 (1937)
- H.M. Wiseman, G.J. Milburn, *Quantum Measurement and Control* (Cambridge University Press, Cambridge, 2010)
- P.-E. Wolf, G. Maret, Weak localization and coherent backscattering of photons in disordered media. Phys. Rev. Lett. **55**, 2696–2699 (1985)
- J. Zakrzewski, D. Delande, A. Buchleitner, Ionization via chaos assisted tunneling. Phys. Rev. E 57, 1458–1474 (1998)
- T. Zech, Hidden symmetries of quantum transport in photosynthesis. Diploma thesis, Albert-Ludwigs Universität Freiburg, Freiburg, 2013
- T. Zech, M. Walschaers, T. Scholak, R. Mulet, T. Wellens, A. Buchleitner, Quantum transport in biological functional units: noise, disorder, structure. Fluct. Noise Lett. 12, 1340007 (2013)
- T. Zech, R. Mulet, T. Wellens, A. Buchleitner, Centrosymmetry enhances quantum transport in disordered molecular networks. New J. Phys. 16, 055002 (2014)

Chapter 5 Scattering Approach to Efficient Transport



A common mistake that people make when trying to design something completely foolproof is to underestimate the ingenuity of complete fools.

Douglas Adams in (1993)

5.1 Introduction

In Chap. 4 we extensively discussed how one can efficiently map a given initial state to a given final state—these states are referred to as "input" and "output" or "donor" and "acceptor"—on a fast time scale. We did not consider the matter of the excitation entering or leaving the system and therefore could explicitly consider the system closed: Neither particles, nor energy, not even entropy were allowed to enter or leave the system. In this chapter, we study one potential approach to let the external world talk to the systems of Chap. 4.

The approach chosen is the one from Sect. 2.6, a choice which allows us to still treat the problem in a single-particle setting. In this setup, we consider the system, described by a Hilbert space \mathbb{C}^N (given that we consider the single-excitation space on N sites), and attach scattering leads to it. A scattering lead is generally described by a space of the form $\mathcal{L}^2(\mathbb{R}^3)$, and attaching a set of scattering channels to the system thus leads to a description of the form $\mathcal{L}^2(\mathbb{R}^3) \oplus \mathbb{C}^N$, although the continuum can in principle have a substructure by appointing a separate Hilbert space to each channel $\mathcal{H}_c \subset \mathcal{L}^2(\mathbb{R}^3)$, such that we can describe $\mathcal{H}_{\text{total}} = \mathbb{C}^N \bigoplus_c \mathcal{H}_c$.

¹We choose $\mathcal{L}^2(\mathbb{R}^3)$ because we generally consider wave propagation in three spatial dimensions.

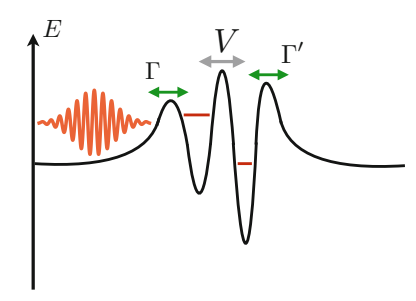


Fig. 5.1 Sketch of a wave packet which travels inside a continuum at the lefthand side, collides with the scattering system, which contains two bound states. The bound states which constitute the system under consideration are coupled to one another in a double well potential, characterised by and effective direct coupling V. The couplings between the bound states of the internal system and the continuum of states in the scattering channels is described by Γ and Γ'

Physically this means that we consider a set of bound states, which form our system, and are coupled to a continuum. This leads us to the setting of nuclear and atomic physics as studied by Fano (1961), Feshbach (1958, 1962, 1967). The central idea it that a freely roaming wave packet hits the system from one of the connected channels, subsequently creates an excitation within the system, which may decay again into one of the channels. A sketch of such a setup, by means of a potential landscape is shown in Fig. 5.1: For simplicity, we show a double well system in a 1D setting (similar to Celardo and Kaplan 2009). The continuum stretching out at, both, the far left and the far right can be interpreted as two different scattering channels, a setting which allows us to treat the scattering process in terms of transmission and reflection coefficients.

Figure 5.1 nicely indicates the different parameters which play a role in the problem: The internal system's level structure—which here requires us to diagonalise the effective two level system Hamiltonian generated by the double-well potential—, the coupling of the external channels' continuum of states to the internal system, and the energy of the incoming wave packet (in case of broadband wave packets, this would be an energy distribution) (Hunn 2013; Hunn et al. 2013). Specially the latter two parameters are new in this scattering setting and therefore we specifically study their impact on the transfer.

5.2 Transfer Probability and Dwell Time

As described in Sect. 2.6, we model such scattering problems in the scattering matrix formalism, which is well-established and can be applied to an enormously wide range of problem settings. As much of our modelling in Chap. 4 was inspired by results from the quantum chaos community, we continue our endeavour and exploit the same toolbox.

A broad subfield of quantum chaos considers these open systems in a framework called *quantum chaotic scattering* (Gaspard 2014). We formulate the scattering matrix setup as defined in Brouwer et al. (1997), Celardo and Kaplan (2009), Haake et al. (1992), Lewenkopf and Weidenmüller (1991), Šeba et al. (1996), Stöckmann et al. (2002):

$$S(E) = \mathbb{1} - 2\pi i \hat{W}^{\dagger} \frac{1}{E - H_{\text{eff}}} \hat{W}, \qquad (5.1)$$

which was already obtained in Eq. (2.83). The scattering matrix thus depends on the energy of the incoming wave, E, and its dimensions must correspond to the number of channels, n_c . The matrix $H_{\rm eff}$ is an operator on the Hilbert space of the closed system, describing the bound states in a resonance framework. This implies that $H_{\rm eff}$ is *non-hermitian* (Rotter 2009). As is standard in this form of scattering theory, $H_{\rm eff}$ is obtained from a Fano–Feschbach projection (Fano 1961; Feshbach 1958, 1962, 1967) and reads

$$H_{\text{eff}} := H - i\pi \hat{W}\hat{W}^{\dagger}. \tag{5.2}$$

The operator H is the Hamiltonian describing the *bound states* and throughout this chapter it is treated as an $N \times N$ matrix, reflecting the existence of N single-particle bound states. Notice that we ignore the Lamb shift (Cohen-Tannoudji et al. 1998). As was mentioned briefly in Sect. 2.6, the operator \hat{W} is also obtained from a projection procedure which describes how the coupling Hamiltonian defined on $\mathcal{H}_{\text{total}}$ is projected down to couple the scattering channels to the internal system. In principle, \hat{W} itself can be energy dependent, although we will here assume it to lack such dependency. This implies that \hat{W} is an $n_c \times N$ matrix, with N the dimension of the internal system (the number of bound states) and n_c the number of external channels. Notice that this is indeed consistent with the fact that S(E) is an $n_c \times n_c$ matrix and $(E - H_{\text{eff}})^{-1}$ an $N \times N$ matrix. For further simplicity, we define a new operator $W := \sqrt{\pi} \hat{W}$, which eliminates the necessity to drag around π factors throughout all calculations.

In Sect. 2.6, we described that by its very definition (2.75), the scattering matrix describes the asymptotic mapping of an initial wave packet $|\phi_i\rangle$ onto a final wave packet $|\phi_f\rangle$ via $\langle\phi_i,S(E)\phi_f\rangle$. Here we approximate that initial and final wave packets are close to plane wave fronts, which implies that their spread in energy can safely be ignored. We assume that there is no additional structure in the channels, and thus the basis of plane waves can be described by a set of wave functions $|c,E\rangle$, where c is the channel index and E the energy of the inserted plane wave, which implies that we effectively treat the scattering channels as one dimensional leads. Therefore, one

²This assumption implies that, within the range of relevant energies, all incoming plane waves interact with the system in the same way. This approximation is common, both in light-matter interactions (Cohen-Tannoudji et al. 1998) and in mesoscopic physics (Lewenkopf and Weidenmüller 1991).

³If this were not the case, one would have to integrate over the relevant energy range, which would make the explanation more technical and less transparent.

may describe the probability for having transfer from a given channel c to another channel c' at a given energy E by

$$p_{c \to c'}(E) := \left| S_{c,c'}(E) \right|^2. \tag{5.3}$$

Wave functions of the form $|c, E\rangle$ can only be transferred to wave functions of the form $|c', E\rangle$, implying that for the dynamics in the full Hilbert space \mathcal{H}_{total} , we have energy conservation. Equation (5.3) defines the *transfer probability* and therefore is the main workhorse of this chapter.

Making the connection to Chap. 4, one can interpret Eq. (5.3) as the "open system", or scattering equivalent of the efficiency treated in Sect. 4.2. However, Chap. 4 focussed strongly on fast transfer and therefore on transfer time scales. Hence, it is natural to wonder whether there is a similar notion available in the open system setting. This issue is not as straightforward as for the closed systems, since by its very definition $p_{c \to c'}(E)$ is an asymptotic quantity. Nevertheless, a considerable amount of work has been done on defining the *delay time* or *dwell time* (Berkolaiko and Kuipers 2010; Brouwer et al. 1997; Kuipers and Sieber 2008; Šeba et al. 1996; Smith 1960). As we specifically are interested in the time it takes an incoming wave front at energy E to transfer from channel c to channel c', the suitable quantity is Brouwer et al. (1997), Smith (1960)

$$\tau_{c \to c'}(E) = \text{Im} \left\{ S_{c,c'}(E)^{-1} \frac{d}{dE} S_{c,c'}(E) \right\}.$$
 (5.4)

In Smith (1960), it is explained, using wave packet dynamics arguments, that $\tau_{c \to c'}(E)$ can be interpreted as the time it takes for the scattering peak in the $c \to c'$ channel to appear. As read in Brouwer et al. (1997), one can also connect the dwell time to a phase shift in the AC signal,⁴ when considering conductance in chaotic cavities. More generally, it can be stated that the dwell time investigates the phase shifts that are introduced in the plane wave as a consequence of the scattering process. Because these dwell times fluctuate in chaotic systems (Lewenkopf and Weidenmüller 1991), they are of particular interest in relation to conductance fluctuations (Jalabert et al. 1994).

Another relevant time scale is the *resonance lifetime* (Gaspard 2014), which is extracted from the eigenvalues of $H_{\rm eff}$. Because $H_{\rm eff}$ is non-hermitian, its eigenvalues are generically given by $\mathcal{E}_i = E_i - i\Gamma_i/2$. As we will see in the following sections, these *resonances* \mathcal{E}_i contain information on the position of the resonance peak, i.e. E_i , and on its *width*, i.e. Γ_i . As shown in Gaspard (2014), these widths are closely related to decay rates and therefore $1/\Gamma_i$ describes the resonance lifetime. This quantity is

⁴Condensed-matter physics commonly studies scattering problems in the sense of currents, leaving open the option to probe a mesoscopic cavity either with alternating current (AC) or direct current (DC). It is argued that, although DC signals only depend on scattering amplitudes, AC signals are sensitive to phase factors (Brouwer et al. 1997). The transfer of an AC signal through a scattering cavity hence introduces a phase shift, which is what we here refer to as the dwell time.

both conveniently easy to handle and insightful, but it has the disadvantage that it only serves to probe the resonance energies E_i .

As long as we are in a regime where different resonances are not overlapping, i.e. Γ_i , $\Gamma_j \ll |E_i - E_j|$ for all i and j, we can safely conclude that the dwell time and the lifetime are narrowly related (see (5.17) and (5.29)). However, once the resonances overlap, one can no longer make this association (see e.g. Lyuboshitz 1977). We here employ the dwell time as an estimate for the time it takes the excitation to be transferred from the input to the output channel, building on Smith (1960), although it must be stressed that this interpretation is only valid when we consider plane waves with well-defined energy.

Having defined both the transfer efficiency $p_{c \to c'}(E)$ and the dwell time $\tau_{c \to c'}(E)$, we can discuss fast and efficient excitation transfer in these open systems. To start this discussion, we present basic calculations for the two-level system of Fig. 5.1. They can be considered textbook knowledge, but serve as a benchmark system to gauge the performance of the disordered systems we will deal with subsequently.

5.3 The Two Level System*

This section reviews textbook knowledge on scattering of two-level systems, which is extensively used throughout the remainder of this chapter.

5.3.1 The Model*

The closed two-level system was already discussed in Sects. 4.2 and 4.4, where we showed that the main structure of the Hamiltonian is given by

$$H = \begin{pmatrix} E_1 & V \\ V & E_2 \end{pmatrix}. \tag{5.5}$$

We assume that this is the Hamiltonian in the site basis and that the system is time reversal invariant, implying that the matrix' components are real. In the philosophy of Chap. 4, where we referred to these two sites as "input" and "output", it is only logical to attach the external channels to the states localised on these sites, *ergo*

$$W = \sqrt{\Gamma/2} |\text{in}\rangle \langle c_1, E| + \sqrt{\Gamma'/2} |\text{out}\rangle \langle c_2, E|.$$
 (5.6)

To visualise this setup, let us point out that this is exactly the scenario sketched in Fig. 5.1. With this choice of system-channel interaction, the effective non-hermitian Hamiltonian reads

$$H_{\text{eff}} = \begin{pmatrix} E_1 - i\frac{\Gamma}{2} & V \\ V & E_2 - i\frac{\Gamma'}{2} \end{pmatrix}. \tag{5.7}$$

From here it can be directly calculated⁵ that

$$S_{c_1,c_2}(E) = -i\sqrt{\Gamma \Gamma'} \frac{V}{\left(E - E_1 + i\frac{\Gamma}{2}\right)\left(E - E_2 + i\frac{\Gamma'}{2}\right) - V^2}.$$
 (5.8)

By (5.3), this leads to a transfer efficiency (now omitting the channel indices, since there are only two channels under consideration)

$$p_0(E) = \frac{\Gamma \Gamma' V^2}{\left((E - E_1)(E - E_2) - V^2 - \frac{\Gamma \Gamma'}{4} \right)^2 + \left(\frac{\Gamma}{2}(E - E_2) + \frac{\Gamma'}{2}(E - E_1) \right)^2}.$$
(5.9)

The dwell time already reduces to a rather complicated expression

$$\tau_{0}(E) = \frac{(2E - E_{1} - E_{2}) \left(\frac{\Gamma}{2}(E - E_{2}) + \frac{\Gamma'}{2}(E - E_{1})\right)}{\left((E - E_{1})(E - E_{2}) - V^{2} - \frac{\Gamma\Gamma'}{4}\right)^{2} + \left(\frac{\Gamma}{2}(E - E_{2}) + \frac{\Gamma'}{2}(E - E_{1})\right)^{2}} - \frac{\left((E - E_{1})(E - E_{2}) - V^{2} - \frac{\Gamma\Gamma'}{4}\right)\left(\frac{\Gamma}{2} + \frac{\Gamma'}{2}\right)}{\left((E - E_{1})(E - E_{2}) - V^{2} - \frac{\Gamma\Gamma'}{4}\right)^{2} + \left(\frac{\Gamma}{2}(E - E_{2}) + \frac{\Gamma'}{2}(E - E_{1})\right)^{2}}.$$
(5.10)

To gain a better understanding for the behaviour of this system one therefore needs to understand the role of five different parameters: Γ , Γ' , E_1 , E_2 and V.

5.3.2 The Symmetric Case*

To disentangle the problem, we treat a much simpler situation by setting $E' = E_1 = E_2$ and $\Gamma = \Gamma'$. Although this seems like a technicality to allow for more transparent manipulations, it nicely connects to the results of Chap. 4, since it renders $H_{\rm eff}$ in Eq. (5.7) *centrosymmetric*. We thus obtain the simpler results

$$p_0(E) = \frac{\Gamma^2 V^2}{\left((E - E')^2 - V^2 - \frac{\Gamma^2}{4} \right)^2 + \Gamma^2 (E - E')^2},$$
 (5.11)

and

$$\tau_0(E) = \frac{\left((E - E')^2 + V^2 + \frac{\Gamma^2}{4} \right) \Gamma}{\left((E - E')^2 - V^2 - \frac{\Gamma^2}{4} \right)^2 + \Gamma^2 (E - E')^2}.$$
 (5.12)

⁵The result follows directly from diagonalising $E1 - H_{\text{eff}}$ and using its spectral decomposition in (5.1).

 $p_0(E)$ accordingly exhibits well-known resonance profiles as shown in Figs. 5.2 and 5.3, ubiquitous in many branches of physics. To interpret such images, we find the extremal points of $p_0(E)$. The calculation is straightforward and leads us to the resonance energies

$$E = E' \pm V \sqrt{1 - \left(\frac{\Gamma}{2V}\right)^2},\tag{5.13}$$

$$E = E', (5.14)$$

where

$$p_0\left(E' \pm V\sqrt{1 - \left(\frac{\Gamma}{2V}\right)^2}\right) = 1,\tag{5.15}$$

$$p_0(E') = \left(\frac{\Gamma}{V}\right)^2 \frac{1}{\left(1 + \left(\frac{\Gamma}{2V}\right)^2\right)^2},\tag{5.16}$$

whereas

$$\tau_0 \left(E' \pm V \sqrt{1 - \left(\frac{\Gamma}{2V}\right)^2} \right) = \frac{2}{\Gamma},\tag{5.17}$$

$$\tau_0(E') = \frac{4}{\Gamma} \left[\left(\frac{\Gamma}{2V} \right)^2 \frac{1}{1 + \left(\frac{\Gamma}{2V} \right)^2} \right]. \tag{5.18}$$

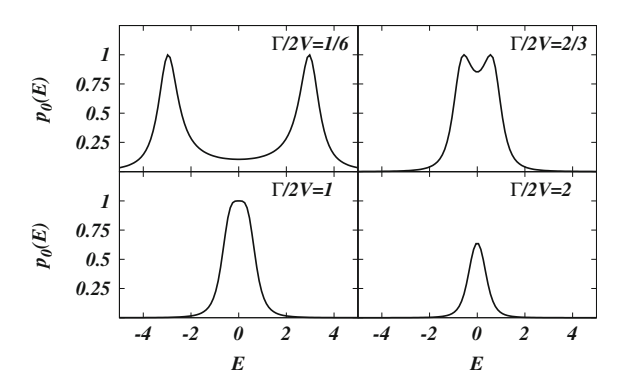


Fig. 5.2 Resonance profiles for the transport from input to output channel across the two level system (5.7), with both levels' on-site energy E'=0. The structure of the transfer probability profiles is controlled by the ratio of the internal coupling V and of the external coupling Γ . Here, this ratio is changed from panel to panel by altering V, while keeping $\Gamma=1$ constant

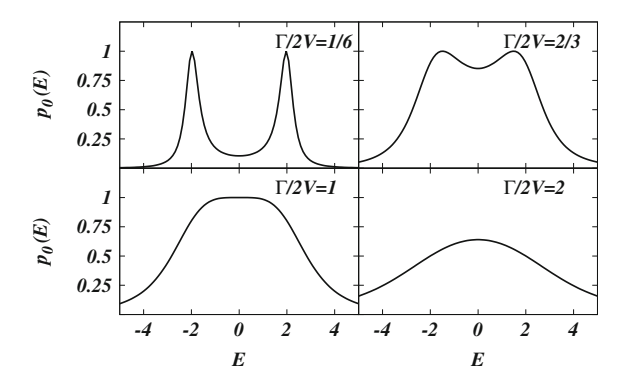


Fig. 5.3 Resonance profiles for the transport from input to output channel in a two level system (5.7), where both levels have on-site energy E'=0. The structure of the transfer probability profile is determined by the ratio of the internal coupling V to the external coupling Γ . This ratio is changed from panel to panel by altering Γ , while keeping V=2 constant

Whenever $2V > \Gamma$ the three energies are well-defined, energies (5.13) indicate the maxima in the resonance profiles of Figs. 5.2 and 5.3, whereas energy (5.14) is a local minimum. Studying $p_0(E)$, we even find a remarkably strong result in Eq. (5.15): Whenever the time scale of the internal coherent dynamics (controlled by V) is faster than the incoherent rate $\Gamma/2$ which connects system and channels, $ergo\ 2V > \Gamma$, the transmission probability is 100%. On the other hand, slow coherent dynamics, which implies $2V < \Gamma$ and thus that energies (5.13) are no longer well-resolved, yields a different behaviour. In this case, Figs. 5.2 and 5.3 show a transition from a regime with two scattering resonances to a situation where both peaks merge into one. Under such circumstances, the previous minimum at E = E' (5.14) takes over as the local maximum. Importantly, we now see that the maximal transfer probability, Eq. (5.16), depends on $\Gamma/2V$ and decreases as $2V \ll \Gamma$. A naive explanation for this effect is that an excitation which enters the system at the input site, via the attached channel, immediately decays into that same channel before it can be be transferred to the output site.

The dwell times impose more subtleties that need to be taken into account. The transfer probability at the resonant energies only depends on the ratio $\Gamma/2V$, not on both parameters independently —this is different for the dwell times. For $2V > \Gamma$, the dwell time, for systems probed at resonance energies (5.13), is simply given by $2/\Gamma$, i.e. by the inverse of the width of the resonance peaks in Figs. 5.2 and 5.3. Even on resonance, the coupling to the channels is the dominant parameter that determines the transport time scale. No clever design, through an effective modification of V can make the transfer faster, only a direct change of Γ can serve this goal. Moreover, we see that, in the regime of merging resonances $2V < \Gamma$, where the maximal transfer efficiency is reached at E = E', the time scales are only slowed down, to ultimately reach the limit $4/\Gamma$ as $2V \ll \Gamma$.

These results imply that, for excitation transfer on resonance, an optimum is reached at $2V = \Gamma$. That is, for a given coherent input-output coupling V, $\Gamma_{\text{opt}} = 2V$ sets the strongest possible channel coupling which still guarantees 100% transfer efficiency. This Γ_{opt} also sets the fastest possible transfer time at $\tau_0 = 2/\Gamma_{\text{opt}} = 1/V$.

On he other hand, for a given Γ , one should strive to make $2V > \Gamma$. Once this objective is reached, both the transfer probability and the dwell time are optimal, at least when the system is probed on resonance.

Having a closer look at the energies (5.13) for which these resonance peaks are obtained in the regime where $2V > \Gamma$, we notice that they are exactly the closed system energy levels $E' \pm V$ (see (4.8)), with the additional correction factor $\sqrt{1-(\Gamma/2V)^2}$. This correction factor can safely be forgotten whenever $2V \gg \Gamma$; then the two resonance peaks are completely isolated and are just located on the eigenstates of the closed system. However, when the system and the channels couple strongly and the resonances start to overlap, as seen in Figs. 5.2 and 5.3, the energy at which the maximal transfer is reached, is shifted closer to E', until $2V = \Gamma$ and the two peaks merge. In this case, the information about the internal system eigenstates is completely washed out by the dominating coupling to the channels.

Of course, one may probe the system at different energies than at resonance. Although we noticed that the maximum transfer probability p_0 , see (5.15), (5.16), only depends on $\Gamma/2V$, as observed in Figs. 5.2 and 5.3, the overall profile of the transfer probability as a function of the incoming energy E strongly depends both on Γ and V separately. Specifically, it becomes clear that increasing Γ increases the width of the resonances, whereas increasing V changes their relative distance on the energy axis. In this sense, one can consider $\Gamma/2V$ as a comparison between the width and relative distance of the peaks, thus quantifying overlap.

Taking Figs. 5.4 and 5.5 into the picture, where we know that even at the resonant energy the dwell time is governed mainly by Γ , we see a similar effect of widening for increasing Γ , and change in relative distance for changing V. However, looking at the dwell times when probing at off-resonant energies, we see that the dwell time typically decreases. On the other hand, Figs. 5.2 and 5.3 indicate that at these energies also the transfer efficiency goes down. In other words, there is always a trade-off observed between speed and efficiency in the transfer through this two-level system.

In summary, as long as $\Gamma/2V$ is smaller than one we find energies for which p_0 is 100%. On the other hand, it is beneficial to make Γ as large as possible, because it dominantly determines the time that an excitation spends in the system. The straightforward way of getting very fast and efficient transfer from the input to the output channel is therefore to increase both Γ and V in a way such that $\Gamma/2V \approx 1$. However, increasing the direct coupling V between input and output states can for many reasons be physically unfeasible, e.g. if the coupling is distance dependent, such as for molecules with dipole-dipole coupling, since this amounts to putting these molecules ever closer together. Therefore, one may wonder whether we can increase the transfer probability in the regime where $\Gamma \gg 2V$, by adding additional complexity to the system.

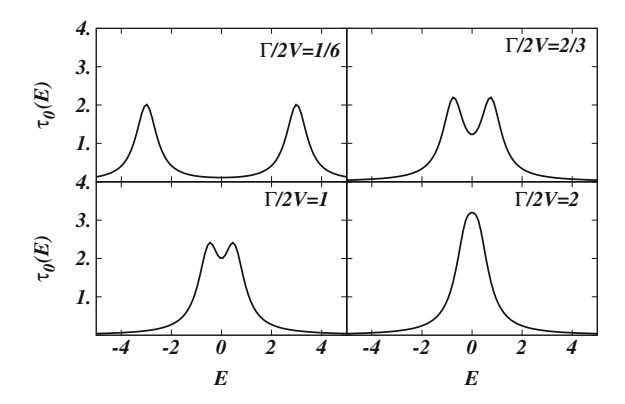


Fig. 5.4 Dwell time profiles derived from (5.12), for the transport from the input to the output channel in a two level system (5.7), where both levels have on-site energy E' = 0. The structure of the transfer probability profile is governed by the ratio of the internal coupling V to the external coupling V. This ratio is varied from panel to panel by altering V, while keeping $\Gamma = 1$ constant

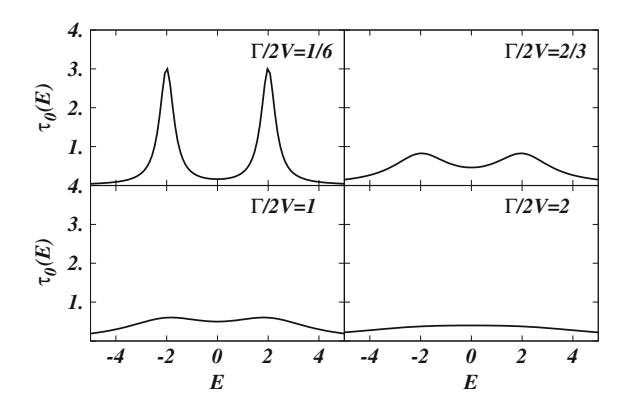


Fig. 5.5 Dwell time profiles derived from (5.12), for the transport from the input to the output channel in a two level system (5.7), where both levels have on-site energy E' = 0. The structure of the transfer probability profile is governed by the ratio of the internal coupling V to the external coupling V. This ratio is varied over the different panels by altering V, while keeping V = 2 constant

5.4 Designing the System

We now extend the system described in Sect. 5.3.2 by adding extra sites, in a way which is analogous to the model described in Sect. 4.4. This implies that we extend the system Hamiltonian to the one represented in Eq. (4.81), and the additional sites translate to more bound states in the scattering picture. Moreover, it is possible to include more external channels; however, we choose to keep the picture of a single input and output site intact. This implies that we have one input channel, attached to one site |in) from which quanta of energy are inserted into the system, and one output

channel, attached to |out⟩, to which these energy quanta should be transmitted. This leads to an effective, non-Hermitian Hamiltonian in the site basis,

$$H_{\text{eff}} = \begin{pmatrix} E' - i\frac{\Gamma}{2} v_1 \dots v_n & V \\ v_1 & v_n \\ \vdots & H_{\text{int}} & \vdots \\ v_n & v_1 \\ V & v_n \dots v_1 E' - i\frac{\Gamma'}{2} \end{pmatrix},$$
(5.19)

where H_{int} is now a centrosymmetric matrix describing the couplings between the newly added intermediate sites. As we strive to generalise the model of Sect. 5.3.2, we choose $\Gamma = \Gamma'$, which turns H_{eff} into a non-Hermitian centrosymmetric matrix.

One may wonder whether the addition of multiple sites potentially changes the transfer probability and dwell time. A wide variety of complicated phenomena can occur when we simply sample $H_{\rm eff}$ using the recipe of (4.61), hence *not* imposing the dominant doublet condition, for a fixed value of Γ . Figure 5.6 shows a typical resonance profile thus generated, which exhibits diverse phenomena: We observe a minority of line shapes which are typical for asymmetric resonances (e.g. at $E \approx 1.5$), and several symmetric resonances. The widths of the resonances tend to vary strongly and also the heights of the peaks fluctuate. However, we must emphasise that we *do* find many resonance peaks that go all the way up to p = 1. These phenomena remind strongly of the typical fluctuations (generally grouped under the term "Ericson fluctuations") which are known as hallmarks of quantum chaotic scattering (Gaspard 2014; Jalabert et al. 1994; Lyuboshitz 1977; Madroñero and Buchleitner 2005; Stöckmann 2007).

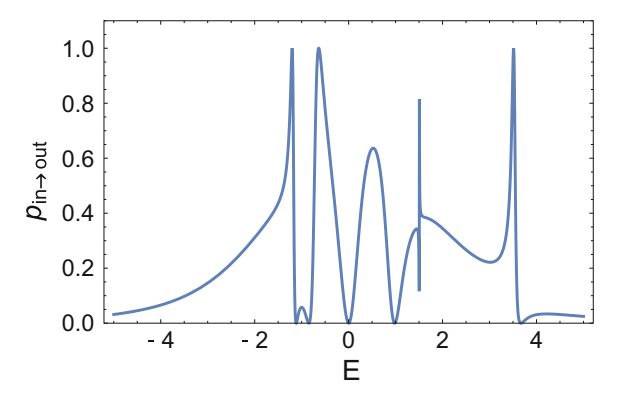
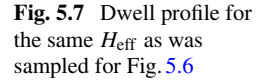
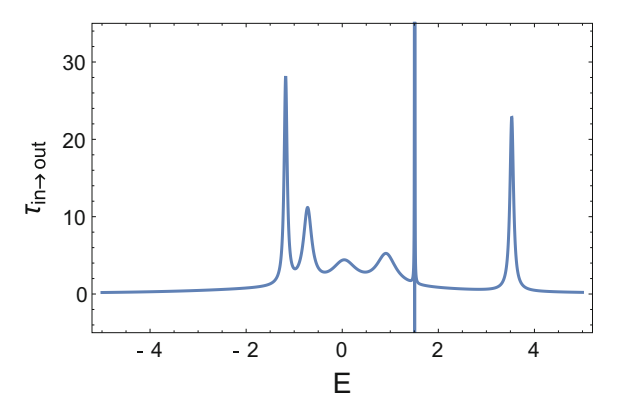


Fig. 5.6 Resonance profile for a randomly sampled effective Hamiltonian $H_{\rm eff}$ as defined in (5.19), using the prescription (4.61) to sample the bound system Hamiltonian, implying that v_i follows the same statistics as $(H_{\rm int})_{jk}$. We set $\xi=1$ and $\Gamma=5$ in (5.19), (5.40), whereas E'=0 and V=1, such that the additional random couplings are really seen as fluctuations around these values. The system contains a total of N=8 sites





Shifting the focus to the dwell time profiles⁶ as shown in Fig. 5.7 several features are observed: At first we see that the narrowest resonance peaks in Fig. 5.6 indeed are associated with very long dwell times, which implies that, even though transfer is highly efficient, the time scales at which it occurs are extremely long. In addition, there is the remarkable feature that the dwell time becomes negative at a given point. This is clearly a consequence of the dwell time actually being based on phase information, rather than it really being a pure time scale. In this case, the interpretation in Smith (1960), based on wave packet dynamics, does not provide the correct image and the dwell time becomes a more subtle quantity.

Although the features seen in Figs. 5.6 and 5.7 are clearly both useful and interesting, they lack an understandable and robust structure. It is possible to achieve transfer with high probability, but it is highly unfeasible to *control* these structures to achieve efficient excitation transfer. Indeed, we already emphasised that once many resonances overlap, systems are characterised by *fluctuations* (Gaspard 2014; Madroñero and Buchleitner 2005). Moreover (Lyuboshitz 1977) argues that transfer time scales are slowed down in systems with many overlapping resonances. Thus, in a next step we impose the dominant doublet (4.68) as a design principle to generate an ensemble of statistically controllable and well-understood system conformations.

As extensively discussed in Chap. 4, the *dominant doublet* can be implemented in several non-equivalent ways. Here we do not impose any specific choice, but simply focus on perturbation theory on an abstract level. At the root of our analysis is the centrosymmetric matrix $H_{\rm eff}$ (5.19), which can again be cast in the symmetry eigenbasis

$$H_{\text{eff}} = \begin{pmatrix} E' + V - i\frac{\Gamma}{2} \langle \mathcal{V}^{+} | \\ |\mathcal{V}^{+} \rangle & H_{sub}^{+} \\ & E' - V - i\frac{\Gamma}{2} \langle \mathcal{V}^{-} | \\ |\mathcal{V}^{-} \rangle & H_{sub}^{-} \end{pmatrix}.$$
 (5.20)

⁶Obtained for the same random realisation of $H_{\rm eff}$ with centrosymmetry constraint as in Fig. 5.6.

Under the assumption that a dominant doublet exists, one imposes the constraint that there are two eigenvectors $|\eta^+\rangle$ and $|\eta^-\rangle$ such that $|\langle \eta^\pm, \pm \rangle|^2 = 1 - \epsilon$ with again $|\pm\rangle = (|\text{in}\rangle \pm |\text{out}\rangle)/\sqrt{2}$. This gives rise to perturbative results for the eigenvalues of H_{eff} , much as known for the Hermitian case:

$$\mathcal{E}^{\pm} \approx E' \pm V - i\frac{\Gamma}{2} + s^{\pm}, \quad \text{where} \quad s^{\pm} = \sum_{i} \frac{\left|\left\langle \mathcal{V}^{\pm}, \psi_{i}^{\pm}\right\rangle\right|^{2}}{E' \pm V - e_{i}^{\pm}}.$$
 (5.21)

Using the dominant doublet constraint combined with Eq. (5.21), we can determine the scattering matrix element that maps the input to the output channel:

$$S_{\text{in}\to\text{out}}(E) = -i\Gamma\left(\frac{\langle\text{out},+\rangle\langle+,\text{in}\rangle}{E-\mathcal{E}^+} + \frac{\langle\text{out},-\rangle\langle-,\text{in}\rangle}{E-\mathcal{E}^-}\right) + \mathcal{O}(\epsilon)$$
 (5.22)

$$=-i\frac{\Gamma}{2}\left(\frac{1}{E-\mathcal{E}^{+}}-\frac{1}{E-\mathcal{E}^{-}}\right)+\mathcal{O}(\epsilon). \tag{5.23}$$

From this result, we can now use (5.21) and compute the modulus squared of S to find, according to (5.23), the estimate

$$p(E) \approx \frac{\frac{\Gamma^2}{4} (2V + \Delta s)^2}{\left((E' - V + s^- - E)^2 + \frac{\Gamma^2}{4} \right) \left((E' + V + s^+ - E)^2 + \frac{\Gamma^2}{4} \right)}, \quad (5.24)$$

where we defined the average shift $\Delta s = s^+ - s^-$. Calculation of $\tau(E)$ according to (5.4) does not lead to a particularly transparent result, which we nevertheless state for completeness:

$$\tau(E) \approx \frac{4\Gamma\left(\Gamma^{2} + 4E'^{2} + 4E'\left(s^{-} + s^{+} - 2E\right)\right)}{\left(\Gamma^{2} + 4\left(E' + s^{-} - V - E\right)^{2}\right)\left(\Gamma^{2} + 4\left(E' + s^{+} + V - E\right)^{2}\right)} + \frac{8\Gamma\left(-2s^{-}(V + E) + s^{-2} + 2\left(V\left(s^{+} + V\right) - s^{+}E + E^{2}\right) + s^{+2}\right)}{\left(\Gamma^{2} + 4\left(E' + s^{-} - V - E\right)^{2}\right)\left(\Gamma^{2} + 4\left(E' + s^{+} + V - E\right)^{2}\right)}.$$
(5.25)

Just as for the two-level system, we can now focus on the energies which define the maximum of the resonance peaks and therefore imply the highest transfer probabilities.

The calculation of the energies which maximise the transfer probability p is straightforward and leads to the result

$$E = E' + \overline{s} \pm \left(V + \frac{\Delta s}{2}\right) \sqrt{1 - \left(\frac{\Gamma}{2V + \Delta s}\right)^2},\tag{5.26}$$

$$E = E' + \overline{s},\tag{5.27}$$

where we defined $\bar{s} := (s^+ + s^-)/2$ as the average shift of the resonance energy. The result is similar to that obtained in Eqs. (5.15) and (5.16), only did we now correct for the shift of energy levels induced by the coupling of the input and output sites to the sites in the bulk.

To assess the transmission properties, we need to compare the coupling Γ to the channels to the actual dominant doublet level splitting $|2V+\Delta s|$. As long as $\Gamma<|2V+\Delta s|$, we obtain two maxima in the resonance profile, located at the energies given by (5.26). Moreover, we see that as $\Gamma\ll|2V+\Delta s|$, the resonances are approximately located at $E^\pm=E\pm V+s^\pm$. Indeed, as one may have expected, the resonance profile is largely dominated by the actual dominant doublet energy levels such as discussed in Chap. 4. The quantity $\Gamma/(2V+\Delta s)$ compares the typical width of the two dominant resonance peaks to the distance between them, which is, to good approximation, the distance between the closed system's dominant doublet energy levels. However, as $\Gamma>|2V+\Delta s|$, the peaks merge as in the case of the two-level system studied in Sect. 5.3, and the new maximum is located at $E=E'+\overline{s}$.

At these resonant energies, the transfer efficiency can be directly obtained as

$$p(E' + \overline{s}) \approx \frac{\Gamma^2}{V^2} \frac{(2V + \Delta s)^2}{\left(\Gamma^2 + (2V + \Delta s)^2\right)^2},$$

$$p\left(E' + \overline{s} \pm \frac{1}{2}\sqrt{(2V + \Delta s)^2 - \Gamma^2}\right) \approx 1,$$
(5.28)

and the dwell time reads

$$\tau(E' + \overline{s}) \approx \frac{4\Gamma}{\Gamma^2 + (2V + \Delta s)^2},$$

$$\tau\left(E' + \overline{s} \pm \frac{1}{2}\sqrt{(2V + \Delta s)^2 - \Gamma^2}\right) \approx \frac{2}{\Gamma}.$$
(5.29)

At first, we can conclude from these results that, whenever $\Gamma < |2V + \Delta s|$, there is an energy, given by Eq. (5.26), at which we can probe the system with 100% transfer probability. On the other hand, once $\Gamma > |2V + \Delta s|$ the two resonance peaks merge, the maximal transfer probability is achieved at $E = E' + \overline{s}$, and the transfer probability gradually decreases as the ratio between Γ and $|2V + \Delta s|$ increases. The phenomenology is exactly the same as in Figs. 5.2 and 5.3, although the additional Δs term can be detrimental, as it can make the difference between optimal- and (strongly) reduced transfer probability. We also observe that the dwell times τ are still mainly governed by the parameter Γ , and, therefore, one strives to have Γ as large as possible. Making sure that one remains in the regime where $|2V + \Delta s| > \Gamma$, this guarantees the possibility of both efficient (height transfer probability) and fast (short dwell time) transfer. Again, we notice that when the two peaks merge, not only does the transfer probability decline, also the dwell time increases.

The entire derivation presented above shows that the results for the dominant doublet system are comparable to the results for the two-level system, apart from the

spectral shifts, here expressed via Δs and \bar{s} . This is very similar to the discussion in Chap. 4, where we described the dynamics of the dominant doublet as that of a two-level system. However, we did see in Chap. 4 that there were high frequency modes superimposed on the dominating oscillations stemming from the doublet. Much in the same manner, our present derivation ignores additional resonance peaks at other energies, which are present in the spectrum. Just from the perturbative results, it becomes clear that these other resonance peaks must be very narrow: The imaginary part of the complex eigenvalues of $H_{\rm eff}$ determines the widths of the resonance peaks, and for those eigenvalues that are not part of the dominant doublet, these imaginary parts only appear in the higher orders of the perturbative expansion (5.21). This implies that, in general, these states are extremely hard to probe and very long-lived once they are populated. On the other hand, if the real part on these intermediate eigenvalues comes close to one of the dominant doublet levels, there can be pronounced interference effects in the resonance profile. These effects are related to higher order terms in (5.21) and are therefore not contained within the theory as it is presented here, moreover numerical simulations suggest that one only very rarely encounters such realisations of the ensemble.⁸

5.5 Statistical Treatment

The model as described above treats a generic realisation of our scattering problem. However, we wish to ultimately treat these systems as an ensemble, in analogy to Chap. 4. Therefore, we are not merely interested in the possibility to enhance the transfer probability by the inclusion of Δs , but also in the relative volume of such enhancing realisations within a random sample of appropriately designed Hamiltonians (as introduced in the previous section). In order to assess this question, we must rely on a statistical treatment, for which we use results of Sect. 4.5.

5.5.1 The Indirect Treatment

From the results of Sect. 5.4, recall that the key parameter which governs the maximal transfer probability is $\Gamma/|2V+\Delta s|$. Although this is not a direct statistical assessment of the maximal transfer probability $p_{\rm max}$, we know that whenever $\Gamma<|2V+\Delta s|$, we anyway obtain $p_{\rm max}\approx 1$. Therefore, understanding the probability to find realisations with $\Gamma<|2V+\Delta s|$ directly implies understanding the density of efficient realisations.

⁷See for example the perturbative treatment described in Fyodorov and Savin (2012).

⁸These events are not excluded from our numerical simulations and they clearly have no significant influence on the results in Sect. 5.5.3.

The structure of $H_{\rm eff}$ is given by Eq. (5.20), which is equivalent to the structure of the Hamiltonian (4.81), amended by the $-i\Gamma/2$ terms which originate from the coupling to the channels. However, the bulk states are in lowest order perturbation theory not affected by the channels, and therefore we found expression (5.21), where we clearly see that s^{\pm} are exactly the same as those of (4.83). Given that the same mathematical equations have the same solutions, even though they arise in a different physical context, we can use the statistics of Δs as given in Eq. (4.114).

Much of Sect. 4.5 was devoted to the difference between two distinct recipes for the realisation of dominant doublets and to determining in each case the parameters s_0 and σ of the Cauchy distribution. In the present chapter, we work with these two parameters but not necessarily fix them explicitly. Therefore, the results which we will obtain can be applied to both methods to handle the dominant doublet.

We start out with a slight reformulation of the problem, and introduce rescaled variables $\tilde{\Gamma} := \Gamma/2V$ and $\Delta \tilde{s} := \Delta s/2V$. With these quantities, the condition for optimal transfer probability is reformulated as $\tilde{\Gamma} < |1 + \Delta \tilde{s}|$. We can also consider the new distribution

$$\Delta s \sim \text{Cauchy}(\tilde{s}_0, \tilde{\sigma}),$$
 (5.30)

where we introduce the rescaled parameters $\tilde{s}_0 := s_0/2V$ and $\tilde{\sigma} := \sigma/2V$. The advantage of these rescaled quantities is not merely that we eliminate one parameter from the equations, but also that the remaining parameters are all dimensionless.

The goal of this section is to derive the density of realisations for which nearperfect transfer probability is achieved, which is given by

$$\begin{aligned} \operatorname{Prob}(\tilde{\Gamma} < |1 + \Delta \tilde{s}|) &= \operatorname{Prob}(\Delta \tilde{s} > \tilde{\Gamma} - 1) + \operatorname{Prob}(\Delta \tilde{s} < -1 - \tilde{\Gamma}) \\ &= 1 - \int_{-\tilde{\Gamma} - 1}^{\tilde{\Gamma} - 1} d\Delta \tilde{s} \ P(\Delta \tilde{s}) \\ &= 1 - \frac{1}{\pi} \left(\arctan\left(\frac{\tilde{\Gamma} - 1 - \tilde{s}_0}{\tilde{\sigma}}\right) + \arctan\left(\frac{\tilde{\Gamma} + 1 + \tilde{s}_0}{\tilde{\sigma}}\right) \right), \end{aligned} \tag{5.32}$$

and clearly shows the sensitive interplay between $\tilde{\Gamma}$, $\tilde{\sigma}$ and, to a lesser extent, \tilde{s}_0 . Figure 5.8 plots this density as a function of $\tilde{\Gamma}$, for different values of $\tilde{\sigma}$, with \tilde{s}_0 set to zero. The transition from efficient transfer to no transfer at all (*ergo* complete reflection into the input channel) is clearly visible for the three values of $\tilde{\sigma}$, but it smoothens as $\tilde{\sigma}$ increases. Moreover, we see that the transition point also shifts to larger values of $\tilde{\Gamma}$. When we focus on $\tilde{\sigma} \ll 1$, we observe that there is a strong tendency to reproduce the results of the two level system dealt with in Sect. 5.3, thus the sharp transition at $\tilde{\Gamma} \approx 1$. Statistics acquire a more important role once $\tilde{\sigma} \approx 1$, where we observe that even as $\tilde{\Gamma} > 1$, there is still a considerable density of

⁹This parameter is typically much smaller than one, due to the dominant doublet condition (4.68). This is clearly seen in (4.93), (4.131), (4.97) and (4.135).

5.5 Statistical Treatment 161

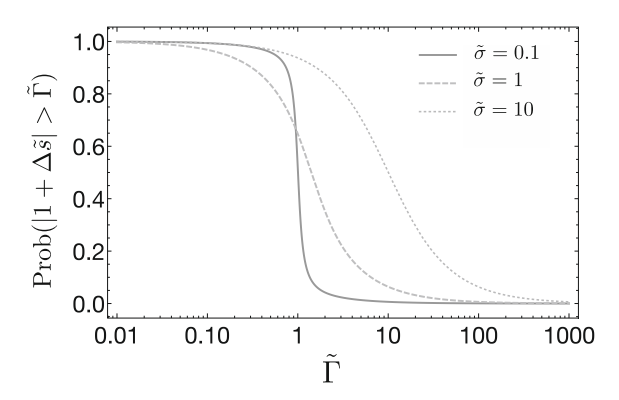


Fig. 5.8 Density (5.33) of efficient realisations, as a function of rescaled coupling to the channels $\tilde{\Gamma} = \Gamma/2V$, for different values of the width of the distribution of energy shifts, relative to the input-output coupling, $\tilde{\sigma} = \sigma/2V$. The parameter $\tilde{s}_0 = s_0/2V$ is set to zero. In the light of the dominant doublet condition (4.68), (4.93), (4.131), (4.97), and (4.135) this is most reasonable

realisations which manifest near-optimal transfer through the system. On the other hand, there is a downside: For $\tilde{\Gamma} < 1$, we find a non-zero density of realisations where the additional (bulk) sites have a negative impact on the transfer. This, however, can be counteracted by an increase of $\tilde{\sigma} \gg 1$, such that the transition from high density of efficient realisations to a low density only occurs at $\tilde{\Gamma} \gg 1$. In this case, the bulk sites can almost deterministically provide optimal transfer in the regime where $\tilde{\Gamma} \approx 1$.

The interest to shift the transition zone in Fig. 5.8 to larger values of $\tilde{\Gamma}$ lies in the fact that Γ determines the dwell times (and lifetimes, for separated resonance peaks). Therefore, $\tilde{\Gamma}\gg 1$ represents a system where the direct transfer in the two-level system is very fast, but also very unlikely, due to the merging resonance peaks. The additional bulk sites push these peaks apart by statistically shifting their resonance energies, whereas the transfer time scale remains essentially controlled by Γ . Therefore, the addition of bulk sites allows us to generate an ensemble where a considerable subset is able to mediate efficient energy transfer on much faster time scales. The prize to pay is that we abandon the deterministic approach, and, instead, elaborate a statistical theory. Consequently, also the resonance energies will fluctuate for different elements of the ensemble.

Although this approach provides us with a strong method to estimate the density of realisations where the two resonance peaks of the dominant doublet levels are not completely overlapping and hence where transfer probabilities of approximately 100% can be expected, it does not provide any information about the transfer probabilities themselves once the resonances merge. Therefore, it is desirable to have a direct statistical treatment of $p_{\rm max}$, as a complementary tool to understand the transfer characteristics.

5.5.2 The Direct Treatment

A statistical analysis on p_{max} directly is unfeasible for various reasons: This maximal transfer efficiency is achieved at the in general distinct resonance energies (5.26) and (5.27), and changes from a constant value in a given parameter region, to being a function of Γ , V and Δs in another. To deal with this inconvenience, one may attempt to circumvent the problem by probing the system slightly off-resonance.

For this idea to be successful, we require an energy which is well defined for all values of $\tilde{\Gamma}/|1+\Delta \tilde{s}|$, and at all times induces a transfer probability close to the actual maximum. Such quantity can be found by considering exactly the energies (5.26) and (5.27): In the discussion following (5.26) we noted that, in the limit where $\tilde{\Gamma}/|1+\Delta \tilde{s}|\ll 1$, the resonance peaks are located at $E\approx E'\pm V+s^\pm$. When $\tilde{\Gamma}/|1+\Delta \tilde{s}|\gg 1$, these energies are a bit off-resonant, but still they may serve as an estimate for p_{max} . More specifically, we find upon explicit evaluation of (5.24), (5.25) for $p(E'\pm V+s^\pm)$ and $\tau(E'\pm V+s^\pm)$ (the result is the same for "+" and "-") that

$$p(E' \pm V + s^{\pm}) \approx \frac{(1 + \Delta \tilde{s})^2}{(1 + \Delta \tilde{s})^2 + \tilde{\Gamma}^2 / 4},\tag{5.34}$$

$$\tau(E' \pm V + s^{\pm}) \approx \frac{2}{\Gamma} \left(1 + \frac{\tilde{\Gamma}^2/4}{(1 + \Delta \tilde{s})^2 + \tilde{\Gamma}^2/4} \right), \tag{5.35}$$

for convenience already expressed in the rescaled variables $\tilde{\Gamma}$ and $\Delta \tilde{s}$. One may argue, moreover, that the use of these energies is, rather than a technicality also a natural strategy, since the choice above exactly coincides with the actual energy levels of the closed system, ignoring the coupling to the external channels. Again, we see that also here the parameter which governs the dwell time is Γ —notice that this is *not* the rescaled variable. Because Γ is not influenced by the fluctuations in the ensemble, we cannot hope to severely influence the time scales in the statistical approach, therefore we focus on the statistics of the transfer probability p.

We consider p as a stochastic variable, to obtain its probability density function by using that it is a function of another stochastic variable $\Delta \tilde{s}$ of which we know the probability distribution from Eqs. (4.114) and (5.30). Exploiting the statistics of $\Delta \tilde{s}$, we can obtain the probability distribution of p as

$$P(p) = \int_{\mathbb{R}} d\Delta s P(\Delta s) \delta \left(p - \frac{(1 + \tilde{\Delta s})^2}{(1 + \tilde{\Delta s})^2 + \tilde{\Gamma}^2/4} \right). \tag{5.36}$$

To evaluate this expression, we use that, for the Dirac-delta function (Wolfram Research 2001),

5.5 Statistical Treatment 163

$$\delta(f(x)) = \sum_{j=1}^{m} \frac{\delta(x - x_j)}{|f'(x_j)|}$$
 (5.37)

where $f(x_j) = 0$ and $f'(x_j) \neq 0$. Inserting this identity in Eq. (5.36), we ultimately find

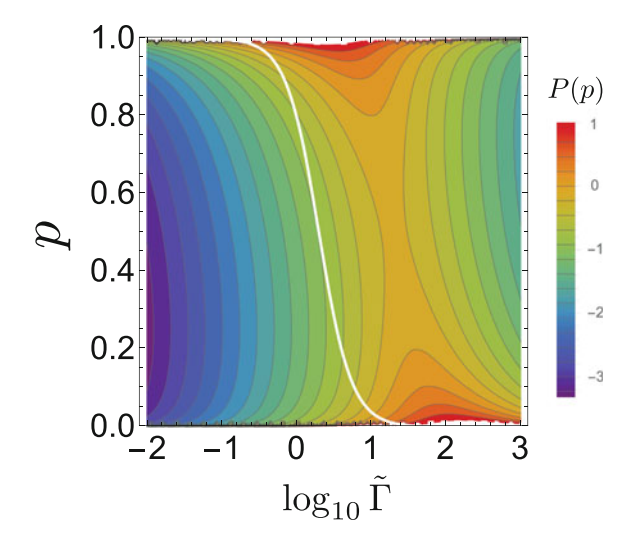
$$P(p) = \frac{\tilde{\Gamma}}{4\pi\sqrt{p}(1-p)^{3/2}} \left(\frac{\tilde{\sigma}}{\tilde{\sigma}^2 + \left(1 + \tilde{s}_0 - \frac{\tilde{\Gamma}}{2}\sqrt{\frac{p}{1-p}}\right)^2} + \frac{\tilde{\sigma}}{\tilde{\sigma}^2 + \left(1 + \tilde{s}_0 + \frac{\tilde{\Gamma}}{2}\sqrt{\frac{p}{1-p}}\right)^2} \right). \tag{5.38}$$

Note that the condition $f'(x_j) \neq 0$ is violated exactly on the edges of the interval [0, 1] on which the distribution is defined. This implies that the resulting distribution (5.38) is strictly speaking only valid for $p \in [\epsilon, 1 - \epsilon]$. These divergences are an artefact which is inherited from the power-law statistics that governs $\Delta \tilde{s}$.

The behaviour of Eq. (5.38) for different values of $\tilde{\Gamma}$ is given in Fig. 5.9, for $\tilde{\sigma} = 10$. Comparing to the isolated two-level system as given by the white curve, we observe that the transition form highly efficient transfer to the region with low transition probability is shifted towards larger values of $\tilde{\Gamma}$, in agreement with our above discussion of Fig. 5.8. Additionally, the probability density smears out in this transition region, implying that all values of p occur with comparable probability.

Even though this result provides us with a direct quantification of the statistics of transfer probabilities throughout the ensemble, it still heavily relies on some assumptions: At first, we ignored higher order terms of the perturbative expansion (5.21) in the derivation of the scattering matrix elements $S_{\text{in}\to\text{out}}(E)$, see (5.23). In addition, we neglected interference effects caused by other resonance peaks possibly lingering close to the resonances associated with the dominant doublet. In order to verify that the assumptions we made are reliable, we compare our results to numerical simulations.

Fig. 5.9 Probability density P(p) of the transfer efficiency (as logarithmically scaled density plot), as given by Eq. (5.38), as a function of $\tilde{\Gamma}$, for $\tilde{\sigma} = 10$. The parameter \tilde{s}_0 is set to zero. The white curve indicates $p_0(E' + V)$, the transfer probability (5.11) for the two-level system (5.7) without intermediate sites



5.5.3 Numerical Results

In our numerical simulations, we explicitly evaluate

$$p_{\text{in}\to\text{out}}(E) = |S_{\text{in}\to\text{out}}(E)|^2$$
 (5.39)

for the probing energy $E = E' + V + s^+$, see (5.34). To do so, we generate the non-Hermitian Hamiltonians H_{eff} randomly in the site-basis, as given by (5.19), and we choose to work in the *averaged dominant doublet ensemble* (recall our definition (4.71) and the statistics (4.93), (4.131) in Chap. 4). ¹⁰ For a system with n intermediate sites, the statistics of the Hamiltonian's entries is given by

$$(H_{\text{int}})_{i,j} \sim \text{Normal}\left(0, (1+\delta_{i,j})\frac{\xi^2}{N}\right),$$
 (5.40)

$$v_i \sim \text{Normal}\left(0, \frac{\chi^2}{N}\right),$$
 (5.41)

$$E' \sim \text{Normal}\left(0, 2\frac{\xi^2}{N}\right).$$
 (5.42)

Therefore, the parameters which are directly controlled while performing the simulations are N, ξ , χ , V, and Γ . Notice that these are the relevant parameters of the theoretical model, therefore we have the freedom to probe all the regimes and verify the statistics. Furthermore, we make sure that the root mean square (RMS) coupling ξ/\sqrt{N} among the bulk sites, and the RMS coupling χ/\sqrt{N} between the input/output and the bulk, are chosen in such a way that

$$\langle \left| \left\langle \pm, \tilde{\pm} \right\rangle \right|^2 \rangle_{\text{realisations}} \approx 1$$

according to Eq. (4.93).

The data are obtained by choosing different values for Γ which are adopted to logarithmic scaling of the data represented in Figs. 5.10 and 5.11 (for practical purposes we chose $\Gamma_{i+1}=1.2\,\Gamma_i$). For each value of Γ , we sample 10,000 random Hamiltonians $H_{\rm eff}$, calculate the shift s^+ by explicit diagonalisation, and thus obtain $p_{\rm in \to out}(E'+V+s^+)$. To finally generate Fig. 5.10, we insert the numerically obtained data points in the extrapolation method SmoothKernelDistribution of Mathematica.

Figure 5.10 shows that there is good qualitative agreement between the analytically predicted probability density (5.38) and the numerically extracted one. The parameters to generate the different numerical results where also varied 11: The results where $\tilde{\sigma} = 0.1$ and $\tilde{\sigma} = 1$ where obtained for N = 8, whereas those for $\tilde{\sigma} = 10$ where

 $^{^{10}\}mathrm{When}$ doing numerics we are bound to make and explicit choice on which dominant doublet ensemble is used.

¹¹This way we make sure that we are not accidentally probing any special parameter regime.

5.5 Statistical Treatment 165

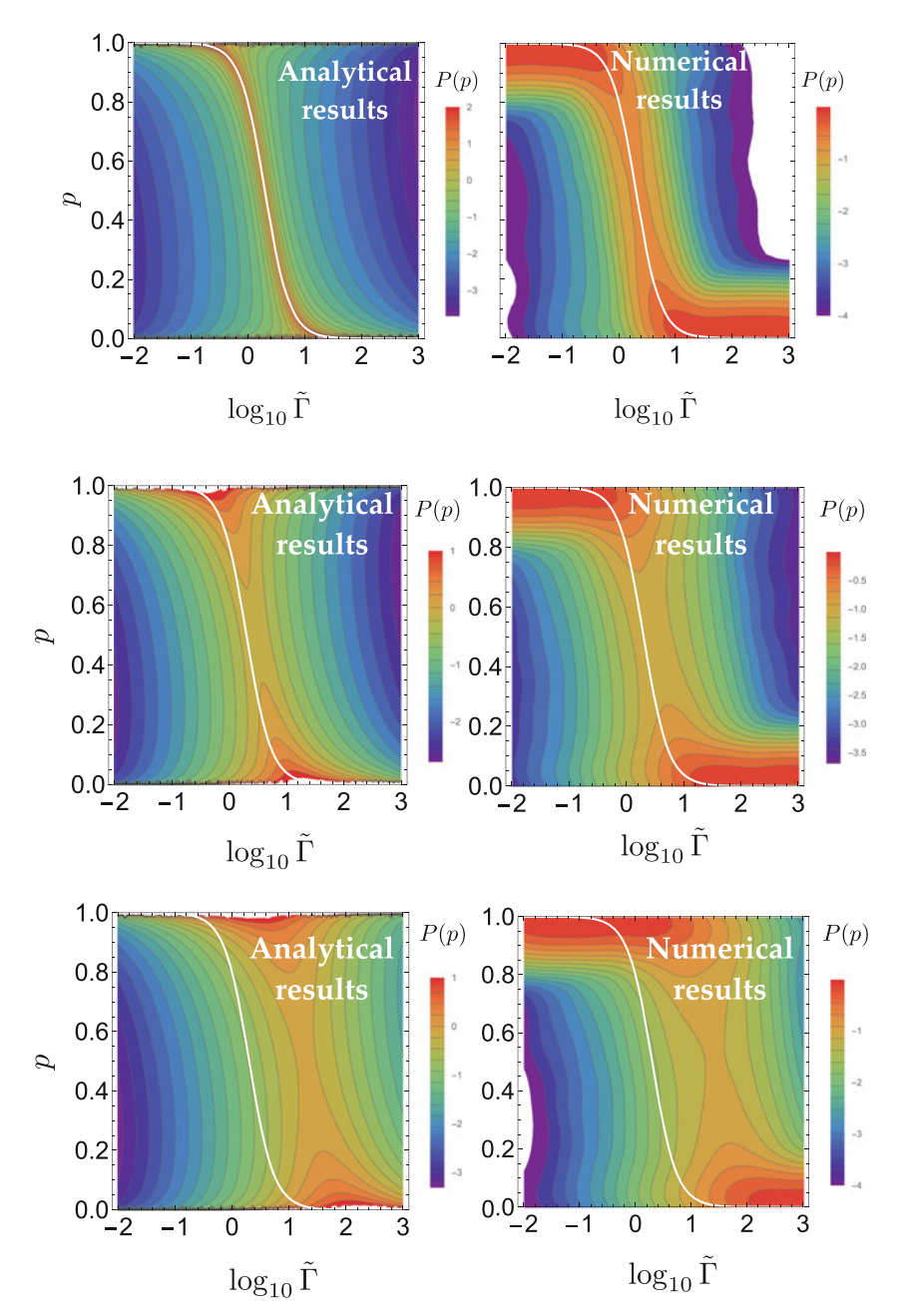


Fig. 5.10 Probability density P(p) of transfer efficiencies (as logarithmically scaled density plot), as given by Eq. (5.38) (left) and as variable $\tilde{\Gamma}$. Different values for $\tilde{\sigma}$ are shown in different rows: $\tilde{\sigma}=0.1$ (top), $\tilde{\sigma}=1$ (middle) and $\tilde{\sigma}=10$ (bottom). The white curve indicates $p_0(E'+V)$, the transfer probability (5.11) for the two-level system (5.7) without intermediate sites

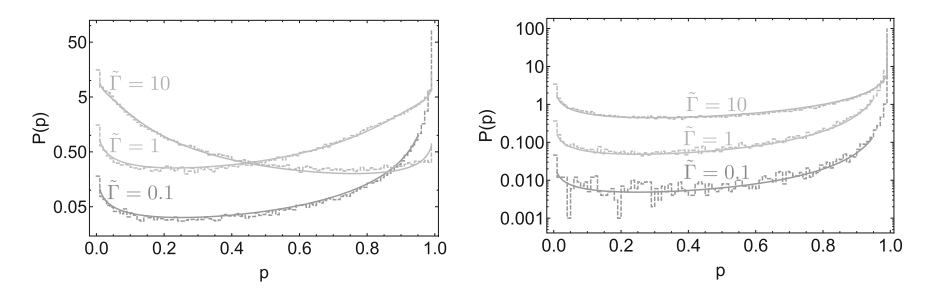


Fig. 5.11 Probability distribution as predicted theoretically by Eq.(5.38) (solid lines), and as obtained (histograms, dashed lines) from numerical simulations. The width of the shift distribution, relative to the coupling between input and output sites, was chosen as $\tilde{\sigma}=1$ (left) and $\tilde{\sigma}=10$ (right). In each panel, results are shown for three different values of the rescaled coupling strength $\tilde{\Gamma}$ to the leads: $\tilde{\Gamma}=0.1$, $\tilde{\Gamma}=1$ and $\tilde{\Gamma}=10$

generated with N=10. Moreover the parameter ξ is changed such that the $\tilde{\sigma}=0.1$ numerical run was conducted with $\xi=20$, $\tilde{\sigma}=1$ with $\xi=50$ and $\tilde{\sigma}=10$ with $\xi=150$. The dominant doublet demand (4.93), where we set $\alpha'=0.95$, with the given values for $\tilde{\sigma}$ and ξ , fix all other parameters in the RMT ensembles and therefore completely determine the theoretical model. The qualitative agreement between the analytical and numerical results prevails for all these different choices of parameters, which as such confirms the theoretical prediction that $\tilde{\sigma}$ and $\tilde{\Gamma}$ are ultimately the only parameters that matter. The parameter ξ sets a general energy scale, determining the typical (as in RMS) coupling between two intermediate sites as ξ/\sqrt{N} . This overall energy scale turns out to be of no importance, because the relevant physics is contained in ratios of coupling strengths (i.e. $\tilde{\sigma}$ and $\tilde{\Gamma}$).

Observing Fig. 5.10, there is an obvious shift of the transition zone from highly probable optimal transfer, to rather poor transfer probabilities. This transition zone initially coincides with the white curve indicating the result without intermediate sites, and it gradually shifts to larger values of $\tilde{\Gamma}$ with increasing $\tilde{\sigma}$, indicating a transition from transport dominated by the direct coupling V to transport dominated by intermediate sites as controlled by the width σ of the shift distribution.

Strikingly, the values $\tilde{\Gamma}$ at which this transition zone is located do agree quantitatively in the analytical and numerical treatment. The main difference between analytical and numerical results is that the latter exhibit all the features of the analytical result, though slightly smeared out and broadened. This can either be due to a lack of statistics, or to some oversimplification of the theory. To discriminate between these two possibilities, we consider several slices of the plots of Fig. 5.10, for different values of $\tilde{\Gamma}$, mainly probing the interesting transition zone. Sampling 100,000 realisations for each choice of $\tilde{\Gamma}$, we compare the actual histograms to the analytical prediction (5.38) of the probability density in Fig. 5.11. The agreement for each value of $\tilde{\Gamma}$ and $\tilde{\sigma}$ is clear, at least on the semi-log scale. This implies that, indeed, our analytical model is very successful in reproducing the correct statistics, and that the smeared out features in the numerical results of Fig. 5.10 result from a lack of statistics.

5.6 Summary and Outlook

We started out by showing that for a two-level system, which consists of an input and an output site, each attached to a different external channel, has its maximal transmission properties determined by the ratio $\tilde{\Gamma}$ between Γ and 2V—with Γ the coupling between input/output channel and input/output site, and V the direct coherent coupling between these two sites. The breakdown of efficient transfer occurs when $\tilde{\Gamma} > 1$, which implies that the two scattering resonance peaks are broader than their relative separation, causing them to strongly interact.

This destructive interaction can be fought by introducing additional disordered sites into the system, following the recipe of Sects. 4.4 and 5.4. These design principles impose a spectral shift between the *dominant doublet's* energy levels. When this shift is strong enough, it pushes apart the resonance peaks such that their mutual separation is greater than their width. The success of this protocol is determined by the statistics of the spectral shifts Δs , which follow a Cauchy distribution as shown in Eqs. (4.114) and (5.30).

In order to characterise the statistical properties of the transfer probability $p_{\text{in}\to\text{out}}$ we imposed both a direct and an indirect treatment in Sect. 5.5. The conclusions in both approaches are the same: The main parameters which govern the transport are $\tilde{\Gamma}$ and $\tilde{\sigma}=\sigma/2V$. If we want any beneficial effect from the additional sites, we must have $\tilde{\sigma}>1$, implying that the indirect transfer mediated by intermediate sites is dominant over the transfer dominated by the direct coupling between input and output states. However, when $\tilde{\Gamma}\gg\tilde{\sigma}>1$, there is only a very small probability to enhance the transfer probability. Nevertheless the main downside of the intermediate sites occurs when $\tilde{\Gamma}$ is slightly smaller than one and $\tilde{\sigma}\approx 1$. In this range of parameters, one has a considerable probability to push the peaks closer together and actually make the transfer worse than it initially was. Ergo, mainly in the regime where $\tilde{\Gamma}\gg 1$ we can make a huge difference by engineering a system such that $\tilde{\sigma}\gg 1$, specially by making $\tilde{\sigma}>\tilde{\Gamma}$. Notice that even though $\tilde{\sigma}$ is a parameter which controls the statistics, it can actually lead to near-deterministic optimal transfer probability when tailored properly.

With or without intermediate states, the transfer dwell time $\tau_{\text{in}\to\text{out}}$, estimating the time needed for the excitation to be transferred from one channel to the other, is dominated by the parameter Γ (not $\tilde{\Gamma}$). Therefore, it is useful to strive for a setting where the systems interact as strongly as possible with the external channels. Since physical constraints may limit us from designing systems such that V is sufficiently large to lead to fast and efficient transfer in a simple double-well setup, one can couple additional degrees of freedom such that $\tilde{\sigma}$ be sufficiently large to push the peaks sufficiently far apart. One may also argue that a system relying on a single direct coupling between two sites in a double-well type system lacks robustness. Indeed, if there is an error in manufacturing which decreases V, transport would break down, whereas the statistical nature of the ensemble with intermediate sites provides a statistical sense of robustness.

The use of such a statistical model comes at a price; although we can exploit the mechanism to obtain an ensemble where a large subset manifests near perfect transfer from the input to the output channel, we are confronted with the statistical distribution of the resonance energies. The statistical shifts in the resonance peaks can lead to a variety of different energies at which the peaks are localised, which induces an effect which in the spectroscopy community is known as *inhomogeneous broadening* (Mandel and Wolf 1995; Mukamel 2009). It is a direct consequence of the disordered nature of the systems under consideration; in principle the Cauchy distribution (4.114) can again be used to understand this effect.

Now that we completed this discussion on fast and efficient single-particle quantum transport in complex systems, we are in the perfect position to study its potential concrete applications. As already mentioned in Sect. 4.1, our central motivation is that of transport processes in biological systems. In the following chapter we therefore investigate how the design principles of Chap. 4 and this chapter can be applied to the context of energy transfer in photosynthetic organisms.

References

- D. Adams, Mostly Harmless (Pan in association with Heinemann, London, 1993)
- G. Berkolaiko, J. Kuipers, Moments of the Wigner delay times. J. Phys. A Math. Theor. 43, 035101 (2010)
- P.W. Brouwer, K.M. Frahm, C.W.J. Beenakker, Quantum mechanical time-delay matrix in Chaotic scattering. Phys. Rev. Lett. **78**, 4737–4740 (1997)
- G.L. Celardo, L. Kaplan, Superradiance transition in one-dimensional nanostructures: an effective non-Hermitian Hamiltonian formalism. Phys. Rev. B 79, 155108 (2009)
- C. Cohen-Tannoudji, J. Dupont-Roc, and G. Grynberg, *Atom-Photon Interactions: Basic Processes and Applications* (Wiley, New York, 1998)
- U. Fano, Effects of configuration interaction on intensities and phase shifts. Phys. Rev. 124, 1866–1878 (1961)
- H. Feshbach, Unified theory of nuclear reactions. Ann. Phys. 5, 357–390 (1958)
- H. Feshbach, A unified theory of nuclear reactions. II. Ann. Phys. 19, 287–313 (1962)
- H. Feshbach, The unified theory of nuclear reactions: III. Overlapping resonances. Ann. Phys. 43, 410–420 (1967)
- Y.V. Fyodorov, D.V. Savin, Statistics of resonance width shifts as a signature of Eigenfunction nonorthogonality. Phys. Rev. Lett. 108, 184101 (2012)
- P. Gaspard, Quantum chaotic scattering. Scholarpedia 9, 9806 (2014)
- F. Haake, F. Izrailev, N. Lehmann, D. Saher, H.-J. Sommers, Statistics of complex levels of random matrices for decaying systems. Z. Phys. B Condens. Matter 88, 359–370 (1992)
- S. Hunn, Microscopic theory of decaying many-particle systems. Ph.D. thesis, Albert-Ludwigs-Universität Freiburg, Freiburg, 2013
- S. Hunn, K. Zimmermann, M. Hiller, A. Buchleitner, Tunneling decay of two interacting bosons in an asymmetric double-well potential: a spectral approach. Phys. Rev. A 87, 043626 (2013)
- R.A. Jalabert, J.-L. Pichard, C.W.J. Beenakker, Universal quantum signatures of Chaos in ballistic transport. EPL 27, 255 (1994)
- J. Kuipers, M. Sieber, Semiclassical relation between open trajectories and periodic orbits for the Wigner time delay. Phys. Rev. E 77, 046219 (2008)
- C.H. Lewenkopf, H.A. Weidenmüller, Stochastic versus semiclassical approach to quantum chaotic scattering. Ann. Phys. 212, 53–83 (1991)

V.L. Lyuboshitz, On collision duration in the presence of strong overlapping resonance levels. Phys. Lett. B **72**, 41–44 (1977)

- J. Madroñero, A. Buchleitner, Ericson fluctuations in an open deterministic quantum system: theory meets experiment. Phys. Rev. Lett. 95, 263601 (2005)
- L. Mandel, E. Wolf, Optical Coherence and Quantum Optics (Cambridge University Press, Cambridge, 1995)
- S. Mukamel, *Principles of Nonlinear Optical Spectroscopy*. Oxford Series in Optical and Imaging Sciences, vol. 6 (Oxford University Press, New York, 2009)
- I. Rotter, A non-Hermitian Hamilton operator and the physics of open quantum systems. J. Phys. A Math. Theor. **42**, 153001 (2009)
- P. Šeba, K. Życzkowski, J. Zakrzewski, Statistical properties of random scattering matrices. Phys. Rev. E **54**, 2438–2446 (1996)
- F.T. Smith, Lifetime matrix in collision theory. Phys. Rev. 119, 2098–2098 (1960)
- H.-J. Stöckmann, *Quantum Chaos: An Introduction* (Cambridge University Press, Cambridge, 2007)
- H.-J. Stöckmann, E. Persson, Y.-H. Kim, M. Barth, U. Kuhl, I. Rotter, Effective Hamiltonian for a microwave billiard with attached waveguide. Phys. Rev. E 65, 066211 (2002)
- I. Wolfram Research, Dirac delta function: Identities (formula 14.03.17.0001) (2001)

Chapter 6 Quantum Effects in Biological Systems



One of the profoundest enigmas of nature is the contrast of dead and living matter

Hermann Weyl (1949)

6.1 From Schrödinger to "Quantum Biology"

Life, a manifestly non-equilibrium process that cleverly defies thermodynamics by reproduction, is often simply too difficult to be described with the mathematical precision an generality that we, physicists, consider the ultimate goal of our field. Nevertheless, the tremendous efforts done by life scientists, ranging from ecology (Debecker et al. 2015), over evolution (Geerts et al. 2015), to system biology (Kollmann et al. 2005) are remarkably successful in applying statistical tools (Pugesek 2009; Zuur 2009) to disentangle the mysteries presented by the topics they study. The emergence of the field of biophysics taught us that biology and physics can be combined and find a common basis exactly via these statistical descriptions, which are reconcilable with statistical mechanics. Moreover, on the molecular level, developments in physics have lead to a wide range of spectroscopic techniques which were crucial for many discoveries in biology (Deisenhofer et al. 1985; Franklin and Gosling 1953; Schluenzen et al. 2000; Watson and Crick 1953; Wilkins et al. 1953). It is the goal of this chapter and this text to point out that physicists have many reasons to be excited about biology, although differences in jargon and methodology also impose barriers that need to be overcome.

Biophysics was arguably born at the end of the 19th century, with fundamental work on statistics and the rise of statistical mechanics. In this period, notable

¹Here we also consider stochastic processes, such as those underlying rate equations (Marcus and Sutin 1985) as part of the field of statistical mechanics.

physicists such as Helmholtz delivered contributions to physiology (Helmholtz and Southall 1910; Helmholtz 1850) and the statisticians Pearson and Fisher constructed the mathematical foundations of the theory of evolution (Fisher 1930; Pearson 1894). The field later received an enormous boost when Schrödinger, then already celebrated as one of the founders of quantum mechanics, turned his attention to biology with his "What is life" (Schrödinger 1944). This work had considerable impact, for example by providing a molecular basis for genetics. Although the concept of "genes" was discussed much earlier by Muller (1922), who called them "ultra-microscopic particles", it can be argued that Schrödinger was among the first to realise that large, complex molecules could be the carriers of genetic information. It must be noted, however, that Schrödinger himself was inspired by earlier work (Timoféeff-Ressovsky et al. 1935) which already concluded that genes needed to have a complicated structure.

The impact of "What is life?" was increased when in the same year the first experimental indications for the existence of DNA (Avery et al. 1944) were published. Moreover, Schrödinger's description provided by far the most detailed proposal for a molecular structure of genes, which he proposed to be an "aperiodic crystal". Metaphorically, he states that this structure could be interpreted as a code that encrypts all genetic information. Therefore, it may be said that Schrödinger effectively predicted the existence of DNA before its experimental discovery. The genuine scientific value of Schrödinger's book and the originality of the arguments therein is still topic of debate.² It was, however, clearly an important inspiration for molecular biologists at the time: both Watson (1969) and Crick (1988) explicitly acknowledge being influenced by "What is life?" and Wilkins even explicitly acknowledged Schrödinger's work in his Nobel lecture (Wilkins 1962).³ Moreover, the work also had an impact in the field of medicine (Nordling 1953).

Even though Schrödinger inspired the discovery of DNA and discussed the importance of mutations thereof (Schrödinger 1944), the role of quantum mechanics in this discussion is today considered "trivial": The molecular level of biology is governed by chemistry—and chemistry, on its turn, is fundamentally governed by quantum physics. The extent to which quantum effects are now identified in biology, was probably beyond the imagination of 1944's Erwin Schrödinger.⁴

It has taken the scientific community decades to push non-trivial quantum mechanics beyond the realm of extremely tedious proof of principle experiments. Until the early 21st century, the increasing insights in the effects of decoherence suggested that quantum effects can only manifest themselves in systems that are strongly shielded from their environment (i.e. extremely low temperature, high vacuum, et cetera). Hence, quantum mechanics would be practically irrelevant in biophysics, mainly due to high temperatures and an enormous number of environmental degrees of freedom.

²An overview of opinions can be found in Dronamraju (1999).

³Watson and Crick even wrote an explicit letter to thank Schrödinger for inspiring them. The Royal Irish Academy recently uploaded a copy of the letter on Twitter (RIAdawson 2014).

⁴Nevertheless, Schrödinger did also consider (Schrödinger 1944) more intricate quantum effects. It is even proposed that quantum uncertainty may be a solution to unify a human body governed by the laws of nature with the notion of free-will. However, this is currently still considered (Davies 2004) closer to science fiction than to scientific fact.

Nevertheless, such decoherence effects need time to destroy all the coherences in the system, below such decoherence time scale, quantum mechanics can manifest itself. Given such time scales in widely open systems, it is clear that the only biological processes that can be influenced are ultrafast, i.e. sub-picosecond time scale. Potential candidate-processes are often found in the realm of charge and energy transfer. A modest influence of quantum structures was already present in the earliest theoretical descriptions for such processes, provided by Marcus and Förster (Förster 1948; Marcus and Sutin 1985; Marcus 1993; May and Kühn 2000). However, these quantum mechanical effects are only important to determine rates that enter rate equations and can therefore be considered "trivial". The idea that quantum mechanics may be more important came gradually, for example by studies of charge transfer in proteins and DNA (Skourtis and Mukamel 1995). Another such example is photosynthesis. where quantum phenomena such as excitons, delocalised over several chlorophyll molecules (Pullerits et al. 1996), and even super-radiance (Monshouwer et al. 1997) have been considered since the nineties. The theoretical models to describe energy transfer processes in these systems have gradually evolved from rate equations to Redfield theory (Redfield 1965), taking quantum effects explicitly into account.

Although Redfield theory is reasonably successful, it still describes a model where essentially classical transport is dominant because of decoherence. Significant new insight was obtained with the introduction of 2D electronic spectroscopy (Fuller and Ogilvie 2015; Hamm and Zanni 2011; Mukamel 2000, 2009), which one may interpret as an extension of pump-probe spectroscopy (Stolow et al. 2004) or a translation of multidimensional NMR techniques (Aue et al. 1976) to the optical domain. Using these techniques, a new perspective was proposed by pioneering work such as Brixner et al. (2005), Collini et al. (2010), Engel et al. (2007), when it was suggested that the transport of energy in photosynthesis actually exploits quantum coherence in a very non-trivial way. Earlier evidence in this direction had already been obtained using other experimental techniques (Chachisvilis et al. 1997). The authors of these works suggest that the energy transfer is governed by quantum coherence that persists up to almost a picosecond (Collini et al. 2010; Engel et al. 2007) and carries the excitons across a network of (bacterio) chlorophylls. Even though these claims have been refined and tempered down considerably ever since, these results attracted much attention from quantum physics communities (Alicki and Miklaszewski 2012; Aubry 2014; Hoyer et al. 2010; Jesenko and Žnidarič 2012, 2013; Manzano 2013; Mohseni et al. 2008; Plenio and Huelga 2008; Scholak et al. 2010, 2011a; Walschaers et al. 2013; Zech et al. 2013, 2014; Zech 2013). Contemporary discussions on accurate models of energy transfer in photosynthesis are situated at two fronts: On the one side, there are the models which are remarkably successful at reproducing experimental data, but lack predictive power (Ishizaki and Tanimura 2005; Kreisbeck and Kramer 2012). On the other side, there are more simplified "toy" models that try to

⁵Redfield's model describes transport in terms of a quantum master equation (Breuer and Petruccione 2007). Generically, systems described by these equations undergo decoherence, such that on sufficiently long time scales (which depend on the decay rates in the system) the dynamics converge to those described by classical rate equations.

single out underlying mechanisms and use them to make predictions. A real match between these two sides of the medal is still lacking. We will extensively come back to this point later in this chapter.

The discovery of non-trivial quantum effects in photosynthesis increased debate about quantum effects in the broader field of biology. A particularly cute proposal was that the European Robin's avian compass exploit entanglement to generate an extremely sensitive quantum sensor for the earth magnetic field (Gauger et al. 2011; Katsoprinakis et al. 2010; Ritz et al. 2000; Wiltschko and Wiltschko 1972). Other effects, such as quantum effects in ion channels (Vaziri and Plenio 2010) and even in the brain (Hameroff and Penrose 1996), have attracted attention, although they remain highly speculative. It must be stressed that even though aesthetically appealing, most of these models lack experimental verification.

Excited quantum physicists like to put all these different topics under one label: "quantum biology", as to represent the dawn of a new era in biology. But is there really such a thing as "quantum biology"? First, let us put some emphasis on connotation: Phrasing a term as "quantum biology" puts it in a list next to "quantum mechanics", "quantum electrodynamics", "quantum information", "quantum chaos", et cetera. Although these different fields are very diverse, rich, and interdisciplinary, they have one fundamental thing in common: There is a universal theory that lies at their basis. This underlines the very core of the *physicist's* way of thinking, the search for *universality* in nature. Presenting the term "quantum biology" insinuates the existence of a universal quantum backbone of biology. This is at least far beyond what can currently be substantiated by actual (experimental) evidence—while science is still to be considered evidence-based by its very methodology.

Even though universal rules are also found in life sciences, they have a very different status as the universal laws of physics. One of the main quests of biology is exactly to understand the deviations from these rules, i.e. biodiversity. These deviations are generally understood in terms of evolutionary pathways, which are governed by a complicated interplay between all the steps on the hierarchical ladder which ranges from the molecular to the ecological level. In this sense, "quantum biology" currently undermines the very load of that term, since it neglects these foundations of biology.⁶

It is a fact that quantum mechanics is an available tool for life to exploit just as any other law of physics is. Given that the cut between quantum physics and classical physics is most probably a human construct, it is reasonable to assume that nature does not care to think about whether something is quantum or classical. In this sense, if quantum mechanics would offer an evolutionary advantage to an organism, it may very well be exploited. After all, in all abstraction living organisms are simply solving an evolutionary optimisation problem. However, this is again where problems with the physicist's perspective kick in: Given that everything from molecules up to the ecosystem constitute this optimisation problem, it is almost impossible to know what

⁶An interesting question is whether the non-trivial quantum effects, which were observed up to now, are a manifestation of a general universal rule or rather a deviation thereof. At present, there is insufficient material to answer that question.

is actually being optimised.⁷ For example, if we consider quantum effects in photosynthesis, we—physicists—may assume that fast and efficient transfer is "optimal". However, it can be beneficial for some organisms to be inefficient in transporting energy, such that a lot of heat is generated, providing them with an ecological advantage (Herbert et al. 2007). This emphasises the far-reaching consequences of the hierarchical structure of functionality and of diversity in biology.

The fact that nature and life confront us with so much diversity, should be seen as a warning to remain cautious when modelling any biological system. When one considers the enormous difference between different light harvesting complexes, such as LHII, LHCII, and the FMO⁸ complex (Blankenship 2002), one cannot simply conclude that they are similar. It may well be that, although they share common origins from the evolutionary point of view, they have evolved to optimise very different fitness functions (Orr 2009), and potentially use very different physics to do so. This is by no means an argument against quantum effects in photosynthesis (or biology as a whole for that matter), but a warning that one should not jump to conclusions.

In the following sections, we present in some more detail the efforts that were specifically undertaken to develop quantum mechanical transport models which may be applicable in a photosynthesis context. The key resources at hand are disorder and noise. We first provide an overview of how they may be exploited and subsequently we explain how the design principles, developed in the previous chapters, can find applications in the photosynthetic realm.

6.2 Photosynthesis: Disorder Versus Noise

Let us now focus on the problem of quantum effects in photosynthesis and specifically on the quest for simple models to underpin the physical mechanisms that govern the energy transport in such systems. Here, one usually does not worry about the ways in which long-lived quantum coherence in maintained; one assumes that it is simply there and studies its influence on the transport. By merely looking at a system such as the FMO complex (Blankenship 2002), one directly sees that these systems are far away from the clean, periodic structures that we know from idealised solid-state models, or from the highly controlled, engineered set-ups in quantum optics. One can therefore say that these systems are *disordered*, but since they occur in biology with a serious degree of reproducibility, there is also a degree of design. Because

⁷In biological jargon one may state that the "fitness function" (Orr 2009) is unknown. In optimisation problems, one strives to find parameters for which a function is maximal/minimal (or reaches sufficiently high/low values). Understanding the behaviour such problems is, however, difficult without any knowledge of the function which is optimised.

⁸The green sulphur bacteria, in which this complex is found, are only occurring in sludge in ponds. From a purely biological and ecological point of view, this system is therefore of quite marginal importance. From a molecular perspective, it is by far one of the easiest photosynthetic complexes to handle, hence its popularity in photosynthesis research.

we consider biological processes, we work at approximately room temperatures and hence a serious amount of *noise* should be present, after all there obviously is a huge environment (e.g. proteins) around to generate a bath into which energy can be dissipated. If the excitation were to stay in the system long enough, these effects would certainly lead to dynamics that can be described by rate equations. The noise acts on many time scales, some of them as long as micro- or milliseconds (Krüger et al. 2012), time scales much longer than those at which the energy transfer processes occur. Therefore, these slow configurational fluctuations can also be interpreted as different disorder realisations.

These two fundamental effects, *disorder* and *noise*, lead to two opposing views on the possible mechanisms of the energy transfer in photosynthetic complexes. Both proposed paradigms start from the assumption that the transport in these systems is fast (sub-picosecond time scales) and efficient. The latter is usually quantified via the quantum efficiency (4.5), which is claimed to be around 95% (Blankenship 2002). These claims can be traced back to Chain and Arnon (1977), Wraight and Clayton (1974), and by modern standards one may challenge whether these are really direct measurements of the relevant quantum efficiency. Nevertheless, the starting point of all models is that the excitations which enter the systems reach their destinations, the photosynthetic reaction centre, with very high probability.

The first line of thought can be summarised by the term *noise assisted transfer*, which is inspired (Plenio and Huelga 2008) by stochastic resonance (Gammaitoni et al. 1998; Huelga and Plenio 2007; Wellens et al. 2004). The starting premise of these models is that ultimately disorder is bad for quantum transport (one often refers to Anderson localisation Anderson 1958), but because the negative effects arise from destructive interference, they can be counteracted by decoherence (Blümel et al. 1991; d'Arcy et al. 2004; Steck et al. 2000). The first models with import this principle to the photosynthesis context (Mohseni et al. 2008; Plenio and Huelga 2008) refer to a regime between coherent and incoherent transport, where the energy transfer appears to be optimal. It was initially claimed that these models provided good agreement to experimental results, but given the large amount of free parameters, this is hardly surprising. It is, however, reasonable to question several of the initial assumptions.

First of all, one often starts running the model from the so-called Hamiltonian of the system (Adolphs et al. 2007; Moix et al. 2011; Schmidt am Busch et al. 2011). This Hamiltonian describes the inter-site couplings and on-site energies by combining a multitude of spectroscopic data with structure data, quantum chemistry and a serious amount of fitting. However, since spectroscopy data always result from experiments on an ensemble of molecular complexes, we cannot claim to have *the* Hamiltonian of the system. What *is* observed, is an ensemble averaged Hamiltonian. It is very dangerous to do quantum dynamics calculations with such an object, because obviously

$$\mathbb{E}_{\mathrm{dis}}\left(e^{-itH}\right) \neq e^{-it\,\mathbb{E}_{\mathrm{dis}}(H)} \tag{6.1}$$

⁹During a talk at the Freiburg Institute for Advanced Studies in Summer 2015, this 95% figure was challenged by Richard Cogdell, who reported that new, currently still unpublished, measurements suggests efficiencies that are roughly 20% lower.

and thus the dynamics is not self averaging. This implies that, under the assumption that there is disorder in a quantum transport setting, we should rather consider the fluctuations in transfer properties, which result from the variations in H over different disorder realisations. One can even show that quantum dynamical maps, obtained for ensemble averaged dynamics, are on their own no longer unitary, but can be described by a non-Markovian master equation (Gneiting et al. 2016; Kropf et al. 2016).

A second point of criticism targets the very assumption that disorder is necessarily disadvantageous in quantum transport. We showed explicitly by formulating a full-fledged theory in Chaps. 4 and 5 that the right design can actually exploit disorder to achieve good, even near-optimal excitation transfer, but also earlier, largely computational work (Scholak 2011; Scholak et al. 2010, 2011a,b,c, 2014) has proven that, in finite size systems, the belief that disorder is always destructive is wrong. Due to the finite size of the system, it is possible to find realisations which lead to good transport, even when randomly sampling spatially disordered dipole-dipole networks. ¹⁰ It was moreover shown that these realisations are reasonably abundant. This line of argumentation immediately leads to the second paradigm.

The competing point of view, in contrast to the *noise-assisted* philosophy, is that quantum interference, even in disordered systems, serves as a resource for good transport (Alicki and Miklaszewski 2012; Manzano 2013; Mostarda et al. 2013; Scholak et al. 2010, 2011a). The fundamental underlying idea of this disorder assisted transport is the concept of design principles. The naive point of view is that, due to the finite size of the system, searching long and hard enough (and nature had hundreds of millions of years to do so), one can always find configurations that foster constructive interference. Ultimately this simply boils down to matching an enormous amount of phases, but as long as this amount is finite, it can be done. That the system seems disordered to our eye, may simply imply that such realisations are highly non-trivial (Scholak 2011; Scholak et al. 2011b,c). However, these systems are extremely sensitive to very small perturbations and as much as nature might be able to design systems, an unrealistic amount of control would be required to secure the functionality. In a later stage the research on design principles shifted from the idea of specially designed controlled structures to design principles which allow for statistical control, such as we presented in Chaps. 4 and 5. By construction, these models allow for disorder to be present and they even exploit spectral fluctuations as a resource for enhanced transport. Needless to say, such approach is more appropriate for applications in biology than its highly fine-tuned predecessor due to its intrinsic robustness. We further elaborate on this idea in the next section.

Although we, as strong proponents of this particular view, see more merit in the design principle approach than in the noise-assisted approach, we must be mindful of its limitations. Beautiful as the idea of incorporating disorder rather than fight-

¹⁰This line of reasoning was originally imported from condensed matter theory, where it is known that fluctuations have a dominant role in quantum transport. A profound example is that of conductance fluctuations in mesoscopic systems (Jalabert et al. 1994), but also the "Anderson regime" leads to strong fluctuation in finite size systems (Kramer and MacKinnon 1993). This *phenomenology* lies at the heart of the present approach.

ing it may seem, there are problems to find experimental smoking guns. Models which propose control of statistics are generically difficult to check, since statistical information is nontrivially available in experiments. Nevertheless, advances in single-molecule experiments (Hildner et al. 2013) indicate a wide spread in the observed energy transfer time scales, which is consistent with the results of Chap. 4. However, the statistics in these experiments is insufficient for a quantitative comparison. Additionally, an issue of models which exploit random matrix theory is that they are built to reproduce statistical features of spectra. They are not intended to model the microscopic structure of the system, which is a serious paradigmatic shift compared to the common approaches in physical chemistry (May and Kühn 2000).

In the meantime, most of these simple models have grown considerably in complexity, as it was realised that they were not correctly capturing the relevant physics in the system. It is fair to conclude that ultimately the two views have strongly converged throughout the course of time. The noise-assisted picture evolved from structured environments (Rey et al. 2013), over non-markovian effects (Ishizaki and Fleming 2009; Sarovar et al. 2010) to vibration-assisted transfer (Christensson et al. 2012). The latter has gained a lot of traction since it considers some vibrational (and thus environmental) degrees of freedom, but ultimately treats them in an essentially coherent fashion (actually "dressing" the exciting spectrum).

The role of vibrations was also recently recognised in coherent models, since they require a resonance between on-site energies to obtain near-optimal transfer. The level structures of light-harvesting systems, however, do not show such resonances and therefore the energy difference must somehow be bridged. Recent work (Brugger 2015) showed that a treatment of some vibrational degrees of freedom in Floquet framework (Shirley 1965) actually can overcome this energy gap in an effective way. This approach also requires a fine interplay between electronic and vibrational degrees of freedom and is hence in philosophy very close to the vibration-assisted framework.

As a final remark, we note that the idea of vibrationally assisted transfer was recently challenged (Fujihashi et al. 2015). The authors claim that, even though the vibrational effects strongly influence the spectroscopy, the small Franck–Condon factors would diminish these effects in energy transport.

There is one philosophical difference between noise-assisted and the disorder-assisted paradigms, which will remain hard to reconcile. In the one framework, disorder is really assumed to be the overall enemy and the weapon to attack it is noise, whereas the other framework sees noise as the enemy and fights it through disorder enhanced transport (to make transport much faster than decoherence time scales). On the other hand, given our previous discussion on the importance of diversity in biology and the rich variety of time scales treated in Chap. 4, it is not unreasonable that both effects actually play a role. Indeed, it was already pointed out that realisations with poor coherent transport properties do benefit from noise, whereas those with good coherent properties see a disadvantage (Scholak et al. 2011a). However, specifically the good realisations also show a degree of robustness against noise (Fernández de Cossío Díaz 2013), which implies that actually in one ensemble, there are several realisations which exploit coherent quantum transport. Others, where the

disorder does not have a positive effect, get enhanced by noise. In terms of Fig. 4.16, this implies that noise-assisted transfer affects the lefthand side of the distribution, shifting it to faster time scales, whereas the righthand side of the distribution is left untouched. Such scenario is feasible, but clearly requires further study to reach conclusions.

6.3 Design Principles in Photosynthesis

The model presented in Chaps. 4 and 5 was explicitly inspired by the discovery of quantum effects in photosynthesis (and also by excitation transport in cold Rydberg gasses Scholak et al. 2014). In this section, we elaborate on the indications that these design principles may already be implemented by nature. Moreover, we also stress some of the problem with which our model is confronted and how these can be overcome. We focus our attention on the well-known FMO complex (Blankenship 2002).

As stressed in the previous section, it is currently difficult to obtain statistics of transfer time scales or transfer efficiencies. Although we have beautiful theoretical frameworks, which lead to analytical results such as Eq. (4.135), relevant experimental data for comparison are currently lacking. To explain what really happens in nature, we are strongly limited by those data which are experimentally available: A wide range of spectroscopic results (all ensemble experiments, hence leading to ensemble averaged information), structure data (obtain by crystallising the complexes and doing X-ray spectroscopy, thus providing "pictures" of the complexes taken under conditions *distinct* from their natural habitat). In addition, we can also employ a wide range of data analysis tools.

Combinations of structure and spectroscopy data lead to what is often called "the Hamiltonian of the system". We know that, due to the many noise processes that act on slow time scales, there are effectively many disorder realisations. In principle one can go quite far in simulating these effects via molecular dynamics (Humphrey et al. 1996; Leach 2001; Strümpfer et al. 2012), but computational overhead would be enormous. The underlying idea is that vibrational degrees of freedom in the bacteriochlorophylls, ¹¹ proteins, and all other surrounding molecules can act quite strongly on the bacteriochlorophyll molecules' electronic degrees of freedom, changing for example the orientation of their dipole moments and on-site energies. These effects lead to variations in the Hamiltonians of the in situ light harvesting complexes where the energy transport is actually taking place. Furthermore, the variations in Hamiltonians can lead to strong fluctuations in transport time scales and efficiencies.

¹¹The photosynthetic pigments in phototrophic bacteria are called bacteriochlorophylls and are narrowly related to the chlorophylls that appear in plants, algae, and cyanobacteria. They typically have different light absorption profiles than chlorophylls (see for example Fig. 6.2 in Scholes et al. 2012).

We start by studying the ensemble averaged Hamiltonian that is obtained in the literature¹² (Schmidt am Busch et al. 2011)

$$H_{\text{lit}} = \begin{pmatrix} 505. & 37.5 & 7.5 & 1.7 & 4.5 & -9.7 & -11.4 & 1.5 \\ 37.5 & 310. & -97.9 & -5.8 & 6.7 & -12.1 & -10.3 & 5.5 \\ 7.5 & -97.9 & 230. & 7.3 & 2. & 11.5 & 4.8 & 30.1 \\ 1.7 & -5.8 & 7.3 & 180. & -64.9 & -17.4 & -64.4 & -58.8 \\ 4.5 & 6.7 & 2. & -64.9 & 405. & 89. & -6.4 & -1.5 \\ -9.7 & -12.1 & 11.5 & -17.4 & 89. & 320. & 31.7 & -9.6 \\ -11.4 & -10.3 & 4.8 & -64.4 & -6.4 & 31.7 & 270. & 4.7 \\ 1.5 & 5.5 & 30.1 & -58.8 & -1.5 & -9.6 & 4.7 & 0. \end{pmatrix}$$
 cm⁻¹, (6.2)

where the first row and column relate to the input and the last row and column to the output site, respectively. In order to compare the results to efficiencies provided in the literature, we need to gauge the dynamics against a suitable benchmark time scale. Due to the high temperatures, fast decoherence times are expected and we set

$$T_B = \frac{0.1\pi\hbar}{|2(H_{\text{lit}})_{1,8}|} \approx 3.5 \,\text{ps},$$
 (6.3)

to make sure that the transfer occurs on time scales where there can still be coherent phenomena.

First of all, we notice that the choice of $|e_1\rangle$ as input and $|e_8\rangle$ as output state vectors (see (4.1)) leads to very poor transport properties; we find an efficiency (as defined by (4.6)) of $\mathcal{P}_H \sim 10^{-3}$. Conjecturing that the reason for this low efficiency is the energy mismatch between input and output site, we can simplify the model by ignoring the on-site energies —after all, these energies are a consequence of the local coupling of the site-network to environmental degrees of freedom. This implies that simply considering the bacteriochlorophyll molecules' positions and orientations leads to the Hamiltonian $H_{\rm lit}^0$, which is essentially $H_{\rm lit}$, but with zeroes on the diagonal. Now we have a model where all the couplings are exactly what is obtained in literature, but where resonant, coherent transport is possible. With this Hamiltonian, we find a significant increase in efficiency, up to $\mathcal{P}_H = 0.12$, which is much better than for the Hamiltonian with on-site energies, but still far bellow any enhanced efficiencies as described in the literature.

We can take disorder effects into account on several levels, ranging from the simplest possible white noise model, to far more realistic models where we deal with a network of dipoles and permute their positions and orientations. Both methods have been implemented (Scholak 2011; Zech 2013) and were fruitful tools to learn about the potential of disorder, e.g. the results in Zech (2013), Zech et al. (2014) directly influenced our choice in Chap. 4 of centrosymmetry as a design principle. However, the dominant doublet provides a new design principle that was not discussed earlier and thus we probe its relevance in quantum transport in complex systems, based on $H_{\rm lit}^0$. Our first approach is a white noise model, where we consider a family of

 $^{^{12}}$ In spectroscopy literature, it is common to express energies in wave numbers, cm $^{-1}$, the conversion to SI units is given by 1cm $^{-1} = 1.98630 \times 10^{-23}$ J.

Hamiltonians H, generated such that

$$\begin{cases} H_{ij} = (H_{\text{lit}}^0)_{ij} + \Xi, & \Xi \sim \text{Normal}(0, \lambda), \quad i \neq j \\ H_{ii} = 0. \end{cases}$$
(6.4)

There are no correlations between the fluctuations in the different elements of the generated Hamiltonians, and the parameter λ indicates the typical strength of the disorder. For all of these Hamiltonians, we can now run the dynamics and obtain the value \mathcal{P}_H .

Apart from the efficiency, we also evaluate whether the systems have a tendency to be centrosymmetric and to form a dominant doublet, and we need to design measures for these properties. The measure for centrosymmetry was already described in Zech (2013), Zech et al. (2014); it reads

$$\epsilon := \min_{S} ||H - JHJ||, \tag{6.5}$$

where we consider the Hilbert-Schmidt norm $||A|| = \sqrt{\operatorname{tr} A^{\dagger} A}$ (Reed and Simon 1980). J denotes the symmetry matrix $J_{ij} = \delta_{i,N-j+1}$ and we minimise over any possible labelling of the intermediate sites, indicated by S. Notice that the range of this measure inconveniently depends on H.¹³

The dominant doublet strength is more straightforward to measure, since it can practically be quantified by $|\langle \pm, \pm \rangle|^2$. Notice, however, that it is not a priori clear which eigenvectors are the candidate dominant doublet vectors and therefore we must maximise over all possible choices. This implies that we consider $\max_i |\langle \eta_i, \pm \rangle|^2$, with η_i the eigenvectors of H, which gives us a value for the overlap with $|+\rangle$ and with $|-\rangle$. We want both of these overlaps to be large, therefore we consider the minimum of both, this leads us to the final measure

$$\alpha := \min_{\pm} \max_{i} |\langle \eta_i, \pm \rangle|^2, \tag{6.7}$$

where η_i are the eigenvectors of H. Contrary to ϵ , the range of the measure α is independent of H.

In Fig. 6.1, we see how this uncorrelated disorder model impacts the transport properties. The density maps show that even this simplistic way of modelling disorder can increase the transfer efficiency. However, very few realisations pass $\mathcal{P}_H = 0.5$. We acquire an insight in the manifestation of design principles: There is a correlation

$$\epsilon' := 1 - \min_{S} \frac{\|H - JHJ\|'}{2\|H\|}$$
 (6.6)

which has the more intuitive properties that $\epsilon'=1$ implies a highly centrosymmetric system and $\epsilon'=0$ implies the system is far from centrosymmetric. This insight however only came after the simulations had already been conducted, with the measure ϵ .

¹³Using the triangle inequality, we could have defined the measure as

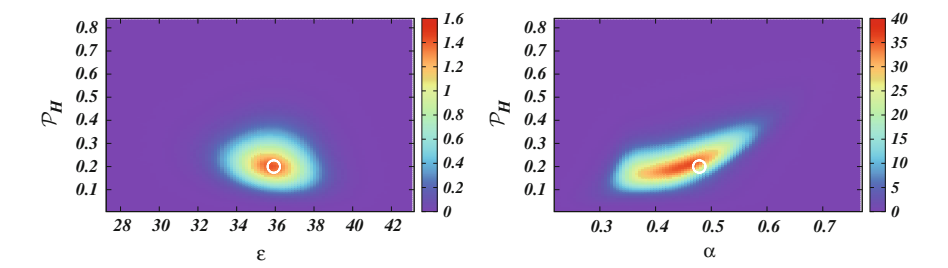


Fig. 6.1 Density maps of the transport efficiency \mathcal{P}_H against the centrosymmetry measure ϵ (left), Eq. (6.5), and against the dominant doublet measure α (right), Eq. (6.7), when sampled over a white noise distribution around the literature Hamiltonian, according to (6.4). The colour code depicts the density of realisations, normalised to the actual probability density function. The middle of the white circle indicates the position of H^0_{lit} (see text). The strength of the fluctuations was chosen $\lambda = 5 \, \text{cm}^{-1}$

between \mathcal{P}_H and α , although it is not strongly pronounced for these low efficiencies. In a more statistical jargon, we can quantify this using the Pearson correlation coefficient (Edwards 1976; Pearson 1895), ¹⁴ which is

$$r := \frac{\mathbb{E}(\alpha \mathcal{P}_H) - \mathbb{E}(\alpha) \mathbb{E}(\mathcal{P}_H)}{\left(\mathbb{E}(\alpha^2) - \mathbb{E}(\alpha)^2\right) \left(\mathbb{E}(\mathcal{P}_H^2) - \mathbb{E}(\mathcal{P}_H)^2\right)} = 0.621341.$$

Contrary to what is expected from Zech et al. (2014), we do not see a correlation between \mathcal{P}_H and ϵ . A plausible explanation for this discrepancy is that our small perturbations (i.e. the parameter in (6.4) is chosen $\lambda=5\,\mathrm{cm}^{-1}$) completely ignore the physical dipole-dipole structure of Zech et al. (2014). This structure is particularly relevant because it induces correlations between the entries of the Hamiltonian upon changing the spatial structure of the network of dipoles. These correlations are completely overlooked by our white noise model, although they may be related to the positive impact of centrosymmetry. In addition, several studies on disorder enhanced transport also used genetic optimisation algorithms to specifically generate efficient realisations (Scholak 2011; Zech 2013), which creates a family of highly efficient systems by probing disorder realisations in a more directed way. Indeed, the white noise model does not strive for efficient transport, hence the resulting efficiencies remain low. It is possible that the correlation between centrosymmetry ϵ and efficiency \mathcal{P}_H only manifests itself for sufficiently high efficiencies.

To implement a more extended protocol that probes the potential of disorder, we collaborated with the complex systems group in Havana (Fernández de Cossío Díaz 2013; Walschaers et al. 2013), to develop a genetic algorithm that optimises the FMO structure in a realistic way. The algorithm is seeded with the spatial coordinates of the FMO complex' bacteriochlorophyll molecules (Table 6.1), together with

¹⁴This coefficient measures how close the data points are to forming a line. If they would form a perfect line, we find r = 1, when they form a "round cloud" we find r = 0.

2015)				
Site	x	у	z	
1	26.51	2.597	-11.349	
2	15.607	-1.517	-17.246	
3	3.389	-13.614	-13.851	
4	6.678	-20.848	-6.036	
5	19.378	-18.571	-1.076	
6	21.834	-7.175	0.634	
7	10.274	-8.207	-5.544	
8	21.766	13.748	-7.718	

Table 6.1 Spatial coordinates of the BChl*a* molecules of the FMO (in Ångstroms), extracted from file 3ENI.pdb1 in the Protein Data Bank (Tronrud et al. 2009). Table taken from Walschaers et al. (2013)

Table 6.2 Normalized dipole components of the BChla molecules of the FMO complex, extracted from file 3ENI.pdb1 in the Protein Data Bank (Tronrud et al. 2009). Table taken from Walschaers et al. (2013)

Site	S_x	S_y	S_z
1	0.741006	0.560602	0.369644
2	0.857141	-0.503776	0.107329
3	0.197121	-0.95741	0.210971
4	0.760508	0.593481	0.263453
5	0.736925	-0.655762	-0.164065
6	0.135017	0.879218	-0.456887
7	0.495115	0.708341	0.503105
8	0.553292	0.138385	-0.821412

the associated eight dipole moments \vec{d}_i , $i=1,\ldots,8$ (Table 6.2). These data determine the off-diagonal elements of the Hamiltonian H via dipole-dipole interaction (Schmidt am Busch et al. 2011). When we label the dipoles we follow the standard notation (Tronrud et al. 2009). The genetic algorithm works as follows:

1. Each one of the intermediate (i = 1, 2, 4, 5, 6, 7) sites' dipole moments' orientations is subject to 100 random perturbations, to generate new dipoles \vec{d}_i^{new} from the old ones \vec{d}_i^{old} , according to the following procedure:

$$\vec{b}_i = \vec{d}_i^{\text{old}} + r_i \vec{n}_i \tag{6.8}$$

$$\vec{d}_i^{\text{new}} = \vec{b}_i / \left| \vec{b}_i \right| . \tag{6.9}$$

Here r_i is a random Gaussian variable with zero mean and standard deviation σ (initially set to $\sigma = 0.005$), and \vec{n}_i is a randomly oriented unit vector generated

with the GSL (GNU Scientific Library Galassi 2009) routine $gsl_ran_dir_3d$, with the additional condition $|\vec{b}_i| \ge 0.1$.

- 2. These new dipole configurations define 100 new Hamiltonians H and, correspondingly, 100 new, different values of the quantum transfer efficiency \mathcal{P} , from input site 8 to output site 3.
- 3. That configuration which mediates the largest efficiency defines the new set of dipole moments \vec{d}_i .
- 4. We repeat steps 1–3 above, with the new \vec{d}_i , and reduce σ to σ/k , in the kth iteration.
- 5. The algorithm stops when $\mathcal{P}_H > 0.99$, or when k = 100.15

When seeded with the experimental FMO data, the algorithm generates efficient configurations very rapidly, typically convergence is reached in less than 20 iterations.

The results of this algorithm are shown in Fig. 6.2, this time in a scatter plot. The blue points indicate the family of optimised realisations that result from optimising the FMO complex's structure data for efficient transport and therefore high values of \mathcal{P}_H . At first these results imply that it is possible to reach very high efficiencies using disorder in a realistic fashion, by simply changing the dipole orientations. Moreover, we note that these blue points are clearly situated in a region where the Hamiltonians are more centrosymmetric and where a dominant doublet structure is present. Additionally, the fast convergence indicates that these realisations are reasonably easy to find.

It is natural to wonder whether these properties are typical for any dipolar network, or whether there is something special about the FMO data. When the algorithm is seeded with a random dipole configuration, there is no tendency to converge rapidly to high efficiencies. In this case, the algorithm regularly saturates at low values of \mathcal{P}_H , as seen from the wide spread of \mathcal{P}_H outcomes in Fig. 6.2 (crosses). Although we observe a wide spread in the efficiencies which are reached, there is still a correlation between \mathcal{P}_H and α . This time, we also observe a correlation between \mathcal{P}_H and ϵ : there are several possible reasons why this correlation appears in this simulation and not in the one with the simpler disorder model (see Fig. 6.1 above): First, we observe that the FMO Hamiltonian $H_{\rm lit}^0$ is more centrosymmetric than the majority of random Hamiltonians that manifest similar efficiencies. A reasonable conjecture is that the centrosymmetry facilitates the presence of a dominant doublet, and this relation between dominant doublet and centrosymmetry may simply be more pronounced in networks of coupled dipoles. However, in Chap. 9, we will see that centrosymmetry is also beneficial for quantum transport in absence of a dominant doublet. Even though that result may be due to a completely different underlying mechanism, it does suggest that the centrosymmetry does more than facilitating the presence of a dominant doublet.

If anything, the data in Fig. 6.2 explicitly show that the optimisation algorithm works extraordinarily well for the FMO literature data. The FMO structure is unambiguously easier to optimise than a random structure (even when the dipoles are

¹⁵There is no deep reason for choosing these specific conditions.

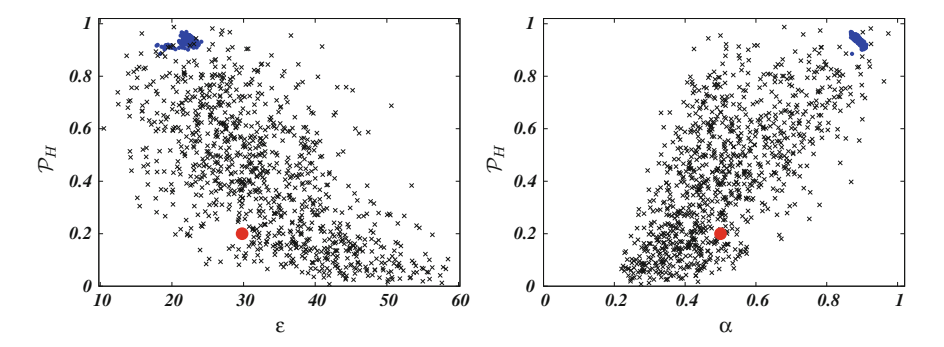


Fig. 6.2 Scatter plots of transfer efficiency \mathcal{P}_H versus centrosymmetry ϵ (left) and dominant doublet strength α (right). Evolutionary optimisation as achieved by a genetic algorithm is indicated by the small filled circles, upon seeding of the algorithm with the documented FMO structure (large filled circles) as listed in Tables 6.1 and 6.2. A benchmark ensemble generated by the algorithm when seeded with randomised dipole orientations is shown as reference (crosses). Figures use the data from Walschaers et al. (2013)

placed at the same positions and only the orientations are randomised). All these data and the fast convergence combined suggest that the optimal structure is actually not very different from the FMO structure as known in literature. To check this conjecture, we compare the orientations of the dipoles in the published structure, shown here in Table 6.2, to the dipole orientations of the optimised structures. The results of such comparison are shown in Fig. 6.3, where the centre of each circle indicates the original solid angle of the dipole moment. The density map indicates how the dipole moment of each of these specific bacteriochlorophyll molecules is altered in the various members of the optimised family of realisations. We observe that all but one dipole remain almost in the same orientation, the deviations with respect to the original structure are below 7%. The one exception is the dipole of the bacteriochlorophyll molecule which in the standard literature labelling is referred to as bacteriochlorophyll 4, with deviations of up to roughly 20% with respect to the original structure.

We cannot exclude that the striking similarity between the literature data and these highly efficient realisations is a coincidence, but it is remarkable to say the least. Moreover, it is surprising that only the orientation of one dipole moment must be changed to obtain these realisations with highly efficient transport properties. One may speculate that these data indicate a molecular switching mechanism, built into this one molecule, or that even the literature data for this one molecule are mistaken. These questions arise by analysing quantum transport properties, but most likely quantum physics will not provide the final answer. We can only hope that these data motivate molecular physicists, physical chemists and biochemists and provide them with directions for future experimental research.

In this setting, where on-site energies are ignored, there are clear indications that the design principles from the previous chapters can be used to generate efficient quantum transport. More remarkably, we show that the structure of the FMO's

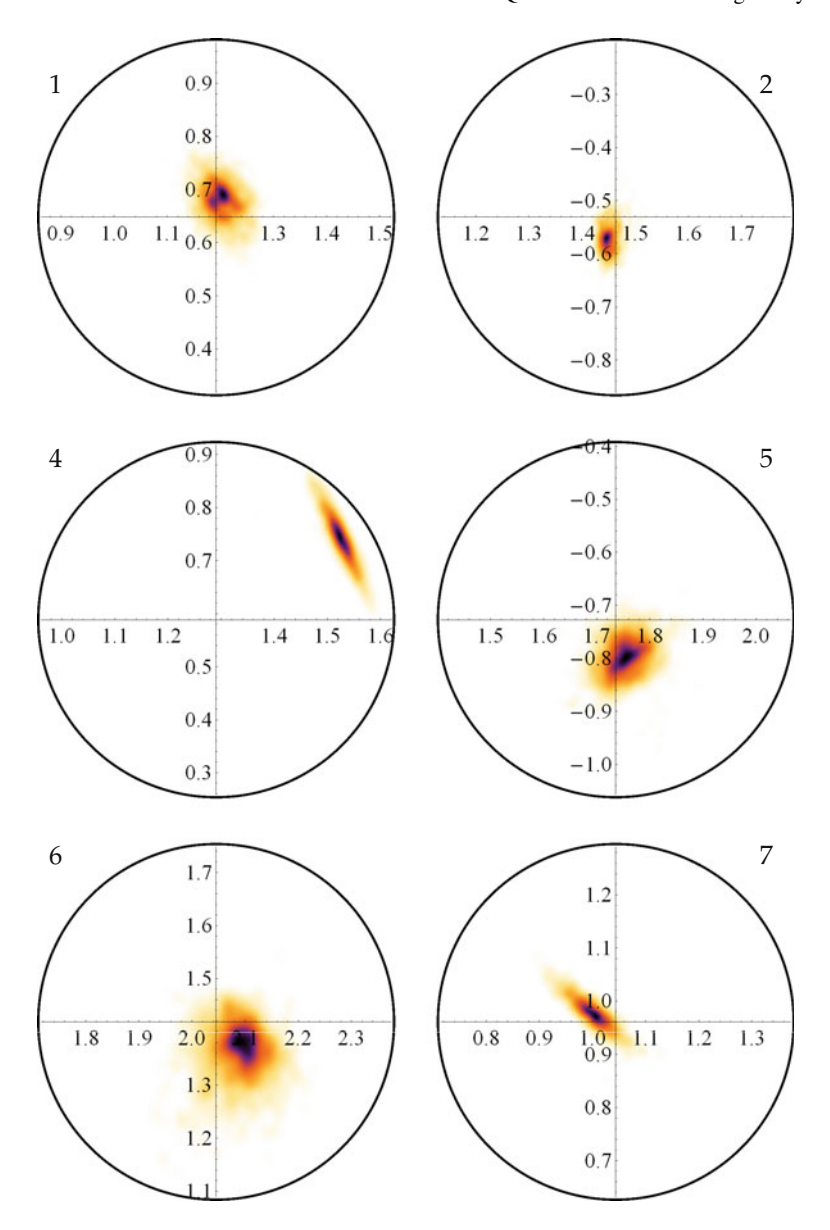


Fig. 6.3 Linearly scaled probability density of the genetically optimised FMO dipole orientations (dark colours indicating high densities), in spherical coordinates (ϕ, θ) (in radians). Dipoles 1, 2, 4, 5, 6, 7 are listed from left to right and top to bottom, and the experimental dipole orientation extracted from Table 6.2 defines the origin of each plot. Dipoles 8 (input) and 3 (output) are not shown since we keep their orientations fixed during optimisation. Figure taken from Walschaers et al. (2013)

dipole-dipole networks seems to facilitate these mechanisms. Nevertheless, when we introduce the diagonal elements to the Hamiltonian, the analysis presented above breaks down and we cannot even reach high values of \mathcal{P}_H anymore, mainly due to the mismatch in input and output energy levels. The beautiful structure of the system in absence of onsite energies, however, made us wonder whether nature may have exploited a trick to help overcome these energy gradients to still be able to exploit these design principles. We believe that this trick consists in using vibrations of the right frequency to shift the energy level into resonance (Brugger 2015). These are, however, prospects for future work, which brings us to the many other open problems in this type of research and the outlook on potential solutions.

6.4 Outlook

In the previous sections, we extensively discussed the ongoing efforts to describe photosynthesis in the context of quantum transport theory, exploiting the quantum coherence as observed in sophisticated experiments. Although we focussed on the knowledge gained throughout the past years, both in our own line of research and in the broader field, there are still many open problems that have not yet been mentioned. Here, we list several of these problems; for a much more detailed overview we refer to Scholes et al. (2017).

A first problem lies in the initial and final states. Whenever a quantum transport model is described, there must be a state in which the system is initialised and an ultimate target state that is to be reached. Many open problems revolve around the fact that it is not really understood what these states are. It is understood that everything starts with a photon and ends with a charge separation process, but all steps in between, and the multiple interfaces between them are being debated.

A first discussion relates to the light-matter interaction, where it is unclear what exactly the states are that are typically being populated by the incoming light. It is often argued that due to the limited spatial resolution, ¹⁶ the light does not resolve single chlorophylls, but sees the whole complex. This implies that the light field interacts with the eigenstates of the Hamiltonian and thus initially generates a delocalised exciton (Monshouwer et al. 1997). ¹⁷ This is in strong contrast with the model we presented here, where the initial exciton is localised on a single chlorophyll molecule. However, assuming that eigenstates of the Hamiltonian are populated, which are by definition stationary states, one could never obtain coherent transport. One solution is that there are additional, coherently coupled, degrees of freedom with no dipole moment, such that they do not couple with the light field but still affect the transport.

 $^{^{16}}$ The resolution of such optical experiments is diffraction-limited (Aeschlimann et al. 2011), hence the resolution is several hundreds of nanometers (a back-of-the-envelope calculations puts the estimate at \sim 350 nm).

¹⁷New results, however, indicate that collective coupling of dipoles to the photon bath can play a significant role in complexes consisting out of several molecules. This slightly distorts the idea of the light field interacting with the eigenstates of the Hamiltonian (Shatokhin et al. 2016).

In addition, excitations are not only travelling within a single light harvesting complex, but typically are transferred from one to the other before they eventually reach the reaction centre. Furthermore, light harvesting complexes are often arranged in some superstructure, and there is evidence that this (variable) superstructure has functional relevance (Zimmermann 2015). When we thus focus on quantum transport within a single light harvesting complex, we can wonder whether there is a difference between the initial state which described a particle that came from another light harvesting system, or one that was created by interaction with the light field. Moreover, we do not know how these different complexes couple to each other and whether we should describe these couplings in a coherent way or not. In a sense, the FMO complex, which we so eagerly studied, is an exception to the general picture: It is understood that in the actual organism, the excitons that travel through the FMO are always being transmitted via an antenna complex, the chlorosome, which actually takes care of all light-matter interaction (Moix et al. 2011). The chlorosome as such is not particularly well understood and neither it its actual interaction with the FMO complex. The latter only has one task: transmitting excitons from the antenna to the reaction centre. Because this is a very different role than played by most other light harvesting complexes, e.g. LHCII and LHII, which function both as antenna complexes and exciton transfer channels, it is not implausible were the FMO to function in a somewhat different way. This means that it is possible that the design principles for the FMO complexes are *different* from those of most other complexes.

Furthermore, there is an ongoing debate on differences arising from interaction with different types of light (Brumer and Shapiro 2012). It is argued that the light used in photon-echo experiments, being coherent light, is highly different from actual solar light, which is thermal. Therefore, it is argued that the understanding gained from nonlinear spectroscopy experiments cannot simply be extrapolated to living organisms. The main line of argument is that coherent light is able to generate quantum coherence in a system, whereas thermal light is not. Naively or at least formally, this is of course the case, which is simply a consequence of descriptions using master equations, but on the other hand, this line of argumentation is overly simplified. The discussion on coherent transport starts after the absorption of a photon, which implies some temporal resolution (to start after the absorption of a photon, we must know when a photon is absorbed). Such temporal resolution does not exist in a master equation approach (see also Chap. 9), which implies an additional, classical type of uncertainty; a classical randomness over which one must average. Master equation approaches do much more averaging than actually is desirable to describe these models for photosynthesis. This averaging over classical randomness in the time at which the exciton is created is a source of additional decoherence. In this sense, it is obvious that such models are not reproducing as much coherence. On the other hand, as long as we pump the system in different channels than those where we extract the energy, our discussion in Chap. 9 clearly shows that generically a current will flow through the system. Such a current is associated with coherence, as explained in Sect. 9.3.4. Therefore, no matter how one chooses to treat the problem, the argument that we cannot have coherence because we drive the system with incoherent light is

6.4 Outlook 189

simply wrong—certainly so for coherence on transient time scales, but even for the non-equilibrium steady state (Shatokhin et al. 2016).

This leads us to the debate on the final state. Many models incorporate a sink (Alicki and Miklaszewski 2012; Manzano 2013; Mohseni et al. 2008; Plenio and Huelga 2008; Scholak et al. 2011a), such that a single excitation is coupled out via an incoherent channel, typically attached to one site. The ultimate goal is to get the system in the state where it is empty. In our model, we simply strive to localise all the energy at one point in the system, which we identify with the output state, however one may argue that it is more important to have high average population in this output site. It is, on the other hand, unclear whether any of these "sink-models" makes much sense, there may for example be a coherent coupling between the reaction centre and the complex.

It is arguably the case that one should try to present models where one carries out all steps from the photon absorption from the light field until the ultimate step of charge separation. Such models are, however, currently out of reach.

This brings us to the biggest open problem of all. The whole debate on quantum effects in photosynthesis and even the whole hype around "quantum biology" was sparked by the discovery of quantum coherence in the signal obtained from photonecho experiments. However there is no direct indication that these effects are at all relevant for the biological functionality of light harvesting complexes. For all we know, they might simply be artefacts, although that seems improbable, since the observed coherences do last longer than they can be reasonably expected to, on the basis of general considerations of quantum open system theory (Collini et al. 2010; Engel et al. 2007). This indicates that a protection mechanism might be in place, and if that would be the case, it most probably implies that the coherences are used in one way or the other. 18 To make these statements more accurate, there is need for an experimental smoking gun of coherent transport. The large quest for the future of this type of research is clearly the identification of forms of manipulation of the system that allow us to unambiguously determine whether transport is coherent or not. One can here think of another purely coherent effect in disordered systems, coherent backscattering: It is know that when additional non-linear effects are included in the system, the coherence is destroyed and the effect vanishes (Muskens et al. 2012). We require a similar operation for light harvesting complexes, which unambiguously destroys coherence in the system but has negligible effects beyond that. If the excitation transfer dies with the coherence, one can be sure that coherence is really of importance.

Even if one understands that coherence is important for transport, it is still not clear in what way exactly it influences the final quantum efficiency. This is probably the holy grail of quantum transport models for photosynthesis: the development of a model that actually predicts quantum efficiencies and shows how the coherence properties influence it. For example, it may be that all quantum effects only serve to set a given rate for the transport, as suggested by Jesenko and Žnidarič (2013). It may be that there is a function for quantum coherence that has to make sure that a

¹⁸Notice that there is a lot of speculation in this sentence.

non-zero rate can exist. Such a scenario would reserve a profound role for quantum physics, but still the dynamics would be classical. Of course, the hope is that quantum effects are important to generate a full-blown quantum transport mechanism. For the time being, we can only guess for the final outcome, but advances are being made (Roden et al. 2016). However, there is also a growing stream of scepticism regarding the role of quantum effects in photosynthesis (Wilkins and Dattani 2015; Duan et al. 2017).

In closing this chapter on quantum effects in Biology, we also conclude Part II of this dissertation, which dealt with single-particle quantum transport in complex systems. In the systems studied throughout this part the complexity appeared via the topological structure of the Hamiltonian. In Part III of this dissertation we will elaborate on a second way to significantly increase the complexity of the system: the introduction of *many* particles. Systems with many particles require a significant amount of additional formalism to describe all the relevant phenomenology. Therefore Chap. 7 is fully devoted to introducing the many-particle description of bosonic and fermionic states, and observables. In Chap. 8, we focus more specifically on the dynamics of a fixed number of non-interacting particles. In concreto, we will study a new type of many-particle interference which appears due to indistinguishability. Finally, in Chap. 9, we open the system such that particles can be exchanged by environments. We specifically study the currents which arise in these systems when they are far from equilibrium and we show that also here, *centrosymmetry* in the system Hamiltonian can profoundly impact the particle current.

References

- R.I. Adawson, Letter from Crick and Watson to Erwin Schrodinger dated 12 Aug 1953 (2014)
- J. Adolphs, F. Müh, M. El-Amine Madjet, T. Renger, Calculation of pigment transition energies in the FMO protein. Photosynth. Res. 95, 197–209 (2007)
- M. Aeschlimann, T. Brixner, A. Fischer, C. Kramer, P. Melchior, W. Pfeiffer, C. Schneider, C. Strüber, P. Tuchscherer, D.V. Voronine, Coherent two-dimensional nanoscopy. Science 333, 1723–1726 (2011)
- R. Alicki, W. Miklaszewski, A resonance mechanism of efficient energy transfer mediated by Fenna–Matthews–Olson complex. J. Chem. Phys. 136, 134103 (2012)
- P.W. Anderson, Absence of diffusion in certain random lattices. Phys. Rev. 109, 1492–1505 (1958)
- S. Aubry, A semiclassical non-adiabatic theory for elementary chemical reactions (2014). arXiv: 1411.5989
- W.P. Aue, E. Bartholdi, R.R. Ernst, Two-dimensional spectroscopy. Application to nuclear magnetic resonance. J. Chem. Phys. **64**, 2229–2246 (1976)
- O.T. Avery, C.M. MacLeod, M. McCarty, Studies on the chemical nature of the substance inducing transformation of Pneumococcal types induction of transformation by a desoxyribonucleic acid fraction isolated from Pneumococcus type Iii. J. Exp. Med. **79**, 137–158 (1944)
- R.E. Blankenship, Molecular Mechanisms of Photosynthesis (Blackwell Science, Oxford, 2002)
- R. Blümel, A. Buchleitner, R. Graham, L. Sirko, U. Smilansky, H. Walther, Dynamical localization in the microwave interaction of Rydberg atoms: the influence of noise. Phys. Rev. A 44, 4521– 4540 (1991)

H.-P. Breuer, F. Petruccione, *The Theory of Open Quantum Systems* (Oxford University Press, Oxford, 2007)

- T. Brixner, J. Stenger, H.M. Vaswani, M. Cho, R.E. Blankenship, G.R. Fleming, Two-dimensional spectroscopy of electronic couplings in photosynthesis. Nature **434**, 625–628 (2005)
- J. Brugger, Phononen-assistierter Quantentransport auf endlichen Netzwerken. Bachelor thesis, Albert-Ludwigs-Universität Freiburg, Freiburg, 2015
- P. Brumer, M. Shapiro, Molecular response in one-photon absorption via natural thermal light versus pulsed laser excitation. PNAS **109**, 19575–19578 (2012)
- M. Chachisvilis, O. Kühn, T. Pullerits, V. Sundström, Excitons in photosynthetic purple bacteria: wavelike motion or incoherent hopping? J. Phys. Chem. B 101, 7275–7283 (1997)
- R.K. Chain, D.I. Arnon, Quantum efficiency of photosynthetic energy conversion. PNAS 74, 3377–3381 (1977)
- N. Christensson, H.F. Kauffmann, T. Pullerits, T. Mančal, Origin of long-lived coherences in light-harvesting complexes. J. Phys. Chem. B 116, 7449–7454 (2012)
- E. Collini, C.Y. Wong, K.E. Wilk, P.M.G. Curmi, P. Brumer, G.D. Scholes, Coherently wired light-harvesting in photosynthetic marine algae at ambient temperature. Nature 463, 644–647 (2010)
- F. Crick, What Mad Pursuit: A Personal View of Scientific Discovery (Basic Books, New York, 1988)
- M.B. d'Arcy, R.M. Godun, G.S. Summy, I. Guarneri, S. Wimberger, S. Fishman, A. Buchleitner, Decoherence as a probe of coherent quantum dynamics. Phys. Rev. E **69**, 027201 (2004)
- P.C.W. Davies, Does quantum mechanics play a non-trivial role in life? Biosystems **78**, 69–79 (2004)
- S. Debecker, R. Sommaruga, T. Maes, R. Stoks, Larval UV exposure impairs adult immune function through a trade-off with larval investment in cuticular melanin. Funct. Ecol. 29, 1292–1299 (2015)
- J. Deisenhofer, O. Epp, K. Miki, R. Huber, H. Michel, Structure of the protein subunits in the photosynthetic reaction centre of Rhodopseudomonas viridis at 3 Å resolution. Nature 318, 618– 624 (1985)
- M. del Rey, A.W. Chin, S.F. Huelga, M.B. Plenio, Exploiting structured environments for efficient energy transfer: the phonon antenna mechanism. J. Phys. Chem. Lett. 4, 903–907 (2013)
- K.R. Dronamraju, Erwin Schrödinger and the origins of molecular biology. Genetics 153, 1071–1076 (1999)
- H.-G. Duan, V.I. Prokhorenko, R.J. Cogdell, K. Ashraf, A.L. Stevens, M. Thorwart, R.J.D. Miller, Nature does not rely on long-lived electronic quantum coherence for photosynthetic energy transfer. PNAS 114, 8493–8498 (2017)
- A.L. Edwards, An Introduction to Linear Regression and Correlation. A Series of Books in Psychology (Freeman, San Francisco, 1976)
- G.S. Engel, T.R. Calhoun, E.L. Read, T.-K. Ahn, T. Mančal, Y.-C. Cheng, R.E. Blankenship, G.R. Fleming, Evidence for wavelike energy transfer through quantum coherence in photosynthetic systems. Nature **446**, 782–786 (2007)
- J. Fernández de Cossío Díaz, Mecanismo de transporte de energía en el complejo molecular de Fenna-Matthews-Olson. Master thesis, Universidad de La Habana, Habana, Cuba, 2013
- R.A. Fisher, *The Genetical Theory of Natural Selection: A Complete Variorum Edition* (Oxford University Press, Oxford, 1930)
- T. Förster, Zwischenmolekulare Energiewanderung und Fluoreszenz. Ann. Phys. 437, 55–75 (1948)
- R.E. Franklin, R.G. Gosling, Molecular configuration in sodium thymonucleate. Nature **171**, 740–741 (1953)
- Y. Fujihashi, G.R. Fleming, A. Ishizaki, Impact of environmentally induced fluctuations on quantum mechanically mixed electronic and vibrational pigment states in photosynthetic energy transfer and 2d electronic spectra. J. Chem. Phys. 142, 212403 (2015)
- F.D. Fuller, J.P. Ogilvie, Experimental implementations of two-dimensional Fourier transform electronic spectroscopy. Ann. Rev. Phys. Chem. **66**, 667–690 (2015)
- M. Galassi (ed.), *GNU Scientific Library: Reference Manual*. A GNU Manual, 3rd edn. (Network Theory, s.l., 2009)

- L. Gammaitoni, P. Hänggi, P. Jung, F. Marchesoni, Stochastic resonance. Rev. Mod. Phys. 70, 223–287 (1998)
- E.M. Gauger, E. Rieper, J.J.L. Morton, S.C. Benjamin, V. Vedral, Sustained quantum coherence and entanglement in the avian compass. Phys. Rev. Lett. **106**, 040503 (2011)
- A.N. Geerts, J. Vanoverbeke, B. Vanschoenwinkel, W. Van Doorslaer, H. Feuchtmayr, D. Atkinson,
 B. Moss, T.A. Davidson, C.D. Sayer, L. De Meester, Rapid evolution of thermal tolerance in the water flea Daphnia. Nat. Clim. Chang. 5, 665–668 (2015)
- C. Gneiting, F.R. Anger, A. Buchleitner, Incoherent ensemble dynamics in disordered systems. Phys. Rev. A 93, 032139 (2016)
- S. Hameroff, R. Penrose, Orchestrated reduction of quantum coherence in brain microtubules: a model for consciousness. Math. Comput. Simul. **40**, 453–480 (1996)
- P. Hamm, M.T. Zanni, Concepts and Methods of 2D Infrared Spectroscopy (Cambridge University Press, Cambridge, 2011)
- H. Helmholtz, Ueber die Fortpflanzungsgeschwindigkeit der Nervenreizung. Ann. Phys. **155**, 329–330 (1850)
- R.A. Herbert, A. Gall, T. Maoka, R.J. Cogdell, B. Robert, S. Takaichi, S. Schwabe, Phototrophic purple sulfur bacteria as heat engines in the South Andros Black Hole. Photosynth. Res. 95, 261–268 (2007)
- R. Hildner, D. Brinks, J.B. Nieder, R.J. Cogdell, N.F. van Hulst, Quantum coherent energy transfer over varying pathways in single light-harvesting complexes. Science 340, 1448–1451 (2013)
- S. Hoyer, M. Sarovar, K.B. Whaley, Limits of quantum speedup in photosynthetic light harvesting. New J. Phys. 12, 065041 (2010)
- S.F. Huelga, M.B. Plenio, Stochastic resonance phenomena in quantum many-body systems. Phys. Rev. Lett. 98, 170601 (2007)
- W. Humphrey, A. Dalke, K. Schulten, VMD: visual molecular dynamics. J. Mol. Graph. Model 14, 33–38 (1996)
- A. Ishizaki, G.R. Fleming, Theoretical examination of quantum coherence in a photosynthetic system at physiological temperature. PNAS 106, 17255–17260 (2009)
- A. Ishizaki, Y. Tanimura, Quantum dynamics of system strongly coupled to low-temperature colored noise bath: reduced hierarchy equations approach. J. Phys. Soc. Jpn. 74, 3131–3134 (2005)
- R.A. Jalabert, J.-L. Pichard, C.W.J. Beenakker, Universal quantum signatures of chaos in ballistic transport. EPL **27**, 255 (1994)
- S. Jesenko, M. Žnidarič, Optimal number of pigments in photosynthetic complexes. New J. Phys. **14**, 093017 (2012)
- S. Jesenko, M. Žnidarič, Excitation energy transfer efficiency: equivalence of transient and stationary setting and the absence of non-Markovian effects. J. Chem. Phys. 138, 174103 (2013)
- G.E. Katsoprinakis, A.T. Dellis, I.K. Kominis, Coherent triplet excitation suppresses the heading error of the avian compass. New J. Phys. 12, 085016 (2010)
- M. Kollmann, L. Løvdok, K. Bartholomé, J. Timmer, V. Sourjik, Design principles of a bacterial signalling network. Nature 438, 504–507 (2005)
- B. Kramer, A. MacKinnon, Localization: theory and experiment. Rep. Prog. Phys. **56**, 1469 (1993)
- C. Kreisbeck, T. Kramer, Long-lived electronic coherence in dissipative exciton dynamics of light-harvesting complexes. J. Phys. Chem. Lett. 3, 2828–2833 (2012)
- C.M. Kropf, C. Gneiting, A. Buchleitner, Effective dynamics of disordered quantum systems. Phys. Rev. X 6, 031023 (2016)
- T.P. Krüger, C. Ilioaia, M.P. Johnson, A.V. Ruban, E. Papagiannakis, P. Horton, R. van Grondelle, Controlled disorder in plant light-harvesting complex II explains its photoprotective role. Biophys. J. 102, 2669–2676 (2012)
- A.R. Leach, *Molecular Modelling: Principles and Applications*, 2nd edn. (Prentice Hall, Harlow, 2001)
- D. Manzano, Quantum transport in networks and photosynthetic complexes at the steady state. PLoS ONE **8**, e57041 (2013)

R.A. Marcus, Electron transfer reactions in chemistry. Theory and experiment. Rev. Mod. Phys. 65, 599–610 (1993)

- R.A. Marcus, N. Sutin, Electron transfers in chemistry and biology. Biochim. Biophys. Acta 811, 265–322 (1985)
- V. May, O. Kühn, Charge and Energy Transfer Dynamics in Molecular Systems: A Theoretical Introduction, 1st edn. (Wiley-VCH, Berlin, 2000)
- M. Mohseni, P. Rebentrost, S. Lloyd, A. Aspuru-Guzik, Environment-assisted quantum walks in photosynthetic energy transfer. J. Chem. Phys. 129, 174106 (2008)
- J. Moix, J. Wu, P. Huo, D. Coker, J. Cao, Efficient energy transfer in light-harvesting systems, III: the influence of the eighth bacteriochlorophyll on the dynamics and efficiency in FMO. J. Phys. Chem. Lett. 2, 3045–3052 (2011)
- R. Monshouwer, M. Abrahamsson, F. van Mourik, R. van Grondelle, Superradiance and exciton delocalization in bacterial photosynthetic light-harvesting systems. J. Phys. Chem. B 101, 7241– 7248 (1997)
- S. Mostarda, F. Levi, D. Prada-Gracia, F. Mintert, F. Rao, Structure–dynamics relationship in coherent transport through disordered systems. Nat. Commun. 4, 2296 (2013)
- S. Mukamel, Multidimensional femtosecond correlation spectroscopies of electronic and vibrational excitations. Ann. Rev. Phys. Chem. **51**, 691–729 (2000)
- S. Mukamel, *Principles of Nonlinear Optical Spectroscopy*. Oxford Series in Optical and Imaging Sciences, vol. 6 (Oxford University Press, New York, 2009)
- H.J. Muller, Variation due to change in the individual gene. Am. Nat. 56, 32–50 (1922)
- O.L. Muskens, P. Venn, T. van der Beek, T. Wellens, Partial nonlinear reciprocity breaking through ultrafast dynamics in a random photonic medium. Phys. Rev. Lett. **108**, 223906 (2012)
- C.O. Nordling, A new theory on the cancer-inducing mechanism. Br. J. Cancer 7, 68–72 (1953)
- H.A. Orr, Fitness and its role in evolutionary genetics. Nat. Rev. Genet. 10, 531–539 (2009)
- K. Pearson, Contributions to the mathematical theory of evolution. Philos. Trans. R. Soc. A 185, 71–110 (1894)
- K. Pearson, Note on regression and inheritance in the case of two parents. Proc. R. Soc. Lond. 58, 240–242 (1895)
- M.B. Plenio, S.F. Huelga, Dephasing-assisted transport: quantum networks and biomolecules. New J. Phys. 10, 113019 (2008)
- B.H. Pugesek (ed.), Structural Equation Modeling: Applications in Ecological and Evolutionary Biology (Digitally printed version edition) (Cambridge University Press, Cambridge, 2009)
- T. Pullerits, M. Chachisvilis, V. Sundström, Exciton Delocalization length in the B850 antenna of rhodobacter sphaeroides. J. Phys. Chem. 100, 10787–10792 (1996)
- A.G. Redfield, The theory of relaxation processes, in *Advances in Magnetic and Optical Resonance*, Advances in Magnetic Resonance, ed. by J.S. Waugh, vol. 1 (Academic Press, New York, 1965), pp. 1–32
- M. Reed, B. Simon, *Methods of Modern Mathematical Physics I: Functional Analysis*, 1st edn. (Academic Press, New York, 1980)
- T. Ritz, S. Adem, K. Schulten, A model for photoreceptor-based magnetoreception in birds. Biophys. J. **78**, 707–718 (2000)
- J.J.J. Roden, D.I.G. Bennett, K.B. Whaley, Long-range energy transport in photosystem ii. J. Chem. Phys. 144, 245101 (2016)
- M. Sarovar, A. Ishizaki, G.R. Fleming, K.B. Whaley, Quantum entanglement in photosynthetic light-harvesting complexes. Nat. Phys. 6, 462–467 (2010)
- F. Schluenzen, A. Tocilj, R. Zarivach, J. Harms, M. Gluehmann, D. Janell, A. Bashan, H. Bartels, I. Agmon, F. Franceschi, A. Yonath, Structure of functionally activated small ribosomal subunit at 3.3 å resolution. Cell **102**, 615–623 (2000)
- M. Schmidt am Busch, M. El-Amine Madjet, T. Renger, The eighth bacteriochlorophyll completes the excitation energy funnel in the FMO protein. J. Phys. Chem. Lett. 2, 93–98 (2011)
- T. Scholak, Transport and coherence in disordered networks. Ph.D. thesis, Albert-Ludwigs Universität Freiburg, Freiburg, 2011

- T. Scholak, F. Mintert, T. Wellens, A. Buchleitner, Transport and entanglement, in *Biomolecular Systems*, ed. by E.R. Weber, M. Thorwart, U. Würfel. Quantum Efficiency in Complex Systems. 1st edn. (Elsevier, Oxford, 2010)
- T. Scholak, F. de Melo, T. Wellens, F. Mintert, A. Buchleitner, Efficient and coherent excitation transfer across disordered molecular networks. Phys. Rev. E 83, 021912 (2011a)
- T. Scholak, T. Wellens, A. Buchleitner, Optimal networks for excitonic energy transport. J. Phys. B: At. Mol. Opt. Phys. **44**, 184012 (2011b)
- T. Scholak, T. Wellens, A. Buchleitner, The optimization topography of exciton transport. EPL 96, 10001 (2011c)
- T. Scholak, T. Wellens, A. Buchleitner, Spectral backbone of excitation transport in ultracold Rydberg gases. Phys. Rev. A 90, 063415 (2014)
- G.D. Scholes, T. Mirkovic, D.B. Turner, F. Fassioli, A. Buchleitner, Solar light harvesting by energy transfer: from ecology to coherence. Energy Environ. Sci. 5, 9374 (2012)
- G.D. Scholes, G.R. Fleming, L.X. Chen, A. Aspuru-Guzik, A. Buchleitner, D.F. Coker, G.S. Engel, R. van Grondelle, A. Ishizaki, D.M. Jonas, J.S. Lundeen, J.K. McCusker, S. Mukamel, J.P. Ogilvie, A. Olaya-Castro, M.A. Ratner, F.C. Spano, K.B. Whaley, X. Zhu, Using coherence to enhance function in chemical and biophysical systems. Nature 543, 647 EP (2017)
- E. Schrödinger, What is Life? The Physical Aspect of the Living Cell (Cambridge University Press, Cambridge, 1944)
- V. Shatokhin, M. Walschaers, F. Schlawin, A. Buchleitner, Coherence turned on by incoherent light (2016). arXiv:1602.07878
- J.H. Shirley, Solution of the Schrödinger equation with a Hamiltonian periodic in time. Phys. Rev. 138, B979–B987 (1965)
- S.S. Skourtis, S. Mukamel, Superexchange versus sequential long range electron transfer; density matrix pathways in Liouville space. Chem. Phys. 197, 367–388 (1995)
- D.A. Steck, V. Milner, W.H. Oskay, M.G. Raizen, Quantitative study of amplitude noise effects on dynamical localization. Phys. Rev. E 62, 3461–3475 (2000)
- A. Stolow, A.E. Bragg, D.M. Neumark, Femtosecond time-resolved photoelectron spectroscopy. Chem. Rev. 104, 1719–1758 (2004)
- J. Strümpfer, M. Şener, K. Schulten, How quantum coherence assists photosynthetic light-harvesting. J. Phys. Chem. Lett. 3, 536–542 (2012)
- N.W. Timoféeff-Ressovsky, K.G. Zimmer, M. Delbrück, Über die Natur der Genmutation und der Genstruktur. Nachrichten von der Gesellschaft der Wissenschaften zu Göttingen 1, 189–215 (1935)
- D.E. Tronrud, J. Wen, L. Gay, R.E. Blankenship, The structural basis for the difference in absorbance spectra for the FMO antenna protein from various green sulfur bacteria. Photosynth. Res. 100, 79–87 (2009)
- H. van Helmholtz, J.P.C. Southall, *Treatise on Physiological Optics* (Dover phoenix editions) (Dover Publications, Mineola, 1910)
- A. Vaziri, M.B. Plenio, Quantum coherence in ion channels: resonances, transport and verification. New J. Phys. 12, 085001 (2010)
- M. Walschaers, J.F.-d.-C. Diaz, R. Mulet, A. Buchleitner, Optimally designed quantum transport across disordered networks. Phys. Rev. Lett. 111, 180601 (2013)
- J.D. Watson, *The Double Helix. A Personal Account of the Discovery of the Structure of DNA* (Penguin Books, Harmondsworth, 1969)
- J.D. Watson, F.H.C. Crick, Molecular structure of nucleic acids: a structure for deoxyribose nucleic acid. Nature 171, 737–738 (1953)
- T. Wellens, V. Shatokhin, A. Buchleitner, Stochastic resonance. Rep. Prog. Phys. 67, 45–105 (2004)
- H. Weyl, *Philosophy of Mathematics and Natural Science* (Princeton University Press, Princeton, 1949)
- M. Wilkins, The Molecular Configuration of Nucleic Acids (1962)
- D.M. Wilkins, N.S. Dattani, Why quantum coherence is not important in the fenna-matthews-olsen complex. J. Chem. Theory Comput. 11, 3411–3419 (2015)

M.H.F. Wilkins, A.R. Stokes, H.R. Wilson, Molecular structure of nucleic acids: molecular structure of deoxypentose nucleic acids. Nature 171, 738–740 (1953)

- W. Wiltschko, R. Wiltschko, Magnetic compass of European robins. Science 176, 62–64 (1972)
- C.A. Wraight, R.K. Clayton, The absolute quantum efficiency of bacteriochlorophyll photooxidation in reaction centres of Rhodopseudomonas spheroides. Biochim. Biophys. Acta 333, 246–260 (1974)
- T. Zech, Hidden symmetries of quantum transport in photosynthesis. Diploma thesis, Albert-Ludwigs Universität Freiburg, Freiburg, 2013
- T. Zech, M. Walschaers, T. Scholak, R. Mulet, T. Wellens, A. Buchleitner, Quantum transport in biological functional units: noise, disorder, structure. Fluct. Noise Lett. 12, 1340007 (2013)
- T. Zech, R. Mulet, T. Wellens, A. Buchleitner, Centrosymmetry enhances quantum transport in disordered molecular networks. New J. Phys. 16, 055002 (2014)
- J. Zimmermann, Random walks with nonlinear interactions on heterogeneous networks. Ph.D. thesis, Albert-Ludwigs-Universität Freiburg, Freiburg, 2015
- A.F. Zuur (ed.), *Mixed Effects Models and Extensions in Ecology with R*. Statistics for Biology and Health (Springer, New York, 2009)

Part III Many-Particle Quantum Transport

Chapter 7 Describing Many-Particle Quantum Systems



More is different Philip W. Anderson in (1972)

This chapter is mainly based on the lectures presented by Mark Fannes at the COST Physics School on "New trends in many-particle quantum transport" of February 2015. These lecture notes were, in turn, based on several rather technical textbooks (Alicki and Fannes 2001; Benatti et al. 2010; Bratteli and Robinson 1987, 1997; Davidson 1996; Dereziński 2006; Evans and Kawahigashi 1998; Petz 1990) and we refer the interested reader to these works for more mathematical background on the results presented here. Our goal is to bring these results from the mathematical quantum physics community closer to the current mainstream quantum physics research.

7.1 Introduction

In Part II of this dissertation all attention was focused on the potential effects of quantum interference phenomena on the transport of a single particle (an exciton, a photon, an electron, et cetera), ignoring all possible complications which arise when another particle is encountered. Multiple particles can indeed give rise to an interesting zoology of possibilities: Most familiarly two particles—such as two negatively charged electrons—can interact with one another. However, many particles may behave strangely merely due to their mutual indistinguishability which, in quantum mechanics, leads to effects such as Bose-Einstein condensation (Anderson et al. 1995; Bose 1924; Davis et al. 1995; Einstein 2005; Verbeure 2011), superfluidity (Kapitza 1938; Landau 1941; London 1938) or the Hong-Ou-Mandel dip (Hong et al. 1987). Indeed, even mere indistinguishability without any need for actual interaction is sufficient to enforce Anderson's statement "more is different" (Anderson 1972). The main goal of this part of the dissertation is to investigate the additional

interference phenomena which arise in many-particle systems solely due to indistinguishability. These effects are dynamical in nature and become rather intriguing (and computationally intractable) once we turn to complex systems as for example described by random evolution.

Before we address the open questions related to the physics of many-particle interference, we require a whole additional framework to deal with many-body systems. Several elements of this mathematical structure have already been introduced in Chap. 2, where we briefly mention the description of quantum mechanics in terms of algebras of observables. It turns out that many-particle systems are particularly suited for a description in terms of the Heisenberg picture imposed on C^* -algebras. In this chapter, we will gradually build up the theory towards such a description and pinpoint its need.

At the time when much of this mathematical framework was developed, many-body quantum physics was still mainly an object of the imagination. Even though the condensed-matter (Bardeen et al. 1957; Mott 1949) and mesoscopic physics (Fulton and Dolan 1987; Laughlin 1983) communities have long been aware of the importance of many-particle effects, the controllable parameters in these fields of study are usually limited. Since the 1980's there has been an enormous amount of experimental progress regarding controllability, mainly due to the birth of ultra-cold atom physics (Ashkin et al. 1986; Chu et al. 1986; Dalibard and Cohen-Tannoudji 1985, 1989; Lett et al. 1988; Phillips and Metcalf 1982), which became enormously successful thanks to optical lattices (Andrews et al. 1997; Bloch 2005; Bloch et al. 2008; Goldman and Dalibard 2014; Hemmerich and Hänsch 1993; Karski et al. 2009; Mandel et al. 2003; Paredes et al. 2004). On the other hand, also the field of photonics flourished, providing us with optical tools to explore many-particle physics (Armstrong et al. 2012; Metcalf et al. 2013; Mosley et al. 2008; Peruzzo et al. 2010; Ra et al. 2013a, b; Sansoni et al. 2012; Tichy et al. 2010, 2011).

The baseline for the underlying physics is that nature does not tend to be very creative at its foundations, given that all matter is built from a few fundamental building blocks, contained in the standard model (Cheng and Li 1984; Griffiths 2004). This leads us to the concept of *identical* particles: particles which have all the same internal degrees of freedom, e.g. two left-handed electrons can be considered identical, whereas a left-handed electron and a left-handed positron can be told apart via their electrical charge. Notice, however, that identical does not necessarily imply *indistinguishable*; when the two left-handed electrons are placed in different corners of the universe, that information on position—an external degree of freedom—can be used to distinguish them. The concept of indistinguishability only comes into play when the particles meet each other in a way that intertwines their external degrees of freedom: When for example two photons jointly enter a beamsplitter, it is impossible to relate a single incoming photon to a single outgoing photon. To observe the effect of the beamsplitter, we must perform measurements. Therefore we must stress that not only the action of the beamsplitter, but also the choice of the

7.1 Introduction 201

measurement apparatus¹ is an important factor when discussing indistinguishability (Tichy et al. 2013). A detailed discussion on these issues can be found in Sect. 8.3.4.

In this dissertation, we will not deal with any subtleties or specific details of the standard model and the particles described there, rather we focus on a more abstract and broadly applicable understanding of quantum mechanical particles in a non-relativistic framework. It turns out that such quantum particles really come in two fundamentally different kinds: bosons and fermions. In quantum field theory, one can formally relate (Pauli 1940, 1950; Schwinger 1951) these particle species to the particles' integer or half-integer spin, respectively, but when focussing on physical features, there are other hallmarks to describe these particle types: Many identical bosons can occupy the same single-particle quantum state and thus form a Bose-Einstein Condensate (BEC), whereas fermions must all occupy different single-particle quantum states. Interestingly, in the following chapter, we show that there is much more phenomenology hidden in both sectors of particles, which becomes apparent in a dynamical setup.

Finally it must be noted that these models are applicable to many forms of matter, both fundamental and composite. Indeed, one may study many-boson systems using photons, which are fundamental particles, but it is also possible to use, for example, atoms. Although atoms are composite particles, made up from fermions, this substructure is often unresolved in experiments. The ultra-cold atoms community has managed to show time over time again that atoms with an integer atomic spin really do behave as bosons in experimental settings (Anderson et al. 1995; Andrews et al. 1997; Bloch 2005; Bloch et al. 2008; Davis et al. 1995; Hänsel et al. 2001). Therefore, the mathematical framework developed in this chapter does serve as an effective model for such systems.

7.2 Postulates for Bosons and Fermions

7.2.1 The Two-Particle System

To introduce the mathematical formalism required to model systems of identical particles it is useful to return to the basic foundations of quantum mechanics as a probabilistic theory, as described in Chap. 2. There, we identified the actual physically relevant objects in the theory as the moments of the probability distribution for the observable(s) of interest. This brings us to the quantity $\langle O^n \rangle_{\psi}$ as starting point of the discussion. Let us start from a system of two particles, where each particle has its own degrees of freedom. For a single particle, these degrees of freedom are well-described by using a Hilbert space \mathcal{H} . Remember that the observables were contained in the

¹In a mathematical phrasing, one may think of the observable which describes the measurement.

algebra of bounded operators $\mathcal{B}(\mathcal{H})$ on this Hilbert space,² whereas the quantum states are the normalised, positive functionals defined on this algebra. Introducing an additional, identical particle into the system, *in principle* implies doubling all the degrees of freedom,³ which in quantum mechanics is described via a tensor product structure of the Hilbert space:

$$\mathcal{H}_{\text{total}} = \mathcal{H} \otimes \mathcal{H}. \tag{7.1}$$

However, this description is flawed by a problem engraved deeply within the nature of these identical particles. When we assume that one particle's quantum state is accurately described by a wave function $\psi_1 \in \mathcal{H}$ and the other by a wave function $\psi_2 \in \mathcal{H}$ we naively describe the total wave function of the system as $\psi_1 \otimes \psi_2 \in \mathcal{H}_{total}$. The problem of this description is that both particles are identical and therefore, interchanging the label of the particles must leave the *physics* completely intact. On the other hand, in general $\psi_1 \otimes \psi_2 \neq \psi_2 \otimes \psi_1$. This implies that (7.1) is not the correct structure to describe such identical particles. However, we can use (7.1) to construct such a structure, by additionally imposing that there be no effect measurable upon permutation of the particles.

The first required ingredient is the act of permuting particles, which can be done by defining the action of the permutation group S_2 (Dixon and Mortimer 1996). A way of describing the permutation of particles on the level of the Hilbert space $\mathcal{H} \otimes \mathcal{H}$ is by construction of the operation U, which acts as

$$U\psi_1 \otimes \psi_2 := \psi_2 \otimes \psi_1. \tag{7.2}$$

Therefore, any vector $\Psi \in \mathcal{H} \otimes \mathcal{H}$ which describes a two-particle state must fulfil

$$U\Psi = e^{i\theta}\Psi. (7.3)$$

This allows us to formally connect the structure of the two-particle space to the representation theory of the permutation group S_2 , by associating the state vectors Ψ with eigenvectors of the group representations.⁴ Given that permuting the particles twice leads to the identity operation, the only two possible eigenvalues are given by phases $\theta = 0$ and $\theta = \pi$. This excludes anyon formalisms as natural candidates for many-particle system descriptions and leaves us which the choices

$$U\Psi = \pm \Psi, \tag{7.4}$$

²For single-particle systems there typically is no need to proceed to more abstract algebras of observables, since there usually the GNS construction (see Sect. 2.3.2) does lead to a unique Hilbert space.

³Classically this would be connected to an increase of the dimensions of phase-space.

⁴Because the group S_2 contains only two elements, one of which is the identity, it is sufficient to focus on the action of U.

implying that the full Hilbert space of two-particle state vectors is given by either

$$\mathcal{H}_{s}^{\otimes 2} := \{ \Psi \mid U\Psi = \Psi \}, \quad \text{or}$$
 (7.5)

$$\mathcal{H}_a^{\otimes 2} := \{ \Psi \mid U\Psi = -\Psi \},\tag{7.6}$$

respectively the subspaces of vectors which are symmetric or antisymmetric under permutations of particles. It is now specifically useful to introduce the vectors

$$|\psi_1; \psi_2\rangle_s := \frac{1}{\sqrt{2}}(\psi_1 \otimes \psi_2 + \psi_2 \otimes \psi_1), \tag{7.7}$$

$$|\psi_1; \psi_2\rangle_a := \frac{1}{\sqrt{2}}(\psi_1 \otimes \psi_2 - \psi_2 \otimes \psi_1), \tag{7.8}$$

to directly obtain

$$\mathcal{H}_{s}^{\otimes 2} \cong \operatorname{span}\{|\psi_{1}; \psi_{2}\rangle_{s} \mid \psi_{1}, \psi_{2} \in \mathcal{H}\},\tag{7.9}$$

$$\mathcal{H}_a^{\otimes 2} \cong \operatorname{span}\{|\psi_1; \psi_2\rangle_a \mid \psi_1, \psi_2 \in \mathcal{H}\}. \tag{7.10}$$

Both of these Hilbert space constructions are physically realised. Although they fulfil the same basic condition to lead to invariant physics under permutations of the particles, they are fundamentally different. Indeed, the wave functions $|\psi;\psi\rangle_s$ are normalisable, whereas $|\psi;\psi\rangle_a=0$. The former set of particles, described by the symmetric wave functions, represent *bosons*, whereas the antisymmetric ones describe *fermions*.

As discussed in Sect. 2.3.1, we can now use the Hilbert space structures $\mathcal{H}_s^{\otimes 2}$ and $\mathcal{H}_a^{\otimes 2}$ to define the bosonic and fermionic observables, respectively. Moreover, when we choose any observable $O = O^{\dagger}$, we can consider the permutation of particles as a unitary operation in the Heisenberg picture (see Chap. 2) and find

$$O \mapsto U^{\dagger}OU.$$
 (7.11)

From the structure of the Hilbert spaces of identical particles (7.5), (7.6) it is now clear that the permutation of particles acts on moments $\langle O^q \rangle$ as

$$\langle O^q \rangle \to \langle U^\dagger O^q U \rangle = \langle O^q \rangle, \quad q \in \mathbb{N},$$
 (7.12)

and thus leaves the physics invariant.

In a more formal mathematical setting, we can discuss the actions of the group S_2 on $\mathcal{H} \otimes \mathcal{H}$ using representation theory as contained in (Fulton 1997; Hamermesh 1989). From the *Schur-Weyl duality* (Hamermesh 1989; Weyl 1928) between the group S_2 and the general linear group GL(k) (Hamermesh 1989; Weyl 1928),⁵ where k is the dimension of \mathcal{H} , we obtain

 $^{^{5}}$ In the next section, the Schur-Weyl duality is more generally formulated in Eq. (7.22).

$$\mathcal{H} \otimes \mathcal{H} \cong \mathcal{H}_a^{\otimes 2} \oplus \mathcal{H}_s^{\otimes 2}, \tag{7.13}$$

where we used that the irreducible representations of S_2 are one-dimensional. A simple calculation, for dim $\mathcal{H} = k$, indicates that

$$\dim \mathcal{H}_a^{\otimes 2} = \binom{k}{2}$$
 and $\dim \mathcal{H}_s^{\otimes 2} = \binom{k+1}{2}$. (7.14)

This implies that the two-fermion space \mathcal{H}_a and the two-boson space \mathcal{H}_s are sufficient to reproduce the full tensor product $\mathcal{H}^{\otimes 2}$.

Given that physical reality seems to force particles to either adopt bosonic or fermionic properties, one cannot describe a system of two identical particles as $\mathcal{H}^{\otimes 2}$, but rather one is restricted to dwell in either \mathcal{H}_a (for fermions) or \mathcal{H}_s (for bosons).

7.2.2 The N-Particle System

Generalising the above results to n-particle systems seems straightforward by using group theory methods based on Young diagrams (Fulton 1997; Walschaers 2011). These objects characterise the irreducible representations of the group S_n . Young diagrams are related to *partitions* of n, in the sense that they are composed of several rows which represent the terms in the partition. The length of each row represents the value of the specific term in the partition. Usually the diagrams are built such that the length of the rows does not increase from top to bottom. As an illustration, we consider the partition n = 9 = 5 + 3 + 1, which would lead to a Young frame



This structure is connected to permutations by filling it up with labels

This is typically called a Young tableau, which allows us to define two important classes of permutations:

$$R(\mu) = \{ \sigma \in S_n \mid \sigma \text{ permutes entries of the rows of tableau } \mu \text{ into the same rows} \}, (7.17)$$

 $C(\mu) = \{ \sigma \in S_n \mid \sigma \text{ permutes entries of the columns of tableau } \mu \text{ into the same columns} \}.$
(7.18)

In our example (7.16), this implies that $\sigma \in R(\mu)$ permutes the elements in each set $\{1, 2, 3, 4, 5\}$, $\{6, 7, 8\}$ and $\{9\}$, without mixing the elements of these different sets. On the other hand, $\sigma \in C(\mu)$ permutes the elements of the sets $\{1, 6, 9\}$, $\{2, 7\}$, $\{3, 8\}$, $\{4\}$ and $\{5\}$, without intermixing the sets. The irreducible representations can be constructed via what is called a *Young symmetriser*, c_{μ} , which is defined by

$$c_{\mu} := \sum_{\sigma \in C(\mu)} \operatorname{sign}(\sigma) \sigma \circ \sum_{\pi \in R(\mu)} \pi. \tag{7.19}$$

In other words, one symmetrises over all rows and antisymmetrises over all columns. These results are all formalised and proven in (Fulton 1997). For the narrative, the important result is that each of these Young symmetrisers, which represent the action of the group S_n , is uniquely defined by one Young frame μ .

Considering a system of n particles, each described by a single particle wave function $\psi_k \in \mathcal{H}$, embedded in total Hilbert space $\mathcal{H}^{\otimes n}$ in principle provides a wide range of possibilities. Let us start by defining a general action of the group S_n as

$$U(\pi)\psi_1 \otimes \psi_2 \otimes \cdots \otimes \psi_n = \psi_{\pi(1)} \otimes \psi_{\pi(2)} \otimes \cdots \otimes \psi_{\pi(n)}. \tag{7.20}$$

When we now assume that n-particle states are connected to the irreducible representations of S_n , we can for example construct 3-particle objects of the form

$$\begin{array}{c}
\boxed{\chi \mid \psi} \\
\phi
\end{array} = \chi \otimes \psi \otimes \phi + \psi \otimes \chi \otimes \phi - \phi \otimes \psi \otimes \chi - \psi \otimes \phi \otimes \chi$$
(7.21)

It is easily understood that one can generalise this construction method to any number of particles n and any young diagram μ . This procedure again provides a method to break $\mathcal{H}^{\otimes n}$ up in various sub-structures, leading to the *Schur-Weyl duality*

$$\mathcal{H}^{\otimes n} = \bigoplus_{\mu} \mathcal{H}_{\mu},\tag{7.22}$$

where each μ represents a different Young diagram for S_n . Were we to follow this line of reasoning, any amount of particles n would lead to new types of particles, which might behave differently under permutations. After all, each Young diagram would present a different set of rules for interchanging particles. More intriguingly, single-particle states could be multiply occupied by putting them in the same row of (7.21), however, different columns could never contain the same single-particle states. This would ultimately lead to very peculiar physical phenomena. For example, in (7.21), the particles described by wave functions χ and ψ behave as bosons with respect to one another. However, the particles described by wave functions χ and ϕ act as fermions under permutation. This indicates that the particle statistics described by general Young symmetrisers would mix fermionic and bosonic behaviour. These

phenomena are not observed in real physical systems and therefore the *Pauli principle* postulates that they do not exist.

Indeed, several of these mathematical structures do not seem to apply to the physical reality we expect from n-particle systems. The reason can again be found by considering the actual quantities $\langle O^n \rangle$ which are accessible by measurement. We demand that this quantity should remain invariant under permutations of particles, because the particles are identical. This implies that

$$\langle O^n \rangle = \langle U(\pi^{-1})O^n U(\pi) \rangle, \quad \text{for all } \pi \in S_n.$$
 (7.23)

When we, again, consider the special, though elementary, case where $\langle . \rangle$ is determined by a wave function $\Psi \in \mathcal{H}^{\otimes n}$, we must fulfil

$$U(\pi)\Psi = e^{i\theta_{\pi}}\Psi,\tag{7.24}$$

where the phase θ_π can depend on the specific permutation which is being considered. The only consistent options are given by $e^{i\theta_\pi}=1$ for all π , or by $e^{i\theta_\pi}=\mathrm{sign}(\pi)$. It is certainly not a coincidence that these two options relate to either the fully symmetrised wave functions or to the fully antisymmetrised ones, which relate to Young diagrams of the form

and
$$(7.25)$$

respectively. This has profound consequences for the structure of the physical theory: For two particles, we deduced that the bosons and fermions together constituted the full space $\mathcal{H}^{\otimes 2}$. Even though we find that Eq. (7.22) must hold, it turns out that for a system of identical particles, only two of these many subspaces \mathcal{H}_{μ} actually make physical sense. These are exactly the ones given by the Young diagrams as given by the shapes in (7.25). Hence, the system is either fermionic or bosonic, described by the respective Hilbert spaces

$$\mathcal{H}_a^{\otimes n} := \{ \Psi \in \mathcal{H}^{\otimes n} \mid U(\pi)\Psi = \operatorname{sign}(\pi)\Psi, \text{ for all } \pi \in S_n \}, \tag{7.26}$$

$$\mathcal{H}_{s}^{\otimes n} := \{ \Psi \in \mathcal{H}^{\otimes n} \mid U(\pi)\Psi = \Psi, \text{ for all } \pi \in S_n \}.$$
 (7.27)

We see that for dim $\mathcal{H} = k$,

$$\dim \mathcal{H}_a^{\otimes n} = \binom{k}{n}$$
 and $\dim \mathcal{H}_s^{\otimes n} = \binom{k+n-1}{n}$, (7.28)

which clearly does not add up to dim $\mathcal{H}^{\otimes n} = k^n$.

7.2.3 Permanents and (Slater) Determinants

Only the two most extreme Young diagrams—and therefore only the spaces $\mathcal{H}_a^{\otimes n}$ and $\mathcal{H}_s^{\otimes n}$ —are relevant for n-particle systems. One may wonder whether there is a more straightforward and consistent way to define the fundamental wave functions that make up these spaces. Although in principle we may always use the actions of the relevant Young symmetrisers c_{μ} , for μ either the single-column (fermions) and single-row (bosons) Young diagram, the framework of representation theory is overly intricate to deal with systems where we only require full symmetrisation or full antisymmetrisation. Therefore, with a set of vectors $\psi_1, \ldots, \psi_n \in \mathcal{H}$, we define

$$\psi_1 \wedge \psi_2 \wedge \dots \wedge \psi_n := \frac{1}{\sqrt{n!}} \sum_{\pi \in S_n} \operatorname{sign}(\pi) \psi_{\pi(1)} \otimes \psi_{\pi(2)} \otimes \dots \otimes \psi_{\pi(n)}, \quad (7.29)$$

$$\psi_1 \odot \psi_2 \odot \cdots \odot \psi_n := \frac{1}{\sqrt{n!}} \sum_{\pi \in S_n} \psi_{\pi(1)} \otimes \psi_{\pi(2)} \otimes \cdots \otimes \psi_{\pi(n)}. \tag{7.30}$$

These vectors are indeed a *total set* 6 in $\mathcal{H}_{a/s}^{\otimes n}$, but their inner-products are non-trivial. It should be noted that the fermionic vectors (7.29) are often referred to as *Slater determinants*. It can be shown that

$$\langle \phi_1 \wedge \phi_2 \wedge \dots \wedge \phi_n, \psi_1 \wedge \psi_2 \wedge \dots \wedge \psi_n \rangle = \det \left([\langle \phi_i, \psi_j \rangle] \right)$$
 (7.31)

$$\langle \phi_1 \odot \phi_2 \odot \cdots \odot \phi_n, \psi_1 \odot \psi_2 \odot \cdots \odot \psi_n \rangle = \operatorname{perm} \left(\left[\left\langle \phi_i, \psi_j \right\rangle \right] \right),$$
 (7.32)

with perm the *permanent* of the matrix. The permanent of an $n \times n$ matrix A is defined as

perm
$$A := \sum_{\pi \in S_n} A_{1\pi(1)} A_{2\pi(2)} \dots A_{n\pi(n)},$$
 (7.33)

which may seem very similar to the determinant and therefore rather innocent. However, permanents are not invariant under unitary transformations of the matrix, typically making them extremely hard to compute. The reason is that det A is determined only by the eigenvalues of A, whereas perm A also depends on the chosen basis. In the language of complexity theory (Moore and Mertens 2011) this implies that the complexity of a standard algorithm for the evaluation of a determinant is $\mathcal{O}(n^3)$, whereas a permanent belongs to complexity class #P (Moore and Mertens 2011). Ultimately this means that one can prove that permanents are much harder to compute than determinants, a problem which propagates to the physics of many-boson interference. The physical implications of (7.31) and (7.32) are core elements of our

⁶A total set in the context of topological vector spaces is a set, the linear span of which is dense in the full topological vector space. In a Hilbert space this becomes equivalent to stating that the only vector orthogonal to all the vectors in the set is the zero-vector.

work on many-particle interference as described in Chap. 8, where we briefly come back to the computational problems which arise in bosonic systems (see Sects, 8.3.5 and 8.5).

These results imply that only in the case where the normalised $\psi_1, \ldots, \psi_n \in \mathcal{H}$ are all orthogonal to one another the vectors (7.29), (7.30) are normalised. Therefore, in order to describe wave functions, we must not only use (7.29), (7.30), but also introduce a normalisation factor.

For completeness, we mention that the products \odot and \wedge can be extended in a natural way to

$$\wedge: \mathcal{H}_{a}^{\otimes n} \times \mathcal{H}_{a}^{\otimes m} \to \mathcal{H}_{a}^{\otimes n+m}: (\psi_{n}, \psi_{m}) \mapsto \psi_{n} \wedge \psi_{m} \tag{7.34}$$

$$\wedge : \mathcal{H}_{a}^{\otimes n} \times \mathcal{H}_{a}^{\otimes m} \to \mathcal{H}_{a}^{\otimes n+m} : (\psi_{n}, \psi_{m}) \mapsto \psi_{n} \wedge \psi_{m}$$

$$\odot : \mathcal{H}_{s}^{\otimes n} \times \mathcal{H}_{s}^{\otimes m} \to \mathcal{H}_{s}^{\otimes n+m} : (\psi_{n}, \psi_{m}) \mapsto \psi_{n} \odot \psi_{m},$$
(7.34)

such that

$$(\psi_1 \wedge \dots \wedge \psi_n) \wedge (\psi_{n+1} \wedge \dots \wedge \psi_{n+m}) = \psi_1 \wedge \dots \wedge \psi_n \wedge \psi_{n+1} \wedge \dots \wedge \psi_{n+m},$$
(7.36)

$$(\psi_1 \odot \cdots \odot \psi_n) \odot (\psi_{n+1} \odot \cdots \odot \psi_{n+m}) = \psi_1 \odot \dots \psi_n \odot \psi_{n+1} \odot \cdots \odot \psi_{n+m}.$$
(7.37)

This shows that in essence, bosons and fermions are in many ways remarkably similar in structure. On the other hand, in the following chapters, we will show that the difference between symmetrisation and antisymmetrisation can make a considerable difference in physical phenomenology.

7.3 **Fock Space**

Constructing Fock Space

In the constructions above, one fundamental assumption was made: The number of particles was assumed to be known and fixed. However, in many physical contexts, this may not be the case; systems can be made of unstable particles or be connected to reservoirs with which they exchange particles. Depending whether in a dynamical, non-equilibrium setting or rather describing equilibrium states, one resorts to different types of modelling these systems, e.g. using the grand canonical ensemble (Bratteli and Robinson 1997; Kardar 2007), response theory (Martin 2004), master equations (Breuer and Petruccione 2007), et cetera. No matter which models are used, one requires a setting in which the particle number can fluctuate. In this section we present the construction of Fock space, which is a first step on the route towards a rigorous description of many-boson and many-fermion systems. It must be emphasised that the Fock space is not the end of the story. As a matter of fact, there is

7.3 Fock Space 209

typically no such thing as a uniquely defined Fock space for a full-blown many-body system.

In several ways, building Fock space is similar to playing with Lego. We have a set of fundamental building blocks at our disposal and we use them to build up a larger construct. Many of these fundamental building blocks have been introduced in Sect. 7.2, since there we presented the structure for an n-particle system. We want to consider a space in which the number of particles can fluctuate, which means that the Hilbert space must be equipped to describe from a single up to hundreds of particles, and even the empty system. This implies that $\mathcal{H}_{a/s}^{\otimes n}$ for all possible values of n must be contained within the joint structure. This can be done by gluing these blocks together using direct sums, thus defining Fock spaces

$$\Gamma^{f}(\mathcal{H}) := \mathbb{C} \oplus \mathcal{H} \oplus \mathcal{H}_{a}^{\otimes 2} \oplus \dots, \tag{7.38}$$

$$\Gamma^b(\mathcal{H}) := \mathbb{C} \oplus \mathcal{H} \oplus \mathcal{H}_s^{\otimes 2} \oplus \dots \tag{7.39}$$

We refer to the different terms in the direct sum as *sectors*. The first sector, denoted \mathbb{C} , describes the empty system. Although the fermionic Fock space (7.38) and the bosonic Fock space (7.39) look very similar, there is already a huge difference between both whenever \mathcal{H} is finite dimensional: Whenever a fermionic system is built on top of a finite dimensional single-particle Hilbert space, it can house at most as many particles as the dimension of \mathcal{H} . This implies that the series of direct sums in (7.38) is finite when we deal with a finite dimensional \mathcal{H} . However, due to the symmetric properties of bosonic wave functions, there is no limit to the number of bosons that can be accommodated in a single system, as several of them can be represented by the same single-particle wave functions. However, there typically are also *physical constraints* to be taken into account.

The most fundamental object in this Fock space is the vacuum vector Ω , which represents the empty system. This vector is, both in fermionic and in bosonic Fock space, given by

$$\Omega = 1 \oplus 0 \oplus 0 \oplus \dots \tag{7.40}$$

Of course, a general vector Ψ in such a Fock space can straightforwardly be written down as

$$\Psi = \psi^{(0)} \oplus \psi^{(1)} \oplus \psi^{(2)} \oplus \dots \text{ with } \psi^{(n)} \in \mathcal{H}_{a/s}^{\otimes n}. \tag{7.41}$$

It is important to demand that⁷

$$\|\Psi\|^2 = \sum_{n} \|\psi^{(n)}\|^2 < \infty \tag{7.42}$$

because we want these vectors to be normalisable. We can now interpret $\psi^{(n)}$ as the n-particle component of the general wave function Ψ .

 $^{^7}$ The norm structure is straightforwardly inherited from the norm that lies on the single-particle Hilbert space \mathcal{H} .

A useful and consistent way to build vectors such as Ψ from the vacuum state is by using *creation operators* $a^{\dagger}(\phi)$, where $\phi \in \mathcal{H}$. These operators connect the n-particle sectors to (n+1)-particle spaces. For a fermionic system, the action of a creation operator on the vector Ψ as defined in (7.41) is given by

$$a^{\dagger}(\phi)\Psi := 0 \oplus \left(\psi^{(0)}\phi\right) \oplus \left(\phi \wedge \psi^{(1)}\right) \oplus \left(\phi \wedge \psi^{(2)}\right) \oplus \dots,$$
 (7.43)

such that $a^{\dagger}(\phi)$ literally takes a single-particle wave function $\phi \in \mathcal{H}$ and adds it to the system. For example the two-particle component $\psi^{(2)}$ of Ψ gets an additional particle with wave function ϕ glued to it, which turns it into a three-particle component $\phi \wedge \psi^{(2)}$ of the new vector $a^{\dagger}(\phi)\Psi$.

The action of a bosonic creation operator is identical, except for the fact that it attaches the new single-particle wave functions using "①". This slight change can nevertheless lead to serious problems, since

$$\|\phi \odot \psi^{(n)}\| \leqslant \sqrt{n+1} \|\phi\| \|\psi^{(n)}\| \tag{7.44}$$

is the best possible bound. Thus, when we deal with a bosonic system, we may write

$$a^{\dagger}(\phi)\Psi = 0 \oplus \left(\psi^{(0)}\phi\right) \oplus \left(\phi \odot \psi^{(1)}\right) \oplus \left(\phi \odot \psi^{(2)}\right) \oplus \dots,$$
 (7.45)

but this only results in a well-defined and normalisable wave function if

$$\sum_{n=0}^{\infty} n \|\psi^{(n)}\|^2 < \infty. \tag{7.46}$$

The additional factor *n* typically puts strong restrictions on the allowed states and points towards a rather fundamental problem of bosonic creation operators: They are *unbounded*.

Given these creation operators $a^{\dagger}(\phi)$, together with the specific Hilbert space \mathcal{H} and the vacuum Ω , we now have all the tools at hand to consistently populate Fock space. Indeed, many-particle wave functions can simply be generated by letting creation operators act on the vacuum. Be mindful, though, these wave functions are typically not normalised. One may simply realise that we can construct an n-particle state in Fock space by applying creation operators to the vacuum, since

⁸Note that the component $\psi^{(0)}$ on the zero-particle sector of Ψ is simply a complex number, describing the component of the wave function that does not contain any particle. Upon acting with the creation operator, a particle is created, hence there is no longer any fraction of the wave function that contains no particle, and the zero-particle component of Ψ acquires one particle with wave function ϕ .

7.3 Fock Space 211

$$a^{\dagger}(\psi_1)a^{\dagger}(\psi_2)\dots a^{\dagger}(\psi_n)\Omega = 0 \oplus \dots \oplus 0 \oplus \left(\psi_1 \wedge \psi_2 \wedge \dots \wedge \psi_n\right) \oplus 0 \oplus \dots$$
(7.47)

Clearly this approach can be extended to more intricate constructions of wave functions which live on multiple particle sectors.

Another useful tool in Fock space is the number operator \hat{N} , which quite literally counts the number of particles. It acts on a vector Ψ , as given by (7.41), as

$$\hat{N}\Psi = 0 \oplus \psi^{(1)} \oplus 2\psi^{(2)} \oplus 3\psi^{(3)} \oplus \dots, \quad \text{with } \sum_{n=0}^{\infty} n^2 \|\psi^{(n)}\|^2 < \infty.$$
 (7.48)

Thus each component of each particle sector is multiplied by its respective number of particles.

7.3.2 Structuring Fock Space

A seemingly innocent, though fundamental aspect of Fock spaces is that they naturally inherit structures engraved in the single-particle Hilbert spaces on which they are constructed. Specifically, direct sum structures in the single-particle Hilbert space can be expressed by tensor product structures of Fock spaces. This is represented by the natural isomorphism U,

$$U:\Gamma^{f/b}(\mathcal{H}_1\oplus\mathcal{H}_2)\to\Gamma^{f/b}(\mathcal{H}_1)\otimes\Gamma^{f/b}(\mathcal{H}_2). \tag{7.49}$$

Actually, the unitary operator U has additional structure and can be seen as a block-diagonal, following the direct sum structure of Fock space

$$U = \bigoplus_{n} U_n, \tag{7.50}$$

where U_n acts on the n-particle sector. Since we break up the Fock space in the tensor product structure (7.49), each particle of the n-particle sector has the possibility to live in either one of the two constituents of the tensor product. Therefore, in order to accommodate all possibilities, we find a binomial formula for Hilbert spaces

$$U_n: \left(\mathcal{H}_1 \oplus \mathcal{H}_2\right)_{a/s}^{\otimes n} \to \bigoplus_{k=0}^n \mathcal{H}_{1}{}_{a/s}^{\otimes k} \otimes \mathcal{H}_{2}{}_{a/s}^{\otimes n-k}, \tag{7.51}$$

these different unitaries act explicitly on bosons as

$$U_{1}(\psi_{1} \oplus \psi_{2}) = \psi_{1} \oplus \psi_{2}$$

$$U_{2}((\psi_{1} \oplus \psi_{2}) \odot (\phi_{1} \oplus \phi_{2})) = ((\psi_{1} \odot \phi_{1}) \otimes 1) \oplus (\psi_{1} \otimes \phi_{2} + \phi_{1} \otimes \psi_{2}) \oplus (1 \otimes (\psi_{2} \odot \phi_{2}))$$

$$\vdots$$
while for fermions the result is slightly different
$$(7.52)$$

$$U_{1}(\psi_{1} \oplus \psi_{2}) = \psi_{1} \oplus \psi_{2}$$

$$U_{2}((\psi_{1} \oplus \psi_{2}) \wedge (\phi_{1} \oplus \phi_{2})) = ((\psi_{1} \wedge \phi_{1}) \otimes 1) \oplus (\psi_{1} \otimes \phi_{2} - \phi_{1} \otimes \psi_{2}) \oplus (1 \otimes (\psi_{2} \wedge \phi_{2}))$$

$$\vdots$$

$$(7.53)$$

It is useful to pinpoint the special case where we consider the two-particle vector $(\psi \oplus 0) \odot (0 \oplus \phi)$ for which we find

$$U_2(\psi \oplus 0) \odot (0 \oplus \phi) = \psi \otimes \phi. \tag{7.54}$$

This implies that, although the two bosons are *identical*, they can effectively be described by a tensor product state and are therefore *distinguishable*. A natural example is that of two free bosons, which are spatially separated, e.g. the one is on Venus, the other on Mars. The particles' wave functions are contained in the Hilbert space of square integrable functions in 3D Euclidean space $\mathcal{L}^2(\mathbb{R}^3)$. We can describe this space as $\mathcal{L}^2(\mathbb{R}^3) = \mathcal{L}^2(\Lambda_{\text{Venus}}) \oplus \mathcal{L}^2(\mathbb{R}^3 \setminus \Lambda_{\text{Venus}})$, where Λ_{Venus} can be seen as an interval in 3D space that only contains Venus. This direct sum structure now allows us to ultimately describe the system with the state $\psi_{\text{Venus}} \otimes \psi_{\text{Mars}}$, i.e. although the particles are identical, they can clearly be distinguished because they are on different planets. We extensively come back to this point when discussing distinguishability in Sect. 8.3.4.

To globally describe the action of U, we can use the knowledge that creation operators and the vacuum state are sufficient to populate the Fock spaces. The action of U on these objects is thus the only relevant ingredient which is required. It holds that

$$U\Omega_{12} = \Omega_1 \otimes \Omega_2, \tag{7.55}$$

$$Ua^{\dagger}(\psi_1 \oplus \psi_2)U^{\dagger} = a^{\dagger}(\psi_1) \otimes \mathbb{1} + \mathbb{1} \otimes a^{\dagger}(\psi_2) \quad \text{for bosons}, \tag{7.56}$$

$$Ua^{\dagger}(\psi_1 \oplus \psi_2)U^{\dagger} = a^{\dagger}(\psi_1) \otimes \mathbb{1} + (-\mathbb{1})^{\hat{N}} \otimes a^{\dagger}(\psi_2)$$
 for fermions, (7.57)

where Ω_{12} is the vacuum of Hilbert space $\Gamma(\mathcal{H}_1 \oplus \mathcal{H}_2)$ and the operator $(-1)^{\hat{N}}$ imposes a minus sign for those states which have an odd number of particles (Jordan and Wigner 1928). As these results may seem a little abstract, we emphasise what they imply for some more concrete examples of systems: At the bottom line of

⁹One can employ exactly the same argument for distinguishable, though identical, fermions.

7.3 Fock Space 213

the above structures is the fact that we can either structure our Fock space using layers of different particle numbers, or factors of different modes. Typically, the considered modes represent the basic structure of \mathcal{H} : When we focus on any type of finite dimensional system, $\mathcal{H} \cong \mathbb{C}^k$. Of course, we can break up \mathbb{C}^k in many direct sum structures, as many as there are partitions of k to be precise. However, the most fundamental building block is simply \mathbb{C} , and thus we can represent any k-dimensional Hilbert space as $\mathcal{H} \cong \bigoplus_{i=1}^k \mathbb{C}$. This, on its turn, implies that we can derive

$$\Gamma^{b/f}(\mathcal{H}) \cong \left(\Gamma^{b/f}(\mathbb{C})\right)^{\otimes k} \quad \text{if } \mathcal{H} \text{ is } k\text{-dimensional.}$$
(7.58)

This result has a fundamental consequence when it comes to interpretations. It implies that there are essentially two equivalent ways to describe a many-particle system: either we take the particle perspective and describe which modes contribute to each particle's state, or we start from the mode perspective and describe how many particles occupy each mode. The fundamental building blocks of the system in the mode perspective are given by $\Gamma^{b/f}(\mathbb{C})$. Let us take a closer look at these structures.

Bosons and Harmonic Oscillators

In the case of bosons, $\Gamma^b(\mathbb{C})$ is given, according to (7.39), by

$$\Gamma^{b}(\mathbb{C}) = \mathbb{C} \oplus \mathbb{C} \oplus \mathbb{C}_{s}^{\otimes 2} \oplus \dots$$

$$= \mathbb{C} \oplus \mathbb{C} \oplus \mathbb{C} \oplus \dots$$
(7.59)

which is still an infinite dimensional system. Because $\mathbb C$ is a one dimensional space, there is only one unique creation operator a^{\dagger} . It can now be shown that

$$\Gamma^b(\mathbb{C}) \cong \mathcal{L}^2(\mathbb{R}),\tag{7.60}$$

the space of square integrable functions. To do so, we first construct the operators P and Q on $\mathcal{L}^2(\mathbb{R})$:

$$(Q\psi)(x) = x \psi(x)$$
 and $(P\psi)(x) = -i \frac{\partial}{\partial x} \psi(x)$ (7.61)

for all $\psi \in \mathcal{L}^2(\mathbb{R})$ and all $x \in \mathbb{R}$. Note that in order to construct an isomorphism $u : \Gamma^b(\mathbb{C}) \to \mathcal{L}^2(\mathbb{R})$, we simply need to find a consistent image for Ω and a^{\dagger} . These are given by

 $^{^{10}}$ We will use the term *modes* to describe the degrees of freedom which are seen by each individual particle in the system. In other words, the single-particle Hilbert space $\mathcal H$ can be seen as the structure that describes the quantum mechanics for these modes.

$$(u\Omega)(x) = \frac{1}{\pi^{1/4}} e^{-x^2/2} \tag{7.62}$$

$$ua^{\dagger}u^{-1} = \frac{1}{\sqrt{2}}(Q - iP). \tag{7.63}$$

With [Q, P] = i from (7.61), we know that these operators are the well-known and fundamental position and momentum operators for $\mathcal{L}^2(\mathbb{R})$. The mapping u directly establishes the connection between the bosonic creation operator and the creation operator for excitations of the harmonic oscillator. In other words, $\Gamma^{b/f}(\mathcal{H})$ can be interpreted as a *chain of harmonic oscillators*.

Note that this equivalence lies at the heart of the early algebraic approach to quantum mechanics (von Neumann 1931), which showed the equivalence between Schrödinger's wave mechanics and Heisenberg's matrix mechanics.

Fermions and Spin Systems

For fermions the structure of $\Gamma^f(\mathbb{C})$ is considerably simpler

$$\Gamma^f(\mathbb{C}) = \mathbb{C} \oplus \mathbb{C} \cong \mathbb{C}^2. \tag{7.64}$$

This is logical, given that a single fermionic mode can contain at most one particle and can therefore be treated similarly to a two-level system. The isomorphism

$$u:\Gamma^f(\mathbb{C})\to\mathbb{C}^2$$
 (7.65)

is straightforwardly given by

$$u\Omega = \begin{pmatrix} 0\\1 \end{pmatrix},\tag{7.66}$$

$$ua^{\dagger}u^{-1} = \begin{pmatrix} 0 & 1 \\ 0 & 0 \end{pmatrix}. \tag{7.67}$$

The latter is nothing else than σ^+ , which allows us to directly make a connection to the Pauli matrices and thereby interpret the single fermionic mode as a spin.

However, there is a serious subtlety when we embed this into a larger structure as set forth by Eq. (7.57). Considering

$$a_i^{\dagger} := a^{\dagger} \left(\left(\bigoplus_{i=1}^{i-1} 0 \right) \oplus 1 \oplus \left(\bigoplus_{j=1}^{k-i} 0 \right) \right)$$
 (7.68)

we have to take into account the $(-1)^{\hat{N}}$ described in Eq. (7.57) when implementing the isomorphism. For \mathbb{C}^2 this operator is described by

$$(-1)^{\sigma^{+}\sigma^{-}} = \begin{pmatrix} 1 & 0 \\ 0 & -1 \end{pmatrix} = \sigma^{z}$$
 (7.69)

7.3 Fock Space 215

and this now leads to the Jordan-Wigner transformation

$$Ua_i^{\dagger}U^{-1} = \sigma^z \otimes \cdots \otimes \sigma^z \otimes \sigma^+ \otimes \mathbb{1} \otimes \cdots \otimes \mathbb{1}, \tag{7.70}$$

where the $\sigma^+ = ua^{\dagger}u^{-1}$ is positioned as the *i*th factor in the tensor product.

The Jordan–Wigner transformation allows to connect a system of multiple fermionic modes to a *quantum spin chain*. This may seem like a rather artificial and unpractical identity due to the σ^z components, however the mapping has its merits: Most remarkable and surprising is probably that one can use fermionic systems and the Jordan–Wigner isomorphism to study the 2D Ising model (Araki and Evans 1983; Bratteli and Robinson 1997), clearly highlighting the use of these identities.

7.3.3 Exponential Vectors

In our list of useful tools for calculation, we ultimately devote the last fraction of this section on Fock space structures to a particularly useful type of objects: the so-called exponential vectors. These objects are particularly useful for bosons: An exponential vector in $\Gamma^b(\mathcal{H})$ is constructed using a single-particle wave function $\psi \in \mathcal{H}$, and is given by

$$\exp(\psi) := 1 \oplus \psi \oplus \frac{1}{\sqrt{2!}} \psi \otimes \psi \oplus \dots \tag{7.71}$$

It can directly be seen that

$$\exp(\psi) = \exp(a^{\dagger}(\psi)) \,\Omega. \tag{7.72}$$

Given the typical normalisation issues which were addressed for bosonic systems, it is useful to note that the exponential vectors are normalisable. Moreover, they form a linearly independent set and their linear combinations are dense in $\Gamma^b(\mathcal{H})$. They also offer computational advantages such as

$$\langle \exp(\phi), \exp(\psi) \rangle = \left\langle 1 \oplus \phi \oplus \left(\frac{1}{\sqrt{2!}} \phi \otimes \phi \right) \oplus \dots, 1 \oplus \psi \oplus \left(\frac{1}{\sqrt{2!}} \psi \otimes \psi \right) \oplus \dots \right\rangle$$

$$= 1 + \langle \phi, \psi \rangle + \frac{1}{2!} \langle \phi, \psi \rangle^2 + \frac{1}{3!} \langle \phi, \psi \rangle^3 + \dots$$

$$= e^{\langle \phi, \psi \rangle}$$
(7.73)

In the context of Fock space structures, the isomorphism (7.49) acts in a very natural way

$$U \exp(\psi_1 \oplus \psi_2) = \exp(\psi_1) \otimes \exp(\psi_2) \tag{7.74}$$

Due to all these nice properties, one may wonder whether it is not more natural to describe bosonic systems with such vectors rather than the standard symmetric wave

functions. It turns out that this intuition is correct, this does provide technical advantages. The exponential vectors also prove to be fundamental tools in the interpretation of bosonic coherent states. We extensively come back to this point in the following sections. First, however, we plunge deeper in the structure of creation operators and their antagonists, the annihilation operators.

7.4 Commutation Relations

It is no coincidence that the creation operator is indicated with a "†", as it is, indeed, the adjoint of another type of operator, denoted by $a(\psi)$, the annihilation operator. As suggested by its destructive name, the annihilation operator destroys particles. This action is, however, slightly more subtle to define than the creation of a particle. After all, it is straightforward to destroy a particle with wave function $\psi_1 \in \mathcal{H}$ from the two fermion wave function $\psi_1 \wedge \psi_2$ (at least assuming $\langle \psi_1, \psi_2 \rangle = 0$), but how would one annihilate a particle with wave function $\phi \in \mathcal{H}$ from the very same two-fermion wave function? Ultimately, we can compute the action of $a(\phi)$ from (7.43), which results in the mapping ϕ 1

$$\psi_1 \wedge \psi_2 \wedge \dots \wedge \psi_{n+1} \mapsto \sum_{j=1}^{n+1} (-1)^{j+1} \langle \phi, \psi_j \rangle \psi_1 \wedge \dots \wedge \psi_{j-1} \wedge \psi_{j+1} \wedge \dots \wedge \psi_{n+1}.$$
(7.75)

For fermions it is not surprising that sign-bookkeeping is required, but their bosonic counterpart saves us from such cumber and we obtain the mapping

$$\psi_1 \odot \psi_2 \odot \cdots \odot \psi_{n+1} \mapsto \sum_{j=1}^{n+1} \langle \phi, \psi_j \rangle \psi_1 \odot \cdots \odot \psi_{j-1} \odot \psi_{j+1} \cdots \odot \psi_{n+1}.$$
(7.76)

Thus we defined the operator $a(\phi)$ for $\phi \in \mathcal{H}$ and have the possibility to make transitions from n particle space to (n-1)-particle space. For completeness, let us also mention that $a(\phi)\Omega = 0$ for any $\phi \in \mathcal{H}$.

Having constructed both creation and annihilation operators, we now explore their mutual relation, which is notoriously captured by the *commutation relations* for bosons and the *anticommutation relations* for fermions. By using for example any *n*-particle wave function, it can be directly verified that for bosons

¹¹Equation (7.43) can be thought of as a block diagonal representation. Therefore, we can restrict ourselves to considering $a^{\dagger}(f):\mathcal{H}^{(n)}\to\mathcal{H}^{(n+1)}$. We can now consider $\Psi\in\mathcal{H}^{(n)}$ and $\Phi\in\mathcal{H}^{(n+1)}$, with $\Psi=\psi_1\wedge\dots\wedge\psi_n$ and $\Phi=\phi_1\wedge\dots\wedge\phi_{n+1}$, and compute $\langle a^{\dagger}(f)\Psi,\Phi\rangle=\sum_{\pi\in S_{n+1}}\langle f,\phi_{\pi(1)}\rangle\langle\psi_1,\phi_{\pi(2)}\rangle\dots\langle\psi_n,\phi_{\pi(n+1)}\rangle$. The adjoint is now defined by demanding that $\langle a^{\dagger}(f)\Psi,\Phi\rangle=\langle\Psi,a(f)\Phi\rangle$ for all $\Psi\in\mathcal{H}^{(n)}$ and $\Phi\in\mathcal{H}^{(n+1)}$. Because the Slater determinants form a total set, we can define the annihilation operator by means of its action on such vectors. The result (7.75) follows from the evaluation of the inner products.

$$[a^{\dagger}(\psi_1), a^{\dagger}(\psi_2)] = 0$$
 and $[a(\psi_1), a^{\dagger}(\psi_2)] = \langle \psi_1, \psi_2 \rangle$, (7.77)

whereas for fermions

$$\{a^{\dagger}(\psi_1), a^{\dagger}(\psi_2)\} = 0 \text{ and } \{a(\psi_1), a^{\dagger}(\psi_2)\} = \langle \psi_1, \psi_2 \rangle.$$
 (7.78)

It is appealing to note at this stage that these operators act similarly to the ladder operators which are know from the theory of angular momentum in quantum mechanics (Basdevant and Dalibard 2002). Formally, angular momentum degrees of freedom can be related to the rotation group and its representations (Hamermesh 1989). Fock space can be constructed in a very analogous way (Bratteli and Robinson 1997).

A final crucial property of the creations and annihilation operators is their behaviour with respect to the linear combinations of single-particle wave functions. From the definitions of these operators, we see that they are \mathbb{C} -linear, which implies that for all $\psi_1, \psi_2 \in \mathcal{H}$ and $\alpha \in \mathbb{C}$

$$a^{\dagger}(\alpha\psi_1 + \psi_2) = \alpha a^{\dagger}(\psi_1) + a^{\dagger}(\psi_2), \tag{7.79}$$

$$a(\alpha\psi_1 + \psi_2) = \overline{\alpha} \, a(\psi_1) + a(\psi_2). \tag{7.80}$$

This property will, for example, be quite fundamental to obtain the results of Sect. 7.5. Although we have constructed the creations and annihilation operators in a consistent way, the results for bosons are not completely satisfactory, since the creation and annihilation operators are unbounded, which follows directly from (7.46), and therefore hard to control. To overcome this inconvenience, it is common to work with another class, known as *Weyl operators*. These unitary—thus bounded—operators can be used to avoid technical difficulties. They also satisfy a bounded version of the bosonic (canonical) commutation relations. Let us start by defining them in terms of the bosonic creation and annihilation operators:

$$W(\psi) := \exp\left(a^{\dagger}(\psi) - a(\psi)\right), \quad \psi \in \mathcal{H}. \tag{7.81}$$

There are several different names and conventions for these operators, depending on the field that uses them. We choose to follow (Alicki 2010), which is most fit for quantum optics applications (Grynberg et al. 2010; Mandel and Wolf 1995; Schleich 2001; Scully and Zubairy 1997). One can prove the following properties

$$W(0) = 1, (7.82)$$

$$W^{\dagger}(\psi) = W(-\psi), \tag{7.83}$$

$$W(\psi_1)W(\psi_2) = \exp(i\operatorname{Im}\langle\psi_1,\psi_2\rangle) \ W(\psi_1 + \psi_2), \tag{7.84}$$

$$W(\psi)a(\phi)W^{\dagger}(\psi) = a(\phi) - \langle \phi, \psi \rangle, \qquad (7.85)$$

$$W(\psi)a^{\dagger}(\phi)W^{\dagger}(\psi) = a^{\dagger}(\phi) - \langle \psi, \phi \rangle. \tag{7.86}$$

For the last three properties, one uses the Baker-Campbell-Hausdorff formula (Alicki 2010).

7.5 Second Quantisation

Now that the creation and annihilation operators are defined and their fundamental structure is known, we explain how they can be used to construct more intricate objects. We already know they can be used to construct wave functions on Fock space, but they serve other purposes when combined: They form observables on Fock space.

Up to now, we focussed attention on the structure of Fock space and on the wave functions defined on it. On the level of observables, we only introduced the number operator \hat{N} . To broaden the discussion to general, though tractable classes of observables, we start with what are called *single-particle observables*. These observables are in principle generated by an observable $O \in \mathcal{B}(\mathcal{H})$ on the single-particle Hilbert space. Since our system contains multiple particles, it does not make sense to let the operator act on only one of them, after all, this would single out a special particle which goes against them being identical. Intuitively, we may again consider the physical quantity $\langle \mathfrak{D}^{(n)} \rangle_{1,2,\dots,n}$, where $\mathfrak{D}^{(n)}$ is the observable defined on $\mathcal{H}_{a/s}^{\otimes n}$, generated by $O \in \mathcal{B}(\mathcal{H})$, and conclude that intuitively

$$\langle \mathfrak{D}^{(n)} \rangle_{1,2,\dots,n} = \langle O \rangle_1 + \langle O \rangle_2 + \dots + \langle O \rangle_n. \tag{7.87}$$

This kind of observables is additive, as expected, for example, for a Hamiltonian (energy) without interactions. In other words, an n-particle observable, with an n-particle state acting on it, is broken up in a sum of single-particle observables with single-particle states acting on them. One can obtain such a structure by defining $\mathfrak{D}^{(n)}$ as

$$\mathfrak{D}^{(n)} = \left(O \otimes \mathbb{1}^{\otimes n-1} + \mathbb{1} \otimes O \otimes \mathbb{1}^{n-2} + \dots + \mathbb{1}^{n-1} \otimes O \right) \Big|_{\mathcal{H}_{a/s}^{\otimes n}}, \tag{7.88}$$

such that essentially each particle in $\mathcal{H}_{a/s}^{\otimes n}$ is appointed its own copy of O. These objects are often referred to as single-particle observables, since their action on the many-particle spaces is essentially a trivial extension of their action on a single particle. On the other hand, even though they seem like somewhat trivial objects, they are quite fundamental in the theory of many-particle systems.

The generalisation to the full Fock space is completely straightforward and is given by

$$\Gamma^{f/b}(O) := 0 \oplus \mathfrak{O}^{(1)} \oplus \mathfrak{O}^{(2)} \oplus \dots$$
 (7.89)

However, there is a much more appealing way to write this object, which often proves useful in calculations, using creation and annihilation operators. At first let us consider $\{e_j\}$, a (potentially infinite) basis of the single-particle space \mathcal{H} . The action of $O \in \mathcal{B}(\mathcal{H})$ on any wave function $\psi \in \mathcal{H}$ is given by

$$O\psi = \sum_{i,j} \langle e_i, Oe_j \rangle \langle e_j, \psi \rangle e_i.$$
 (7.90)

This identity can be used to calculate

$$\mathfrak{D}^{(n)}\psi_{1} \wedge \psi_{2} \wedge \cdots \wedge \psi_{n}$$

$$= (O\psi_{1}) \wedge \psi_{2} \wedge \cdots \wedge \psi_{n} + \psi_{1} \wedge (O\psi_{2}) \wedge \cdots \wedge \psi_{n} + \cdots$$

$$+ \psi_{1} \wedge \psi_{2} \wedge \cdots \wedge (O\psi_{n})$$

$$= \left(\sum_{i,j} \langle e_{i}, Oe_{j} \rangle a^{\dagger}(e_{i})a(e_{j}) \right) \psi_{1} \wedge \psi_{2} \wedge \cdots \wedge \psi_{n}.$$

$$(7.91)$$

As this procedure can be carried out for all particle numbers n and all wave functions ψ_k , we conclude that

$$\Gamma^{f}(O) = \sum_{i,j} \langle e_i, Oe_j \rangle a^{\dagger}(e_i) a(e_j). \tag{7.92}$$

Because a random basis $\{e_j\}$ is used, one can in principle choose any basis to carry out this construction. However, usually physics provides a natural basis to treat the problem; if not, mathematics encourages us to use the basis of eigenvectors of O. Of course, a fully analogous calculation is possible for bosons.

These representations of single-particle observables in Fock space have several useful and interesting properties, which one can derive using Eq. (7.92):

$$[\Gamma^{b/f}(O), a^{\dagger}(\psi)] = a^{\dagger}(O\psi), \tag{7.93}$$

$$[\Gamma^{b/f}(O), a(\psi)] = -a(O^{\dagger}\psi), \tag{7.94}$$

$$[\Gamma^{b/f}(O), \Gamma^{b/f}(M)] = \Gamma^{b/f}([O, M]). \tag{7.95}$$

For this dissertation, these properties are specifically useful when considering dynamics and equations of motion.

Example 7.5.1 Since we claimed that the single-particle operators can be quite fundamental, let us give a concrete example of one very fundamental observable which is actually a single-particle operator: The number operator. It sounds slightly ironical that the operator that counts the number of particles is actually contained in the class of single-particle operators, but when one considers its structure, it is actually logical. Remember that we defined in (7.48):

$$\hat{N}\Psi = 0 \oplus \psi^{(1)} \oplus 2\psi^{(2)} \oplus 3\psi^{(3)} \oplus \dots$$

This definition allows for the very straightforward expression that

$$\hat{N} = 0 \oplus \mathbb{1} \oplus 2\mathbb{1} \oplus 3\mathbb{1} \oplus \dots, \tag{7.96}$$

which directly implies that, actually,

$$\hat{N} = \Gamma^{f/b}(\mathbb{1}). \tag{7.97}$$

Therefore, it is also logical that we can choose any basis $\{e_j\}$ of the single-particle space \mathcal{H} and express

$$\hat{N} = \sum_{i} a^{\dagger}(e_j)a(e_j), \tag{7.98}$$

which is clearly related to the number operators which we know for the harmonic oscillator.

These insights allow for a natural definition and interpretation of other types of "counting operators": One may consider $P_S \in \mathcal{B}(\mathcal{H})$ such that $P_S^2 = P_S$, and, hence, is a projector on a subspace which we label S. By considering

$$\hat{n}_S := \Gamma^{f/b}(P_S) \tag{7.99}$$

we construct an operator which counts exactly how many particles are occupying wave functions contained in S. Specifically interesting is the case where $P = |\psi\rangle\langle\psi|$, which leads to

$$\hat{n}_{\psi} := \Gamma^{f/b}(|\psi\rangle\langle\psi|). \tag{7.100}$$

After our discussion about the structure of Fock space in Sect. 7.3.2, we know that one can typically partition $\mathcal{H} \cong \bigoplus_j \mathbb{C}$ such that each term in the direct sum corresponds to a different mode. Now, we can use operators of the form \hat{n}_k , as the number operators constructed on the kth factor of $\bigotimes_j \Gamma^{f/b}(\mathbb{C})$, to count the number of particles in each mode.

In complete analogy to the single-particle observables, one can also define n-particle observables, which act on each possible combination of n particles. For all sectors with fewer than n particles, the operator simply returns zero, 12 but one clearly sees that for larger particle numbers some combinatorics is required. We will not go into detail here, but simply introduce the two-particle case to sketch the idea.

Let us assume that $A \in \mathcal{B}(\mathcal{H}_{a/s}^{\otimes 2})$, thus turning it into a two-particle observable. We can again embed this observable in an *n*-particle space $\mathcal{H}_{a/s}^{\otimes n}$ (with $n \ge 2$) by the following construction¹³:

$$\mathfrak{A}^{(n)} := \sum_{\{i_1, i_2\}} \left(A_{\{i_1, i_2\}} \otimes \left(\bigotimes_{k \notin \{i_1, i_2\}} \mathbb{1} \right) \right) \Big|_{\mathcal{H}_{als}^{\otimes n}} \tag{7.101}$$

 $^{^{12}}$ Thus, if an m-particle observable acts on an n-wave function, the result will be zero whenever n < m.

 $^{^{13}}$ A word on notation: Whenever we consider an operator A, acting on some Hilbert space \mathcal{H} , we denote $A \mid_{\mathcal{K} \subset \mathcal{H}}$ the restriction of A on the subspace $\mathcal{K} \subset \mathcal{H}$. Such a restriction simply limits the domain of the operator to the smaller subspace.

Notationally, this may look a little complicated, but it represents the idea that one sums over each combination of two particles and lets *A* act on the two-particle space spanned by these two particles. We now define the two-particle observable on the full Fock space as

$$\Gamma^{b/f}(A) := 0 \oplus 0 \oplus \mathfrak{A}^{(2)} \oplus \mathfrak{A}^{(3)} \oplus \dots, \tag{7.102}$$

where $\mathfrak{A}^{(2)} = A$.

As a rather aesthetic alternative we may also write

$$\Gamma^{f}(A) = \frac{1}{2} \sum_{i,j,k,l} \langle e_i \wedge e_j, A e_k \wedge e_l \rangle a^{\dagger}(e_i) a^{\dagger}(e_j) a(e_k) a(e_l) \quad \text{for fermions,}$$
(7.103)

$$\Gamma^{b}(A) = \frac{1}{2} \sum_{i,j,k,l} \langle e_i \odot e_j, A e_k \odot e_l \rangle a^{\dagger}(e_i) a^{\dagger}(e_j) a(e_k) a(e_l) \quad \text{for bosons,}$$
(7.104)

where $\{e_j\}$ forms as basis of the single-particle Hilbert space \mathcal{H} . These identities are computed in a similar way as we did for the single-particle case in Eq. (7.92), but we do not present the details here. It is, however, important to show that, indeed, the action of $\Gamma^{f/b}(A)$ on a single particle wave functions leads to a zero contribution: Let us consider $\psi \in \mathcal{H}$, represented in Fock space by $\Psi = a^{\dagger}(\psi)\Omega$, and $\Gamma^{f/b}(A)$ act on it:

$$\Gamma^{f}(A)\Psi = \frac{1}{2} \sum_{i,j,k,l} \langle e_{i} \wedge e_{j}, A e_{k} \wedge e_{l} \rangle a^{\dagger}(e_{i}) a^{\dagger}(e_{j}) a(e_{k}) a(e_{l}) a^{\dagger}(\psi) \Omega$$

$$= \frac{1}{2} \sum_{i,j,k,l} \langle e_{i} \wedge e_{j}, A e_{k} \wedge e_{l} \rangle a^{\dagger}(e_{i}) a^{\dagger}(e_{j}) a(e_{k}) \left(\langle e_{l}, \psi \rangle - a^{\dagger}(\psi) a(e_{l}) \right) \Omega$$

$$= 0.$$
(7.105)

The last step simply follows from the fact that we end up with an annihilation operator acting on the vacuum.

The procedure described here indicates that any type of observable can be expressed in terms of creation and annihilation operators, which makes these operators much more fundamental than the wave functions in the Fock space. One requires nothing but a vacuum vector Ω and a set of creation and annihilation operators that obey the right commutation (or anticommutation relations) to do physics. Ultimately these creation and annihilation operators are the foundation of many-particle quantum physics, which is extensively discussed in Sect. 7.7.

The transition from *n*-particle observables on the *n*-particle space to the full Fock space, as described in this section, is often referred to as *second quantisation* because it exactly quantises everything in terms of creation and annihilation operators.

There is one additional—and very useful—object that remains to be considered: the *exponential* element (Dierckx et al. 2008). Just as the second quantisation method described above, the exponential element represents a single-particle observable as a bounded operator on Fock space. However, it does so in a fundamentally different way, since it acts multiplicatively. The formal definition of the exponential element is given by

$$E(O) = 1 \oplus O \oplus O \wedge O \oplus O \wedge O \wedge O \oplus \dots \quad \text{for fermions}, \quad (7.106)$$

$$E(O) = 1 \oplus O \oplus O \odot O \oplus O \odot O \odot O \oplus \dots \qquad \text{for bosons.} \tag{7.107}$$

These exponential elements have many useful properties as will be shown in Sect. 8.2.¹⁴ The most important of these properties are listed here, for $A, B \in \mathcal{B}(\mathcal{H})$

$$E(\mathbb{1}_{\mathcal{H}}) = \mathbb{1}_{\Gamma(\mathcal{H})},\tag{7.108}$$

$$E(A^{\dagger}) = E(A)^{\dagger}, \tag{7.109}$$

$$E(A^{\dagger}A) \geqslant 0, \tag{7.110}$$

$$E(A)E(B) = E(AB), \tag{7.111}$$

$$E(A \oplus B) \cong E(A) \otimes E(B),$$
 (7.112)

$$E(A)a^{\dagger}(\phi) = a^{\dagger}(A\phi)E(A), \tag{7.113}$$

$$a(\phi)E(A) = E(A)a(A^{\dagger}\phi), \tag{7.114}$$

$$E(e^A) = e^{\Gamma(A)}. (7.115)$$

Notice that the very last property connects the mapping Γ in a very fundamental way to E. The exponential elements are especially useful for calculations involving dynamics.

7.6 Many-Particle Quantum States

In the previous sections, we built the structure of n-particle spaces and of the "all-inclusive" Fock space. Furthermore, we discussed the structure of some of the most natural types of observables in such systems. What up to now did not receive much attention, are the quantum states living on Fock space. In Sect. 2.3.2 we have seen that states are the positive, normalised functionals defined on the algebra of observables. Here we introduce several well-known classes of states, which one might for example encounter in quantum optics or statistical mechanics.

¹⁴Alternatively, see Dierckx et al. (2008) for applications in quantum information theory.

 $^{^{15}}$ In the next section, however, we sill see that Fock space is not as all-inclusive as it is often presented.

7.6.1 Number States

The first class of states under consideration is already quite known from the previous sections, as they where implicitly considered in much of the construction of Fock space. The *number states* are those which represent a fixed number of particles. Prominent members of this class of states are those of the form

$$\Psi \sim a^{\dagger}(\psi_1) \dots a^{\dagger}(\psi_n) \Omega. \tag{7.116}$$

Logically, for bosons it may be that $\langle \psi_i, \psi_j \rangle = 1$, whereas for fermions this would be impossible and simply result in the zero vector. Notice that we wrote "~", which is because the wave function is not yet normalised. Normalisation can either be obtained from Eqs. (7.31) and (7.32) or from direct computation via creation and annihilation operators. We go into some details of this calculation, since it is crucial for what follows. The quantity to calculate is given by

$$\left\langle a^{\dagger}(\psi_1) \dots a^{\dagger}(\psi_n) \Omega, a^{\dagger}(\psi_1) \dots a^{\dagger}(\psi_n) \Omega \right\rangle = \left\langle \Omega, a(\psi_n) \dots a(\psi_1) a^{\dagger}(\psi_1) \dots a^{\dagger}(\psi_n) \Omega \right\rangle. \tag{7.117}$$

Let us start by going through the calculation for fermions. At the root lies the identity

$$a(\psi_j)a^{\dagger}(\psi_i) = \langle \psi_j, \psi_i \rangle - a^{\dagger}(\psi_i)a(\psi_j) \tag{7.118}$$

which describes two possible scenarios: Either the creation and annihilation operators vanish and lead to a factor $\langle \psi_i, \psi_i \rangle$, or they just switch places. We turn to the monomial

$$a(\psi_n) \dots a(\psi_1) a^{\dagger}(\psi_1) \dots a^{\dagger}(\psi_n),$$

with which we play a game: we try to move all the annihilation operators on the right hand- and all the creation operators on the left hand side. However, since the monomial acts on the vacuum, once an annihilation operator makes it to the right, the associated term gets killed. This means that ultimately only the factors $\langle \psi_j, \psi_i \rangle$ in (7.118) remain. A constructive way to generate the result starts with

$$a(\psi_1)a^{\dagger}(\psi_1)\dots a^{\dagger}(\psi_n)\Omega = \sum_{j} (-1)^{j+1} \langle \psi_1, \psi_j \rangle \prod_{k \neq j} a^{\dagger}(\psi_k)\Omega. \tag{7.119}$$

As a next step, one considers

$$a(\psi_2)a(\psi_1)a^{\dagger}(\psi_1)\dots a^{\dagger}(\psi_n)\Omega = \sum_{j} (-1)^{j+1} \langle \psi_1, \psi_j \rangle a(\psi_2) \prod_{k \neq j} a^{\dagger}(\psi_k)\Omega$$
$$= \sum_{j_1 \neq j_2} (-1)^{j_1+j_2+2} \langle \psi_1, \psi_{j_1} \rangle \langle \psi_2, \psi_{j_2} \rangle \prod_{k \notin \{j_1, j_2\}} a^{\dagger}(\psi_k)\Omega,$$

$$(7.120)$$

and it is obvious that one can continue this way. Each step reduces the length of the monomial

$$a(\psi_n) \dots a(\psi_1) a^{\dagger}(\psi_1) \dots a^{\dagger}(\psi_n)$$

by one creation and one annihilation operator, and ultimately we sum over all possible ways of pairing a creation operator with an annihilation operator. The final result can be summarised as

$$\left\langle \Omega, a(\psi_n) \dots a(\psi_1) a^{\dagger}(\psi_1) \dots a^{\dagger}(\psi_n) \Omega \right\rangle = \sum_{\pi \in S_n} \operatorname{sign}(\pi) \left\langle \psi_1, \psi_{\pi(1)} \right\rangle \left\langle \psi_2, \psi_{\pi(2)} \right\rangle \dots \left\langle \psi_n, \psi_{\pi(n)} \right\rangle
= \det(\left[\left\langle \psi_i, \psi_j \right\rangle\right]).$$
(7.121)

It is interesting to note that actually this object can be related to the so-called *Gram matrix* (Bhatia 2007; Horn and Johnson 2010; Walschaers 2011) G for the n-tuple of wave functions $\{\psi_1, \ldots, \psi_n\}$, which is defined by

$$G = [\langle \psi_i, \psi_j \rangle]. \tag{7.122}$$

Using the Gram matrix, we write the wave function (7.116)

$$\Psi = \frac{1}{\sqrt{\det G}} a^{\dagger}(\psi_1) \dots a^{\dagger}(\psi_n) \Omega, \qquad (7.123)$$

which in turn can now be used to generate a number state $\langle . \rangle_{\Psi}$ which acts on an observable \mathfrak{O} , by means of

$$\langle \mathfrak{O} \rangle = \frac{1}{\det G} \langle a^{\dagger}(\psi_1) \dots a^{\dagger}(\psi_n) \Omega, \mathfrak{O} a^{\dagger}(\psi_1) \dots a^{\dagger}(\psi_n) \Omega \rangle. \tag{7.124}$$

This concludes the calculation for the fermionic case.

For *bosons*, we can almost repeat the above computation, with the difference that, instead of (7.118),

$$a(\psi_j)a^{\dagger}(\psi_i) = \langle \psi_j, \psi_i \rangle + a^{\dagger}(\psi_i)a(\psi_j). \tag{7.125}$$

This leads to the slightly different result that

$$a(\psi_1)a^{\dagger}(\psi_1)\dots a^{\dagger}(\psi_n)\Omega = \sum_{j} \langle \psi_1, \psi_j \rangle \prod_{k \neq j} a^{\dagger}(\psi_k)\Omega, \qquad (7.126)$$

from which we conclude that the signs which were obtained for fermions in (7.119) can be neglected for bosons. Conducting an analogous step-wise calculation leads to the final result

$$\langle \Omega, a(\psi_n) \dots a(\psi_1) a^{\dagger}(\psi_1) \dots a^{\dagger}(\psi_n) \Omega \rangle = \sum_{\pi \in S_n} \langle \psi_1, \psi_{\pi(1)} \rangle \langle \psi_2, \psi_{\pi(2)} \rangle \dots \langle \psi_n, \psi_{\pi(n)} \rangle$$

$$= \text{perm } G,$$
(7.127)

where we now consider the permanent of the Gram matrix G. The number state $\langle . \rangle_{\Psi}$ which acts on an observable \mathfrak{O} is now given by

$$\langle \mathfrak{O} \rangle = \frac{1}{\operatorname{perm} G} \langle a^{\dagger}(\psi_1) \dots a^{\dagger}(\psi_n) \Omega, \mathfrak{O} a^{\dagger}(\psi_1) \dots a^{\dagger}(\psi_n) \Omega \rangle. \tag{7.128}$$

We can quite easily see that the normalisation factors strongly depend on the orthogonality properties of the Gram matrix G for the set of single-particle wave functions $\{\psi_1, \ldots, \psi_n\}$. The first extreme case which one can consider is the one where $\langle \psi_i, \psi_j \rangle = \delta_{i,j}$ and thus $G = \mathbb{1}$. We then obtain that $\det G = \operatorname{perm} G = 1$, omitting the need for the normalisation factor. The other extreme is the case where $\langle \psi_i, \psi_j \rangle = 1$, in other words, where all particles are occupying the same wave function. In this case, we find that $\det G = 0$, which is just again a manifestation of the fact that this situation cannot occur for fermions. However, for bosons these states are physically admissible and we find that $\det G = n!$. There are some additional possibilities for bosons, such as wave functions of the form

$$\Psi = \frac{1}{\sqrt{\det G}} a^{\dagger}(e_1)^{q_1} \dots a^{\dagger}(e_n)^{q_n} \Omega, \tag{7.129}$$

where $\langle e_i, e_j \rangle = \delta_{i,j}$. In this case, G has the form

$$G = \bigoplus_{k=1}^{n} \mathbb{I}_{q_k},\tag{7.130}$$

where we define \mathbb{I}_q as a $q \times q$ matrix, filled with ones. It is now a reasonably simple exercise to see that

perm
$$G = q_1!q_2!\dots q_n!$$
, (7.131)

which gives us the normalisation constant. For a generic set of non-orthogonal single-particle wave functions, the normalisation factor for bosons would be extremely hard to calculate.

Now that we have explicitly studied the properties and normalisation of the state vectors (7.116), we can construct the *full class of number states*. The state vectors of form (7.116) describe a state with n particles, and they form a total set for the number states. However, linear combinations of several vectors of the form (7.116) can in general not be cast in a form given by a monomial of creation operators acting on the vacuum. In other words, when choosing $\psi_1, \ldots, \psi_n, \phi_1, \ldots, \phi_n \in \mathcal{H}$, there typically exists no $\chi_1, \ldots, \chi_n \in \mathcal{H}$ such that

$$\lambda_1 a^{\dagger}(\psi_1) \dots a^{\dagger}(\psi_n) + \lambda_2 a^{\dagger}(\phi_1) \dots a^{\dagger}(\phi_n) = a^{\dagger}(\chi_1) \dots a^{\dagger}(\chi_n),$$

with $\lambda_1, \lambda_2 \in \mathbb{C}$ and $|\lambda_1|^2 + |\lambda_2|^2 = 1$. Nevertheless, these superpositions of different number states are still number states, which becomes apparent when connect the above discussion to the number operator.

Number states can be defined as eigenvectors $\Psi \in \Gamma(\mathcal{H})$ of the number operator:

$$\hat{N}\Psi = n\Psi. \tag{7.132}$$

When we now express the number operator \hat{N} in terms of creation and annihilation operators, we can calculate for *fermionic* states Ψ as in (7.123) that

$$\hat{N}\Psi = \frac{1}{\sqrt{\det G}} \sum_{j} a^{\dagger}(e_{j})a(e_{j})a^{\dagger}(\psi_{1}) \dots a^{\dagger}(\psi_{n})\Omega$$

$$= \frac{1}{\sqrt{\det G}} \sum_{j} \sum_{k=1}^{n} (-1)^{k+1} \langle e_{j}, \psi_{k} \rangle a^{\dagger}(e_{j}) \prod_{l \neq k} a^{\dagger}(\psi_{l})\Omega$$

$$= \frac{1}{\sqrt{\det G}} \sum_{k=1}^{n} (-1)^{k+1} \left(\sum_{j} \langle e_{j}, \psi_{k} \rangle a^{\dagger}(e_{j}) \right) \prod_{l \neq k} a^{\dagger}(\psi_{l})\Omega$$

$$= \frac{1}{\sqrt{\det G}} \sum_{k=1}^{n} (-1)^{k+1} a^{\dagger}(\psi_{k}) \prod_{l \neq k} a^{\dagger}(\psi_{l})\Omega$$

$$= \frac{1}{\sqrt{\det G}} \sum_{k=1}^{n} (-1)^{k+1} a^{\dagger}(\psi_{k}) \prod_{l \neq k} a^{\dagger}(\psi_{l})\Omega$$

$$= \frac{1}{\sqrt{\det G}} \sum_{k=1}^{n} (-1)^{k+1} (-1)^{k-1} a^{\dagger}(\psi_{1}) \dots a^{\dagger}(\psi_{n})\Omega$$

$$= n \frac{1}{\sqrt{\det G}} a^{\dagger}(\psi_{1}) \dots a^{\dagger}(\psi_{n})\Omega = n\Psi.$$

It now becomes clear that n is a highly degenerate eigenvalue of \hat{N} and that therefore the vectors described by the Slater determinants (7.123) span a whole subspace related of eigenvectors associated to n. All these eigenvectors describe a fixed amount of particles n and therefore must all be considered number states.

The computation (7.133) can be conducted in a very similar way for bosons:

$$\hat{N}\Psi = \frac{1}{\sqrt{\operatorname{perm} G}} \sum_{j} a^{\dagger}(e_{j}) a(e_{j}) a^{\dagger}(\psi_{1}) \dots a^{\dagger}(\psi_{n}) \Omega$$

$$= \frac{1}{\sqrt{\operatorname{perm} G}} \sum_{j} \sum_{k=1}^{n} \langle e_{j}, \psi_{k} \rangle a^{\dagger}(e_{j}) \prod_{l \neq k} a^{\dagger}(\psi_{l}) \Omega$$

$$= \frac{1}{\sqrt{\operatorname{perm} G}} \sum_{k=1}^{n} a^{\dagger}(\psi_{1}) \dots a^{\dagger}(\psi_{n}) \Omega$$

$$= n \frac{1}{\sqrt{\operatorname{perm} G}} a^{\dagger}(\psi_1) \dots a^{\dagger}(\psi_n) \Omega = n \Psi.$$
(7.134)

In the bosonic case, there are no signs picked up when the order of creations operators is changed, thus making the computation somewhat easier.

Finally, we note that Chap. 8 is completely devoted to the dynamical properties of the number states discussed throughout this section.

7.6.2 Bosonic Coherent States*

Bosonic coherent states are in a sense the most classical states, as we explain in this section. This dissertation focusses on those effects which are genuinely quantum mechanical in nature and therefore coherent states are of limited interest. They are, however, fundamental in quantum optics and also appear naturally in algebraic quantum field theory. Hence, they are included here for completeness of this overview on many-particle theory.

There are many ways to motivate the use of coherent states and we touch upon several of them in this section, but we start out from a very fundamental notion of quantum mechanics: *Heisenberg's uncertainty relation*, which we already encountered in Sect. 2.2.2. We showed earlier in Sect. 7.3.2 that a bosonic mode can be interpreted as a harmonic oscillator, which implies a natural notion (7.61) of position and momentum. Throughout the previous sections, we defined the annihilation operator, which allows for a more general definition of "position" and "momentum". The operators $P(\psi)$ and $Q(\psi)$ are typical for the bosonic Fock space and are called *quadratures*, they are defined as

$$Q(\psi) := \frac{1}{\sqrt{2}} (a^{\dagger}(\psi) + a(\psi))$$
 and $P(\psi) := \frac{i}{\sqrt{2}} (a^{\dagger}(\psi) - a(\psi)).$ (7.135)

One may immediately note the relations $P(\psi) = Q(i\psi)$, but more crucial is the commutation relation

$$[Q(\psi_1), P(\psi_2)] = i \operatorname{Re} \langle \psi_1, \psi_2 \rangle, \quad \text{with } \psi_1, \psi_2 \in \mathcal{H},$$
 (7.136)

where we note that for any normalised single-particle wave function $\psi \in \mathcal{H}$, one obtains $[Q(\psi), P(\psi)] = i$, as familiar from the harmonic oscillator. When we define the standard deviation of the measurement of the observable A in a given state by

$$\Delta(A) = \sqrt{\langle A^2 \rangle - \langle A \rangle^2},\tag{7.137}$$

one can prove the famous *uncertainty relation* (Heisenberg 1927; Kennard 1927; Robertson 1929; Weyl 1928) for the quadratures (recall also Sect. 2.2.2):

$$\Delta(Q(\psi))\Delta(P(\psi)) \geqslant \frac{1}{2}.\tag{7.138}$$

This inequality is particularly useful since the right hand side is state-independent and thus gives us a universal bound on the intrinsic statistical uncertainty associated with an arbitrary initial state.

The study on coherent states starts from the question how to saturate this inequality (Schrödinger 1926a); which quantum states lead to $\Delta(Q(\psi))\Delta(P(\psi)) = 1/2$? A starting point is to define an operator

$$a(\psi) + \langle \psi, \zeta \rangle a^{\dagger}(\psi), \quad \text{with } \zeta \in \mathcal{H},$$
 (7.139)

the properties of which depend on ζ . For example, one may use the bosonic commutation relation to show that, for any normalised $\Psi \in \Gamma^b(\mathcal{H})$,

$$\|(a(\psi) + \langle \psi, \zeta \rangle a^{\dagger}(\psi) - \lambda)\Psi\|^{2} = \|(a^{\dagger}(\psi) + \langle \zeta, \psi \rangle a(\psi) - \overline{\lambda})\Psi\|^{2} + (|\langle \zeta, \psi \rangle|^{2} - 1)\|\Psi\|^{2},$$
(7.140)

an identity which indicates that for $|\langle \zeta, \psi \rangle| > 1$, we cannot find any eigenvalues of $a(\psi) + \langle \psi, \zeta \rangle \, a^\dagger(\psi)$. On the other hand it turns out that *every complex number* is an eigenvalue of

$$a(\psi) + \langle \psi, \zeta \rangle a^{\dagger}(\psi), \text{ with } |\langle \zeta, \psi \rangle| < 1.$$
 (7.141)

One may bring up that it is not appealing to have the ψ -dependence in this condition. The Cauchy-Schwarz inequality can be used to obtain the stronger condition that $\|\zeta\| < 1$, but this is more restrictive. Let us start by assuming the existence of an $\alpha \in \mathcal{H}$, such that

$$\left(a(\psi) + \langle \psi, \zeta \rangle a^{\dagger}(\psi)\right) \Psi_{\alpha,\zeta} = \langle \psi, \alpha \rangle \Psi_{\alpha,\zeta}, \text{ with } \|\Psi_{\alpha,\zeta}\| = 1.$$
 (7.142)

A direct calculation shows that

$$\langle \Psi_{\alpha,\zeta}, a(\psi) \, \Psi_{\alpha,\zeta} \rangle = \frac{\langle \psi, \alpha \rangle - \langle \alpha, \psi \rangle \, \langle \psi, \zeta \rangle}{1 - |\langle \psi, \zeta \rangle|^2}. \tag{7.143}$$

A rather involved calculation furthermore leads to

$$\Delta^2(Q(\psi)) = \frac{1}{2} \frac{(1 - \langle \psi, \zeta \rangle)(1 - \langle \zeta, \psi \rangle)}{1 - |\langle \psi, \zeta \rangle|^2} \quad \text{and} \quad \Delta^2(P(\psi)) = \frac{1}{2} \frac{(1 + \langle \psi, \zeta \rangle)(1 + \langle \zeta, \psi \rangle)}{1 - |\langle \psi, \zeta \rangle|^2}.$$

Multiplying these quantities, we clearly find that $\Delta^2(Q(\psi))\Delta^2(P(\psi)) = 1/4$, and that therefore any eigenvectors of the operators of (7.141) can be used to construct states that saturate the uncertainty relation.

In the mathematical physics community, one typically denotes all states of the form $\Psi_{\alpha,\zeta}$ as coherent states. In the quantum optics community, one tends to follow the notion of coherence as defined by Glauber (1963a), which is obtained for $\zeta=0$. In this case, we find

$$a(\psi)\Psi_{\alpha} = \langle \psi, \alpha \rangle \, \Psi_{\alpha}, \tag{7.145}$$

such that

$$\Delta^2(Q(\psi)) = \frac{1}{2} \text{ and } \Delta^2(P(\psi)) = \frac{1}{2},$$
 (7.146)

which implies that, indeed

$$\Delta(Q(\psi))\Delta(P(\psi)) = \frac{1}{2}.$$
 (7.147)

However, this definition is slightly stronger: not only does it saturate the uncertainty relations, it does so in a completely symmetric way. A *Glauber coherent state* (Glauber 1963a; Schrödinger 1926a) thus gives us the minimal simultaneous uncertainty in both Q and P, and thus $\Delta(Q(\psi)) = \Delta(P(\psi))$. If the goal is to simply minimise the uncertainty in for example Q, one may use (7.144) and choose ζ appropriately, this allows us to lower the uncertainty on Q, at the price of a higher uncertainty on P. Such states are referred to as *squeezed states* and are extensively discussed in Sect. 7.6.3. This effect lies at the basis of the field of quantum metrology.

We claim that there is another appealing way to generate these Glauber coherent states, which is very similar to generating number states. Remember that it was shown that a number state can simply be generated by acting with a creation operator on the vacuum state. There is a similar class of operators that generates coherent states when acting on the vacuum. We even already introduced these operators earlier in this chapter under the name *Weyl operators* (Alicki 2010; de Almeida 1998). These operators yield the very interesting property that

$$W(\alpha) = \exp(-i\sqrt{2}P(\alpha)) \tag{7.148}$$

In the quantum optics community, it is rather common to refer to these operators as the *displacement operators*. This naming is logical from properties (7.85), (7.86), and even more so when pushed one step further to obtain

$$W(-\alpha)Q(\psi)W(\alpha) = Q(\psi) + \sqrt{2}\operatorname{Re}\langle\psi,\alpha\rangle. \tag{7.149}$$

Let us start by assuming that, indeed,

$$\Psi_{\alpha} = W(\alpha)\Omega \tag{7.150}$$

and check the validity of this claim. This is a rather straightforward procedure, because we must only verify that

$$a(\psi)\Psi_{\alpha} = a(\psi)W(\alpha)\Omega$$

$$= W(\alpha)W(-\alpha)a(\psi)W(\alpha)\Omega$$

$$= W(\alpha)a(\psi)\Omega + \langle \psi, \alpha \rangle W(\alpha)\Omega$$

$$= \langle \psi, \alpha \rangle \Psi_{\alpha},$$
(7.151)

to recover Eq. (7.145). One can even go one step further by considering the exponential vectors (7.71) of Sect. 7.3.3. By using the Baker-Campbell-Hausdorff equality (Baker 1905; Campbell 1897; Hausdorff 1906), we find that

$$\Psi_{\alpha} = W(\alpha)\Omega = \exp\left(a^{\dagger}(\alpha) - a(\alpha)\right)\Omega$$

$$= e^{-\|\alpha\|^{2}/2} \exp(a^{\dagger}(\alpha)) \exp(-a(\alpha))\Omega$$

$$= e^{-\|\alpha\|^{2}/2} \exp(a^{\dagger}(\alpha))\Omega$$

$$= e^{-\|\alpha\|^{2}/2} \exp(\alpha)$$
(7.152)

and therefore Ψ_{α} is nothing more than an exponential vector, normalised by a Gaussian. This remarkable wave function has the property that it remains unchanged when a particle is annihilated from it. Notice, moreover, that $\alpha \in \mathcal{H}$ should not be normalised.

Properties of the particle counting statistics can be read of from this definition, such as

$$\langle \hat{n}_{\psi} \rangle_{\alpha} = \langle \Psi_{\alpha}, a^{\dagger}(\psi)a(\psi)\Psi_{\alpha} \rangle = |\langle \psi, \alpha \rangle|^{2}$$
 (7.153)

and also

$$\langle \hat{n}_{\psi}^2 \rangle_{\alpha} = |\langle \psi, \alpha \rangle|^2 \,. \tag{7.154}$$

One may also consider the expectation value for the total number of particles, by considering the number operator \hat{N} , for which we find

$$\langle \hat{N} \rangle_{\alpha} = \sum_{j} \langle \hat{n}_{e_{j}} \rangle_{\alpha} = \sum_{j} \left| \langle e_{j}, \alpha \rangle \right|^{2} = \|\alpha\|^{2},$$
 (7.155)

and in an analogous fashion, we obtain that

$$\langle \hat{N}^2 \rangle_{\alpha} = \|\alpha\|^2. \tag{7.156}$$

These properties are intimately related to those of classical electromagnetic waves. In order to get the full probability distribution P(n), which describes the probability for finding n particles when the particle number is measured, we can define P_n , the projector on the n-particle space $\mathcal{H}_s^{\otimes n}$. This object is defined by the action on a vector $\Psi \in \Gamma^b(\mathcal{H})$ as

$$P_n \Psi = P_n \psi^{(0)} \oplus \psi^{(1)} \oplus \psi^{(2)} \oplus \dots$$

= $0 \oplus \dots \oplus 0 \oplus \psi^{(n)} \oplus 0 \oplus \dots$ (7.157)

To obtain P(n) we compute

$$P(n) := \langle \Psi_{\alpha}, P_n \Psi_{\alpha} \rangle = \frac{e^{-\|\alpha^2\|}}{n!} \left(\alpha^{\otimes n}, \alpha^{\otimes n} \right) = \frac{e^{-\|\alpha^2\|} \|\alpha\|^{2n}}{n!}, \tag{7.158}$$

which can slightly be rephrased as

$$P(n) = \frac{e^{-\langle n \rangle} \langle n \rangle^n}{n!},\tag{7.159}$$

to represent a Poisson distribution.

A final interesting property of the wave functions which represent coherent states is that they can be used as a "basis" of Fock space. We already stressed that the linear combinations of exponential vectors are dense in the bosonic Fock space, thus the coherent state wave functions clearly inherit this property. A useful fact in for example semiclassical treatments of many-boson systems (Engl et al. 2014) or in many branches of quantum optics (Grynberg et al. 2010; Mandel and Wolf 1995; Schleich 2001; Scully and Zubairy 1997) is that the projectors on the vectors Ψ_{α} form a nonorthogonal resolution of the identity. Formally this implies that we can use them to construct a positive operator-valued measure and use the spectral theorem. If It is more common to deal with this kind of objects in single mode systems, which implies that $\mathcal{H} \cong \mathbb{C}$ and therefore $\alpha \in \mathbb{C}$. Here one usually encounters the notation (Alicki 2010; Grynberg et al. 2010; Mandel and Wolf 1995; Schleich 2001)

$$\frac{1}{\pi} \int d^2 \alpha |\Psi_{\alpha}\rangle \langle \Psi_{\alpha}| = 1. \tag{7.160}$$

These operators can now also be used in the context of spectral decompositions, which leads for example to the Glauber-Sudarshan representation (Glauber 1963a, b; Mehta 1967; Mehta and Sudarshan 1965; Sudarshan 1963) of density matrices.

7.6.3 Bosonic Squeezed States*

Due to their important role in quantum optics and natural appearance in algebraic quantum field theory, squeezed states are included for completeness of this overview on many-particle theory.

 $^{^{16}}$ In Sect. 2.3.1, we introduced the spectral theorem with the explicit demand that the spectral measure is *projector-valued*. This demand is, however, not strictly necessary and can be dropped to find a more general form of the spectral theorem. This constructions, in relation to quantum probability theory, are discussed in Holevo (2001) and can be connected to *Naimark's* (\cong *Neumark* mod *transcription*) *dilation theorem* (Neumark 1943; Stinespring 1955) which characterises positive-operator valued measures.

When discussing the coherent states, we discovered that there is a wide set of states which all saturate the uncertainty relations, as given by Eq. (7.144). These states are all related to the wave functions $\Psi_{\alpha,\zeta}$, where the Glauber coherent states were those given by $\zeta=0$. Now we study a class of states for which $\zeta\neq 0$, the *squeezed states*.

It turns out that the parametrisation in terms of ζ may formally be intuitive, in practice it is nevertheless inconvenient. A more practical way of discussing squeezing starts out (Alicki 2010; Mandel and Wolf 1995) from an operator S(z), with $z \in \mathbb{C}$, which squeezes a *single mode* ¹⁷

$$S(z) = \exp\frac{1}{2} \left(\overline{z}a^2 - za^{\dagger 2} \right).$$
 (7.161)

Using that

$$a^{A} B e^{-A} = B + [A, B] + \frac{1}{2!} [A, [A, B]] + \dots$$
 (7.162)

one derives that

$$S(z)^{\dagger} a S(z) = (\cosh r) a - (e^{i\theta} \sinh r) a^{\dagger}, \tag{7.163}$$

where we rewrote $z = re^{i\theta}$. We can define two natural classes of states (Alicki 2010; Mandel and Wolf 1995)¹⁸: the *squeezed coherent states* $\Psi_{z,\alpha}$ and the *coherent squeezed states* $\Psi_{\alpha,z}$, which are given by

$$\Psi_{z,\alpha} = S(z)W(\alpha)\Omega$$
 and $\Psi_{\alpha,z} = W(\alpha)S(z)\Omega$. (7.164)

These wave functions are intrinsically different, for example

$$\langle \Psi_{\alpha,z}, a\Psi_{\alpha,z} \rangle = \alpha,$$
 (7.165)

whereas

$$\langle \Psi_{z,\alpha}, a\Psi_{z,\alpha} \rangle = \alpha \cosh r - \overline{\alpha} e^{i\theta} \sinh r$$
 (7.166)

Even though the result for coherent squeezed states seems identical to that of Glauber coherent states, there is a subtle difference in the quadratures:

$$\Delta^{2} Q = \frac{1}{2} \left((\cosh r)^{2} + (\sinh r)^{2} - 2\cos(\theta)\cosh(r)\sinh(r) \right)$$
 (7.167)

$$\Delta^{2}P = \frac{1}{2} \left((\cosh r)^{2} + (\sinh r)^{2} + 2\cos(\theta)\cosh(r)\sinh(r) \right). \tag{7.168}$$

¹⁷Hence, we consider single-particle Hilbert space $\mathcal{H} \cong \mathbb{C}$.

¹⁸Note that Mandel and Wolf (1995) uses different names for these states.

This result is independent of α and it therefore follows that there is a serious difference between the squeezed vacuum $\Psi_{0,z}$ and the actual standard vacuum $\Omega = \Psi_{0,0}$. One might now focus on the special case where $\theta = 0$, such that

$$\Delta^2 Q = \frac{1}{2} e^{-2r}$$
 and $\Delta^2 P = \frac{1}{2} e^{2r}$. (7.169)

Here we clearly see that a strong decrease in uncertainty on the Q quadrature operator comes at the price of a proportionally increased uncertainty on the P observable. With or without θ , we ultimately find

$$\Delta Q \,\Delta P = \frac{1}{2}.\tag{7.170}$$

Similarly, we can consider the squeezed coherent states $\Psi_{z,\alpha}$ in the context of the uncertainty relation. To do so, we start by noting that

$$((\cosh r)a + (e^{i\theta}\sinh r)a^{\dagger})\Psi_{z,\alpha} = S(z)aS(z)^{\dagger}S(z)W(\alpha)\Omega = \alpha S(z)W(\alpha)\Omega,$$
(7.171)

which allows us to conclude that

$$\left(a + (e^{i\theta}\tanh r)a^{\dagger}\right)\Psi_{z,\alpha} = \frac{\alpha}{\cosh r}\Psi_{z,\alpha}.$$
 (7.172)

This is exactly the expression which previously defined a general coherent state in (7.142). We see that the parameter¹⁹ ζ is given by $\zeta = e^{i\theta} \tanh r$, and that indeed $|\zeta| < 1$. We use Eq. (7.144) to obtain

$$\Delta^{2}(Q(\psi)) = \frac{1}{2} \frac{(1 - e^{i\theta} \tanh r)(1 - e^{-i\theta} \tanh r)}{1 - (\tanh r)^{2}}$$
(7.173)

$$\Delta^{2}(P(\psi)) = \frac{1}{2} \frac{(1 + e^{i\theta} \tanh r)(1 + e^{-i\theta} \tanh r)}{1 - (\tanh r)^{2}}.$$
 (7.174)

This implies that, for $\theta = 0$, we again find

$$\Delta^2 Q = \frac{1}{2} e^{-2r}$$
 and $\Delta^2 P = \frac{1}{2} e^{2r}$, (7.175)

which allows us to conclude that even though the states are in principle different, both the coherent squeezed states and the squeezed coherent states from (7.164) give rise to the same uncertainties on the quadratures.

To implement squeezing in a more general Hilbert space is not so straightforward. We can of course define $\zeta, \psi \in \mathcal{H}$ and $\|\psi\| = 1$, and introduce squeezing in mode ψ as

¹⁹In this case, we are just dealing with a parameter $\zeta \in \mathbb{C}$, since we only consider a single-mode space.

$$S(\zeta, \psi) = \exp \frac{1}{2} \left(\langle \zeta, \psi \rangle \, a(\psi)^2 - \langle \psi, \zeta \rangle \, a^{\dagger}(\psi)^2 \right), \tag{7.176}$$

which is a trivial embedding of the single-mode discussion in a multi-mode language and exactly reproduces all the results, as long as $a(\psi)$, $P(\psi)$ and $Q(\psi)$ are considered. The action on generic operators $a(\phi)$ is somewhat involved and unpractical. One thus concludes that there is need for a different generalisation.

The advantage of unitary operations, such as S(z), is that we can relate them to a Hamiltonian and therefore a *physical* setup. However, this does not mean that it has direct *mathematical* advantages. Indeed, it was much more fundamental to have an operation \mathcal{B}_z which carries out the mapping

$$\mathcal{B}_{z}(a(\psi)) = (\cosh r)a(\psi) - e^{i\theta}(\sinh r)a^{\dagger}(\psi), \tag{7.177}$$

$$\mathcal{B}_z(a^{\dagger}(\psi)) = (\cosh r)a^{\dagger}(\psi) - e^{-i\theta}(\sinh r)a(\psi). \tag{7.178}$$

This operation describes exactly how the squeezing operators act on the creation and annihilation operators of the bosonic field and, although their definition seems handwaving, these operations are a simple case of a much more fundamental class of operations: the *Bogoliubov transformation* (Bratteli and Robinson 1997). These transformations are essentially defined as operations that mix creation and annihilation operators, without increasing the order. We crucially demand that $\mathcal{B}_z(a(\psi))$ and $\mathcal{B}_z(a^\dagger(\psi))$ can themselves be interpreted as new creation and annihilation operators such that

$$\left[\mathcal{B}_{z}(a(\psi)), \mathcal{B}_{z}(a^{\dagger}(\psi))\right] = 1 \quad \text{and} \quad \left[\mathcal{B}_{z}(a(\psi)), \mathcal{B}_{z}(a(\psi))\right] = 0, \quad (7.179)$$

A direct calculation shows that this is indeed the case for the transformations (7.177), (7.178). Considering this to be the fundamental squeezing operation allows a wide range of extensions; one can define $\mathcal{B}_{U,V}$, with $U, V \in \mathcal{B}(\mathcal{H})$, as

$$\mathcal{B}_{U,V}(a(\psi)) = a(U\psi) + a^{\dagger}(VJ\psi), \tag{7.180}$$

$$\mathcal{B}_{U,V}(a^{\dagger}(\psi)) = a^{\dagger}(U\psi) + a(VJ\psi). \tag{7.181}$$

A subtle point pops up here, since we have to include a *complex structure*, i.e. the operator $J: \mathcal{H} \to \mathcal{H}$. This operator is subtle because it is *conjugate linear*, defined by the properties (for $\psi, \phi \in \mathcal{H}$) (Petz 1990)

$$J^2 = 1, (7.182)$$

$$\langle J\phi, J\psi\rangle = \langle \psi, \phi\rangle, \tag{7.183}$$

$$\langle \psi, J^{\dagger} \phi \rangle = \langle \phi, J \psi \rangle = \langle J^2 \psi, J \phi \rangle = \langle \psi, J \phi \rangle.$$
 (7.184)

²⁰We already introduced this type of operator in Chap. 3 to describe time-reversal.

Ultimately, the transformations (7.180), (7.181), together with the fact that

$$\left[\mathcal{B}_{U,V}(a(\psi)), \mathcal{B}_{U,V}(a^{\dagger}(\psi))\right] = 1 \quad \text{and} \quad \left[\mathcal{B}_{U,V}(a(\psi)), \mathcal{B}_{U,V}(a(\psi))\right] = 0,$$
(7.185)

lead to the additional conditions that

$$U^{\dagger}U - V^{\dagger}V = 1 \quad \text{and} \quad U^{\dagger}V + V^{\dagger}U = 0. \tag{7.186}$$

Whenever these conditions are fulfilled, we have defined a reasonable operation. To define the full class of states we formally write

$$W_{\alpha}(.) := W(-\alpha) \cdot W(\alpha), \tag{7.187}$$

which allows us to define a generalised form of squeezed coherent and coherent squeezed states. Remember that the *state* is a functional that maps observables to numbers and, therefore, we can define a state $\langle . \rangle_{U,V,\alpha}$ by simply considering

$$\langle . \rangle_{U,V,\alpha} := (\langle . \rangle_{\Omega} \circ \mathcal{B}_{U,V} \circ \mathcal{W}_{\alpha})(.) \tag{7.188}$$

and notice that $\mathcal{B}_{U,V} \circ \mathcal{W}_{\alpha} \neq \mathcal{W}_{\alpha} \circ \mathcal{B}_{U,V}$, such that we may also define the class of states where one first displaces and only squeezes afterwards.

Once one mixes different modes (Braunstein 2005; De Valcarcel et al. 2006), the uncertainties on the quadratures become much more subtle (Roslund et al. 2014). Because this would become a very long and technical discussion once we go into calculating these uncertainties, such endeavour is omitted here.

We note that the treatment presented here is strongly mathematically inspired, its realm of physical applications is situated at the boarder between quantum optics (Grynberg et al. 2010), quantum chaos (de Almeida 1998), condensed-matter physics (Orzel et al. 2001), and theoretical chemistry (Miller 2002). Even though these are simple constructs from a mathematical physics perspective, the potential applications of such states in communication, computation, et cetera is still being uncovered (Armstrong et al. 2012; Cai et al. 2017; Chen et al. 2014; Ferrini et al. 2013; Gerke et al. 2015; Roslund et al. 2014; Su et al. 2012; Yoshikawa et al. 2016).

7.6.4 Representing Bosonic States*

We discuss several techniques for representing bosonic states. These techniques are not explicitly used throughout the remainder of the dissertation. Nevertheless, they are included due to their relevance for many-particle physics. Furthermore, they provide an important connection to the field of quantum chaos.

In many situations, there is the natural urge to come up with a suitable representation of quantum states in terms of the probability distributions they characterise. Of course, probability distributions depend on the variables which are measured and therefore we always require some form of operator for which the distribution is defined. However, to make the connection to classical physics, one ultimately wants to represent quantum states as probability distribution on phase space (Moyal 1949; Schleich 2001).²¹ With the quadrature and coherent wave functions as discussed in the previous chapters, we have an ideal toolbox at hand to discuss such representation.

We start by considering some straightforward representations for normal states; remember that these are the functionals on the algebra of observables, which can be characterised by a density operator ρ . These formulations allow a generalisation to the more abstract algebraic language of Sect. 7.7 (Fannes and Verbeure 1975), such that the representations can be extended to bosonic quantum field theories.

Husimi Representation*

The Husimi representation²² (Husimi 1940) is by far the easiest representation to comprehend as we can simply define the relevant Husimi function as

$$\tilde{Q}(\alpha) := \frac{1}{\pi^n} \langle \Omega, W(-\alpha) \rho W(\alpha) \Omega \rangle, \qquad (7.189)$$

where we write \tilde{Q} to indicate that we consider a function, $\tilde{Q}:\mathcal{H}\to[0,1/\pi)$, rather than an operator. We must assume that the single-particle Hilbert space (or mode space in quantum optics language) \mathcal{H} is finite dimensional, as n in the definition is given by $n=\dim\mathcal{H}$.

We make the connection to phase space by the identifications

$$q_{\psi} = \langle \Omega, W(-\alpha) Q(\psi) W(\alpha) \Omega \rangle = \sqrt{2} \operatorname{Re} \langle \psi, \alpha \rangle,$$
 (7.190)

$$p_{\psi} = \langle \Omega, W(-\alpha) P(\psi) W(\alpha) \Omega \rangle = \sqrt{2} \operatorname{Im} \langle \psi, \alpha \rangle.$$
 (7.191)

Since we consider a finite dimensional modes space, which implies that $\mathcal{H} \cong \mathbb{C}^n$, we can consider a basis $\{e_i\}$ with $j \in \{e_1, \dots, e_n\}$ to construct

$$q_i = \sqrt{2} \operatorname{Re} \langle e_i, \alpha \rangle,$$
 (7.192)

$$p_j = \sqrt{2} \operatorname{Im} \langle e_j, \alpha \rangle. \tag{7.193}$$

We can now parameterise α as

$$\mathbb{R}^{2n} \to \mathbb{C}^n : (q_1, p_1, \dots, q_n, p_n) \mapsto \frac{1}{\sqrt{2}} (q_1 - ip_1, \dots, q_n - ip_n),$$
 (7.194)

which allows us to interpret the Husimi function as a quasi-probability distribution on phase space.

²¹This also is a common topic in single-particle systems (Bohigas et al. 1993; de Almeida 1998; Heller 1984; Leboeuf and Saraceno 1990).

²²Also known as *Q representation* or *Glauber Q representation*.

A useful property of the Husimi function, next to its positivity, is the fact that it is a normalised function

 $\int d^2 \alpha \, \tilde{Q}(\alpha) = 1, \tag{7.195}$

hence the interpretation as quasi-probability distribution.

Glauber-Sudarshan P-Representation*

This representation is based on the idea (Glauber 1963a, b; Mehta 1967; Mehta and Sudarshan 1965; Sudarshan 1963) that we can define a (non-orthogonal (Holevo 2001)) resolution of the identity using projectors on coherent states P_{α} . The idea is to consider density matrices ρ , which are diagonal in this over-complete basis of coherent wave functions, such that, for a single-mode system (i.e. $\mathcal{H} \cong \mathbb{C}$), one may write

$$\rho = \int d\alpha |\Psi_{\alpha}\rangle \langle \Psi_{\alpha}| \tilde{P}(\alpha), \qquad (7.197)$$

as a type of spectral decomposition. This now implies that $\tilde{P}(\alpha)$, which is a function on phase space using a suitable parametrisation of α , determines the state.

The function $\tilde{P}(\alpha)$ can be interpreted as a quasi-probability distribution, in the sense that it can be used to capture the statistics contained within the density matrix ρ . Nevertheless, it is not a genuine probability distribution, since it can become negative. Therefore, one can conclude that any normal state²⁴ can be seen a *linear* combination rather than a convex combination of coherent states.

Bosonic states which cannot be written as a convex combination of coherent states are commonly referred to as non-classical. To intuitively understand this idea, it is useful to remember that the coherent states are the most classical pure states that can be constructed (remember Sect. 7.6.2). Convex combinations represent a mixture of distributions as we know from classical probability theory and thus this definition of non-classicality seems sensible.

The P-representation is elegant and useful from a theoretical point of view, but it has particular difficulties in connecting it to (quantum optics) experiments. There is no specific experimentally accessible observable related to the representation, and the possible singularities in $\tilde{P}(\alpha)$ make it notoriously hard to reconstruct the functions based on experimental measurements. There are ways to work around these problems

$$P_{\alpha} := \frac{1}{\pi^d} \int_{\mathcal{H}} \langle \Psi_{\alpha}, W(-\phi)\Psi_{\alpha} \rangle W(\phi) d\phi. \tag{7.196}$$

This result can also be extended to innfinite-dimensional single-particle spaces (Fannes and Verbeure 1975).

 $^{^{23}}$ To extend this notion to a framework of many degrees of freedom, some effort is required to actually define this projector. The ultimate result (Fannes and Verbeure 1975; Petz 1990) for a single-particle Hilbert space $\mathcal H$ of dimension d is given by

²⁴Remember that in Chap. 2 we introduced the normal states as those states which allow for a density matrix representation. More specifically, we would here refer to a normal state with respect to the Fock representation (see Sect. 7.7.2).

(Kiesel and Vogel 2010), but the most common solution is to consider a different representation: the *Wigner function*.

Wigner-Weyl Representation*

In the perspective of this dissertation, which strongly builds on algebraic structures and probability theory, it is natural to start the discussion on the Wigner–Weyl representation from the *quantum characteristic function*. This object is appealing from a mathematical point of view because it allows us to connect our quantum mechanical structure directly to an object which is well-know in probability theory. In general, a characteristic function is defined for a stochastic variable \hat{X} , living on a probability space, as²⁵

$$\varphi(t) = \mathbb{E}\left(e^{-it\hat{X}}\right). \tag{7.198}$$

The quantum characteristic function is a straightforward generalisation to quantum probability theory, which one may think of as simply replacing the expectation value with a quantum state and the stochastic variable with a suitable quantum mechanical observable.

We use the Weyl operators and/or quadratures, (7.81), (7.135), respectively, to define the *quantum characteristic function* as

$$\tilde{\chi}(\alpha) := \langle \exp(iQ(\alpha)) \rangle = \left\langle W\left(-\frac{i}{\sqrt{2}}\alpha\right) \right\rangle,$$
 (7.199)

which can be done for any possible state $\langle . \rangle$. ²⁶ In classical probability theory, knowledge of the characteristic function implies knowledge of the full probability distribution, as the two are related via Fourier transformation. For the quantum characteristic function, we can also define a function via Fourier transformation, although then it is a quasi-probability distribution, baptised the *Wigner function* $\tilde{W}(\beta)$. This function is given by

$$\tilde{W}(\beta) := \frac{1}{(2\pi)^{2n}} \int d^{2n} \alpha \, \tilde{\chi}(\alpha) e^{-i\langle \alpha, \beta \rangle}, \tag{7.200}$$

which, just as the P-representation, may become negative. There is a lot a work done (Banaszek and Wódkiewicz 1998, 1999; Corney and Olsen 2015; Park et al. 2015; Walschaers et al. 2017) on Wigner functions and specifically on interpreting this negativity. It turns out that states with a non-positive Wigner function are impossible to reproduce by any classical process and hence the negativity of the Wigner function can be considered an indication of "quantumness". Wigner functions which are positive are therefore sometimes considered classical states. There is a theorem classifying the possible classical *pure* states by Hudson, Soto and Claverie (Hudson 1974; Soto and Claverie 1983), proving that the only possible non-negative Wigner

 $^{^{25}\}mathbb{E}$ denotes the expectation value.

²⁶The Q and W in equation (7.199) denote operators on Fock space and should not be confused with the Husimi function \tilde{Q} and Wigner function \tilde{W} .

functions for those states are (multivariate) Gaussians, the states for which they are achieved are therefore also called *Gaussian states*. There have been attempts (Mandilara et al. 2009) to extend or amend the theorem for mixed states, however up to present not much is known about the properties of the Wigner functions of such mixed states.

By calculating the characteristic function for a Glauber coherent state via (7.84), one finds

$$\tilde{\chi}(\alpha) = \left\langle \Psi_{\alpha'}, W\left(-\frac{i}{\sqrt{2}}\alpha\right) \Psi_{\alpha'} \right\rangle = e^{-\|\alpha\|^2/4 - i\sqrt{2}\operatorname{Re}\langle\alpha',\alpha\rangle},\tag{7.201}$$

from which we find that also the Wigner function is a Gaussian. It is a completely symmetric Gaussian distribution, with the same standard deviation in all directions. A slightly more involved calculation shows that the squeezed states which we discussed earlier are also Gaussian states, but with standard deviations which are stretched in one direction and squeezed in the other.

Number states do *not* fall into the class of Gaussian states, giving them typical quantum properties which Gaussian states lack, such as the possibility to manifest many-particle interference. This is extensively discussed in the following chapter of this dissertation.

7.6.5 Thermal States for Non-interacting Particles

The last standard set of states which we discuss has its origin in equilibrium statistical mechanics, they are usually referred to as *thermal states* (Bratteli and Robinson 1997). For many-particle systems, it is common to use the grand canonical ensemble to describe the equilibrium states at finite temperature T and chemical potential μ . In quantum mechanics, there is a standard way to express the grand canonical ensemble states as a so-called *Gibbs states*, described via the density matrix (Bratteli and Robinson 1997; Kardar 2007)

$$\rho = \frac{e^{-(\mathcal{H} - \mu \hat{N})/k_b T}}{\mathcal{Z}},\tag{7.202}$$

where \mathcal{H} is the Hamiltonian of the system and \mathcal{Z} the partition function. It is common in statistical mechanics to focus attention on this partition function, since one can derive all other properties from it. Remember that, due to normalisation of the state,

$$\mathcal{Z} := \operatorname{tr}\left(e^{-(\mathcal{H} - \mu \hat{N})/k_b T}\right). \tag{7.203}$$

To calculate the partition function, we insert the system Hamiltonian, which in our cases is chosen to describe non-interacting particles. The lack of interactions means

that there can be no higher order terms that shift energy levels in many-particle situations, which implies that the Hamiltonian is a single-particle observable in second quantisation. In other words, $\mathcal{H} = \Gamma^{b,f}(H)$ with $H \in \mathcal{B}(\mathcal{H})$. This allows to rewrite

$$\mathcal{Z} = \operatorname{tr} e^{\Gamma^{b,f} \left(-(H - \mu \mathbb{1})/k_b T \right)}$$

$$= \operatorname{tr} E \left(e^{-(H - \mu \mathbb{1})/k_b T} \right). \tag{7.204}$$

where we used the exponential element (7.106), (7.107) as defined at the end of Sect. 7.5. Up to this point, no assumptions were made on the type of particles, all steps were valid both for bosons and fermions. To proceed, there is, however, the need to differentiate, because there are two useful identities that can be exploited: First, if we assume $A \in \mathcal{H}$, it generally holds (Bratteli and Robinson 1997; Dereziński 2006; Dierckx et al. 2008) that

$$tr E(A) = det(1 + A)$$
 for fermions, (7.205)

$$tr E(A) = det(1 - A)^{-1}$$
 for bosons. (7.206)

Using the identity (7.205) for fermions, we obtain that

$$\mathcal{Z} = \det\left(\mathbb{1} + e^{-(H - \mu\mathbb{1})/k_b T}\right) = \prod_{k} \left(1 + e^{-(\epsilon_k - \mu)/k_b T}\right),\tag{7.207}$$

with ϵ_k the eigenvalues of H. To uncover the statistics of the particle density, we use the statistical mechanics result (Kardar 2007)

$$\langle \hat{N} \rangle = k_b T \frac{1}{\mathcal{Z}} \left(\frac{\partial \mathcal{Z}}{\partial \mu} \right)_{V,T} = \sum_k \frac{1}{1 + e^{(\epsilon_k - \mu)/k_b T}},$$
 (7.208)

which is the famous Fermi-Dirac statistics.

Finally, from the identity (7.206) for bosons, it can be seen that

$$\mathcal{Z} = \det\left(\mathbb{1} - e^{-(H - \mu\mathbb{1})/k_b T}\right)^{-1} = \prod_k \frac{1}{1 - e^{-(\epsilon_k - \mu)/k_b T}},\tag{7.209}$$

such that

$$\langle \hat{N} \rangle = \sum_{k} \frac{1}{e^{(\epsilon_k - \mu)/k_b T} - 1},\tag{7.210}$$

which is the well-known *Bose-Einstein statistics*. From monotonicity arguments which are applicable to such functions, we can ultimately derive the possibility to form a Bose-Einstein condensate. Here we do not go into the full details, but refer the reader to a particularly elegant argumentation presented in Verbeure (2011).

We finally mention that in the case of non-interacting particles, the states given by density matrices (7.202) also belong to the broader set of non-pure Gaussian states. Thermal states, however, do not saturate the uncertainty relations, ²⁷ which makes sense since they are by definition sensitive to additional thermal fluctuations. Still, these states do lead to Wigner functions which describe a (multivariate) Gaussian distributions.

7.7 Abstract Algebraic Description

Although the text contains many references to the algebraic description, most of this dissertation can be understood using the Fock representation (i.e.the methods of the previous sections). Since, however, the difference between bosons and fermions is one of the main themes throughout Part III, this discussion is included to provide extra depth. The C*-algebra framework clearly indicates that there is also a very fundamental, mathematical difference between bosons and fermions. Moreover, this section serves to stress that many-particle physics entails much more than Fock space. Finally, this section also attempts to provide an accessible introduction to the algebraic approach to quantum mechanics.

Up to this point, the whole chapter was constructed based on bosonic and fermionic Fock space. However, it cannot be stressed enough that Fock space is in its very essence a mostly empty space, only harbouring few particles, which became painfully clear when we discussed the problems of normalisability of many-boson wave functions (see Sect. 7.3.1 above). The problems could be solved by using the Weyl operators (7.81) and coherent states (7.145) as fundamental objects rather than the number states (7.132) when dealing with bosonic system. Nevertheless, in Chap. 2, we discussed quantum probabilistic structures in a framework that goes beyond Hilbert spaces and it is only logical to try and accomplish the same by describing many-particle spaces beyond the limitations of Fock space. This leads us to the realm of C^* -algebras and many of the results discussed in the previous section can directly be generalised to this framework.

The foundation of this approach lies in the idea that, ultimately, the algebra of observables is the most fundamental structure available in our quantum mechanical theory, and hence we describe our systems of bosons and fermions by a C^* -algebra \mathcal{A} , in which all observables are contained. In standard quantum physics, one has the habit of considering algebras of observables, which are composed of bounded operators on a Hilbert space. This is however not necessary to reach a consistent physical model. In Sect. 2.3 we provided a brief introduction to C^* -algebras and the states living on them, here we explain why such structures are useful —and even required— to describe general many-particle systems.

²⁷In contrast to the coherent states of Sect. 7.6.2.

²⁸See Appendix A for several formal definitions.

7.7.1 The CAR Algebra

Structure

First, we treat the fermionic structures, which are formally defined via the *canonical* anticommutation relations (CAR), which we already came across in Sect. 7.4 as the anticommutation relation for creation and annihilation operators. Now, rather than to deal with creation and annihilation operators which act on a specific Fock space, we simply consider them as abstract elements of a C^* -algebra. The CAR algebra \mathcal{A}^{CAR} is defined on top of a single-particle Hilbert space \mathcal{H} which provides the structure on which a single particle lives. The algebra is unital, which implies the existence of a unit element $\mathbf{1} \in \mathcal{A}^{CAR}$ such that for all $x \in \mathcal{A}^{CAR}$ we obtain that $\mathbf{1}x = x\mathbf{1} = x$. Apart from the $\mathbf{1}$, the algebra is completely generated by a class of elements given by $c(\psi) \in \mathcal{A}^{CAR}$, with $\psi \in \mathcal{H}$, which are defined such that

$$c: \mathcal{H} \to \mathcal{A}^{CAR}: \psi \mapsto c(\psi)$$
 is \mathbb{C} -antilinear, (7.211)

$$\{c(\psi), c(\phi)\} = 0, \qquad \psi, \phi \in \mathcal{H}, \tag{7.212}$$

$$\{c(\psi), c^*(\phi)\} = \langle \psi, \phi \rangle \mathbf{1}, \quad \psi, \phi \in \mathcal{H}. \tag{7.213}$$

These anticommutation relations can be abstractly defined to construct our algebra and therefore are a generalisation of the creation and annihilation operators on $\Gamma^f(\mathcal{H})$. To obtain a well-defined C^* -algebra, we must verify the boundedness of these generators. From a quick calculation using the C^* -property (see Sect. A.4), we find

$$||c(\psi)||^4 = ||c^*(\psi)c(\psi)||^2 = ||c^*(\psi)c(\psi)c^*(\psi)c(\psi)||$$

$$= ||c^*(\psi)(||\psi||^2 \mathbf{1} - c^*(\psi)c(\psi))c(\psi)|| = ||\psi||^2 ||c^*(\psi)c(\psi)||$$

$$= ||\psi|||c(\psi)||^2,$$
(7.214)

and therefore

$$||c(\psi)|| = ||\psi||. \tag{7.215}$$

This serves as a verification that the proposed structure correctly manifests the properties of a C^* -algebra, such that we can consider *observables* $o \in \mathcal{A}^{CAR}$, which must have the property that $o = o^*$, and thus a spectrum $\sigma(o) \subset \mathbb{R}$. However, before we can associate elements of an abstract algebra to measurement outcomes, we require additional structures: the quantum states on the algebra.

Structuring States

In the most rigorous formulation, quantum states are normalised, positive functionals on a C^* -algebra. Therefore we consider

$$\omega: \mathcal{A}^{\text{CAR}} \to \mathbb{C},$$
 (7.216)

such that

$$x \in \mathcal{A}^{\text{CAR}} \mapsto \omega(x)$$
 is \mathbb{C} -linear, (7.217)

$$\omega(x^*x) \geqslant 0$$
, for all $x \in \mathcal{A}^{CAR}$, (7.218)

$$\omega(\mathbf{1}) = 1. \tag{7.219}$$

Formally, with these rules we have defined all possible states on \mathcal{A}^{CAR} . However, such definition is far from practical to perform actual calculations and therefore we again (recall our discussion in Sect. 2.3.2) emphasise the GNS-construction: For any pair (ω, \mathcal{A}) there exists a unique Hilbert space \mathcal{K} , vectors $\Omega \in \mathcal{K}$, and a representation $\pi: \mathcal{A} \to \mathcal{B}(\mathcal{K})$, such that

$$\pi(x^*) = \pi(x)^{\dagger}, \quad \text{for all } x \in \mathcal{A}, \tag{7.220}$$

$$\omega(x) = \langle \Omega, \pi(x)\Omega \rangle, \text{ for all } x \in \mathcal{A},$$
 (7.221)

$$\pi(A)\Omega$$
 is dense in K . (7.222)

When we apply the GNS construction to any state ω , we obtain the crucial fact that $\pi(c(\psi))^{\dagger}$ and $\pi(c(\psi))$, for all $\psi \in \mathcal{H}$, play the role of creation and annihilation operators, respectively. Several applications of these operators can populate the whole Hilbert space \mathcal{K} . However, we must strongly emphasise that Ω as defined by the GNS construction for a general state ω is typically not the vacuum state, and \mathcal{K} is generally not the Fock space which was discussed in the first sections of this chapter!

When one considers the so-called Fock state, given by

$$\omega_{\Gamma}(c^*(\psi_1)\dots c^*(\psi_n)c(\phi_m)\dots c(\phi_1))_{\Gamma} = 0$$
 for any monomial, (7.223)

it can be shown that the GNS construction connects $(\omega_{\Gamma},\mathcal{A}^{\mathrm{CAR}})$ to $\Gamma^f(\mathcal{H})$ such that

$$\pi(c(\psi)) = a(\psi) \text{ and } \Omega = 1 \oplus 0 \oplus 0 \oplus \dots \in \Gamma^f(\mathcal{H}).$$
 (7.224)

However, there are states ω on the CAR algebra which *cannot* be captured by the Fock space formalism. Sadly, there is no formalism to describe all the states on the algebra, but there are structures which are particularly useful to pursue this objective.

From elementary probability theory, we know that knowledge of a probability measure is equivalent to knowledge of all moments (or correlation functions). Since ω is ultimately the quantum equivalent of a probability measure (Holevo 2001; Maassen 2010), we may consider an analogous method. To assess all correlation functions we consider all *Wick monomials*²⁹ and calculate

$$\omega(c^*(\psi_1)\dots c^*(\psi_n)c(\phi_m)\dots c(\phi_1)), \tag{7.225}$$

²⁹A *Wick monomial* is a monomial of creation and annihilation operators, e.g. $c^*(\psi_1) \dots c^*(\psi_n) c(\phi_m) \dots c(\phi_1)$ (Davies 1977).

as we already did to characterise ω_{Γ} . One can show that positivity can be guaranteed by the requirement

$$\omega(p^*p) \geqslant 0$$
, for all polynomials p in c and c^* from (7.211). (7.226)

A remarkably useful construct to understand quantum states on such abstract algebras are the *truncated correlation functions* (Bratteli and Robinson 1997),³⁰ which are defined as³¹

$$\langle c^{\#}(\psi_{1})\rangle_{T} = \omega(c^{\#}(\psi_{1})),$$

$$\langle c^{\#}(\psi_{1}); c^{\#}(\psi_{2})\rangle_{T} = \omega(c^{\#}(\psi_{1})c^{\#}(\psi_{2})) - \omega(c^{\#}(\psi_{1}))\omega(c^{\#}(\psi_{2})),$$

$$\langle c^{\#}(\psi_{1}); c^{\#}(\psi_{2}); c^{\#}(\psi_{3})\rangle_{T} = \omega(c^{\#}(\psi_{1})c^{\#}(\psi_{2})c^{\#}(\psi_{3})) - \omega(c^{\#}(\psi_{1})c^{\#}(\psi_{2}))\omega(c^{\#}(\psi_{3}))$$

$$+ \omega(c^{\#}(\psi_{1})c^{\#}(\psi_{3}))\omega(c^{\#}(\psi_{2})) - \omega(c^{\#}(\psi_{1}))\omega(c^{\#}(\psi_{2})c^{\#}(\psi_{3})),$$

$$\vdots$$

$$(7.227)$$

where we must pay attention to the fact that c and c^* fulfil anti-commutation relations. A useful relation is given by considering a partition \mathcal{P} of $\{1,\ldots,n\}$, given by $\mathcal{P}=\{\mathcal{C}_1,\ldots,\mathcal{C}_k\}$, such that $\mathcal{C}_j=\{i_{j,1},\ldots,i_{j,n_j}\}$ with $i_{j,l}< i_{j,l+1}$ and $i_{j,1}< i_{j+1,1}$. Assuming that $l\neq m$, we additionally must demand that $\mathcal{C}_l\cap\mathcal{C}_m=$ and $\bigcup_l\mathcal{C}_l=\{1,\ldots n\}$. This notation essentially expresses that we take an ordered set of natural numbers and cut it into pieces, in such a way that every piece is again an ordered set of numbers. The additional order of the different pieces is based the smallest number they contain. It is necessary to keep track of the ordering due to the anticommutation relations, which lead to minus signs. Hence we must do specific sign bookkeeping, and therefore we define $\mathrm{sign}(\mathcal{P})$ as the sign of the permutation $1,\ldots,n\mapsto i_{1,1},i_{1,2},\ldots,i_{1,n_1},i_{2,1},\ldots i_{k,n_k}$. This now finally allows us to write

$$\omega(c^{\#}(\psi_{1})c^{\#}(\psi_{2})\dots c^{\#}(\psi_{n})) = \sum_{\mathcal{P}} \operatorname{sign}(\mathcal{P}) \prod_{j} \langle c^{\#}(\psi_{i_{j,1}}); \dots; c^{\#}(\psi_{i_{j,n_{j}}}) \rangle_{T}.$$
 (7.228)

The expressions for general $\langle c^{\#}(\psi_1); c^{\#}(\psi_2); \dots; c^{\#}(\psi_n) \rangle_T$ can be obtained recursively from (7.228). In what follows, we consider some specific classes of fermionic quantum states, which are particularly useful and reasonably simple to describe.

Fermionic Gaussian States*

Gauge Invariant Quasi-Free States — The first class of states on our menu are states which are gauge invariant, meaning that the statistics governed by the state does not depend on phase factors in the single-particle Hilbert space. In order to understand

³⁰Truncated correlation functions are the multivariate version of cumulants and are also regularly referred to as "joint cumulants".

 $^{^{31}}$ "c*" as a collective term to denote both "c" and "c*", e.g. each c* in (7.227) can be replaced by c or by c*.

such states, we must start by defining the gauge transformation, a *-automorphism $\alpha_{\theta}: \mathcal{A}^{CAR} \to \mathcal{A}^{CAR}$ which acts as³²

$$\alpha_{\theta}(c(\psi)) = c(e^{i\theta}\psi), \quad \psi \in \mathcal{H}, \ \theta \in [0, 2\pi).$$
 (7.229)

A state which is *gauge invariant* is a functional ω which has all properties of a state and additionally follows the rule

$$\omega \circ \alpha_{\theta} = \omega \quad \text{for all } \theta \in [0, 2\pi).$$
 (7.230)

This implies that for a gauge invariant state

$$\omega(c^*(\psi_1)\dots c^*(\psi_n)c(\phi_m)\dots c(\phi_1)) = 0, \quad \text{whenever } m \neq n.$$
 (7.231)

In addition, we want the states to be *quasi-free*, which mathematically implies that

$$\langle c^{\#}(\psi_1); \dots; c^{\#}(\psi_n) \rangle_T = 0$$
 whenever $n \neq 2$. (7.232)

Physically, this demand implies that we consider systems where all the correlations between particles are negligible. Combining the two demands to obtain *gauge invariant quasi-free states*, leads us to only *one* non-vanishing truncated correlation function, of the form

$$\langle c^*(\psi); c(\phi) \rangle_T = \omega(c^*(\psi)c(\phi)) := \langle \phi, Q\psi \rangle. \tag{7.233}$$

We can always associate an operator $Q \in \mathcal{B}(\mathcal{H})$ on the single-particle space with a state ω to describe $\omega(c^*(\psi)c(\phi))$ such as done in (7.233). It is straightforward to see that positivity of the state requires $Q \geqslant 0$, and the fact that we consider fermions leads to $Q \leqslant 1$. For a general state, Q alone would not provide a lot of useful statistical information, apart for what can be interpreted as the second moment. For the gauge invariant quasi-free states, however, all information about the state is encrypted in Q. We already encountered examples of such states, most notably the Fock state ω_{Γ} , but one may also construct an abstraction of the thermal state for non-interacting fermions by defining

$$Q_{FD} = \left(1 + \exp\left((H - \mu 1)/k_b T\right)\right)^{-1},\tag{7.234}$$

which defines a gauge invariant quasi-free state governed by Fermi-Dirac statistics.

 $^{^{32}}$ Technically, these are gauge transformations with respect to the group U(1), as commonly encountered in quantum electrodynamics (Cheng and Li 1984), where these gauge transformations refer to different choices of vector potentials. In principle, we can define more general gauge transformations with respect to other groups (Bratteli and Robinson 1987, 1997), but when we here refer to gauge-invariant states the relevant group is U(1).

One can use (7.228) to conclude that

$$\omega_{Q}(c^{*}(\psi_{1})\dots c^{*}(\psi_{n})c(\phi_{m})\dots c(\phi_{1})) = \delta_{n,m}\det[\langle \phi_{i}, Q\psi_{j}\rangle]. \tag{7.235}$$

Considering terminology, it is common to refer to Q as the *symbol* (Dierckx et al. 2008; Helsen 2015). It can be proven that these states are pure states if (and only if) their symbols are projectors such that $Q^2 = Q$. The case where Q = 1 can somehow be interpreted as the Fermi-sea in which one does not create particles, but rather vacancies, known as *holes*.

General Quasi-Free States — Dropping the demand that the state be gauge invariant leads to additional properties. We still assume that $\omega(c^{\#}(\psi)) = 0$ for all $\psi \in \mathcal{H}$, however, we allow $\omega(c(\psi)c(\phi)) \neq 0$. We characterise the state through

$$\omega(c^*(\psi)c(\phi)) = \langle \phi, Q\psi \rangle$$
 and $\omega(c^*(\psi)c(\phi)) := \langle \phi, R\psi \rangle$. (7.236)

Again, $0 \le Q \le 1$, but the conditions on R are more subtle, it must be a *conjugate linear map* on \mathcal{H} and it must obey $R^{\dagger} = -R$ due to the anticommutation relations (7.212). These conditions on Q and R simply make sure that the identities in (7.236) make sense. However, they do not imply that ω is a well-defined state. In order for this to be the case, we must demand that for any choice of ψ , $\phi \in \mathcal{H}$

$$\omega\Big(\big(c^*(\phi) + c(\psi)\big)\big(c(\phi) + c^*(\psi)\big)\Big) \geqslant 0. \tag{7.237}$$

This leads us to the condition that

$$\langle \phi, Q\phi \rangle + \langle \phi, R\psi \rangle + \langle R\phi, \psi \rangle + \langle \psi, (\mathbb{1} - Q)\psi \rangle \geqslant 0 \, \psi, \, \phi \in \mathcal{H}, \tag{7.238}$$

which implies that

$$Q \geqslant 0$$
 and $Q + R^{\dagger} Q^{-1} R \leqslant \mathbb{1}$. (7.239)

We can consider all partitions of the form $\mathcal{P}_{QF} = \{\{i_1, j_1\}, \{i_n, j_n\}, \dots, \{i_k, j_k\}\}$ of $\{1, \dots, 2n\}$, which are special cases of those used to obtain (7.228), and write

$$\omega\left(c^{\#}(\psi_{1})\dots c^{\#}(\psi_{2n})\right) = \sum_{\mathcal{P}}\operatorname{sign}(\mathcal{P})\,\omega\left(c^{\#}(\psi_{i_{1}})c^{\#}(\psi_{j_{1}})\right)\dots\omega\left(c^{\#}(\psi_{i_{n}})c^{\#}(\psi_{j_{n}})\right)$$
(7.240)

which is consistent with the demand (7.232) used to define quasi-free states.

Bogoliubov Transformations for Fermions*

In Sect. 7.6.3 we described the Bogoliubov transformations as a general form of squeezing. However, these transformation are also fundamental from a mathematical perspective, since they are the only *-automorphisms on \mathcal{A}^{CAR} that consistently map polynomials in $c^{\#}$ to polynomials of the same order. More specifically, when considering a monomial

$$c^{\sharp}(\psi_1)\ldots c^{\sharp}(\psi_n),$$

it will be mapped to a sum of terms of the same length in $c^{\#}$. However, there typically do arise terms with more c^{*} 's and fewer c's and the other way around.

These transformations are not only fit to describe squeezing, they can also be used to describe other classes of states and dynamics. Let us start by defining the general Bogoliubov transformation $\mathcal{B}_{A,B}:\mathcal{A}^{CAR}\to\mathcal{A}^{CAR}$ by means of its action on $c(\psi)$:

$$c(\psi) \mapsto c(A\psi) + c^*(B\psi), \quad \psi \in \mathcal{H}.$$
 (7.241)

To define everything in a consistent fashion, we must demand that $A \in \mathcal{B}(\mathcal{H})$ and is therefore linear. On the other hand, $B : \mathcal{H} \to \mathcal{H}$ is considered to be *antilinear* and therefore it holds that

$$\langle \phi, B^{\dagger} \psi \rangle = \langle \psi, B \phi \rangle, \quad \psi, \phi \in \mathcal{H}.$$
 (7.242)

For this to lead to a consistent automorphism on the algebra, we must demand that for all $\psi, \phi \in \mathcal{H}$

$$\left\{\mathcal{B}_{A,B}\left(c(\phi)\right),\mathcal{B}_{A,B}\left(c(\psi)\right)\right\} = 0 \quad \text{ and } \quad \left\{\mathcal{B}_{A,B}\left(c(\phi)\right),\mathcal{B}_{A,B}\left(c^*(\psi)\right)\right\} = \left\langle\phi,\psi\right\rangle,\tag{7.243}$$

respectively, leading to the general requirement that

$$A^{\dagger}B + B^{\dagger}A = 0$$
 and $A^*A + B^*B = 1$. (7.244)

Because $\mathcal{B}_{A,B}$ is an automorphism, it should be invertible and the inverse should be well-defined. An interesting trick, traced back to Araki (1971) is to consider a class of transformations on the space $\mathcal{H} \oplus \mathcal{H}^*$, where \mathcal{H}^* is the dual of \mathcal{H} . The dual space contains all functionals $\phi^* : \mathcal{H} \to \mathbb{C}$. Riesz showed in his classic representation theorem (Conway 1997) that it is possible to relate $\phi^* \in \mathcal{H}^*$ to $\phi \in \mathcal{H}$ by means of

$$\phi^*(\psi) = \langle \phi, \psi \rangle, \quad \psi \in \mathcal{H}. \tag{7.245}$$

This implies two conjugate linear isomorphisms

$$\mathcal{I}: \mathcal{H} \to \mathcal{H}^*: \phi \mapsto \phi^* \text{ and } \mathcal{J}: \mathcal{H}^* \to \mathcal{H}: \phi^* \mapsto \phi,$$
 (7.246)

and it directly follows that their combination leads to the identities $\mathcal{J} \circ \mathcal{I} = \mathbb{1}_{\mathcal{H}}$ and $\mathcal{I} \circ \mathcal{J} = \mathbb{1}_{\mathcal{H}^*}$. We can equivalently express the Bogoliubov transformation (7.241) in terms of a transformation on $\mathcal{H} \oplus \mathcal{H}^*$ by associating

$$\gamma: \mathcal{H} \oplus \mathcal{H}^* \to \mathcal{A}^{CAR}: \psi \oplus \phi^* \mapsto c(\psi) + c^*(\phi).$$
 (7.247)

The Bogoliubov transformation (7.241) is given by $\mathcal{B}_{A,B} = \gamma \circ U \circ \gamma^{-1}$, with U given by

$$U = \begin{pmatrix} A & B\mathcal{J} \\ \mathcal{I}B & \mathcal{I}A\mathcal{J} \end{pmatrix}. \tag{7.248}$$

Indeed, it is directly calculated that

$$\gamma \circ U \circ \gamma^{-1}(c(\psi)) = \gamma \circ U(\psi \oplus 0) = \gamma(A\psi \oplus \mathcal{I}(B\psi))\gamma(A\psi \oplus (B\psi)^*) = c(A\psi) + c^*(B\psi). \tag{7.249}$$

Invertibility comes for free when ${\cal H}$ is finite dimensional, but when it is not, we must additionally impose that

$$AB^{\dagger} + BA^{\dagger} = 0$$
 and $AA^{\dagger} + BB^{\dagger} = 1$. (7.250)

The inverse map is then given by

$$\mathcal{B}_{AB}^{-1}(c^*(\psi)) = c^*(A^{\dagger}\psi) + c(B^{\dagger}\psi), \quad \psi \in \mathcal{H}. \tag{7.251}$$

Combining (7.244) and (7.250), we obtain a quite extensive and formal definition of these transformations.

In addition, we see that these transformations also form a group \mathcal{G}_b . When we characterise the transformations $\mathcal{B}_{A,B}$ as (A,B), we can define the group operation \circ as

$$(A_1, B_1) \circ (A_2, B_2) = (A_1 A_2 + B_1 B_2, A_1 B_2 + B_1 A_2).$$
 (7.252)

Moreover, a group needs an inverse for each element (hence the effort to go through Araki's trick) and a neutral element. These are, respectively, given by

$$(A, B)^{-1} = (A^{\dagger}, B^{\dagger}),$$
 (7.253)

$$e = (1, 0). (7.254)$$

The possibility to implement a group structure is of course crucial with possible dynamical applications in mind. Let us stress that $\mathcal{U}(\mathcal{H})$, the unitary group on the single particle space \mathcal{H} , can naturally be represented by

$$U \in \mathcal{U}(\mathcal{H}) \mapsto (U, 0). \tag{7.255}$$

We conclude with the observation that the general quasi-free states remain general quasi-free states under Bogoliubov transformations, or in other words

$$\omega$$
 is quasi-free $\Longrightarrow \omega \circ \mathcal{B}_{A,B}$ is quasi-free, (7.256)

and that the mapping $\mathcal{B}_{A,B}$ can be described on the level of operators Q and R, that describe the states, by means of

$$Q \mapsto A^{\dagger}QA + A^{\dagger}RB - B^{\dagger}RA + B^{\dagger}(\mathbb{1} - Q)B,$$

$$R \mapsto A^{\dagger}RA + B^{\dagger}(\mathbb{1} - Q)A + A^{\dagger}OB - B^{\dagger}RB.$$
(7.257)

Notice that gauge invariant states (R=0) are generally not mapped into other gauge invariant states. This is only the case when either B=0 or A=0. We may associate these fermionic Bogoliubov transformations to a form of squeezing operations, and as such we can also interpret the general quasi-free states with $R \neq 0$ as some form of fermionic squeezed states. However, there are many problems in connecting such notions from quantum optics to fermionic systems. Notice for example that

$$c(\psi) \mapsto c(\psi) + \langle \psi, \alpha \rangle$$
 (7.258)

does *not* form a good *-automorphism on the CAR algebra because it does not conserve the canonical anticommutation relations. Therefore it is extremely difficult to define fermionic coherent states (Helsen 2015).

7.7.2 The CCR Algebra*

In the following chapters, all bosonic systems are treated in a specific representation of the CCR algebra. Hence, these discussions can be understood without the formal details presented in this section. This discussion on the formal structure of the CCR algebra is included for completeness and context.

This discussion on the CCR algebra borrows many elements from Manuceau (1968), Manuceau and Verbeure (1968), Petz (1990), Verbeure (2011). Throughout this section, we will not enter details on more pathological cases. Unless explicitly mentioned otherwise, we assume analytic states, non-degenerate symplectic forms, et cetera.

Structure*

The abstract version of the bosonic algebra is in several ways more subtle than the fermionic counterpart. We already discussed the relation between bosons and harmonic oscillators in Sects. 7.3.2 and 7.6.2. Also in Sect. 2.2.1 we referred to the canonical commutation relations (2.7) as the so-called "quantum condition". It is remarkable that so many different types of physics are essentially described by fundamentally isomorphic mathematics. The subtlety, however, arises when we study the different expressions

$$PQ - QP = \frac{h}{2\pi i} \mathbb{1},\tag{2.7}$$

$$[a^{\dagger}(\psi_1), a^{\dagger}(\psi_2)] = 0$$
 and $[a(\psi_1), a^{\dagger}(\psi_2)] = \langle \psi_1, \psi_2 \rangle$, (7.77)

$$[Q(\psi_1), P(\psi_2)] = i \operatorname{Re} \langle \psi_1, \psi_2 \rangle \quad \text{with } \psi_1, \psi_2 \in \mathcal{H}. \tag{7.136}$$

Starting from the first equation (2.7), we can see that it is impossible to fulfil the relation by choosing either P or Q a bounded operator and the other one a trace class operator: Under these assumptions, we may consider the trace of the full expression, which implies that $0 = -i\hbar \text{tr} \mathbb{1}$. This can only hold for $\hbar = 0$. It turns out that we can only fulfil these equations by using *unbounded* operators. Hence, these specific operator forms cannot be used as a basic structure to construct an abstract C^* -algebra. To achieve this goal, we must follow a different path. However, we will ultimately explain how this path leads to the above commutators.

The C^* -algebra of the CCR is generally constructed on a *symplectic space* (\mathcal{S}, σ) , which in several physical applications would be the *phase space*. Here we consider \mathcal{S} a *real* Hilbert space and σ the symplectic (or canonical) form $\sigma: \mathcal{S} \times \mathcal{S} \mapsto \mathbb{R}$, such that $\sigma(f,g) = -\sigma(g,f)$ for all $f,g \in \mathcal{S}$. We also assume that the symplectic space is non-degenerate, ergo if $\sigma(f,g) = 0$ for all $f \in \mathcal{S}, g$ must be the zero vector.

On top of this symplectic space (S, σ) , we define the objects w(f), with $f \in S$, which fulfil the Weyl-relations

$$w(f)^* = w(-f), \quad f \in \mathcal{S},$$
 (7.259)

$$w(f)w(g) = e^{i\sigma(f,g)}w(f+g), \quad f,g \in \mathcal{S}. \tag{7.260}$$

We can now consider the *-algebra $\Delta(\mathcal{S},\sigma)$ generated by $\{w(f) \mid f \in \mathcal{S}\}$, which becomes a C^* -algebra upon completion under the norm topology. This latter statement directly introduces the following problem: A priori, it is not obvious with which norm $\Delta(\mathcal{S},\sigma)$ is equipped. Already here, we see that the CCR algebra inherits most of its properties by virtue of its representations (see Appendix A). Let us consider $\mathcal{R}(\mathcal{S},\sigma)$, the space of all representations $\pi:\Delta(\mathcal{S},\sigma)\to\mathcal{L}(\mathcal{H}_\pi)$, with $\mathcal{L}(\mathcal{H}_\pi)$ the linear operators on a Hilbert space \mathcal{H}_π , such that $\lambda\in\mathbb{R}\to\pi(w(\lambda f))$ is weakly continuous $\mathcal{L}(\mathcal{H}_\pi)$ for all $f\in\mathcal{S}$. The space $\mathcal{L}(\mathcal{H}_\pi)$ is naturally equipped with a norm and therefore the following definition makes sense (Manuceau 1968):

$$||a|| := \sup_{\mathcal{R}} ||\pi(a)||, \quad \forall a \in \Delta(\mathcal{S}, \sigma).$$
 (7.261)

It can be proven that actually $\|\pi(a)\| = \|\pi'(a)\|$ for all $a \in \Delta(\mathcal{S}, \sigma)$ and all $\pi, \pi' \in \mathcal{R}(\mathcal{S}, \sigma)$ (Manuceau 1968). Therefore, we may simply consider one specific representation to construct the norm, i.e. $\|a\| = \|\pi(a)\|$ for all $a \in \Delta(\mathcal{S}, \sigma)$ and all $\pi \in \mathcal{R}(\mathcal{S}, \sigma)$. The C^* -algebra for the CCR is now obtained upon completion for this norm, which we denote $\overline{\Delta(\mathcal{S}, \sigma)}$. A very important result (Slawny 1972) in this context is the uniqueness of this algebra (up to *-isomorphisms), which implies that it makes sense to refer to *the* C^* -algebra of the CCR.

Although this structure is mathematically appealing, it is highly abstract and it is far from obvious how it connects to the actual CCR (2.7), (7.77), (7.136). The connection is facilitated by the fact that there is a unique representation π which

³³For a definition, see the footnote on p. 39 or (Conway 1997; Pedersen 1989).

maps $\overline{\Delta(S, \sigma)}$ to the operators of the type (7.81). In what follows, we make this argument more explicit.

We now define the general Weyl system $W: \mathcal{S} \to \mathcal{B}(\mathcal{H}): f \mapsto W(f)$, where W(f) follows the rules

$$W(0) = 1, (7.262)$$

$$W^{\dagger}(f) = W(-f), \tag{7.263}$$

$$W(f_1)W(f_2) = \exp(i\sigma(f_1, f_2)) \ W(f_1 + f_2), \tag{7.264}$$

clearly rendering these operators unitary. We define $\mathcal{W}(\mathcal{S}, \sigma)$ as the set of all such possible Weyl systems (so implying that we also consider all possible $\mathcal{B}(\mathcal{H})$ on which these structures can be constructed).

In the representation $\pi \in \mathcal{R}(\mathcal{S}, \sigma)$ an element $w(f) \in \overline{\Delta(\mathcal{S}, \sigma)}$ is obviously given by $\pi(w(f)) = W(f)$ with $W \in \mathcal{W}(\mathcal{S}, \sigma)$. However, what is more remarkable is that any $W \in \mathcal{W}(\mathcal{S}, \sigma)$ also gives rise to a *unique* $\pi \in \mathcal{R}(\mathcal{S}, \sigma)$, such that $W(f) = \pi(w(f))$ for all $f \in \mathcal{S}$. In other words, the *set of representations of the C*-algebra is isomorphic to the set of Weyl systems*. This means that, for *any* representation π , we can find a unique W_{π} such that $\pi(w(f)) = W_{\pi}(f)$, which is always a unitary operator on a Hilbert space. Invoking Stone's theorem (Stone 1930, 1932; von Neumann 1932), we can always construct a set of hermitian operators $q_{\pi}(f)$ on the relevant Hilbert space, such that $W_{\pi}(tf) = \exp(itq_{\pi}(f))$, for all $t \in \mathbb{R}$. These operators fulfil the commutation relation

$$[q_{\pi}(f), q_{\pi}(g)] = -2i\sigma(f, g), \quad f, g \in \mathcal{S},$$
 (7.265)

such that the symplectic space (\mathbb{R}^2, σ) allows us to choose two basis vectors e_1, e_2 , with $q_{\pi}(e_1) = Q$ and $q_{\pi}(e_2) = P$, such that

$$[Q, P] = -2i. (7.266)$$

There is one thing that feels odd about the description, because we in the end want to make the abstraction for *bosonic systems*. As we have seen, a bosonic system is built upon a *complex Hilbert space* (the single-particle Hilbert space), rather than upon a symplectic space. The reason is that a Hilbert space is actually a symplectic space with additional structure, to end up with a positive definite sesquilinear form, i.e. the Hilbert space's inner product. The complex structure is crucial to define creation and annihilation operators as we will see in Eq. (7.273). Let us therefore elaborate on the connection between symplectic spaces and Hilbert spaces.

Given a Hilbert space $\mathcal{H}_{\mathcal{S}}$ with inner product $\langle ., . \rangle$, we may express

$$\langle \phi, \psi \rangle = \operatorname{Re} \langle \phi, \psi \rangle + i \operatorname{Im} \langle \phi, \psi \rangle$$

:= \alpha(\phi, \psi) + i \sigma(\phi, \psi), (7.267)

³⁴This directly follows from (7.259) and (7.260).

where α is a *symmetric*, real bilinear form, whereas σ is *symplectic* and real. We can now think of the underlying (S, σ) in the sense that $\mathcal{H}_S = S$ as sets (in the same way as $\mathbb{C} = \mathbb{R}^2$ as sets) and $\sigma(.,.) = \operatorname{Im} \langle .,. \rangle$. In other words, any Hilbert space has an underlying symplectic structure. As it turns out, we can also extend any symplectic space to a complex Hilbert space. Let us therefore define a *complex structure* $J: S \to S$ with the properties

$$J^2 = -1 (7.268)$$

$$\sigma(f, Jf) \leqslant 0, \quad f \in \mathcal{S} \tag{7.269}$$

$$\sigma(Jf, Jg) = \sigma(f, g), \quad f, g \in \mathcal{S}. \tag{7.270}$$

We can turn S into a complex space by defining the scalar product as

$$(t+is)f = tf + sJf, \quad s, t \in \mathbb{R}, f \in \mathcal{S}. \tag{7.271}$$

To turn it into a Hilbert space, we define the inner product

$$\langle f, g \rangle := \sigma(f, Jg) + i\sigma(f, g).$$
 (7.272)

The main reason why we can consider $\overline{\Delta(S,\sigma)}$ as the C^* -algebra of the CCR was in some sense already shown in Sect. 7.4: The Weyl operators as defined for a bosonic system only use the *symplectic* structure underlying the Hilbert space. If we now define a complex structure J on (S,σ) , we can define the following two operators in any specific representation π :

$$a_{\pi}^{\dagger}(f) := \frac{1}{2}(q_{\pi}(f) - iq_{\pi}(Jf))$$
 and $a_{\pi}(f) := \frac{1}{2}(q_{\pi}(f) + iq_{\pi}(Jf)),$ (7.273)

such that

$$[a_{\pi}(f), a_{\pi}^{\dagger}(g)] = \sigma(f, Jg) + i\sigma(f, g), \quad f, g \in \mathcal{S}$$
 (7.274)

or, in the more common Hilbert space notation,

$$[a_{\pi}(\phi), a_{\pi}^{\dagger}(\psi)] = \langle \phi, \psi \rangle. \tag{7.275}$$

This leads to the well-known creation and annihilation operators. We can interpret this in the following way: Equipping a symplectic space (such as phase space) with the CCR C^* -algebra and choosing a representation allows us to construct the quantum analog of a classical system. If the symplectic space is on top equipped with a complex structure, and is hence a complex Hilbert space, we can build a bosonic system on top. Given that the creation and annihilation operators only make sense if constructed on a Hilbert space, the term *second quantisation* is somewhat intuitive. For example, we may start from a phase space (\mathbb{R}^2 , σ), build a C^* -algebra $\Delta(\mathbb{R}^2, \sigma)$ on it and choose the appropriate representation. This representation gives rise to an associated Hilbert

space \mathcal{H} and we can *again* construct a C^* -algebra $\overline{\Delta(\mathcal{H}, \operatorname{Im}\langle .,. \rangle)}$ on it, which under an appropriate representation allows us to study bosonic systems.

The reason why we call $\overline{\Delta(\mathcal{S},\sigma)}$ the C^* -algebra of the CCR is because *any* structure which fulfils the canonical commutation relations can ultimately be related to a representation of $\overline{\Delta(\mathcal{S},\sigma)}$. Another important result, shown by von Neumann (von Neumann 1931, 1932), is that, for dim $\mathcal{S}<\infty$, all these representations π are unitarily equivalent. This really means that for a finite number of phase space coordinates, we can find position and momentum operators which are uniquely determined (up to unitary transformations). However, for bosons in infinite-dimensional single-particle Hilbert space, the creation and annihilation operators are no longer uniquely determined, and we are forced to choose the correct representation.

In the previous section, we have seen that states and representations go hand in hand, given the importance of representations in studying the CCR. Let us now consider the states on the C^* -algebra of the CCR.

Structuring States*

As we consider the abstract mathematical description of many-boson systems, it is logical to focus attention to the most feasible structure to describe these systems and the states that live on them. We described any quantum observable in a consistent way by defining the algebra of observables in terms of $w(\psi)$, as given by (7.259), (7.260). Therefore, we describe states as normalised, positive functionals ω on $\overline{\Delta(\mathbb{R}^{2d}, \sigma)}$. The functionals are commonly understood in terms of the expectation values $\omega(w(\psi))$.

By means of (7.260), we can see that actually any element $x \in \overline{\Delta(\mathbb{R}^{2d}, \sigma)}$ is of the form $x = \sum_j a_j w(f_j)$ with $a_j \in \mathbb{C}$ and $f_j \in \mathcal{S}$. Due to linearity, one may realise that a state is fully characterised by knowledge of

$$\tilde{\xi}(f) = \omega(w(f)), \text{ for all } f \in \mathcal{S}.$$
 (7.276)

The normalisation condition implies that

$$\omega(w(0)) = 1, \tag{7.277}$$

whereas positivity can be expressed by the demand

$$\omega(x^*x) = \sum_{i,j} a_i \overline{a_j} e^{-i\sigma(f_i, f_j)} \tilde{\xi}(f_i - f_j) \geqslant 0, \tag{7.278}$$

for any set of complex numbers $\{a_i\}$ and any set of vectors $\{f_i\}$. Even though it is sufficient to know the function $\tilde{\xi}: \mathcal{S} \to \mathbb{C}$ as a characterisation of the state, it is not trivial to verify that (7.278) holds.

 $^{^{35}}$ The consequence of this theorem is fundamental in the sense that it formalises the equivalence of Schrödinger's wave mechanics and Heisenberg's matrix mechanics. Moreover, the fact that this theorem only holds for dim $\mathcal{S}<\infty$ implies that in quantum field theories this equivalence breaks down.

For the CAR algebra, we introduced the truncated correlation functions (7.228) as useful tools to describe structures of quantum states. Let us try to import this idea to the CCR setting. Obviously it does not make much sense to do so for products of Weyl elements, but we may use a result originally derived by Robinson (1965). However, to do so, we must choose a *specific representation* to work in. As we have seen before in Chap. 2, the fact that we study states already fixes the relevant representation by means of the GNS construction (7.220)–(7.222). For the state ω , we consider the GNS-triplet (π_{ω} , \mathcal{H}_{ω} , Ω_{ω}), such that it makes sense to consider the related quadratures $q_{\omega}(\psi)$ as discussed in the previous section.³⁶

To understand the connection between bosonic states and truncated correlation functions, we first define the function

$$f(t) := \omega(w(tf)), \quad t \in \mathbb{R}, f \in \mathcal{S},$$
 (7.279)

for which it can be directly shown that

$$f(t) = \langle \Omega_{\omega}, e^{itq_{\omega}(f)} \Omega_{\omega} \rangle = \sum_{n=0}^{\infty} \frac{i^n z^n}{n!} \langle \Omega_{\omega}, q_{\omega}(f)^n \Omega_{\omega} \rangle.$$
 (7.280)

By defining the bosonic truncation scheme as

$$\langle \Omega_{\omega}, q_{\omega}(f_1) \dots q_{\omega}(f_n) \rangle = \sum_{\mathcal{D}} \prod_{k} \langle q(f_{i_{k,1}}); \dots; q(f_{i_{k,n_k}}) \rangle_T,$$
 (7.281)

we can now write that

$$f(t) = \exp\left(\sum_{n=1}^{\infty} \frac{i^n t^n}{n!} \langle q_{\omega}(f)^n \rangle_T\right). \tag{7.282}$$

This implies that, indeed, knowledge of all truncated correlation functions (7.281) implies knowledge of the state. In what follows, we focus attention to a very specific set of states, for which the truncated correlation functions have a very specific form.

Bosonic Gaussian States*

Let us start our study of quasi-free states without the use of their induced GNS representation. We have argued in (7.276) that any state ω on $\overline{\Delta(\mathcal{S},\sigma)}$ can be understood in terms of the quantum characteristic function $\tilde{\xi}: f \in \mathcal{S} \mapsto z \in \mathbb{C}$. Therefore, we can identify a state by defining this function. When we now construct a symmetric bilinear form $\alpha: \mathcal{S} \times \mathcal{S} \to \mathcal{R}$ on the symplectic space (\mathcal{S}, σ) , we can define a bosonic quasi-free state through its quantum characteristic function

³⁶Note that we introduced the quadratures (7.135) as induced by a specific representation. Since each state naturally gives rise to a GNS representation, we may label the quadratures by the state ω .

$$\tilde{\xi}(f) = \omega(w(f)) = \exp\left(-\frac{1}{2}\alpha(f, f)\right), \quad f \in \mathcal{S}.$$
 (7.283)

In order for a state to be well-defined, we must fulfil both conditions (7.277) and (7.278). Condition (7.277) is obviously true, whereas (7.278) imposes an additional condition on α . Indeed, we must choose α such that it fulfils the demand

$$\sigma(f,g)^2 \leqslant \alpha(f,f)\alpha(g,g). \tag{7.284}$$

When we now turn to the specific representation induced by the state ω , we can see that

$$\langle \Omega_{\omega}, q_{\omega}(f) q_{\omega}(g) \Omega_{\omega} \rangle = \alpha(f, g) - i\sigma(f, g). \tag{7.285}$$

The gauge-invariance can easily be broken by means of a specific class of *-automorphisms τ_{χ} , which describes a natural action of the functional $\chi: \mathcal{S} \to \mathbb{R}$. We define this *-automorphism via

$$\tau_{\chi}(w(f)) := e^{i\chi(f)}w(f), \quad f \in \mathcal{S}. \tag{7.286}$$

We can thus define a new state $\omega':=\omega\circ\tau_\chi$, such that the associated quantum characteristic function reads

$$\tilde{\xi}'(f) = \omega\Big(\tau_{\chi}\big(w(f)\big)\Big) = \exp\Big(-\frac{1}{2}\alpha(f,f) - i\chi(f)\Big), \quad f \in \mathcal{S}. \tag{7.287}$$

Because τ_{χ} is a well-defined *-automorphism and ω is a well-defined state, we can conclude that ω' is also a well-defined state. States characterised by quantum characteristic functions of the form (7.287) can be seen as general *bosonic Gaussian states*.

These new states ω' can be be understood via the representation of the quasi-free state ω . We consider the Weyl operators $W_{\omega}(f) = \pi_{\omega}(w(f))$ for all $f \in \mathcal{S}$ and the vector $W_{\omega}(c)\Omega_{\omega}$ for any given $c \in \mathcal{S}$. This allows us to evaluate

$$\langle W_{\omega}(c)\Omega_{\omega}, W_{\omega}(f)W_{\omega}(c)\Omega_{\omega}\rangle = \langle \Omega_{\omega}, W_{\omega}(f)\Omega_{\omega}\rangle e^{2i\sigma(f,c)}.$$
 (7.288)

Therefore, we can use the functional $\chi_c := -2\sigma(c, .)$, to obtain that

$$\pi(\tau_{\chi_c}(x)) = W_{\pi}(-c)\pi(x)W_{\pi}(c) \tag{7.289}$$

for all $x \in \overline{\Delta(S, \sigma)}$. Thus, we see that also in this more abstract framework, the general Gaussian states can be seen as displaced quasi-free states and the Weyl operators obtained in the specific representation of the quasi-free state act as displacement operators.

When we use the GNS representation to define quadrature operators, we see that bosonic Gaussian states are those states for which all truncated correlation functions of orders n > 2 vanish. Hence, the only non-vanishing contributions are given by

$$\langle q(f)\rangle_{T} = \langle \Omega_{\omega}, q_{\omega}(f)\Omega_{\omega}\rangle, \tag{7.290}$$

$$\langle q(f); q(g)\rangle_{T} = \langle \Omega_{\omega}, q_{\omega}(f)q_{\omega}(g)\Omega_{\omega}\rangle - \langle \Omega_{\omega}, q_{\omega}(f)\Omega_{\omega}\rangle \langle \Omega_{\omega}, q_{\omega}(g)\Omega_{\omega}\rangle. \tag{7.291}$$

This implies that all higher order correlation functions $\omega(q(f_1)...q(f_n))$ can be expressed as a sum of products of correlation functions of order at most two. We can then use (7.282) and it turns out that

$$\tilde{\xi}(f) = \exp\left(i\langle\Omega_{\omega}, q_{\omega}(f)\Omega_{\omega}\rangle - \frac{1}{2}\langle q_{\omega}(f); q_{\omega}(f)\rangle_{T}\right). \tag{7.292}$$

It should not come as a surprise that this result is highly similar to the result obtained in (7.201), up to the factor $\sqrt{2}$ difference in the definition (7.148) of the quadrature.

In the more structured case where the symplectic structure arises from a complex Hilbert space $\mathcal{H}_{\mathcal{S}}$, with $\sigma := \text{Im } \langle ., . \rangle$, and $\langle ., . \rangle$ the Hilbert space's inner product, we can consider a special type of quasi-free state, the Fock state.³⁷ First of all, we note that Re $\langle ., . \rangle$ is in fact a symmetric linear form on $\mathcal{H}_{\mathcal{S}}$ and that, moreover,

$$\|\psi\|^2 = \langle \psi, \psi \rangle = \text{Re } \langle \psi, \psi \rangle. \tag{7.293}$$

In the sense of (7.283), we can then define the *Fock state* ω_{Γ} as

$$\tilde{\xi}_{\Gamma}(\psi) = \omega_{\Gamma}(w(\psi)) = \exp\left(-\frac{1}{2}\|\psi\|^2\right), \quad \psi \in \mathcal{H}_{\mathcal{S}}.$$
 (7.294)

When we now consider the GNS-triplet for the Fock state, we find

$$(\pi_{\Gamma}, \Omega_{\Gamma}, \Gamma(\mathcal{H}_{\mathcal{S}})),$$
 (7.295)

where π_{Γ} is referred to as the *Fock representation*, $\Gamma(\mathcal{H}_{\mathcal{S}})$ is the well-known Fock space (7.39) with vacuum Ω_{Γ} . Moreover, we can define creation and annihilation operators $a_{\Gamma}^{\dagger}(\psi)$ and $a_{\Gamma}(\psi)$, using (7.273), such that

$$[a_{\Gamma}(\phi), a_{\Gamma}^{\dagger}(\psi)] = \langle \phi, \psi \rangle, \quad \text{and} \quad [a_{\Gamma}(\phi), a_{\Gamma}(\psi)] = 0, \quad \psi, \phi \in \mathcal{H}_{\mathcal{S}},$$

$$(7.296)$$

$$a_{\Gamma}(\psi)\Omega_{\Gamma} = 0, \quad \psi \in \mathcal{H}_{\mathcal{S}}.$$

$$(7.297)$$

Thus we have recovered the Fock space $\Gamma(\mathcal{H}_{\mathcal{S}})$ with vacuum Ω_{Γ} .

³⁷Let us directly note that the term "Fock state" in mathematical physics does not refer to the "Fock state" in for example quantum optics. What quantum opticians refer to as a Fock state is rather a number state with respect to the Fock representation.

Note that the definition of a Fock state is in this case rather broad. For example, for any Fock state ω_{Γ} , the *-automorphism

$$u_U(w(\psi)) := w(U\psi), \quad U \in \mathcal{B}(\mathcal{H}), \ U^{\dagger}U = UU^{\dagger} = \mathbb{1},$$
 (7.298)

defines the same Fock state $\omega_u := \omega \circ u_U$. We can extend this logic to a symplectic transformation S, such that

$$s_S(w(\psi)) = w(S\psi), \quad \text{Im } \langle S\psi, S\phi \rangle = \text{Im } \langle \psi, \phi \rangle.$$
 (7.299)

The transformation s_S is an alternative representation of the Bogoliubov transformations (7.180), (7.181), which we discussed earlier. They define a *squeezed state* $\omega_s := \omega_{\Gamma} \circ s_S$, with

$$\tilde{\xi}_s(\psi) = \omega_{\Gamma}(w(S\psi)) = \exp\left(-\frac{1}{2}\|S\psi\|^2\right), \quad \psi \in \mathcal{H}_{\mathcal{S}}.$$
 (7.300)

It can be shown (Petz 1990) that whenever $(S^{\dagger}S - 1)^{\dagger}(S^{\dagger}S - 1)$ has finite trace, we can find a unitary transformation U such that $\pi_s(x) = U^{\dagger}\pi_{\Gamma}(x)U$ for all $x \in \overline{\Delta(\mathcal{H}_S, \operatorname{Im}\langle.,.\rangle)}$. Thus, although the states are not the same, they are equivalent up to unitary transformations (which are the representations of the Bogoliubov transformations (7.299)). Finally we can also combine the Fock state ω_{Γ} with the displacement τ_{χ} (7.286), where we can now associate the functional with an element in \mathcal{H}_S , such that we write

$$\tau_{\chi}(w(\psi)) = e^{i\langle \chi, \psi \rangle} w(\psi), \tag{7.301}$$

which leads us to the states $\omega_c := \omega_\Gamma \circ \tau_\chi$, which are the *Glauber coherent states*. Moreover, $\omega_\Gamma \circ s_S \circ \tau_\chi$ are the *coherent squeezed states*. Notice that all these states are *pure* (Petz 1990).

Let us finally come back to the more general quasi-free states and now assume a Hilbert space structure. We will here limit ourselves to considering the specific GNS-construction (7.220)–(7.222) of the state and the identities defined there. In the GNS representation, we can construct creation and annihilation operators (7.273) by virtue of the Hilbert space structure. For these operators we write the resulting bilinear forms as

$$\langle \Omega_{\omega}, a_{\omega}^{\dagger}(\psi) a_{\omega}(\phi) \Omega_{\omega} \rangle := \langle \psi, Q \phi \rangle, \quad \text{and} \quad \langle \Omega_{\omega}, a_{\omega}(\psi) a_{\omega}(\phi) \Omega_{\omega} \rangle := \langle \psi, T \phi \rangle.$$
(7.302)

We must now demand that $Q \in \mathcal{B}(\mathcal{H}) \geqslant 0$, to guarantee that the state is positive and $T: \mathcal{H} \to \mathcal{H}$ must be conjugate linear to fulfil the CCR. The conditions for positivity then read

$$Q(\mathbb{1} + Q) - T^{\dagger}T \geqslant 0, \tag{7.303}$$

which concludes our definition of bosonic Gaussian states.

7.8 Concluding Remarks

In this chapter we provided a construction of many-particle quantum physics and the way in which it is described. The formalism as developed in Sects. 7.2–7.6 is ultimately limited to systems which have either a finite number of particles or are constructed on a finite-dimensional Hilbert space. A more general treatment leads us more in the direction of algebraic quantum field theory, and here we see that the treatment of bosonic systems, as described in Sect. 7.7.2, is completely different from that of the fermionic counterparts, as described in Sect. 7.7.1.

We learn in Sect. 7.7 that not only the algebra, but also the state is crucial to describe the problem. A state fixes a representation on a specific Hilbert space by means of the GNS construction. In general, this Hilbert space is simply too small to contain all the possible states on the algebra, hence the importance of the GNS construction. In this sense, a Fock space is actually a very small space, which can only harbour a finite amount of particles. The GNS construction teaches us, however, that we can locally perturb states by creating and annihilating (quasi-)particles by using the creation and annihilation operators in the relevant representation.

One of the most profound differences between the CAR and the CCR structure is that the bosonic creation and annihilation operators are not even defined in an abstract way. Due to the lack of boundedness, they cannot be contained within a C^* -algebraic structure. We did explain, however, that Stone's theorem (Stone 1930, 1932; von Neumann 1932) allows us to define a set of such operators in each representation, i.e. for every state.

Studying a physical problem therefore does not only boil down to choosing the correct algebra of observables, but also the specific state and hence a specific representation. The importance of representations in systems with infinite-dimensional mode spaces is implicitly shown by results such as (Chenu et al. 2015), where it is claimed that thermal states cannot be represented by a convex mixture of coherent states. This result appears to be in grave contradiction to our previous claims in Sect. 7.6.4. However, the single-particle Hilbert space that is considered in Chenu et al. (2015) is infinite-dimensional, such that a typical thermal state is not contained within the Fock representation. Hence, it should not come as a surprise that such a thermal state cannot be represented by a mixture of coherent states in the Fock representation. The algebraic approach provides solutions (Fannes and Verbeure 1975) for such paradoxical results, which highlights its importance beyond mere mathematical elegance. Often in fields such as quantum optics, the mode spaces are controlled sufficiently well (Armstrong et al. 2012; Cai et al. 2017; Chen et al. 2014; De Valcarcel et al. 2006; Gerke et al. 2015; Ra et al. 2017; Roslund et al. 2014; Su et al. 2012), such that it is sufficient to consider the bosonic Fock representation. The work in the following chapters is therefore typically conducted in the Fock representation. Nevertheless, the central topic of study in Part III of this thesis is the difference between the quantum mechanics of bosons and fermions and thus it is instructive to also understand their fundamental difference on a deeper algebraic level.

The structures which we discussed throughout this chapter form the basis of Chaps. 8 and 9. In the former, we focus on the dynamical properties of of fixed number of particles, i.e. the number states of Sect. 7.6.1, and elaborate on many-particle interference phenomena. In Chap. 9, the number of particles is allowed to fluctuate and we investigate the behaviour of single-particle observables (recall Sect. 7.5) in the non-equilibrium steady state.

References

- R. Alicki, Field-theoretical methods, in *Quantum Information, Computation and Cryptography*, ed. by F. Benatti, M. Fannes, R. Floreanini, D. Petritis. Lecture Notes in Physics, vol. 808 (Springer, Berlin, 2010), pp. 151–174
- R. Alicki, M. Fannes, Quantum Dynamical Systems (Oxford University Press, Oxford, 2001)
- P.W. Anderson, More is different. Science **177**, 393–396 (1972)
- M.H. Anderson, J.R. Ensher, M.R. Matthews, C.E. Wieman, E.A. Cornell, Observation of Bose-Einstein condensation in a dilute atomic vapor. Science **269**, 198–201 (1995)
- M.R. Andrews, C.G. Townsend, H.-J. Miesner, D.S. Durfee, D.M. Kurn, W. Ketterle, Observation of interference between two Bose condensates. Science 275, 637–641 (1997)
- H. Araki, On quasifree states of CAR and bogoliubov automorphisms. Publ. Res. Inst. Math. Sci. 6, 385–442 (1971)
- H. Araki, D.E. Evans, On a C*-algebra approach to phase transition in the two-dimensional Ising model. Commun. Math. Phys. 91, 489–503 (1983)
- S. Armstrong, J.-F. Morizur, J. Janousek, B. Hage, N. Treps, P.K. Lam, H.-A. Bachor, Programmable multimode quantum networks. Nat. Commun. 3, 1026 (2012)
- A. Ashkin, J.M. Dziedzic, J.E. Bjorkholm, S. Chu, Observation of a single-beam gradient force optical trap for dielectric particles. Opt. Lett. 11, 288 (1986)
- H. Baker, Alternants and continuous groups. Proc. Lond. Math. Soc. 3(2), 24–27 (1905)
- K. Banaszek, K. Wódkiewicz, Nonlocality of the Einstein-Podolsky-Rosen state in the Wigner representation. Phys. Rev. A 58, 4345–4347 (1998)
- K. Banaszek, K. Wódkiewicz, Testing quantum nonlocality in phase space. Phys. Rev. Lett. 82, 2009–2013 (1999)
- J. Bardeen, L.N. Cooper, J.R. Schrieffer, Theory of superconductivity. Phys. Rev. 108, 1175–1204 (1957)
- J.-L. Basdevant, J. Dalibard, *Quantum Mechanics* (Springer, Berlin, 2002)
- F. Benatti, M. Fannes, R. Floreanini, D. Petritis, *Quantum Information, Computation and Cryptography: An Introductory Survey of Theory, Technology and Experiments* (Springer Science & Business Media, Berlin, 2010)
- R. Bhatia, *Positive Definite Matrices* (Princeton University Press, Princeton, 2007)
- I. Bloch, Ultracold quantum gases in optical lattices. Nat. Phys. 1, 23–30 (2005)
- I. Bloch, J. Dalibard, W. Zwerger, Many-body physics with ultracold gases. Rev. Mod. Phys. 80, 885 (2008)
- O. Bohigas, S. Tomsovic, D. Ullmo, Manifestations of classical phase space structures in quantum mechanics. Phys. Rep. 223, 43–133 (1993)
- S.N. Bose, Plancks Gesetz und Lichtquantenhypothese, Z. Phys. 26, 178–181 (1924)
- O. Bratteli, D.W. Robinson, Operator Algebras and Quantum Statistical Mechanics, vol. 1 (Springer, Berlin, 1987)
- O. Bratteli, D.W. Robinson, Operator Algebras and Quantum Statistical Mechanics Equilibrium States. Models in Quantum Statistical Mechanics (Springer, Berlin, 1997)
- S.L. Braunstein, Squeezing as an irreducible resource. Phys. Rev. A 71, 055801 (2005)

- H.-P. Breuer, F. Petruccione, *The Theory of Open Quantum Systems* (Oxford University Press, Oxford, 2007)
- Y. Cai, J. Roslund, G. Ferrini, F. Arzani, X. Xu, C. Fabre, N. Treps, Multimode entanglement in reconfigurable graph states using optical frequency combs. Nat. Commun. 8, 15645 EP (2017)
- J.E. Campbell, On a law of combination of operators bearing on the theory of continuous transformation groups. Proc. Lond. Math. Soc. 28, 381–390 (1897)
- M. Chen, N.C. Menicucci, O. Pfister, Experimental realization of multipartite entanglement of 60 modes of a quantum optical frequency comb. Phys. Rev. Lett. 112, 120505 (2014)
- T.-P. Cheng, L.-F. Li, *Gauge Theory of Elementary Particle Physics* (Oxford Science Publications, Clarendon Press, Oxford University Press, Oxford [Oxfordshire], New York, 1984)
- A. Chenu, A.M. Brańczyk, G.D. Scholes, J.E. Sipe, Thermal light cannot be represented as a statistical mixture of single pulses. Phys. Rev. Lett. **114**, 213601 (2015)
- S. Chu, J.E. Bjorkholm, A. Ashkin, A. Cable, Experimental observation of optically trapped atoms. Phys. Rev. Lett. **57**, 314–317 (1986)
- J.B. Conway, *A Course in Functional Analysis*. Graduate Texts in Mathematics, vol. 96, 2nd edn. (Springer, New York, 1997)
- J.F. Corney, M.K. Olsen, Non-Gaussian pure states and positive Wigner functions. Phys. Rev. A 91, 023824 (2015)
- J. Dalibard, C. Cohen-Tannoudji, Dressed-atom approach to atomic motion in laser light: the dipole force revisited. J. Opt. Soc. Am. B 2, 1707 (1985)
- J. Dalibard, C. Cohen-Tannoudji, Laser cooling below the Doppler limit by polarization gradients: simple theoretical models. J. Opt. Soc. Am. B 6, 2023 (1989)
- K.R. Davidson, C*-Algebras by Example. Fields Institute Monographs, vol. 6 (American Mathematical Society, Providence, 1996)
- E.B. Davies, Irreversible dynamics of infinite fermion systems. Commun. Math. Phys. **55**, 231–258 (1977)
- K.B. Davis, M.O. Mewes, M.R. Andrews, N.J. van Druten, D.S. Durfee, D.M. Kurn, W. Ketterle, Bose-Einstein condensation in a gas of sodium atoms. Phys. Rev. Lett. **75**, 3969–3973 (1995)
- A.M.O. de Almeida, The Weyl representation in classical and quantum mechanics. Phys. Rep. **295**, 265–342 (1998)
- G.J. De Valcarcel, G. Patera, N. Treps, C. Fabre, Multimode squeezing of frequency combs. Phys. Rev. A 74, 061801 (2006)
- J. Dereziński, Introduction to representations of the canonical commutation and anticommutation relations, in *Large Coulomb Systems*, ed. by J.D.P. Dr, H.S.P. Dr. Lecture Notes in Physics, vol. 695 (Springer, Berlin, 2006), pp. 63–143
- B. Dierckx, M. Fannes, M. Pogorzelska, Fermionic quasifree states and maps in information theory. J. Math. Phys. **49**, 032109 (2008)
- J.D. Dixon, B. Mortimer, *Permutation Groups*. Graduate Texts in Mathematics, vol. 163 (Springer, New York, 1996)
- A. Einstein, Quantentheorie des einatomigen idealen Gases. Zweite Abhandlung, in *Albert Einstein: Akademie-Vorträge*, ed. by E.D. Simon (Wiley-VCH Verlag GmbH & Co. KGaA, 2005), pp. 245–257
- T. Engl, J. Dujardin, A. Argüelles, P. Schlagheck, K. Richter, J.D. Urbina, Coherent backscattering in Fock space: a signature of quantum many-body interference in interacting bosonic systems. Phys. Rev. Lett. **112**, 140403 (2014)
- D.E. Evans, Y. Kawahigashi, *Quantum Symmetries on Operator Algebras*. Oxford Mathematical Monographs (Clarendon Press, Oxford, 1998)
- M. Fannes, A. Verbeure, Gauge transformations and normal states of the CCR. J. Math. Phys. 16, 2086–2088 (1975)
- G. Ferrini, J.P. Gazeau, T. Coudreau, C. Fabre, N. Treps, Compact Gaussian quantum computation by multi-pixel homodyne detection. New J. Phys. 15, 093015 (2013)
- W. Fulton, Young Tableaux: With Applications to Representation Theory and Geometry. London Mathematical Society Student Texts, vol. 35 (Cambridge University Press, Cambridge, 1997)

References 261

T.A. Fulton, G.J. Dolan, Observation of single-electron charging effects in small tunnel junctions. Phys. Rev. Lett. **59**, 109–112 (1987)

- S. Gerke, J. Sperling, W. Vogel, Y. Cai, J. Roslund, N. Treps, C. Fabre, Full multipartite entanglement of frequency-comb Gaussian states. Phys. Rev. Lett. 114, 050501 (2015)
- R.J. Glauber, Coherent and incoherent states of the radiation field. Phys. Rev. **131**, 2766–2788 (1963a)
- R.J. Glauber, The quantum theory of optical coherence. Phys. Rev. 130, 2529–2539 (1963b)
- N. Goldman, J. Dalibard, Periodically driven quantum systems: effective Hamiltonians and engineered gauge fields. Phys. Rev. X 4, 031027 (2014)
- D. Griffiths, Introduction to Elementary Particles (WILEY-VCH, Weinheim, 2004)
- G. Grynberg, A. Aspect, C. Fabre, *Introduction to Quantum Optics: From the Semi-classical Approach to Quantized Light* (Cambridge University Press, Cambridge, 2010)
- M. Hamermesh, *Group Theory and Its Application to Physical Problems. Dover Books on Physics and Chemistry* (Dover Publications, New York, 1989)
- W. Hänsel, P. Hommelhoff, T.W. Hänsch, J. Reichel, Bose-Einstein condensation on a microelectronic chip. Nature 413, 498–501 (2001)
- F. Hausdorff, Die symbolische Exponentialformel in der Gruppentheorie. Leipz. Berichte **58**, 19–48 (1906)
- W. Heisenberg, Über den anschaulichen Inhalt der quantentheoretischen Kinematik und Mechanik.
 Z. Phys. 43, 172–198 (1927)
- E.J. Heller, Bound-state eigenfunctions of classically chaotic Hamiltonian systems: scars of periodic orbits Phys. Rev. Lett. 53, 1515–1518 (1984)
- J. Helsen, Structure of coherent fermionic states. Master thesis, KU Leuven, Leuven, 2015
- A. Hemmerich, T.W. Hänsch, Two-dimesional atomic crystal bound by light. Phys. Rev. Lett. **70**, 410–413 (1993)
- A.S. Holevo, Statistical Structure of Quantum Theory (Springer Science & Business Media, Berlin, 2001)
- C.K. Hong, Z.Y. Ou, L. Mandel, Measurement of subpicosecond time intervals between two photons by interference. Phys. Rev. Lett. **59**, 2044–2046 (1987)
- R.A. Horn, C.R. Johnson, *Matrix Analysis*, 23rd edn. (Cambridge University Press, Cambridge, 2010)
- R. Hudson, When is the wigner quasi-probability density non-negative? Rep. Math. Phys. **6**, 249–252 (1974)
- K. Husimi, Some formal properties of the density matrix. J. Phys. Soc. Jpn. 22, 264–314 (1940)
- P. Jordan, E. Wigner, Über das Paulische äquivalenzverbot. Z. Phys. 47, 631–651 (1928)
- P. Kapitza, Viscosity of liquid helium below the λ -point. Nature **141**, 74–74 (1938)
- M. Kardar, Statistical Physics of Particles (Cambridge University Press, Cambridge, 2007)
- M. Karski, L. Förster, J.-M. Choi, A. Steffen, W. Alt, D. Meschede, A. Widera, Quantum walk in position space with single optically trapped atoms. Science **325**, 174–177 (2009)
- E.H. Kennard, Zur Quantenmechanik einfacher Bewegungstypen. Z. Phys. 44, 326–352 (1927)
- T. Kiesel, W. Vogel, Nonclassicality filters and quasiprobabilities. Phys. Rev. A 82, 032107 (2010)
- L. Landau, Theory of the superfluidity of helium II. Phys. Rev. 60, 356–358 (1941)
- R.B. Laughlin, Anomalous quantum hall effect: an incompressible quantum fluid with fractionally charged excitations. Phys. Rev. Lett. 50, 1395–1398 (1983)
- P. Leboeuf, M. Saraceno, Eigenfunctions of non-integrable systems in generalised phase spaces. J. Phys. A: Math. Gen. 23, 1745 (1990)
- P.D. Lett, R.N. Watts, C.I. Westbrook, W.D. Phillips, P.L. Gould, H.J. Metcalf, Observation of atoms laser cooled below the Doppler limit. Phys. Rev. Lett. 61, 169–172 (1988)
- F. London, The λ -phenomenon of liquid helium and the Bose-Einstein degeneracy. Nature **141**, 643–644 (1938)
- H. Maassen, Quantum probability and quantum information theory, in *Quantum Information, Computation and Cryptography*, ed. by F. Benatti, M. Fannes, R. Floreanini, D. Petritis. Lecture

- Notes in Physics, vol. 808 (Springer, Berlin, 2010), pp. 65–108. https://doi.org/10.1007/978-3-642-11914-9_3
- L. Mandel, E. Wolf, Optical Coherence and Quantum Optics (Cambridge University Press, Cambridge, 1995)
- O. Mandel, M. Greiner, A. Widera, T. Rom, T.W. Hänsch, I. Bloch, Coherent transport of neutral atoms in spin-dependent optical lattice potentials. Phys. Rev. Lett. **91**, 010407 (2003)
- A. Mandilara, E. Karpov, N.J. Cerf, Extending Hudson's theorem to mixed quantum states. Phys. Rev. A **79**, 062302 (2009)
- J. Manuceau, C*-algèbre de relations de commutation. Annales de l'I.H.P. Physique théorique 8, 139–161 (1968)
- J. Manuceau, A. Verbeure, Quasi-free states of the \$C.C.R.\$-algebra and Bogoliubov transformations. Commun. Math. Phys. 9, 293–302 (1968)
- P.A. Martin, Physique Statistique des Processus Irreversibles (Lecture Notes) (2004)
- C.L. Mehta, Diagonal coherent-state representation of quantum operators. Phys. Rev. Lett. 18, 752–754 (1967)
- C.L. Mehta, E.C.G. Sudarshan, Relation between quantum and semiclassical description of optical coherence. Phys. Rev. 138, B274–B280 (1965)
- B.J. Metcalf, N. Thomas-Peter, J.B. Spring, D. Kundys, M.A. Broome, P.C. Humphreys, X.-M. Jin, M. Barbieri, W. Steven Kolthammer, J.C. Gates, B.J. Smith, N.K. Langford, P.G.R. Smith, I.A. Walmsley, Multiphoton quantum interference in a multiport integrated photonic device. Nat. Commun. 4, 1356 (2013)
- W.H. Miller, On the relation between the semiclassical initial value representation and an exact quantum expansion in time-dependent coherent states. J. Phys. Chem. B 106, 8132–8135 (2002)
- C. Moore, S. Mertens, The Nature of Computation (Oxford University Press, Oxford, 2011)
- P.J. Mosley, J.S. Lundeen, B.J. Smith, P. Wasylczyk, A.B. U'Ren, C. Silberhorn, I.A. Walmsley, Heralded generation of ultrafast single photons in pure quantum states. Phys. Rev. Lett. 100, 133601 (2008)
- N.F. Mott, The basis of the electron theory of metals, with special reference to the transition metals. Proc. Phys. Soc. A **62**, 416 (1949)
- J.E. Moyal, Quantum mechanics as a statistical theory. Math. Proc. Camb. 45, 99–124 (1949)
- M. Neumark, On a representation of additive operator set functions. C. R. (Dokl.) Acad. Sci. URSS 41, 359–361 (1943)
- C. Orzel, A.K. Tuchman, M.L. Fenselau, M. Yasuda, M.A. Kasevich, Squeezed states in a Bose-Einstein condensate. Science 291, 2386–2389 (2001)
- B. Paredes, A. Widera, V. Murg, O. Mandel, S. Fölling, I. Cirac, G.V. Shlyapnikov, T.W. Hänsch, I. Bloch, Tonks-Girardeau gas of ultracold atoms in an optical lattice. Nature **429**, 277–281 (2004)
- J. Park, J. Zhang, J. Lee, S.-W. Ji, M. Um, D. Lv, K. Kim, H. Nha, Testing nonclassicality and non-Gaussianity in phase space. Phys. Rev. Lett. 114, 190402 (2015)
- W. Pauli, The connection between spin and statistics. Phys. Rev. 58, 716–722 (1940)
- W. Pauli, On the connection between spin and statistics. Prog. Theor. Phys. 5, 526–543 (1950)
- G.K. Pedersen, Analysis Now (Springer, New York, 1989)
- A. Peruzzo, M. Lobino, J.C.F. Matthews, N. Matsuda, A. Politi, K. Poulios, X.-Q. Zhou, Y. Lahini, N. Ismail, K. Wörhoff, Y. Bromberg, Y. Silberberg, M.G. Thompson, J.L. OBrien, Quantum walks of correlated photons. Science 329, 1500–1503 (2010)
- D. Petz, An Invitation to the Algebra of Canonical Commutation Relations. Leuven Notes in Mathematical and Theoretical Physics Series A, vol. 2 (Leuven University Press, Leuven, 1990)
- W.D. Phillips, H. Metcalf, Laser deceleration of an atomic beam. Phys. Rev. Lett. 48, 596–599 (1982)
- Y.-S. Ra, M.C. Tichy, H.-T. Lim, O. Kwon, F. Mintert, A. Buchleitner, Y.-H. Kim, Nonmonotonic quantum-to-classical transition in multiparticle interference. PNAS 110, 1227–1231 (2013a)
- Y.-S. Ra, M.C. Tichy, H.-T. Lim, O. Kwon, F. Mintert, A. Buchleitner, Y.-H. Kim, Observation of detection-dependent multi-photon coherence times. Nat. Commun. 4, 2451 (2013b)

References 263

Y.-S. Ra, C. Jacquard, A. Dufour, C. Fabre, N. Treps, Tomography of a mode-tunable coherent single-photon subtractor. Phys. Rev. X 7, 031012 (2017)

- H.P. Robertson, The uncertainty principle. Phys. Rev. 34, 163–164 (1929)
- D.W. Robinson, A theorem concerning the positive metric. Commun. Math. Phys. 1, 89–94 (1965)
- J. Roslund, R.M. de Araújo, S. Jiang, C. Fabre, N. Treps, Wavelength-multiplexed quantum networks with ultrafast frequency combs. Nat. Photonics8, 109–112 (2014)
- L. Sansoni, F. Sciarrino, G. Vallone, P. Mataloni, A. Crespi, R. Ramponi, R. Osellame, Two-particle bosonic-fermionic quantum walk via integrated photonics. Phys. Rev. Lett. **108**, 010502 (2012)
- W. Schleich, Quantum Optics in Phase Space (Wiley-VCH, Berlin, 2001)
- E. Schrödinger, Der stetige übergang von der Mikro- zur Makromechanik. Naturwissenschaften 14, 664–666 (1926a)
- J. Schwinger, The theory of quantized fields. I. Phys. Rev. 82, 914–927 (1951)
- M.O. Scully, M.S. Zubairy, Quantum Optics (Cambridge University Press, Cambridge, 1997)
- J. Slawny, On factor representations and theC*-algebra of canonical commutation relations. Commun. Math. Phys. 24, 151–170 (1972)
- F. Soto, P. Claverie, When is the Wigner function of multidimensional systems nonnegative? J. Math. Phys. 24, 97–100 (1983)
- W. Stinespring, Positive functions on C*-algebras. Proc. Am. Math. Soc. 6, 211 (1955)
- M.H. Stone, Linear transformations in Hilbert space: III. Operational methods and group theory. PNAS 16, 172–175 (1930)
- M.H. Stone, On one-parameter unitary groups in Hilbert space. Ann. Math. 33, 643 (1932)
- X. Su, Y. Zhao, S. Hao, X. Jia, C. Xie, K. Peng, Experimental preparation of eight-partite cluster state for photonic qumodes. Opt. Lett. 37, 5178–5180 (2012)
- E.C.G. Sudarshan, Equivalence of semiclassical and quantum mechanical descriptions of statistical light beams. Phys. Rev. Lett. **10**, 277–279 (1963)
- M.C. Tichy, M. Tiersch, F. de Melo, F. Mintert, A. Buchleitner, Zero-transmission law for multiport beam splitters. Phys. Rev. Lett. 104, 220405 (2010)
- M.C. Tichy, H.-T. Lim, Y.-S. Ra, F. Mintert, Y.-H. Kim, A. Buchleitner, Fourphoton indistinguishability transition. Phys. Rev. A 83, 062111 (2011)
- M.C. Tichy, F. de Melo, M. Kuś, F. Mintert, A. Buchleitner, Entanglement of identical particles and the detection process. Fortschr. Phys. 61, 225–237 (2013)
- A. Verbeure, Many-Body Boson Systems: Half a Century Later, Theoretical and Mathematical Physics (Springer, London, 2011)
- J. von Neumann, Die Eindeutigkeit der Schrödingerschen Operatoren. Math. Ann. **104**, 570–578 (1931)
- J. von Neumann, Über Einen Satz Von Herrn M. H. Stone. Ann. Math. 33, 567 (1932)
- M. Walschaers, Counting messages of quantum sources. Master thesis, KU Leuven, 2011
- M. Walschaers, C. Fabre, V. Parigi, N. Treps, Entanglement and wigner function negativity of multimode non-gaussian states. Phys. Rev. Lett. 119, 183601 (2017)
- H. Weyl, Gruppentheorie und Quantenmechanik (Hirzel, Leipzig, 1928)
- J.-I. Yoshikawa, S. Yokoyama, T. Kaji, C. Sornphiphatphong, Y. Shiozawa, K. Makino, A. Furusawa, Invited article: generation of one-million-mode continuous-variable cluster state by unlimited time-domain multiplexing. APL Photonics 1, 060801 (2016)

Chapter 8 Many-Particle Interference



"O brave new world!"

John in "Brave new World" (Huxley 1932)

8.1 Introduction

After the extensive discussion of bosonic and fermionic structures, we now dig deeper into the dynamical properties of these particles. More specifically, we focus on the concept of true indistinguishability and the additional interference effects arising because of it—even in the absence of physical interaction between the particles (Tichy 2011; Tichy et al. 2010, 2012). These many-body interferences are still rather poorly understood and not too much research has been done on them. The reason is that there are few many-particle systems with sufficient control that allow to treat non-Gaussian states (e.g. number states), which are required to see such fundamental quantum effects. For example, in well-controlled settings as photonics it is very difficult to generate number states, since one usually starts out from coherent or thermal light sources (Aspect et al. 1982; Ates et al. 2009; Eibl et al. 2003; Grice et al. 1998; Grice and Walmsley 1997; Huang et al. 2011; Kwiat et al. 1995; Metcalf et al. 2013; Mosley et al. 2008; Ou et al. 1999; Ra et al. 2013a; Santori et al. 2001, 2002; Tichy et al. 2011). On the other hand, ultra-cold atoms setups usually lack sufficient control to resolve these interference effects, because they suffer from a lot of decoherence (Anderson et al. 1995; Andrews et al. 1997; Bloch et al. 2008; Chu 2002; Davis et al. 1995; Deslauriers et al. 2006; Harber et al. 2003; Turchette et al. 2000). More recently, however, both photonics (Crespi et al. 2013; Metcalf et al. 2013; Peruzzo et al. 2010; Sansoni et al. 2012; Spagnolo et al. 2014; Spring et al. 2013) and ultra-cold atom (or ion) experiments (Ahlbrecht et al. 2012; Genske et al. 2013; Köhl et al. 2005; Leibfried et al. 2004; Müller et al. 2011; Preiss et al. 2015; Schneider et al. 2012; Sherson et al. 2010) have started to reach regimes where such effects can be probed, urging also for deeper theoretical understanding.

On the theory side, there has been some work in the context of the Hong-Ou-Mandel effect (Hong et al. 1987). However, for a long time this remained limited to a two-particle setting. There was never much interest in solving truly *many*-body problems. Even though the condensed-matter and chemical physics communities deal with the dynamics of genuine many-body systems, they usually try to avoid full-blown many-body calculations by using density functional theory (Burke et al. 2005) or Hartree-Fock (Alicki and Fannes 2001; Negele and Orland 1998). These methods make approximations on the quantum states, and, in the latter case, push them to the Gaussian realm.

Nevertheless, in the mathematical physics, quantum statistical mechanics, quantum chaos, and quantum information communities interest has reached out to complicated many-body states, via the development of, for example, finitely-correlated states (Fannes et al. 1994, 1992; Verstraete et al. 2008). However, most of these works focus on determining ground- and thermal states, rather than on dynamical applications (Schuch et al. 2011; Verstraete and Cirac 2006). On the other hand, several fields, such as nuclear (Benet and Weidenmüller 2003; Benet et al. 2001; Bethe and Bacher 1936) and atomic (Tanner et al. 2000) physics naturally deal with genuine n-particle wave functions. Moreover, n-particle dynamics has been studied in relation to quantum chaos, both for cold atoms (Buchleitner and Kolovsky 2003; Kolovsky and Buchleitner 2003; Ponomarev and Kolovsky 2006; Ponomarev et al. 2006) and in a more abstract RMT setting (Kaplan and Papenbrock 2000). Recently, attention for the dynamical properties of many-particle dynamics was boosted significantly when topics such as quantum walks (Ahlbrecht et al. 2012; Genske et al. 2013; Hamilton et al. 2014; Hein and Tanner 2010; Peruzzo et al. 2010; Preiss et al. 2015) and boson sampling (Aaronson and Arkhipov 2013; Broome et al. 2013; Crespi et al. 2013; Shen et al. 2014; Spagnolo et al. 2014; Spring et al. 2013; Tillmann et al. 2013) appeared on the stage.

Also from a fundamental quantum transport and complex systems point of view, the dynamics in systems described by number states is remarkably interesting and fascinating. The Hong-Ou-Mandel (HOM) effect, which we consider in detail throughout Sect. 8.3.4, indicates that bosons which meet in a beamsplitter (see Sect. 8.2.2) always have an enhanced probability of coming out in the same direction, thus they bunch. The opposite is true for fermions, which actually can never come out in the same direction, hence two fermions antibunch. One therefore sees completely opposite behaviour for two fermions and two bosons. This no longer holds when we consider larger beamsplitter arrays in which more than two particles are injected. One of the first systematic studies of these effects can be found in the PhD work of Malte C. Tichy (Tichy 2011), where notably a suppression law was proven: In beamsplitter arrays with specific symmetry properties, transitions from a given class of input states to a given class of output states are completely suppressed (Tichy et al. 2010, 2014). Intriguingly, there are events which are suppressed both for fermions and for bosons, and, hence, although bosons and fermions clearly behave differently from each other, they are not as complementary as the HOM scenario suggests. There is much more to bosons than HOM-like bunching behaviour: One witnesses a wide range of novel many-particle interference phenomena, exclusively due to the indistinguishability

8.1 Introduction 267

of the particles, and in the absence of any interaction between the particles (Mayer 2012; Tichy 2014): These phenomena still lack a unified understanding, which motivated this chapter of the current dissertation.

We explore the properties of many-body interferences in a complex systems setup, and mainly focus on the unitary evolution or scattering of non-interacting particles, either fermions or bosons. We start the chapter by reviewing some aspects of closed system dynamics of non-interacting particles in the framework of Fock space, and we focus our attention on optical implementations. There are two different frameworks how to deal with these many-particle interference effects: The one strongly focusses on the initial and final wave function, treating the problem in a Schrödinger picture, whereas the other focusses on the process of measuring the output event. A measurement-inspired approach makes the logical connection to correlation functions and decoherence. These aspects are crucial for the final purpose we are after: the certification of *boson sampling*.

Apart from aspects presented in Sect. 8.4, and the results on the certification of boson sampling in Sect. 8.5, the physics described in this chapter is known. However, it is here treated in a slightly different, and original, mathematical framework, which eases the treatment, for example, of non-orthogonal modes. Not only is this chapter therefore complementary to much of what is known from the common atomic and optical physics literature dealing with many-particle quantum systems. By sticking to a basis-independent description as much as possible this text can also be considered a generalisation of most of these known results to sets of particles with non-orthogonal wave functions.

8.2 Dynamics of Non-interacting Particles

Throughout this chapter we consider a system that is closed and where the dynamics or the transport of particles can therefore be treated as a unitary channel (recall (2.48)). At the very foundations of such an approach lies a Hamiltonian equation of motion, be it in Schrödinger, von Neumann or Heisenberg form. We first derive the formalism to treat Hamiltonian dynamics, and later on divert to a more general picture. Since we assume to deal with states containing a finite, well-controlled number of particles, it is sufficient to limit ourselves to a Fock space description of the system and its dynamics.

¹Later in Chap. 9 we explore particle transport properties in open systems where the number of particles is allowed to fluctuate.

8.2.1 Unitary Dynamics

We start out by considering a single-particle Hilbert space \mathcal{H} on which we construct the Fock space $\Gamma^{b/f}(\mathcal{H})$. As discussed in Chap. 2, we may consider the Hamiltonian dynamics of any observable \mathcal{D} (in this case acting on Fock space) as generated by the *Heisenberg* equation of motion

$$\frac{\mathrm{d}}{\mathrm{d}t}\mathfrak{O} = i[\mathcal{H}, \mathfrak{O}]. \tag{8.1}$$

Here, \mathcal{H} is a self-adjoint, time-independent operator on Fock space, $\mathcal{H}=\mathcal{H}^{\dagger}$, which we consider to be a polynomial in creation and annihilation operators. Formally we may solve equation (8.1) by defining a unitary map $\mathcal{U}_t: \mathcal{B}(\Gamma^{b/f}(\mathcal{H})) \to \mathcal{B}(\Gamma^{b/f}(\mathcal{H}))$, which propagates observables according to the dynamics described by Eq. (8.1). This mapping is given by

$$\mathfrak{O} \mapsto \mathcal{U}_t(\mathfrak{O}) := \exp(it[\mathfrak{H}, .])\mathfrak{O} = e^{it\mathfrak{H}}\mathfrak{O}e^{-it\mathfrak{H}}.$$
 (8.2)

All relevant information about the dynamics is hidden in the unitary operator $\mathfrak{U}(t) := e^{-it\mathcal{H}}$. For a general Hamiltonian, the explicit evaluation of the action of such a propagator can be expected to range from tricky to simply impossible, but under given conditions, we can cast the object in a far more useful form: In this chapter we deal with the dynamics of *non-interacting* particles, which considerably simplifies both the Hamiltonian \mathcal{H} and the unitary propagator $\mathfrak{U}(t)$.

Assuming that the particles are *non-interacting* implies that there can be no terms in $\mathcal H$ which couple different particles. In other words, each particle sees exactly the same Hamiltonian and this automatically brings us to the choice

$$\mathcal{H} = \Gamma(H), \quad H \in \mathcal{B}(\mathcal{H}).$$
 (8.3)

Hence (recall (7.89) and (7.92) and our discussion in Sect. 7.5), the Hamiltonian is a single-particle observable in second quantisation.³ This allows us to use the properties of the second quantisation, more specifically the one captured in Eq. (7.115), to obtain

$$\mathfrak{U}(t) = e^{-it\Gamma(H)} = E\left(e^{-itH}\right). \tag{8.4}$$

This leads to the more general idea that a *single-particle unitary channel* on Fock space, given by " \mathfrak{U}_1^{\dagger} . \mathfrak{U}_1 ", can always be described by a propagator

$$\mathfrak{U}_1 = E(U), \tag{8.5}$$

²Because the creation and annihilation operators are generators of the algebra of observables, this requirement is logical.

³Since the derivations in this section hold both for fermions and bosons, we omit, for the time being, the index f/b in the second quantisation operators Γ , originally defined in (7.89).

where U is a unitary operator on \mathcal{H} . We can perform a consistency check by using (7.108)–(7.115) to obtain

$$\mathfrak{U}_1^{\dagger}\mathfrak{U}_1 = E(U)^{\dagger}E(U) = E(U^{\dagger}U) = E(\mathbb{1}_{\mathcal{H}}) = \mathbb{1}_{\Gamma(\mathcal{H})}.$$
 (8.6)

Let us focus on the transformation of creation or annihilation operators under (8.5). By virtue of (7.108)–(7.115), the unitary channel acts, for any $\psi \in \mathcal{H}$, as

$$a^{\dagger}(\psi) \mapsto \mathfrak{U}_{1}^{\dagger} a^{\dagger}(\psi) \mathfrak{U}_{1} = E(U^{\dagger}) a^{\dagger}(\psi) E(U) = a^{\dagger}(U^{\dagger}\psi) E(U^{\dagger}) E(U) = a^{\dagger}(U^{\dagger}\psi) \tag{8.7}$$

Notice that a completely similar calculation leads to

$$a(\psi) \mapsto a(U^{\dagger}\psi), \quad \psi \in \mathcal{H}.$$
 (8.8)

We may now use (7.108)–(7.115) to directly generalise this mapping for any normally ordered monomial⁴ of creation and annihilation operators. A simple calculation shows that

$$E(U^{\dagger})a^{\dagger}(\psi_{1})\dots a^{\dagger}(\psi_{n})a(\psi_{m})\dots a(\psi_{1})E(U)$$

$$= a^{\dagger}(U^{\dagger}\psi_{1})\dots a^{\dagger}(U^{\dagger}\psi_{n})a(U^{\dagger}\psi_{m})\dots a(U^{\dagger}\psi_{1}).$$
(8.9)

This implies that we can consistently identify such a single-particle unitary channel with the *-automorphism $a(\psi) \mapsto a(U^{\dagger}\psi)$, which is actually completely equivalent to the Bogoliubov transformations (7.180) or (7.241)—depending on which particle type we consider—with V=0 or B=0, respectively. To connect these results back to the original idea of single-particle dynamics, generated by a Hamiltonian $\Gamma(H)$, with $H \in \mathcal{B}(\mathcal{H})$, we describe the evolution by means of the evolution of creation and annihilation operators⁵

$$a^{\#}(\psi) \mapsto a^{\#}(e^{itH}\psi), \tag{8.10}$$

or, equivalently, via the Bogoliubov transformation $\mathcal{B}_{e^{itH},0}$ (recall (7.180), (7.181) and (7.241)).

Alternatively, in the *Schrödinger* picture, we focus on the dynamics of functionals on our relevant *-algebra of observables. This is typically a difficult task to accomplish, but under certain circumstances and for specific initial states, it turns out to be a very suitable approach. Indeed, the single-particle unitary channels which we consider throughout this chapter provide exactly such circumstances. The dynamics of a wave function is generated by Schrödinger's equation as

$$\frac{\partial}{\partial t}\Psi = -i\Gamma(H)\Psi,\tag{8.11}$$

^{4&}quot;Normally ordered" (Davies 1977a) refers to monomials where all creation operators are ordered on the left, whereas all annihilation operators are on the right.

⁵Note that $a^{\#}$ is a collective term for a^{\dagger} and a, i.e. (8.10) holds for, both, creation and annihilation operators.

what implies

$$\Psi(t) = \exp(-it\Gamma(H))\Psi_0 = E(e^{-itH})\Psi_0, \tag{8.12}$$

such that we again find the familiar propagator. Instead of such continuous description of the time evolution we can consider a general unitary channel⁶ defined by the map

$$\Psi \mapsto \mathfrak{U}_1 \Psi, \quad \Psi \in \Gamma(\mathcal{H}), \quad \|\Psi\| < \infty.$$
 (8.13)

Now let us assume that our initial wave function describes an n-particle number state given as

$$\Psi_0 = a^{\dagger}(\psi_1) \dots a^{\dagger}(\psi_n) \Omega. \tag{8.14}$$

We may again use property (7.113) to derive that

$$\mathfrak{U}_1 \Psi_0 = E(U) a^{\dagger}(\psi_1) \dots a^{\dagger}(\psi_n) \Omega = a^{\dagger}(U\psi_1) \dots a^{\dagger}(U\psi_n) E(U) \Omega. \tag{8.15}$$

Let us now write the explicit expressions for E(U) and Ω , according to (7.106), (7.107) and (7.40), respectively, such that

$$E(U)\Omega = \Big(1 \oplus U \oplus (U \otimes U)|_{s/a} \oplus \dots\Big)\Big(1 \oplus 0 \oplus 0 \oplus \dots\Big) = \Omega.$$
 (8.16)

Consequently, the channel's action on the number state Ψ_0 reads

$$\Psi_0 \mapsto \mathfrak{U}_1 \Psi_0 = a^{\dagger}(U\psi_1) \dots a^{\dagger}(U\psi_n) \Omega. \tag{8.17}$$

This implies that we can in principle also describe the dynamics as

$$a^{\dagger}(\psi) \mapsto a^{\dagger}(U\psi), \quad \psi \in \mathcal{H}.$$
 (8.18)

The U in (8.18) appears to be in contrast to the U^{\dagger} in (8.8). Note that, both, in the Heisenberg and in the Schrödinger picture, we are able to connect a mapping (8.8) or (8.18) of the creation and annihilation operators, depending on the picture, to a transformation on the single-particle Hilbert space \mathcal{H} , given by $\psi \mapsto U^{\dagger}\psi$ in the Heisenberg picture, and $\psi \mapsto U\psi$ in the Schrödinger picture. This is exactly what is needed, since the physically relevant objects are expectation values $\langle \mathfrak{D} \rangle$ of observables. To obtain a physically reasonable mapping, we must make sure that it consistently describes the transformation of $\langle \mathfrak{D} \rangle$ under \mathfrak{U}_1 :

$$\langle \mathfrak{O} \rangle \mapsto \langle \mathfrak{O} \rangle_{\mathfrak{U}_1}.$$
 (8.19)

To provide a plausible argument that (8.8) and (8.18) are indeed consistent, let us consider a very simple example, which can easily be extended to more complicated

⁶In the Schrödinger picture.

situations. Assume that we consider $\mathfrak{O}=a^{\dagger}(\psi_1)a(\psi_2)^7$ and a state $\langle . \rangle$ generated by the wave function $a^{\dagger}(\phi)\Omega$. This implies that, in the Heisenberg picture,

$$\langle \mathfrak{O} \rangle \mapsto \langle a^{\dagger}(\phi)\Omega, a^{\dagger}(U^{\dagger}\psi_{1})a(U^{\dagger}\psi_{2})a^{\dagger}(\phi)\Omega \rangle = \langle \phi, U^{\dagger}\psi_{1} \rangle \langle U^{\dagger}\psi_{2}, \phi \rangle, \quad (8.20)$$

whereas in the Schrödinger picture

$$\langle \mathfrak{O} \rangle \mapsto \langle a^{\dagger}(U\phi)\Omega, a^{\dagger}(\psi_1)a(\psi_2)a^{\dagger}(U\phi)\Omega \rangle = \langle U\phi, \psi_1 \rangle \langle \psi_2, U\phi \rangle.$$
 (8.21)

Indeed, the two pictures are consistent, and the apparent contradiction between (8.8) and (8.18) is actually a necessity for the consistency of both pictures.

8.2.2 Beamsplitters*

Beamsplitters are very standard in quantum optics, but to those not familiar with this field there are several details which are easily overlooked. Because these details are important to our discussion, we explicitly present them here. Ultimately, the key result of this section is the structure of the complete Hilbert space (8.34), and the beamsplitter's action (8.35). Often the additional $\mathcal{L}^2(\mathbb{R})$ degree of freedom of the beam is treated implicitly. However, these additional degrees of freedom are crucial for our discussion on partial distinguishability in Sects. 8.3.4, 8.4.2 and 8.5.3.

We zoom in on one of the most important objects in (quantum) optics: the beam-splitter. As the name suggests the main action of a beamsplitter on an electromagnetic field is splitting it in two (Born and Wolf 1999; Stokes 1849). The incoming electric field \vec{E} is split in a reflected (under a given angle) component \vec{E}_r and a transmitted component \vec{E}_t . We can denote that for the *amplitudes*

$$E_r = RE$$
 and $E_t = TE$, (8.22)

where *R* and *T* are the reflection and transmission coefficients, respectively. A sketch of this process is presented in Fig. 8.1. Since the total energy in the beams should be conserved if there is no absorption in the dielectric medium, we obtain the relation

$$|E|^2 = |E_r|^2 + |E_t|^2$$
, and thus $|T|^2 + |R|^2 = 1$. (8.23)

One may wonder how one can quantise such an operation in a correct way. A standard way of doing this is to quantise the classical light field and derive the action of the beamsplitter starting out from (8.22) (Campos et al. 1989; Grynberg et al. 2010; Mandel and Wolf 1995; Schleich 2001). Alternatively, however, one may also start from quantum theory and propose a reasonable model, which can later on be shown to

⁷Which is actually not an observable, but rather a coherence (between the particles in modes ψ_1 and ψ_2).

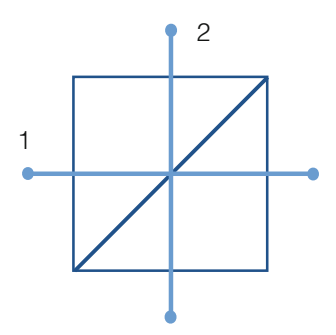


Fig. 8.1 Sketch of a beamsplitter. An input beam may be injected from either side 1 or 2 (or from both simultaneously) and will de divided in two outgoing beams, travelling on in both directions. The amount of a beam which is reflected versus the amount that is transmitted is governed by the transmission and reflection coefficients T and R, respectively (see main text)

be consistent with the classical approach. We opt for the latter method and omit rigour for the time being. Notice that, since we consider an optics setting, we automatically assume to be working with bosons, unless explicitly stated otherwise.

To reach a reasonable quantum mechanical model for the beamsplitter, we must realise what it actually does: It divides a single beam of light into two outgoing beams. The frequency of the electromagnetic wave typically remains the same for the incoming and outgoing beam, as long as we assume that there is no additional nonlinear optics involved, and the intensity of the incoming light beam is equal to the sum of the intensities of the outgoing beam (in the absence of absorption and other losses). Without going into quantum field theory, we ask the very basic question what a beam of light intuitively is. Typically, this question is answered by saying that a light beam is an ensemble of photons. The intensity of a light beam is then proportional to the number of photons, which means that, when an ensemble of n(with $n \gg 1$) photons hits the beamsplitter, $|T|^2 n$ of them are transmitted, whereas $|R|^2 n$ of them are reflected. To reach the limit of classical light, we typically need huge quantities of photons (hence $n \gg 1$), but we might wonder what happens when we make n smaller. The quantum nature of light makes sure that on average $|T|^2 n$ photons are transmitted, whereas $|R|^2 n$ of them are reflected. Now going even further down in particle number, we ultimately reach the regime with a single particle. What happens as one single photon collides with the beamsplitter? It is either transmitted or reflected, and quantum mechanically this means that a photon with the input wave function ψ is transferred to

$$\psi \mapsto r\psi_r + t\psi_t \qquad |r|^2 + |t|^2 = 1,$$
 (8.24)

where ψ_r is the reflected wave function and ψ_t the transmitted one. We assume that the two outgoing states are as different as they can be, such that $\langle \psi_t, \psi_r \rangle = 0$. This implies that we treat the photons as (Gaussian) wave packets with a well-defined momentum. This is consistent to the picture of a beam which is confined in

the transverse direction. In our effective description, $\langle \psi_t, \psi_r \rangle = 0$ thus implies that outgoing wave packets in direction 1 do not have overlap with those in direction 2. The whole process can be described using pure states and we work in a Schrödinger picture. The quantum mechanical probability amplitudes r and t must now be such that they consistently reproduce the classical behaviour (8.23) in the large n limit.

Approaching the large n limit can be done by lifting everything to a Fock space description, hence describing the action of the beamsplitter as

$$a^{\dagger}(\psi) \mapsto a^{\dagger}(r\psi_r + t\psi_t) = r a^{\dagger}(\psi_r) + t a^{\dagger}(\psi_t),$$
 (8.25)

which can be extended for a bunch of photons $\Psi = \frac{1}{\sqrt{n!}} a^{\dagger} (\psi)^n \Omega$ to

$$\Psi \mapsto \frac{1}{\sqrt{n!}} \left(r \, a^{\dagger}(\psi_r) + t \, a^{\dagger}(\psi_t) \right)^n \Omega = \frac{1}{\sqrt{n!}} \sum_{k=0}^n \binom{n}{k} r^k t^{n-k} a^{\dagger}(\psi_r)^k a^{\dagger}(\psi_t)^{n-k} \Omega, \tag{8.26}$$

which ultimately implies that the expected number $\langle \hat{n}_r \rangle$ of particles which is reflected is given by $n |r|^2$, where n is the total number of particles in the initial state. If we now enter the regime of large n, the central limit theorem makes the fluctuations around the average smaller and we recover that, indeed, $|R|^2 = |r|^2$, and, equivalently, $|T|^2 = |t|^2$. However, one may wonder whether the description of a classical light field in terms of a number state is really the correct classical limit. It turns out that this is not really the case.

When introducing the Wigner representation in Sect. 7.6.4, we argued that the classical pure states are actually the Gaussian states. Due to its similarity to a point in phase space, it can be argued that the coherent state is nearest to the typical setting of classical physics. Therefore, Eq. 8.26 does not lead to the most classical behaviour, because it does not start from the most classical input state. Nevertheless, we assume that relation (8.25) defines the action of the beamsplitter on a creation operator. It follows from (7.71), (7.152) that a coherent pure state $\Psi_{\alpha} \in \Gamma^b(\mathcal{H})$, which is generated in the input mode of the beamsplitter, can be represented as

$$\Psi_{\alpha} = e^{-|\alpha|^2/2} \exp\left(\alpha a^{\dagger}(\psi)\right) \Omega, \quad \alpha \in \mathbb{C}. \tag{8.27}$$

To make the discussion on beamsplitters more realistic, we must treat the problem in terms of *beams*. A beam describes light with a clear direction of propagation, whereas in the transverse direction, the intensity of the light is confined within a given shape. We limit ourselves to Gaussian beams, where its transverse intensity profile is described by a Gaussian with a given width. We assume that the waists of the incoming and outgoing beams in Fig. 8.1 are small, such that outside of the beamsplitter these beams do not interfere with each other. Having made this

⁸It will turn out that the output state of (8.26) describes very similar counting statistics to that of the output state for coherent light (8.31). This is a straightforward consequence of the law of large numbers.

assumption, we will not go into further detail on the transverse spatial modes and simply assume that these are the same for all photons in the beam.

Therefore, we may effectively model the structure of a beam by a single-particle Hilbert space $\mathcal{H}=\mathcal{L}^2(\mathbb{R})$, describing the propagation degree of freedom. Because we study two such beams, we effectively describe the full system as $\mathcal{H}_{tot}=\mathcal{L}^2(\mathbb{R})\oplus \mathcal{L}^2(\mathbb{R})$, where the first term in the direct sum describes direction 1 and the second term direction 2 of Fig. 8.1. Assuming there is only a beam injected from direction 1, we may rewrite Eq. (8.24) as

$$\begin{pmatrix} \psi \\ 0 \end{pmatrix} \mapsto \begin{pmatrix} t & \psi \\ r & \psi \end{pmatrix}. \tag{8.28}$$

This implies that the action of the beamsplitter on a coherent state

$$\Psi_{\alpha} = e^{-|\alpha|^2/2} \exp\left(\alpha a^{\dagger}(\psi \oplus 0)\right) \Omega, \quad \alpha \in \mathbb{C}, \tag{8.29}$$

is given by

$$\Psi_{\alpha} \mapsto e^{-|\alpha|^2/2} \exp\left\{\alpha \left(a^{\dagger} (r \psi \oplus t \psi)\right)\right\} \Omega. \tag{8.30}$$

We can now exploit the Fock space structure and the isomorphism $\Gamma^b(\mathcal{L}^2(\mathbb{R})) \oplus \mathcal{L}^2(\mathbb{R}) \cong \Gamma^b(\mathcal{L}^2(\mathbb{R})) \otimes \Gamma^b(\mathcal{L}^2(\mathbb{R}))$, with the specific mappings (7.55) and (7.56). To find an explicit description in terms of this tensor product structure, where each component in the product relates to a beam in a different direction, we may write that the beamsplitter actually acts as

$$\Psi_{\alpha} \mapsto \left(e^{-|t \, \alpha|^2/2} \exp\left\{\alpha \, t \, a^{\dagger}(\psi)\right\} \Omega_1 \right) \otimes \left(e^{-|r \, \alpha|^2/2} \exp\left\{\alpha \, r \, a^{\dagger}(\psi)\right\} \Omega_2 \right) = \Psi_{t \, \alpha} \otimes \Psi_{r \, \alpha}. \tag{8.31}$$

Notice that we simply split a coherent beam of light into a product of two coherent beams of light. To finally check consistency of this action with the classical beam splitter, we must understand how the energy is split. As the energy depends on the intensity, which is the expectation value of the particle number in each beam, we easily verify that the number of particles in the incoming beam is

$$\langle \hat{N}_{in} \rangle = |\alpha|^2 \,, \tag{8.32}$$

whereas for the reflected and transmitted beams, we obtain

$$\langle \hat{N}_r \rangle = |r|^2 |\alpha|^2$$
 and $\langle \hat{N}_t \rangle = |t|^2 |\alpha|^2$. (8.33)

This indeed confirms that it is consistent to state that |r| = |R| and |t| = |T|. The action of a beamsplitter is nothing else than a scattering process such as those described in Sect. 2.6. One should note that, in principle, in a microscopic derivation (by considering the beamsplitter as a box potential for example) one obtains that t and r are actually frequency-dependent. For perfectly monochromatic light, this is

not problematic, but once we inject wave packets, one may see some effects. For the bandwidths used in many optical experiments, these effects are typically negligible for single beamsplitters.

Although the description using $\mathcal{H}_{tot} = \mathcal{L}^2(\mathbb{R}) \oplus \mathcal{L}^2(\mathbb{R})$ for the Fock space is convenient, we can consider a different approach which is less spatially oriented and more based on the actual degrees of freedom for the single particle. Notice that, indeed.

$$\mathcal{L}^2(\mathbb{R}) \oplus \mathcal{L}^2(\mathbb{R}) \cong \mathbb{C}^2 \otimes \mathcal{L}^2(\mathbb{R}), \tag{8.34}$$

and we clearly have a Hilbert space that labels the beams (\mathbb{C}^2) and another Hilbert space that describes the degree of freedom within the beam $(\mathcal{L}^2(\mathbb{R}))$. We can extend such a setup to so called multiport beamsplitters or beamsplitter arrays, which are discussed later in this chapter, by choosing \mathbb{C}^m rather than \mathbb{C}^2 . On the other hand, we may also replace the $\mathcal{L}^2(\mathbb{R})$ side, which is unaffected by the beamsplitter, by any other Hilbert space. The notation on the right hand side of (8.34) is particularly interesting, because we can describe the action of the beamsplitter by means of an operator $B \in \mathcal{M}_2$ (the space of 2×2 matrices),

$$B = \begin{pmatrix} t & r' \\ r & t' \end{pmatrix}. \tag{8.35}$$

No action is applied by (8.35) on the $\mathcal{L}^2(\mathbb{R})$ space, meaning that a typical photon travelling through the beamsplitter can be described by

$$\begin{pmatrix} 1 \\ 0 \end{pmatrix} \otimes \psi \mapsto (B \otimes 1) \left\{ \begin{pmatrix} 1 \\ 0 \end{pmatrix} \otimes \psi \right\} = \begin{pmatrix} t \\ r \end{pmatrix} \otimes \psi. \tag{8.36}$$

If we now assume that the beamsplitter can be used from the two input directions (labeled with 1 and 2 in Fig. 8.1) and also in the reversed direction, we obtain several consistency rules, which can all be summarised by the requirement that

$$B^{\dagger}B = BB^{\dagger} = 1. \tag{8.37}$$

In other words, the beamsplitter is described by a unitary transformation mixing the different beams. In this sense, the beamsplitter is nothing more than a single-particle unitary process, implying it is a special type of Bogoliubov transformation. This allows us to not only define it for bosons, but also for fermions.

Notice that we may consider the action of the beamsplitter on bosons in various equivalent ways:

$$a^{\dagger}(\psi) \mapsto a^{\dagger}(B\psi), \quad \psi \in \mathbb{C}^2.$$
 (8.38)

$$W(\psi) \mapsto W(B\psi), \quad \psi \in \mathbb{C}^2.$$
 (8.39)

We simplified the description somewhat, by ignoring the additional (spatial) degree of freedom and simply focusing on the beamsplitter's input modes \mathbb{C}^2 .

8.3 Many-Particle Interference: The Wave Function Approach

Now that we have extensively discussed the dynamics and transformations of noninteracting particles, and specifically studied beamsplitters as a paradigmatic example coming from the optics community, we can understand the interference phenomena which arise in such setups. There are essentially two methods for doing so, one is the wave function approach (which is represented in the Schrödinger picture) and the other, considered in the next section, is the measurement approach (which is treated in the Heisenberg picture). To understand which pathways, or different probability amplitudes, do interfere, we must consider a well-defined input and output state. ⁹ The paradigmatic example for a single-particle interference process is Young's doubleslit experiment. Classically, we expect the particle to go through one of the two slits with a certain probability. However, in quantum mechanics, as shown in Figs. 1.1 and 1.2, the final probability distribution on the detection screen is not an incoherent mixture of two probability distributions, but rather we see a spiked structure in the intensity profile. Young (Young 1804) originally identified these fringes as an unambiguous wave-like phenomenon which arises due to interference. The key point of this section is to convince the reader that Young's double slit experiment provides insufficient phenomenology to understand the interference phenomena in manyparticle processes, even when the particles are non-interacting.

Throughout this chapter, we devote our attention to number states of the specific type (7.116), which one may refer to as *elementary tensors*. In Appendix C we highlight the changes when one considers more general types of number states. More specifically, we show that, in this setting, some type of higher-order many-particle interference appears.

8.3.1 From Single-Particle to Many-Particle Interference

In Sect. 2.5, we provided the mathematical introduction to the main topic of interest in this dissertation: quantum interference. We learned that the phenomenology of the double slit in Sect. 1.1 and of Example 2.5.1 in Sect. 2.5, or the networks in Chap. 4, are clearly influenced by such interference effects. In those specific cases, the interferences occur between different single-particle pathways. This means that a particle's probability to be detected at a given position (or site) is not the same as the sum of the probabilities of individual pathways. In the networks this implies that we cannot add up different hopping processes, but have to solve Schrödinger's equation (recall (4.2)). In the scattering approach of Chap. 5, these pathways appear

⁹We were also confronted with this issue in Chap. 4, see e.g. p. 79.

as contributions to the scattering matrix. In all those discussions, we finally projected the system's state on a specific measurement state vector, which was localised at a specific position, and only then do we see the manifestation of interference effects in the *probability* density.

There is no reason, however, to limit this approach to single-particle Hilbert spaces. In what follows throughout this chapter, we focus on many-particle interference, which implies that we must translate (2.73) to the Fock space setting. Therefore, the initial state (.) is henceforth generated by a many-particle wave function $\Psi \in \Gamma(\mathcal{H})$. The final projector P_a is a projector on Fock space, which in Sect. 8.3 is considered a projector on a single state vector $\Xi \in \Gamma(\mathcal{H})$. We specifically study the influence of a single-particle unitary operation, as introduced in (8.5), on the interference pattern which arises. The most subtle aspect is to formally define the projectors $\{P_{h_i}\}\$, which contrast the obtained transition probability to what is expected from classical probability theory. We know that classically we can combine single-particle processes to a many-particle process via combinatorics. This approach is exact for distinguishable particles, as we will see in Sect. 8.3.4, but for indistinguishable particles additional interference terms appear. Rather than explicitly describing a set of projectors $\{P_{b_i}\}\$, which render particles distinguishable, we will use the incoherent mixture of combined single-particle probabilities to represent the expected outcome in the absence of interference effects.

In concreto, we classically consider a set of occupied input modes $I = \{\psi_1, \ldots, \psi_n\}$ and a set of occupied output modes $J = \{\xi_1, \ldots, \xi_n\}$. Between these modes, there are single-particle transition probabilities $p_{\psi_i \to \xi_j}$. Note that these probabilities $p_{\psi_i \to \xi_j}$ generically contain single-particle interferences. To determine the classical probability $p_{I \to J}^d$ to transfer the particles from the input to the output modes, we combine single-particle processes:

$$p_{I \to J}^{d} = \sum_{\pi \in S_n} p_{\psi_1 \to \xi_{\pi(1)}} \dots p_{\psi_n \to \xi_{\pi(n)}}.$$
 (8.40)

In Sect. 8.3.4, we prove that this is the limit obtained for distinguishable particles. However, when dealing with indistinguishable particles in the bosonic or fermionic Fock space, additional interference terms show up. We find specifically that

$$p_{I \to I}^{b/f} = p_{I \to I}^d + \text{interference terms},$$
 (8.41)

and the remainder of the chapter is devoted to understanding the phenomenology induced by these interference terms. Note also that this is yet another realisation of the general relation (2.73).

8.3.2 Many-Boson Interference

Since we work in a Schrödinger picture, the correct object to propagate is the wave function that describes a given, (pure) quantum state in Fock space. When dealing with bosons, there is a wide range of states that can be considered, most notably the number states (7.132) and Glauber coherent states (7.145). We know that the latter are Gaussian states which saturate the uncertainty relation in a symmetric way. Therefore, they are the closest we can get to a point in phase space, and we do not expect to see any strong interference effects for these states, as they are the closest we can get to classical physics. If we were to see many-particle interference for coherent states, this would imply that we can generate these effects with classical light, going against the idea that this is a genuine quantum phenomenon. Number states, on the other hand, have a very pronounced non-classical character and therefore are expected to show more interesting interference properties. We start by discussing the dynamical properties of number states, introducing many-boson interference in a concrete fashion. Later we briefly comment on the lack of such interference effects in Glauber coherent states.

Number States

Let us start with number states, which are expected to exhibit interesting quantum effects since they do not belong to the class of Gaussian states (see Sect. 7.6.4). We thus use them as input for our interference setup. Note that we will focus on the specific vector of type (7.116), a special class of number states. Hence, we prepare the initial state

$$\Psi = \frac{1}{\sqrt{\text{perm } G}} a^{\dagger}(\psi_1) a^{\dagger}(\psi_2) \Omega, \quad \text{with } \psi_1, \psi_2 \in \mathbb{C}^2$$
 (8.42)

and inject it into a beamsplitter:

$$\Psi \mapsto \frac{1}{\sqrt{\operatorname{perm} G}} a^{\dagger} (B\psi_1) a^{\dagger} (B\psi_2) \Omega. \tag{8.43}$$

In relation to (8.41), we consider the probability to observe the particles in modes ξ_1 and $\xi_2 \in H$, which is now given by the transition probability to the state

$$\Xi = \frac{1}{\sqrt{\text{perm }G'}} a^{\dagger}(\xi_1) a^{\dagger}(\xi_2) \Omega. \tag{8.44}$$

Thus we compute

$$\begin{split} p_{\Psi \to \Xi}^{b} &= \frac{1}{\operatorname{perm} G \operatorname{perm} G'} \left| \left\langle \Omega, a(\xi_{2}) a(\xi_{1}) a^{\dagger} (B\psi_{1}) a^{\dagger} (B\psi_{2}) \Omega \right\rangle \right|^{2} \\ &= \frac{1}{\operatorname{perm} G \operatorname{perm} G'} \left| \left\langle \Omega, a(\xi_{2}) \left(\langle \xi_{1}, B\psi_{1} \rangle + a^{\dagger} (B\psi_{1}) a(\xi_{1}) \right) a^{\dagger} (B\psi_{2}) \Omega \right\rangle \right|^{2} \\ &= \frac{1}{\operatorname{perm} G \operatorname{perm} G'} \left| \left\langle \xi_{1}, B\psi_{1} \right\rangle \left\langle \Omega, a(\xi_{2}) a^{\dagger} (B\psi_{2}) \Omega \right\rangle \right| \\ &+ \left\langle \Omega, a(\xi_{2}) a^{\dagger} (B\psi_{1}) \left(\langle \xi_{1}, B\psi_{2} \rangle + a^{\dagger} (B\psi_{2}) a(\xi_{1}) \right) \Omega \right\rangle \right|^{2} \\ &= \frac{1}{\operatorname{perm} G \operatorname{perm} G'} \left| \left\langle \xi_{1}, B\psi_{1} \right\rangle \left\langle \Omega, a(\xi_{2}) a^{\dagger} (B\psi_{2}) \Omega \right\rangle \right| \\ &+ \left\langle \xi_{1}, B\psi_{2} \right\rangle \left\langle \Omega, a(\xi_{2}) a^{\dagger} (B\psi_{1}) \Omega \right\rangle \right|^{2} \\ &= \frac{1}{\operatorname{perm} G \operatorname{perm} G'} \left| \left\langle \xi_{1}, B\psi_{1} \right\rangle \left\langle \Omega, \left(\langle \xi_{2}, B\psi_{2} \rangle + a^{\dagger} (B\psi_{2}) a(\xi_{2}) \right) \Omega \right\rangle \right| \\ &+ \left\langle \xi_{1}, B\psi_{2} \right\rangle \left\langle \Omega, \left(\langle \xi_{2}, B\psi_{1} \rangle + a^{\dagger} (B\psi_{1}) a(\xi_{2}) \right) \Omega \right\rangle \right|^{2} \\ &= \frac{1}{\operatorname{perm} G \operatorname{perm} G'} \left| \left\langle \xi_{1}, B\psi_{1} \right\rangle \left\langle \xi_{2}, B\psi_{2} \right\rangle + \left\langle \xi_{1}, B\psi_{2} \right\rangle \left\langle \xi_{2}, B\psi_{1} \right\rangle \right|^{2}. \end{split}$$

Summarising everything in one simple expression, we find that

$$p_{\Psi \to \Xi}^b = \frac{\left| \text{perm} \left[\left\langle \xi_i, B \psi_j \right\rangle \right] \right|^2}{\text{perm } G \text{ perm } G'}.$$
 (8.46)

To explicitly show that many-particle interference effects indeed show up, let us finally express

$$\begin{split} p_{\Psi \to \Xi}^{b} &= \frac{1}{\operatorname{perm} G \operatorname{perm} G'} \bigg(\left| \langle \xi_{1}, B\psi_{1} \rangle \right|^{2} \left| \langle \xi_{2}, B\psi_{2} \rangle \right|^{2} + \left| \langle \xi_{1}, B\psi_{2} \rangle \right|^{2} \left| \langle \xi_{2}, B\psi_{1} \rangle \right|^{2} \\ &+ \langle \xi_{1}, B\psi_{1} \rangle \left\langle \psi_{1}, B^{\dagger} \xi_{2} \right\rangle \left\langle \xi_{2}, B\psi_{2} \rangle \left\langle \psi_{2}, B^{\dagger} \psi_{1} \right\rangle \\ &+ \langle \xi_{1}, B\psi_{2} \rangle \left\langle \psi_{2}, B^{\dagger} \xi_{2} \right\rangle \left\langle \xi_{2}, B\psi_{1} \rangle \left\langle \psi_{1}, B^{\dagger} \psi_{1} \right\rangle \bigg). \end{split}$$

Upon comparison with (8.41), with the identification $p_{\psi_i \to \xi_j} = |\langle \xi_j, B\psi_i \rangle|^2$, the final two terms are seen to represent the interferences.

To indicate how drastic these interference effects may be, let us assume that we consider orthogonal wave functions, such that $\langle \psi_1, \psi_2 \rangle = 0$ and $\langle \xi_1, \xi_2 \rangle = 0$. To connect this to Fig. 8.1, it would imply for example that the particle with wave function ψ_1 enters the beamsplitter from direction 1 and another one, with wave function ψ_2 , enters from direction 2. The final state on which we project (see Sect. 8.3.1) represents the case where both particles exit the beamsplitter in different directions. Let us assume that B is given by

$$B = \begin{pmatrix} \langle \xi_1, B\psi_1 \rangle & \langle \xi_1, B\psi_2 \rangle \\ \langle \xi_2, B\psi_1 \rangle & \langle \xi_2, B\psi_2 \rangle \end{pmatrix} = \begin{pmatrix} \sqrt{1-\lambda} & \sqrt{\lambda} \\ \sqrt{\lambda} & -\sqrt{1-\lambda} \end{pmatrix}, \quad \lambda \in [0, 1], \quad (8.48)$$

such that expression (8.47) simplifies to

$$p_{1,2} := p_{\Psi \to \Xi}^b = (2\lambda - 1)^2. \tag{8.49}$$

The notation $p_{1,2}$ (Hong et al. 1987) implies the probability to observe a coincidence measurement where one outgoing photon is detected in direction 1 and the other one in direction 2. When we now consider the unbiased beamsplitter ($\lambda = 1/2$), we find that $p_{1,2} = 0$. This is in contrast to the result (8.40) obtained from classical probability and combinatorics, which results in $p_{1,2} = 1/2$. Hence, the interference terms in (8.47) cause the two bosons to *bunch* together while *jointly* travelling through an unbiased beamsplitter.

The beamsplitter-scenario is naturally generalised to a generic n-particle setup, with the initial state

$$\Psi = \frac{1}{\sqrt{\text{perm } G}} a^{\dagger}(\psi_1) \dots a^{\dagger}(\psi_n) \Omega, \tag{8.50}$$

which is propagated by a single-particle unitary channel E(U), $U \in \mathcal{B}(\mathcal{H})$ (recall (8.15)). Setting up a measurement which allows us to detect the state

$$\Xi = \frac{1}{\sqrt{\text{perm }G'}} a^{\dagger}(\xi_1) \dots a^{\dagger}(\xi_n) \Omega, \tag{8.51}$$

gives us the transition probability

$$p_{\Psi \to \Xi}^{b} = \frac{1}{\operatorname{perm} G \operatorname{perm} G'} \left| \left\langle a^{\dagger}(\xi_{1}) \dots a^{\dagger}(\xi_{n}) \Omega, a^{\dagger}(U\psi_{1}) \dots a^{\dagger}(U\psi_{n}) \Omega \right\rangle \right|^{2}.$$
(8.52)

It is reasonably straightforward to see that the arithmetic of the calculation (8.45) can be generalised for this setting. A stepwise treatment of such a computation was also presented in Sect. 7.6.1, when we discussed the normalisation of number states. Ultimately, one finds that

$$p_{\Psi \to \Xi} = \frac{\left| \text{perm} \left[\left\langle \xi_i, U \psi_j \right\rangle \right] \right|^2}{\text{perm } G \text{ perm } G'}, \tag{8.53}$$

what forces us to consider the permanent of an $n \times n$ matrix $[\langle \xi_i, U\psi_j \rangle]$, which can be interpreted as a sub-matrix of U. Just as in the previous setup with the beamsplitter, we can rewrite the modulus-squared in (8.53) to make the interference terms explicit:

$$p_{\Psi \to \Xi}^{b} = \frac{1}{\operatorname{perm} G \operatorname{perm} G'} \left(\sum_{\pi \in S_{n}} \left| \left\langle \xi_{1}, U \psi_{\pi(1)} \right\rangle \right|^{2} \left| \left\langle \xi_{2}, U \psi_{\pi(2)} \right\rangle \right|^{2} \dots \left| \left\langle \xi_{n}, U \psi_{\pi(n)} \right\rangle \right|^{2} + \sum_{\substack{\pi, \sigma \in S_{n} \\ \pi \neq \sigma}} \left\langle \xi_{1}, U \psi_{\pi(1)} \right\rangle \left\langle \psi_{\sigma(1)}, U^{\dagger} \xi_{1} \right\rangle \dots \left\langle \xi_{n}, U \psi_{\pi(n)} \right\rangle \left\langle \psi_{\sigma(n)}, U^{\dagger} \xi_{n} \right\rangle \right).$$

$$(8.54)$$

The sum in the second line runs over all pairs of unequal permutations and clearly contains many interference terms, whereas the sum on the first line is expected from combinatorics (8.40). Indeed, notice that when we consider just one-particle transitions, we find

$$p_{\psi \to \xi}^b = \left| \left\langle \Omega, a(\xi) a^{\dagger}(U\psi) \Omega \right\rangle \right|^2 = \left| \left\langle \xi, U\psi \right\rangle \right|^2, \tag{8.55}$$

thus the first term in (8.54) represents simply the result from classical probability theory, as given by (8.40). The second sum in (8.54), however, runs over the permutations π , $\sigma \in S_n$ of the selected output modes with $\pi \neq \sigma$. This implies that there are n!(n!-1) interference terms that need to be taken into account. It should therefore be stressed that these many-particle interferences are of paramount importance to understand the propagation of many particles through unitary channels as (8.15).

Before we proceed to the discussion of (the lack of) many-particle interference phenomena for coherent states, let us stress that a general single-particle unitary channel as (8.15) is far from an idealisation. At least in bosonic systems, it has been shown (Reck et al. 1994) that *any* such single-particle unitary operation can be engineered with the help of sufficiently many¹⁰ beamsplitters (with variable transmission and reflection coefficients) and phase shifters. The latter simply act as $a^{\dagger}(\psi) \mapsto a^{\dagger}(e^{i\theta}\psi)$. Figure 8.2 sketches such a setup for the specific case of a 4 × 4 single-particle unitary channel.

Glauber Coherent States*

This section shows that Glauber coherent states, in contrast to number states, do not exhibit many-particle interference. This serves as an indication that many-particle interference is a genuine quantum phenomenon which cannot be obtained from classical waves.

Let us now briefly study the behaviour of a general Glauber coherent state when being transmitted through a beamsplitter (8.39). The action of a beamsplitter on a coherent state is given by

$$\Psi_{\alpha} = W(\alpha)\Omega \mapsto W(B\alpha)\Omega = \Psi_{B\alpha}, \quad \alpha \in \mathbb{C}^2,$$
(8.56)

and in order to see interference effects, we follow (2.73) and evaluate the expectation value of a projector on the Fock space. Let us, in analogy to the previous section, choose a projector $|\Phi\rangle\langle\Phi|$, with Φ given by

 $^{^{10}}$ More specifically (Reck et al. 1994) shows that this amount is N(N-1)/2 when one wishes to describe an $N \times N$ unitary operation.

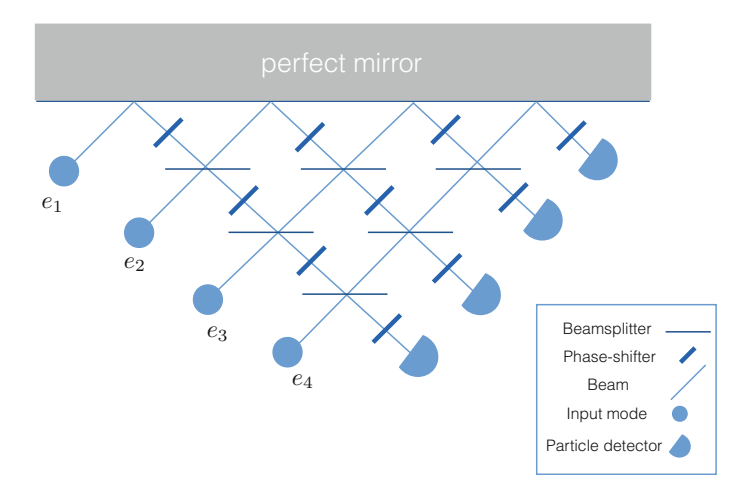


Fig. 8.2 Sketch of a pyramid-shaped beamsplitter array. A total of four different input modes are connected to four different output detectors. The maze of six beamsplitters (each described by its own 2×2 unitary B, see (8.48)) and a set of additional phase-shifters provide a variety of different pathways for the bosons to travel to the detectors. During this dynamical process, there are single-particle interferences because of the multitude of different pathways, but also many-particle interferences because of the bosonic, indistinguishable nature of the particles

$$\Phi = \frac{1}{\sqrt{\text{perm } G}} a^{\dagger}(\psi) a^{\dagger}(\phi) \Omega, \tag{8.57}$$

with ψ , $\phi \in \mathcal{H}$. We want to find exactly one particle in state ψ and one in state ϕ . Therefore we must calculate

$$p_{\psi,\phi}^{\alpha} = \frac{1}{\operatorname{perm} G} \left| \left\langle a^{\dagger}(\psi) a^{\dagger}(\phi) \Omega, \Psi_{B\alpha} \right\rangle \right|^{2}$$

$$= \frac{e^{-\|\alpha\|^{2}}}{2 \operatorname{perm} G} \left| \left\langle \psi \odot \phi, B\alpha \otimes B\alpha \right\rangle \right|^{2}$$

$$= \frac{e^{-\|\alpha\|^{2}}}{\operatorname{perm} G} \left| \left\langle \psi, B\alpha \right\rangle \right|^{2} \left| \left\langle \phi, B\alpha \right\rangle \right|^{2}.$$
(8.58)

The calculation can easily be generalised to any single-particle unitary process, where we compute the probability of finding a state $a^{\dagger}(\psi_1) \dots a^{\dagger}(\psi_n) \Omega$ and find that

$$p_{\psi_1,\dots\psi_n}^{\alpha} = \frac{e^{-\|\alpha\|^2} \|\alpha\|^{2n}}{\operatorname{perm} G} \left| \langle \psi_1, Ue_{\alpha} \rangle \right|^2 \dots \left| \langle \psi_n, Ue_{\alpha} \rangle \right|^2, \tag{8.59}$$

with U a unitary operator in $\mathcal{B}(\mathcal{H})$ and $e_{\alpha} = \alpha/\|\alpha\|$. Indeed, one does not find any many-particle interferences, but simply a multiplication of probabilities: The factor

$$\frac{e^{-\|\alpha\|^2}\|\alpha\|^{2n}}{\operatorname{perm} G}$$

is the probability to find n particles in the coherent state Ψ_{α} , and the latter factors $|\langle \psi_j, Ue_{\alpha} \rangle|^2$ describe single-particle transition probabilities for these n particles to be detected in the selected output modes. This is nothing but expression (8.40), where all particles occupy the same initial mode e_{α} , additionally multiplied by the probability to sample n particles from the coherent state.

8.3.3 Many-Fermion Interference

It should not come as a surprise, given what we already calculated throughout this dissertation, that the technical details for fermions are very similar to those of bosons. However, this does *not* imply that the resulting physical phenomenology is similar, too. We have seen in the previous chapter that simply replacing commutators by anticommutators results ultimately in algebras with quite different properties: Not only do we witness Bose-Einstein condensation for bosons, in sharp contrast to Pauli's exclusion principle for fermions. We also learned that coherent states arise naturally for bosons, whereas they are rather exotic for fermions (Helsen 2015). It was shown that Glauber coherent states do not give rise to many-boson interference effects. For fermions, we cannot generalise this line of thought, due to the profoundly different nature of fermionic coherent states. In this sense, the only quantity which allows for a consistent comparison between bosons and fermion is the transition probability from number states to number states (where we limit ourselves to Slater determinants—recall Sect. 7.6.1). Note, however, that Slater determinants are in fact quasi-free states, which implies that mathematically they are expected to have more controllable behaviour than the non-Gaussian bosonic number states. To explore this, we again start from the easily tractable beamsplitter (i.e. a two mode system), which we then generalise to a single-particle unitary channel.

We prepare our setup to initially describe a two-particle number state

$$\Phi = a^{\dagger}(\psi_1)a^{\dagger}(\psi_2)\Omega, \quad \psi_1, \psi_2 \in \mathbb{C}^2, \ \langle \psi_1, \psi_2 \rangle = 0, \tag{8.60}$$

that is injected into a beamsplitter. Because we are now considering fermions, the creation and annihilation operators have to obey the canonical anticommutation relations (7.78). This also has the profound effect that the only possible way to reach a two-particle state in \mathbb{C}^2 is to prepare the particles in two orthogonal modes, because $a^{\dagger}(\psi)a^{\dagger}(\psi)=0$ for any $\psi\in\mathbb{C}^2$. This orthogonal preparation condition automatically takes care of normalisation.

To picture a fermionic beamsplitter, we can consider a matter-wave picture where a beamsplitter is a device that splits such a wave in two parts. Thus, the device mediates the following mapping

$$\Psi \mapsto a^{\dagger} (B\psi_1) a^{\dagger} (B\psi_2) \Omega. \tag{8.61}$$

Completely consistently with what was done for bosons, we now assume a measurement setup that allows for a measurement in the number state

$$\Xi = a^{\dagger}(\xi_1)a^{\dagger}(\xi_2)\Omega, \quad \xi_1, \xi_2 \in \mathbb{C}^2, \ \langle \xi_1, \xi_2 \rangle = 0, \tag{8.62}$$

and the transition probability is therefore given by

$$p_{\Psi \to \Xi}^{f} = \left| \left\langle \Omega, a(\xi_{2})a(\xi_{1})a^{\dagger}(B\psi_{1})a^{\dagger}(B\psi_{2})\Omega \right\rangle \right|^{2}$$

$$= \left| \left\langle \Omega, a(\xi_{2})\left(\left\langle \xi_{1}, B\psi_{1} \right\rangle - a^{\dagger}(B\psi_{1})a(\xi_{1}) \right) a^{\dagger}(B\psi_{2})\Omega \right\rangle \right|^{2}$$

$$= \dots$$

$$= \left| \det[\left\langle \xi_{i}, B\psi_{j} \right\rangle] \right|^{2}.$$
(8.63)

The calculation is fully analogous to the one in (8.45), apart from the minus signs that appear for fermions, as indicated in the one step of the calculation which we explicitly state in (8.63). To highlight that interference terms indeed emerge in this setup, let us rewrite

$$p_{\Psi \to \Xi}^{f} = |\langle \xi_{1}, B\psi_{1} \rangle|^{2} |\langle \xi_{2}, B\psi_{2} \rangle|^{2} + |\langle \xi_{1}, B\psi_{2} \rangle|^{2} |\langle \xi_{2}, B\psi_{1} \rangle|^{2} - \langle \xi_{1}, B\psi_{1} \rangle \langle \psi_{1}, B^{\dagger} \xi_{2} \rangle \langle \xi_{2}, B\psi_{2} \rangle \langle \psi_{2}, B^{\dagger} \psi_{1} \rangle - \langle \xi_{1}, B\psi_{2} \rangle \langle \psi_{2}, B^{\dagger} \xi_{2} \rangle \langle \xi_{2}, B\psi_{1} \rangle \langle \psi_{1}, B^{\dagger} \psi_{1} \rangle,$$
(8.64)

which ultimately seems very similar to the bosonic case (8.47), apart from the minus signs. This may seem like an insignificant change, though actually has a considerable impact, as directly evident from the determinant formulation in (8.63). Because we automatically have our two-particle system prepared in an orthogonal basis, we know that $[\langle \xi_i, B\psi_j \rangle]$ is nothing more than B in this specific basis. Here the crucial difference between the determinant and the permanent (obtained for bosons in (8.46)) pops up: The determinant is a unitary invariant, which follows directly from the fact that, for $X, Y \in \mathcal{B}(\mathcal{H})$, on any finite dimensional Hilbert space \mathcal{H} ,

$$\det(XY) = \det X \det Y. \tag{8.65}$$

$$\det(X^{-1}) = \frac{1}{\det X}. (8.66)$$

This directly has as the consequence that the determinant is nothing more than the product of all eigenvalues in the case of a diagonalisable matrix. The permanents acquired in bosonic interference problems do not exhibit *any* of these useful properties.

In the context of our present problem of two fermions transmitted through a beamsplitter, this has the simple consequence that

$$p_{\Psi \to \Xi}^f = \left| \det[\langle \xi_i, B\psi_j \rangle] \right|^2 = \left| \det B \right|^2. \tag{8.67}$$

Of course, B is a unitary matrix, thus it is diagonalisable and its eigenvalues are generically of the form $u \in \mathbb{C}$, with |u| = 1. We thus obtain

$$p_{\Psi \to \Xi}^f = 1. \tag{8.68}$$

Independently of which exact specific pair of orthogonal modes we choose on output from the beamsplitter, we *deterministically* detect one particle in one, and the remaining particle in the other mode. In other words, two fermions *never* leave the beamsplitter in the same direction, an effect which is baptised *antibunching*. Of course, this is not at all a dynamical effect, it is simply a manifestation of Pauli's exclusion principle. Notice the contrast with the bosonic case: There the bunching effect was dependent on the details of the beamsplitter, such that it can actually be understood as a dynamical effect. It is rather straightforward to see that this scenario can easily be generalised to larger systems where the number of particles equals the number of modes.

We now treat the generalisation of the beamsplitter to a generic single-particle unitary channel E(U), with unitary operator $U \in \mathcal{B}(\mathcal{H})$. Consider a general number state $\Psi \in \Gamma^f(\mathcal{H})$, given by

$$\Psi = \frac{1}{\sqrt{\det G}} a^{\dagger}(\psi_1) \dots a^{\dagger}(\psi_n) \Omega, \tag{8.69}$$

and mapped on

$$\Psi \mapsto \frac{1}{\sqrt{\det G}} a^{\dagger}(U\psi_1) \dots a^{\dagger}(U\psi_n) \Omega. \tag{8.70}$$

If we measure in the output state

$$\Xi = \frac{1}{\sqrt{\det G'}} a^{\dagger}(\xi_1) \dots a^{\dagger}(\xi_n) \Omega, \tag{8.71}$$

we again obtain, in a straightforward way,

$$p_{\Psi \to \Xi}^f = \frac{\left| \left[\left\langle \xi_i, U \psi_j \right\rangle \right] \right|^2}{\det G \det G'}.$$
(8.72)

It should be stressed that now, in general $[\langle \xi_i, U\psi_j \rangle]$ is a *submatrix* of U, rather than the full operator. Repeating another one of the computations which we already performed for bosons in Sect. 8.3.2, we can explicitly express the occurring interferences by

$$p_{\Psi \to \Xi}^{f} = \frac{1}{\det G \det G'} \left(\sum_{\pi \in S_{n}} \left| \left\langle \xi_{1}, U \psi_{\pi(1)} \right\rangle \right|^{2} \left| \left\langle \xi_{2}, U \psi_{\pi(2)} \right\rangle \right|^{2} \dots \left| \left\langle \xi_{n}, U \psi_{\pi(n)} \right\rangle \right|^{2} \right. \\ + \sum_{\substack{\pi, \sigma \in S_{n} \\ \pi \neq \sigma}} \operatorname{sign}(\pi) \operatorname{sign}(\sigma) \left\langle \xi_{1}, U \psi_{\pi(1)} \right\rangle \left\langle \psi_{\sigma(1)}, U^{\dagger} \xi_{1} \right\rangle \dots \left\langle \xi_{n}, U \psi_{\pi(n)} \right\rangle \left\langle \psi_{\sigma(n)}, U^{\dagger} \xi_{n} \right\rangle \right).$$

$$(8.73)$$

Comparison of (8.54)–(8.73) shows that the terms in the first sum of both equations are identical and reflect the classical summation (8.40), because also for fermions

$$p_{\psi \to \xi}^{f} = \left| \left\langle \Omega, a(\xi) a^{\dagger}(U\psi) \Omega \right\rangle \right|^{2} = \left| \left\langle \xi, U\psi \right\rangle \right|^{2}. \tag{8.74}$$

The second sum, however, is different from (8.54), due to the factor $sign(\pi)sign(\sigma)$. The actual differences between bosons and fermions depend strongly on the specificities of the unitary operator U and on the specific input and output states. Essentially the interference terms in (8.54) and (8.73) are given as products of matrix elements of the unitary matrix U, whereas the difference between both is given by the additional factors $sign(\pi)sign(\sigma)$ in (8.73). In the two-particle case, the only interference terms in (8.63) appear with factor $sign(\pi)sign(\sigma) = -1$, leaving the impression that many-boson interference and many-fermion interference are complementary effects (see e.g. also Fig. 8.5). In the *many*-particle case this is no longer the case, since it is conceivable that the unitary operator U and the input state are chosen such that in (8.73) only the terms with $sign(\pi)sign(\sigma) = 1$ contribute to the interference effect. This implies that for such unitary channel and that specific input state, the many-fermion interference leads to exactly the same transmission probability as many-boson interference. Ergo, in that specific case we find that $p_{\Psi \to \Xi}^f = p_{\Psi \to \Xi}^b$. Even though such setup is in practice hard to engineer, examples can be found, specifically in the case where U is highly symmetric, such as for the Fourier matrix (Tichy et al. 2010, 2012).

8.3.4 Distinguishability and the Hong-Ou-Mandel Effect

Throughout the discussion on many-particle interference, we stressed that the phenomenon is closely related to the indistinguishability of the particles. In the beginning of Chap. 7, we mentioned that *identical* particles are not necessarily *indistinguishable*. A simple example may be given by two photons, both with vertical polarisation, where one is on Venus and the other on Mars. Although internally these particles are fully the same, obeying the same algebra of canonical commutation relations (CCR) (7.77), they can easily be distinguished, simply by referring to their position. Another external degree of freedom that can be exploited is time: Two identical photons, that are detected by a human eye, can be told apart when the first one was "seen" on Monday and the other one on Friday. Of course, once the photons differ in their internal degrees of freedom, for example because of different polarisation or frequency, we can always tell them apart, no matter how close we pack them in

time and space. However, here we must enter a discussion on semantics, because one would probably not call particles that differ in an internal degree of freedom identical anymore. Nevertheless, the key message is that distinguishability can arise via *any* degree of freedom (possibly an auxiliary one) where the particles are different. This implies that, in order to see indistinguishability-induced effects, the particles must get together in time and space (which is exactly what happens when they are jointly travelling through a beamsplitter array). But this leads to an interesting question: How "close" should these particles get, and how can the purely quantum mechanical phenomenology of indistinguishable particles be continuously transformed into that of the classical probability theory of distinguishable particles? It turns out that measurement and, effectively, decoherence are crucial aspects for answering this question.

Part of the transition from distinguishable to indistinguishable is baked into the structure of Fock space and even in the CCR and CAR (canonical anticommutation relations) algebras, although this interpretation is rarely spelled out.

Let us focus on bosons for the time being. The expression (7.77) indeed has the transition from distinguishable to indistinguishable behaviour encrypted into it. When the two states $\psi, \phi \in \mathcal{H}$ are parallel, the creation and annihilation operator are as far away from commutation as possible, and therefore one may say that the particles which they create manifest strong bosonic properties and are as indistinguishable as they can get. On the other hand, when ψ and ϕ are orthogonal, their creation and annihilation operators commute, implying that the particles are actually distinguishable. In other words, the distinguishability of two particles is simply determined by the overlap of their single-particle wave functions, ¹¹ which directly allows for a continuous interpolation between fully parallel and fully orthogonal single-particle wave functions via the inner product.

To make this idea explicit, let us recall Sect. 7.3.2. It is sometimes argued that indistinguishable particles require symmetrisation or anti-symmetrisation of the composite tensor product structure, whereas distinguishable particles are simply described by tensor products. It may immediately be argued that this is simply a consequence of a misconception between *identical* and *indistinguishable*, but the reality is *much* more subtle: All particles are either bosons or fermions and therefore all particles are ultimately ruled by either the CCR or the CAR. To make this more concrete, one may pose the question as follows: Consider two distinguishable particles, one described by the single-particle wave function $\psi \in \mathcal{H}$, the other by $\phi \in \mathcal{H}$, such that $\langle \psi, \phi \rangle = 0$. According to the previous paragraph, these particles are *distinguishable*, but still their joint wave function in Fock space is described by

$$\Psi = a^{\dagger}(\phi)a^{\dagger}(\psi)\Omega \in \Gamma^{b}(\mathcal{H}), \tag{8.75}$$

which now implies that we can equivalently describe this state by

¹¹Thus the concept of "exchange interaction" e.g. in the structure theory of helium (Madroñero 2004).

$$\Psi = \phi \odot \psi \in \mathcal{H}_s^{\otimes 2}. \tag{8.76}$$

Where is the expected tensor product structure? The answer to this question is that it is standing right in front of our nose, but we are simply treating the problem on a wrong basis. Indeed, we already discussed in Sect. 7.3.2 that the structure of the single-particle space induces structure of the Fock space, more specifically we can show that

$$\Gamma^b(\mathcal{H}_1 \oplus \mathcal{H}_2) \cong \Gamma^b(\mathcal{H}_1) \otimes \Gamma^b(\mathcal{H}_2). \tag{8.77}$$

To stick to the specific example of two particles, we use the isomorphism

$$\left(\mathcal{H}_1 \oplus \mathcal{H}_2\right)_s^{\otimes 2} \cong \mathcal{H}_{1s}^{\otimes 2} \oplus \left(\mathcal{H}_1 \otimes \mathcal{H}_2\right) \oplus \mathcal{H}_{2s}^{\otimes 2}, \tag{8.78}$$

where all explicit constructions were already provided in Sect. 7.3.2. The orthogonality between ψ and ϕ now naturally defines a direct sum structure via a *corollary of the Hilbert projection theorem* (Conway 1997; Pedersen 1989): Any linear subspace $\mathcal{K} \subset \mathcal{H}$ naturally defines an orthogonal complement \mathcal{K}^{\perp} as

$$\mathcal{K}^{\perp} = \{ x \in \mathcal{H} \mid \langle y, x \rangle = 0 \text{ for all } y \in \mathcal{K} \}, \tag{8.79}$$

and it can be shown that $\mathcal{H} \cong \mathcal{K} \oplus \mathcal{K}^{\perp}$. Note that the proof is simple for finite dimensional spaces;¹² for general Hilbert space, the Hilbert's projection theorem (Conway 1997; Pedersen 1989) itself offers the outcome.

To come back to our specific two-particle system, without going into detail, we thus can always define \mathcal{H}_1 and \mathcal{H}_2 such that $\psi \in \mathcal{H}_1$, $\phi \in \mathcal{H}_2$ and $\mathcal{H} \cong \mathcal{H}_1 \oplus \mathcal{H}_2$, simply because $\langle \phi, \psi \rangle = 0$. Formally, we may now make the direct sum structure in the vectors explicit by writing $\psi \in \mathcal{H}_1 \mapsto \psi \oplus 0 \in \mathcal{H}$ and $\phi \in \mathcal{H}_2 \mapsto 0 \oplus \phi \in \mathcal{H}$ and this leads us to what we already derived in (7.54):

$$a^{\dagger}(\phi)a^{\dagger}(\psi)\Omega \in \Gamma^{b}(\mathcal{H}) \cong \phi \otimes \psi \in \mathcal{H}_{1} \otimes \mathcal{H}_{2}.$$
 (8.80)

A more schematic representation of this equivalence is shown in Fig. 8.3. We must stress that, in the case of fermions, the story is somewhat more subtle due to the $(-1)^{\hat{N}}$ in (7.57). However, in case of full distinguishability, these factors are of no importance; they appear as an overall phase in a tensor product wave function, but this will not have any measurable impact. Yet, when $\langle \phi, \psi \rangle \neq 0$, this is no longer an issue of just a global phase. For the technical details, see Sect. 7.3.2.

Now that we have understood that distinguishability is implied by orthogonality, and that orthogonality can be understood in terms of a direct sum structure in the single-particle Hilbert space, which, in turn, implies a tensor product structure on the level of the Fock space, we may start wondering about the physical implications.

¹²One can simply use that all spaces of equal, finite dimension are isomorphic (Igodt and Veys 2011).

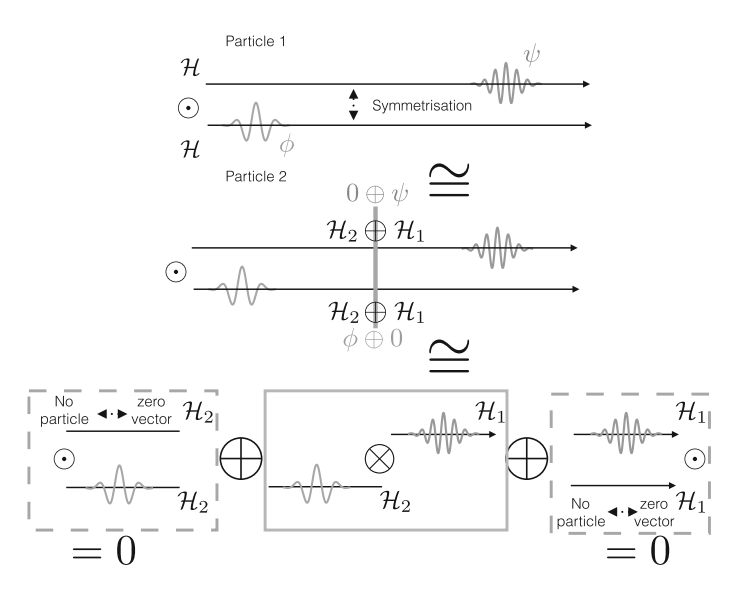


Fig. 8.3 Schematic representation of the possible ways to structure two-particle space $\mathcal{H}_s^{\otimes 2}$, with a direct sum structure on the single-particle level $\mathcal{H} \cong \mathcal{H}_1 \oplus \mathcal{H}_2$. The present example represents $\mathcal{H} \subset \mathcal{L}^2(\mathbb{R})$. The single-particle wave functions of each particle differ in structure and by their positions in space such that the particles are *de facto* distinguishable. The tensor product structure of the state is made explicit as indicated by the blue with the filled frame. The terms indicated by the boxes with the dashed frames contain a wave packet multiplied by the zero function, and therefor vanish

In other words, how do we see this distinguishability arising and how does it impact interferometric setups such as the ones we discussed in the context of many-boson and many-fermion interference in Sects. 8.3.2 and 8.3.3?

The naive expectation, given the single-particle transition probabilities (8.55) and (8.74), is that, whenever the particles are travelling through the beamsplitter array (or whichever device is used to implement the channel) one after the other, implying a sufficient separation in time to tell them apart, we can simply do classical probability theory, and combine these single-particle transition probabilities as in (8.40). We therefore expect that

$$p_{\Psi \to \Xi}^{d} = \sum_{\pi \in S_n} \left| \left\langle \xi_1, U \psi_{\pi(1)} \right\rangle \right|^2 \left| \left\langle \xi_2, U \psi_{\pi(2)} \right\rangle \right|^2 \dots \left| \left\langle \xi_n, U \psi_{\pi(n)} \right\rangle \right|^2, \tag{8.81}$$

which ignores any many-particle interference all together. However, much more can be said about (partial) distinguishability.

There is beautiful and elegant way to extrapolate from Eq. (8.81) to Eq. (8.54) or (8.73), which is effectively via a decoherence process that specifically targets the many-particle interference. The physics behind the presented results was recently explored by several authors (Shchesnovich 2015a, b; Tichy 2015), but methods used

in this dissertation to derive the final results are different from those found in these works, thus our contribution here provides an interesting and complementary view to what is already known in the literature.

The first step of our method is to extend the system by additional degrees of freedom, all contained within a Hilbert space \mathcal{H}_{add} . They may either be internal, such as spin or polarisation, or external, such as the $\mathcal{L}^2(\mathbb{R})$ degree of freedom in (8.34), which accounts for the particle's motion along the beam axis in a beamsplitter setup. In a setup with m modes (e.g. defined by the input modes of a beamsplitter array), this implies that we have to consider the full single-particle Hilbert space

$$\mathcal{H} = \bigoplus_{j=1}^{m} \mathcal{H}_{\text{add}} \cong \mathbb{C}^{m} \otimes \mathcal{H}_{\text{add}}.$$
 (8.82)

The direct sum structure in the mode space implies that particles in different input directions of such a beamsplitter array can actually be considered distinguishable. ¹³ They only have indistinguishable character when they *simultaneously* travel through the channel and the modes get mixed. We will assume throughout our entire calculation that the mode degree of freedom is not entangled with the additional degrees of freedom, hence that single-particle states are all of the form $\psi_i \otimes \chi_i$, where $\psi_i \in \mathbb{C}^m$ and $\chi_i \in \mathcal{H}_{\mathrm{add}}$. Thus, the total input state in the full Fock space reads

$$\Psi = \frac{1}{\mathcal{N}} a^{\dagger} (\psi_1 \otimes \chi_1) \dots a^{\dagger} (\psi_n \otimes \chi_n) \Omega, \tag{8.83}$$

where N denotes whichever necessary normalisation factor.

A crucial assumption is that the dynamics preserves the tensor product structure (i.e. does not couple mode and additional degrees of freedom), such that the single-particle unitary channel is seen to act as $E(U \otimes U')$ with $U \in \mathcal{B}(\mathbb{C}^m)$ and $U' \in \mathcal{B}(\mathcal{H}_{add})$. In other words, the channel acts as

$$\Psi \mapsto \frac{1}{N} a^{\dagger} (U\psi_1 \otimes U'\chi_1) \dots a^{\dagger} (U\psi_n \otimes U'\chi_n) \Omega. \tag{8.84}$$

Now let us start to calculate the probability to detect a specific output state

$$\Xi = \frac{1}{\mathcal{N}} a^{\dagger} (\xi_1 \otimes \zeta_1) \dots a^{\dagger} (\xi_n \otimes \zeta_n) \Omega, \quad \xi_i \in \mathbb{C}^m, \ \zeta_i \in \mathcal{H}_{add}. \tag{8.85}$$

With $\langle \xi_i \otimes \zeta_i, U\psi_j \otimes U'\chi_j \rangle = \langle \xi_i, U\psi_j \rangle \langle \zeta_i, U'\chi_j \rangle$, we can insert (8.84), (8.85) into Eq. (8.54) or (8.73), because all we did was structuring the single-particle space. We find, for bosons,

¹³This makes sense, because they can be told apart by the input direction they are following.

$$p_{\Psi \to \Xi}^{b} = \frac{1}{\mathcal{N} \mathcal{N}'} \left(\sum_{\pi \in S_{n}} \left| \left\langle \xi_{1}, U \psi_{\pi(1)} \right\rangle \right|^{2} \left| \left\langle \zeta_{1}, U' \chi_{\pi(1)} \right\rangle \right|^{2} \dots \left| \left\langle \xi_{n}, U \psi_{\pi(n)} \right\rangle \right|^{2} \left| \left\langle \zeta_{n}, U' \chi_{\pi(n)} \right\rangle \right|^{2} + \sum_{\substack{\pi, \sigma \in S_{n} \\ \pi \neq \sigma}} \left\langle \xi_{1}, U \psi_{\pi(1)} \right\rangle \left\langle \psi_{\sigma(1)}, U^{\dagger} \xi_{1} \right\rangle \dots \left\langle \xi_{n}, U \psi_{\pi(n)} \right\rangle \left\langle \psi_{\sigma(n)}, U^{\dagger} \xi_{n} \right\rangle \times \left\langle \zeta_{1}, U' \chi_{\pi(1)} \right\rangle \left\langle \chi_{\sigma(1)}, U'^{\dagger} \zeta_{1} \right\rangle \dots \left\langle \zeta_{n}, U' \chi_{\pi(n)} \right\rangle \left\langle \chi_{\sigma(n)}, U'^{\dagger} \zeta_{n} \right\rangle \right),$$

$$(8.86)$$

and, for fermions,

$$p_{\Psi \to \Xi}^{f} = \frac{1}{\mathcal{N} \mathcal{N}'} \left(\sum_{\pi \in S_{n}} \left| \left\langle \xi_{1}, U \psi_{\pi(1)} \right\rangle \right|^{2} \left| \left\langle \zeta_{1}, U' \chi_{\pi(1)} \right\rangle \right|^{2} \dots \left| \left\langle \xi_{n}, U \psi_{\pi(n)} \right\rangle \right|^{2} \left| \left\langle \zeta_{n}, U' \chi_{\pi(n)} \right\rangle \right|^{2} \\ + \sum_{\substack{\pi, \sigma \in S_{n} \\ \pi \neq \sigma}} \operatorname{sign}(\pi) \operatorname{sign}(\sigma) \left\langle \xi_{1}, U \psi_{\pi(1)} \right\rangle \left\langle \psi_{\sigma(1)}, U^{\dagger} \xi_{1} \right\rangle \dots \left\langle \xi_{n}, U \psi_{\pi(n)} \right\rangle \left\langle \psi_{\sigma(n)}, U^{\dagger} \xi_{n} \right\rangle \\ \times \left\langle \zeta_{1}, U' \chi_{\pi(1)} \right\rangle \left\langle \chi_{\sigma(1)}, U'^{\dagger} \zeta_{1} \right\rangle \dots \left\langle \zeta_{n}, U' \chi_{\pi(n)} \right\rangle \left\langle \chi_{\sigma(n)}, U'^{\dagger} \zeta_{n} \right\rangle \right). \tag{8.87}$$

So far, this only makes Eqs. (8.54) or (8.73) look a little longer, but nothing new has happened. However, this assumes that the measurement setup resolves both, the state of the mode degree of freedom, and the *specific state* of all other degrees of freedom. This is in contrast with a beamsplitter array where one simply mounts a photon counter on each output mode. A realistic setup is always bound to finite resolution, making it impossible to fully resolve all additional degrees of freedom (see e.g. the supplementary material of Crespi et al. 2013). Therefore, there generally is some structure \mathcal{H}_{add} left which is not resolved in the measurement. In other words, we only measure in \mathbb{C}^m and have to effectively trace out \mathcal{H}_{add} . To do so, we fix a basis $\{f_i\}$ of \mathcal{H}_{add} and sum over it. This needs to be done for each individual particle, and results in

$$P_{\Psi \to \Xi}^{b} := \frac{1}{\mathcal{N} \mathcal{N}'} \sum_{i_{1}, i_{2}, \dots i_{n}} \left(\sum_{\pi \in S_{n}} \left| \left\langle \xi_{1}, U \psi_{\pi(1)} \right\rangle \right|^{2} \left| \left\langle f_{i_{1}}, U' \chi_{\pi(1)} \right\rangle \right|^{2} \dots \left| \left\langle \xi_{n}, U \psi_{\pi(n)} \right\rangle \right|^{2} \left| \left\langle f_{i_{n}}, U' \chi_{\pi(n)} \right\rangle \right|^{2}$$

$$+ \sum_{\substack{\pi, \sigma \in S_{n} \\ \pi \neq \sigma}} \left\langle \xi_{1}, U \psi_{\pi(1)} \right\rangle \left\langle \psi_{\sigma(1)}, U^{\dagger} \xi_{1} \right\rangle \dots \left\langle \xi_{n}, U \psi_{\pi(n)} \right\rangle \left\langle \psi_{\sigma(n)}, U^{\dagger} \xi_{n} \right\rangle$$

$$\times \left\langle \chi_{\sigma(1)}, U'^{\dagger} f_{i_{1}} \right\rangle \left\langle f_{i_{1}}, U' \chi_{\pi(1)} \right\rangle \dots \left\langle \chi_{\sigma(n)}, U'^{\dagger} f_{i_{n}} \right\rangle \left\langle f_{i_{n}}, U' \chi_{\pi(n)} \right\rangle \right),$$

$$(8.88)$$

where every index i_k runs over the entire basis.¹⁴ Our notation is not fully precise here, in the sense that the sums over the i_k may be finite or infinite. One can in principle even sum over continuous bases, which implies that the sum would be and integral. The essence of the expression is that we run over a full basis of \mathcal{H}_{add} and thus sum up all possible measurement outcomes on the additional degrees of freedom that are not resolved in the experiment. Now it remains to simply use that

¹⁴Note that in principle the normalisation factor \mathcal{N}' depends only on $\xi_1, \ldots \xi_n$ in this case, because $\langle f_i, f_j \rangle = \delta_{ij}$.

$$\sum_{i} \langle \chi_1, f_i \rangle \langle f_i, \chi_2 \rangle = \langle \chi_1, \chi_2 \rangle \quad \text{for any } \chi_1, \chi_2 \in \mathcal{H}_{\text{add}}, \tag{8.89}$$

together with the normalisation of the χ_i and the unitarity of U', to obtain

$$P_{\Psi \to \Xi}^{b} = \frac{1}{\mathcal{N} \mathcal{N}'} \left(\sum_{\pi \in S_{n}} \left| \left\langle \xi_{1}, U \psi_{\pi(1)} \right\rangle \right|^{2} \dots \left| \left\langle \xi_{n}, U \psi_{\pi(n)} \right\rangle \right|^{2} + \sum_{\substack{\pi, \sigma \in S_{n} \\ \pi \neq \sigma}} \left\langle \xi_{1}, U \psi_{\pi(1)} \right\rangle \left\langle \psi_{\sigma(1)}, U^{\dagger} \xi_{1} \right\rangle \dots \left\langle \xi_{n}, U \psi_{\pi(n)} \right\rangle \left\langle \psi_{\sigma(n)}, U^{\dagger} \xi_{n} \right\rangle$$

$$\times \left\langle \chi_{\sigma(1)}, \chi_{\pi(1)} \right\rangle \dots \left\langle \chi_{\sigma(n)}, \chi_{\pi(n)} \right\rangle \right). \tag{8.90}$$

Exactly the same computation can be done for fermions, where we find

$$P_{\Psi \to \Xi}^{f} = \frac{1}{\mathcal{N} \mathcal{N}'} \left(\sum_{\pi \in S_{n}} \left| \left\langle \xi_{1}, U \psi_{\pi(1)} \right\rangle \right|^{2} \dots \left| \left\langle \xi_{n}, U \psi_{\pi(n)} \right\rangle \right|^{2} \right. \\ + \sum_{\substack{\pi, \sigma \in S_{n} \\ \pi \neq \sigma}} \operatorname{sign}(\pi) \operatorname{sign}(\sigma) \left\langle \xi_{1}, U \psi_{\pi(1)} \right\rangle \left\langle \psi_{\sigma(1)}, U^{\dagger} \xi_{1} \right\rangle \dots \left\langle \xi_{n}, U \psi_{\pi(n)} \right\rangle \left\langle \psi_{\sigma(n)}, U^{\dagger} \xi_{n} \right\rangle \\ \times \left\langle \chi_{\sigma(1)}, \chi_{\pi(1)} \right\rangle \dots \left\langle \chi_{\sigma(n)}, \chi_{\pi(n)} \right\rangle \right). \tag{8.9}$$

Notice that when $\langle \chi_i, \chi_j \rangle = \delta_{ij}$, and thus the different particles are *fully distinguishable*, we obtain

$$P_{\Psi \to \Xi}^b = P_{\Psi \to \Xi}^f = \sum_{\pi \in S_n} \left| \left\langle \xi_1, U \psi_{\pi(1)} \right\rangle \right|^2 \dots \left| \left\langle \xi_n, U \psi_{\pi(n)} \right\rangle \right|^2, \tag{8.92}$$

which is exactly what we naively expected. Additionally, when $\langle \chi_i, \chi_j \rangle = 1$ for all i and j, we recover the results in Eqs. (8.54) and (8.73). However, all other possible choices of inner products between the states describing additional degrees of freedom lead to different probabilities and hence different interference phenomena.

The most straightforward example imaginable is that of the beamsplitter in which two particles are injected (recall Sect. 8.2.2 and Fig. 8.1). We assume that the beamsplitter is unbiased and that the particles are prepared in orthogonal modes which we denote e_1 , $e_2 \in \mathbb{C}^2$. Moreover, we assume that the detectors are also mounted on two orthogonal output modes m_1 , $m_2 \in \mathbb{C}^2$. We can then describe the beamsplitter by

$$B = \begin{pmatrix} \langle m_1, Ue_1 \rangle & \langle m_1, Ue_2 \rangle \\ \langle m_2, Ue_1 \rangle & \langle m_2, Ue_2 \rangle \end{pmatrix} = \frac{1}{\sqrt{2}} \begin{pmatrix} 1 & 1 \\ 1 & -1 \end{pmatrix}.$$
 (8.93)

Eqs. (8.90) and (8.91) were obtained under the assumption that we cannot resolve any additional degree of freedom except that associated with the modes, *upon detection*. On the other hand, we do have to care about such additional degrees of free-

dom for the initial state. As a realistic choice for \mathcal{H}_{add} we consider $\mathcal{H}_{add} = \mathcal{L}^2(\mathbb{R})$, i.e. we restrict the particles to move along a one dimensional "line", which implies that we fully ignore the transverse modes of our light beam and completely focus on the longitudinal properties (a reasonable approximation when they are photons, travelling through a waveguide or an optical fibre). Schematically, one may again think of Fig. 8.1 and consider particles as freely propagating wave functions on the lines depicted in blue. In the beamsplitter, the lines physically intersect, and the thus induced coupling of the different modes creates all the interference effects described so far. In this specific case of Fig. 8.1, the total Hilbert space is given by $\mathcal{H} = \mathbb{C}^2 \otimes \mathcal{L}^2(\mathbb{R})$, and the measurement traces out $\mathcal{L}^2(\mathbb{R})$.

By virtue of Eqs. (8.90) and (8.91), it remains to specify the properties of the wave functions $\chi_1, \chi_2 \in \mathcal{L}^2(\mathbb{R})$. We assume these wave functions to be Gaussian wave packets which come in with a fixed time-delay Δt . Moreover, since the single photons are produced via parametric down-conversion (Hong et al. 1987), they have uncertainty-related frequency distributions of ω_1 and ω_2 , which are correlated due to energy conservation, since $\omega_1 + \omega_2 = \omega_0$, with ω_0 the pump frequency. With some additional assumptions on the properties of ω_1, ω_2 , and on the bandwidth $\Delta \omega$, such as in Ra et al. (2013a), Tichy et al. (2011), we find that

$$|\langle \chi_1(t_1), \chi_2(t_2) \rangle|^2 = \exp\left(-\frac{(\Delta \omega \Delta t)^2}{2}\right),\tag{8.94}$$

which may be interpreted as the blue-shaded area indicated in Fig. 8.4. The insertion of (8.94) in the expressions (8.90) and (8.91), gives the probability of a coincidence event, i.e. the probability that one particle is simultaneously detected in each of the two output modes. For bosons, we find

$$p_{1,1}^b = \frac{1}{2} - \frac{1}{2} \exp\left(-\frac{(\Delta\omega\Delta t)^2}{2}\right)$$
 (8.95)

and for fermions

$$p_{1,1}^f = \frac{1}{2} + \frac{1}{2} \exp\left(-\frac{(\Delta\omega\Delta t)^2}{2}\right).$$
 (8.96)

As one may expect from the beamsplitter results (8.49) and (8.68), bosons and fermions behave in opposite ways. However, once Δt becomes too large and the overlap in Fig. 8.4 vanishes, the particles become distinguishable and the results for fermions and bosons collapse onto the same result $p_{1,1}^d = 1/2$ expected from classical probability theory. This transition, shown in Fig. 8.5, from bosonic (or fermionic) interference to the statistics of distinguishable particles is called the *Hong-Ou-Mandel effect* and has become a standard tool in quantum optics labs to certify the preparation of pairs of indistinguishable photons.

In the literature the Hong-Ou-Mandel effect occurs frequently, but it is only very recently that one started to consider more general instances of the transition probabilities (8.90) and (8.91). As one rather unexpected result, it was shown that the

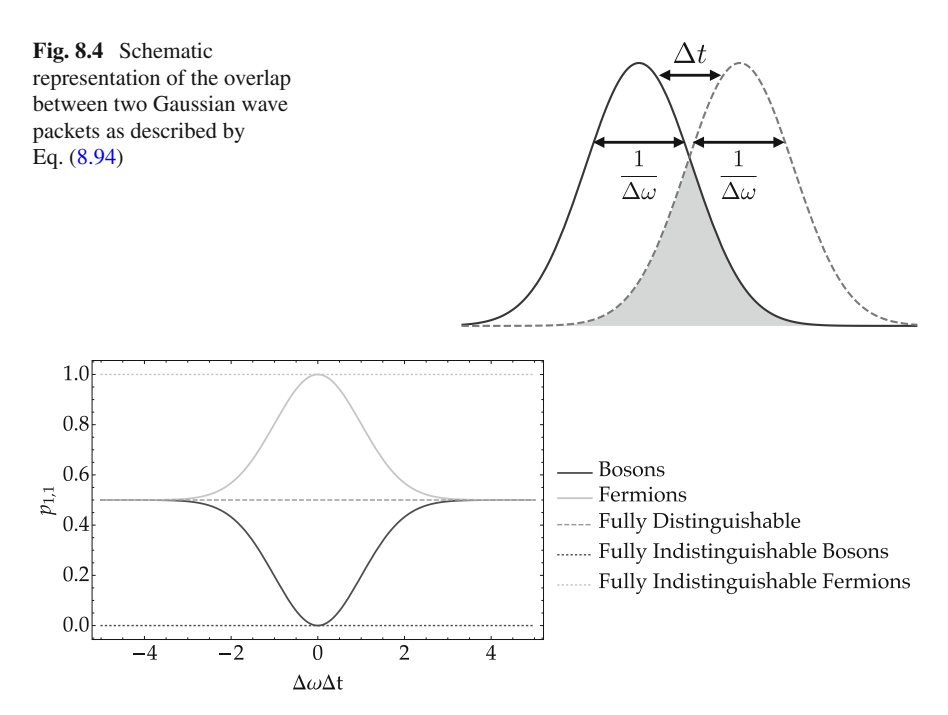


Fig. 8.5 Bosonic, Eq. (8.95), and fermionic, Eq. (8.96), coincidence probability for the simultaneous detection of one photon in each of the output modes of a HOM setup (see Fig. 8.1)

transition from bosonic to distinguishable particles is no longer associated with a monotonic dependence of generic (many-particle) interference patterns on Δt once one considers three or four particles instead of two (Ra et al. 2013a; Tichy et al. 2011).

Theoretical activities to formulate general transmission probabilities in the regime of *partial distinguishability* are a rather recent development (Mayer et al. 2011; Tamma and Laibacher 2014; Tan et al. 2013; Tichy et al. 2011) and were intensified in the context of the boson sampling debate (Shchesnovich 2015a; Tichy 2015). The problem can be formulated in terms of permanents of rank-three tensors (Tichy 2015), or in a quantum optics-inspired language (Shchesnovich 2015a). The pathway followed in this section remains close to the approach of Tichy (2015), but is formulated in the language of Chap. 7. Many more results, e.g. on measures of distinguishability, are provided in Tichy (2015). Furthermore, several properties of partial distinguishability have recently been observed experimentally (Menssen et al. 2017; Ra et al. 2013a, b).

8.3.5 Boson Sampling

Apart from the Hong-Ou-Mandel effect, the more general concept of many-particle interference was not widely recognised in literature until recently. There have been

efforts inspired by entanglement theory and quantum transport (Tichy et al. 2010; Tichy 2011; Tichy et al. 2012, 2013; Tichy 2014) or in the context of transport on discrete lattices, nowadays labeled *quantum walks* (Ahlbrecht et al. 2012; Mayer et al. 2011; Mayer 2012; Peruzzo et al. 2010; Preiss et al. 2015; Sansoni et al. 2012). A potential reason is that many groups working on many-particle systems usually choose to consider systems of interacting particles, where the genuine dynamical effects of indistinguishability are combined with the effects of interactions (Ahlbrecht et al. 2012; Genske et al. 2013; Preiss et al. 2015). Up to the present day, there have not been any studies where the combination of many-particle interference and particle interactions was investigated in a systematic way. It is in general hard to obtain a detailed understanding of the effects generated by interactions and therefore it is an intricate task to disentangle the physical phenomenology in such systems.

The quantum optics and photonics community in principle had many of the desired tools at hand, since one requires linear optics and single photons. It is, nevertheless, far from straightforward to generate enough single photons, but it has been feasible to go beyond two in a well-controlled way for quite a while (Eibl et al. 2003; Huang et al. 2011; Ou et al. 1999; Ra et al. 2013a, b; Tichy et al. 2011; Yao et al. 2012). The interest in the generation of many-photon number states was not only motivated by fundamental physics questions; it got boosted by the prospect of applications in metrology (Kok et al. 2002) and quantum computation (Knill et al. 2001).

The most recent boost of interest in many-particle interference came from the computer science community. Even though there have been several proposals of quantum algorithms which are better at solving specific problems than their classical counterparts, e.g. prime factorisation (Shor 1997), it is far less clear how quantum computing fits in formal complexity theory (Nielsen and Chuang 2010). Recent advances (Aaronson and Arkhipov 2013; Bremner et al. 2010) have shed some light on this debate. Specifically (Aaronson and Arkhipov 2013) made the explicit connection between this formal debate in complexity theory and many-boson interference through the idea of *boson sampling*.

Because this dissertation focusses on the physics of many-particle interference rather than complexity theory of quantum information, we restrict ourselves to a brief sketch of the main result in Aaronson and Arkhipov (2013). We focus on the aspects of the work which are of relevance from the physics perspective and avoid the rigorous jargon of complexity theory.

The key ingredients in such a boson sampling setup are bosonic number states Ψ (8.50), a single-particle unitary channel \mathfrak{U}_1 (8.5) and a selected output measurement state Ξ (8.51). The initial state is transferred via the unitary channel, at each output mode, a photon counter is mounted and the photons are detected according to a certain probability distribution (see also Fig. 8.6). The probability to detect a specific set of output modes, determined by Ξ , is given by the distribution $p_{\Psi \to \Xi}^b$ (8.54). With the results obtained above on many-particle interference, we observe that, in the absence of exploitable symmetries in the channel \mathfrak{U}_1 , brute force evaluation of this probability distribution is unfeasible: The number of possible choices for output states grows unpleasantly fast with the number of particles and the number of modes,

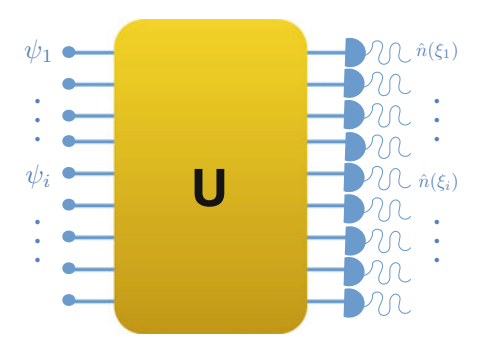


Fig. 8.6 Schematic representation of the generic measurement setup. A set of initial input modes $\{\psi_1, \ldots, \psi_m\}$ are connected to a set of output modes $\{\xi_1, \ldots, \xi_m\}$ via a single-particle unitary operation, given by E(U) as in (8.5). Each of these output modes is equipped with a counter, described by $\hat{n}(\xi_i) = a^{\dagger}(\xi_i)a(\xi_i)$, which measures the number of particles in the mode

and for each such choice $p_{\Psi \to \Xi}^b$ itself scales in a very unfavourable way with the number of particles.

In physics this type of problems are not uncommon, since we regularly encounter ensembles for which partition functions, and hence probability distributions, are hard to access. A popular way to circumvent these difficulties is via Monte Carlo simulations (Landau and Binder 2009), which exploits the idea that it may still be possible to faithfully sample from a distribution without actually knowing all its details. When one approaches the boson sampling problem from a physics perspective it seems natural to employ similar techniques, i.e. one simulates the sampling directly. It is exactly on this level that the results of Aaronson and Arkhipov (2013) have their impact: They "prove" that even a simulation of the sampling procedure for the many-boson setup is a computationally hard problem.

In the context of computational complexity theory, this result is important because it goes beyond the level of specific algorithms. Indeed, Aaronson and Arkhipov argue that it is impossible to come up with *any* algorithm that lets a classical computer efficiently simulate the boson sampling procedure. ¹⁶

For our work in this dissertation, an aspect of the boson sampling setup is the requirement of a unitary $m \times m$ matrix (where m is the number of modes), which describes the single-particle unitary channel \mathfrak{U}_1 (8.5), to be sampled from the *Haar measure*.

¹⁵The proof relies on the "permanent-of-Gaussians conjecture" and on the "permanent anticoncentration conjecture" (see Aaronson and Arkhipov (2013) for details). Therefore it is formally not completely correct to refer to the result as a closed proof.

¹⁶In computational complexity theory jargon the result states that the existence of an efficient simulation scheme for boson sampling implies a collapse of the polynomial hierarchy up to the third order. For details on this statement, we refer the reader to Aaronson and Arkhipov (2013), Moore and Mertens (2011). For the context of this dissertation, it suffices to know that this is a complexity theorist's way of stating that it is highly unlikely to be possible.

In general, the Haar measure is defined as the natural uniform probability measure μ on a compact topological group \mathcal{G} , which is characterised (Conway 1997) by the properties

$$\mu(\mathcal{G}) = 1,\tag{8.97}$$

$$\mu(\mathcal{O}) > 0$$
 for every non-empty open set $\mathcal{O} \subset \mathcal{G}$, (8.98)

$$\mu(g\mathcal{M}) = \mu(\mathcal{M}g) = \mu(\mathcal{M})$$
 for all $g \in \mathcal{G}$ and every measurable set $\mathcal{M} \subset \mathcal{G}$.
(8.99)

In our specific context, the compact topological group \mathcal{G} is the group of all $m \times m$ unitary matrices, $\mathcal{U}(m)$.¹⁷

To Aaronson and Arkhipov, the use of a random unitary matrix appears to be a mathematical trick. For their proof to work, one must avoid any symmetries in the unitary matrix, since they may be exploited to sample efficiently. Because of the random choice of U, the probability that exploitable symmetries are present in the system is negligible.

However, from a physics point of view, the choice of a unitary matrix from the Haar measure makes a connection (Urbina et al. 2016) to the theory of scattering in chaotic cavities (recall also Chap. 5). The combination of the structured interplay of many-particle interference amplitudes, combined with the random scattering medium, moreover, allows us to treat the boson sampler as a genuine complex system (recall Sect. 3.1.1). *Ergo*, boson sampling is essentially many-particle interference in complex systems (i.e. the setup as sketched (b) of Fig. 1.2). In addition, the connection to RMT allows us to use the tools and ideas of Sect. 3.3, which will be the basis of our main results in Sect. 8.5.

Soon after the proposal of Aaronson and Arkhipov, several attempts of an experimental implementation (though of rather modest size, i.e. far from the regime of true complexity) followed (Bentivegna et al. 2015; Broome et al. 2013; Crespi et al. 2013; Shen et al. 2014; Spagnolo et al. 2014; Spring et al. 2013; Tillmann et al. 2013). Even though there recently were several innovations on the level of integrated photonic circuits (Broome et al. 2013; Bunyk et al. 2014; Metcalf et al. 2013; Spring et al. 2013), the main problem remains: The difficulty to generate and control number states of a sufficiently large number of indistinguishable photons, which can be fed into arbitrary initial modes. So far, experiments have provided good results for up to four photons, and there have been reports of the productions of states with up to eight photons, but this is still far away from the realm of boson sampling that lies outside the reach of a classical computer. Recent advances in this direction include scattershot sampling (Bentivegna et al. 2015), improved photon sources (Loredo et al. 2017; Wang et al. 2017), microwave photonics (Barends et al. 2013; Kelly et al. 2015;

¹⁷In random matrix theory (RMT), the set of unitary matrices equipped with its Haar measure is also referred to as the *Circular Unitary Ensemble* (Akemann et al. 2011).

¹⁸Think for example of Tichy et al. (2010), Tichy (2011), Tichy et al. (2014) to see that symmetries can make many-boson interference much more tractable.

Peropadre et al. 2016), and variations of Gaussian boson sampling (Chakhmakhchyan and Cerf 2017; Chabaud et al. 2017; Hamilton et al. 2017). Nevertheless, it remains an open question (Latmiral et al. 2016; Lund et al. 2017) at what point one may claim to have realised a process that is intractable on a classical computer. This question has even lead to the development (Clifford and Clifford 2018; Neville et al. 2017) of better classical algorithms to simulate boson sampling.¹⁹

Another problem lies in the construction of circuits with sufficiently many modes. Here the problem is that the length of the pathways in the photonic circuit grows, and therefore the setup gets more sensitive to losses and several types of decoherence. Therefore, especially when we approach regimes which are really intractable by simulations, we require tools to check that the devices actually work the way they should. This bridges to the more general problem of *certification* of quantum simulations. We ultimately address this issue in Sect. 8.5, but first we must slightly alter the paradigm in which these problems were formulated. More specifically, we claim that it is more useful to start from a measurement-based Heisenberg picture than from a wave-function-based Schrödinger picture to make further progress.

8.4 Many-Particle Interference: The Measurement Approach

In the previous section, we reviewed the central results on many-particle interference, the distinguishability transition and finally boson sampling. These topics are usually treated in the Schrödinger picture, investigating the dynamics of states and their transition probabilities to other states. From a theoretical physics perspective, this is all formally correct, but we argue that there is an alternative point of view: Rather than focusing on the dynamics of the input state and considering "some projective measurement" on the final output state, we shift focus to the measurement process. The measurement is one of the most fundamental and well-controlled steps in the experiment and it is our goal to gain better understanding of how such measurement can be described. One of the big advantages of such treatment is that we can deal with a broader range of initial states when working in the Heisenberg picture.

We start out with a measurement-based treatment of sampling experiments to precisely formulate the questions which we want our theory to answer.

¹⁹Even though these algorithms still have an unfavourable scaling with increasing numbers of particles, they are much more capable of simulating small systems. One can, for example, apply them to simulate boson sampling with several dozens of particles on a normal laptop.

8.4.1 Many-body Measurement*

The main purpose of this section is to shift the perspective to a more operational, measurement-based framework, and to explain how this connects to the wave function approach. To some readers, specifically those familiar with sampling experiments, this section may be redundant. Nevertheless, it does also provide additional results, such as (8.111), which evaluates the probability to find a specific number of particles in a specific mode. This quantity is useful when we want to describe post-selection experiments.

Initially, we assume that the extra degrees of freedom can be safely ignored and all particles considered are in the same state on \mathcal{H}_{add} .

To correctly describe the measurement setup of a sampling experiment, we must identify the relevant measurement operator. Since we stressed in Sect. 7.4 that the creation and annihilation operators generate the algebra of observables, we know that the relevant operator must be a polynomial of these creation and annihilation operators.

Describing a Counter

To come to a meaningful construction, it is useful to take one step back and focus on the physical realisation of a measurement setup as sketched in Fig. 8.6. The main goal is to detect photons in selected output modes, which essentially implies that we mount a counter on each mode. We already treated the operator (7.100) that has the required properties, the local number operator $\hat{n}(\xi) = a^{\dagger}(\xi)a(\xi) = \Gamma(|\xi\rangle \langle \xi|)$, with $\xi \in \mathcal{H}$. Indeed, this operator is exactly the mathematical tool that describes *one* detector in the setup in Fig. 8.6.

The advantage of the operator $\hat{n}(\xi)$ is that it is well-defined, no matter how many particles are considered in the problem setup, which is also engraved in the fact that it is a single-particle observable in second quantisation (recall Sect. 7.5). It simply counts the number of photons that it receives, independently of how many photons landed in any other detector. Because we treat a single-particle unitary channel, and $\hat{n}(\xi)$ is a dynamical object in the Heisenberg picture, it undergoes dynamics given by

$$\hat{n}(\xi) \mapsto E(U^{\dagger})\hat{n}(\xi)E(U) = \hat{n}(U^{\dagger}\xi). \tag{8.100}$$

This object can now be paired with the initial state in which the system is prepared. This may be a number state such as in (8.50), but could just as well be any quantum state $\langle . \rangle$ (see Eq.2.22). We can obtain the expected number of particles that are detected by the particle counter at mode ξ , by evaluation of $\langle \hat{n}(U^{\dagger}\xi) \rangle$. If $\langle . \rangle$ is generated by a wave function with n_i particles in the ith mode,

²⁰Experimentally, such a counter is rather difficult to construct. Standard photodetectors just click upon detection of one or more photons, e.g. the single-photon avalanche diodes (Cova et al. 1996) that are commonly used cannot resolve the photon number at a given time. The number of photons in a single mode is much harder to resolve, but efforts are being made (Humphreys et al. 2015). We are somewhat ambitious in the text and assume that full counting is feasible.

$$\Psi = \prod_{i=1}^{m} \frac{\left(a^{\dagger}(e_i)\right)^{n_i}}{\sqrt{n_i!}} \Omega, \tag{8.101}$$

the result reads

$$\langle \hat{n}(U^{\dagger}\xi) \rangle = \frac{\left\langle \Omega, \prod_{j=1}^{m} \left(a(e_{j}) \right)^{n_{j}} a^{\dagger}(U^{\dagger}\xi) a(U^{\dagger}\xi) \prod_{i=1}^{m} \left(a^{\dagger}(e_{i}) \right)^{n_{i}} \Omega \right\rangle}{\prod_{i} n_{i}!}$$

$$= \sum_{j=1}^{m} n_{j} \left| \left\langle U^{\dagger}\xi, e_{j} \right\rangle \right|^{2} = \sum_{j=1}^{m} n_{j} \left| \left\langle \xi, Ue_{j} \right\rangle \right|^{2}.$$
(8.102)

The reason for considering states where all particles are initialised in *orthogonal* modes is a purely technical one. It turns out that counting statistics becomes substantially more intricate once non-orthogonal modes are considered. A detailed treatment of these initial states is left for Sect. 8.4.2.

Interestingly, a single-particle wave function $a^{\dagger}(\psi)\Omega$, $\psi \in \mathcal{H}$, has an expected count

$$\langle \hat{n}(U^{\dagger}\xi)\rangle = |\langle \xi, U\psi \rangle|^2 = p_{\psi \to \xi},$$
 (8.103)

ergo, the expected number of clicks in a single-particle experiment is given by the single-particle transition probability. This implies naturally that we can interpret (8.102) in the context of classical probability theory. When we choose $n_i \in \{0, 1\}$, the result (8.102) is identical for fermions, therefore such a single particle quantity is not a good identification tool for bosonic and fermionic many-particle interference in the transmission signal.

In the light of Chap. 2, we can understand much more using this observable than only the expected number of particles in a given mode. We can also determine moments of the probability distribution of possible outcomes, but, more fundamentally, we may even understand the spectral properties of $\hat{n}(\xi)$ as an operator on Fock space, and use these to describe the full probability distribution. In an operational language, this means that the state $\langle . \rangle$ and the spectral decomposition of $\hat{n}(\xi)$ can be used to describe the probability to obtain specific measurement outcomes.

The probability to measure n photons in mode ξ in such a sampling experiment is given by

$$p_{n\xi} = \langle E(U^{\dagger}) P_{n\xi} E(U) \rangle, \tag{8.104}$$

where E(U) is as in (7.106), (7.107) and

$$P_{n\xi} := \sum_{j} |\Psi_{j}\rangle\langle\Psi_{j}|, \quad \Psi_{j} \in \{\Psi \in \Gamma(\mathcal{H}) \mid \hat{n}(\xi)\Psi = n\Psi\}. \tag{8.105}$$

To understand the spectral properties of $\hat{n}(\xi)$, and therefore the form of the Ψ_j which enter (8.105), we consider the action of the operator in some simple examples. It is straightforward to see that

$$\hat{n}(\xi)\Omega = 0, \tag{8.106}$$

and hence the vacuum is already an eigenstate of $\hat{n}(\xi)$ with eigenvalue zero. Additionally, we consider single-particle wave functions, thus

$$\hat{n}(\xi)a^{\dagger}(\psi)\Omega = \langle \xi, \psi \rangle a^{\dagger}(\xi)\Omega, \quad \psi \in \mathcal{H}, \tag{8.107}$$

where it is also straightforward to see that in general $a^\dagger(\psi)\Omega$ is not an eigenvector. However, when $\langle \xi, \psi \rangle = 0$, we do find that the wave function is an eigenvector with eigenvalue 0; in the opposite extreme, where $\langle \xi, \psi \rangle = 1$, and essentially $\xi = \psi$, we obtain that $a^\dagger(\xi)\Omega$ is an eigenvector with eigenvalue 1. Because $\hat{n}(\xi)$ acts on the full Fock space, we may also look for many-particle eigenvectors. In the two-particle sector, this leads to

$$\hat{n}(\xi)a^{\dagger}(\phi)a^{\dagger}(\psi)\Omega = \frac{1}{\mathcal{N}} \langle \xi, \phi \rangle a^{\dagger}(\xi)a^{\dagger}(\psi)\Omega + \langle \xi, \psi \rangle a^{\dagger}(\xi)a^{\dagger}(\phi)\Omega, \quad \psi, \phi \in \mathcal{H},$$
(8.108)

which is, again, generally not an eigenvector. However, for $\langle \xi, \psi \rangle = \langle \xi, \phi \rangle = 0$, (8.108) defines an eigenvector with eigenvalue 0. Alternatively, we may assume that $\psi = \phi = \xi$, such that we obtain an eigenvector with eigenvalue 2. The last possibility is to set $\langle \xi, \psi \rangle = 1$ and $\langle \xi, \phi \rangle = 0$ (or vice versa), where we obtain an eigenvalue 1. This can straightforwardly be generalised to the *n*-particle case: In general, any $n \in \mathbb{N}$ can be an eigenvalue and the corresponding eigenvectors are given by²¹

$$\Psi_{n\xi} \in \operatorname{span}\left\{\frac{1}{\mathcal{N}}a^{\dagger}(\xi)^{n}a^{\dagger}(\psi_{1})\dots a^{\dagger}(\psi_{q})\Omega \mid \psi_{j} \in \mathcal{H}\left\langle \xi, \psi_{j} \right\rangle = 0\right\}. \tag{8.109}$$

When we assume that the system is prepared in a number state such as (8.101), we must only consider other number states with the same number of particles²² in the sum (8.105). When we define the space

$$\xi^{\perp} := \{ \psi \in \mathcal{H} \mid \langle \psi, \xi \rangle = 0 \}, \tag{8.110}$$

²¹More formal proofs can be constructed in various ways. An appealing construction exploits the equivalence of a bosonic system with a tensor product of harmonic oscillators (see Sect. 7.3.2), to explicitly construct eigenstates of a number operator acting on one of these oscillators.

 $^{^{22}}$ In principle, for each eigenvalue n, we obtain an enormous eigenspace on which to project. This implies that we must consider all wave functions which have a non-zero component in the n-particle sector. However, because we consider a projector on the whole eigenspace, we ultimately find that the only wave functions which are relevant in the sum (8.105) are those which are n-particle wave functions.

we find that

$$p_{n\xi} = \sum_{j_1,\dots,j_r} \frac{1}{\mathcal{N}' n_1! \dots n_m!} \times \left| \left\langle \left(a^{\dagger}(e_1) \right)^{n_1} \dots \left(a^{\dagger}(e_m) \right)^{n_m} \Omega, \left(a^{\dagger}(U^{\dagger}\xi) \right)^n a^{\dagger}(U^{\dagger}x_{j_1}) \dots a^{\dagger}(U^{\dagger}x_{j_r}) \Omega \right\rangle \right|^2,$$
(8.111)

where a lot of notational overhead is required: the set $\{x_j\}$ is a basis of ξ^\perp , over which is summed for each index j_k . The label m denotes the total number of modes, and n_i is the number of particles in a given mode i, $\sum_i n_i$ is therefore the total number of particles in the system. The label r is given by $r = \left(\sum_i n_i\right) - n$, the total number of particles which are *not* detected in mode ξ . We can indeed calculate this probability using the permanents (or determinants for fermions) discussed in Sect. 8.3; wave function approach and measurement approach essentially describe the same objects. However, since we here describe only one single detector, we do not perform a full sampling experiment. Indeed, we actually trace out r particles! In order to accurately describe the full wave function approach, we need to come up with a treatment of several detectors at a time.

Describing an Array of Counters

To describe sampling experiments, we want to interrogate several detectors at the same time, and are specifically interested in finding the particles in predefined modes. Combinations of several detectors can be formed in two ways: additive and multiplicative. In our context, the multiplicative route is the way to go, since we are asking questions of the type "what is the probability to detect one particle in ξ_1 and one particle in ξ_2 ?". Given that $\hat{n}(\xi_j) = \Gamma(|\xi_j\rangle\langle\xi_j|)$ is a single-particle observable, it directly follows that $\hat{n}(\xi_1) + \hat{n}(\xi_2) = \Gamma(|\xi_1\rangle\langle\xi_1| + |\xi_2\rangle\langle\xi_2|)$ still is a single-particle observable. However, $\hat{n}(\xi_1)\hat{n}(\xi_2)$ is clearly not a single-particle observable.

Now, let us start with a set $f_1, \ldots, f_n \in \mathcal{H}, \langle f_i, f_j \rangle = \delta_{ij}$, and consider the measurement operator

$$\mathfrak{O} = \hat{n}(f_1) \dots \hat{n}(f_n) = a^{\dagger}(f_1) \dots a^{\dagger}(f_n) a(f_n) \dots a(f_1), \tag{8.112}$$

where the last step is only valid because of the *orthogonality* of the f_i . Expression (8.112) now identifies $\mathfrak O$ as a clear n-particle observable. What we do in such an experimental setting is literally multiplying the number of photons measured in the selected detectors. Given that we consider n detectors, it is only logical that, for less than n input particles, there is always at least one detector that does not detect any particle. This implies a zero measurement for the product of all detectors.

Looking back at Sect. 7.7, bearing many-particle correlation functions in mind, a Wick monomial (definition on p. 243) as the one in (8.112) should immediately seem familiar. Indeed, if we consider the dynamics

$$\mathfrak{O} \mapsto E(U^{\dagger})\mathfrak{O}E(U) = a^{\dagger}(U^{\dagger}f_1) \dots a^{\dagger}(U^{\dagger}f_n)a(U^{\dagger}f_n) \dots a(U^{\dagger}f_1) \quad (8.113)$$

and pair this object with a general quantum state $\langle . \rangle$, we obtain

$$\langle a^{\dagger}(U^{\dagger}f_1)\dots a^{\dagger}(U^{\dagger}f_n)a(U^{\dagger}f_n)\dots a(U^{\dagger}f_1)\rangle$$
 (8.114)

as the expected measurement outcome. This exactly probes the *correlation* between outcomes in the different measurement modes, under a specific single-particle unitary channel, for a specific initial state $\langle . \rangle$. The study of these objects is reserved for Sect. 8.4.2. Here we focus on the connection to the wave functions approach.

To study the actual probabilities of given events, we must interpret the measurement outcomes in the correct context, as we did in (8.105). To generalise Eq. (8.109) to describe eigenvectors of \mathfrak{D} as in (8.112), let us define

$$\mathcal{F} := \operatorname{span}\{f_1, \dots, f_n\}. \tag{8.115}$$

The general eigenvalues of (8.112) are given by $\nu := \nu_1 \nu_2 \dots \nu_n$, with $\nu_j \in \mathbb{N}$, with the associated eigenvectors

$$\Psi_{\nu_1\dots\nu_n} \in \operatorname{span}\left\{\frac{1}{\mathcal{N}}a^{\dagger}(f_1)^{\nu_1}\dots a^{\dagger}(f_n)^{\nu_n}a^{\dagger}(\psi_1)\dots a^{\dagger}(\psi_q)\Omega \mid \psi_1,\dots,\psi_q \in \mathcal{F}^{\perp}\right\}. \tag{8.116}$$

However, this is not completely correct, in the sense that there are many choices of ν_1, \ldots, ν_n that lead to the same measurement outcome ν . This implies that the measurement outcomes are as such highly degenerate. Therefore, simply considering $\mathfrak O$ as in (8.112) may not always be sufficient.

It is, nevertheless, illuminating to interpret the scenario where we prepare the system in an initial state

$$a^{\dagger}(e_1) \dots a^{\dagger}(e_n)\Omega, \quad \langle e_i, e_j \rangle = \delta_{ij}.$$
 (8.117)

When we now measure the observable $\hat{n}(f_1) \dots \hat{n}(f_n)$, and ask for the probability to obtain measurement outcome 1, we find

$$p_1 = \sum_{i} \langle E(U^{\dagger}) P_1 E(U) \rangle, \tag{8.118}$$

where P_1 projects on all wave functions $\Xi \in \Gamma(\mathcal{H})$ with the property

$$\hat{n}(f_1)\dots\hat{n}(f_n)\Xi=\Xi. \tag{8.119}$$

In the light of (8.109) this is a huge set, but when $\langle . \rangle$ describes a number state with exactly n particles, where n is also the number of independent detectors considered, only the projection on one specific $\Psi \in \Gamma(\mathcal{H})$ gives a non-vanishing contribution to Eq. (8.118). Due to the Hilbert projection theorem (see (8.79) and related discussion), this non-vanishing contribution must come from an n-particle wave function with

property (8.119). There is only one single wave function fulfilling this criterium, given by

$$\Xi^{(n)} = a^{\dagger}(f_1) \dots a^{\dagger}(f_n) \Omega. \tag{8.120}$$

Consequently, we find for bosons that

$$p_{1} = \left| \left\langle a^{\dagger}(e_{1}) \dots a^{\dagger}(e_{n}) \Omega, a^{\dagger}(U^{\dagger}f_{1}) \dots a^{\dagger}(U^{\dagger}f_{n}) \Omega \right\rangle \right|^{2} = \left| \operatorname{perm}\left[\left\langle f_{i}, U e_{j} \right\rangle \right] \right|^{2}, \tag{8.121}$$

which is exactly the transition probability $p_{\Psi \to \Xi}^b$ from Eq. (8.53). Also for fermions one obtains the familiar result

$$p_1 = \left| \det[\left\langle f_i, U e_j \right\rangle] \right|^2 = p_{\Psi \to \Xi}^f. \tag{8.122}$$

On the matter of interpretation, we may consider this situation to be special, in the sense that we consider n specific detectors for an n-particle initial state. Since the number of particles is conserved in the process, there are only two possible measurement outcomes for observables \mathfrak{D} (8.112): "0" or "1". We interpret these as "No" or "Yes" respectively, answering the question "Were the particles detected by this specifically selected set of modes?". This implies that the probability p_1 is indeed exactly the probability to detect a particle in each of these specific modes and therefore making p_1 equivalent to the previously obtained probabilities (8.54) or (8.73).

There is one difficulty which was so far hidden under the rug: The case where several particles are detected by the same mode. The logical suggestion is to consider operators of the n-detector type, such as described by Eq. (8.112), and simply consider eigenvalues which go beyond "1". This, however, leads to a problem: Even for an (n+1)-particle number state and an n-detector setup, the eigenvalue 2 is n-fold degenerate. We may use these operators to identify whether *one of the n detectors* detected two particles, but we cannot determine *which* detector.

To adjust our interrogation technique for specific questions such as: "Did we find exactly one particle in modes $f_1, \ldots f_{n-1}$, two particles in mode f_n , and no particles anywhere else?", we may already feel the need for the construction of specific operators with outcomes "0" or "1" ("No" or "Yes") in the (n + 1)-particle sector, because the question implies that we consider a setup with n + 1 particles. The direct proposal is to simply consider an operator

$$\mathfrak{O} = \hat{n}(f_1) \dots \hat{n}(f_{n-1})\hat{n}(f_n)\hat{n}(f_n), \tag{8.123}$$

but there is a problem: The operator is not strictly an n + 1-particle operator. This is traced back to

$$\hat{n}(f_n)\hat{n}(f_n) = a^{\dagger}(f_n)a(f_n) + a^{\dagger}(f_n)a^{\dagger}(f_n)a(f_n)a(f_n),$$
 (bosons) (8.124)

$$\hat{n}(f_n)\hat{n}(f_n) = a^{\dagger}(f_n)a(f_n) - a^{\dagger}(f_n)a^{\dagger}(f_n)a(f_n)a(f_n), \quad \text{(fermions)} \quad (8.125)$$

which clearly contains a single-particle term. This issue immediately suggests an alternative definition of \mathfrak{O} , since we see that the true n+1-particle observable is rather given by

$$\mathfrak{D} = a^{\dagger}(f_1) \dots a^{\dagger}(f_{n-1}) a^{\dagger}(f_n) a^{\dagger}(f_n) a(f_n) a(f_n) a(f_{n-1}) \dots a(f_1). \tag{8.126}$$

These are the formal operators which ask questions about specific (n + 1)-particle events. Nevertheless, it is not obvious that one can simply generalise these results to a set of general non-orthogonal modes, due to eigenvector structures which are considerably more complicated. Although we formally know how to describe the operators (8.126), we pay the price that we can no longer connect in an obvious fashion the interpretation of such an operator to a physical detector array.

We established that observables and a concrete measurement-based description are correctly reproducing the results of the wave function approach for sets of orthogonal output modes. However, as we showed, the measurement-based setup is capable to address a broader class of questions: It provides a theoretical framework to study moments, such as expectation values of the number of particles in a given mode, or correlations between different independent modes. Moreover, it can in principle do so for any initial state. Additionally, it allows us to investigate few-particle properties of many-particle states; exactly this will prove crucial to gain a deeper understanding of many-particle interference. Although, computationally, we cannot keep track of complete sampling events, ²³ we can use few-particle and/or few mode observations to probe many-particle properties.

8.4.2 Many-Body Correlations

Correlations functions are fundamental objects that allow us to learn a great deal about quantum states and quantum systems in general. We discussed in Sect. 7.7 that knowledge of all correlation functions implies knowledge of the full quantum state. In the present section, we specifically follow this line of thought and describe correlations between different detectors. Initially, we do not consider the additional complication of additional degrees of freedom that are not detected, hence discard \mathcal{H}_{add} . As a first step, we use the measurement based language to describe correlation functions of orthogonal modes, and later we treat more general correlation functions to emphasise some of the subtleties that arise due to the lack of orthogonality. In Sect. 8.5, we use these quantities as the foundation of a *practical* certification scheme for boson sampling setups.

Orthogonal Modes

As the observable to be measured, we consider $\hat{n}(f_1) \dots \hat{n}(f_q)$, where f_i are the modes on which detectors are mounted. Action of the dynamical map upon this observable leads to

²³And it is obviously unreasonable to hope to do so.

$$\hat{n}(f_1)\dots\hat{n}(f_q) \mapsto \hat{n}(U^{\dagger}f_1)\dots\hat{n}(U^{\dagger}f_q), \quad f_i \in \mathcal{H}, \langle f_i, f_i \rangle = \delta_{ij}, \quad (8.127)$$

such that we can combine this object with the initial quantum state (.) to obtain

$$c_{1,\dots,q} := \langle \hat{n}(U^{\dagger}f_1)\dots\hat{n}(U^{\dagger}f_q)\rangle = \langle a^{\dagger}(U^{\dagger}f_1)\dots a^{\dagger}(U^{\dagger}f_q)a(U^{\dagger}f_q)\dots a(U^{\dagger}f_1)\rangle.$$
(8.128)

These are exactly the correlation functions as treated in Sect. 7.7, for a general state $\langle . \rangle$, but here we consider the specific Fock space representation rather than the abstract CCR or CAR algebras. Nevertheless, the correlation functions $c_{1,...,q}$ will serve to characterise the state.

In principle, this approach is feasible for any possible input state $\langle . \rangle$, but we choose to deal with number states and, more specifically, number states which are of the form (8.101). This leads to the explicit expression

$$c_{1,\dots,q} = \left\langle \prod_{i=1}^{m} \frac{\left(a^{\dagger}(e_{i})\right)^{n_{i}}}{\sqrt{n_{i}!}} \Omega, a^{\dagger}(U^{\dagger}f_{1}) \dots a^{\dagger}(U^{\dagger}f_{q}) a(U^{\dagger}f_{q}) \dots a(U^{\dagger}f_{1}) \prod_{i=1}^{m} \frac{\left(a^{\dagger}(e_{i})\right)^{n_{i}}}{\sqrt{n_{i}!}} \Omega \right\rangle. \tag{8.129}$$

The main technical difficulty in the evaluation of this quantity is the correct treatment of the combinatorics. A brute force attack on this front would lack transparency and therefore we first treat a simple example:

Example 8.4.1 The simplest possible example consists in only one initially occupied mode and two detectors at modes f_i and f_j , such that we need to evaluate

$$c_{i,j} = \frac{1}{n!} \left\langle a(U^{\dagger} f_i) a(U^{\dagger} f_j) a^{\dagger}(e_l)^n \Omega, a(U^{\dagger} f_i) a(U^{\dagger} f_j) a^{\dagger}(e_l)^n \Omega \right\rangle. \tag{8.130}$$

To carry out the calculation, we need the crucial step

$$a(U^{\dagger}f_{j})a(U^{\dagger}f_{i})a^{\dagger}(e_{l})^{n} = n(n-1) \langle f_{i}, Ue_{l} \rangle \langle f_{j}, Ue_{l} \rangle a^{\dagger}(e_{l})^{n-2}$$

$$+ a^{\dagger}(e_{l})^{n} a(U^{\dagger}f_{j})a(U^{\dagger}f_{i})$$

$$+ n \langle f_{i}, Ue_{l} \rangle a^{\dagger}(e_{l})^{n-1} a(U^{\dagger}f_{j})$$

$$+ n \langle f_{i}, Ue_{l} \rangle a^{\dagger}(e_{l})^{n-1} a(U^{\dagger}f_{i}).$$

$$(8.131)$$

Using this identity, we find that the final correlation is given by

$$c_{i,j} = \frac{n^2(n-1)^2}{n!} \left| \langle f_i, Ue_l \rangle \left\langle f_j, Ue_l \right\rangle \right|^2 \left\langle \Omega, a(e_l)^{n-2} a^{\dagger}(e_l)^{n-2} \Omega \right\rangle$$

$$= n(n-1) \left| \langle f_i, Ue_l \rangle \right|^2 \left| \left\langle f_j, Ue_l \right\rangle \right|^2,$$
(8.132)

since only the first term in (8.131) survives the encounter with the vacuum.

Let us now assume that we are dealing with bosons. To make further progress on (8.129), we consider the situation where the particles are prepared in different initial

modes $e_1, \ldots, e_m \in \mathcal{H}$ (for m modes in total), such that the wave function

$$\Psi = \prod_{i=1}^{m} \frac{\left(a^{\dagger}(e_i)\right)^{n_i}}{\sqrt{n_i!}} \Omega \tag{8.133}$$

describes the state. The general expression (8.129) is actually an inner product of the vector

$$a(U^{\dagger}f_q)\dots a(U^{\dagger}f_1)\frac{\left(a^{\dagger}(e_1)\right)^{n_1}}{\sqrt{n_1!}}\dots\frac{\left(a^{\dagger}(e_m)\right)^{n_m}}{\sqrt{n_m!}}\Omega\tag{8.134}$$

with itself. The problem is that the expression is a Wick monomial in anti-normal order, which implies we must reshuffle it to cast it into normal ordering. This operation is useful since in normal order only the terms without any annihilation operators survive when acting on the vacuum Ω (see also Example 8.4.1). The canonical commutation relations (7.77) imply that

$$a(U^{\dagger}f_i)a^{\dagger}(e_j) = \langle U^{\dagger}f_i, e_j \rangle + a^{\dagger}(e_j)a(U^{\dagger}f_i), \tag{8.135}$$

which implies that *either creation and annihilation operators switch place, or they disappear.* Since we only deal with terms where there are no annihilation operators left, it means that they have all paired up with a creation operator to form an inner product, as schematically represented in Fig. 8.7. Of course, there are many ways of pairing creation operators and annihilation operators and we must sum over all these possibilities.

This procedure implies that we can rewrite (8.134), using additional notational tools for index bookkeeping: We define the $\textit{multiset}^{24} \ \mathcal{D}(\Psi)$, for a specific $\Psi \in \Gamma^b(\mathcal{H})$ as given by (8.133), as

$$\mathcal{D}(\Psi) = (\underbrace{1, \dots, 1}_{n_1}, \underbrace{2, \dots, 2}_{n_2}, \dots, \underbrace{m, \dots, m}_{n_m}). \tag{8.136}$$

We now consider sums over different indices as sums over different choices of subsets. However, since elements in $\mathcal{D}(\Psi)$ come with given multiplicities, it is crucial to also count the number of different ways to construct these subsets. As a simple example, assume that $\mathcal{D}(\Psi) = \{1, 1, 2, 2\}$ and we want to consider the subset $\{1, 2\}$. One clearly sees that there are four ways to do reduce $\{1, 1, 2, 2\}$ to $\{1, 2\}$. Defining $\mathcal{C}_{\mathcal{U}}$ as the number of ways in which one can sample subset \mathcal{U} from $\mathcal{D}(\Psi)$, we find that

 $^{^{24}}$ Multisets are very similar to sets, but are an extension in that sense that elements can occur several times. For example $\{1, 2, 3\}$ is a set, but $\{1, 1, 2, 3\}$ is a multiset. For an overview of the theoretical framework, see Blizard (1988)

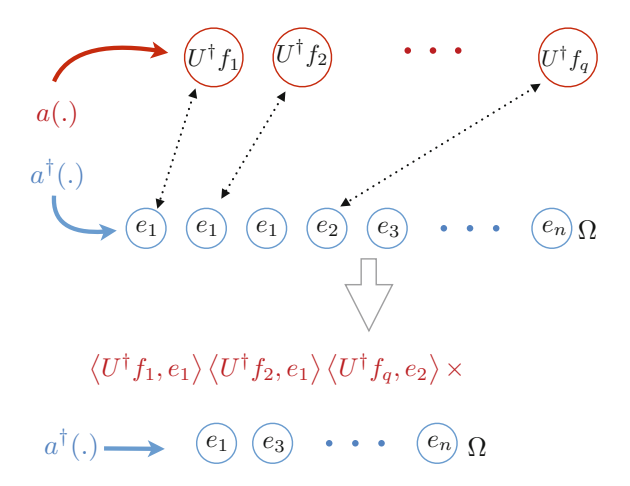


Fig. 8.7 Schematic representation of the pairing of creation and annihilation operators as generated by (8.135), to rewrite (8.134). In this concrete case the Wick monomial $a(U^{\dagger}f_1)\dots a(U^{\dagger}f_q)a^{\dagger}(e_1)\dots a^{\dagger}(e_n)$ acts on the vacuum Ω . Upon reordering to normal order, the monomial will become a polynomial and all potential pairings of annihilation operators with creation operators need to be considered. Each pairing of an annihilation and creation operator ultimately leads to a factor which is given by the inner product of their arguments, multiplied by the remaining creation operators

$$a(U^{\dagger}f_{q})\dots a(U^{\dagger}f_{1})\frac{\left(a^{\dagger}(e_{1})\right)^{n_{1}}}{\sqrt{n_{1}!}}\dots\frac{\left(a^{\dagger}(e_{m})\right)^{n_{m}}}{\sqrt{n_{m}!}}\Omega$$

$$=\frac{1}{\sqrt{n_{1}!\dots n_{m}!}}\sum_{\substack{\mathcal{U}\subset\mathcal{D}(\Psi)\\|\mathcal{U}|=q}}\mathcal{C}_{\mathcal{U}}\sum_{\pi\in\mathcal{S}_{q}}\prod_{\substack{r=1\\j_{r}\in\mathcal{U}}}^{q}\left\langle f_{r},Ue_{j_{\pi(r)}}\right\rangle\prod_{k\in\mathcal{D}(\Psi)\backslash\mathcal{U}}a^{\dagger}(e_{k})\Omega.$$
(8.137)

Using this result in the general expression (8.129), we find ultimately that

$$c_{1,\dots,q}^{b} = \frac{1}{n_{1}!\dots n_{m}!} \sum_{\substack{\mathcal{U}',\mathcal{U}\subset\mathcal{D}(\Psi)\\|\mathcal{U}'|=|\mathcal{U}|=q}} \mathcal{C}_{\mathcal{U}}\mathcal{C}_{\mathcal{U}'} \sum_{\substack{\pi,\sigma\in S_{q}\\j_{r}\in\mathcal{U}\\j_{r}'\in\mathcal{U}'}} \prod_{\substack{r=1\\j_{r}\in\mathcal{U}\\j_{r}'\in\mathcal{U}'}} \left\langle f_{r},Ue_{j_{\pi(r)}}\right\rangle \left\langle e_{j_{\sigma(r)}'},U^{\dagger}f_{r}\right\rangle \times \left\langle \prod_{k\in\mathcal{D}(\Psi)\backslash\mathcal{U}'} a^{\dagger}(e_{k})\Omega, \prod_{l\in\mathcal{D}(\Psi)\backslash\mathcal{U}} a^{\dagger}(e_{l})\Omega\right\rangle. \tag{8.138}$$

It remains to gain deeper understanding of

$$\left\langle \prod_{k \in \mathcal{D}(\Psi) \setminus \mathcal{U}'} a^{\dagger}(e_{k}) \Omega, \prod_{l \in \mathcal{D}(\Psi) \setminus \mathcal{U}} a^{\dagger}(e_{l}) \Omega \right\rangle$$

$$= \sum_{\pi \in S_{n-q}} \left\langle e_{k_{1}}, e_{l_{\pi(1)}} \right\rangle \left\langle e_{k_{2}}, e_{l_{\pi(2)}} \right\rangle \dots \left\langle e_{k_{n-q}}, e_{l_{\pi(n-q)}} \right\rangle$$
(8.139)

with $n = \sum_{i=1}^m n_i$ the total number of particles. We labeled the indices such that $\mathcal{D}(\Psi) \setminus \mathcal{U}' := \{k_1, k_2, \dots, k_{n-q}\}$ and $\mathcal{D}(\Psi) \setminus \mathcal{U} := \{l_1, l_2, \dots, l_{n-q}\}$. In words this notation means that the pairing of creation and annihilation operators lowers the particle number of the total wave-function. However, since we do this pairing both on the "bra" and on the "ket" side of (8.129), we need to consider what happens to the remaining creation and annihilation operators. Obviously, when we take out $a^{\dagger}(e_j)$ from the "bra" side, but leave an $a^{\dagger}(e_j)$ on the "ket" side, the orthogonality of all other single-particle wave-functions kills the entire factor (8.139). Mathematically formulated, due to the *orthogonality* conditions $\langle e_i, e_j \rangle = \delta_{ij}$, we obtain from (8.139) that

$$\mathcal{D}(\Psi) \setminus \mathcal{U}' \neq \mathcal{D}(\Psi) \setminus \mathcal{U} \implies \left\langle \prod_{k \in \mathcal{D}(\Psi) \setminus \mathcal{U}'} a^{\dagger}(e_k) \Omega, \prod_{l \in \mathcal{D}(\Psi) \setminus \mathcal{U}} a^{\dagger}(e_l) \Omega \right\rangle = 0.$$
(8.140)

This implies that the number of terms that have a non-zero contribution in (8.138) drastically decreases.

We are discussing a multiset that does bookkeeping for *indices*, and this is nothing else than a list of natural numbers. Since we only consider terms where

$$\mathcal{D}(\Psi) \setminus \mathcal{U}' = \mathcal{D}(\Psi) \setminus \mathcal{U}, \tag{8.141}$$

we only need to consider those terms where

$$\mathcal{U}' \subset \mathcal{D}(\Psi) = \mathcal{U} \subset \mathcal{D}(\Psi). \tag{8.142}$$

Hence, the sum (8.138) can be rewritten as

$$c_{1,\dots,q}^{b} = \frac{1}{n_{1}!\dots n_{m}!} \sum_{\substack{\mathcal{U}\subset\mathcal{D}(\Psi)\\|\mathcal{U}|=q}} (\mathcal{C}_{\mathcal{U}})^{2} \sum_{\pi,\sigma\in\mathcal{S}_{q}} \prod_{\substack{r=1\\j_{r}\in\mathcal{U}}}^{q} \left\langle f_{r}, Ue_{j_{\pi(r)}} \right\rangle \left\langle e_{j_{\sigma(r)}}, U^{\dagger}f_{r} \right\rangle \times \left\langle \prod_{k\in\mathcal{D}(\Psi)\backslash\mathcal{U}} a^{\dagger}(e_{k})\Omega, \prod_{l\in\mathcal{D}(\Psi)\backslash\mathcal{U}} a^{\dagger}(e_{l})\Omega \right\rangle. \tag{8.143}$$

Let us introduce one final tool to simplify the expression (8.143). The multiplicity $\mathbb{M}_{\mathcal{A}}(x)$ counts the number of times that an element x occurs in \mathcal{A} , and we therefore

may rewrite

$$\mathcal{C}_{\mathcal{U}} = \prod_{k \in \mathcal{U} \cap \mathbb{N}} \frac{\mathbb{M}_{\mathcal{D}(\Psi)}(k)!}{\mathbb{M}_{\mathcal{D}(\Psi) \setminus \mathcal{U}}(k)!},$$
(8.144)

where we introduced the natural object $\mathcal{U} \cap \mathbb{N}$: We directly interpret this $\mathcal{U} \cap \mathbb{N}$ as a subset of a set of indices \mathcal{U} , which contains all the *different* elements of \mathcal{U} , but all occurring with multiplicity one.²⁵ This notation, together with the orthogonality conditions on the vectors $e_k \in \mathcal{H}$, leads to

$$\left\langle \prod_{k \in \mathcal{D}(\Psi) \setminus \mathcal{U}} a^{\dagger}(e_k) \Omega, \prod_{l \in \mathcal{D}(\Psi) \setminus \mathcal{U}} a^{\dagger}(e_l) \Omega \right\rangle = \prod_{k \in \left(\mathcal{D}(\Psi)\right) \setminus \mathcal{U} \cap \mathbb{N}} \mathbb{M}_{\mathcal{D}(\Psi) \setminus \mathcal{U}}(k)!, \quad (8.145)$$

and, ultimately,

$$c_{1,\dots,q}^{b} = \sum_{\substack{\mathcal{U} \subset \mathcal{D}(\Psi) \\ |\mathcal{U}| = q}} \prod_{k \in \mathcal{U} \cap \mathbb{N}} \frac{\mathbb{M}_{\mathcal{D}(\Psi)}(k)!}{\mathbb{M}_{\mathcal{D}(\Psi) \setminus \mathcal{U}}(k)!} \sum_{\pi,\sigma \in S_q} \prod_{\substack{r=1 \\ j_r \in \mathcal{U}}}^{q} \left\langle f_r, U e_{j_{\pi(r)}} \right\rangle \left\langle e_{j_{\sigma(r)}}, U^{\dagger} f_r \right\rangle.$$

$$(8.146)$$

Specifically, for $c_{1,2}$, with two selected modes f_1 , f_2 , (8.146) turns into

$$c_{1,2}^{b} = \sum_{\substack{j_{1},j_{2} \in \mathcal{D}(\Psi) \cap \mathbb{N} \\ j_{1} \neq j_{2}}} n_{j_{1}} n_{j_{2}} \left(\langle f_{1}, U e_{j_{1}} \rangle \langle e_{j_{1}}, U^{\dagger} f_{1} \rangle \langle f_{2}, U e_{j_{2}} \rangle \langle e_{j_{2}}, U^{\dagger} f_{2} \rangle \right)$$

$$+ \langle f_{1}, U e_{j_{1}} \rangle \langle e_{j_{2}}, U^{\dagger} f_{1} \rangle \langle f_{2}, U e_{j_{1}} \rangle \langle e_{j_{2}}, U^{\dagger} f_{2} \rangle$$

$$+ \sum_{j \in \mathcal{D}(\Psi) \cap \mathbb{N}} n_{j} (n_{j} - 1) \langle f_{1}, U e_{j} \rangle \langle e_{j}, U^{\dagger} f_{1} \rangle \langle f_{2}, U e_{j} \rangle \langle e_{j}, U^{\dagger} f_{2} \rangle.$$

$$(8.147)$$

The results (8.146), (8.147) are identical to those obtained in Mayer et al. (2011), Mayer (2012), although the techniques used here are slightly different. Also the above multiset techniques to do the bookkeeping of indices are different from other approaches.

In order to interpret these results in terms of many-particle interference, we compare our final q-point correlation function (8.146) to the transfer probability (8.54) from many-boson input state Ψ to measurement state Ξ , upon transmission through the unitary channel. We note that the correlation function (8.146) is essentially a sum over over q-particle processes which connect a set of q particles, which are selected from the total of n input particles to the q selected output modes. In those cases with multiple particles per input mode, additional combinatorics is required, as contained in $\mathbb{M}_{\mathcal{D}(\Psi)}(k)!/\mathbb{M}_{\mathcal{D}(\Psi)\setminus\mathcal{U}}(k)!$.

²⁵To give a simple example, when we consider the set $A = \{1, 1, 2, 3\}$, then we find that $A \cap \mathbb{N} = \{1, 2, 3\}$.

Let us finally touch upon the analogous scenario for *fermions*. One sees directly that the above calculations can be repeated for fermionic systems. There is however a *huge* advantage in fermionic systems: We can have no more than a single particle per input mode, which avoids the need for multisets and combinatorics, but simply allows us to consider sets. The price to be paid is additional sign bookkeeping, such that we ultimately find, for $n_j \in \{0, 1\}$,

$$a(U^{\dagger}f_{q}) \dots a(U^{\dagger}f_{1}) \frac{\left(a^{\dagger}(e_{1})\right)^{n_{1}}}{\sqrt{n_{1}!}} \dots \frac{\left(a^{\dagger}(e_{m})\right)^{n_{m}}}{\sqrt{n_{m}!}} \Omega$$

$$= \frac{1}{\sqrt{n_{1}! \dots n_{m}!}} \sum_{\substack{\mathcal{U} \subset \mathcal{D}(\Psi) \\ |\mathcal{U}| = q}} \sum_{\pi \in S_{q}} \operatorname{sign}(\pi) \prod_{\substack{r=1 \\ j_{r} \in \mathcal{U}}}^{q} \left\langle f_{r}, U e_{j_{\pi(r)}} \right\rangle \prod_{k \in \mathcal{D}(\Psi) \setminus \mathcal{U}} a^{\dagger}(e_{k}) \Omega.$$
(8.148)

Repeating the reasoning for bosons leads us to the following final result for fermions:

$$c_{1,\dots,q}^{f} = \sum_{\substack{\mathcal{U} \subset \mathcal{D}(\Psi) \\ |\mathcal{U}| = q}} \sum_{\pi,\sigma \in S_q} \operatorname{sign}(\pi) \operatorname{sign}(\sigma) \prod_{\substack{r=1 \\ j_r \in \mathcal{U}}}^{q} \left\langle f_r, U e_{j_{\pi(r)}} \right\rangle \left\langle e_{j_{\sigma(r)}}, U^{\dagger} f_r \right\rangle. \tag{8.149}$$

and notably to the specific two-point correlation function of modes f_1 and f_2 :

$$c_{1,2}^{f} = \sum_{\substack{j_{1}, j_{2} \in \mathcal{D}(\Psi) \\ j_{1} \neq j_{2}}} \left(\langle f_{1}, U e_{j_{1}} \rangle \langle e_{j_{1}}, U^{\dagger} f_{1} \rangle \langle f_{2}, U e_{j_{2}} \rangle \langle e_{j_{2}}, U^{\dagger} f_{2} \rangle - \langle f_{1}, U e_{j_{1}} \rangle \langle e_{j_{2}}, U^{\dagger} f_{1} \rangle \langle f_{2}, U e_{j_{1}} \rangle \langle e_{j_{2}}, U^{\dagger} f_{2} \rangle \right).$$

$$(8.150)$$

Also these results are consistent with Mayer et al. (2011); Mayer (2012). Notice also that whenever we prepare input states for bosons which have at most one particle per mode, very similar results as in the fermionic case are obtained.

Non-Orthogonal Modes

In this section, we consider a setting where both the prepared state and the observable are composed from *non-orthogonal* modes. As mentioned in Sect. 8.4.1, this will blur the immediate connection between the thus constructed observable and an actual measurement setup. One may therefore consider this a mere theoretical generalisation of our previous discussion on orthogonal modes. Nevertheless, we argued that one requires *all* correlation functions of the form (7.225) or (7.281) in order to characterise a state, hence the generalisation is important from a theoretical perspective.

Let us start with a general set of modes $W = \{\xi_1, \dots \xi_q\}, \xi_j \in \mathcal{H}$, which we correlate. We then must consider the correlation function (we, again, consider the bosonic case)

$$c_W^b := \langle a^{\dagger}(U^{\dagger}\xi_1) \dots a^{\dagger}(U^{\dagger}\xi_a) a(U^{\dagger}\xi_a) \dots a(U^{\dagger}\xi_1) \rangle. \tag{8.151}$$

The state $\langle . \rangle$ is again a bosonic number state, generated by a wave function with particles prepared in a set of modes $V = \{\psi_1, \dots \psi_n\}, \psi_j \in \mathcal{H}$, such that the wave function $\Psi \in \Gamma^b(\mathcal{H})$ is given by

$$\Psi = \frac{1}{\sqrt{\text{perm } G^{V,V}}} a^{\dagger}(\psi_1) \dots a^{\dagger}(\psi_n) \Omega. \tag{8.152}$$

Here we introduce a new notation for a slightly generalised Gram matrix,

$$G^{A,B} := [\langle \alpha_i, \beta_j \rangle], \quad \alpha_i \in A, \ \beta_j \in B, \tag{8.153}$$

where A and B are n-tuples of elements from a Hilbert space, i.e. sets of non-orthogonal modes which we select. While A = B = V in (8.152), the general case $A \neq B$ will become useful. Note that there are crucial properties that a Gram matrix $G^{A,A}$ has and $G^{A,B}$ lacks, most notably positive semi-definiteness.

We insert the state given by wave function (8.152) into (8.151) and obtain

$$c_W^b = \frac{\left\langle a(U^\dagger \xi_q) \dots a(U^\dagger \xi_1) a^\dagger(\psi_1) \dots a^\dagger(\psi_n) \Omega, a(U^\dagger \xi_q) \dots a(U^\dagger \xi_1) a^\dagger(\psi_1) \dots a^\dagger(\psi_n) \Omega \right\rangle}{\operatorname{perm} G^{V,V}}.$$
(8.154)

To evaluate this expression, we must again re-express the Wick monomial in the numerator of (8.154) in normal order. By virtue of expression (8.135)—analogous to the derivation of (8.137)—we find

$$a(U^{\dagger}\xi_{q})\dots a(U^{\dagger}\xi_{1})a^{\dagger}(\psi_{1})\dots a^{\dagger}(\psi_{n})\Omega$$

$$= \sum_{\substack{j_{1},\dots,j_{q}=1\\j_{1}>j_{2}>\dots>j_{q}}}^{n} \sum_{\pi\in\mathcal{S}_{q}} \left\langle \xi_{1},U\psi_{j_{\pi(1)}}\right\rangle \dots \left\langle \xi_{q},U\psi_{j_{\pi(q)}}\right\rangle \prod_{k\notin\{j_{1},\dots,j_{n}\}} a^{\dagger}(\psi_{k})\Omega.$$
(8.155)

With this result, (8.154) turns into

$$c_{W}^{b} = \frac{1}{\operatorname{perm} G^{V,V}} \sum_{\substack{j_{1},j'_{1},\dots,j_{q},j'_{q}=1\\j_{1}>j_{2}>\dots>j_{q}\\j'_{1}>j'_{2}>\dots>j'_{q}}} \left(\sum_{\pi,\sigma\in S_{q}} \left\langle \psi_{j'_{\sigma(1)}}, U^{\dagger}\xi_{1} \right\rangle \left\langle \xi_{1}, U\psi_{j_{\pi(1)}} \right\rangle \right. \\ \left. \dots \left\langle \psi_{j'_{\sigma(q)}}, U^{\dagger}\xi_{q} \right\rangle \left\langle \xi_{q}, U\psi_{j_{\pi(q)}} \right\rangle \right) \\ \times \left\langle \prod_{l\notin\{j'_{1},\dots,j'_{n}\}} a^{\dagger}(\psi_{l})\Omega, \prod_{k\notin\{j_{1},\dots,j_{n}\}} a^{\dagger}(\psi_{k})\Omega \right\rangle.$$

$$(8.156)$$

We can now use (7.32) and the definition (8.153), to obtain

$$\left\langle \prod_{l \notin \{j'_1, \dots, j'_n\}} a^{\dagger}(\psi_l) \Omega, \prod_{k \notin \{j_1, \dots, j_n\}} a^{\dagger}(\psi_k) \Omega \right\rangle = \operatorname{perm} G^{V \setminus \{\psi_{j'_1}, \dots, \psi_{j'_q}\}, V \setminus \{\psi_{j_1}, \dots, \psi_{j_q}\}}.$$
(8.157)

This is a generalisation of the discussion following (8.139) where the orthogonality condition on the modes allowed us to conclude that perm $G^{V\setminus \{\psi_{j_1}',\dots,\psi_{j_q}'\},V\setminus \{\psi_{j_1},\dots,\psi_{j_q}\}}$ is zero whenever $\{\psi_{j_1'},\dots,\psi_{j_q'}\}\neq \{\psi_{j_1},\dots,\psi_{j_q}\}$. This is no longer the case for non-orthogonal modes ψ_j , and the final expression for (8.154) therefore reads

$$\begin{split} c_W^b &= \sum_{\substack{j_1,j_1',\ldots,j_q,j_q'=1\\j_1>j_2>\cdots>j_q\\j_1'>j_2'>\cdots>j_q'\\} \sum_{\substack{m,\sigma\in S_q\\j_1'>j_2'>\cdots>j_q'\\perm\ G^{V\backslash\{\psi_{j_1'},\ldots,\psi_{j_q'}'\},V\backslash\{\psi_{j_1},\ldots,\psi_{j_q}\}\\perm\ G^{V,V}}} \\ &\times \frac{\operatorname{perm} G^{V\backslash\{\psi_{j_1'},\ldots,\psi_{j_q'}'\},V\backslash\{\psi_{j_1},\ldots,\psi_{j_q}\}}}{\operatorname{perm} G^{V,V}}. \end{split} \tag{8.158}$$

No further simplification is possible unless additional assumptions are made on the input and output mode tuples V and W, respectively. Note, however, that we can apply the same interpretation as in our discussion on p. 310: The correlation function is essentially a sum of all q-particle pathways that lead to the q elected output modes. In other words, these correlation functions characterise all "sub processes" of order q.

Without going through the entire calculation, which is again fully analogous to the bosonic case (see Appendix D), we also provide the result for the *fermionic correlation function*:

$$c_{W}^{f} = \sum_{\substack{j_{1}, j'_{1}, \dots, j_{q}, j'_{q} = 1 \\ j_{1} > j_{2} > \dots > j_{q} \\ j'_{1} > j'_{2} > \dots > j'_{q}}} \left(\sum_{\pi, \sigma \in S_{q}} \operatorname{sign}(\pi) \operatorname{sign}(\sigma) \left\langle \psi_{j'_{\sigma(1)}}, U^{\dagger} \xi_{1} \right\rangle \left\langle \xi_{1}, U \psi_{j_{\pi(1)}} \right\rangle \right. \\ \left. \dots \left\langle \psi_{j'_{\sigma(q)}}, U^{\dagger} \xi_{q} \right\rangle \left\langle \xi_{q}, U \psi_{j_{\pi(q)}} \right\rangle \right) \\ \times \frac{\det G^{V \setminus \{\psi_{j'_{1}}, \dots, \psi_{j'_{q}}\}, V \setminus \{\psi_{j_{1}}, \dots, \psi_{j_{q}}\}}}{\det G^{V, V}}.$$

$$(8.159)$$

Indeed, the transition from orthogonal to non-orthogonal modes very considerably enhances the complexity of our transmission problem: Not only can we no longer interpret the correlation functions $c_W^{b,f}$ as simple products of number operators on given modes, we also find that computations become much more intricate. This is seen from the fact that (8.158), (8.159) sum over a great quantity of terms, many of which are zero due to the orthogonality condition (8.140) in (8.146), (8.149).

Partial Distinguishability

Just as in Sect. 8.3.4, we find that in the current setting of correlation functions, the problem of (partial) distinguishability comes about when we consider additional degrees of freedom which are not observed by the measurement apparatus.

Let us consider a similar setup as in our above discussions of orthogonal and non-orthogonal modes, but now structure the single-particle Hilbert space as $\mathbb{C}^m \otimes \mathcal{H}_{\mathrm{add}}$, i.e. as a composite system which consists of a mode space garnished by additional degrees of freedom. The measurement setup is constructed by a set of single-particle wave functions $W = \{\xi_1 \otimes \zeta_1, \ldots \xi_q \otimes \zeta_q\}$, where $\xi_j \in \mathbb{C}^m$ and $\zeta_j \in \mathcal{H}_{\mathrm{add}}$. At a first instance, we may simply calculate $c_W^{b/f}$ as given by (8.158) or (8.159), which is, however, not yet what we are ultimately interested in. We assume that the detectors are only observing the mode space \mathbb{C}^m and hence we must trace over $\mathcal{H}_{\mathrm{add}}$. In practice, this implies the choice of an arbitrary orthogonal basis $\{\eta_j\}$ of $\mathcal{H}_{\mathrm{add}}$ (which may be infinite and even continuous), to evaluate

$$c_W^{b/f} = \sum_{i_1, \dots, i_q} \langle a^{\dagger} (U^{\dagger} \xi_1 \otimes U'^{\dagger} \eta_{i_1}) \dots a^{\dagger} (U^{\dagger} \xi_q \otimes U'^{\dagger} \eta_{i_q})$$

$$a(U^{\dagger} \xi_q \otimes U'^{\dagger} \eta_{i_q}) \dots a(U^{\dagger} \xi_1 \otimes U'^{\dagger} \eta_{i_1}) \rangle, \tag{8.160}$$

for any state $\langle . \rangle$ and a unitary channel, given by (8.84). In our setup, we will be essentially interested in the case where $\langle . \rangle$ is a number state, and, more specifically, we will focus on number states which are prepared such that the set of *modes* $\{\psi_j\}$ and $\{\xi_j\}$ are orthogonal. *In concreto*, this implies that $\langle . \rangle$ is determined by a wave function $\Psi \in \Gamma^b(\mathbb{C}^m \otimes \mathcal{H}_{add})$, given by

$$\Psi = a^{\dagger}(e_1 \otimes \chi_1)a^{\dagger}(e_2 \otimes \chi_2) \dots a^{\dagger}(e_n \otimes \chi_n)\Omega, \quad e_j \in \mathbb{C}^m, \ \chi_j \in \mathcal{H}_{add}, \ \langle e_i, e_j \rangle = \delta_{i,j},$$
(8.161)

such that we prepare at most one single particle per mode e_j . This is mainly a choice of simplicity, we later comment on the more general setup. We similarly also demand that the detectors are mounted on orthogonal modes $\{f_1, \ldots, f_q\}$. The calculation of

$$\left\langle \Psi, \hat{n}(U^{\dagger}f_1 \otimes U'^{\dagger}\eta_{i_1}) \dots \hat{n}(U^{\dagger}f_q \otimes U'^{\dagger}\eta_{i_q})\Psi \right\rangle$$

is known from (8.138): The tensor product structure is easily inserted in the setup, but it remains relevant to evaluate

$$\left\langle \prod_{k \in \mathcal{D}(\Psi) \setminus \mathcal{U}} a^{\dagger}(e_k \otimes \chi_k) \Omega, \prod_{l \in \mathcal{D}(\Psi) \setminus \mathcal{U}'} a^{\dagger}(e_l \otimes \chi_l) \Omega \right\rangle,$$

with $\mathcal{D}(\Psi)$ as in (8.136) and $\mathcal{U}', \mathcal{U} \subset \mathcal{D}(\Psi)$ as in (8.138). This evaluation is feasible exactly because we have at most one single particle per *orthogonal* input mode, which allows us to conclude that

$$\mathcal{D}(\Psi) \setminus \mathcal{U} \neq \mathcal{D}(\Psi) \setminus \mathcal{U}' \implies \left\langle \prod_{k \in \mathcal{D}(\Psi) \setminus \mathcal{U}} a^{\dagger}(e_k \otimes \chi_k) \Omega, \prod_{l \in \mathcal{D}(\Psi) \setminus \mathcal{U}'} a^{\dagger}(e_l \otimes \chi_l) \Omega \right\rangle = 0,$$
(8.162)

and also that

$$\left\langle \prod_{k \in \mathcal{D}(\Psi) \setminus \mathcal{U}} a^{\dagger}(e_k \otimes \chi_k) \Omega, \prod_{l \in \mathcal{D}(\Psi) \setminus \mathcal{U}} a^{\dagger}(e_l \otimes \chi_l) \Omega \right\rangle = \operatorname{perm} \mathbb{1} = 1.$$
 (8.163)

Thus we obtain for the bosonic version of (8.160):

$$c_{W}^{b} = \sum_{i_{1},\dots,i_{q}} \sum_{\substack{j_{1},\dots,j_{q}=1\\j_{1}>j_{2}>\dots>j_{q}}} \sum_{\pi,\sigma\in S_{q}} \langle f_{1},Ue_{j_{\pi(1)}}\rangle\langle e_{j_{\sigma(1)}},U^{\dagger}f_{1}\rangle\dots\langle f_{q},Ue_{j_{\pi(q)}}\rangle\langle e_{j_{\sigma(q)}},U^{\dagger}f_{q}\rangle$$

$$\times \langle \chi_{j_{\sigma(1)}},U'^{\dagger}\eta_{i_{1}}\rangle\langle \eta_{i_{1}},U'\chi_{j_{\pi(1)}}\rangle\dots\langle \chi_{j_{\sigma(q)}},U'^{\dagger}\eta_{i_{q}}\rangle\langle \eta_{i_{q}},U'\chi_{j_{\pi(q)}}\rangle$$

$$= \sum_{\substack{j_{1},\dots,j_{q}=1\\j_{1}>j_{2}>\dots>j_{q}}} \sum_{\pi,\sigma\in S_{q}} \langle f_{1},Ue_{j_{\pi(1)}}\rangle\langle e_{j_{\sigma(1)}},U^{\dagger}f_{1}\rangle\dots\langle f_{q},Ue_{j_{\pi(q)}}\rangle\langle e_{j_{\sigma(q)}},U^{\dagger}f_{q}\rangle$$

$$\times \langle \chi_{j_{\sigma(1)}},\chi_{j_{\pi(1)}}\rangle\dots\langle \chi_{j_{\sigma(q)}},\chi_{j_{\pi(q)}}\rangle,$$

$$(8.164)$$

where the last equality follows from the completeness of the $\{\eta_i\}$, such that we can again exploit (8.89). For the pair of $W = \{f_1, f_2\}$, i.e. the *two-point correlation function*, we obtain

$$c_{W}^{b} = \sum_{\substack{j_{1}, j_{2}=1\\j_{1} \neq j_{2}}} \left(\left| \left\langle f_{1}, U e_{j_{1}} \right\rangle \right|^{2} \left| \left\langle f_{2}, U e_{j_{2}} \right\rangle \right|^{2} + \left| \left\langle \chi_{j_{1}}, \chi_{j_{2}} \right\rangle \right|^{2} \left\langle f_{1}, U e_{j_{1}} \right\rangle \left\langle e_{j_{2}}, U^{\dagger} f_{1} \right\rangle \left\langle f_{2}, U e_{j_{2}} \right\rangle \left\langle e_{j_{1}}, U^{\dagger} f_{2} \right\rangle \right).$$

$$(8.165)$$

The results for fermionic results are again computed completely analogously, starting from (8.149), and therefore we simply provide the result

$$c_{W}^{f} = \sum_{\substack{j_{1}, \dots, j_{q}=1\\j_{1} > j_{2} > \dots > j_{q}}} \sum_{\substack{\pi, \sigma \in S_{q}}} \operatorname{sign}(\pi) \operatorname{sign}(\sigma) \left\langle f_{1}, U e_{j_{\pi(1)}} \right\rangle \left\langle e_{j_{\sigma(1)}}, U^{\dagger} f_{1} \right\rangle \dots \left\langle f_{q}, U e_{j_{\pi(q)}} \right\rangle \times \left\langle e_{j_{\sigma(q)}}, U^{\dagger} f_{q} \right\rangle \left\langle \chi_{j_{\sigma(1)}}, \chi_{j_{\pi(1)}} \right\rangle \dots \left\langle \chi_{j_{\sigma(q)}}, \chi_{j_{\pi(q)}} \right\rangle. \tag{8.166}$$

which for $W = \{f_1, f_2\}$ reduces to

$$c_{W}^{f} = \sum_{\substack{j_{1}, j_{2}=1\\j_{1} \neq j_{2}}} \left(\left| \left\langle f_{1}, U e_{j_{1}} \right\rangle \right|^{2} \left| \left\langle f_{2}, U e_{j_{2}} \right\rangle \right|^{2} - \left| \left\langle \chi_{j_{1}}, \chi_{j_{2}} \right\rangle \right|^{2} \left\langle f_{1}, U e_{j_{1}} \right\rangle \left\langle e_{j_{2}}, U^{\dagger} f_{1} \right\rangle \left\langle f_{2}, U e_{j_{2}} \right\rangle \left\langle e_{j_{1}}, U^{\dagger} f_{2} \right\rangle \right).$$

$$(8.167)$$

Note that, in the limit where $|\langle \chi_i, \chi_j \rangle|^2 = \delta_{ij}$, such that all particles are distinguishable by their additional degree of freedom, (8.164), (8.166) turn into

$$c_{W}^{d} = \sum_{\substack{j_{1}, \dots, j_{q} = 1 \\ j_{1} > j_{2} > \dots > j_{q}}} \sum_{\pi \in S_{q}} \left| \left\langle f_{1}, U e_{j_{\pi(1)}} \right\rangle \right|^{2} \dots \left| \left\langle f_{q}, U e_{j_{\pi(q)}} \right\rangle \right|^{2}$$

$$= \sum_{\substack{j_{1}, \dots, j_{q} = 1 \\ j_{1} > j_{2} > \dots > j_{q}}} \sum_{\pi \in S_{q}} p(e_{j_{\pi(1)}} \to f_{1}) \dots p(e_{j_{\pi(q)}} \to f_{q}). \tag{8.168}$$

This limit is reached both when starting initially from bosonic or fermionic correlation functions. The result is consistent with the correlation function which one would expect from basic classical probability theory.

When we allow several bosons in the same mode, we add an additional layer of difficulty. In the above discussion we could assume that all particles were described by mutually orthogonal single-particle wave functions. This is no longer the case when we consider multiple particles in the same mode. For the input state, let us therefore consider the n-tuple

$$V = \{e_1 \otimes \chi_{1,1}, \dots, e_1 \otimes \chi_{1,n_1}, e_2 \otimes \chi_{2,1}, \dots, e_2 \otimes \chi_{2,n_2}, \dots, e_r \otimes \chi_{r,n_r}\}$$

such that the total number of particles is given by $n = \sum_{j=1}^{r} n_r$. We still consider the modes in which we measure to be orthogonal, such that $W = \{f_1, \dots f_q\}$. We can use (8.156) to calculate c_W^b , since this is the most general result that one may come up with. The trace over the additional measurement degrees of freedom is straightforward and leads to the result

$$c_{W}^{b} = \sum_{\substack{\mathcal{V}, \mathcal{V}' \subset V \\ |\mathcal{V}| = |\mathcal{V}| = q}} \left(\sum_{\substack{\pi, \sigma \in S_{q} \\ e_{i_{j}} \otimes \chi_{i_{j}} \in \mathcal{V} \\ e_{i'_{j}} \otimes \chi_{i'_{j}} \in \mathcal{V}'}} \prod_{j=1 \atop e_{i_{j}} \otimes \chi_{i_{j}} \in \mathcal{V}} \left\langle e_{i_{\sigma(j)}}, U^{\dagger} f_{j} \right\rangle \left\langle f_{j}, U e_{i'_{\pi(j)}} \right\rangle \left\langle \chi_{i_{\sigma(j)}}, \chi_{i'_{\pi(j)}} \right\rangle \right) \frac{\operatorname{perm} G^{V \setminus \mathcal{V}, V \setminus \mathcal{V}'}}{\operatorname{perm} G^{V, V}},$$

$$(8.169)$$

where we use the notation $e_{i_j} \otimes \chi_{i_j}$ simply to indicate one of the q elements of \mathcal{V} . Notice, however, that it may be that e_{i_1} and e_{i_2} are one and the same vector. The difficulty is now that the object perm $G^{V \setminus \mathcal{V}, V \setminus \mathcal{V}'}$ /perm $G^{V,V}$ does not allow for a simple expression. However, there is a considerable amount of structure in $G^{V,V}$, since it is a block matrix,

$$G^{V,V} = \begin{pmatrix} [\langle \chi_{1,i}, \chi_{1,j} \rangle] & 0 & \dots & 0 \\ 0 & [\langle \chi_{2,i}, \chi_{2,j} \rangle] & \dots & 0 \\ \vdots & & \ddots & \vdots \\ 0 & & \dots & [\langle \chi_{r,i}, \chi_{r,j} \rangle] \end{pmatrix}, \tag{8.170}$$

where each block refers to a different mode. We can easily see that the permanent of this matrix takes the form

$$\operatorname{perm} G^{V,V} = \prod_{k=1}^{r} \operatorname{perm} \left[\left\langle \chi_{k,i}, \chi_{k,j} \right\rangle \right]. \tag{8.171}$$

The structure of $G^{V\setminus \mathcal{V},V\setminus \mathcal{V}'}$ is a bit more complicated. In any non-vanishing contribution, $V\setminus \mathcal{V}$ contains the same number of wave functions, the component in \mathbb{C}^m of which is given by e_i as $V\setminus \mathcal{V}'$. In order to notationally grasp this, we exploit the structure of the vectors in V, V and V'. For this purpose, we define the sets

$$V_i := \{ e_i \otimes \chi_{i,1}, \dots, e_i \otimes \chi_{i,n_i} \}, \tag{8.172}$$

such that $V = \bigcup_i V_i$. This allows us to define

$$\mathcal{V}_i := V_i \cap \mathcal{V} \quad \text{and} \quad \mathcal{V}'_i := V_i \cap \mathcal{V}', \tag{8.173}$$

such that $\mathcal{V} = \bigcup_i \mathcal{V}_i$ and $\mathcal{V}' = \bigcup_i \mathcal{V}'_i$. Given these conditions, terms with $|\mathcal{V}'_i| = |\mathcal{V}'_i|$ contribute to the sum in (8.169). In these terms, we can rewrite

$$G^{V \setminus \mathcal{V}, V \setminus \mathcal{V}'} = \bigoplus_{i} G^{V_{i} \setminus \mathcal{V}_{i}, V_{i} \setminus \mathcal{V}'_{i}}, \tag{8.174}$$

$$G^{V,V} = \bigoplus_{i} G^{V_i,V_i}, \tag{8.175}$$

which transforms (8.169) into

$$c_{W}^{b} = \sum_{\substack{\mathcal{V}, \mathcal{V}' \subset V \\ |\mathcal{V}| = |\mathcal{V}'| = q \\ |\mathcal{V}_{i}| = |\mathcal{V}'_{i}| \forall i}} \left(\sum_{\substack{\pi, \sigma \in S_{q} \\ e_{i_{j}} \otimes \chi_{i_{j}} \in \mathcal{V} \\ e_{i_{j}'} \otimes \chi_{i_{j}'} \in \mathcal{V}'}} \prod_{j=1}^{q} \left\langle e_{i_{\sigma(j)}}, U^{\dagger} f_{j} \right\rangle \left\langle f_{j}, U e_{i_{\pi(j)}'} \right\rangle \left\langle \chi_{i_{\sigma(j)}}, \chi_{i_{\pi(j)}'} \right\rangle \right) \times \prod_{i} \frac{\operatorname{perm} G^{V_{i} \setminus \mathcal{V}_{i}, V_{i} \setminus \mathcal{V}'_{i}}}{\operatorname{perm} G^{V_{i}, V_{i} \setminus \mathcal{V}'_{i}}}.$$

$$(8.176)$$

Although there are considerably less terms and more structure in (8.176) than in (8.169), we do not gain much to provide a more explicit expression, or to ease the intuitive understanding of the transmission signal.

²⁶Were this not the case, we would find a row of zeroes in $G^{V\setminus V,V\setminus V'}$.

This concludes our section on many-particle correlations, a section that was mainly intended to establish a broad range of mathematical tools which may be employed to characterise many-particle interferometry experiments. However, we also stressed that these correlation functions have a natural interpretation: The q-point correlation function, between q selected output modes, summarises all q-particle interference processes which send q particles from the input state to the q selected output modes. This interpretation makes it particularly useful to exploit these tools in the following section, in our effort to certify boson sampling.²⁷ Ultimately, this allows us to define accessible (i.e. scalable with system size) characteristics of many-particle interference phenomena.

8.5 Certification of Boson Sampling

In Sect. 8.3.5 we explained that the intractability of many-particle interference lies at the heart of the bosons sampling problem. The important implication is that it becomes practically impossible to predict the exact probability with which specific many-particle events will occur. In other words, the interference pattern has a very rich, complicated structure, which cannot be *deterministically* probed by standard computational or analytical techniques. This leads us to the natural question: *how do we certify the functioning of a many-particle interferometer?*

Certification is a delicate topic, partially because the terminology has a different meaning to different communities. As physicists, we are typically concerned about setting up experiments which are intended to function correctly. Certification of such experimental devices implies avoiding unintended malfunction. This attitude is in contrast with computer science, a field which is forced to avoid potential security breaches (think for example about cryptography). To computer scientists, certification also implies protection against intentional misconduct, i.e. a person who knows the certification protocol should not be able to mislead it. In the original formulation of the bosons sampling problem (Aaronson and Arkhipov 2013), the authors focus on a problem in the theory of computational complexity, relating many-particle interference to the context of quantum information. This has lead to mathematical debates on the latter type of certification (Aaronson and Arkhipov 2014; Aolita et al. 2015; Gogolin et al. 2013), which tend to loose sight of the underlying physical problem. Moreover, a strong focus on rigorous, high-fidelity certification, as appropriate for a rigorous computer scientific perspective, is overly restrictive and comes at the price of impractical implementation. As a profound example, Aolita et al. (2015) proposes an method which, for n particles in m modes requires the measurement of $\mathcal{O}(m(4d^2+1)^n)^{28}$ multi-particle correlation functions, the latter involving up to 2n + 1 modes. Even though this method allows for a highly accurate certification of

²⁷Which actually implies finding benchmarks of many-particle interference.

 $^{^{28}}d < m$ is an integer which depends on the specific unitary scattering matrix.

the output state, it still requires many, intricate measurements and has an unfavourable scaling with the number of particles.

In contrast, we will here focus on the physics perspective of certification and add an important ingredient: *Statistics* (Walschaers et al. 2016b). Indeed, one may argue that a *direct* certification is obviously rather unfeasible, and that it therefore appears rather absurd to attempt such certification in the first place, unless we consider very few particles (which in turn would invalidate the complexity argument which motivates boson sampling). Our method was inspired by the results of Mayer et al. (2011), Mayer (2012) and touches upon the proposal of Aolita et al. (2015) in the sense that we, too, exploit multimode correlation functions. Nevertheless, we drop the demand of strict, deterministic certification that cannot be cheated upon and rather focus on the physics of many-particle interference. The addition of statistical methods such as RMT (recall Sect. 3.3) allow us to design more concrete, implementable schemes for the certification of many-particle interference experiments (Giordani et al. 2018). Similar methods have been applied in complementary work (Rigovacca et al. 2016) to obtained bounds for the correlations in classical setups, that can be violated with non-classical input states.

A treatment based on correlation functions has the enormous advantage of being scalable. When we consider for example the correlation function in (8.146), ²⁹ there is a sum over permutations that needs to be considered, making the object potentially difficult to evaluate. However, these correlation functions provide a crucial difference to the probability distribution (8.88): They consider permutations of q elements, where q is the number of detectors we monitor and ultimately correlate. In other words, a bosonic q-point correlation function (at least of orthogonal modes) requires us to calculate a sum of permanents of $q \times q$ matrices. We see that actually the number of particles determines the number of terms in the sum (8.146), but it does not lead to any contributions of higher complexity (Laibacher and Tamma 2015; Mayer et al. 2011; Mayer 2012).

In concreto, we can interpret our method as the study of q-particle interference sub-processes which are concealed within the full n-particle interference signal. Because there are many such sub-processes, we can additionally obtain statistical features by averaging over all of them. The question which we must now ask is exactly what this value q must be to obtain a sufficient amount of information to do the certification. Throughout this section, we argue that it is sufficient to consider sub-processes of only few (i.e. two or three) particles, and therefore correlations of as many output modes. This implies that our method not only is implementable, but also has a very favourable scaling with the number n of particles and the number m of modes.

We start, however, by introducing an additional strategy for sampling which uses fully distinguishable particles to mimic a particular bosonic phenomenology, i.e. bunching.

²⁹Or any other correlation function that we derived for that matter.

8.5.1 Bunching and Simulated Bosons

Certification procedures that rely more on physical properties of many-particle interference only appeared quite recently. One attempt suggested to use bosonic clouding as a benchmark for many-boson interference (Carolan et al. 2014). This clouding effect relies on the idea that there is a type of generalised Hong-Ou-Mandel effect, which encourages the particles to bunch together: The events where the particles end up in the same mode are statistically enhanced as compared to sampling distinguishable particles. Although the effect of bosonic clouding can indeed be observed in experiments, it relies on the strong conjecture that there are no other particle types that give rise to the same bunching-type effect when sampled over. This conjecture was falsified by Tichy et al. (2014), where it was indicated that a mean-field sampler (introduced in more detail in the following paragraph) can exactly reproduce all effects related to bunching using distinguishable particles without any many-particle interference. Hence, even though bunching is a consequence of many-particle interference, it is insufficient to be used as a hallmark since it can also be achieved without many-particle interference. This highlights that many-particle interference is much more subtle than mere bunching.

The mean-field sampler's means of operation are strongly inspired by the literature on BECs, where one often uses a semiclassical³⁰ mean-field model to describe interfering condensates (Cennini et al. 2005; Hadzibabic et al. 2004). The main idea of these methods is to assume distinguishable particles, which all occupy the same single-particle wave function, but with random phases ascribed to them. In many senses, this approach resembles the methods that are used to understand interference between distinct beams of coherent light (Mandel 1964, 1983; Paul 1986; Pfleegor and Mandel 1967; Rarity et al. 2005; Radloff 1971). These methods are capable of reproducing the Hong-Ou-Mandel effect, but with a significantly reduced visibility (with a maximal visibility proven to be 50%) (Ou 1988). In these works, the random fluctuations in the phase of the laser impose a phase-averaging procedure that is essential to obtain the final interference fringe.

To implement the mean-field sampler, we must consider a system with internal degrees of freedom, such that $\mathcal{H}=\mathbb{C}^m\otimes\mathcal{H}_{add}$. The core idea is to treat all particles in the same way, ignoring intricate correlations between the particles. To simulate the bosonic bunching signature of a state

$$\Psi = a^{\dagger}(e_{i_1} \otimes \xi) \dots a^{\dagger}(e_{i_n} \otimes \xi) \Omega, \quad e_{i_1}, \dots, e_{i_n} \in \mathbb{C}^m, \ \xi \in \mathcal{H}_{add},$$
 (8.177)

we "macroscopically" occupy a single-particle state

$$\psi = \frac{1}{\sqrt{n}} \sum_{j=1}^{n} \exp(i\theta_j) e_{i_j},$$
(8.178)

³⁰The term "semiclassical" is here not interpreted in the same sense as in Engl et al. (2014). We rather use the terminology in the same, mean-field sense as Gessner et al. (2016).

which we use to construct a "mean-field" wave function

$$\Psi_{\mathrm{mf}} := a^{\dagger}(\psi \otimes x_{1}) \dots a^{\dagger}(\psi \otimes x_{n}) \Omega,$$
with $x_{i} \in \mathcal{H}_{\mathrm{add}}, \langle x_{i}, x_{i} \rangle = \delta_{ij}.$

$$(8.179)$$

A crucial additional element is that throughout the sampling procedure, we allow the phases $\{\theta_j\}$ to vary. It can now be shown Tichy (2011); Tichy et al. (2014) that the probability for a particle to travel to output mode q in the mean-field sampler is given by

$$p_q^{\text{mf}} = \frac{1}{n} \left| \sum_{j=1}^n e^{i\theta_j} \langle q, Ue_{i_j} \rangle \right|^2.$$
 (8.180)

The particles are now classically correlated and gather where $p_q^{\rm mf}$ is highest. In Mayer (2012), Tichy (2011), Tichy et al. (2014) it was shown that this type of particles can reproduce bunching effects.

To understand the procedure in some more detail, let us compute the probability $p_{q_1,\ldots,q_n}^{\text{mf}}$ that the *n* particles are detected in modes q_1,\ldots,q_n . Because the particles are distinguishable, we directly find that

$$p_{q_1,\dots,q_n}^{\text{mf}} = n! \prod_{j=1}^n p_{q_j}^{\text{mf}}.$$
 (8.181)

The factor n! must be included because it counts the number of different ways in which we can distribute the particles over the selected modes. To simplify notation, let us introduce

$$U_{ri_k} := \langle f_r, Ue_{i_k} \rangle, \tag{8.182}$$

such that when we insert (8.180) into (8.181), we find³¹

$$p_{q_{1},...,q_{n}} = \frac{n!}{n^{n}} \left| \sum_{j=1}^{n} U_{q_{1}j} \exp(i\theta_{j}) \right|^{2} \left| \sum_{j=1}^{n} U_{q_{2}j} \exp(i\theta_{j}) \right|^{2} ... \left| \sum_{j=1}^{n} U_{q_{n}j} \exp(i\theta_{j}) \right|^{2},$$

$$= \frac{n!}{n^{n}} \sum_{j_{1},...,j_{n},k_{1},...,k_{n}=1}^{n} U_{q_{1}j_{1}} ... U_{f=q_{n}j_{n}} \overline{U}_{q_{1}k_{1}} ... \overline{U}_{q_{n}k_{n}} \exp\left(i\sum_{l} \theta_{j_{l}} - i\sum_{l} \theta_{k_{l}}\right).$$
(8.183)

This result provides the probability that the particles are detected in modes q_1, \ldots, q_n for a fixed set of randomly sampled phases $\{\theta_i\}$.

The following crucial step to simulate bosonic bunching effects is to evaluate the average over these random phases. To do so, let us introduce the operation \mathbb{E}_{θ} , defined by

 $^{^{31}}$ To avoid indices of indices of indices, we simply write j rather than i_j in the following step.

$$\mathbb{E}_{\theta}(X) := \frac{1}{(2\pi)^n} \int_0^{2\pi} d\theta_1 d\theta_2 \dots d\theta_n X. \tag{8.184}$$

From a straightforward calculation, we find that

$$\mathbb{E}_{\theta}\left(\exp\left(i\sum_{l}\theta_{j_{l}}-i\sum_{l}\theta_{k_{l}}\right)\right) = \sum_{\sigma\in\mathcal{S}_{n}}\delta_{\sigma(j_{1}),k_{1}}\dots\delta_{\sigma(j_{n}),k_{n}},\tag{8.185}$$

and thus it follows that

$$\mathbb{E}_{\theta}(p_{q_1,\dots,q_n}^{\mathrm{mf}}) = \frac{n!}{n^n} \sum_{\sigma \in S_n} \sum_{j_1,\dots,j_n=1}^n U_{q_1j_1} \dots U_{q_nj_n} \overline{U}_{q_1\sigma(j_1)} \dots \overline{U}_{q_n\sigma(j_n)}.$$
(8.186)

When we now compare $\mathbb{E}_{\theta}(p_{q_1,\dots,q_n}^{\mathrm{mf}})$ in (8.186)–(8.90), we see that the main difference lies in the index set: In (8.186) we sum over all possible j_1,\dots,j_n , whereas in (8.90) we are confronted with the additional demand that all indices be different from each other. Note that, even though the averaging over the phases drastically reduces the interfering terms as seen by comparing (8.183)–(8.186), there are additional interference terms in (8.186) compared to (8.90). Even though this highlights the similarities and differences between the boson sampling and mean-field sampling, we refer to the results in Tichy et al. (2014) to see how the mean-field sampler reproduces bunching effects.

Given that the mean-field sampler thus *simulates bosons* with distinguishable particles, an actual certification scheme for boson sampling should do more than simply test for bunching. Indeed, the mean-field sampler is by construction free of any manyparticle inference effects and it nevertheless induces bunching. An effective method which was proposed in Tichy et al. (2014) exploits the suppression law (Tichy 2011; Tichy et al. 2012, 2010), for the (highly symmetric and non-random) Fourier matrix. The authors propose to use the specific circuit that implements the Fourier matrix in order to validate whether there is actual bosonic interference present. They show that this method effectively distinguishes bosons from simulated bosons, obtained from mean-field sampling, which makes their method far preferential over clouding. This has led to a range of additional works (Crespi 2015; Crespi et al. 2016; Viggianiello et al. 2018; Dittel et al. 2018b, 2017) on totally destructive interference in other setups. The disadvantage of any of these suppression law certification schemes is that they strongly rely on the specific scattering law inscribed into a specific unitary transformation, and therefore cannot be directly related to the random scattering setup (realised through a unitary scattering matrix distributed according to the Haar measure (Aaronson and Arkhipov 2013)) of the original boson sampling proposal. Consequently, more advanced methods, which can be directly implemented on circuits that describe Haar measure unitaries, are required to certify boson sampling. Moreover, we must make sure that such methods can successfully tell genuine bosonic many-particle interference apart from the mere bunching effects which are

observed for simulated bosons. In the remainder of this chapter, we propose such a method, based on truncated many-particle correlation functions and RMT.

Let us also note that, even if one simply wishes to tell bosons apart from distinguishable particles, it is still very inefficient to use bunching-based methods such as clouding. The reason is that, in systems where the number m of modes is significantly larger than the number n of particles, events with several particles in the same output mode (i.e. bunching events) can be considered rare events. To certify an enhanced probability of these events, one must acquire a sufficient amount of statistics. The related overhead can be expected to scale unfavourably, 32 because most measurement outcomes do not contribute as the size of the problem increases.

8.5.2 Correlations meet Random Matrix Theory

As indicated in Sect. 8.4.2, many-particle correlation functions contain specific information that is closely related to many-particle interference. Indeed, the appearance of a factor

$$\sum_{\pi,\sigma\in\mathcal{S}_q}\prod_{\substack{r=1\\j_r\in\mathcal{U}}}^q\big\langle f_r,Ue_{j_{\pi(r)}}\big\rangle\big\langle e_{j_{\sigma(r)}},U^\dagger f_r\big\rangle$$

in the correlation function (8.146) indicates that similar effects contribute also in many-particle interference probabilities as, for example, given by (8.54). The appeal of correlation functions in comparison to probability distributions, is that not only the numbers of modes and particles appear as parameters, but also *the order* of the correlation function.

It is well-known from probability theory that knowledge of all moments (or correlation functions) of a distribution is equivalent to knowledge of the probability distribution itself. However, this also implies that *all* correlation functions encrypt information on the probability distribution. In many many-particle scattering setups it may be feasible to obtain correlation functions of variable order, but not the entire probability distribution. The boson sampling setup defines precisely such an instance, and the *relevant* question is therefore up to which order we must know the correlation functions (or which orders) in order to certify *bosonic many-particle interference* (rather than bunching).

The intriguing aspect of the method we present in this section is that it only requires *low order* correlation functions. As shown in (8.54) (and all its generalisations in Sect. 8.4.2), these low order correlation functions contain *many-particle interference*

 $^{^{32}}$ As an example, consider the bunching event where all particles are detected in a single mode. There are only m such events which can occur for a total of m!/n!(m-n)! possible outcomes. Even with an enhanced probability, a lot of sampling is required to probe the relative frequency of such events.

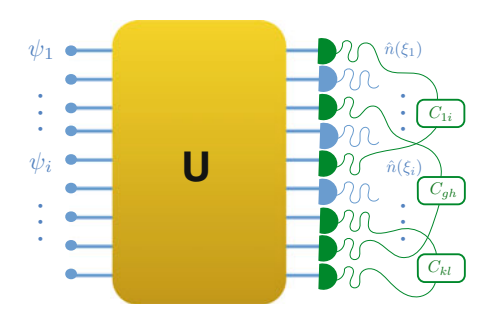


Fig. 8.8 Schematic representation of the measurement setup (recall Fig. 8.6), with additional correlators C_{ij} that constitute the certification scheme (8.193)–(8.195). Modes on the left can be populated with particles to form a many-particle input state, to be transmitted via the unitary channel E(U) as in (8.5) to a set of output modes $\{\xi_1,\ldots,\xi_m\}$. Each of these output modes is equipped with a counter, described by $\hat{n}(\xi_j) = a^{\dagger}(\xi_j)a(\xi_j)$, which measures the number of particles in the mode. We certify boson sampling by correlating the measurement outcomes of all pairs of detectors

pathways of low order.³³ As a first step, we wonder whether it is possible to get enough information from a single two-point correlation function to certify many-boson interferometry (with n particles and m modes).

It turns out that the strict answer is negative, in the sense that we must not rely on *one specific* two-point correlation function, but rather on all of them, as indicated in Fig. 8.8. Indeed, a fundamental aspect of the study of correlations between different pairs of modes is that we have m(m-1)/2 combinations, which gives us a large dataset. We baptise this statistical sample the *C-dataset*. The second fundamental ingredient in our certification protocol, next to the correlation functions themselves, is the *statistical* treatment of this C-dataset. We handle this dataset using analytical methods from RMT (Brouwer and Beenakker 1996; Collins and Śniady 2006; Berkolaiko and Kuipers 2010, 2011) to separate bosonic C-datasets from other datasets.

In what follows, we assess the statistical features of C-datasets as robust tools to certify boson sampling. Additionally, we investigate the potential to extract further information from higher order correlation functions, by explicitly considering the three-point case. To validate the sensitivity of these data for genuine (dynamical) many-particle interference, we statistically compare the obtained C-datasets to those generated by distinguishable particles and simulated bosons. Moreover, we compare bosonic C-datasets to fermionic C-datasets, in an effort to enhance our understanding of *dynamical* properties of fundamentally indistinguishable particles in quantum mechanics.

Two-Point Correlation Functions

In order to certify with the help of two-point correlation functions, we first need to specify the initial state and the measurement setup. To approach the experimental

³³"Low" order is an order which is significantly smaller than the number of particles. In this Dissertation, we focus on second and third order.

setting in a realistic fashion, we choose input states of n particles prepared in orthogonal modes. To be able to compare bosonic to fermionic results, we populate each input mode with at most one particle, i.e. we consider the initial state

$$\Psi = a^{\dagger}(e_{i_1}) \dots a^{\dagger}(e_{i_n}) \Omega, \quad \langle e_{i_k}, e_{i_l} \rangle = \delta_{jk}. \tag{8.187}$$

The measurement apparatus be mounted on two orthogonal modes f_r and f_s . Because this section is not as much about technical details and methods as the previous one, we again use the notation (8.182) to express (8.147) as

$$c_{rs}^{b} = \langle \hat{n}(f_r)\hat{n}(f_s)\rangle = \sum_{\substack{k,l=1\\k\neq l}}^{n} \left[U_{ri_k} U_{si_l} \overline{U}_{ri_k} \overline{U}_{si_l} + U_{ri_k} U_{si_l} \overline{U}_{ri_l} \overline{U}_{si_k} \right], \quad (8.188)$$

and (8.150) as

$$c_{rs}^{f} = \sum_{\substack{k,l=1\\k\neq l}}^{n} \left[U_{ri_k} U_{si_l} \overline{U}_{ri_k} \overline{U}_{si_l} - U_{ri_k} U_{si_l} \overline{U}_{ri_l} \overline{U}_{si_k} \right]. \tag{8.189}$$

For comparison, we will also consider the outcome (8.168) for particles which are fully distinguishable, which reads

$$c_{rs}^{d} = \sum_{\substack{k,l=1\\k\neq l}}^{n} U_{ri_{k}} U_{si_{l}} \overline{U}_{ri_{k}} \overline{U}_{si_{l}}.$$
 (8.190)

As we see, the genuine many-particle contributions are hidden in the second ("cross") term of c_{rs}^b and c_{rs}^f (recall (2.73) and (8.41)), the first terms which sum products of transmission probabilities $\left|U_{ri_k}\right|^2\left|U_{si_l}\right|^2$ are common to all these cases (8.188)–(8.190). Therefore, a more logical certification quantifier for boson sampling actually is $c_{rs}^b - c_{rs}^d$, which leaves the terms purely related to bosonic (two-particle) interference (recall our discussion on p. 310). However, this quantity has a considerable disadvantage: It cannot be extracted in one measurement run. One must either compute c_{rs}^d numerically and do post-processing of the C-data, or one must do a separate experimental run where the particles are made distinguishable. Therefore, it is interesting to wonder whether we can make the measurement more sensitive compared to $c_{rs}^{b/f}$ by simply using the data collected by the detectors *while* performing boson sampling.

Such a procedure is possible and is naturally given by exactly the type of objects discussed in Sect. 7.7, the *truncated correlation functions*³⁴

³⁴Keep in mind that these are multivariate analog of cumulants. They also occurs under the name *joint cumulants*, but we will follow the terminology of the quantum statistical mechanics community (Bratteli and Robinson 1997).

$$C_{rs} := \langle \hat{n}(f_r)\hat{n}(f_s)\rangle - \langle \hat{n}(f_r)\rangle\langle \hat{n}(f_s)\rangle$$

= $c_{rs} - \langle \hat{n}(f_r)\rangle\langle \hat{n}(f_s)\rangle$ (8.191)

which is perfect to perform the given task, since

$$\langle \hat{n}(f_r) \rangle \langle \hat{n}(f_s) \rangle = \sum_{k,l=1}^{n} U_{ri_k} U_{si_l} \overline{U}_{ri_k} \overline{U}_{si_l}. \tag{8.192}$$

These objects only differ from c^d_{rs} by the index set of the summation. Notice that, indeed, c^d_{rs} has the additional constraint that $k \neq l$ in the sum. This implies

$$C_{rs}^{b} = \sum_{\substack{k,l=1\\k \neq l}}^{n} U_{ri_k} U_{si_l} \overline{U}_{ri_l} \overline{U}_{si_k} - \sum_{k=1}^{n} U_{ri_k} U_{si_k} \overline{U}_{ri_k} \overline{U}_{si_k}, \tag{8.193}$$

$$C_{rs}^{f} = -\sum_{\substack{k,l=1\\k\neq l}}^{n} U_{ri_k} U_{si_l} \overline{U}_{ri_l} \overline{U}_{si_k} - \sum_{k=1}^{n} U_{ri_k} U_{si_k} \overline{U}_{ri_k} \overline{U}_{si_k}, \tag{8.194}$$

$$C_{rs}^d = -\sum_{k=1}^n U_{ri_k} U_{si_k} \overline{U}_{ri_k} \overline{U}_{si_k}, \tag{8.195}$$

and even though the correlations from classical probability theory, i.e. c_{rs}^d , are not completely erased, they are considerably decreased in order, ³⁵ compared to the many-particle interference terms.

Let us now verify whether the C-datasets constructed from the C_{rs}^b can convey useful and unambiguous information on many-boson interference. We do so by choosing a U from the Haar measure and subsequent generation of the C-dataset (which is a computationally simple task, due to the low order of the considered correlation function). The result is portrayed as a histogram of events in Fig. 8.9, which indicates that there is indeed a considerable difference between bosons and both fermions and distinguishable particles: Apparently, truncated correlation functions for fermions

$$\sum_{k=1}^{n} U_{ri_k} U_{si_k} \overline{U}_{ri_k} \overline{U}_{si_k}$$

which appears in all truncated correlation functions $C_{rs}^{b,f,d}$. This summation only contains n terms, which is a considerable decrease compared to the n(n-1) terms which appear in

$$\sum_{\substack{k,l=1\\k\neq l}}^{n} U_{ri_k} U_{si_l} \overline{U}_{ri_k} \overline{U}_{si_l},$$

for the correlation functions $c_{rs}^{b,f,d}$.

³⁵The decrease in order is seen by the term

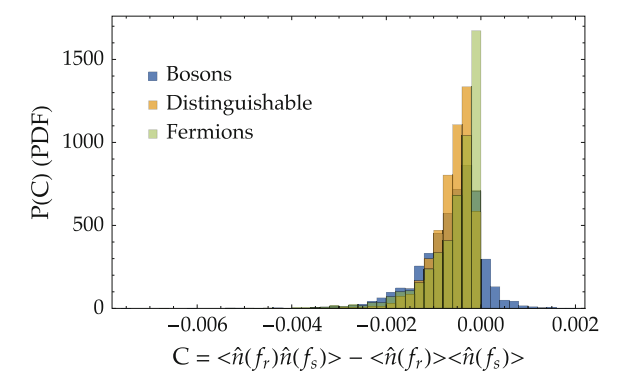


Fig. 8.9 Normalised (as probability density function (PDF)) histograms of the correlator data built from truncated two-point correlation functions $C_{rs}^{b/f/d}$ (8.193)–(8.195) of six particles injected into 100 modes for all possible mode combinations. Bosons are compared to fermions and distinguishable particles. All histograms are obtained from one single circuit by evaluating $C_{rs}^{b/f/d}$ for all pairs r and s of output modes, using the same input state Ψ , given by (8.187). In particular this implies that for distinct particle types the same components of U were used

and distinguishable particles can never be positive, whereas for bosons they can. For distinguishable particles, this result is clear from the very expression of C_{rs}^d (which is just a sum over products of probabilities, garnished with a global minus sign), but for fermions a further computation is required: We may rewrite

$$C_{rs}^{f} = -\sum_{\substack{k,l=1\\k\neq l}}^{n} U_{ri_{k}} U_{si_{l}} \overline{U}_{ri_{l}} \overline{U}_{si_{k}} - \sum_{k=1}^{n} U_{ri_{k}} U_{si_{k}} \overline{U}_{ri_{k}} \overline{U}_{si_{k}}$$

$$= -\sum_{k,l=1}^{n} U_{ri_{k}} U_{si_{l}} \overline{U}_{ri_{l}} \overline{U}_{si_{k}} = -\sum_{k=1}^{n} U_{ri_{k}} \overline{U}_{si_{k}} \sum_{l=1}^{n} U_{si_{l}} \overline{U}_{ri_{l}}$$

$$= -\left| \sum_{k=1}^{n} U_{ri_{k}} \overline{U}_{si_{k}} \right|^{2} \leq 0,$$

$$(8.196)$$

which proves that also $C_{rs}^f \leq 0$. This suggests that whenever we measure a C-dataset from an unknown source, positive truncated correlations are a signature of bosonic many-particle interference. This, however, turns out to be untrue. More specifically, positive C-data actually appear to be a signature of bunching effects, since we will show (see Fig. 8.10) that they also pop up in the mean-field sampler that simulates bosonic bunching (but cannot—by construction (8.179)—exhibit interference of many-particle transmission amplitudes).

The mean-field sampler's correlation functions have not been specifically studied in the previous section, but they are easy enough to derive. At the basis lies a combination of the correlation functions (8.158) for non-orthogonal modes with the

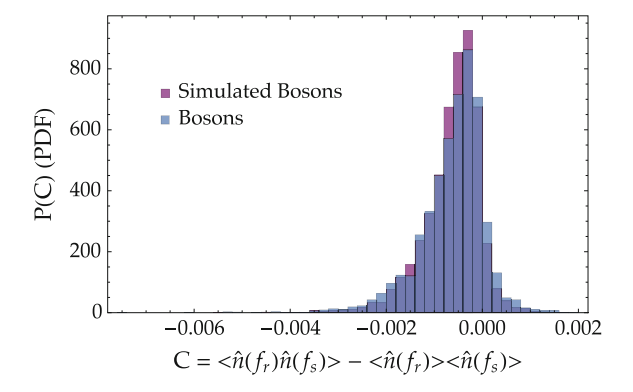


Fig. 8.10 Normalised (PDF) histograms of the correlator data built from truncated two-point correlation functions $C_{rs}^{b/mf}$ (8.193), (8.200) of six particles injected into 100 modes for all possible mode combinations. Bosonic many-particle interference is compared to bunching phenomena generated by the mean-field sampler. The histograms are obtained from the same circuit as used in Fig. 8.9, evaluating $C_{rs}^{b/mf}$ for all pairs r and s of output modes, using the same input state Ψ , given by (8.187). In particular this again implies that for distinct particle types the same components of U were used

corresponding result (8.176) for partial distinguishability. Indeed, the situation is in a sense opposite to that for actual bosons: Bosons are prepared in orthogonal modes and are indistinguishable in all additional degrees of freedom,³⁶ whereas simulated boson are prepared in the same mode, but are distinguishable by their additional degrees of freedom.

To derive the results for simulated bosons, we consider a state (8.179) such that the components of the single-particle wave functions related to \mathcal{H}_{add} are orthogonal, which leads to full distinguishability. However, the component of the single-particle wave functions in \mathbb{C}^m is the same for all particles. We insert this structure for the single-particle wave functions into (8.176), and subsequently exploit the orthogonality of the x_i in (8.179), to obtain:

$$c_{rs,\{\theta\}}^{mf} = \sum_{\substack{k,l=1\\k\neq j}}^{n} |\langle f_r, U\psi \rangle|^2 |\langle f_s, U\psi \rangle|^2, \quad \psi = \frac{1}{\sqrt{n}} \sum_{j=1}^{n} \exp(i\theta_j) e_{i_j}$$
 (8.197)

which, after insertion of the explicit expression for ψ and with the notation of (8.182) is cast into

³⁶The full single-particle Hilbert space is described by $\mathcal{H} \cong \mathbb{C}^m \otimes \mathcal{H}_{add}$. To observe interference patterns of indistinguishable bosons in the interferometer, each particle much be described by the same single-particle wave function in \mathcal{H}_{add} . For an extended discussion, see Sect. 8.3.4.

$$c_{rs,\{\theta\}}^{mf} = \frac{(n-1)}{n} \left| \sum_{j_1,j_2=1}^{n} e^{i(\theta_{j_1} + \theta_{j_2})} U_{ri_{j_1}} U_{si_{j_2}} \right|^2$$

$$= (n-1) \sum_{j_1,j_2,j'_1,j'_2=1}^{n} e^{i(\theta_{j_1} + \theta_{j_2} - \theta_{j'_1} - \theta_{j'_2})} U_{ri_{j_1}} U_{si_{j_2}} \overline{U}_{ri_{j'_1}} \overline{U}_{si_{j'_2}}.$$
(8.198)

A crucial property of the mean-field sampler giving rise to (8.198) is to acquire many different random phases $\{\theta\}$, such that, ultimately, the object of interest is given by $c_{rs}^{mf} = \mathbb{E}_{\theta}(c_{rs,\{\theta\}}^{mf})$. In complete analogy to (8.185), a straightforward calculation shows that $\mathbb{E}_{\theta}(e^{i(\theta_{j_1}+\theta_{j_2}-\theta_{j_1'}-\theta_{j_2'})}) = \delta_{j_1,j_1'}\delta_{j_2,j_2'} + \delta_{j_1,j_2'}\delta_{j_2,j_1'}$. Inserting this result into (8.198), we find

$$c_{rs}^{mf} = \mathbb{E}_{\theta}(c_{rs,\{\theta\}}^{mf}) = \frac{(n-1)}{n} \sum_{\substack{j_{1}, j_{2}=1\\j_{1} \neq j_{2}}}^{n} \left(U_{ri_{j_{1}}} U_{si_{j_{2}}} \overline{U}_{ri_{j_{1}}} \overline{U}_{si_{j_{2}}} + U_{ri_{j_{1}}} U_{si_{j_{2}}} \overline{U}_{ri_{j_{2}}} \overline{U}_{si_{j_{1}}} \right)$$

$$+ \frac{(n-1)}{n} \sum_{j=1}^{n} U_{ri_{j}} U_{si_{j}} \overline{U}_{ri_{j}} \overline{U}_{si_{j}},$$
(8.199)

and for the truncated correlation function:

$$C_{rs}^{mf} = \frac{(n-1)}{n} \sum_{\substack{j_1, j_2 = 1 \\ j_1 \neq j_2}}^{n} U_{ri_{j_1}} U_{si_{j_2}} \overline{U}_{ri_{j_2}} \overline{U}_{si_{j_1}} - \frac{1}{n} \sum_{j_1, j_2 = 1}^{n} U_{ri_{j_1}} U_{si_{j_2}} \overline{U}_{ri_{j_1}} \overline{U}_{si_{j_2}}.$$
(8.200)

Now that we have an expression for C_{rs}^{mf} , we can sample a unitary matrix Ufrom the Haar measure and compute the C-dataset. While, from expression (8.200) and (8.193), C_{rs}^{mf} and C_{rs}^{b} are certainly different, they also contain many identical terms (recall (8.186)). These terms, however, appear with slightly different weights, and we thus wonder how different the associated C-datasets effectively are. Judging from Fig. 8.10 they are very similar. Moreover, we see that both C-datasets contain positive truncated correlations. As already mentioned earlier, we may relate positive correlations to bunching rather than bosonic interference. Following the results (Ou 1988) for classical beams with random phases, it should not come as a surprise that the mean-field sampler can reproduce a qualitatively similar set of correlations between detectors. Therefore, we need more refined tools to quantify particle-type specific signatures of genuine many-particle interference, and investigate the moments of the C-dataset. Not only can we easily generate these moments numerically,³⁷ we can also analytically predict them. The machinery to be used for the analytical treatment is RMT. However, while extremely successful and versatile, RMT does not allow us to compute exactly what we want. The main issue with RMT is that it is built to evaluate

 $^{^{37}}$ In the sense that we can obtain them from a simulation of a circuit described by a random unitary matrix U.

averages over different realisations of the random matrix under consideration, tough results for one single realisation is out of the theory's reach. Nevertheless, from other fields in physics where RMT is used, such as quantum chaos (Stöckmann 2007), we do know that, often, averages of the ensemble provide good estimates for properties of a single matrix, sampled from the ensemble. An example was encountered in Sect. 3.3.3, where we treated the normalised density of states $\rho(E)$ and its ensemble average $\langle \rho(E) \rangle$. For a randomly sampled GOE matrix, which is sufficiently large (i.e. lives on a sufficiently large Hilbert space), we typically find that $\rho(E)$, and $\langle \rho(E) \rangle$ are very similar. Moreover, individual $\rho(E)$ are typically similar for distinct realisations, chosen from the same ensemble.

Our C-dataset is in many ways similar to the set of eigenvalues from which we computed $\rho(E)$ in Sect. 3.3.3. Notice that there is no mathematical equivalence, but rather an approach which is similar in philosophy. Two-point correlation functions for Gaussian ensembles in RMT neglect many higher order correlations inscribed in the spectrum. Nonetheless, already this strongly coarse grained information contains a significant amount of information on the specific RMT ensemble; we can, for example, distinguish GOE from, GUE. Interestingly, we also know that the two-point correlation function as obtained from a single GOE matrix is close to the ensemble average, provided the matrix is large enough. We now follow a similar type of reasoning for our boson sampling problem, which can be mathematically described by unitary matrices distributed according to the Haar measure.

Objects which are easily accessible from an experimental point of view are the low-order moments of the actual C-dataset. This implies an average of the C_{rs} (we omit the superscripts) over all possible choices of two *distinct* output modes r and s. In concreto, the defining expressions read

$$m_1^{\text{exp}} = \frac{2}{m(m-1)} \sum_{\substack{r,s=1\\r>s}}^{m} C_{rs},$$
 (8.201)

$$m_2^{\text{exp}} = \frac{2}{m(m-1)} \sum_{\substack{r,s=1\\r>s}}^{m} C_{rs}^2,$$
 (8.202)

$$m_3^{\exp} = \frac{2}{m(m-1)} \sum_{\substack{r,s=1\\r>s}}^{m} C_{rs}^3.$$
 (8.203)

In this work, we limit ourselves to the first three moments and see how much information can be obtained from them. The restriction to low-order moments is due to the increasing overhead when the order is increased, which makes analytical computation tedious (see also Berkolaiko and Kuipers 2011; Kuipers and Sieber 2008; Urbina et al. 2016). For these lower order moments, we can derive analytical estimates with the help RMT. Formally, one may write these analytical moments as

$$m_1 = \mathbb{E}_U(C_{rs}), \tag{8.204}$$

$$m_2 = \mathbb{E}_U\left(C_{rs}^2\right),\tag{8.205}$$

$$m_3 = \mathbb{E}_U\left(C_{rs}^3\right). \tag{8.206}$$

The averaging procedure, even though straightforward, is technically tedious and is therefore left for Appendix B; here we only present the main ideas of the computational procedure. There is a generally applicable technique for averaging products of components of unitary matrices over the ensemble of all unitary matrices distributed according to the Haar measure. At the heart of this computation lies the identity

$$\mathbb{E}_{U}(U_{a_{1},b_{1}}\dots U_{a_{n},b_{n}}\overline{U}_{\alpha_{1},\beta_{1}}\dots\overline{U}_{\alpha_{n},\beta_{n}})$$

$$=\sum_{\sigma,\pi\in\mathcal{S}_{n}}V_{m}(\sigma^{-1}\pi)\prod_{k=1}^{n}\delta(a_{k}-\alpha_{\sigma(k)})\delta(b_{k}-\beta_{\pi(k)}),$$
(8.207)

which as such can be traced back to the representation theory of groups, and specifically to the Schur-Weyl duality (Collins and Śniady 2006; Hamermesh 1989). After going through the computation, we finally obtain, for n particles injected into m modes, and an initial state of the form (8.177) for bosons:

$$m_1^b = -\frac{n(m+n-2)}{m(m^2-1)},\tag{8.208}$$

$$m_2^b = \frac{2n\left(m^2n + m^2 + 9mn - 11m + n^3 - 2n^2 + 5n - 4\right)}{m^2(m+2)(m+3)\left(m^2 - 1\right)},$$
(8.209)

$$\begin{split} m_3^b &= -2n \left(\frac{m^3n^2 + 15m^3n + 2m^3 + 3m^2n^3 + 6m^2n^2 + 213m^2n - 222m^2 - 3mn^4}{m^2(m+1)(m+2)(m+3)(m+4)(m+5)\left(m^2 - 1\right)} \right. \\ &\quad \left. + \frac{45mn^3 + 32mn^2 + 372mn - 464m + 3n^5 - 6n^4 + 45n^3 + 78n^2 + 168n - 288}{m^2(m+1)(m+2)(m+3)(m+4)(m+5)\left(m^2 - 1\right)} \right), \end{split}$$

for fermions

$$m_1^f = \frac{n(n-m)}{m(m^2-1)},$$
 (8.211)

$$m_2^f = \frac{2n(n+1)(m-n)(m-n+1)}{m^2(m+2)(m+3)(m^2-1)},$$
(8.212)

$$m_3^f = -\frac{6n(n+1)(n+2)(m-n)(m-n+1)(m-n+2)}{m^2(m+1)(m+2)(m+3)(m+4)(m+5)(m^2-1)},$$
 (8.213)

for distinguishable particles

$$m_1^d = -\frac{n}{m(m+1)},\tag{8.214}$$

$$m_2^d = \frac{n\left(m^2n + 3m^2 + mn - 5m + 2n - 2\right)}{m^2(m+2)(m+3)\left(m^2 - 1\right)},$$
(8.215)

$$m_2^d = -\frac{n\left(m^2n^2 + 9m^2n + 26m^2 + 5mn^2 + 21mn - 62m + 12n^2 + 60n - 72\right)}{m^2(m+2)(m+3)(m+4)(m+5)\left(m^2 - 1\right)},$$
(8.216)

and, finally, for the mean-field sampler, which simulates bosonic bunching though *no* many-particle interference,

$$\begin{split} m_1^{mf} &= -\frac{n(m+n-2)}{m(m^2-1)}, \\ m_2^{mf} &= \frac{4mn-m-14n^2+8n-2}{m^2(m+2)(m+3)(m^2-1)n} \\ &+ \frac{2m^2n^3-m^2n^2+4m^2n-m^2+18mn^3-25mn^2+2n^5-4n^4+10n^3}{m^2(m+2)(m+3)(m^2-1)n}, \\ m_3^{mf} &= \left(\frac{-2m^3n^5-21m^3n^4+30m^3n^3-41m^3n^2-10m^3n+8m^3-6m^2n^6-3m^2n^5}{(m-1)m^2(m+1)^2(m+2)(m+3)(m+4)(m+5)n^2} \right. \\ &+ \frac{-285m^2n^4+261m^2n^3+75m^2n^2-66m^2n+24m^2+6mn^7-90mn^6-55mn^5}{(m-1)m^2(m+1)^2(m+2)(m+3)(m+4)(m+5)n^2} \\ &+ \frac{-360mn^4+591mn^3+8mn^2-128mn+64m}{(m-1)m^2(m+1)^2(m+2)(m+3)(m+4)(m+5)n^2} \\ &+ \frac{-6n^8+12n^7-90n^6-120n^5-24n^4+396n^3-168n^2-48(n-1)}{(m-1)m^2(m+1)^2(m+2)(m+3)(m+4)(m+5)n^2} \\ &+ \frac{-6n^8+12n^7-90n^6-120n^5-24n^4+396n^3-168n^2-48(n-1)}{(m-1)m^2(m+1)^2(m+2)(m+3)(m+4)(m+5)n^2} \\ \end{split}$$

Before we continue to show that our approach is remarkably fruitful to acquire statistical signatures of many-particle interference, we remark that the moments in the above expression all scale with m and n, which is unpractical if we wish to compare different system sizes. As a solution we use rescaled moments, which have leading order terms independent of m and n. These moments are given by the Normalised Mean NM, which we defined ourselves, and the Coefficient of Variation CV and the Skewness S, which are common in the statistical literature and are narrowly related to cumulants (Everitt 1998). The defining expressions read

$$NM = \frac{\mathbb{E}_U(C)m^2}{n} \tag{8.220}$$

$$CV = \frac{\sqrt{\mathbb{E}_U(C^2) - \mathbb{E}_U(C)^2}}{\mathbb{E}_U(C)},$$
(8.221)

$$S = \frac{\mathbb{E}_{U}(C^{3}) - 3\mathbb{E}_{U}(C)\mathbb{E}_{U}(C^{2}) + 2\mathbb{E}_{U}(C)^{3}}{\left(\mathbb{E}_{U}(C^{2}) - \mathbb{E}_{U}(C)^{2}\right)^{3/2}}.$$
(8.222)

Given the rescaled moments of the C-dataset, we can now compare the statistical features of many-particle interference upon transmission across the boson sampler, as done in Fig. 8.11. Different mode numbers are compared for an input state (8.177) with six particles; the solid lines indicate the analytical predictions, whereas the error bars indicate the standard deviation for a set of moments obtained from numerically generated C-datasets derived from 500 distinct random unitaries. Clearly the numerical results are spread around the analytical prediction. Importantly, however, we see that in several cases the error bars do not overlap, indicating that the moments are statistically well separated. More specifically, we observe that the first moment is very effective to distinguish the interference structures as produced by the fundamental particle types of quantum statistics, but is completely useless to differentiate bunching from many-boson interference (because we find that $m_1^b = m_1^{mf}$, and as a consequence also NM coincides). This deficiency is compensated for by the second and third rescaled moments CV and S, which do resolve the structural differences of the interference patterns produced by true and simulated bosons (at least once we consider circuits which are sufficiently large).

To indicate the functionality of the certification method, we show several scatter plots in Fig. 8.12, which visualise how the moments of an actual C-dataset, each obtained from a single random unitary chosen from the Haar measure, scatter around the RMT result. As to be expected given Fig. 8.11, we see the spread of the data points decrease with increasing mode number. Figure 8.12 indicates that, indeed, the normalised mean NM is sufficient to distinguish bosons from fermions and distinguishable particles. Again in agreement with Fig. 8.11, the coefficient of variation CV turns out to be a useful quantity to differentiate simplistic bunching from genuine many-boson interference. The combination of CV with the skewness S offers the clearest distinction of the interference patterns produced by the various particle types. Also note the clear correlation between CV and S for different C-datasets, which we have so far not elucidated.

As evident from Figs. 8.11, 8.12 and 8.13, our certification method produces unambiguous results once the mode and particle numbers become sufficiently large. This clearly is an important advantage, because this is exactly the regime where direct certification of boson sampling becomes practically unfeasible because of the rapidly increasing complexity of the multiple interference patterns in the transmission signal. Since we observe that the *spread* of the different C-dataset quantifiers (8.220)–(8.222) shrinks relative to the distance between the RMT predictions, we can conclude that the RMT predictions become more accurate for growing mode number.

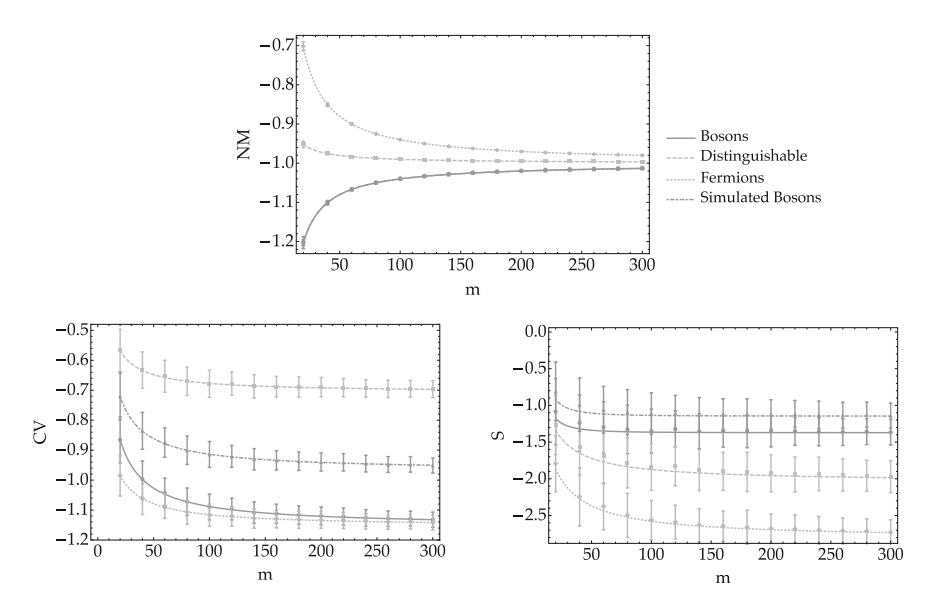


Fig. 8.11 Theoretical RMT predictions (solid lines) as given in (8.220)–(8.222), with (8.208)–(8.219), for the normalised mean (NM; top), the coefficient of variation (CV; bottom left) and the skewness (S; bottom right) of the C-dataset are compared to numerically generated NM, CV and S values for the six-particle state (8.177) injected into a random scattering compound of a variable number m of modes. For mode numbers $m = 20, 40, \ldots, 300$, we sampled over 500 matrices U. For each of these, NM, CV, and S were calculated and their mean and standard deviation indicated by marker (that depends on the particle type) and the error bars, respectively

Figure 8.13 indicates that our method of certification of many-particle interference becomes more intricate once the numbers of modes and particles are reasonably small. Even though NM still serves as a suitable quantifier to distinguish the fundamental particle types in this regime, the spread on CV and S is clearly too large to extract unambiguous information from them. As a consequence, our method appears to be unsuited to distinguish genuine bosonic many-particle interference from the mere bunching effects generated by the mean-field sampler for small system sizes.

A first potential solution to this problem is depicted in Fig. 8.14 and boils down to generating a *full scatter plot* for a single experiment. We show that averaging over twenty CV - S data points for bosonic many-particle interference provides a mean value which is significantly (as quantified by standard errors) closer to the bosonic RMT result than to that of the mean-field sampler. Thus even in this regime, genuine many-boson inference patterns contain a distinct fine-structure from patterns generated by the mean-field sampler, and this difference is encrypted in the C-dataset. Such full scatter plots can be achieved by either changing the scattering circuit, i.e. U, or the initial state Ψ (8.177), where we inject the particles in different initial modes to obtain different data points.

Ultimately, however, the C-datasets for bosons and simulated bosons are very similar (recall Fig. 8.10). The underlying cause for this similarity is that two-point truncated correlation functions are strongly influenced by bunching effects. Remem-

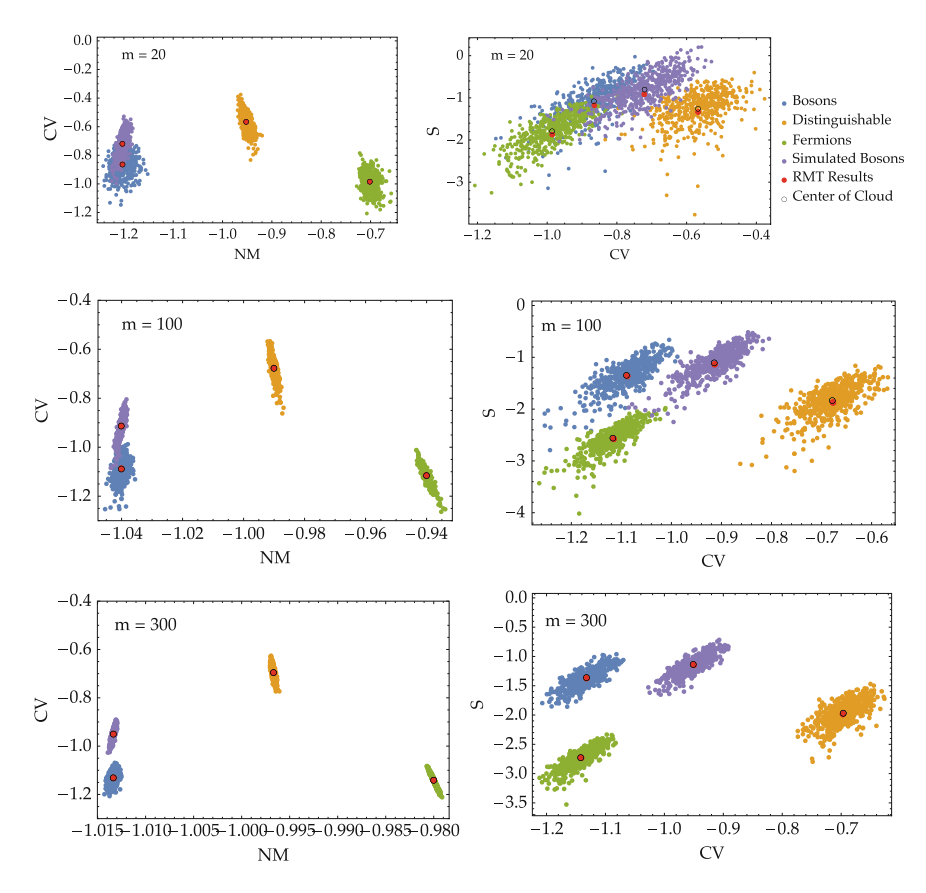


Fig. 8.12 Scatter plots indicating the normalised mean (NM; left), the coefficient of variation (CV; left) and the skewness (S; right) as given in (8.220)-(8.222). For a six-particle state (8.177), injected in 500 random unitary scattering compounds U of m=20, 100 and 300 modes, C-datasets are generated (8.193)-(8.195), (8.200) for interference patterns associated with different particle types ("bosons", "distinguishable", "fermions" and "simulated bosons"). The numerically achieved rescaled moments NM, CV and S with (8.201)-(8.203) are averaged (black circle) and compared to the RMT predictions which make use of (8.208)-(8.219); red dot)

ber that two-point correlation functions essentially sum up all underlying two-particle interference pathways in (see the discussion on p. 310) and we know from (8.49) that bunching effects are very pronounced in two-particle processes. Therefore, the natural next step is to determine a method which is more sensitive to many-particle inference and effectively filters out these bunching effects. A potential way to do so, is to treat *higher order correlation functions*.

Three-Point Correlation Functions

In our quest for a more sensitive method to distinguish genuine many-boson interference from bunching effects, the most straightforward step is to increase the order of the correlation functions. From the techniques discussed in Sect. 8.4.2, we already

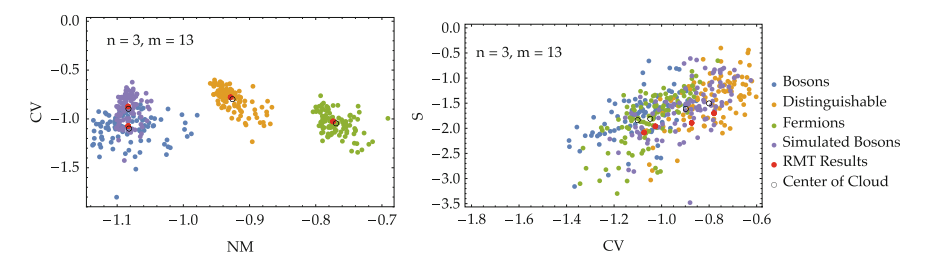


Fig. 8.13 Scatter plots indicating the normalised mean (NM; left), the coefficient of variation (CV; left) and right) and the skewness (S; right) as given in (8.220)–(8.222). For a three-particle state (8.177), injected in 100 random unitary scattering compounds U of m=13 modes, C-datasets are generated (8.193)–(8.195), (8.200) for interference patterns associated with different particle types ("bosons", "distinguishable", "fermions" and "simulated bosons"). The numerically generated rescaled moments NM, CV and S, with (8.201)–(8.203), are averaged (black circle) and compared to the RMT predictions which make use of (8.208)–(8.219); red dot). The choice of particle and mode number is motivated by state of the art experiments (Spagnolo et al. 2014)

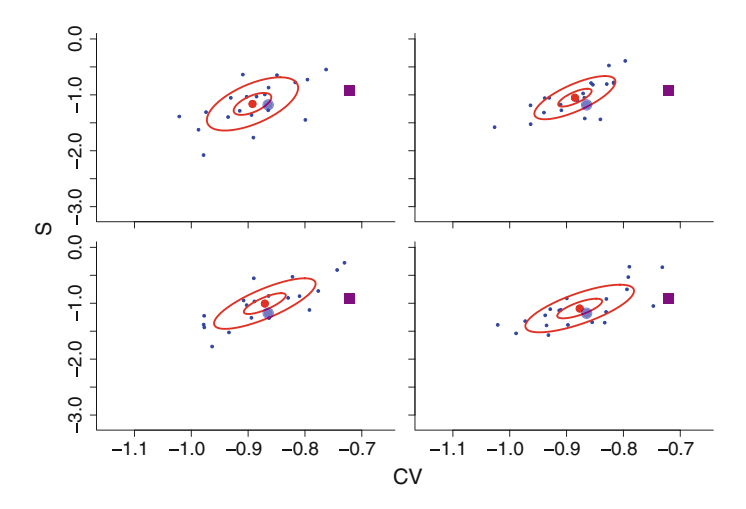


Fig. 8.14 Scatter plots indicating (small blue dots) the coefficient of variation (CV) and the skewness (S) as given in (8.221), (8.222). For a six-particle state (8.177), injected in 20 random unitary scattering compounds U of m=20 modes, C-datasets are generated for many-boson interference (8.193). The numerically generated rescaled moments CV and S, with (8.202)–(8.203), are averaged (red dot) and the regions associated with two and four standard errors are indicated (red circles). The RMT prediction for bosons (large blue dot) is shown to be significantly closer to the numerical average than the RMT prediction for the mean-field sampler (filled purple square). This figure is taken from Walschaers et al. (2016b)

have all the tools at hand. We again consider detectors mounted on orthogonal modes f_q , f_r and f_s , and moreover assume that the input states are of the form (8.187), such that we can use expression (8.146), which for bosons translates into

$$c_{qrs}^{b} = \sum_{\substack{j,k,l=1\\j\neq k\neq l}}^{n} U_{qi_{j}} U_{ri_{k}} U_{si_{l}} \overline{U}_{qi_{j}} \overline{U}_{ri_{k}} \overline{U}_{si_{l}} + U_{qi_{j}} U_{ri_{k}} U_{si_{l}} \overline{U}_{qi_{j}} \overline{U}_{ri_{l}} \overline{U}_{si_{k}}$$

$$+ U_{qi_{j}} U_{ri_{k}} U_{si_{l}} \overline{U}_{qi_{l}} \overline{U}_{ri_{k}} \overline{U}_{si_{j}} + U_{qi_{j}} U_{ri_{l}} U_{si_{k}} \overline{U}_{qi_{k}} \overline{U}_{ri_{j}} \overline{U}_{si_{l}}$$

$$+ U_{qi_{j}} U_{ri_{k}} U_{si_{l}} \overline{U}_{qi_{l}} \overline{U}_{ri_{j}} \overline{U}_{si_{k}} + U_{qi_{j}} U_{ri_{l}} U_{si_{l}} \overline{U}_{qi_{k}} \overline{U}_{ri_{l}} \overline{U}_{si_{l}}.$$

$$(8.223)$$

For fermions, we find

$$c_{qrs}^{f} = \sum_{\substack{j,k,l=1\\j\neq k\neq l}}^{n} U_{qi_{j}} U_{ri_{k}} U_{si_{l}} \overline{U}_{qi_{j}} \overline{U}_{ri_{k}} \overline{U}_{si_{l}} - U_{qi_{j}} U_{ri_{k}} U_{si_{l}} \overline{U}_{qi_{j}} \overline{U}_{ri_{l}} \overline{U}_{si_{k}}$$

$$- U_{qi_{j}} U_{ri_{k}} U_{si_{l}} \overline{U}_{qi_{l}} \overline{U}_{ri_{k}} \overline{U}_{si_{j}} - U_{qi_{j}} U_{ri_{l}} U_{si_{k}} \overline{U}_{qi_{k}} \overline{U}_{ri_{j}} \overline{U}_{si_{l}}$$

$$+ U_{qi_{j}} U_{ri_{k}} U_{si_{l}} \overline{U}_{qi_{l}} \overline{U}_{ri_{j}} \overline{U}_{si_{k}} + U_{qi_{l}} U_{ri_{k}} U_{si_{l}} \overline{U}_{qi_{k}} \overline{U}_{ri_{l}} \overline{U}_{si_{l}},$$

$$(8.224)$$

and for distinguishable particles we obtain

$$c_{qrs}^{d} = \sum_{\substack{j,k,l=1\\j\neq k\neq l}}^{n} U_{qi_j} U_{ri_k} U_{si_l} \overline{U}_{qi_j} \overline{U}_{ri_k} \overline{U}_{si_l}. \tag{8.225}$$

Just as for the two-point correlation function, the mean-field sampler imposes extra subtleties due to the accumulated random phases. For a given set $\{\theta\}$ of phases, the three-point correlation function is given by

$$c_{qrs,\{\theta\}}^{mf} = \frac{(n-1)(n-2)}{n^2} \sum_{j,k,l,j',k',l'=1}^{n} e^{i(\theta_j + \theta_k + \theta_l - \theta_{j'} - \theta_{k'} - \theta_{l'})} U_{qi_j} U_{ri_k} U_{si_l} \overline{U}_{qi'_j} \overline{U}_{ri'_k} \overline{U}_{si'_l}.$$
(8.226)

Just as before, while we accumulate statistics of detector outcomes, we are effectively averaging over the random phases. Again only those terms in the sum survive where all terms cancel. These are the terms where the set of indices $\{i, j, k\}$ equals the set $\{j', k', l'\}$. There are 3! ways to equate these sets, leading to the final result

$$c_{qrs}^{mf} = \frac{(n-1)(n-2)}{n^{2}} \left(\sum_{\substack{j,k,l=1\\k\neq l\neq m}}^{n} \left(U_{qi_{j}} U_{ri_{k}} U_{si_{l}} \overline{U}_{qi_{j}} \overline{U}_{ri_{k}} \overline{U}_{si_{l}} + U_{qi_{j}} U_{ri_{k}} U_{si_{l}} \overline{U}_{qi_{j}} \overline{U}_{ri_{l}} \overline{U}_{si_{k}} \right.$$

$$+ U_{qi_{j}} U_{ri_{k}} U_{si_{l}} \overline{U}_{qi_{l}} \overline{U}_{ri_{k}} \overline{U}_{si_{j}} + U_{qi_{j}} U_{ri_{l}} U_{si_{k}} \overline{U}_{qi_{k}} \overline{U}_{ri_{j}} \overline{U}_{si_{l}}$$

$$+ U_{qi_{j}} U_{ri_{k}} U_{si_{l}} \overline{U}_{qi_{l}} \overline{U}_{ri_{j}} \overline{U}_{si_{k}} + U_{qi_{j}} U_{ri_{k}} U_{si_{l}} \overline{U}_{qi_{l}} \overline{U}_{ri_{l}} \overline{U}_{si_{j}} \right)$$

$$+ \sum_{\substack{k,l=1\\k\neq l}}^{n} \left(U_{qi_{k}} U_{ri_{k}} U_{si_{l}} + U_{qi_{l}} U_{ri_{k}} U_{si_{k}} + U_{qi_{k}} U_{ri_{l}} U_{si_{k}} \right)$$

$$\times \left(\overline{U}_{qi_{k}} \overline{U}_{ri_{k}} \overline{U}_{si_{l}} + \overline{U}_{qi_{l}} \overline{U}_{ri_{k}} \overline{U}_{si_{k}} + \overline{U}_{qi_{k}} \overline{U}_{ri_{l}} \overline{U}_{si_{k}} \right)$$

$$+ \sum_{l=1}^{n} U_{qi_{l}} U_{ri_{l}} U_{si_{l}} \overline{U}_{qi_{l}} \overline{U}_{ri_{l}} \overline{U}_{si_{l}} \right). \tag{8.227}$$

The correlation functions (8.223)–(8.227) lead to similar problems as already encountered with the two-point correlation functions; they contain genuine three-particle interference-like terms:

$$U_{qi_i}U_{ri_k}U_{si_l}\overline{U}_{qi_l}\overline{U}_{ri_i}\overline{U}_{si_k}$$
 and $U_{qi_i}U_{ri_k}U_{si_l}\overline{U}_{qi_k}\overline{U}_{ri_l}\overline{U}_{si_i}$,

but they are also polluted by single-particle

$$U_{qi_i}U_{ri_k}U_{si_l}\overline{U}_{qi_i}\overline{U}_{ri_k}\overline{U}_{si_l},$$

and two-particle contributions (i.e. all the remaining ones). To filter out the low-order contributions we, again, resort to truncated correlation functions, as above, though the resulting expressions are now considerably more cumbersome:

$$C_{qrs} = \langle \hat{n}(f_q)\hat{n}(f_r)\hat{n}(f_s)\rangle - \langle \hat{n}(f_q)\hat{n}(f_r)\rangle\langle \hat{n}(f_s)\rangle - \langle \hat{n}(f_r)\hat{n}(f_s)\rangle\langle \hat{n}(f_q)\rangle - \langle \hat{n}(f_q)\hat{n}(f_s)\rangle\langle \hat{n}(f_r)\rangle + 2\langle \hat{n}(f_q)\rangle\langle \hat{n}(f_r)\rangle\langle \hat{n}(f_s)\rangle = \langle \hat{n}(f_q)\hat{n}(f_r)\hat{n}(f_s)\rangle - C_{qr}\langle \hat{n}(f_s)\rangle - C_{rs}\langle \hat{n}(f_q)\rangle - C_{qs}\langle \hat{n}(f_r)\rangle - \langle \hat{n}(f_q)\rangle\langle \hat{n}(f_r)\rangle\langle \hat{n}(f_s)\rangle.$$
(8.228)

Because the number of terms in these expressions grows quickly, we introduce some additional notation in order to keep the resulting expressions somewhat compact.³⁸ We start by considering sums over different indices, which have the specific form

$$T_{\pi} = \sum_{\substack{j,k,l=1\\j\neq k\neq l}}^{n} U_{qi_{j}} U_{ri_{k}} U_{si_{l}} \overline{U}_{qi_{\pi(j)}} \overline{U}_{ri_{\pi(k)}} \overline{U}_{si_{\pi(l)}},$$
(8.229)

³⁸This notation was introduced by J.-D. Urbina and J. Kuipers in private communication.

where $\pi \in S_3$ is a permutation. We split these terms in three classes: G, H, and I, where G describes permutations with cycle³⁹ lengths are (1, 1, 1), H represents permutations given by cycles (1, 2) and I are those with cycle lengths (3). This produces the terms

$$G = \sum_{\substack{j,k,l=1\\i\neq k\neq l}}^{n} U_{qi_j} U_{ri_k} U_{si_l} \overline{U}_{qi_j} \overline{U}_{ri_k} \overline{U}_{si_l}, \tag{8.230}$$

$$H_1 = \sum_{\substack{j,k,l=1\\j\neq k\neq l}}^n U_{qi_j} U_{ri_k} U_{si_l} \overline{U}_{qi_j} \overline{U}_{ri_l} \overline{U}_{si_k}, \tag{8.231}$$

$$H_2 = \sum_{\substack{j,k,l=1\\j\neq k\neq l}}^n U_{qi_j} U_{ri_k} U_{si_l} \overline{U}_{qi_k} \overline{U}_{ri_j} \overline{U}_{si_l}, \tag{8.232}$$

$$H_3 = \sum_{\substack{j,k,l=1\\j\neq k\neq l}}^n U_{qi_j} U_{ri_k} U_{si_l} \overline{U}_{qi_l} \overline{U}_{ri_k} \overline{U}_{si_j}, \tag{8.233}$$

$$I_{1} = \sum_{\substack{j,k,l=1\\i\neq k\neq l}}^{n} U_{qi_{j}} U_{ri_{k}} U_{si_{l}} \overline{U}_{qi_{l}} \overline{U}_{ri_{j}} \overline{U}_{si_{k}}, \tag{8.234}$$

$$I_2 = \sum_{\substack{j,k,l=1\\i\neq k\neq l}}^n U_{qi_j} U_{ri_k} U_{si_l} \overline{U}_{qi_k} \overline{U}_{ri_l} \overline{U}_{si_j}. \tag{8.235}$$

With this notation, we find that

$$c_{qrs}^b = G + \sum H + \sum I, \tag{8.236}$$

$$c_{qrs}^f = G - \sum H + \sum I, \tag{8.237}$$

$$c_{ars}^d = G. (8.238)$$

³⁹The cycle notation of permutations is commonly used in abstract algebra and discrete mathematics (Biggs 1989). A *cycle* of *length* n (i_1, \ldots, i_n) represents a cyclic permutation $i_1 \rightarrow i_2 \rightarrow \cdots \rightarrow i_n \rightarrow i_1$. It turns out that any permutation can be interpreted as combination of several cycles. As an example, we may consider the set of three elements $\{a, b, c\}$ and consider the permutation $\{a, b, c\} \mapsto \{a, b, c\}$, which can be written as a combination of three cycles of length one: (a)(b)(c). As a second example, we consider $\{a, b, c\} \mapsto \{c, b, a\}$ which is denoted by (b)(a, c) in cycle nations. As a final example, $\{a, b, c\} \mapsto \{c, a, b\}$ is written as (a, b, c) in cycle notation. In representation theory, it is common to classify permutations based on cycle lengths (Hamermesh 1989). To use the examples of before, we could characterise (a)(b)(c) as a permutation with *cycle lengths* (1, 1, 1), whereas (b)(a, c) has cycle lengths (1, 2), and finally (a, b, c) has cycle length (3).

Clearly, to deal with either mean-field sampling (8.227) or truncated correlation functions of the form (8.228), we need additional terms, where some of the indices coincide. This leads to classes of terms with only two distinct indices. We first find

$$J_{l} = \sum_{\substack{k,l=1\\k \neq l}}^{n} U_{qi_{k}} U_{ri_{k}} U_{si_{l}} \overline{U}_{qi_{k}} \overline{U}_{ri_{k}} \overline{U}_{si_{l}}, \tag{8.239}$$

$$J_k = \sum_{\substack{j,k=1\\j\neq k}}^n U_{qi_j} U_{ri_k} U_{si_j} \overline{U}_{qi_j} \overline{U}_{ri_k} \overline{U}_{si_j}, \tag{8.240}$$

$$J_{j} = \sum_{\substack{j,k=1\\i\neq k}}^{n} U_{qi_{j}} U_{ri_{k}} U_{si_{k}} \overline{U}_{qi_{j}} \overline{U}_{ri_{k}} \overline{U}_{si_{k}}, \tag{8.241}$$

where the index on the left hand side always indicates which index is different from the other two. Moreover, we must consider permutations of the remaining distinct indices, leading to two additional classes, which each refer to a specific choice of the repeated index⁴⁰: First,

$$K_{l,1} = \sum_{\substack{k,l=1\\k \neq l}}^{n} U_{qi_k} U_{ri_k} U_{si_l} \overline{U}_{qi_k} \overline{U}_{ri_l} \overline{U}_{si_k}, \tag{8.242}$$

$$K_{k,1} = \sum_{\substack{j,k=1\\i\neq k}}^{n} U_{qi_j} U_{ri_k} U_{si_j} \overline{U}_{qi_k} \overline{U}_{ri_j} \overline{U}_{si_j}, \tag{8.243}$$

$$K_{j,1} = \sum_{\substack{j,k=1\\i\neq k}}^{n} U_{qi_j} U_{ri_k} U_{si_k} \overline{U}_{qi_k} \overline{U}_{ri_k} \overline{U}_{si_j}, \tag{8.244}$$

and, second,

$$K_{l,2} = \sum_{\substack{k,l=1\\k \neq l}}^{n} U_{qi_k} U_{ri_k} U_{si_l} \overline{U}_{qi_l} \overline{U}_{ri_k} \overline{U}_{si_k},$$
(8.245)

$$K_{k,2} = \sum_{\substack{j,k=1\\j\neq k}}^{n} U_{qi_j} U_{ri_k} U_{si_j} \overline{U}_{qi_j} \overline{U}_{ri_j} \overline{U}_{si_k}, \tag{8.246}$$

⁴⁰Let us consider the difference between $K_{l,1}$ and $K_{l,2}$ in more depth to emphasise the idea: Both $K_{l,1}$ and $K_{l,2}$ start from the index set $\{i_k, i_k, i_l\}$, however to represent the permutation of k and l, there are two possible choices for k. $K_{l,1}$ represents the permutation $\{i_k, i_k, i_l\} \rightarrow \{i_k, i_l, i_k\}$, whereas $K_{l,2}$ represents $\{i_k, i_k, i_l\} \rightarrow \{i_l, i_k, i_k\}$.

$$K_{j,2} = \sum_{\substack{j,k=1\\j\neq k}}^{n} U_{qi_j} U_{ri_k} U_{si_k} \overline{U}_{qi_k} \overline{U}_{ri_j} \overline{U}_{si_k}.$$
 (8.247)

The final class of contributions to C_{qrs} is given by the case where there is only one free index to sum over,

$$L = \sum_{i}^{n} U_{qi_j} U_{ri_j} U_{si_j} \overline{U}_{qi_j} \overline{U}_{ri_j} \overline{U}_{si_j}, \qquad (8.248)$$

such that we can now use all these terms to write

$$c_{qrs}^{mf} = \frac{(n-1)(n-2)}{n^2} \Big(G + \sum H + \sum I + \sum J + \sum K + L \Big).$$
 (8.249)

Intriguingly, the only genuine three-particle terms in all these expressions are those of the *I*-type. They are the only terms which contain cyclic permutations of length three (such permutations can be considered irreducible in the sense that it is impossible to divide them in permutations of subgroups). It therefore is interesting to see whether these terms are indeed more dominant in the truncated correlation function. After a straightforward calculation where one groups the terms appropriately, we find that

$$C_{qrs}^b = \sum I - \sum K + 2L,$$
 (8.250)

$$C_{qrs}^{f} = \sum I + \sum K + 2L,$$
 (8.251)

$$C_{qrs}^d = 2L, (8.252)$$

for direct sampling from orthogonal modes. The result for mean-field sampling is considerably more complicated:

$$C_{qrs}^{mf} = \sum I - \left(\frac{3}{n} - \frac{2}{n^2}\right) \left(G + \sum I\right) - \frac{2}{n} \left(1 - \frac{1}{n}\right) \left(\sum H + \sum J + \sum K\right) + \frac{2}{n^2} L.$$
 (8.253)

We see that, in the mean-field sampler, all the different types of terms contribute to the final, truncated correlation function, but they do so in different orders. More specifically, in the limit of many particles, $n \to \infty$, we obtain that

$$\lim_{n \to \infty} C_{qrs}^{mf} = \sum I, \tag{8.254}$$

which essentially implies that we do see signatures of three-particle trajectories which are very pronounced. One may actually argue that these signatures are too pronounced, since, in this limit, we completely overlook the $\sum K$ terms that express

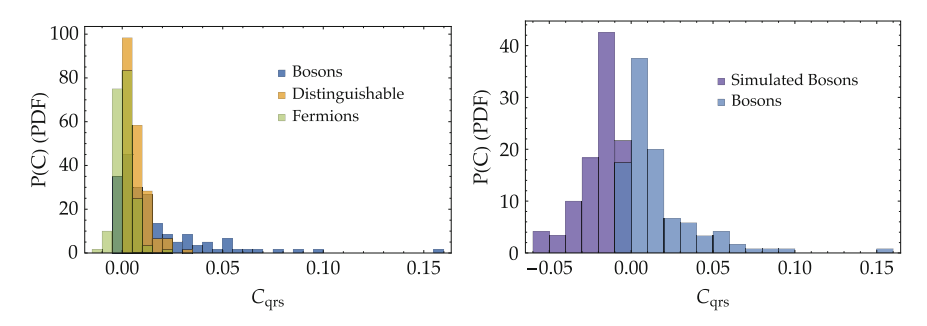


Fig. 8.15 Normalised (PDF) histograms of the correlator data built from truncated three-point correlation functions $C_{qrs}^{b/f/d/mf}$ (8.250)–(8.253) of four particles injected into ten modes for all possible mode combinations. Bosons are compared to fermions and distinguishable particles (left), and to the sampling from the mean-field sampler which simulates bunching effects, but not genuine many-partial interference (right). All histograms are obtained from one single circuit by evaluating $C_{qrs}^{b/f/d/mf}$ for all combinations q, r and s of three output modes, using the same input state Ψ given by (8.187). In particular this implies that for distinct particle types the same components of U were used

the difference between bosons and fermions, as well as the L term, which essentially gives the underlying classical truncated correlation.

To analyse the effectiveness of these three-point truncated correlation functions to differentiate interference patterns of particle types, we again consider histograms in Fig. 8.15. Notice that these histograms are obtained from a system with only four particles and *ten* modes. This is a regime where it was impossible for the two-point truncated correlation function to distinguish genuine bosonic interference from bunching effects generated by the mean-field sampler (recall Fig. 8.13). However, the right panel of Fig. 8.15 clearly highlights a considerable difference between the two histograms, suggesting that certification is feasible.

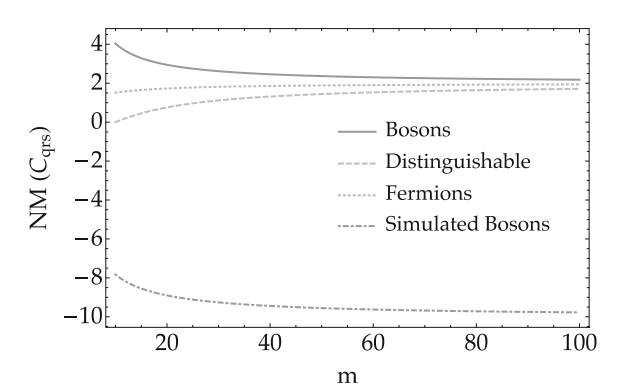
To verify this qualitative hypothesis, inferred from the histograms, we again use RMT as a tool for the derivation of moments. Interestingly, it turns out that the first moment of the distribution of C_{qrs} already provides a considerable amount of information. To calculate the first moment, i.e. the average value of C_{qrs} , we exploit the specific definitions (8.230)–(8.248) of all terms. Indeed, each different class of terms leads to the same expectation value when we average over the Haar measure. Using again the identity (8.207) and the functions $V_m(\sigma^{-1}\pi)$ from Brouwer and Beenakker (1996), we find

$$\mathbb{E}_{U}(G) = \frac{n(n-1)(n-2)(m^2-2)}{m(m^2-1)(m^2-4)},$$
(8.255)

$$\mathbb{E}_{U}(H) = -\frac{n(n-1)(n-2)}{(m^2-1)(m^2-4)},$$
(8.256)

$$\mathbb{E}_{U}(I) = \frac{2n(n-1)(n-2)}{m(m^2-1)(m^2-4)},$$
(8.257)

Fig. 8.16 Theoretical RMT predictions (8.261)–(8.264) for the normalised mean (NM; (8.265)) of the three-point truncated correlation functions (8.250)–(8.253) for a five-particle state (8.177) injected into a random scattering compound with variable number m of modes



$$\mathbb{E}_{U}(J) = \frac{n(n-1)}{m(m-1)(m+2)},\tag{8.258}$$

$$\mathbb{E}_{U}(K) = -\frac{n(n-1)}{m(m^2 - 1)(m+2)},\tag{8.259}$$

$$\mathbb{E}_{U}(L) = \frac{n}{m(m+1)(m+2)}.$$
(8.260)

These expressions can now straightforwardly be inserted in the expressions (8.250)–(8.253) for the truncated correlation functions C_{qrs} , to obtain the RMT expectation values

$$\mathbb{E}_{U}(C_{qrs}^{b}) = \frac{2n(m^2 + 3nm + 2n^2 - 6m - 12n + 12)}{m(m^2 - 1)(m^2 - 4)},$$
(8.261)

$$\mathbb{E}_{U}(C_{qrs}^{f}) = \frac{2n(m^2 - 3nm + 2n^2)}{m(m^2 - 1)(m^2 - 4)},$$
(8.262)

$$\mathbb{E}_{U}(C_{qrs}^{d}) = \frac{2n}{m(m+1)(m+2)},$$
(8.263)

$$\mathbb{E}_{U}(C_{qrs}^{mf}) = \frac{-3m^{2}n^{2} + 5m^{2}n + 6mn^{2} - 6mn - 6m + 4n^{3} - 18n^{2} + 18n}{m(m^{2} - 1)(m^{2} - 4)},$$
(8.264)

which clearly predicts a profound difference between the mean-field sampler and the other particle types, which is also expressed in Fig. 8.16, where we define the normalised mean NM as

$$NM = \mathbb{E}_U(C_{qrs}) \frac{m^3}{n}.$$
 (8.265)

Although it appears hard to separate boson sampling from the sampling of fermions or distinguishable particles, by the three-point correlator, the latter is remarkably distinctive when validating boson sampling against mean-field sampling.

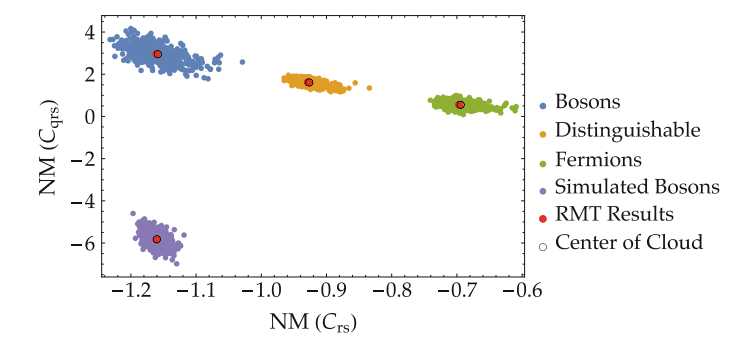


Fig. 8.17 Scatter plot indicating the normalised means NM (8.220), (8.265) of C_{rs} (8.193)–(8.195), (8.200) and C_{qrs} (8.250)–(8.253). For a four-particle state (8.177), injected in 500 random unitary scattering compounds U of m=10 modes, C-datasets are generated for interference patterns associated with different particle types ("bosons", "distinguishable", "fermions" and "simulated bosons"). The numerically generated NM, with (8.201)–(8.203), are averaged (black circle) and compared to the RMT predictions which make use of (8.208)–(8.219), (8.264); red dot)

Ergo, the three-point truncated correlation function is a useful tool to distinguish bunching effects from genuine many-particle interference.

Remember that the normalised mean of the C-dataset of *two-point* truncated correlation functions was a good certification tool for different particle types such that we were able to efficiently distinguish bosonic- from fermionic interference and from distinguishable particles' statistics. Hence, we can use a combination of both the normalised mean for the two-point truncated correlation functions *and* the normalised mean of the three-point correlation functions. This combined information leads to scatter plots as in Fig. 8.17, which presents data for only four particles injected into no more than ten modes. Even in the regime which is haunted by finite size effects (recall Fig. 8.13), we see that this combination of two- and three-point truncated correlation data provides a very strong tool for certification. The clouds of data points are so well separated that the RMT results have strong predictive power. Consequently, the position of a single measurement point on such plot, combined with just the RMT predictions should be enough for reliable certification!

We thus showed that statistical information on low order (second and third order) correlations between output modes suffices to certify boson sampling for any numbers of modes and particles. We must stress that these methods strongly rely on the random matrix ensemble from which the unitaries are sampled, using both the notion that such sampled random matrices are "generic", and therefore statistical results can successfully be applied to provide robust, analytical results. Unitaries which have specific symmetries in them and therefore do not follow the Haar measure, lead to very different C-datasets, such that the here derived RMT results are no longer applicable. Therefore, the method which we provide is also suitable for verifying whether an ensemble of devices (e.g. beamsplitter arrays, photonics waveguides, *et cetera*) are correctly generated according to the Haar measure in the sense that they manifest the correct statistical properties and hence the correct C-datasets.

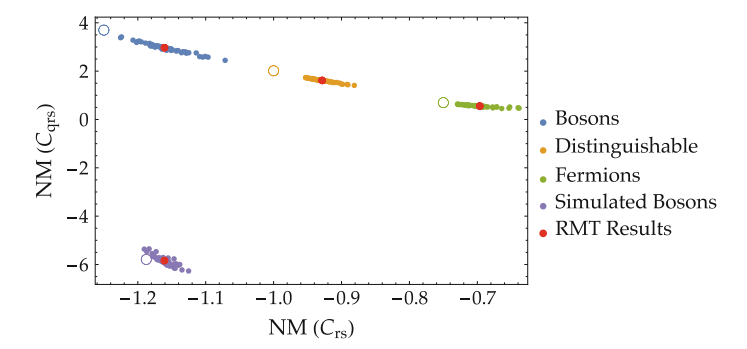


Fig. 8.18 Scatter plot indicating the normalised means NM (8.220), (8.265) of C_{rs} (8.193)–(8.195), (8.200), and C_{qrs} (8.250)–(8.253,) C-datasets. A four-particle state (8.177) is injected in 100 random unitary scattering compounds U (dots) and the scatterer describe by the Fourier matrix $U_{jk} = \exp(2\pi i j k/m)$ (circle), both for m = 13 modes. For each scattering compound, the C-datasets is numerically generated for interference patterns associated with different particle types ("bosons", "distinguishable", "fermions" and "simulated bosons"). The numerically achieved NM with (8.201)–(8.203) are averaged (black circle) and compared to the RMT predictions which make use of (8.208)–(8.219), (8.264)–(8.264); red dot)

Nevertheless, C-datasets of low order correlation functions, in general, provide an enormous amount of information about the system. This is even the case for the highly symmetric Fourier matrix, whose components are given by $U_{jk} = \exp(2\pi i j k/m)$, with m the number of modes. Indeed, in Fig. 8.18 we see that the normalised means 41 of C_{rs} and C_{qrs} datasets as induced by the Fourier matrix fall outside of scattered data points obtained from random scattering unitaries chosen with respect to the Haar measure. However, also in the scattering process generated by the Fourier matrix, the normalised means associated with interference patterns generated by different particle types are very distinct, which allows efficient certification of many-particle interference types, also for scattering problems which are strongly dominated by symmetries.

8.5.3 Partial Distinguishability and Correlation Spectroscopy

Now that we managed to certify the extreme cases of many-particle interference, from bosonic to fermionic, compared to purely classical probability theory, set forth by distinguishable particles, and learned how to differentiate between genuine many-boson interference and simple bunching effects, we can treat transition regimes. It can be argued that, from the physics perspective, there is only one relevant transition to be considered: When discussing the concept of distinguishability in Sects. 7.3.2 and 8.3.4, we argued that, in essence, there are only two types of particles in nature (related

⁴¹For the Fourier matrix, the normalised means of both C_{rs} and C_{qrs} are completely independent of the chosen input state (8.177). The physical interpretation of this result is currently unclear to us.

to two fundamental algebras), bosons and fermions. Alternations in the interference patterns related to the distinguishability of particles is rooted in additional, often external degrees of freedom which remain unresolved, thus destroying specifically the coherence between them (and hence their capacity to interfere, as discussed in Sect. 8.3.4).

This distinguishability transition is, moreover, of considerable importance in experimental settings, where one rarely reaches complete indistinguishability (see, for example, the supplementary material of Spagnolo et al. 2014). Therefore, we must understand how such partial distinguishability influences the interference patterns which we study. More specifically, the sensitivity of our certification method with respect to the distinguishability of the injected bosons is a profound point of interest. Hence, in the current section, we focus on the specific transition from indistinguishable bosons to fully distinguishable particles, and study how this transition impacts the C-dataset.

The relevant two-point correlation function (8.165) was already derived earlier and, using the shorter notation (8.182), is given by

$$c_{rs}^{pd} = \sum_{\substack{k,l=1\\k\neq l}}^{n} U_{ri_k} U_{si_l} \overline{U}_{ri_k} \overline{U}_{si_l} + |\langle \chi_k, \chi_l \rangle|^2 U_{ri_k} U_{si_l} \overline{U}_{ri_l} \overline{U}_{si_k}. \tag{8.266}$$

Moreover, by virtue of Eq. (8.164), we can also derive the three-point correlation function

$$c_{qrs}^{pd} = \sum_{\substack{j,k,l=1\\j\neq k\neq l}}^{n} U_{qi_{j}} U_{ri_{k}} U_{si_{l}} \overline{U}_{qi_{j}} \overline{U}_{ri_{k}} \overline{U}_{si_{l}} + |\langle \chi_{k}, \chi_{l} \rangle|^{2} U_{qi_{j}} U_{ri_{k}} U_{si_{l}} \overline{U}_{qi_{j}} \overline{U}_{ri_{l}} \overline{U}_{si_{k}}$$

$$+ |\langle \chi_{j}, \chi_{l} \rangle|^{2} U_{qi_{j}} U_{ri_{k}} U_{si_{l}} \overline{U}_{qi_{l}} \overline{U}_{ri_{k}} \overline{U}_{si_{j}} + |\langle \chi_{j}, \chi_{k} \rangle|^{2} U_{qi_{j}} U_{ri_{l}} U_{si_{k}} \overline{U}_{qi_{k}} \overline{U}_{ri_{j}} \overline{U}_{si_{l}}$$

$$+ \langle \chi_{j}, \chi_{l} \rangle \langle \chi_{k}, \chi_{j} \rangle \langle \chi_{l}, \chi_{k} \rangle U_{qi_{j}} U_{ri_{k}} U_{si_{l}} \overline{U}_{qi_{l}} \overline{U}_{ri_{j}} \overline{U}_{si_{k}}$$

$$+ \langle \chi_{j}, \chi_{k} \rangle \langle \chi_{k}, \chi_{l} \rangle \langle \chi_{l}, \chi_{j} \rangle U_{qi_{j}} U_{ri_{k}} U_{si_{l}} \overline{U}_{qi_{k}} \overline{U}_{ri_{l}} \overline{U}_{si_{j}},$$

$$(8.267)$$

Converting the above expressions to the more sensitive truncated correlation functions (see (8.191) and (8.228) above) is straightforward for the two-point case:

$$C_{rs}^{pd} = \sum_{\substack{k,l=1\\k \neq l}}^{n} |\langle \chi_k, \chi_l \rangle|^2 U_{ri_k} U_{si_l} \overline{U}_{ri_l} \overline{U}_{si_k} - \sum_{k=1}^{n} U_{ri_k} U_{si_k} \overline{U}_{ri_k} \overline{U}_{si_k}.$$
(8.268)

For the three-point case, however, one must take into account that two-point terms, which are also influenced by the degree of distinguishability, are subtracted. To capture all these effects correctly, we define G', H', I', J', K', and L' class terms, the analogs of the terms (8.230)–(8.248) introduced in our earlier discussion (see the previous section) on three-point truncated correlation functions. First, we can define

$$G' = G = \sum_{\substack{j,k,l=1\\j\neq k\neq l}}^{n} U_{qi_j} U_{ri_k} U_{si_l} \overline{U}_{qi_j} \overline{U}_{ri_k} \overline{U}_{si_l},$$
(8.269)

$$H_{1}' = \sum_{\substack{j,k,l=1\\j\neq k\neq l}}^{n} |\langle \chi_{k}, \chi_{l} \rangle|^{2} U_{qi_{j}} U_{ri_{k}} U_{si_{l}} \overline{U}_{qi_{j}} \overline{U}_{ri_{l}} \overline{U}_{si_{k}},$$
(8.270)

$$H_2' = \sum_{\substack{j,k,l=1\\j\neq k\neq l}}^{n} \left| \left\langle \chi_j, \chi_k \right\rangle \right|^2 U_{qi_j} U_{ri_k} U_{si_l} \overline{U}_{qi_k} \overline{U}_{ri_j} \overline{U}_{si_l}, \tag{8.271}$$

$$H_3' = \sum_{\substack{j,k,l=1\\i\neq k\neq l}}^n \left| \left\langle \chi_j, \chi_l \right\rangle \right|^2 U_{qi_j} U_{ri_k} U_{si_l} \overline{U}_{qi_l} \overline{U}_{ri_k} \overline{U}_{si_j}, \tag{8.272}$$

$$I_{1}' = \sum_{\substack{j,k,l=1\\i\neq k\neq l}}^{n} \langle \chi_{j}, \chi_{l} \rangle \langle \chi_{k}, \chi_{j} \rangle \langle \chi_{l}, \chi_{k} \rangle U_{qi_{j}} U_{ri_{k}} U_{si_{l}} \overline{U}_{qi_{l}} \overline{U}_{ri_{j}} \overline{U}_{si_{k}}, \tag{8.273}$$

$$I_{2}' = \sum_{\substack{j,k,l=1\\j\neq k\neq l}}^{n} \langle \chi_{j}, \chi_{k} \rangle \langle \chi_{k}, \chi_{l} \rangle \langle \chi_{l}, \chi_{j} \rangle U_{qi_{j}} U_{ri_{k}} U_{si_{l}} \overline{U}_{qi_{k}} \overline{U}_{ri_{l}} \overline{U}_{si_{j}}.$$
(8.274)

We now find that, indeed,

$$c_{qrs}^{pd} = G + \sum H' + \sum I',$$
 (8.275)

but, to obtain the truncated correlation functions, we also need to consider the J' and K' class terms. It is directly seen that J' = J because this term is governed only by a product of single-particle transition probabilities, implying there is no many-particle interference present.⁴² Therefore, we can restrict to the K' class and obtain

$$K'_{l,1} = \sum_{\substack{k,l=1\\k\neq l}}^{n} |\langle \chi_k, \chi_l \rangle|^2 U_{qi_k} U_{ri_k} U_{si_l} \overline{U}_{qi_k} \overline{U}_{ri_l} \overline{U}_{si_k}, \tag{8.276}$$

$$K'_{k,1} = \sum_{\substack{j,k=1\\i\neq k}}^{n} \left| \left\langle \chi_j, \chi_k \right\rangle \right|^2 U_{qi_j} U_{ri_k} U_{si_j} \overline{U}_{qi_k} \overline{U}_{ri_j} \overline{U}_{si_j}, \tag{8.277}$$

$$K'_{j,1} = \sum_{\substack{j,k=1\\j\neq k}}^{n} \left| \left\langle \chi_j, \chi_k \right\rangle \right|^2 U_{qi_j} U_{ri_k} U_{si_k} \overline{U}_{qi_k} \overline{U}_{ri_k} \overline{U}_{si_j}, \tag{8.278}$$

⁴²Mathematically, J=J' simply follows because the factor associated with the factor related to the additional degrees of freedom is of the type $|\langle \chi_k, \chi_k \rangle|^2 \langle \chi_l, \chi_l \rangle$, which is equal to one due to normalisation.

$$K'_{l,2} = \sum_{\substack{k,l=1\\k\neq l}}^{n} |\langle \chi_k, \chi_l \rangle|^2 U_{qi_k} U_{ri_k} U_{si_l} \overline{U}_{qi_l} \overline{U}_{ri_k} \overline{U}_{si_k},$$
(8.279)

$$K'_{k,2} = \sum_{\substack{j,k=1\\j\neq k}}^{n} \left| \left\langle \chi_j, \chi_k \right\rangle \right|^2 U_{qi_j} U_{ri_k} U_{si_j} \overline{U}_{qi_j} \overline{U}_{ri_j} \overline{U}_{si_k}, \tag{8.280}$$

$$K'_{j,2} = \sum_{\substack{j,k=1\\j\neq k}}^{n} \left| \left\langle \chi_j, \chi_k \right\rangle \right|^2 U_{qi_j} U_{ri_k} U_{si_k} \overline{U}_{qi_k} \overline{U}_{ri_j} \overline{U}_{si_k}. \tag{8.281}$$

Finally, also L' = L (for the same reason as J' = J) and a straightforward calculation, analogous to (8.250), leads to

$$C_{qrs}^{pd} = \sum I' - \sum K' + 2L. \tag{8.282}$$

We note that, for $\langle \chi_i, \chi_j \rangle = 1$, for all i, j, (8.282) reduces to C_{qrs}^b , and, when $\langle \chi_i, \chi_j \rangle = \delta_{ij}$, we indeed find C_{qrs}^d .

From the above considerations, it is clear that one needs a thorough understanding of the additional degrees of freedom, i.e. the set $\{\chi_j\}$, of the incoming particles in order to achieve anything. To illustrate the power of the certification method, using the above truncated correlation functions, we will study specific choices for the set $\{\chi_j\}$. The first choice, a sequence of Gaussian wave packets with a fixed time delay, is considered for theoretical merit, as it builds intuition. This setup is slightly inspired by non-linear spectroscopy (Mukamel 2009; Schlawin et al. 2012b) where one injects pulses into a medium with a variable, controlled, time delay. The second choice for $\{\chi_j\}$, where random deviations from the expected arrival time at the detector are considered, is intended to be closer to the interferometric experimental setting.

A sequence of particles with a fixed time delay is considered as a first specific setup. Here, we focus on the situation where these particles (which we assume to be photons) are Gaussian wave packets in $\mathcal{H}_{add} = \mathcal{L}^2(\mathbb{R})$. This implies that one particle's internal wave function can be described by Ra et al. (2013a)

$$\chi_j(t) = \frac{1}{\pi^{1/4} \sqrt{\Delta \omega}} \int_{\mathbb{R}} d\omega \exp\left(-\frac{(\omega - \omega_0)^2}{2\Delta \omega} + i(t + t_j)\omega\right) |\omega\rangle, \qquad (8.283)$$

where we choose to work in the frequency-time domain rather than the position-momentum picture. Note that t_j in the expression can be related to an initial position, which only becomes important when we consider several particles. When performing an experiment, $t_j - t_k$ is the difference between the times at which the particles j and k are detected. We see that these different detection times not only (obviously) physically, but also formally render distinguishability, since

$$\left\langle \chi_j(t), \chi_k(t) \right\rangle = \exp\left(-\frac{\Delta\omega^2 (t_k - t_j)^2}{4} - i\omega_0 (t_k - t_j)\right) = \left\langle \chi_j(0), \chi_k(0) \right\rangle. \tag{8.284}$$

Obviously, only the time delays between the different particles are relevant, such that we can always take the first particle to trigger the detector and set the corresponding arrival time $t_j=0$. This implies that, when we have n particles, there are still n-1 time delays that are variable, which naturally leads to a wide range of possibilities. In order to structure our discussion, we assume a train of particles, in the sense that the particles are detected with fixed time intervals between them, or, in other words, $t_{j+1}-t_j=\Delta t$ for $j=1,\ldots n-1$. This setup is convenient, since it allows us to simply use $\Delta\omega\Delta t$ as a measure for subsequent particles' mutual distinguishability.

Indeed, Fig. 8.19 points out that increasing values of $\Delta\omega\Delta t$ imply larger degrees of distinguishability. Moreover, considering for example $\Delta\omega\Delta t=1$, we see that χ_1 and χ_2 have a strong overlap, whereas the overlap between χ_1 and χ_6 is negligible. In this sense, we can expect two-particle interference processes between χ_i and χ_{i+1} to have stronger contributions than three-particle interference processes, which are on their turn dominant over four-particle interference processes, *et cetera*. *Ergo*, by virtue of this sequence of wave packets, we can carefully investigate the importance of each of these processes by varying $\Delta\omega\Delta t$.

Because all the input modes are randomly coupled to all the output modes when the unitary scattering matrix is sampled from the Haar measure, statistical features of the interference pattern are not expected to depend on the modes in which the particles are injected. In other words, the statistics of the C-dataset does not depend on how the particles in Fig. 8.19 are distributed over the different input modes.

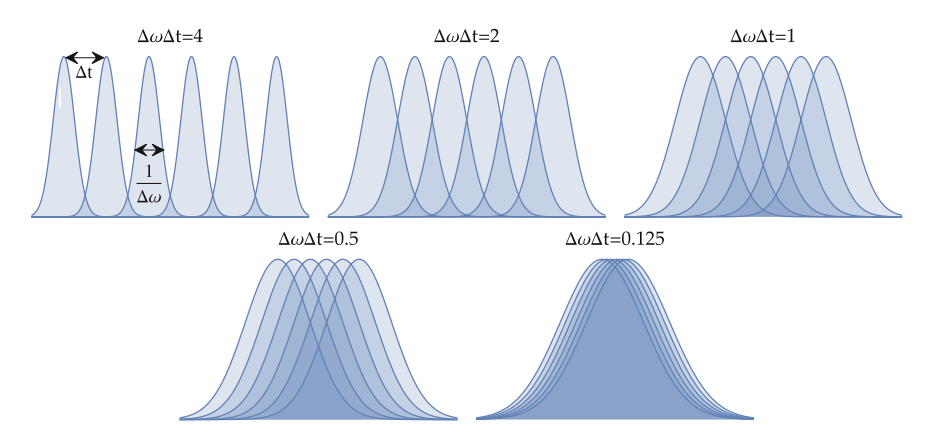


Fig. 8.19 Gaussian probability distributions for the detection of bosons, described by single-particle wave functions $\chi_j(t) \in \mathcal{H}_{add}$ (8.283), at specific times. The wave packets are characterised by a bandwidth $\Delta\omega$ and are subject to fixed time delays Δt between mean detection times t_j (for particle with wave-function χ_j) and t_{j+1} . The degree of indistinguishability is characterised by the overlap of the probability distributions (8.284), which is fully determined by dimensionless parameter $\Delta\omega\Delta t$, which takes values $\Delta\omega\Delta t = 4, 2, 1, 0.5, 0.125$ from very well distinguishable to essentially indistinguishable, respectively

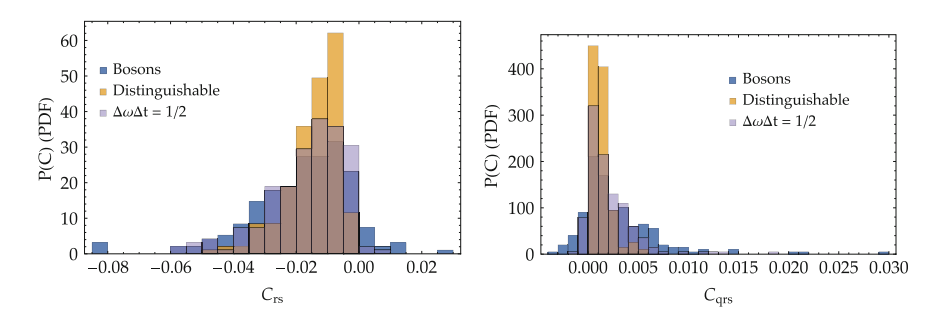


Fig. 8.20 Normalised (PDF) histograms of the correlator data built from truncated two-point, $C_{rs}^{b/d/pd}$ (8.193), (8.195), (8.268; left) and three-point, $C_{qrs}^{b/d/pd}$, correlation functions (8.250), (8.252), (8.282); right). Six partially distinguishable particles with wave packets $\chi_j \in \mathcal{H}_{\rm add}$ (8.283) for the additional degrees of freedom are injected in twenty modes, with fixed time delay such that $\Delta\omega\Delta t=1/2$ (see Fig. 8.19) and are compared to bosonic interference ($\Delta\omega\Delta t=0$) and to the signal for fully distinguishable particles ($\Delta\omega\Delta t\to\infty$). All histograms are obtained from one single circuit by evaluating $C_{rs}^{b/d/pd}$ for all pairs r and s, and $C_{qrs}^{b/d/pd}$ for all triplets q, r and s of output modes. We always use the same input state Ψ , given by (8.187)

All pieces are thus collected to study these C-datasets for the two-point and three-point truncated correlation functions, and we can start with a comparison of the histograms for a train of particles with $\Delta\omega\Delta t=1/2$ (recall Fig. 8.19) to those which we already know for bosons ($\Delta t \Delta\omega=0$) and distinguishable particles ($\Delta t \Delta\omega\gg1$). In Fig. 8.20 we see that the histogram for the train of mutually delayed particles indeed exhibits a somewhat intermediate structure that shares features with both the bosonic and the distinguishable case.

The story becomes much more interesting when we quantitatively analyse the distributions in Fig. 8.20 through their lowest-order moments. The averaging procedure of the unitary scattering matrices over the Haar measure is fully analogous to the previous sections (see Appendix B), such that we find

$$\mathbb{E}_{U}(C_{rs}^{pd}) = -\frac{1}{m(m^{2} - 1)} \sum_{\substack{k,l = 1 \\ k \neq l}}^{n} |\langle \chi_{k}, \chi_{l} \rangle|^{2} - \frac{n}{m(m + 1)}.$$
 (8.285)

Comparing (8.285) to the earlier result (8.268), we see that each term related to a two-particle interference process leads to the same average (see Appendix B) and that $|\langle \chi_k, \chi_l \rangle|^2$ provides a means of counting how many such two-particle interference terms contribute to the correlation function. From Fig. 8.19, we can understand that this implies counting the different pairings of wave packets, weighted by their degree of overlap. For our specific choice of χ_j , (8.285) reduces to

$$\mathbb{E}_{U}(C_{rs}^{pd}) = -\frac{2}{m(m^2 - 1)} \sum_{k=1}^{n-1} (n - k)e^{-k^2(\Delta\omega\Delta t)^2/2} - \frac{n}{m(m+1)}.$$
 (8.286)

After a much more complicated computation (following the same procedure as Appendix B), we can also find the second moment expectation value

$$\mathbb{E}_{U}(C_{rs}^{pd^{2}}) = \frac{2A - 2B(m-5) + 2D(2 + 6m - n + mn) + C(10 + m + m^{2})}{(m-1)m^{2}(m+1)(m+2)(m+3)} + \frac{(m-2)(1+3m)n + 2n^{2} + mn^{2} + m^{2}n^{2})}{(m-1)m^{2}(m+1)(m+2)(m+3)},$$
(8.287)

with

$$A = \sum_{\substack{k_1, k_2, l_1, l_2 \\ k_1 \neq k_2 \neq l_1 \neq l_2}} \left| \left\langle \chi_{k_1}, \chi_{l_1} \right\rangle \right|^2 \left| \left\langle \chi_{k_2}, \chi_{l_2} \right\rangle \right|^2, \tag{8.288}$$

$$B = \sum_{\substack{k,l_1,l_2\\k\neq l_1\neq l_2}} |\langle \chi_k, \chi_{l_1} \rangle|^2 |\langle \chi_k, \chi_{l_2} \rangle|^2,$$
 (8.289)

$$C = \sum_{\substack{k,l\\k\neq l}} |\langle \chi_k, \chi_l \rangle|^4, \qquad (8.290)$$

$$D = \sum_{\substack{k,l\\k \neq l}} |\langle \chi_k, \chi_l \rangle|^2.$$
 (8.291)

For the three-point truncated correlation functions, we again consider the different terms

$$\mathbb{E}_{U}(I_{1}') = \frac{2}{m(m^{2}-1)(m^{2}-4)} \sum_{\substack{j,k,l=1\\i\neq k\neq l}}^{n} \langle \chi_{j}, \chi_{l} \rangle \langle \chi_{k}, \chi_{j} \rangle \langle \chi_{l}, \chi_{k} \rangle \tag{8.292}$$

$$\mathbb{E}_{U}(I_{2}') = \frac{2}{m(m^{2}-1)(m^{2}-4)} \sum_{\substack{j,k,l=1\\i\neq k\neq l}}^{n} \left\langle \chi_{j}, \chi_{k} \right\rangle \left\langle \chi_{k}, \chi_{l} \right\rangle \left\langle \chi_{l}, \chi_{j} \right\rangle \tag{8.293}$$

$$\mathbb{E}_{U}(K') = -\frac{1}{m(m^2 - 1)(m + 2)} \sum_{\substack{k, l = 1 \\ k \neq l}}^{n} |\langle \chi_k, \chi_l \rangle|^2$$
 (8.294)

$$\mathbb{E}_{U}(L) = \frac{n}{m(m+1)(m+2)},\tag{8.295}$$

from which we ultimately find that

$$\mathbb{E}_{U}(C_{qrs}^{pd}) = \frac{4}{m(m^{2} - 1)(m^{2} - 4)} \sum_{\substack{j,k,l = 1 \\ j \neq k \neq l}}^{n} \operatorname{Re}\left(\langle \chi_{j}, \chi_{l} \rangle \langle \chi_{k}, \chi_{j} \rangle \langle \chi_{l}, \chi_{k} \rangle\right) + \frac{6}{m(m^{2} - 1)(m + 2)} \sum_{\substack{k,l = 1 \\ k \neq l}}^{n} |\langle \chi_{k}, \chi_{l} \rangle|^{2} + \frac{2n}{m(m + 1)(m + 2)}.$$
(8.296)

The above expressions (8.285)–(8.287), (8.296) provide us with several quantities that may be used for the characterisation of partial distinguishability. Fist, the ubiquitous appearance of inner products $\langle \chi_j, \chi_k \rangle$, $j \neq k$, implies a strong dependence on the exact structure of the wave functions in \mathcal{H}_{add} . Here we focus on the train of Gaussian wave packets (8.283), with $\Delta\omega\Delta t$ as a single-particle quantifier of the degree of distinguishability (recall Fig. 8.19), and witness nice transitions from the indistinguishable bosonic behaviour to fully distinguishable in Figs. 8.21 (for varying number n of particles) and 8.22 (for varying number m of modes), which depict the RMT results (8.285)–(8.287), (8.296).

Let us first focus on Fig. 8.21, which explores the scaling behaviour of the normalised means NM of both C_{rs} and C_{qrs} , and the coefficient of variation CV of C_{rs} for increasing numbers n of particles, for a fixed number m=50 of modes. We see, interestingly, that the *visibility* of the distinguishability transition in the normalised means increases with the number n of particles. Specifically for (8.285) this can directly be connected to the number of interference terms that contribute. The contribution of the many-particle interference effects in (8.285) is given by (see also Appendix B) the term

$$-\frac{1}{m(m^2-1)}\sum_{\substack{k,l=1\\k\neq l}}^n |\langle \chi_k,\chi_l\rangle|^2,$$

such that the only influence of the particle number is contained in

$$\sum_{\substack{k,l=1\\k\neq l}}^{n} |\langle \chi_k, \chi_l \rangle|^2.$$

Ergo, each interference term contributes in the same way to the RMT average, via a term $1/m(m^2-1)$. The number of particles and their indistinguishability determines how many of such contribution need to be counted, information which is encrypted in $\langle \chi_k, \chi_l \rangle$.

Contrary to the change of visibility which we see in both NM plots in Fig. 8.21, the CV plot depicts a different behaviour. The visibility does not change significantly upon increasing the number n of particles, but we do see the total shift of CV to

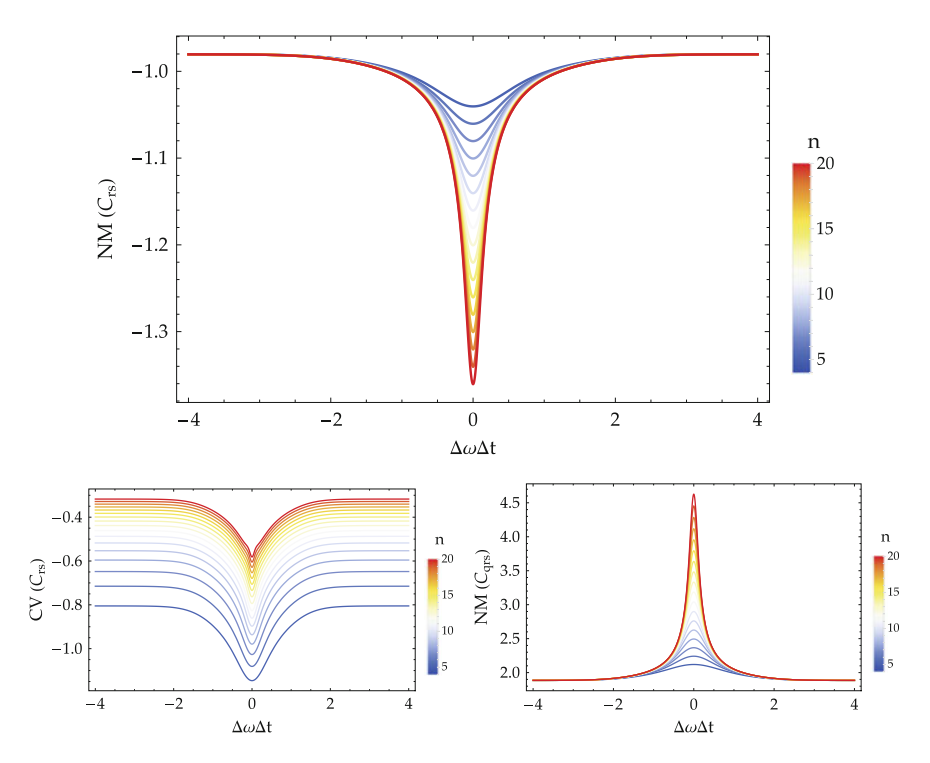


Fig. 8.21 RMT results for the normalised means (NM) of two-point $(C_{rs}; \text{top}; (8.220), (8.285)$ and three-point $(C_{qrs}; \text{bottom right}; (8.265), (8.296)$ truncated correlations functions, and the coefficient of variation of the two-point truncated correlation functions (CV; bottom left; (8.221), (8.287). RMT averages over random unitary scattering compounds of m = 50 modes are obtained for a sequence of bosons, described by Gaussian wave packets $\chi_j \in \mathcal{H}_{\text{add}}$ (8.283), as shown in Fig. 8.19, with $\Delta t \Delta \omega$ varied. The number of injected particles is varied $n = 4, 5, \ldots, 20$ (colour code). Visibility increases with n for both NM plots, whereas no such significant effect is seen in CV

larger values. Nevertheless, the complicated structure of (8.287) makes it hard to gain any specific intuition from this behaviour.

When we shift attention to Fig. 8.22, we observe the opposite effect when the number m of modes is increased for a fixed number n=6 of particles. The visibility of the transition, seen in the normalised means NM of both C_{rs} and C_{qrs} , decreases for an increase in the number of modes. Mathematically, this is directly seen from the structure of (8.285) and (8.296). This is a consequence of the random structure of the scattering compound, which implies that the typical probability amplitude decreases as the total number of accessible modes increases. Again, CV's behaviour is characterised by a shift in the curve (down to lower values of CV), rather than a change in visibility.

In Figs. 8.23, 8.24 and 8.25, we, again (recall Fig. 8.11) compare the analytical RMT predictions (8.285)–(8.287, 8.296) to data points obtained for single unitaries, here with randomly chosen values of $\Delta\omega\Delta t$ (which determine their position along the plots' x-axes).

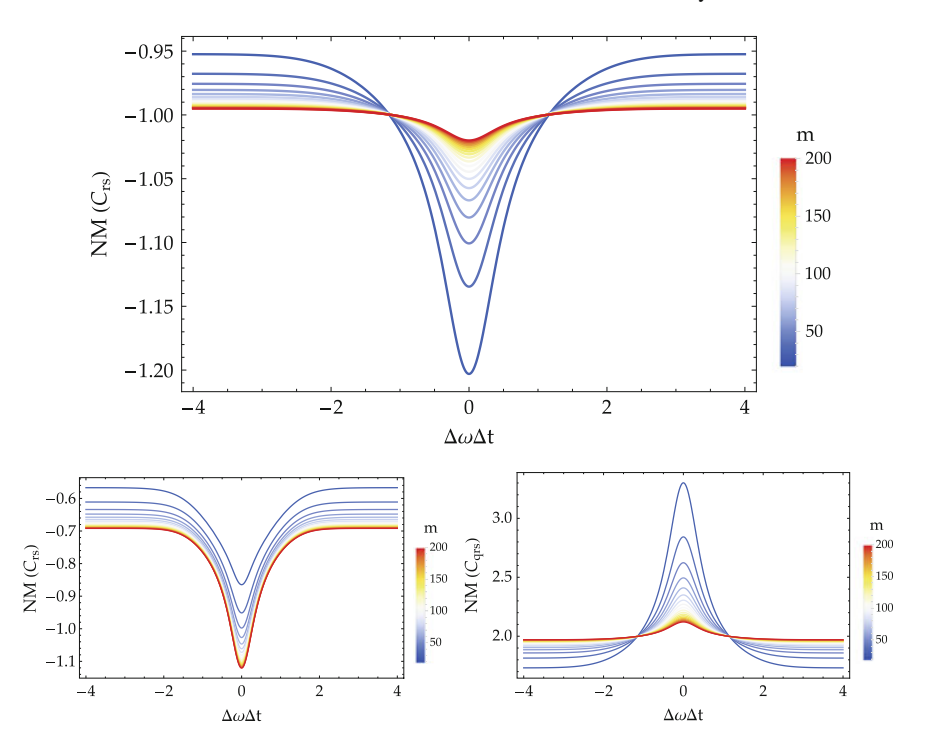


Fig. 8.22 RMT results for the normalised means (NM) of two-point $(C_{rs}; \text{top}; (8.220), (8.285)$ and three-point $(C_{qrs}; \text{bottom right}; (8.265), (8.296)$ truncated correlations functions, and the coefficient of variation of the two-point truncated correlation functions (CV; bottom left; (8.221); (8.287)). RMT averages over random unitary scattering compounds of $m = 20, 30, \ldots, 200$ modes (colour code) are obtained for a sequence of bosons, described by six Gaussian wave packets $\chi_j \in \mathcal{H}_{\text{add}}$ (8.283), as shown in Fig. 8.19, with $\Delta t \Delta \omega$ varied. Visibility decreases for growing m for both NM plots, whereas no such significant effect is seen in CV

From Fig. 8.24, we conclude that in the regime of small mode numbers (e.g. here m=20) there is a considerable spread on the possible outcomes for variable (random) U and thus different circuits. The first moments in Figs. 8.23 and 8.25 are far less sensitive to changes of U, which is in agreement with Fig. 8.11 where we observe a very small standard deviation for NM compared to the RMT predictions. In Fig. 8.24, the spread in CV gets smaller for the m=100 data, but $NM(C_{qrs})$ in Fig. 8.25 for m=100 does not exhibit a clear transition in the data. The lack of accuracy in this latter dataset arises because we consider only 200 randomly selected combinations of three output modes to compute the C-dataset for the three-point truncated correlation functions (8.282). However, since the two-point truncated correlation functions already offer sufficient information in Figs. 8.23 and 8.24, there is no problem with this lack of accuracy, at least with respect to this diagnostic purpose. To indicate that such kind of data can be used to certify the degree of bosonic behaviour, Fig. 8.26 displays a scatter plot, comparable to Figs. 8.12 and 8.13.

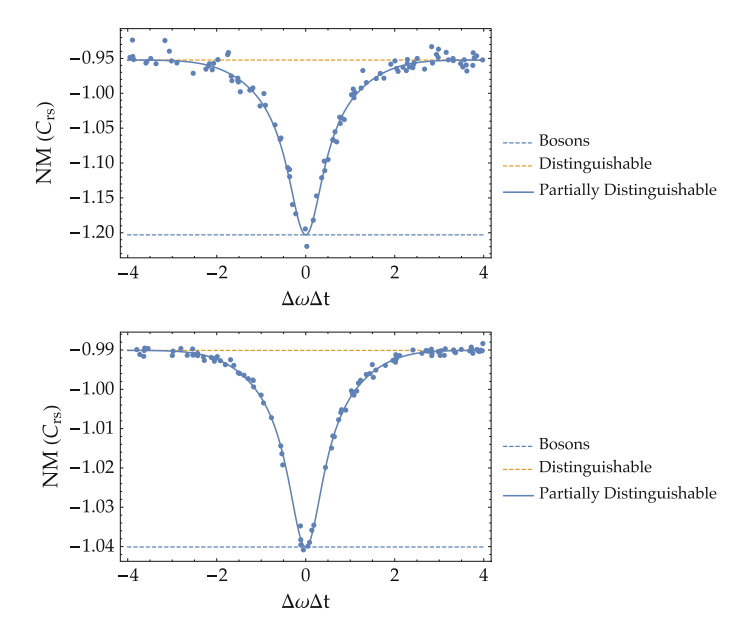


Fig. 8.23 RMT results (solid line) for the normalised mean (NM; (8.220)) of the two-point truncated correlation function C_{rs} (8.268). RMT averages (8.285) over random unitary scattering compounds with m=20 (top) and m=100 (bottom) modes are obtained for an injected sequence of bosons, described by six Gaussian wave packets $\chi_j \in \mathcal{H}_{add}$ (8.283), as shown in Fig. 8.19, with $\Delta t \Delta \omega$ varied. Data points (dots) correspond to the NM of a numerically generated C-dataset for a scattering compound U, randomly chosen from the Haar measure, for Gaussian wave packets with $\Delta \omega \Delta t$ randomly chosen from the uniform distribution on [-4, 4]. RMT predictions for bosonic interference (8.208) and for fully distinguishable particles (8.214) are indicated for reference

A sequence of particles with a random expected detection times is the second example which we consider. In this case, we still consider $\chi_j \in \mathcal{H}_{add}$ as Gaussian wave packets, given by (8.283). However, the times t_j around which these wave packets are centred are now assumed to be randomly distributed according to a *normal distribution* with mean zero and standard deviation δt . We again assume that all wave packets have the same bandwidth $\Delta \omega$, such that we arrive at a scenario as shown in Fig. 8.27, which depicts wave packets centred around randomly drawn times, for different values of δt .

This setup is intended to describe an experimental setting where one aims to inject all particles into the scattering compound at the same time t_0 , but is confronted with an error, which is normally distributed (at least in approximation) and characterised by δt . Because we are only interested in the overlaps $\langle \chi_j, \chi_k \rangle$ (8.284), $j \neq k$, between the wave functions, we directly see that the result should not depend on t_0 (which we therefore set equal to zero).

We study the influence of the error on the moments of the C-datasets as a quantifier for the bosonic many-particle interference. From the previous discussion about the well-controlled sequence of particles with fixed time delay, it is to be expected that small errors, ergo small δt (compared to the bandwidth $\Delta \omega$) keep the features of the

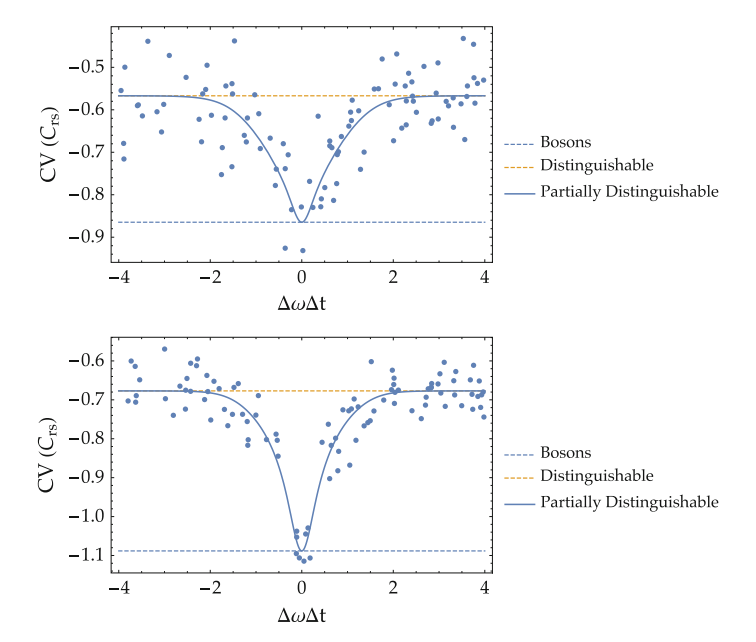


Fig. 8.24 RMT results (solid line) for the normalised mean (CV; 8.221) of the two-point truncated correlation function C_{rs} (8.268). RMT averages (8.287) over random unitary scattering compounds with m=20 (top) and m=100 (bottom) modes are obtained for an injected sequence of bosons, described by six Gaussian wave packets $\chi_j \in \mathcal{H}_{add}$ (8.283), as shown in Fig. 8.19, with $\Delta t \Delta \omega$ varied. Data points (dots) correspond to the CV of a numerically generated C-dataset for a scattering compound U, randomly chosen from the Haar measure, for Gaussian wave packets with $\Delta \omega \Delta t$ randomly chosen from the uniform distribution on [-4, 4]. RMT predictions for bosonic interference (8.209) and for fully distinguishable particles (8.215) are indicated for reference

interference pattern intact. Figure 8.27 suggests a high degree of indistinguishability in this case, which is consistent with this idea. To reach a quantitative description, we, again, resort to RMT. Because we learned in the previous discussion, where we considered fixed time delays, that the two-point truncated correlation functions C_{rs} contain sufficient information for certification, we will not consider the three-point correlation functions for this example.

To obtain the RMT prediction for this scenario, we can reuse the results (8.285) and (8.287) of the sequence with fixed time delays. The quantities $\langle \chi_j, \chi_k \rangle$ are, however, completely different in behaviour since they are also stochastic quantities. To gain a statistical understanding of the moments of the C-dataset, we must therefore also average over the normal distribution for the times t_j . For the first moment (8.285), we thus perform a direct integration to obtain

$$\mathbb{E}_{t}\left(\sum_{\substack{k,l=1\\k\neq l}}^{n}|\langle\chi_{k},\chi_{l}\rangle|^{2}\right) = \frac{n(n-1)}{\sqrt{1+2(\Delta\omega\delta t)^{2}}},\tag{8.297}$$

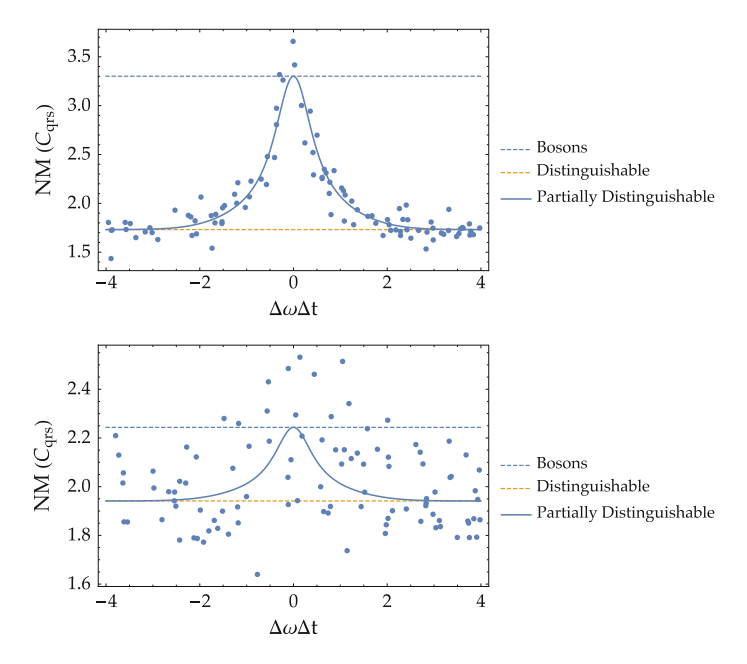


Fig. 8.25 RMT results (solid line) for the normalised mean (NM; 8.265) of the three-point truncated correlation function C_{qrs} (8.282). RMT averages (8.296) over random unitary scattering compounds with m = 20 (top) and m = 100 (bottom) modes are obtained for an injected sequence of bosons, described by six Gaussian wave packets $\chi_i \in \mathcal{H}_{add}$ (8.283), as shown in Fig. 8.19, with $\Delta t \Delta \omega$ varied. Data points (dots) correspond to the NM of a numerically generated C-dataset for 200 randomly selected sets of three output modes of a random scattering compound U, for Gaussian wave packets with $\Delta\omega\Delta t$ randomly chosen from the uniform distribution on [-4, 4]. RMT predictions for bosonic interference (8.261) and for fully distinguishable particles (8.263) are indicated for reference

such that

$$\mathbb{E}_{U,t}(C_{rs}^{pd}) = -\frac{n(n-1)}{m(m^2-1)} \frac{1}{\sqrt{1+2(\Delta\omega\delta t)^2}} - \frac{n}{m(m+1)}.$$
 (8.298)

For the second moment, we must average the different contributions (8.288)– (8.291), which can again be done by direct integration:

$$\mathbb{E}_t(A) = \frac{n(n-1)(n-2)(n-3)}{(1+2(\Delta\omega\delta t)^2)},\tag{8.299}$$

$$\mathbb{E}_{t}(A) = \frac{n(n-1)(n-2)(n-3)}{(1+2(\Delta\omega\delta t)^{2})},$$

$$\mathbb{E}_{t}(B) = \frac{n(n-1)(n-2)}{\sqrt{1+(\Delta\omega\delta t)^{2}}\sqrt{1+3(\Delta\omega\delta t)^{2}}},$$
(8.299)

$$\mathbb{E}_t(C) = \frac{n(n-1)}{\sqrt{1 + 4(\Delta\omega\delta t)^2}},\tag{8.301}$$

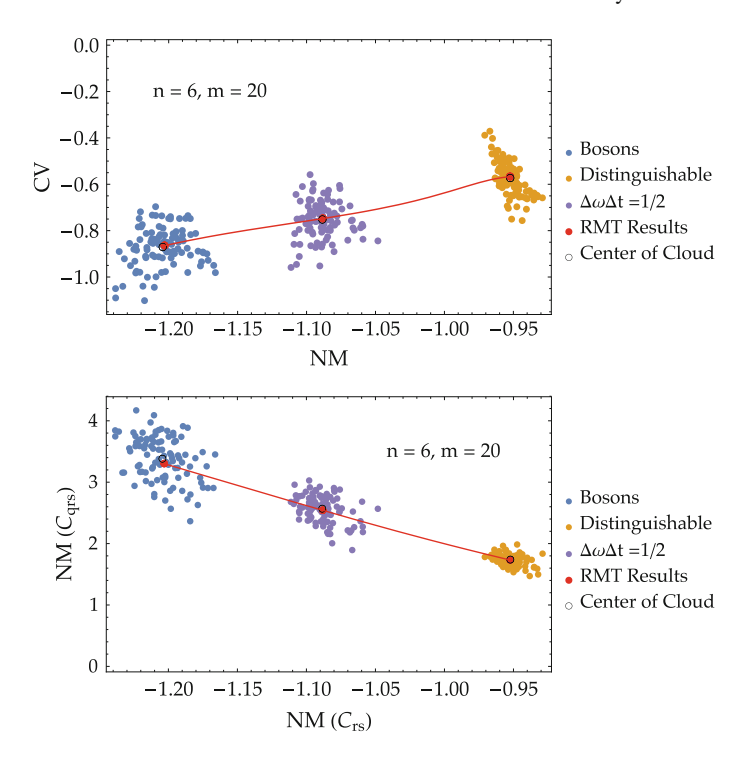


Fig. 8.26 Scatter plots indicating the normalised means (NM; (8.220), (8.265)) of two-point correlators C_{rs} ((8.193), (8.195), (8.268)) and three-point correlators C_{qrs} ((8.250), (8.252), (8.282)), and the coefficient of variation (CV; (8.221)) of C_{rs} . Six partially distinguishable particles with wave packets $\chi_j \in \mathcal{H}_{add}$ (8.283) for the additional degrees of freedom are injected in 100 random unitary scattering compounds U with twenty modes, with fixed time delay such that $\Delta\omega\Delta t = 1/2$ (see Fig. 8.19), $\Delta\omega\Delta t = 0$ (bosons) and $\Delta\omega\Delta t \to \infty$ (fully distinguishable). Associated C-datasets of C_{rs} and C_{qrs} are numerically generated for each choice of U to evaluate NM and CV. The numerically achieved NM and CV are averaged (black circle) and compared to the RMT predictions which make use of ((8.285), (8.287), (8.296); red dot). We continuously vary $\Delta t \Delta \omega$ to indicate (red line) the transition from the RMT prediction for bosons to that for distinguishable particles

$$\mathbb{E}_t(D) = \frac{n(n-1)}{\sqrt{1 + 2(\Delta\omega\delta t)^2}}.$$
(8.302)

We now find that

$$\mathbb{E}_{U,t}(C_{rs}^{pd^2}) = \frac{2\mathbb{E}_t(A) - 2\mathbb{E}_t(B)(m-5) + 2\mathbb{E}_t(D)(2+6m-n+mn) + \mathbb{E}_t(C)(10+m+m^2)}{(m-1)m^2(m+1)(m+2)(m+3)} + \frac{(m-2)(1+3m)n + 2n^2 + mn^2 + m^2n^2)}{(m-1)m^2(m+1)(m+2)(m+3)}.$$
(8.303)

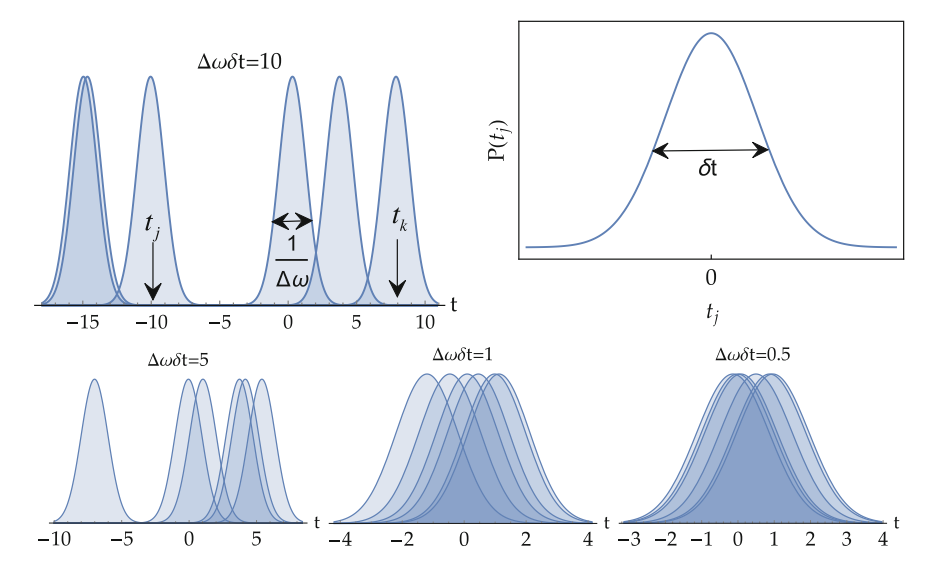


Fig. 8.27 Gaussian probability distributions for the detection of bosons, described by single-particle wave functions $\chi_j(t) \in \mathcal{H}_{add}$ (8.283), at specific times. The wave packets are characterised by a bandwidth $\Delta\omega$ and mean detection time t_j . The mean detection times are randomly chosen from a normal distribution (top right) of zero mean and standard deviation δt . The degree of indistinguishability is characterised by the overlap of the probability distributions (8.284), which is fully determined by dimensionless parameter $\Delta\omega\delta t$, which is varied $\Delta\omega\delta t=10,5,1,0.5$ from essentially distinguishable to essentially indistinguishable, respectively

As important result, we obtain that the RMT predictions ((8.298), (8.303)) for the moments only depend on three parameters: the numbers n and m of particles and modes, respectively, and the quantity $\Delta\omega\delta t$, which characterises the degree of distinguishability (in agreement with the intuition of Fig. 8.27).

In Figs. 8.28 and 8.29 we investigate the dependence of the rescaled moments NM (8.220) and CV (8.221) on variable particle and mode numbers, respectively, according to the specific RMT results (8.298) and (8.303). We observe a phenomenology which is very similar to Figs. 8.21 and 8.22, which show the same quantities for sequences of wave packets with a fixed time delay. Again we see that the distinguishability transition is clearly visible upon changing the parameter which characterises the degree distinguishability, here $\Delta\omega\delta t$. Both in Fig. 8.28 and in Fig. 8.21, we see an increase in visibility of the transition in NM when increasing the number of particles (for a fixed number of modes). For CV the curves in both figures experience a clear shift to higher values due to an increase in particle numbers. A comparison of Figs. 8.29 and 8.22 shows in both cases that the visibility of the distinguishability transition in NM decreases for increasing mode numbers, whereas we again see the characteristic shift in the CV curve.

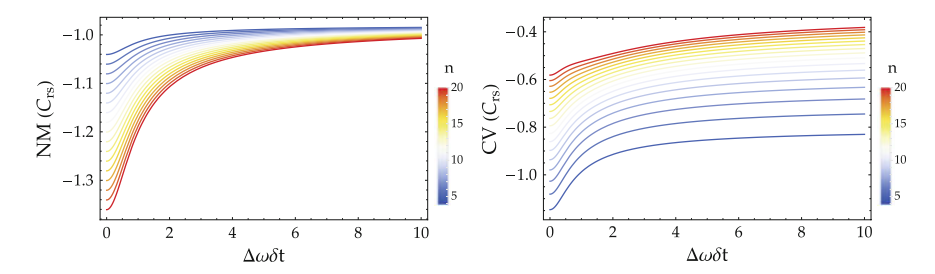


Fig. 8.28 RMT results for the normalised means (NM; top; (8.220)) and the coefficient of variation (CV; bottom; (8.221)) of two-point truncated correlations functions (C_{rs} ; (8.268)). RMT averages ((8.298), (8.303)) over random unitary scattering compounds with m = 50 modes are obtained for a sequence of bosons, described by Gaussian wave packets $\chi_j \in \mathcal{H}_{add}$ (8.283), as shown in Fig. 8.27. The mean detection times are randomly chosen from a normal distribution of zero mean and standard deviation δt , and the parameter $\Delta \omega \delta t$ is varied. The number of injected particles is also varied, $n = 4, 5, \ldots, 20$ (colour code)

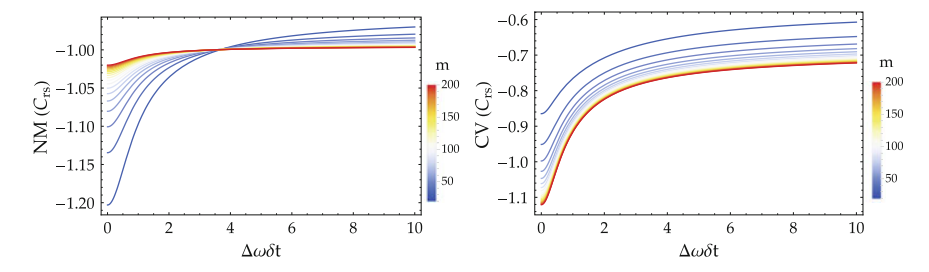


Fig. 8.29 RMT results for the normalised means (NM; top; (8.220)) and the coefficient of variation (CV; bottom; (8.221)) of two-point truncated correlations functions (C_{rs} ; (8.268)). RMT averages ((8.298), (8.303)) over random unitary scattering compounds with $m=20,30,\ldots,200$ modes (colour code) are obtained for a sequence of bosons, described by six Gaussian wave packets $\chi_j \in \mathcal{H}_{add}$ (8.283), as shown in Fig. 8.27. The mean detection times are randomly chosen from a normal distribution of zero mean and standard deviation δt , and the parameter $\Delta \omega \delta t$ is varied

Figure 8.30 indicates that the RMT results (8.298) and (8.303) agree with the numerical trend upon the choice of a random scattering matrix U and a random set of times $\{t_j\}$. However, when we compare Fig. 8.30 to the earlier results in Figs. 8.23, 8.24 and 8.25, we observe larger scatter around the RMT prediction. We can clearly conclude that this is a consequence of the fluctuations in arrival times. Be mindful, the numerical C-dataset is computed for a fixed unitary and a fixed set of chosen $\{t_j\}$, which implies a *structural error* in the arrival times: To experimentally determine a C-dataset, many measurements are required to accumulate statistics. Evaluating the C-dataset for *one* set of chosen $\{t_j\}$ implies that the particles arrive with the same time delays in each measurement.

Alternatively, when the particles arrive at different random times for each measurement, the C-dataset for fixed unitaries already contains an average over the arrival times, which decreases the scatter, as shown in Fig. 8.31. In this case, the time average must be contained in each element C_{rs} of the C-dataset, thus we must consider

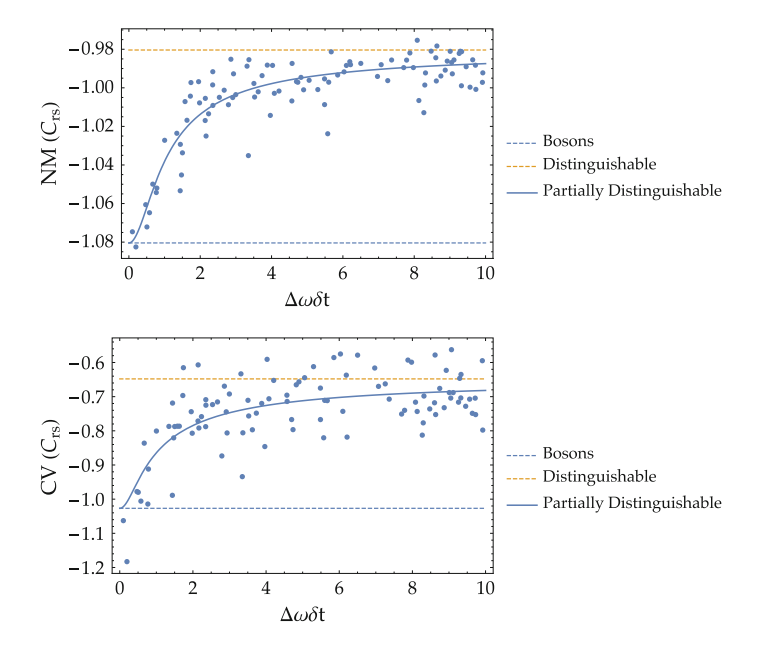


Fig. 8.30 RMT results (solid line) for the normalised mean (NM; top; (8.220)) and coefficient of variation (CV; bottom; (8.221)) of the two-point truncated correlation function C_{rs}^{pd} (8.268). RMT averages ((8.298), (8.303)) over random unitary scattering compounds of fifty modes are obtained for an injected sequence of bosons, described by six Gaussian wave packets $\chi_j \in \mathcal{H}_{add}$ (8.283), as shown in Fig. 8.27. We average over the normal distribution of zero mean and standard deviation δt , which describes the distribution of t_j , and vary the parameter $\Delta\omega\delta t$. Data points (dots) correspond to the NM of a numerically generated C-dataset for a scattering compound U, randomly chosen from the Haar measure, for Gaussian wave packets with six normally distributed mean detection times t_j , with zero mean and standard deviation δt . For each data point the value $\Delta\omega\delta t$ is randomly selected from the interval [0, 10]. RMT predictions for bosonic interference (8.208) and for fully distinguishable particles (8.214) are indicated for reference (dashed lines)

$$\mathbb{E}_{t}\left(C_{rs}^{pd}\right) = \sum_{\substack{k,l=1\\k\neq l}}^{n} \mathbb{E}_{t}\left(\left|\left\langle\chi_{k},\chi_{l}\right\rangle\right|^{2}\right) U_{ri_{k}} U_{si_{l}} \overline{U}_{ri_{l}} \overline{U}_{si_{k}} - \sum_{k=1}^{n} U_{ri_{k}} U_{si_{k}} \overline{U}_{ri_{k}} \overline{U}_{si_{k}} \\
= \frac{1}{\sqrt{1 + 2(\Delta\omega\delta t)^{2}}} \sum_{\substack{k,l=1\\k\neq l}}^{n} U_{ri_{k}} U_{si_{l}} \overline{U}_{ri_{l}} \overline{U}_{si_{k}} - \sum_{k=1}^{n} U_{ri_{k}} U_{si_{k}} \overline{U}_{ri_{k}} \overline{U}_{si_{k}}.$$

(8.304)

This leaves the RMT prediction (8.298) for the first moment of the C-dataset unchanged, but changes the second moment because $\mathbb{E}_U \mathbb{E}_t (C_{rs}^2) \neq \mathbb{E}_U (\mathbb{E}_t (C_{rs})^2)$. A straightforward computation leads to

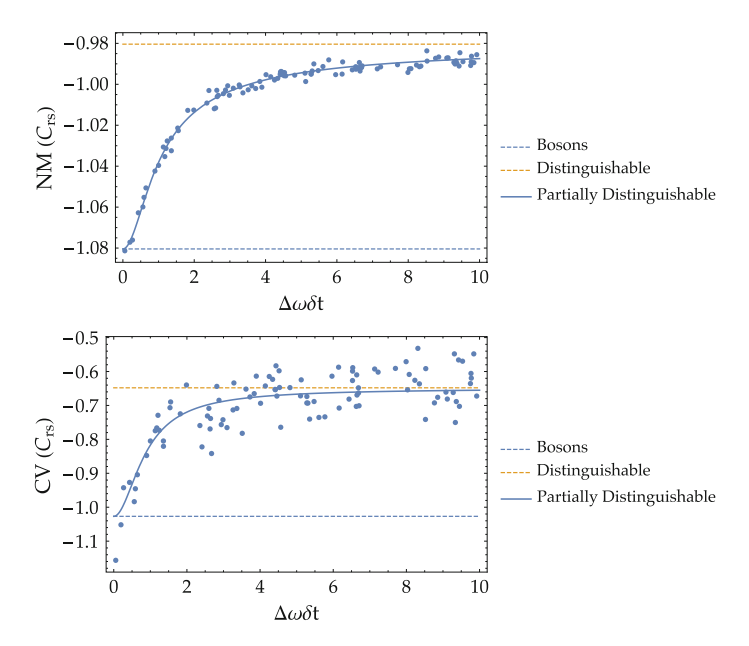


Fig. 8.31 RMT results (solid line) for the normalised mean (NM); top; (8.220)) and coefficient of variation (CV); bottom; (8.221)) of the time averaged two-point truncated correlation function $\mathbb{E}_t(C_{rs}^{pd})$ (8.304). RMT averages ((8.298), (8.305)) over random unitary scattering compounds of fifty modes are obtained for an injected sequence of bosons, described by six Gaussian wave packets $\chi_j \in \mathcal{H}_{add}$ (8.283) which arrive at random times in each measurement. The parameter $\Delta\omega\delta t$ describes the statistics of the overlaps of the wave functions $\langle \chi_j, \chi_k \rangle$ (8.284) and is varied. Data points (dots) correspond to the NM of a numerically generated time averaged C-dataset for a scattering compound U, randomly chosen from the Haar measure. Time averages are numerically generated by averaging of C_{rs}^{pd} (8.268) for 100 sets of six mean detection times which are randomly chosen from the normal distribution with zero mean and standard deviation δt . For each data point the value $\Delta\omega\delta t$ is randomly selected from the interval [0, 10]. RMT predictions for bosonic interference (8.208) and for fully distinguishable particles (8.214) are indicated for reference (dashed lines)

$$\mathbb{E}_{U}(\mathbb{E}_{t}(C_{rs})^{2}) = \frac{2A' - 2B'(m-5) + 2D'(2 + 6m - n + mn) + C'(10 + m + m^{2})}{(m-1)m^{2}(m+1)(m+2)(m+3)} + \frac{(m-2)(1+3m)n + 2n^{2} + mn^{2} + m^{2}n^{2})}{(m-1)m^{2}(m+1)(m+2)(m+3)},$$
(8.305)

with

$$A' = \frac{n(n-1)(n-2)(n-3)}{(1+2(\Delta\omega\delta t)^2)},$$
(8.306)

$$B' = \frac{n(n-1)(n-2)}{(1+2(\Delta\omega\delta t)^2)},$$
(8.307)

$$C' = \frac{n(n-1)}{(1+2(\Delta\omega\delta t)^2)},$$
(8.308)

$$D' = \frac{n(n-1)}{\sqrt{1 + 2(\Delta\omega\delta t)^2}}. (8.309)$$

Let us additionally emphasise that the RMT predictions shown in Figs. 8.21, 8.22, 8.28 and 8.29 all describe *monotonous* distinguishability transitions in the moments of the C-dataset. The similarities in phenomenology for the sequence of wave packets with fixed time delays and the sequence of wave packets arriving at randomly distributed times leads to the conjecture that there may be a more general measure (regardless of the specific details of $\{\chi_j\}$) for the distinguishability of a series of particles, which monotonously describes the distinguishability transition in the moments of the C-dataset.

In addition, the accuracy with which the random matrix predictions describe random scattering media in Figs. 8.23, 8.24, 8.25, 8.30, and 8.31, combined with the monotonicity of the distinguishability transition, present our method as a useful benchmark: the moments of the C-dataset serve as a many-particle and multimode generalisation of the Hong-Ou-Mandel effect as a benchmark for the distinguishability of two particles. Therefore, the techniques we develop here are the first steps towards what one may denote as *multimode correlation spectroscopy*.

8.6 Summary and Outlook

In this chapter, we introduced and discussed essential tools required for the study of many-particle interference. Due to the intricate combination of many probability amplitudes in the transmission signal, *deterministic* information on the fine-structure of the interference patterns is intractable. However, we followed the philosophy of the theory of complex systems (recall Chap. 3) and derived coarse-grained *statistical* signatures of many-particle interferences.

First, we introduced many-particle interference in a wave function approach, associated with the Schrödinger picture. After a review of known results, here translated to the framework which we introduced in Chap. 7, we shifted gears to a measurement-based approach. The main idea here was to treat the problem based on the detectors that are placed on the output modes of the interferometer, and to consider the problem in a Heisenberg picture. After explaining that both approaches produce equivalent results, we implemented the measurement-based framework to consider many-body correlation functions.

Not only did we considerably extend the known properties of correlation functions of multiple output modes to non-orthogonal modes and partially distinguishable particles, we also applied these correlation functions to boson sampling. The most fundamental results in this chapter showed that two-point and three-point truncated correlation functions of the particle numbers in different output modes provide a sufficient amount of information to identify *unambiguous and robust statistical signatures* of particle-type specific many-particle interference structures. This has direct

applications for the certification of boson sampling (Giordani et al. 2018; Walschaers et al. 2016b). We also showed that one can clearly exploit these truncated correlation data to detect partial distinguishability. Exploring different sources of distinguishability, we employed the dataset of truncated correlation functions to emphasise the potential of a novel type of *multimode correlation spectroscopy* (Walschaers et al. 2016a).

One paradigmatic example of many-particle interference effects is set by boson sampling, as extensively discussed throughout the chapter. The results presented in this chapter have also led to several new and interesting questions around the subject.

We showed that the truncated two- and three-point correlation functions of the output modes beautifully show a transition from distinguishable to indistinguishable particles. However, we only considered a specific choice of the wave functions in the single-particle Hilbert space of additional degrees of freedom. We have presented several arguments, e.g. the counting argument based on the structure of (8.285), in favour of the existence of a more general measure of distinguishability which describes the distinguishability transition inscribed in the moments of the C-dataset. We believe that a considerable amount of mathematical tools required to achieve this goal are already at hand (see those presented through this chapter and earlier work (Walschaers 2011) on counting quantum states), and progress is already being made (Tichy 2015; Tillmann et al. 2015).

More practical problems in the light of certification of boson sampling are effects related to losses, although these may be solved by adding additional output channels on which no measurements can be performed (Mayer 2012). Because we quantified the dependence of the C-dataset's moments on the total number of modes, our certification schemes may ultimately be used to identify the number of loss processes. Nevertheless, a more structured study of such scenarios is required.

There are several potential generalisations and adaptations that fall outside the scope of our current work: To begin with we focussed our attention on Gaussian channels (i.e. the single-particle unitary channel (8.15)), which are formally defined as channels which map Gaussian states⁴³ into other Gaussian states. Physically this property implies that no additional correlations between the particles are created upon transmission through the channel. Furthermore, we restricted our discussion to pure number states which already lead to highly non-trivial many-particle interference phenomena. Hence, it is legitimate to wonder what happens when either of these ingredients is changed.

An interesting field of study is that of more intricate non-Gaussian states. A profound problem is that currently no theoretical or experimental tools are known to characterise the full class of non-Gaussian states. Nevertheless, there are experimental tools which can be used to consider well-known Gaussian states and slightly manipulate them, for example by adding or subtracting particles (Averchenko et al. 2016; Ra et al. 2017; Walschaers et al. 2017b). This yields a setup similar to the one considered here, since we can use the GNS construction to substitute the vac-

⁴³The most general definitions of *Gaussian states* are given in Sect. 7.7. However, a simpler introduction for states on the bosonic Fock space can be found in Sect. 7.6.4.

uum state for a more complicated vector on which we create quasi-particles. Efforts have been made in this direction (although they do not consider sophisticated algebraic constructions as we just suggested here) (Lund et al. 2014; Olson et al. 2015; Seshadreesan et al. 2015), but they strongly focus on the impact on computational complexity. A thorough account on the physical properties of many-particle interference patterns induced by such states is still missing. In this context, it is also of interest to consider homodyne detection (Grynberg et al. 2010; Roslund et al. 2014) as a complement to photon counting in the setup, which recently led to several new developments (Chabaud et al. 2017; Chakhmakhchyan and Cerf 2017).

This leads us to consider more minimalistic approaches and wonder when such dynamical sampling problems become tractable in computer simulations. A partial answer (Rahimi-Keshari et al. 2016) to this question was given, based on properties of the phase space representations (see Sect. 7.6.4) of, both, the input state that is sent through the interferometer and the measurement on which we ultimately project. This result suggests that one non-Gaussian research may already be sufficient to render a sampling problem hard to simulate. This suspicion is confirmed by setups where non-Gaussian photon-detectors are replaced by Gaussian homodyne detection (Chabaud et al. 2017; Chakhmakhchyan and Cerf 2017), and by setups (Hamilton et al. 2017) where one uses non-Gaussian detectors to sample from a multimode Gaussian states. The latter is remarkable, given that we argued in Sect. 8.3.2 that Glauber coherent states do not give rise to many-particle interference. Indeed, the Gaussian boson sampling setup (Hamilton et al. 2017) requires a certain amount of squeezing (see Sect. 7.6.3) to be computationally hard. However, the underlying physical mechanisms of these setups are still ambiguous. In particular, it is not clear whether we can interpret these results in the context of many-particle interference. A potential route to answer this question is by exploring versions of the setup where the channel is highly symmetric, such that interference effects become more pronounced (Dittel et al. 2018a).

An alternative extension of these many-particle interference setups is to consider different types of channels. Since all Bogoluibov transformations (i.e. multimode squeezing, recall expressions (7.180), (7.181) in Sect. 7.6.3 and the generalisations in Sect. 7.7) lead to Gaussian channels, the most challenging generalisation is to go beyond this realm and investigate the impact on many-particle interference patterns. One way to generate a non-Gaussian transmission channel is to consider systems where the particles can interact with each other or, in an all optical setting, where there are nonlinearities (Dufour et al. 2017). This leads us to an important open question of many-particle physics: How to disentangling the dynamical contribution of interference, induced by indistinguishability, from the dynamical contribution of interactions within the transmission signal? However, this question is also notoriously difficult to address: It is commonplace to approach systems of interacting particles via perturbative or hierarchical techniques (Negele and Orland 1998), which quickly increase the complexity of the problem. Recent developments (Gessner 2015) based on coarse-grained descriptions may provide a fruitful alternative for studying statistical signatures of many-particle dynamics.

A more tractable route runs via the introduction of intricate forms of decoherence and dephasing. In Sect. 9.6 of the next chapter we will introduce a class of dephasing channels, which are shown to be non-Gaussian, but can can be handled. These dephasing channels may lead to interesting many-particle interference phenomena, on transient time scales.

In this chapter we extensively focussed on understanding interference phenomena in many-particle systems with a *fixed number* of particles. In the following chapter we investigate what happens when we allow systems to exchange non-interacting fermions or bosons with particle reservoirs. We will introduce the concept of particle currents which flow through the system and subsequently study their behaviour in the non-equilibrium steady state. Once again, we will uncover that these currents manifest profoundly different phenomenology, depending on whether the particles are fermions or bosons.

References

- S. Aaronson, A. Arkhipov, The computational complexity of linear optics. Theory Comput. 9, 143–252 (2013). http://dx.doi.org/10.4086/toc.2013.v009a004
- S. Aaronson, A. Arkhipov, Boson sampling is far from uniform. Quantum Info. Comput. 14, 1383–1423 (2014)
- A. Ahlbrecht, A. Alberti, D. Meschede, V.B. Scholz, A.H. Werner, R.F. Werner, Molecular binding in interacting quantum walks. New J. Phys. 14, 073050 (2012)
- G. Akemann, J. Baik, P.D. Francesco (eds.), *The Oxford Handbook of Random Matrix Theory* (Oxford Handbooks in Mathematics, 2011)
- R. Alicki, M. Fannes, Quantum Dynamical Systems (Oxford University Press, Oxford, 2001)
- M.H. Anderson, J.R. Ensher, M.R. Matthews, C.E. Wieman, E.A. Cornell, Observation of Bose-Einstein condensation in a dilute atomic vapor. Science **269**, 198–201 (1995)
- M.R. Andrews, C.G. Townsend, H.-J. Miesner, D.S. Durfee, D.M. Kurn, W. Ketterle, Observation of interference between two bose condensates. Science 275, 637–641 (1997)
- L. Aolita, C. Gogolin, M. Kliesch, J. Eisert, Reliable quantum certification of photonic state preparations. Nat. Commun. 6, 8498 (2015)
- A. Aspect, P. Grangier, G. Roger, Experimental realization of Einstein-Podolsky-Rosen-Bohm Gedanken experiment: a new violation of Bell's Inequalities. Phys. Rev. Lett. 49, 91–94 (1982)
- S. Ates, S.M. Ulrich, S. Reitzenstein, A. Löffler, A. Forchel, P. Michler, Post-selected indistinguishable photons from the resonance fluorescence of a single quantum dot in a microcavity. Phys. Rev. Lett. 103, 167402 (2009)
- V. Averchenko, C. Jacquard, V. Thiel, C. Fabre, N. Treps, Multimode theory of single-photon subtraction. New J. Phys. 18, 083042 (2016)
- R. Barends, J. Kelly, A. Megrant, D. Sank, E. Jeffrey, Y. Chen, Y. Yin, B. Chiaro, J. Mutus, C. Neill, P. O'Malley, P. Roushan, J. Wenner, T.C. White, A.N. Cleland, J.M. Martinis, Coherent Josephson qubit suitable for scalable quantum integrated circuits. Phys. Rev. Lett. 111, 080502 (2013)
- L. Benet, H.A. Weidenmüller, Review of the k-body embedded ensembles of Gaussian random matrices. J. Phys. A: Math. Gen. **36**, 3569 (2003)
- L. Benet, T. Rupp, H.A. Weidenmüller, Spectral properties of the k-body embedded Gaussian ensembles of random matrices. Ann. Phys. 292, 67–94 (2001)

M. Bentivegna, N. Spagnolo, C. Vitelli, F. Flamini, N. Viggianiello, L. Latmiral, P. Mataloni, D.J. Brod, E.F. Galvao, A. Crespi, R. Ramponi, R. Osellame, F. Sciarrino, Experimental scattershot boson sampling. Sci. Adv. 1, e1400255–e1400255 (2015)

- G. Berkolaiko, J. Kuipers, Moments of the Wigner delay times. J. Phys. A: Math. Theor. 43, 035101 (2010)
- G. Berkolaiko, J. Kuipers, Transport moments beyond the leading order. New J. Phys. 13, 063020 (2011)
- H.A. Bethe, R.F. Bacher, Nuclear physics A. Stationary states of nuclei. Rev. Mod. Phys. 8, 82–229 (1936)
- N. Biggs, *Discrete Mathematics*, Rev. edn. Oxford Science Publications (Clarendon Press; Oxford University Press, Oxford [England]: New York, 1989)
- W.D. Blizard, Multiset theory. Notre Dame J. Formal Logic 30, 36–66 (1988)
- I. Bloch, J. Dalibard, W. Zwerger, Many-body physics with ultracold gases. Rev. Mod. Phys. 80, 885 (2008)
- M. Born, E. Wolf, *Principles of Optics: Electromagnetic Theory of Propagation, Interference and Diffraction of Light*, 7th edn. (Cambridge University Press, Cambridge, New York, 1999)
- O. Bratteli, D.W. Robinson, Operator Algebras and Quantum Statistical Mechanics Equilibrium States (Models in Quantum Statistical Mechanics) (Springer, Berlin, 1997)
- M.J. Bremner, R. Jozsa, D.J. Shepherd, Classical simulation of commuting quantum computations implies collapse of the polynomial hierarchy. Proc. R. Soc. A (2010). arXiv:10.1098/rspa.2010.0301
- M.A. Broome, A. Fedrizzi, S. Rahimi-Keshari, J. Dove, S. Aaronson, T.C. Ralph, A.G. White, Photonic boson sampling in a tunable circuit. Science 339, 794–798 (2013)
- P.W. Brouwer, C.W.J. Beenakker, Diagrammatic method of integration over the unitary group, with applications to quantum transport in mesoscopic systems. J. Math. Phys. 37, 4904–4934 (1996)
- A. Buchleitner, A.R. Kolovsky, Interaction-induced decoherence of atomic bloch oscillations. Phys. Rev. Lett. 91, 253002 (2003)
- P. Bunyk, E. Hoskinson, M. Johnson, E. Tolkacheva, F. Altomare, A. Berkley, R. Harris, J. Hilton, T. Lanting, A. Przybysz, J. Whittaker, Architectural considerations in the design of a superconducting quantum annealing processor. IEEE Trans. Appl. Supercond. 24, 1–10 (2014)
- K. Burke, J. Werschnik, E.K.U. Gross, Time-dependent density functional theory: past, present, and future. J. Chem. Phys 123, 062206 (2005)
- R.A. Campos, B.E.A. Saleh, M.C. Teich, Quantum-mechanical lossless beam splitter: SU(2) symmetry and photon statistics. Phys. Rev. A 40, 1371–1384 (1989)
- J. Carolan, J.D.A. Meinecke, P.J. Shadbolt, N.J. Russell, N. Ismail, K. Wörhoff, T. Rudolph, M.G. Thompson, J.L. O'Brien, J.C.F. Matthews, A. Laing, On the experimental verification of quantum complexity in linear optics. Nat. Photon 8, 621–626 (2014)
- G. Cennini, C. Geckeler, G. Ritt, M. Weitz, Interference of a variable number of coherent atomic sources. Phys. Rev. A 72, 051601 (2005)
- U. Chabaud, T. Douce, D. Markham, P. van Loock, E. Kashefi, G. Ferrini, Continuous-variable sampling from photon-added or photon-subtracted squeezed states. Phys. Rev. A 96, 062307 (2017)
- L. Chakhmakhchyan, N.J. Cerf, Boson sampling with Gaussian measurements. Phys. Rev. A 96, 032326 (2017)
- S. Chu, Cold atoms and quantum control. Nature **416**, 206–210 (2002)
- P. Clifford, R. Clifford, The classical complexity of boson sampling, in *Proceedings of the Twenty-Ninth Annual ACM-SIAM Symposium on Discrete Algorithms*, SODA '18 (Society for Industrial and Applied Mathematics, Philadelphia, PA, USA, 2018), pp. 146–155
- B. Collins, P. Śniady, Integration with respect to the haar measure on unitary, orthogonal and symplectic group. Commun. Math. Phys. **264**, 773–795 (2006)
- J.B. Conway, *A Course in Functional Analysis*. Graduate Texts in Mathematics, vol. 96, 2nd edn. (Springer, New York, 1997)

- S. Cova, M. Ghioni, A. Lacaita, C. Samori, F. Zappa, Avalanche photodiodes and quenching circuits for single-photon detection. Appl. Opt. **35**, 1956 (1996)
- A. Crespi, R. Osellame, R. Ramponi, M. Bentivegna, F. Flamini, N. Spagnolo, N. Viggianiello, L. Innocenti, P. Mataloni, F. Sciarrino, Suppression law of quantum states in a 3d photonic fast fourier transform chip. Nat. Commun. 7, 10469 EP (2016)
- A. Crespi, Suppression laws for multiparticle interference in sylvester interferometers. Phys. Rev. A 91, 013811 (2015)
- A. Crespi, R. Osellame, R. Ramponi, D.J. Brod, E.F. Galvão, N. Spagnolo, C. Vitelli, E. Maiorino, P. Mataloni, F. Sciarrino, Integrated multimode interferometers with arbitrary designs for photonic boson sampling. Nat. Photon 7, 545–549 (2013)
- E.B. Davies, Irreversible dynamics of infinite fermion systems. Commun. Math. Phys. **55**, 231–258 (1977a)
- K.B. Davis, M.O. Mewes, M.R. Andrews, N.J. van Druten, D.S. Durfee, D.M. Kurn, W. Ketterle, Bose-Einstein condensation in a gas of sodium atoms. Phys. Rev. Lett. **75**, 3969–3973 (1995)
- L. Deslauriers, S. Olmschenk, D. Stick, W.K. Hensinger, J. Sterk, C. Monroe, Scaling and suppression of anomalous heating in ion traps. Phys. Rev. Lett. 97, 103007 (2006)
- C. Dittel, G. Dufour, M. Walschaers, G. Weihs, A. Buchleitner, R. Keil, Totally destructive interference for permutation-symmetric many-particle states. Phys. Rev. A 97, 062116 (2018a)
- C. Dittel, G. Dufour, M. Walschaers, G. Weihs, A. Buchleitner, R. Keil, Totally destructive many-particle interference. Phys. Rev. Lett. 120, 240404 (2018b)
- C. Dittel, R. Keil, G. Weihs, Many-body quantum interference on hypercubes. Quantum Sci. Technol. 2, 015003 (2017)
- G. Dufour, T. Brünner, C. Dittel, G. Weihs, R. Keil, A. Buchleitner, Many-particle interference in a two-component bosonic Josephson junction: an all-optical simulation. New J. Phys. 19, 125015 (2017)
- M. Eibl, S. Gaertner, M. Bourennane, C. Kurtsiefer, M. Żukowski, H. Weinfurter, Experimental observation of four-photon entanglement from parametric down-conversion. Phys. Rev. Lett. 90, 200403 (2003)
- T. Engl, J. Dujardin, A. Argüelles, P. Schlagheck, K. Richter, J.D. Urbina, Coherent backscattering in fock space: a signature of quantum many-body interference in interacting bosonic systems. Phys. Rev. Lett. **112**, 140403 (2014)
- B. Everitt, *The Cambridge Dictionary of Statistics* (Cambridge University Press, Cambridge, 1998)
- M. Fannes, B. Nachtergaele, R.F. Werner, Finitely correlated states on quantum spin chains. Commun. Math. Phys. 144, 443–490 (1992)
- M. Fannes, B. Nachtergaele, R.F. Werner, Finitely correlated pure states. J. Funct. Anal. 120, 511–534 (1994)
- M. Genske, W. Alt, A. Steffen, A.H. Werner, R.F. Werner, D. Meschede, A. Alberti, Electric quantum walks with individual atoms. Phys. Rev. Lett. 110, 190601 (2013)
- M. Gessner, Dynamics and characterization of composite quantum systems. Ph.D. thesis, Albert-Ludwigs-Universität Freiburg, Freiburg, 2015
- M. Gessner, V.M. Bastidas, T. Brandes, A. Buchleitner, Semiclassical excited-state signatures of quantum phase transitions in spin chains with variable-range interactions. Phys. Rev. B 93, 155153 (2016)
- A. Giannopoulos, V. Milman, Concentration property on probability spaces. Adv. Math. 156, 77– 106 (2000)
- T. Giordani, F. Flamini, M. Pompili, N. Viggianiello, N. Spagnolo, A. Crespi, R. Osellame, N. Wiebe, M. Walschaers, A. Buchleitner, F. Sciarrino, Experimental statistical signature of many-body quantum interference. Nat. Photonics 12, 173–178 (2018)
- C. Gogolin, M. Kliesch, L. Aolita, J. Eisert, Boson-sampling in the light of sample complexity (2013). arXiv:1306.3995 [quant-ph]
- W.P. Grice, I.A. Walmsley, Spectral information and distinguishability in type-II down-conversion with a broadband pump. Phys. Rev. A 56, 1627–1634 (1997)

W.P. Grice, R. Erdmann, I.A. Walmsley, D. Branning, Spectral distinguishability in ultrafast parametric down-conversion. Phys. Rev. A 57, R2289–R2292 (1998)

- G. Grynberg, A. Aspect, C. Fabre, *Introduction to Quantum Optics: From the Semi-classical Approach to Quantized Light* (Cambridge University Press, Cambridge, 2010)
- Z. Hadzibabic, S. Stock, B. Battelier, V. Bretin, J. Dalibard, Interference of an array of independent Bose-Einstein condensates. Phys. Rev. Lett. 93, 180403 (2004)
- M. Hamermesh, Group Theory and its Application to Physical Problems, Dover Books on Physics and Chemistry (Dover Publications, New York, 1989)
- C.S. Hamilton, R. Kruse, L. Sansoni, C. Silberhorn, I. Jex, Driven quantum walks. Phys. Rev. Lett. 113, 083602 (2014)
- C.S. Hamilton, R. Kruse, L. Sansoni, S. Barkhofen, C. Silberhorn, I. Jex, Gaussian boson sampling. Phys. Rev. Lett. 119, 170501 (2017)
- D.M. Harber, J.M. McGuirk, J.M. Obrecht, E.A. Cornell, Thermally induced losses in ultra-cold atoms magnetically trapped near room-temperature surfaces. J. Low Temp. Phys. 133, 229–238 (2003)
- B. Hein, G. Tanner, Quantum search algorithms on a regular lattice. Phys. Rev. A 82, 012326 (2010)
- J. Helsen, Structure of coherent fermionic states. Master thesis, KU Leuven, Leuven, 2015
- C.K. Hong, Z.Y. Ou, L. Mandel, Measurement of subpicosecond time intervals between two photons by interference. Phys. Rev. Lett. 59, 2044–2046 (1987)
- Y.-F. Huang, B.-H. Liu, L. Peng, Y.-H. Li, L. Li, C.-F. Li, G.-C. Guo, Experimental generation of an eight-photon Greenberger-Horne-Zeilinger state. Nat. Commun. 2, 546 (2011)
- P.C. Humphreys, B.J. Metcalf, T. Gerrits, T. Hiemstra, A.E. Lita, J. Nunn, S.W. Nam, A. Datta, W.S. Kolthammer, I.A. Walmsley, Tomography of photon-number resolving continuous-output detectors. New J. Phys. 17, 103044 (2015)
- A. Huxley, Brave New World (Chatto & Windus, 1932)
- P. Igodt, W. Veys, *Lineaire Algebra* (Universitaire Pers, Leuven, 2011)
- L. Kaplan, T. Papenbrock, Wave function structure in two-body random matrix ensembles. Phys. Rev. Lett. 84, 4553–4556 (2000)
- J. Kelly, R. Barends, A.G. Fowler, A. Megrant, E. Jeffrey, T.C. White, D. Sank, J.Y. Mutus, B. Campbell, Y. Chen, Z. Chen, B. Chiaro, A. Dunsworth, I.-C. Hoi, C. Neill, P.J.J. O'Malley, C. Quintana, P. Roushan, A. Vainsencher, J. Wenner, A.N. Cleland, J.M. Martinis, State preservation by repetitive error detection in a superconducting quantum circuit. Nature 519, 66–69 (2015)
- E. Knill, R. Laflamme, G.J. Milburn, A scheme for efficient quantum computation with linear optics. Nature 409, 46–52 (2001)
- M. Köhl, H. Moritz, T. Stöferle, K. Günter, T. Esslinger, Fermionic atoms in a three dimensional optical lattice: observing fermi surfaces, dynamics, and interactions. Phys. Rev. Lett. 94, 080403 (2005)
- P. Kok, H. Lee, J.P. Dowling, Creation of large-photon-number path entanglement conditioned on photodetection. Phys. Rev. A **65**, 052104 (2002)
- A.R. Kolovsky, A. Buchleitner, Floquet-Bloch operator for the Bose-Hubbard model with static field. Phys. Rev. E 68, 056213 (2003)
- J. Kuipers, M. Sieber, Semiclassical relation between open trajectories and periodic orbits for the Wigner time delay. Phys. Rev. E 77, 046219 (2008)
- P.G. Kwiat, K. Mattle, H. Weinfurter, A. Zeilinger, A.V. Sergienko, Y. Shih, New high-intensity source of polarization-entangled photon Pairs. Phys. Rev. Lett. **75**, 4337–4341 (1995)
- S. Laibacher, V. Tamma, From the physics to the computational complexity of multiboson correlation interference. Phys. Rev. Lett. **115**, 243605 (2015)
- D.P. Landau, K. Binder, A Guide to Monte Carlo Simulations in Statistical Physics (Cambridge University Press, Cambridge, 2009)
- L. Latmiral, N. Spagnolo, F. Sciarrino, Towards quantum supremacy with lossy scattershot boson sampling. New J. Phys. 18, 113008 (2016)

- D. Leibfried, M.D. Barrett, T. Schaetz, J. Britton, J. Chiaverini, W.M. Itano, J.D. Jost, C. Langer, D.J. Wineland, Toward heisenberg-limited spectroscopy with multiparticle entangled states. Science 304, 1476–1478 (2004)
- J.C. Loredo, M.A. Broome, P. Hilaire, O. Gazzano, I. Sagnes, A. Lemaitre, M.P. Almeida, P. Senellart, A.G. White, Boson sampling with single-photon fock states from a bright solid-state source. Phys. Rev. Lett. 118, 130503 (2017)
- A.P. Lund, A. Laing, S. Rahimi-Keshari, T. Rudolph, J.L. O'Brien, T.C. Ralph, Boson sampling from a Gaussian state. Phys. Rev. Lett. 113, 100502 (2014)
- A.P. Lund, M.J. Bremner, T.C. Ralph, Quantum sampling problems, boson sampling and quantum supremacy. npj Quantum Inf. 3, 15 (2017)
- J. Madroñero, Spectral properties of planar helium under periodic driving. Ph.D. thesis, Ludwig-Maximilians-Universität München, München, 2004
- L. Mandel, Quantum theory of interference effects produced by independent light beams. Phys. Rev. 134, A10–A15 (1964)
- L. Mandel, Photon interference and correlation effects produced by independent quantum sources. Phys. Rev. A 28, 929–943 (1983)
- L. Mandel, E. Wolf, Optical Coherence and Quantum Optics (Cambridge University Press, Cambridge, 1995)
- K. Mayer, Many-particle quantum walks. Diploma thesis, Albert-Ludwigs Universität Freiburg, Freiburg, 2012
- K. Mayer, M.C. Tichy, F. Mintert, T. Konrad, A. Buchleitner, Counting statistics of many-particle quantum walks. Phys. Rev. A 83, 062307 (2011)
- A.J. Menssen, A.E. Jones, B.J. Metcalf, M.C. Tichy, S. Barz, W.S. Kolthammer, I.A. Walmsley, Distinguishability and many-particle interference. Phys. Rev. Lett. 118, 153603 (2017)
- B.J. Metcalf, N. Thomas-Peter, J.B. Spring, D. Kundys, M.A. Broome, P.C. Humphreys, X.-M. Jin, M. Barbieri, W. Steven Kolthammer, J.C. Gates, B.J. Smith, N.K. Langford, P.G.R. Smith, I.A. Walmsley, Multiphoton quantum interference in a multiport integrated photonic device. Nat. Commun. 4, 1356 (2013)
- C. Moore, S. Mertens, The Nature of Computation (Oxford University Press, Oxford [England]; New York, 2011)
- P.J. Mosley, J.S. Lundeen, B.J. Smith, P. Wasylczyk, A.B. U'Ren, C. Silberhorn, I.A. Walmsley, Heralded generation of ultrafast single photons in pure quantum states. Phys. Rev. Lett. 100, 133601 (2008)
- S. Mukamel, Principles of Nonlinear Optical Spectroscopy. Oxford Series in Optical and Imaging Sciences, vol. 6 (Oxford University Press, New York, 2009)
- M. Müller, K. Hammerer, Y.L. Zhou, C.F. Roos, P. Zoller, Simulating open quantum systems: from many-body interactions to stabilizer pumping. New J. Phys. 13, 085007 (2011)
- J.W. Negele, H. Orland, Quantum Many-particle Systems (Perseus Books, Reading, 1998)
- A. Neville, C. Sparrow, R. Clifford, E. Johnston, P.M. Birchall, A. Montanaro, A. Laing, Classical boson sampling algorithms with superior performance to near-term experiments. Nat. Phys. 13, 1153 EP (2017)
- M.A. Nielsen, I.L. Chuang, Quantum Computation and Quantum Information, 10th edn. (Cambridge University Press, Cambridge, 2010)
- J.P. Olson, K.P. Seshadreesan, K.R. Motes, P.P. Rohde, J.P. Dowling, Sampling arbitrary photon-added or photon-subtracted squeezed states is in the same complexity class as boson sampling. Phys. Rev. A 91, 022317 (2015)
- Z.Y. Ou, Quantum theory of fourth-order interference. Phys. Rev. A 37, 1607–1619 (1988)
- Z.Y. Ou, J.-K. Rhee, L.J. Wang, Photon bunching and multiphoton interference in parametric down-conversion. Phys. Rev. A 60, 593–604 (1999)
- H. Paul, Interference between independent photons. Rev. Mod. Phys. 58, 209–231 (1986)
- G.K. Pedersen, Analysis Now (Springer, New York, 1989)
- B. Peropadre, G.G. Guerreschi, J. Huh, A. Aspuru-Guzik, Proposal for microwave boson sampling. Phys. Rev. Lett. 117, 140505 (2016)

A. Peruzzo, M. Lobino, J.C.F. Matthews, N. Matsuda, A. Politi, K. Poulios, X.-Q. Zhou, Y. Lahini, N. Ismail, K. Wörhoff, Y. Bromberg, Y. Silberberg, M.G. Thompson, J.L. OBrien, Quantum walks of correlated photons. Science 329, 1500–1503 (2010)

- R.L. Pfleegor, L. Mandel, Interference of independent photon beams. Phys. Rev. **159**, 1084–1088 (1967)
- A.V. Ponomarev, A.R. Kolovsky, Dipole and Bloch oscillations of cold atoms in a parabolic lattice. Laser Phys. **16**, 367–370 (2006)
- A.V. Ponomarev, J. Madroñero, A.R. Kolovsky, A. Buchleitner, Atomic current across an optical lattice. Phys. Rev. Lett. **96**, 050404 (2006)
- P.M. Preiss, R. Ma, M.E. Tai, A. Lukin, M. Rispoli, P. Zupancic, Y. Lahini, R. Islam, M. Greiner, Strongly correlated quantum walks in optical lattices. Science **347**, 1229–1233 (2015)
- Y.-S. Ra, M.C. Tichy, H.-T. Lim, O. Kwon, F. Mintert, A. Buchleitner, Y.-H. Kim, Nonmonotonic quantum-to-classical transition in multiparticle interference. PNAS 110, 1227–1231 (2013a)
- Y.-S. Ra, M.C. Tichy, H.-T. Lim, O. Kwon, F. Mintert, A. Buchleitner, Y.-H. Kim, Observation of detection-dependent multi-photon coherence times. Nat. Commun. 4 (2013b)
- Y.-S. Ra, C. Jacquard, A. Dufour, C. Fabre, N. Treps, Tomography of a mode-tunable coherent single-photon subtractor. Phys. Rev. X 7, 031012 (2017)
- W. Radloff, Zur interferenz unabhängiger lichtstrahlen geringer intensität. Annalen der Physik 481, 178–189 (1971)
- S. Rahimi-Keshari, T.C. Ralph, C.M. Caves, Sufficient conditions for efficient classical simulation of quantum optics. Phys. Rev. X 6, 021039 (2016)
- J.G. Rarity, P.R. Tapster, R. Loudon, Non-classical interference between independent sources. J. Opt. B: Quantum Semiclass. Opt. 7, S171 (2005)
- M. Reck, A. Zeilinger, H.J. Bernstein, P. Bertani, Experimental realization of any discrete unitary operator. Phys. Rev. Lett. 73, 58–61 (1994)
- L. Rigovacca, C. Di Franco, B.J. Metcalf, I.A. Walmsley, M.S. Kim, Nonclassicality criteria in multiport interferometry. Phys. Rev. Lett. 117, 213602 (2016)
- J. Roslund, R.M. de Araújo, S. Jiang, C. Fabre, N. Treps, Wavelength-multiplexed quantum networks with ultrafast frequency combs. Nat. Photon 8, 109–112 (2014)
- L. Sansoni, F. Sciarrino, G. Vallone, P. Mataloni, A. Crespi, R. Ramponi, R. Osellame, Two-particle bosonic-fermionic quantum walk via integrated photonics. Phys. Rev. Lett. 108, 010502 (2012)
- C. Santori, M. Pelton, G. Solomon, Y. Dale, Y. Yamamoto, Triggered single photons from a quantum dot. Phys. Rev. Lett. **86**, 1502–1505 (2001)
- C. Santori, D. Fattal, J. Vučković, G.S. Solomon, Y. Yamamoto, Indistinguishable photons from a single-photon device. Nature 419, 594–597 (2002)
- F. Schlawin, K.E. Dorfman, B.P. Fingerhut, S. Mukamel, Manipulation of two-photon-induced fluorescence spectra of chromophore aggregates with entangled photons: a simulation study. Phys. Rev. A **86**, 023851 (2012b)
- W. Schleich, Quantum Optics in Phase Space (Wiley-VCH, Berlin, 2001)
- C. Schneider, D. Porras, T. Schaetz, Experimental quantum simulations of many-body physics with trapped ions. Rep. Prog. Phys. **75**, 024401 (2012)
- N. Schuch, D. Pérez-García, I. Cirac, Classifying quantum phases using matrix product states and projected entangled pair states. Phys. Rev. B 84, 165139 (2011)
- K.P. Seshadreesan, J.P. Olson, K.R. Motes, P.P. Rohde, J.P. Dowling, Boson sampling with displaced single-photon Fock states versus single-photon-added coherent states: the quantum-classical divide and computational-complexity transitions in linear optics. Phys. Rev. A 91, 022334 (2015)
- V.S. Shchesnovich, Partial indistinguishability theory for multiphoton experiments in multiport devices. Phys. Rev. A **91**, 013844 (2015a)
- V.S. Shchesnovich, Tight bound on the trace distance between a realistic device with partially indistinguishable bosons and the ideal boson sampling. Phys. Rev. A **91**, 063842 (2015b)
- C. Shen, Z. Zhang, L.-M. Duan, Scalable implementation of boson sampling with trapped ions. Phys. Rev. Lett. 112, 050504 (2014)

- J.F. Sherson, C. Weitenberg, M. Endres, M. Cheneau, I. Bloch, S. Kuhr, Single-atom-resolved fluorescence imaging of an atomic Mott insulator. Nature **467**, 68–72 (2010)
- P. Shor, Polynomial-time algorithms for prime factorization and discrete logarithms on a quantum computer. SIAM J. Comput. 26, 1484–1509 (1997)
- N. Spagnolo, C. Vitelli, M. Bentivegna, D.J. Brod, A. Crespi, F. Flamini, S. Giacomini, G. Milani, R. Ramponi, P. Mataloni, R. Osellame, E.F. Galvão, F. Sciarrino, Experimental validation of photonic boson sampling. Nat. Photon 8. 615–620 (2014)
- J.B. Spring, B.J. Metcalf, P.C. Humphreys, W.S. Kolthammer, X.-M. Jin, M. Barbieri, A. Datta, N. Thomas-Peter, N.K. Langford, D. Kundys, J.C. Gates, B.J. Smith, P.G.R. Smith, I.A. Walmsley, Boson sampling on a photonic chip. Science 339, 798–801 (2013)
- H.-J. Stöckmann, *Quantum Chaos: An Introduction* (Cambridge University Press, Cambridge, 2007)
- G.G. Stokes, On the perfect blackness of the central spot in Newton's rings, and on the verification of Fresnel's formulae for the intensities of reflected and refracted rays. Camb. Dublin Math. J. 4, 1–14 (1849)
- V. Tamma, S. Laibacher, Multiboson correlation interferometry with multimode thermal sources. Phys. Rev. A **90**, 063836 (2014)
- S.-H. Tan, Y.Y. Gao, H. de Guise, B.C. Sanders, Su(3) quantum interferometry with single-photon input pulses. Phys. Rev. Lett. **110**, 113603 (2013)
- G. Tanner, K. Richter, J.-M. Rost, The theory of two-electron atoms: between ground state and complete fragmentation. Rev. Mod. Phys. **72**, 497–544 (2000)
- M.C. Tichy, Entanglement and interference of identical particles. Ph.D. thesis, Albert-Ludwigs Universität Freiburg, Freiburg, 2011
- M.C. Tichy, Interference of identical particles from entanglement to boson-sampling. J. Phys. B: At. Mol. Opt. Phys. 47, 103001 (2014)
- M.C. Tichy, Sampling of partially distinguishable bosons and the relation to the multidimensional permanent. Phys. Rev. A **91**, 022316 (2015)
- M.C. Tichy, M. Tiersch, F. de Melo, F. Mintert, A. Buchleitner, Zero-transmission law for multiport beam splitters. Phys. Rev. Lett. **104**, 220405 (2010)
- M.C. Tichy, H.-T. Lim, Y.-S. Ra, F. Mintert, Y.-H. Kim, A. Buchleitner, Four-photon indistinguishability transition. Phys. Rev. A 83, 062111 (2011)
- M.C. Tichy, M. Tiersch, F. Mintert, A. Buchleitner, Many-particle interference beyond many-boson and many-fermion statistics. New J. Phys. 14, 093015 (2012)
- M.C. Tichy, F. de Melo, M. Kuś, F. Mintert, A. Buchleitner, Entanglement of identical particles and the detection process. Fortschr. Phys. **61**, 225–237 (2013)
- M.C. Tichy, K. Mayer, A. Buchleitner, K. Mølmer, Stringent and efficient assessment of boson-sampling devices. Phys. Rev. Lett. 113, 020502 (2014)
- M. Tillmann, B. Dakić, R. Heilmann, S. Nolte, A. Szameit, P. Walther, Experimental boson sampling. Nat. Photon 7, 540–544 (2013)
- M. Tillmann, S.-H. Tan, S.E. Stoeckl, B.C. Sanders, H. de Guise, R. Heilmann, S. Nolte, A. Szameit, P. Walther, Generalized multiphoton quantum interference. Phys. Rev. X 5, 041015 (2015)
- Q.A. Turchette, B.E. Kielpinski, D. King, D.M. Leibfried, C.J. Meekhof, M.A. Myatt, C.A. Rowe, C.S. Sackett, W.M. Wood, C. Monroe Itano, D.J. Wineland, Heating of trapped ions from the quantum ground state. Phys. Rev. A 61, 063418 (2000)
- J.-D. Urbina, J. Kuipers, S. Matsumoto, Q. Hummel, K. Richter, Multiparticle correlations in mesoscopic scattering: Boson sampling, birthday paradox, and Hong-Ou-Mandel profiles. Phys. Rev. Lett. 116, 100401 (2016)
- F. Verstraete, J.I. Cirac, Matrix product states represent ground states faithfully. Phys. Rev. B 73, 094423 (2006)
- F. Verstraete, V. Murg, J.I. Cirac, Matrix product states, projected entangled pair states, and variational renormalization group methods for quantum spin systems. Adv. Phys. 57, 143–224 (2008)
- N. Viggianiello, F. Flamini, L. Innocenti, D. Cozzolino, M. Bentivegna, N. Spagnolo, A. Crespi, D.J. Brod, E.F. Galvao, R. Osellame, F. Sciarrino, *Experimental Generalized Quantum Suppression Law in Sylvester Interferometers* (New J, Phys, 2018)

- M. Walschaers, Counting messages of quantum sources. Master thesis, KU Leuven, 2011
- M. Walschaers, J. Kuipers, A. Buchleitner, From many-particle interference to correlation spectroscopy. Phys. Rev. A 94, 020104 (2016a)
- M. Walschaers, J. Kuipers, J.-D. Urbina, K. Mayer, M.C. Tichy, K. Richter, A. Buchleitner, A statistical benchmark for bosonsampling. New. J. Phys. 18, 032001 (2016b)
- M. Walschaers, C. Fabre, V. Parigi, N. Treps, Entanglement and wigner function negativity of multimode non-gaussian states. Phys. Rev. Lett. 119, 183601 (2017b)
- H. Wang, Y. He, Y.-H. Li, Z.-E. Su, B. Li, H.-L. Huang, X. Ding, M.-C. Chen, C. Liu, J. Qin, J.-P. Li, Y.-M. He, C. Schneider, M. Kamp, C.-Z. Peng, S. Höfling, C.-Y. Lu, J.-W. Pan, High-efficiency multiphoton boson sampling. Nat. Photonics 11, 361 EP (2017)
- X.-C. Yao, T.-X. Wang, P. Xu, H. Lu, G.-S. Pan, X.-H. Bao, C.-Z. Peng, C.-Y. Lu, Y.-A. Chen, J.-W. Pan, Observation of eight-photon entanglement. Nat. Photon 6, 225–228 (2012)
- T. Young, The Bakerian lecture: experiments and calculations relative to physical optics. Phil. Trans. R. Soc. Lond. **94**, 1–16 (1804)

Chapter 9 Currents of Indistinguishable Particles



So we beat on, boats against the current, borne back ceaselessly into the past

F. Scott Fitzgerald in "The Great Gatsby" (Fitzgerald 1925)

9.1 Open System Dynamics for Many-body Systems

This chapter is formulated in the algebraic framework of Sect. 7.7 and is somewhat more abstract than the previous chapter. With this formulation, we intend to facilitate generalisations to scenarios with infinitely many particles, e.g. systems in the thermodynamical limit. Furthermore, this more general setting also forces us to make several assumptions more explicit, which highlights the mathematical limits of the model and thus the physical setting which it can describe. Readers who are not mathematically inclined may choose to picture a Fock space on a finite-dimensional single-particle Hilbert space. In the fermionic case, this automatically guaranties that all operators are matrices, which makes them bounded and trace-class.

In the previous chapter we used the many-particle framework of Chap. 7 to extensively study new interference phenomena which were purely related to indistinguishability. These effects even manifested in the absence of any interactions between particles. Even though we developed an understanding for the statistical signatures of many-particle quantum interference, we have not yet addressed the issue of *efficient* quantum transport in the many-particle context. Of specific interest is the question whether the single-particle channels of Sect. 8.2, which describe the dynamics of non-interacting particles, can be designed as optimal conductors.

In this chapter we treat this question by extending the model of Chap. 5 to a many-particle setting. In the light of Chaps. 7 and 8, it is crucial that our model grasps the specific differences between bosons and fermions as contained in the canonical

commutation and anticommutation relations, respectively. An implicit assumption in Chap. 5 is some degree of control over the channels, in the sense that we are scattering single particles on the system. We generalise this picture to the many-particle setting by considering channels as particles reservoirs with which particles can be exchanged. Once we have several such reservoirs we will typically see currents flowing Landauer (1957), unless the system and all reservoirs are in equilibrium. Hence, systems can be forced into a non-equilibrium setting by imposing thermodynamic differences between the reservoirs, e.g. in chemical potential or temperature. Such gradients induce currents through the system, i.e. constant fluxes of particles. Because we specifically consider quantum systems, these currents are a clear quantum transport phenomenon and thus *efficient* quantum transport is associated with large currents.

The contributions in this chapter can be understood in the broader context of currents in quantum mechanical systems. This topic is commonly considered within the context of condensed-matter physics, where it is studied in a variety of settings, e.g. in the framework of heat conduction (Asadian et al. 2013; Casati and Prosen 2003; De Roeck and Maes 2006; Dufour et al. 2017; Manzano et al. 2012; Ruelle 2000). A specific field of experimental applications is that of nanowires and molecular junctions (Agraït et al. 2003; Nitzan and Ratner 2003; Petrov et al. 2011; Segal and Nitzan 2002; Segal et al. 2003; Velizhanin et al. 2008), where both the transport of heat and charge have been considered. Of interest in relation to Chap. 6 is the potential relevance for quantum transport in photosynthetic complexes (Jesenko and Žnidarič 2013; Manzano 2013; Witt and Mintert 2013). Finally, the framework is also relevant for topics which are related to quantum optics, where one may study currents of cold atoms through optical lattices (Ponomarev et al. 2006).

Let us briefly note that also more general advances considering non-equilibrium steady states for spin-systems (Prosen and Žnidarič 2009) and fermionic systems (Prosen 2008) have been presented in recent years.

The connection between single-particle scattering and many-particle currents can be made more explicit by recalling from Chap. 5 that the general single-particle framework was described in a Hilbert space $\mathcal{H}_{total} = \mathcal{H}_s \bigoplus_c \mathcal{H}_c$ —with $\mathcal{H}_c \subset \mathcal{L}^2(\mathbb{R}^3)$ the Hilbert space of a channel and \mathcal{H}_s the Hilbert space describing the system. In Chap. 7, we introduced the Fock space $\Gamma(\mathcal{H}_{total})$ as a framework to describe *finitely many* particles in a system. The discussion in Sect. 7.3.2 now implies that

$$\Gamma(\mathcal{H}_{total}) = \Gamma\left(\mathcal{H}_s \bigoplus_c \mathcal{H}_c\right) \cong \Gamma(\mathcal{H}_s) \bigotimes_c \Gamma(\mathcal{H}_c). \tag{9.1}$$

This is the mathematical way of stating that a many-particle scattering problem allows for an equivalent description in terms of a tensor structure, which is the common framework of the theory of open systems (Alicki 1987; Breuer and Petruccione 2007). In this sense, we can now consider $\Gamma(\mathcal{H}_s)$ as the system and $\Gamma(\mathcal{H}_c)$ as the reservoirs.

To describe the system in a more formally correct way, we must be able to consider the thermodynamic limit (at least for the reservoirs). This leads us to the formalism of Sect. 7.7 which was historically developed to study quantum statistical mechanics. Rather than considering Fock space, we formulate the problem in terms of algebras of observables and throughout most of the chapter do so in the context of fermions. Therefore, we consider the CAR algebra as introduced in Sect. 7.7.1 and we will exploit the Jordan-Wigner transformation (recall Sect. 7.3.2) on the level of the C^* -algebras. From (Alicki and Fannes 2001) one obtains the equivalence

$$\mathcal{A}^{CAR}\Big(\mathcal{H}_s \bigoplus_c \mathcal{H}_c\Big) \cong \mathcal{A}^{CAR}(\mathcal{H}_s) \bigwedge_c \mathcal{A}^{CAR}(\mathcal{H}_c), \tag{9.2}$$

where $\mathcal{A}^{CAR}(\mathcal{H}_{\#})$ is the CAR algebra constructed on single-particle Hilbert space $\mathcal{H}_{\#}$, and " \wedge " is the *graded tensor product*. For our discussion the latter can be thought of in the same way as a normal tensor product. The right hand side of (9.2) provides a structure where we can accommodate infinitely many particles in the reservoirs and describe the full dynamics. However, we here follow the program of open system theory and proceed to a picture where the reservoirs $\mathcal{A}^{CAR}(\mathcal{H}_c)$ are integrated out.

The coarse-graining of the reservoirs can be done explicitly, for example in the weak-coupling limit as in Alicki (1978). However, our goal is not to formally derive a master equation starting from a Hamiltonian description, but rather we consider a phenomenological, exactly solvable model (Alicki 1987; Davies 1977a). Therefore, we simply focus our attention on the algebra of observables associated to the system $\mathcal{A}^{CAR}(\mathcal{H}_s)$ (henceforth denoted \mathcal{A}^{CAR}) and describe the systems dynamics in the Heisenberg picture in terms of a one-parameter semigroup, which means that it is completely irreversible, divisible, and memoryless (recall Sect. 2.4.1). Because we consider the dynamics of a C^* -algebra, we must use Lindblad's more general result (Lindblad 1976) and describe a one-parameter semigroup of completely positive dynamical maps $\Lambda_t = \exp(t\mathcal{L})$, with

$$\mathcal{L}(x) = \Psi(x) + Kx + xK^*, \quad \text{for all } x \in \mathcal{A}^{CAR}, \tag{9.3}$$

where $K \in \mathcal{A}^{\operatorname{CAR}}$ and $\Psi : \mathcal{A}^{\operatorname{CAR}} \to \mathcal{A}^{\operatorname{CAR}}$ a CP map.

The model which we implement here (Davies 1977a), requires a specific CP-map Ψ and operator $K \in \mathcal{A}^{CAR}$ (9.3). We choose

 $^{^1}$ A definition and introduction to the use of the graded tensor product are provided in Sect. 6.2 of Alicki and Fannes (2001). Here we restrict to simply stating that it shares many properties with the normal tensor product, but guarantees that $\{c(\phi\oplus 0),c(0\oplus\psi)\}=0$. If one uses a normal tensor product, rather than a graded one, the CAR cannot hold because a normal tensor product leads to $[c(\phi\oplus 0),c(0\oplus\psi)]=0$. Because we will directly proceed to the dynamical one-parameter semigroup, we will not elaborate further on this object.

$$K = -\frac{1}{2} \sum_{i} L_i^* L_i \tag{9.4}$$

$$\Psi(x) = \sum_{i}^{i} L_{i}^{*}\theta(x)L_{i}, \quad \text{for all } x \in \mathcal{A}^{\text{CAR}},$$
(9.5)

where $L_i \in \mathcal{A}^{\text{CAR}}$ and θ is a *-automorphism, given by $\theta(c(\psi)) = -c(\psi)$. This leads us to the final master equation, which extends the previously considered von Neumann equation $(8.1)^2$

$$\frac{\mathrm{d}}{\mathrm{d}t}x = -i[\Gamma(H), x] + \sum_{i} L_{i}^{*}\theta(x)L_{i} - \frac{1}{2}\{L_{i}^{*}L_{i}, x\}, \quad \text{for all } x \in \mathcal{A}^{\mathrm{CAR}}, \quad (9.6)$$

Expression (9.6) is extremely close to the more well-know Lindblad equation (2.46) (Lindblad 1976), the difference lies in the additional *-automorphism θ , which is necessitated by the CAR (Davies 1977a). Depending on the exact phenomenology which we wish to describe, we must make an explicit choice for the operators L_i .

On top of the coherent dynamics generated by a single-particle Hamiltonian, we include dissipation and absorption of particles (from the system's perspective). We first specify the model and hence the choice of L_i for this specific type of dynamics in Sect. 9.2. Then, in Sect. 9.3, we treat the dynamics for single-particle observables and the resulting currents in the non-equilibrium steady state. More specifically, in Sect. 9.4 we derive a universal bound for these currents, which is valid for all Hamiltonians without interactions, i.e. given by $\Gamma(H)$ with $H \in \mathcal{B}(\mathcal{H})$ (recall Sect. 7.5). Sections 9.5 and 9.6 are devoted to reaching this bound using various possible methods. The final section deals with the translation of our results to a bosonic setup, which requires few, but subtle changes.

9.2 Dissipation and Absorption

In Chap. 8 we introduced the dynamics of a fixed number of non-interacting particles in Sect. 8.2 and explored the interference phenomena which may arise in such dynamics. In this chapter, we extend this framework by allowing the number of particles to change over time. However, we still restrict ourselves to non-interacting particles, such that the system Hamiltonian given by $\Gamma(H)$ (recall (7.5)), with $H \in \mathcal{B}(\mathcal{H})$, and \mathcal{H} the single-particle Hilbert space. Hence, the generalisation extends (8.1) to (9.6).

The Lindblad operators L_i are chosen such that the system absorbs and dissipates particles, one at a time. It turns out that these operators can be stated as

²Note that in (8.1) we restricted ourselves to the Fock space, whereas here we extend this to the more general framework of C^* -algebras. This means that we now consider $\Gamma(H) = \sum_{i,j} \langle e_i, He_j \rangle c^*(e_i) c(e_j)$, for any basis $\{e_j\} \in \mathcal{H}$ and c as in (7.211).

$$L_i^d = \sqrt{\gamma_i^d} c(\delta_i),$$
 for dissipation from mode $\delta_i \in \mathcal{H}$ (9.7)

$$L_i^a = \sqrt{\gamma_i^a} c^*(\alpha_i), \quad \text{for absorption in mode } \alpha_i \in \mathcal{H},$$
 (9.8)

with $\gamma_i^{d,a} \geqslant 0$ the rates at which these processes take place. We choose both the Hamiltonian and the Lindblad operators to be time-independent, hence there are no external driving forces.

Let us first consider the action of the generator $\mathcal{L}^{d,a}$ (9.3), as induced via one such operator $L_i^{d,a}$, on $c^*(\psi)c(\phi)$. With (9.7) we directly find that

$$\mathcal{L}^{d}\left(c^{*}(\psi)c(\phi)\right) = \gamma^{d}\left(c^{*}(\delta)c^{*}(\psi)c(\phi)c(\delta) - \frac{1}{2}\left\{c^{*}(\delta)c(\delta), c^{*}(\psi)c(\phi)\right\}\right). \tag{9.9}$$

With the CAR (7.212, 7.213) it straightforwardly follows that

$$c^*(\delta)c(\delta)c^*(\psi)c(\phi) = \langle \delta, \psi \rangle c^*(\delta)c(\phi) + c^*(\delta)c^*(\psi)c(\phi)c(\delta), \tag{9.10}$$

$$c^*(\psi)c(\phi)c^*(\delta)c(\delta) = \langle \phi, \delta \rangle c^*(\psi)c(\delta) + c^*(\delta)c^*(\psi)c(\phi)c(\delta). \tag{9.11}$$

These terms in (9.9) give:

$$\mathcal{L}^{d}(c^{*}(\psi)c(\phi)) = -\frac{\gamma^{d}}{2} \langle \delta, \psi \rangle c^{*}(\delta)c(\phi) - \langle \phi, \delta \rangle c^{*}(\psi)c(\delta). \tag{9.12}$$

The absorption is dealt with in a strictly analogous manner, and (9.8) in (9.3, 7.212, 7.213) produces

$$\mathcal{L}^{a}\left(c(\phi)c^{*}(\psi)\right) = \gamma^{a}\left(c(\alpha)c(\phi)c^{*}(\psi)c^{*}(\alpha) - \frac{1}{2}\left\{c(\alpha)c^{*}(\alpha), c(\phi)c^{*}(\psi)\right\}\right). \tag{9.13}$$

This can be compactified with the identities

$$c(\alpha)c^*(\alpha)c(\phi)c^*(\psi) = \langle \phi, \alpha \rangle c(\alpha)c^*(\psi) + c(\alpha)c(\phi)c^*(\psi)c^*(\alpha), \tag{9.14}$$

$$c(\phi)c^*(\psi)c(\alpha)c^*(\alpha) = \langle \alpha, \psi \rangle c(\phi)c^*(\alpha) + c(\alpha)c(\phi)c^*(\psi)c^*(\alpha), \tag{9.15}$$

to yield the final result

$$\mathcal{L}^{a}(c(\phi)c^{*}(\psi)) = -\frac{\gamma^{a}}{2} \langle \phi, \alpha \rangle c(\alpha)c^{*}(\psi) - \frac{\gamma^{a}}{2} \langle \alpha, \psi \rangle c(\phi)c^{*}(\alpha). \tag{9.16}$$

When combining the absorptive and the dissipative part of the open system dynamics we still need the action of \mathcal{L}^a on the $c^*(\psi)c(\phi)$ (as in (9.12)) rather than on $c(\phi)c^*(\psi)$ in (9.16):

$$\mathcal{L}^{a}(c^{*}(\psi)c(\phi)) = \langle \phi, \psi \rangle \mathcal{L}^{a}(\mathbf{1}) - \mathcal{L}^{a}(c(\phi)c^{*}(\psi))$$

$$= -\mathcal{L}^{a}(c(\phi)c^{*}(\psi))$$

$$= \frac{\gamma^{a}}{2} \langle \phi, \alpha \rangle c(\alpha)c^{*}(\psi) + \frac{\gamma^{a}}{2} \langle \alpha, \psi \rangle c(\phi)c^{*}(\alpha)$$

$$= -\frac{\gamma^{a}}{2} \langle \phi, \alpha \rangle c^{*}(\psi)c(\alpha) - \frac{\gamma^{a}}{2} \langle \alpha, \psi \rangle c^{*}(\alpha)c(\phi) + \gamma^{a} \langle \phi, \alpha \rangle \langle \alpha, \psi \rangle.$$
(9.17)

Expressions (9.12) and (9.17) are the fundamental building blocks to describe the overall dynamics of a *normally ordered Wick monomial*. The generalisation of (9.12) reads

$$\mathcal{L}^{d}(c^{*}(\phi_{1})\dots c^{*}(\phi_{n})c(\phi_{n+1})\dots c(\phi_{n+m})) = -\frac{\gamma_{i}^{d}}{2} \sum_{j=1}^{n+m} \left\langle \delta_{i}, \phi_{j} \right\rangle \left(\prod_{k=1}^{j-1} c^{\#}(\phi_{k}) \right) c^{\#}(\delta_{i}) \left(\prod_{k'=j+1}^{n+m} c^{\#}(\phi_{k'}) \right),$$
(9.18)

where the # indicates either a creation or an annihilation operator, such that the order of creation and annihilation operators of the original monomial is preserved. The fact that the generator thus maps normally ordered monomials onto normally ordered monomials of the same order will be crucial when we solve the dynamics further down. Analogously, we obtain the generalised absorptive contribution:

$$\mathcal{L}^{a}(c(\phi_{1})\dots c(\phi_{n})c^{*}(\phi_{n+1})\dots c^{*}(\phi_{n+m}))$$

$$= -\frac{\gamma_{i}^{a}}{2} \sum_{j=1}^{n+m} \langle \alpha_{i}, \phi_{j} \rangle \left(\prod_{k=1}^{j-1} c^{\#}(\phi_{k}) \right) c^{\#}(\alpha_{i}) \left(\prod_{k'=j+1}^{n+m} c^{\#}(\phi_{k'}) \right),$$
(9.19)

We can now generalise for n_a absorptive and n_d dissipative channels,³ which we group together in the operators $A, D \in \mathcal{B}(\mathcal{H})$, respectively:

$$A = \sum_{i=1}^{n_a} \frac{\gamma_i^a}{2} |\alpha_i\rangle \langle \alpha_i|, \quad D = \sum_{i=1}^{n_d} \frac{\gamma_i^d}{2} |\delta_i\rangle \langle \delta_i|.$$
 (9.20)

The dissipative part of the dynamics then reads

 $^{^3}$ Even limits $n_a, n_d \to \infty$ can be accommodated. This scenario naturally arises for systems with an infinite dimensional single-particle Hilbert space \mathcal{H} , as treated in Davies (1977a). In principle, one may even replace the sums by integrals, and use the spectral theorem to define A and D. Mathematically, this implies that some care is required to ensure that the dynamics is well-defined (Davies 1977b,1979; Holevo 2001). Physical examples where such treatment becomes relevant are typically found in quantum field theory treatments of unstable particles (Alicki 1987): One may think of fundamental particles or light nuclei, quantised electromagnetic waves in absorbing and radiating media, quasi particles of condensed matter physics, or neutron diffusion (Davies 1977b).

$$\mathcal{L}^{d}(c^{*}(\phi_{1})\dots c^{*}(\phi_{n})c(\phi_{n+1})\dots c(\phi_{n+m}))$$

$$= -\sum_{j=1}^{n+m} \left(\prod_{k=1}^{j-1} c^{\#}(\phi_{k})\right) c^{\#}(D\phi_{j}) \left(\prod_{k'=j+1}^{n+m} c^{\#}(\phi_{k'})\right), \tag{9.21}$$

and the absorptive part

$$\mathcal{L}^{a}(c(\phi_{1})\dots c(\phi_{n})c^{*}(\phi_{n+1})\dots c^{*}(\phi_{n+m}))$$

$$= -\sum_{j=1}^{n+m} \left(\prod_{k=1}^{j-1} c^{\#}(\phi_{k})\right) c^{\#}(A\phi_{j}) \left(\prod_{k'=j+1}^{n+m} c^{\#}(\phi_{k'})\right). \tag{9.22}$$

Once again, (9.22) has to be rewritten in normal order for dynamics à la (9.6) with, both, dissipative and absorptive channels, what adds another layer of computational overhead.

In what follows, we will consider some specific applications of the thus formulated theoretical framework, focussed on the dynamics of single-particle observables as introduced in Sect. 7.5.

9.3 Dynamics of Single-Particle Observables

9.3.1 Solving the Dynamics

The starting point of this section, where we analyse the dynamics of single-particle observables, is the generator \mathcal{L} (9.6) of our dynamics, acting on a general single-particle operator $\Gamma(B)$, $B \in \mathcal{B}(\mathcal{H})$ and $\operatorname{tr} B < \infty$, with

$$\Gamma(B) = \sum_{ij} \langle e_i, Be_j \rangle c^*(e_i) c(e_j). \tag{9.23}$$

Our treatment and formulation will in many ways be similar to Alicki (1987, 1978). We first use (9.21) and (9.22) to evaluate

$$\mathcal{L}(c^{*}(\phi)c(\psi)) = i[\Gamma(H), c^{*}(\phi)c(\psi)] + \mathcal{L}^{d}(c^{*}(\phi)c(\psi)) + \mathcal{L}^{a}(c^{*}(\phi)c(\psi))$$

$$= c^{*}((iH - A - D)\phi)c(\psi) + c^{*}(\phi)c((iH - A - D)\psi) + 2\langle\phi, A\psi\rangle \mathbf{1}.$$
(9.24)

With (9.23) and (9.24) we directly find

$$\mathcal{L}(\Gamma(B)) = \Gamma\left(i[H, B] - \{P, B\}\right) + 2\operatorname{tr}(AB)\mathbf{1},\tag{9.25}$$

where P := A + D. This tells that, because of the absorption of particles, a single-particle operator is mapped onto a new single-particle operator and a multiple of

the identity. Therefore the set $\mathcal{X} = \{\Gamma(B) + z\mathbf{1} \mid B \in \mathcal{B}(\mathcal{H}), z \in \mathbb{C}\}$ is left invariant under the dynamics and $\Gamma(B(t)) + z(t)\mathbf{1}$ can serve as ansatz for a solution:⁴

$$\frac{\mathrm{d}}{\mathrm{d}t}(\Gamma(B(t)) + z(t)\mathbf{1}) = \mathcal{L}(\Gamma(B(t))) + z(t)\mathcal{L}(\mathbf{1}). \tag{9.26}$$

Using that $\mathcal{L}(\mathbf{1}) = 0$ by $(2.38)^5$, and that \mathcal{L} is linear, this can be rewritten as

$$\Gamma(\dot{B}(t)) + \dot{z}(t)\mathbf{1}) = \Gamma(i[H, B(t)] - \{P, B(t)\}) + 2\operatorname{tr}(AB(t))\mathbf{1}, \tag{9.27}$$

which leads to two coupled differential equations:

$$\dot{B}(t) = i[H, B(t)] - \{P, B(t)\}, \tag{9.28}$$

$$\dot{z}(t) = 2\operatorname{tr}(AB(t)),\tag{9.29}$$

with
$$z(t = 0) = z_0$$
, and $B(t = 0) = B_0$. (9.30)

These equations, and hence also (9.27) can be solved to find

$$\Lambda_{t}(\Gamma(B_{0})) = \Gamma\left(e^{t(iH-P)}B_{0}e^{t(-iH-P)}\right) + \operatorname{tr}\left(\int_{0}^{t} ds \ 2Ae^{(iH-P)s}B_{0}e^{(-iH-P)s}\right)\mathbf{1},\tag{9.31}$$

which we will now use to determine the dynamics of several relevant quantities.

9.3.2 The Non-Equilibrium Steady State

We focus on single-particle observables (see Sect. 7.5), and can therefore express their expectation values in *any state* ω using an operator $Q \in \mathcal{B}(\mathcal{H})^6$:

$$\omega(c^*(\phi)c(\psi)) = \langle \phi, Q\psi \rangle. \tag{9.32}$$

Thus, due to linearity of the state ω , whenever we consider an operator B which is trace-class, 7 i.e. $B \in \mathcal{T}(\mathcal{H})$, we find

$$\omega(\Gamma(B)) = \operatorname{tr}(QB). \tag{9.33}$$

Since, in addition, $\omega(1) = 1$ by definition (7.219), we obtain from (9.31) that

 $^{{}^4\}mathcal{L}(\mathcal{X}) \subset \mathcal{X}$ and thus the generated dynamics can never make elements of \mathcal{X} leave the set.

⁵Alternatively, one may insert **1** in the right hand side of (9.6).

⁶This holds because $\omega(c^*(\phi)c(\psi))$ defines a sesquilinear form for ϕ and ψ (Bratteli and Robinson 1997).

⁷Recall the definition in Sect. 2.3.2 or Conway (1997)

$$\omega \circ \Lambda_t(\Gamma(B_0)) = \operatorname{tr}\left(e^{t(iH-P)}B_0e^{t(-iH-P)}Q\right) + \operatorname{tr}\left(B_0\int_0^t \mathrm{d} s \ 2e^{(-iH-P)s}Ae^{(iH-P)s}\right). \tag{9.34}$$

Typically,⁸ in the limit where $t \to \infty$, we arrive at

$$\lim_{t \to \infty} \omega \circ \Lambda_t(\Gamma(B_0)) = 2 \operatorname{tr} \left(B_0 \int_0^\infty \mathrm{d} s \ e^{(-iH - P)s} A e^{(iH - P)s} \right), \tag{9.35}$$

such that we can define the *non-equilibrium steady state* (NESS) $\omega_{\text{NESS}} := \lim_{t \to \infty} \omega \circ \Lambda_t$. It directly follows that

$$\omega_{\text{NESS}}(c^*(\phi)c(\psi)) = \langle \phi, Q_{\text{NESS}}\psi \rangle$$
with $Q_{\text{NESS}} := 2 \int_0^\infty ds \ e^{(-iH-P)s} A e^{(iH-P)s}$, (9.36)

such that the expectation value of a single-particle observable in the NESS can be described as

$$\omega_{\text{NESS}}(\Gamma(B_0)) = \text{tr}(B_0 Q_{\text{NESS}}). \tag{9.37}$$

The physical content of (9.36) is that the *expected* number of particles in every single particle state converges to a constant value. Given that the absorption and dissipation rates $\{\gamma_j^a\}$ and $\{\gamma_j^d\}$ are constant in time, i.e. do not fade away as $t \to \infty$, a current must be flowing even in the NESS, which justifies the terminology.

9.3.3 Normal States

Our above discussion did not depend on any assumptions on the state ω , but the prize we had to pay was the requirement that the single-particle observable $B \in \mathcal{B}(\mathcal{H})$ also fulfils tr $B < \infty$, or, in other words, $B \in \mathcal{T}(\mathcal{H})$. Whenever this is not the case, we risk to encounter problems in systems where the single-particle spaces \mathcal{H} are infinite dimensional. The problem lies in the fact that tr QB is generally infinite in this case, and therefore $\mathcal{L}(\Gamma(B))$ would no longer be well-defined. Fundamentally, the boundedness of $B \in \mathcal{B}(\mathcal{H})$ cannot guarantee the boundedness of $\Gamma(B)$, and therefore in general $\Gamma(B) \notin \mathcal{A}^{CAR}$. A good example is the number operator $\hat{N} = \Gamma(1)$, which is clearly unbounded when the single-particle space \mathcal{H} is infinite dimensional.

Physically, this situation corresponds to the thermodynamic limit, which is commonplace in statistical mechanics. One of the strengths of the algebraic approach to

⁸Formally, this depends on the spectrum of iH - P, which should not contain points which are purely imaginary. Mathematically, the set of operators iH - P which do contain purely imaginary points in their spectrum is negligible. Physically, phrased in the terminology of resonances, this implies that each resonance should have finite width. Also from a physical perspective this demand is typically satisfied, although there may be exceptions which in decoherence theory are termed decoherence-free subspaces (Lidar and Whaley 2003).

many-particle systems—which we introduced in Sect. 7.7—is that it also allows us to describe such types of systems. Nevertheless, global observables (such as $\Gamma(1)$) are typically not suited to describe properties of such systems. This essentially implies that such a system in the thermodynamic limit cannot be contained within one single representation of the algebra. A typical method to deal with these systems uses local sub-algebras to describe local observables. In the thermodynamic limit this method induces a description in terms of densities. The relevant states to consider are then referred to as *locally normal* (Bratteli and Robinson 1987, 1997). Important applications of such techniques are found in the studies of BEC (Araki and Woods 1963; Verbeure 2011), superfluidity (Robinson 1965a) and the BCS model for superconductivity (Balslev and Verbeure 1968; Haag 1962).

We will restrict ourselves to a more straightforward way to avoid mathematical difficulties: We limit ourselves to states which are *normal with respect to the Fock representation* (Bratteli and Robinson 1997). In other words, these states can be seen as well-defined density matrices in the Fock representation (recall Sect. 2.3.2), which implies that they are convex combinations of pure states with finite particle numbers (in the expectation value). More specifically, they are the states ω which satisfy

$$\omega(\hat{N}) = \sum_{i} \omega(c^*(\eta_i)c(\eta_i)) < \infty, \tag{9.38}$$

where $\{\eta_i\}$ forms an orthogonal basis of the single-particle Hilbert space. Using the result (9.32) that we can always find a $Q \in \mathcal{B}(\mathcal{H})$ for which $\omega(c^*(\psi)c(\phi)) = \langle \phi, Q\psi \rangle$, we could also say that the normal states with respect to the Fock representation are those where this Q fulfils the constraint tr $Q < \infty$.

It is not sufficient to limit ourselves to *initial* states which are normal with respect to the Fock representation, but we must also make sure that this property is conserved throughout the dynamics, i.e. in the Schrödinger picture we must map normal states onto normal states. A necessary condition to achieve this goal is clearly that $\text{tr} A < \infty$, and the additional demand that $\text{tr} D < \infty$ is sufficient to guarantee that the number of particles in the system remains finite.

Let us remark that the above actually implies that the entire analysis can be carried out in the Fock space representation $\Gamma^f(\mathcal{H})$.

9.3.4 Currents

To discuss in more detail the stationary currents that manifest in the non-equilibrium steady state, we observe a particularly interesting meaning hidden in the generators of the dynamics. In general, dynamics of the form

 $^{^{9}}$ Hence, the language of C^* -algebras is not strictly necessary, but is here nevertheless used to facilitate future extensions.

$$\frac{\mathrm{d}}{\mathrm{d}t}x(t) = \mathcal{L}(x(t))\tag{9.39}$$

can be interpreted as a *continuity equation*. For a system with initial state ω to ever converge to a steady state, it must hold that

$$\lim_{t \to \infty} \omega \circ \mathcal{L}(x(t)) = 0. \tag{9.40}$$

For a single-particle observable $\Gamma(B_0)$ this is tantamount of

$$\omega_{\text{NESS}}\Big(i[\Gamma(H), \Gamma(B_0)]\Big) + \omega_{\text{NESS}}\Big(\mathcal{L}^d\big(\Gamma(B_0)\big)\Big) + \omega_{\text{NESS}}\Big(\mathcal{L}^d\big(\Gamma(B_0)\big)\Big) = 0,$$
(9.41)

what we can rewrite, using (9.25) and the definition (9.36) of Q_{NESS} , as

$$i \operatorname{tr}([H, Q_{\text{NESS}}]B_0) = \operatorname{tr}((2A - \{A, Q_{\text{NESS}}\})B_0) - \operatorname{tr}(\{D, Q_{\text{NESS}}\}B_0).$$
 (9.42)

The left hand side of this equation grasps all the coherent contributions to the current associated with observable B_0 (Alicki 1976, 1979), 10 and more specifically how this current is distributed within the system. The right hand side accounts for incoherent contributions, which stem from particle exchange with the reservoirs. The latter can be understood in the sense that, for example, $\operatorname{tr}(\{D, Q_{\text{NESS}}\}B_0)$ is obtained by letting \mathcal{L}^d (9.21) act on the observable $\Gamma(B_0)$ in ω_{NESS} . Hence it literally describes how the observable $\Gamma(B_0)$ is expected to change in time as consequence of the dissipation of particles from the system.

Local Currents and Coherence

Local quantities are found via objects such as $\hat{n}(\phi) = \Gamma(|\phi\rangle \langle \phi|)$, which is the observable that describes the number of particles occupying a given mode $\phi \in \mathcal{H}$ (recall Sect. 8.4). When we evaluate (9.42) for $\hat{n}(\phi)$ and find

$$2\operatorname{Im}\langle\phi,HQ\phi\rangle=2\ \langle\phi,A\phi\rangle-2\operatorname{Re}\Big(\langle\phi,AQ\phi\rangle+\langle\phi,DQ\phi\rangle\Big), \tag{9.43}$$

where the lefthand side denotes the current flowing in and out of the state ψ within the system, ¹¹ and the righthand side takes into account all the particles that enter or leave the system via state ϕ . Let us consider a specific example:

Example 9.3.1 To acquire more insight, let us briefly adopt the network picture of Sect. 4.1. Recall that there the single-particle Hamiltonian was represented as

$$H = \sum_{i,j} H_{ij} |e_i\rangle \langle e_j|, \qquad (4.1)$$

¹⁰We can associate currents to several quantities, such as global particle number $(B_0 = 1)$, local particle number $(B_0 = |\psi\rangle \langle \psi|)$, energy $(B_0 = H)$, et cetera.

¹¹This is much like the probability current which arises in the single-particle Schrödinger equation, only do we here consider a many-particle generalisation.

with $\{e_j\}$ as orthogonal basis of the single-particle Hilbert space \mathcal{H} , which we associate with the nodes of a network.

We moreover assume that A and D are both diagonal in this mode basis, which implies that each node in the network is connected to its own reservoir:

$$A = \sum_{j} \gamma_{j}^{a} |e_{j}\rangle\langle e_{j}|, \text{ and } D = \sum_{j} \gamma_{j}^{d} |e_{j}\rangle\langle e_{j}|.$$
 (9.44)

When we now locally study what happens in the *k*th node of the network, we must choose $\phi = e_k$. When we combine (4.1), (9.44), and the orthogonality of $\{e_j\}$ in (9.43), we obtain

$$\sum_{j} 2\operatorname{Im} H_{kj} \langle e_{j}, Q e_{k} \rangle = 2 \gamma_{k}^{a} (1 - \langle e_{k}, Q e_{k} \rangle) + 2 \gamma_{k}^{d} \langle e_{k}, Q e_{k} \rangle. \tag{9.45}$$

Recall from (9.42) that the right hand side can be interpreted as a local change in particle number, induced by Hamiltonian dynamics. Hence in the framework of Alicki (1976, 1979) we consider

$$j_{k \to j} = 2 \operatorname{Im} H_{kj} \langle e_j, Q e_k \rangle \tag{9.46}$$

a local thermodynamic flux of particles from node k to node j. This current is not only mediated by the coherent part of the dynamics, it is also directly proportional to the coherence. Indeed, recall that, by virtue of (9.32), we obtain

$$\langle e_j, Qe_k \rangle = \omega(c^*(e_j)c(e_k)).$$
 (9.47)

Therefore, (9.46) shows us that coherence and local currents go hand in hand.

Example 9.3.1 is not only relevant in relation to our discussion in Chap. 4, it also provides us with a simple intuitive picture to see how local currents are related to coherence. Nevertheless, we needed to make several specific assumptions to arrive at this picture. It is not hard to understand that the network is ultimately nothing more than a mental picture to help us understand the dynamics when we express the problem explicitly in the eigenbasis of A and D. In general, however, A and D will not be diagonal in the same basis. When we then express the problem in the eigenbasis of either A or D, we find additional terms in (9.43). Therefore, we will also find currents related to the real part of $\omega(c^*(e_j)c(e_k))$. In the network picture these are effective currents which are mediated by a reservoir that couples to multiple nodes.

Putting aside subtleties related to specific choices of bases (which usually depend strongly on the concrete physical problem which is considered), we can reach a general conclusion: Whenever currents are flowing through a system, we will find that a current from mode ϕ to mode ψ , for ψ , $\phi \in H$, is associated with a non-vanishing coherence $\omega(c^*(\psi)c(\phi))$. If, in addition, the single-particle Hamiltonian

H is real (recall (9.46)), we can clearly associate the imaginary part of the coherence $\omega(c^*(e_j)c(e_k))$ to a current induced by coherent dynamics. The real part of $\omega(c^*(e_j)c(e_k))$ corresponds to an incoherent current, mediated by the a particle reservoir.

Depending on the exact questions we want to answer, these local currents may not be the most practical objects to work with. However, because we consider systems with finite particle numbers, we can also attempt to discuss the global current that flows trough the system. Moreover, if an overall current flows through the system, is must also induce currents on a local level. In this sense, a global particle current implies that there are coherences present in the system, although we typically cannot gain quantitative details on the individual coherences.

Total Particle Current

To describe the global particle current, the relevant choice of observable is the number operator, $\hat{N} = \Gamma(1)$ (recall (7.97) in Sect. 7.5), and therefore $B_0 = 1$. This reduces (9.42) to

$$2\operatorname{tr}(A(\mathbb{1} - Q_{\text{NESS}})) = 2\operatorname{tr}(DQ_{\text{NESS}}). \tag{9.48}$$

Equation (9.48) says that the total incoming particle current is equal to the total outgoing particle current, the *non-equilibrium steady state particle current J* can therefore be defined as

$$J := 2 \operatorname{tr}(DQ_{\text{NESS}}) = 2 \operatorname{tr}(A(\mathbb{1} - Q_{\text{NESS}})).$$
 (9.49)

J can be interpreted as the rate at which particles are flowing out of the system into the different output channels (as characterised by the eigenvectors of D) (Alicki 1976). This is an immediate consequence of the fact that $J = \omega_{\text{NESS}}(\mathcal{L}^d(\hat{N}))$. An explicit expression for J can be obtained with the help of (9.36):

$$J = 4 \int_0^\infty \mathrm{d}s \, \operatorname{tr} \left(D e^{(-iH - P)s} A e^{(iH - P)s} \right). \tag{9.50}$$

We will now show that J can be bounded under very general conditions, and that there are procedures to saturate this bound.

9.4 The Maximal Current

In this section, we study the characteristics of the total particle current J as given by (9.50). Although (9.50) provides us with an exactly solvable expression for the current, it is highly impractical to use: To study the current in detail, we must solve an integral over operators, which is usually a tough task. Therefore we try to gain a deeper understanding of the structural system properties which determine the current J.

The key result of these considerations will be a universal upper bound for the current J^{12} :

 $J \leqslant 2 \frac{\operatorname{tr}(D)\operatorname{tr}(A)}{\operatorname{tr}(D) + \operatorname{tr}(A)}. \tag{9.51}$

The proof is slightly technical in the sense that the individual steps are in general not necessarily physically motivated. First, we introduce the super-operator

$$G(X) := -i[H, X] + \{P, X\}, \text{ with } P = A + D,$$
 (9.52)

and define the super-operators which describe left and right multiplication, \mathcal{L}_Y and \mathcal{R}_Y , respectively:

$$\mathcal{L}_Y(X) := YX \text{ and } \mathcal{R}_Y(X) := XY.$$
 (9.53)

We can now split \mathcal{G} into a sum of two commuting terms:

$$\mathcal{G} = \mathcal{L}_{P-iH} + \mathcal{R}_{P+iH}. \tag{9.54}$$

Generically, ¹³ \mathcal{G} is invertible, and, for positive definite P, ¹⁴

$$\mathcal{G}^{-1}(X) = \int_0^\infty ds \exp(-s\mathcal{G})(X)$$

$$= \int_0^\infty ds \exp(-s\mathcal{L}_{P-iH}) \circ \exp(-s\mathcal{R}_{P+iH})(X)$$

$$= \int_0^\infty ds \, e^{-s(P-iH)} X \, e^{-s(P+iH)}. \tag{9.55}$$

Furthermore, we compute

$$\mathcal{G}(X^{\dagger}X) - \mathcal{G}(X^{\dagger})X - X^{\dagger}\mathcal{G}(X) = -2X^{\dagger}PX \le 0, \tag{9.56}$$

such that

$$\mathcal{G}(X^{\dagger}X) \le \mathcal{G}(X^{\dagger})X + X^{\dagger}\mathcal{G}(X). \tag{9.57}$$

 $^{^{12}}$ For fermions, one may directly argue that $J \leq 2 \text{tr} A$ (because $Q_{\text{NESS}} \geqslant 0$) and that $J \leq 2 \text{tr} D$ (because $Q_{\text{NESS}} \leq 1$). However, these bounds are never reached since the new bound, which we will prove here, is strictly smaller than both 2 tr A and 2 tr D (unless tr A = 0 or tr D = 0, where all these bounds coincide and there is simply no current).

 $^{^{13}}$ Recall the footnote on p. 382. In a mathematical sense, the set of super-operators \mathcal{G} which are defined according to (9.52) and are not invertible is negligible. Again, there may be physical models (which are arguably often idealised) where H and P are such that \mathcal{G} is not invertible and therefore some extra care is required when attempting to apply our results in this context. We conjecture that continuity arguments can be applied to extend the proof to the mathematically rare cases where \mathcal{G} is not invertible. Nevertheless, the details have not been rigorously studied.

¹⁴One way to obtain this identity is by considering the Laplace transform of $\exp(-s\mathcal{G})$.

9.4 The Maximal Current 389

We now introduce a symmetrised version of the *zero temperature Duhamel (or Bogoliubov) inner product* (Bratteli and Robinson 1997; Petz and Toth 1993):

$$\langle X, Y \rangle_{\sim} := \operatorname{tr}\left(X^{\dagger} \mathcal{G}^{-1}(Y) + \mathcal{G}^{-1}(X^{\dagger})Y\right),$$
 (9.58)

with *X* and *Y* general operators. Positivity of (9.58) follows from the invertibility of \mathcal{G} , from $\mathcal{G}(X^{\dagger}) = (\mathcal{G}(X))^{\dagger}$, from (9.57), and from

$$\operatorname{tr} \mathcal{G}(X^{\dagger}X) = \operatorname{tr} \{P, X^{\dagger}X\} \geqslant 0. \tag{9.59}$$

In the next step, we use the Cauchy-Schwarz inequality

$$|\langle A, P \rangle_{\sim}|^2 \leqslant \langle A, A \rangle_{\sim} \langle P, P \rangle_{\sim} \tag{9.60}$$

and evaluate the different factors. To do so, we observe that

$$\mathcal{L}_{P\pm iH}(\mathbb{1}) + \mathcal{R}_{P\mp iH}(\mathbb{1}) = 2P. \tag{9.61}$$

This yields

$$\langle A, P \rangle_{\sim} = \text{tr}A, \tag{9.62}$$

$$\langle P, P \rangle_{\sim} = \text{tr} P, \tag{9.63}$$

$$\langle A, A \rangle_{\sim} = 2 \int_0^\infty ds \operatorname{tr} \left(A e^{-s(P-iH)} A e^{-s(P+iH)} \right). \tag{9.64}$$

Inserting these results in (9.60), we obtain

$$\left(\operatorname{tr}(A)\right)^{2} \leqslant \left(\operatorname{tr}(A) - J/2\right)\operatorname{tr}(A+D) \tag{9.65}$$

and it then follows that

$$J \leqslant 2 \frac{\operatorname{tr}(A) \operatorname{tr}(D)}{\operatorname{tr}(A+D)} =: J_{\max}.$$
(9.66)

Since this bound J_{max} does not depend on the system Hamiltonian, but only on the properties of the channels (particle reservoirs) A and D as defined in (9.20), it can be considered universal.

Note that the Duhamel inner product (9.58) is fundamental for the above. Indeed, this structure is a common tool in quantum statistical mechanics (Aizenman et al. 2004; Dyson et al. 1976, 1978; Fannes and Verbeure 1977a, b; Hohenberg 1967; Kubo and Kishi 1990; Naudts and Verbeure 1976; Naudts et al. 1975; Roepstorff 1977), but none of these works investigates dynamical problems. The appearence of a non-Hermitian operator, $(P \pm i H)$, in (9.55) is a serious complication: Because of

this non-Hermiticity, the usual Duhamel inner product is no longer well-defined. It is the very reason why we define a new, symmetrised version in (9.58).

Although the bound (9.66) is a rigorous mathematical result, this does not necessarily mean that it is also *sharp*. More specifically, it is not clear whether the coherent contributions, contained with the Hamiltonian H, have any impact on the current in the NESS. To asses such impact, we introduce the continuous tuning parameter $\lambda \in \mathbb{R}^+$, which controls the relative strength of Hamiltonian and incoherent contributions in

$$J = 4 \int_0^\infty ds \operatorname{tr} \left(D e^{(-i\lambda H - P)s} A e^{(i\lambda H - P)s} \right). \tag{9.67}$$

In the following we will refer to the limit $\lambda \to \infty$ as the limit of dominantly coherent dynamics, and to $\lambda \to 0$ as that of dominantly incoherent dynamics. Note that the case $\lambda = 0$ is well-defined and corresponds to

$$J_{\lambda=0} = 4 \int_0^\infty ds \, \text{tr} \Big(De^{-sP} A e^{-sP} \Big).$$
 (9.68)

The proof of the bound (9.66) holds for $J_{\lambda=0}$, and this quantity is completely independent of the Hamiltonian H. Based on continuity of J (9.67) in λ , one may argue that for sufficiently small values of λ , the current will remain close to $J_{\lambda=0}$. In a mathematical formulation, one may argue that " λ sufficiently small" can be gauged against the operator norms $\|P\|$ and $\|H\|$. Without rigorously evaluating limits, $\lambda \ll \|P\|/\|H\|$ is a safe choice for obtaining currents near $J_{\lambda=0}$. Therefore, for any typical P, independent of the Hamiltonian $H \in \mathcal{B}(\mathcal{H})$, we may always find a value λ such that the influence of H is negligible. Physically, one may interpret this argument based on time scales: Coherent dynamics is governed by oscillatory dynamics contained in H, and the incoherent contributions contained in P damp these oscillations. The parameter λ sets an overall scale for the frequencies of oscillatory dynamics. Regardless of how H is designed, we can always choose λ small enough for all oscillatory frequencies to be significantly smaller than their damping rates. In other words, coherence phenomena will never become expressed.

The opposite limit, where $\lambda \to \infty$, is more subtle and will be discussed in more detail throughout Sect. 9.5. Nevertheless, an unambiguous physical understanding of how the coherent contributions influence the NESS behaviour of the system is still lacking.

To verify whether physical systems described by the model (9.6), with (9.7, 9.8), manifest and potentially saturate our bound, we perform additional numerical simulations: We generate random Hamiltonians by sampling matrices from the GOE (recall Chap. 3), as given by (3.26), where we set the typical (i.e. root mean squared) interaction between the different modes equal to v/\sqrt{m} . From (3.46), we know that v governs the width of the spectrum of Hamiltonian H. Because we consider a many-particle setting, we again refer to the dimension of the single-particle Hilbert space

¹⁵Using spectral and perturbation theory, one may come up with more rigorous arguments.

 \mathcal{H} as the number m of modes. Hence, throughout our numerical evaluations, H is an $m \times m$ matrix. We model the reservoir couplings by random positive semi-definite matrices A and D chosen from the Wishart ensemble (Akemann et al. 2011; Wishart 1928). The latter ensembles are solely determined by the numbers of absorption and dissipations channels, m_A and m_D , respectively. For our numerical simulations, we set

$$A = W_a^{\dagger} W_a, \quad \text{and} \quad D = W_d^{\dagger} W_d, \tag{9.69}$$

where W_a and W_d are $m_A \times m$ and $m_D \times m$ matrices, respectively. They are generated by choosing random components according to

$$(W_{a,d})_{ij} \sim \text{Normal}(0,1),$$
 (9.70)

which generates random positive semi-definite matrices A and D, which act on the single-particle Hilbert space \mathcal{H} . A typical eigenvalue of A or D therefore is of the order m_A or m_D , respectively. Finally, the parameter λ is varied randomly over ten orders of magnitude according to:

$$\lambda = 10^x, \quad x \sim \text{Uniform}([-5, 5]).$$
 (9.71)

Alternatively, one may thus say that $\log_{10} \lambda$ is uniformly distributed on the interval [-5, 5].

Although these choices allow an interpretation in the context of random networks (recall Chap. 4) and bear similarities to Fyodorov and Savin (2012), Haake et al. (1992), we do not intend to model any specific type of systems, nor study any statistical properties of the resulting currents. We merely use RMT methods to generate systems where we can control the typical time and energy scales in absence of any symmetries. The primary goal is to investigate whether we can find realisations which closely approach the bound (9.66). As a secondary goal, we set out to gauge the importance of coherent and incoherent effects in the dynamics.

Figures 9.1, 9.2 and 9.3 show the first numerical results on the statistics of the current under changes of λ . Because the bound J_{max} depends on A and D, we rescale all currents with respect to J_{max} . The quantity J/J_{max} can then be compared for any choice of A and D. Qualitatively, all these plots indicate that a strong coherent contribution is needed to saturate the bound (9.66).

$$A_{jj} = \sum_{j=1}^{m_A} ((W_{a,d})_{ij})^2.$$

Due to (9.70) these objects are distributed according to a χ^2 -distribution and hence their expectation value is m_A . As a consequence, we may conclude that $\mathbb{E}(\operatorname{tr} A/m) = m_A$.

 $^{^{16}}$ A simple estimate can be obtained as follows: The mean eigenvalue of A is by definition given by tr A/m (because the trace is the sum of all eigenvalues). Nevertheless, the trace is also the sum of the diagonal entries of A and, according to (9.69), these are given by

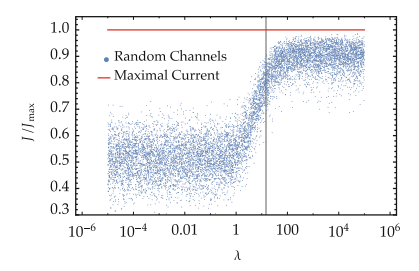


Fig. 9.1 Scatter plot which indicates the stationary current J (9.67) relative to the maximal current J_{max} (9.66). Variable λ (9.67) controls the relative strength of the Hamiltonian and incoherent contributions; for each data point $\log_{10} \lambda$ is randomly chosen from the interval [-5, 5]. For each realisation, Hamiltonians H in (9.67) are chosen from the GOE (3.26), with typical interaction v/\sqrt{m} between modes, with v=1 and mode number m=10, and the channels (9.20) A and D in (9.67) are drawn from a Wishart ensemble (9.69), with $m_A=5$ and $m_D=10$. Data points are compared to the upper bound $J=J_{\text{max}}$ (horizontal line). The value $\lambda=m_A+m_D$ is indicated (vertical line) since it represents the typical incoherent rate as the mean eigenvalue of P=A+D (see discussion of (9.69))

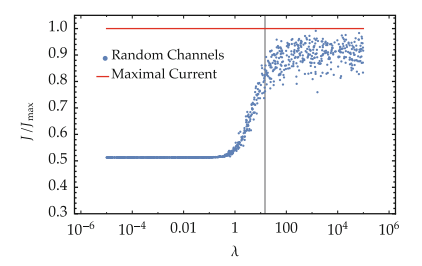


Fig. 9.2 Scatter plot which indicates the stationary current J (9.67) relative to the maximal current J_{max} (9.66). Variable λ (9.67) controls the relative strength of the Hamiltonian and incoherent contributions; for each data point, $\log_{10} \lambda$ is randomly chosen from the interval [-5, 5]. For each realisation, Hamiltonians H in (9.67) are chosen from the GOE (3.26), with typical interaction v/\sqrt{m} between modes, with v=1 and mode number m=10. The channels (9.20) A and D in (9.67) are fixed for all realisations. Therefore, A and D are initially drawn from a Wishart ensemble (9.69), with $m_A=5$ and $m_D=10$. Data points are compared to the upper bound $J=J_{\text{max}}$ (horizontal line). The value $\lambda=m_A+m_D$ is indicated (vertical line) since it represents the typical incoherent rate as the mean eigenvalue of P=A+D (see discussion of (9.69))

In Fig. 9.2, the channel contributions A and D remain unchanged for all realisations of H, and there is definitely a significant effect on the current when the Hamiltonian is changed. However, this effect is only seen in the regime where λ is sufficiently large, i.e. $\lambda \gg m_A + m_D$ (recall that $m_A + m_D$ is the typical incoherent rate). This is logical, because in the limit $\lambda \to 0$ all influence of the coherent dynamics must vanish.

In contrast, Fig. 9.3 investigates the case where the Hamiltonian remains fixed for all random realisations of A and D. Even in the limit $\lambda \gg m_D + m_A$, and where the coherent dynamics is strongly dominant, strong fluctuations are induced by A

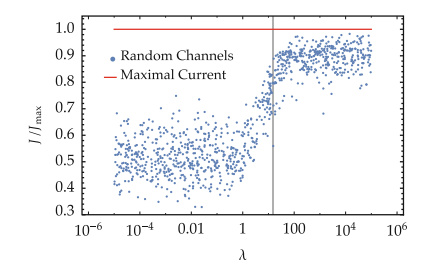


Fig. 9.3 Scatter plot which indicates the stationary current J (9.67) relative to the maximal current J_{max} (9.66). Variable λ (9.67) controls the relative strength of the Hamiltonian and of incoherent contributions; for each data point $\log_{10} \lambda$ is randomly chosen from the interval [-5, 5]. For each realisation the channels (9.20) A and D in (9.67) are drawn from a Wishart ensemble (9.69), with $m_A = 5$ and $m_D = 10$. The Hamiltonian H in (9.67) is kept fixed for all realisations and is initially chosen from the GOE (3.26) with typical interaction v/\sqrt{m} between modes, with v = 1 and mode number m = 10. Data points are compared to the upper bound $J = J_{\text{max}}$ (horizontal line). The value $\lambda = m_A + m_D$ is indicated (vertical line) since it represents the typical incoherent rate as the mean eigenvalue of P = A + D (see discussion of (9.69))

and D. When we consider (9.67), this observation makes perfect sense: even for the $\lambda \to \infty$ limit, the operators A and D still enter non-negligibly in (9.67).

It is natural to wonder whether we can identify some characteristic structure in the Hamiltonians of those realisations that provide $J \approx J_{\rm max}$. Or, more bluntly, whether one can identify design principles that can guarantee to saturate the bound $J_{\rm max}$ (9.66). Recall we achieved this objective in the fully coherent setting of Chap. 4. The following two sections provide an affirmative answer to this question in the current open system setting.

9.5 Symmetry Enhanced Current

In this section, we explain how to reach the upper bound on the fermionic current by engineering the system Hamiltonian in a clever way. However, we argued, following (9.68), that in the regime where $\lambda \to 0$ it is impossible to influence the current by tweaking the Hamiltonian, because its contribution to the dynamics is completely overshadowed by the incoherent dynamics generated by A and D. This mathematical fact was partially confirmed in Fig. 9.2. Nevertheless, in the limit where $\lambda \to 0$, we obtained a current $J_{\lambda=0}$ (9.68) which may still come close to J_{\max} (9.66) upon suitable choice of the channels contained in A and D, ¹⁷ but this limit is obviously independent of the Hamiltonian H. In other words, if we want to engineer the system Hamiltonian such that the current is optimal, while still allowing fluctuations in A and D, we must do so in the regime where λ is sufficiently large. In physical terms, this implies that

¹⁷It is actually not clear whether or not the bound J_{max} (9.66) can be saturated by $J_{\lambda=0}$ (9.68).

there are strong coherent contributions present in the dynamics and that the coherent frequencies are much higher than the rate with which they are damped.

Mathematically, this implies that the regime of interest is that where $\lambda \to \infty$, such that we can treat the problem in perturbation theory. In this limit, rapidly oscillating terms are generated in (9.67) by $\exp(-is\lambda H)$, and, as a consequence of the Riemann-Lebesgue lemma, ¹⁸ many contributions to J cancel. We first write the spectral resolution of the Hamiltonian

$$H = \sum_{k} E_k R_k. \tag{9.72}$$

Here the E_k are the eigenvalues of H and R_k the orthogonal projectors onto the associated eigenspaces. Hence

$$R_k = R_k^* = R_k^2$$
, and $\sum_k R_k = 1$. (9.73)

I first order perturbation theory and with (9.72) we can rewrite (9.67) as

$$\lim_{\lambda \to \infty} J = \lim_{\lambda \to \infty} 4 \int_0^\infty ds \operatorname{tr} \left\{ D e^{-(P+i\lambda H)s} A e^{-(P-i\lambda H)s} \right\}$$

$$= \sum_k 4 \int_0^\infty ds \operatorname{tr} \left\{ D R_k e^{-sR_k P R_k} A e^{-sR_k P R_k} R_k \right\}. \tag{9.74}$$

For given A and D, we therefore have to manipulate the R_k in order to maximise the current.

Recall that the centrosymmetry, introduced as a design principle in Sect. 4.4.1, enhanced constructive interference between network nodes which where connected through the symmetry operator (such as our input and output sites in Chap. 4). This argument motivates the introduction of a symmetry which couples the absorption to the dissipation channels and hence enhances coherent transport between them. *In concreto*, we propose to design the Hamiltonian part of the system such that it allows for a symmetry, given by a *unitary* operator *S*, such that

$$[H, S] = 0. (9.75)$$

$$\int_0^\infty \mathrm{d} s \, e^{-is\lambda} f(s) \to 0, \quad \text{as} \quad \lambda \to \infty.$$

¹⁸The proof and rigorous formulation of the theorem can be found in most standard textbooks on functional or Fourier analysis, e.g. Conway (1997), Pedersen (1989). The theorem comes in several versions, applicable to either Laplace or Fourier transformations and in essence they all contain the message: Rapidly oscillating terms vanish upon integration over a sufficiently large time interval. The version of the theorem which we require states that for any function $f \in L^1(\mathbb{R})$, we find that

In order for the symmetry to enhance the transfer, the operator *S* must also perform a specific task on the channels. In connection to Chap. 4 this implies that each absorptive channel should be partnered with a dissipative channel via the symmetry. More practically, we require

$$S^{\dagger}AS = D. \tag{9.76}$$

Even though the mechanism is clearly based on our earlier work on enhanced coherent transport, it does not grant us complete freedom in the choice of incoherent channels. In other words, the symmetry enhanced transfer does impose constraints on A and D. Furthermore, in this case, trA = trD, and, therefore, the bound (9.66) reduces to

$$J \leqslant \operatorname{tr} A. \tag{9.77}$$

To understand the effect of the symmetry, we must go back to Eq. (9.74) and use that

$$\lim_{\lambda \to \infty} J = \sum_{k} 4 \int_0^\infty \mathrm{d}s \, \mathrm{tr} \left\{ D R_k e^{-sR_k P R_k} A e^{-sR_k P R_k} R_k \right\} \tag{9.78}$$

$$= \sum_{k} 4 \int_{0}^{\infty} ds \operatorname{tr} \left\{ e^{-sR_{k}PR_{k}} R_{k} D R_{k} e^{-sR_{k}PR_{k}} A \right\}. \tag{9.79}$$

Now, we can use that S and H commute according to (9.75), what implies that $S = \bigoplus_k S_k$ is block-diagonal, with blocks living on the the eigenspaces of H. Therefore, we find that

$$\lim_{\lambda \to \infty} J = \sum_{k} 4 \int_0^\infty \mathrm{d}s \, \mathrm{tr} \left\{ e^{-sR_k P R_k} S_k^{\dagger} R_k A R_k S_k e^{-sR_k P R_k} A \right\}. \tag{9.80}$$

In the case where H is *non-degenerate*, all projectors R_k are rank-one operators. This also implies that H and S have the same eigenbasis, such that

$$S_k = e^{i\theta_k} R_k. (9.81)$$

In the limit $\lambda \to \infty$, we therefore obtain, with (9.73) and (9.48),

$$tr(DQ_{\text{NESS}}) = \sum_{k} 4 \int_{0}^{\infty} ds \, tr \left\{ e^{-sR_{k}PR_{k}} R_{k} A R_{k} e^{-sR_{k}PR_{k}} A \right\} = tr(AQ_{\text{NESS}}).$$
(9.82)

Equation (9.48) then leads to

$$\lim_{\lambda \to \infty} \operatorname{tr}(DQ_{\text{NESS}}) = \operatorname{tr} A \quad \Longrightarrow \quad \lim_{\lambda \to \infty} J = J_{\text{max}}, \tag{9.83}$$

and, thus, the bound (9.77) is saturated.

To stress the importance of the non-degeneracy of H (as assumed right after (9.80)), let us focus on the other extreme, which is mimicked by the fully degenerate case $H \sim 1$. In that case, we find ¹⁹ that

$$J = 4 \int_0^\infty ds \operatorname{tr} \left\{ D e^{-(P+i\lambda \mathbb{1})s} A e^{-(P-i\lambda \mathbb{1})s} \right\}$$

$$= 4 \int_0^\infty ds \operatorname{tr} \left\{ D e^{-Ps} A e^{-Ps} \right\}$$

$$= J_{\lambda=0},$$
(9.84)

In other words, the current will always reach the same value, independently of H. The intermediate regime between non-degeneracy and full degeneracy is much more subtle to understand. Crucial, however, is that we cannot proceed beyond step (9.82). As a rule of thumb, one may remember that all symmetries in the system must be represented in the channels. Indeed, degeneracies in H can only arise due to an additional symmetry in the system. If this symmetry also connects A to D, we can re-apply similar logic as we did for a single symmetry to proceed beyond (9.82). This is, however, a rather technical discussion, which we do not elaborate any further.

More relevant is the question at which finite value of λ are we sufficiently close to the limit $\lambda \to \infty$. In physics, limits can often be interpreted in terms of time- or energy scales which are much larger or smaller than all other characteristic scales of the system. In our specific setting, $\lambda \to \infty$ therefore means that the frequencies generated by the Hamiltonian are much faster than all other rates and frequencies in the system, which is exactly what triggered our use of the Riemann-Lebesgue lemma for the evaluation of (9.74) above. Therefore, we expect to see the saturation of the bound emerge once λ is sufficiently large as compared to the eigenvalues of A and D (which determine the other natural time scales of the system). Because the average eigenvalue of A + D is $\sim m_A + m_D$, this limit is identified as the behaviour for $\lambda \gg m_A + m_D$ (see discussion following (9.69)). We validate this intuition via numerical simulations.

In order to conduct simulations, we must make a specific choice for the symmetry operator. It is appealing to consider *centrosymmetry*, which was already central to our work in Chaps. 4 and 5. Therefore, we choose *S* a matrix such that

$$S_{i,j} = \delta_{i,m-j+1} \tag{9.85}$$

with m modes (in other words, m is the dimension of single-particle Hilbert space \mathcal{H}). Moreover, we must then sample H according to (4.61). We can still choose a random A from the Wishart ensemble (9.69), but must then construct

$$D = S^{\dagger} A S. \tag{9.76}$$

¹⁹Because 1 commutes with any operator.

²⁰To some extent, this is analogous to finding a complete set of commuting observables.

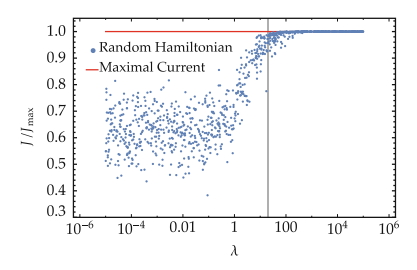


Fig. 9.4 Scatter plot which indicates the stationary current J (9.67) relative to the maximal current $J_{\rm max}$ (9.66). Variable λ (9.67) controls the relative strength of the Hamiltonian and of incoherent contributions. For each data point $\log_{10}\lambda$ is randomly chosen from the interval [-5,5]. Each realisation of the Hamiltonian H in (9.67) is chosen from the centrosymmetric GOE (4.61), with typical interaction v/\sqrt{m} between modes, with v=1 and mode number m=10. For each realisation the absorption operator A (9.20) in (9.67) is drawn from a Wishart ensemble (9.69), with $m_A=10$. The dissipation operator D is determined by condition (9.76) with (9.85). Data points are compared to the upper bound $J=J_{\rm max}$ (horizontal line). The value $\lambda=m_A+m_D$ is indicated (vertical line) since it represents the typical incoherent rate as the mean eigenvalue of P=A+D (see discussion (9.69))

When the system is designed according to these *design principles*, we find scatter plots as in Fig. 9.4: Indeed, in the regime $\lambda \gg m_A + m_D$ (which corresponds to λ significantly larger than the typical rates contained in P), all data points converge towards $J/J_{\text{max}} = 1$. In other words, the saturation regime as defined by suitably designed symmetries (9.75, 9.5), can be reached for finite λ . Let us also emphasise that centrosymmetry, the importance of which was demonstrated numerically in Chaps. 4 and 5, now plays a rigorously understood role for the enhancement of currents in the NESS. This implies that *centrosymmetry is not only relevant for transient time dynamics, it also optimises currents in the non-equilibrium steady state.*

Although it was aesthetically appealing to choose the centrosymmetry operation as a symmetry operator in (9.75, 9.76), this is certainly not the only possibility. A more generic approach is to sample the symmetry operator from the *Haar measure*. This implies that we deal with a random S, from which we can always obtain the spectral decomposition

$$S = \sum_{k=1}^{m} e^{i\theta_k} |s_k\rangle \langle s_k|. \tag{9.86}$$

We now use this decomposition as the basis for the construction of the Hamiltonian, which we define as

$$H = \sum_{k=1}^{m} e_k |s_k\rangle \langle s_k| \qquad e_k \sim \text{Uniform}([-m/2, m/2]), \tag{9.87}$$

where Uniform ([x, y]) denotes the uniform distribution of the interval [x, y]. By construction, it then follows that [H, S] = 0. The choice of the uniform distribution

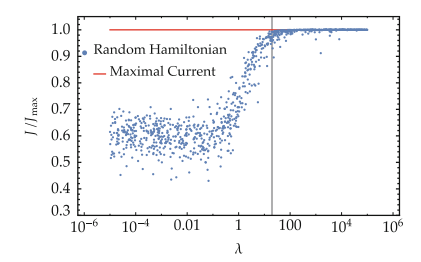


Fig. 9.5 Scatter plot which indicates the stationary current J (9.67) relative to the maximal current J_{max} (9.66). Variable λ (9.67) controls the relative strength of the Hamiltonian and of incoherent contributions. For each data point $\log_{10} \lambda$ is randomly chosen from the interval [-5, 5]. Each realisation of the Hamiltonian H in (9.67) is generated according to (9.87), with mode number m=10 and random symmetry operator S from the Haar measure (recall Sect. 8.3.5). For each realisation, the absorption operator A (9.20) in (9.67) is drawn from a Wishart ensemble (9.69), with $m_A=10$. The dissipation operator D is determined by condition (9.76). Data points are compared to the upper bound $J=J_{\text{max}}$ (horizontal line). The value $\lambda=m_A+m_D$ is indicated (vertical line) since it represents the typical incoherent rate as the mean eigenvalue of P=A+D (see discussion (9.69))

for the eigenvalues e_k is somewhat arbitrary; it simply serves to ensure that the typical level spacing is independent of the system size m.²¹ We can now again sample A from the Wishart ensemble (9.69), but we must account for the constraint (9.76) on D.

This construction provides us with a generic way to verify that the bound is saturated in the $\lambda \to \infty$ regime. Indeed, we see in Fig. 9.5 that the current approaches the bound as predicted. The procedure proposed here can be generalised to multiple symmetry operators, although this may lead to additional constraints on the channels. For the time being, we just remark that, no matter how complex the system is, the presence of one exploitable symmetry can lead to optimal currents. It remains a goal for the future to fully characterise and understand the effects of more intricate symmetries in such systems.

9.6 Dephasing Enhanced Current

Throughout Chap. 4, we noted several times that quantum effects are often not beneficial for transport, especially in the presence of disorder and randomness (recall specifically Sect. 4.3.2). In Fig. 9.1, we see that randomness in the Hamiltonian is also translated to fluctuations of the stationary current in the present setup. Neverthe-

²¹The density of states is given by $\rho = 1/m$, hence using (4.92), we find that $\Delta \approx 1/(m\rho) = 1$. Essentially this is mathematically nothing more than putting points in a box and increasing the size of the box upon increasing the number of points such that the density of points remains the same. One may then argue that for a uniform distribution also the typical distance between neighbouring points remains unchanged under such a scaling.

less, in the limit where coherent contributions can manifest themselves in the system $(\lambda \to \infty)$, we see that currents are typically larger. In contrast to Sect. 9.5, where we exploited coherent effects to our advantage by engineering the Hamiltonian, we now investigate what happens when we destroy the phase coherence in the system.

Literature (Blümel et al. 1991; Arndt et al. 1991; Cohen 1991; Stegmann et al. 2014; Scholak et al. 2010; Steck et al. 2000) teaches us that destructive quantum interference, which leads to localisation phenomena, can be suppressed by dynamical noise. Moreover, the many works (Benzi et al. 1981; Gammaitoni et al. 1998; Huelga and Plenio 2007; Wellens et al. 2004) on *stochastic resonance* indicate that noise can also be used to amplify weak periodic signals, which can be applied to the coherences of quantum systems (Wellens and Buchleitner 2000). These effects were already touched upon in Sect. 6.2, where we discussed the model of dephasing-assisted transport (Plenio and Huelga 2008). The goal of this section is to provide the first steps towards understanding the potential, but also the problems of dephasing in the model which we consider here.

9.6.1 Modelling Dephasing

In our dephasing model, we want phase information to be lost completely, thus the dephasing process must be memoryless. This implies that the framework of one-parameter semigroups and Markovian dynamics is appropriate to describe this type of dynamical noise. The generator of the dephasing dynamics is therefore also given by (9.6), and it remains for us to determine the operators L_i .

In the language of open quantum systems (Cohen-Tannoudji et al. 1998; Loudon 2000; Scully and Zubairy 1997), where one uses qubits (two-level systems or spins), dephasing is modelled by the operator $\sigma^+\sigma^-$, where σ^+ and σ^- are the raising and lowering Pauli matrices, respectively. When working with genuine spin systems, it is also common to use the σ^z Pauli matrix. The crucial assumption here is that the total energy in the system remains conserved, and only phase information is lost. A generalisation to our many-particle setup is essentially given by the condition that the number of particles in the system remains constant, while the phase information should be destroyed, effectively rendering the dynamics more classical (Brouwer and Beenakker 1997; Cohen and Imry 1999). The natural set of Lindblad operators, inspired by (Kordas et al. 2015; Scholak 2011; Manzano et al. 2012; Manzano 2013; Plenio and Huelga 2008; Witt and Mintert 2013), that satisfies these conditions is given by $\{\hat{n}(f_1), \dots \hat{n}(f_m)\}$, where we assume that $\{f_j\}$ form an orthonormal basis of the single-particle Hilbert space \mathcal{H} (which we for simplicity assume to be finite dimensional).

Let us verify that, indeed, the number of particles is conserved. First, notice that $\hat{N} = \Gamma(\mathbb{1}) = \sum_j \hat{n}(f_j)$, where any basis of \mathcal{H} can be used for the sum over local number operators. We directly verify that $[\hat{n}(f_i), \hat{n}(f_j)] = 0$, and $\hat{n}(f_i)\hat{n}(f_i) = \hat{n}(f_i)$. With these results, we insert the Lindblad operators $\hat{n}(f_j)$ in (9.3, 9.4, 9.5) and obtain that

$$\mathcal{L}^{\text{deph}}(\hat{N}) = \sum_{j} \gamma_{j} \left(\hat{n}(f_{j}) \hat{N} \hat{n}(f_{j}) - \frac{1}{2} \{ \hat{N}, \hat{n}(f_{j}) \hat{n}(f_{j}) \} \right)$$

$$= \sum_{j} \gamma_{j} \left(\hat{n}(f_{j}) \hat{N} - \hat{n}(f_{j}) \hat{N} \right) = 0$$
(9.88)

and it follows that the number of particles is conserved.

Now we consider the evolution of a general Wick monomial: We start from the simplest example, $c^*(\psi)c(\phi)$, and compute the action of a single $\hat{n}(f)$, such that

$$\mathcal{L}^{\hat{n}}(c^*(\psi)c(\phi)) = \gamma \left(\hat{n}(f)c^*(\psi)c(\phi)\hat{n}(f) - \frac{1}{2}\{c^*(\psi)c(\phi), \hat{n}(f)\}\right). \tag{9.89}$$

Analysing term after term, first we have

$$\hat{n}(f)c^{*}(\psi)c(\phi)c^{*}(f)c(f) = \langle \phi, f \rangle \hat{n}(f)c^{*}(\psi)c(f) + \hat{n}(f)c^{*}(f)c^{*}(\psi)c(\phi)c(f)$$

$$= \langle \phi, f \rangle \hat{n}(f)c^{*}(\psi)c(f) - \langle f, \psi \rangle \hat{n}(f)c^{*}(f)c(\phi) + \hat{n}(f)c^{*}(\psi)c(\phi)$$

$$= \langle f, \psi \rangle \langle \phi, f \rangle \hat{n}(f) - \langle f, \psi \rangle c^{*}(f)c(\phi) + \hat{n}(f)c^{*}(\psi)c(\phi),$$

$$(9.90)$$

and, secondly,

$$c^*(\psi)c(\phi)\hat{n}(f) = c^*(\psi)c(\phi)c^*(f)c(f)$$

$$= \langle \phi, f \rangle c^*(\psi)c(f) - \langle f, \psi \rangle c^*(f)c(\phi) + \hat{n}(f)c^*(\psi)c(\phi). \tag{9.91}$$

Equations (9.90, 9.91) in (9.89) yield

$$\mathcal{L}^{\hat{n}}(c^*(\psi)c(\phi)) = \gamma \left(\langle f, \psi \rangle \langle \phi, f \rangle \, \hat{n}(f) - \frac{1}{2} \langle f, \psi \rangle \, c^*(f)c(\phi) - \frac{1}{2} \langle \phi, f \rangle \, c^*(\psi)c(f) \right). \tag{9.92}$$

We can now define a dephasing operator $F \in \mathcal{B}(\mathcal{H})$ just as we defined A and D earlier:

$$F = \sum_{j} \frac{\gamma_{j}}{2} |f_{j}\rangle\langle f_{j}|. \tag{9.93}$$

With this, we rewrite the generator (9.88) as

$$\mathcal{L}^{\text{deph}}(c^*(\psi)c(\phi)) = -c^*(F\psi)c(\phi) - c^*(\psi)c(F\phi) + \sum_j \gamma_j \langle f_j, \psi \rangle \langle \phi, f_j \rangle \hat{n}(f_j).$$
(9.94)

The dynamics as described by (9.94) can be generalised in a straightforward manner to higher order monomials as

$$\mathcal{L}^{\text{deph}}(c^{*}(\phi_{1})\dots c^{*}(\phi_{n})c(\phi_{n+1})\dots c(\phi_{n+m}))$$

$$= -\sum_{k=1}^{n+m} \left(\prod_{j=1}^{k-1} c^{\#}(\phi_{j})\right) c^{\#}(F\phi_{k}) \left(\prod_{j'=k+1}^{n+m} c^{\#}(\phi_{j'})\right)$$

$$+ \sum_{i} \sum_{k=1}^{n} \sum_{l=n+1}^{m+n} \gamma_{i} \langle f_{i}, \phi_{k} \rangle \langle \phi_{l}, f_{i} \rangle \left(\prod_{j_{1}=1}^{k-1} c^{*}(\phi_{j_{1}})\right) c^{*}(f_{i})$$

$$\times \left(\prod_{j_{2}=k+1}^{l-1} c^{\#}(\phi_{j_{2}})\right) c(f_{i}) \left(\prod_{j_{3}=l+1}^{n+m} c(\phi_{j_{3}})\right),$$
(9.95)

where $\{k, l\}$ run over all the possible pairs of creation and annihilation operators.

In the remainder of the this section we choose to focus on the dynamics on single-particle observables, in analogy to Sect. 9.3. First, we consider the action of the generator (9.94) on a general single-particle observable $\Gamma(B)$ (9.23), $B \in \mathcal{T}(\mathcal{H})$:

$$\mathcal{L}^{\text{deph}}(\Gamma(B)) = -\Gamma(\{B, F\}) + \sum_{i} \gamma_i \langle f_i, Bf_i \rangle \Gamma(|f_i\rangle \langle f_i|), \qquad (9.96)$$

such that, for whichever state ω , we can use (9.32) to write that

$$\omega \circ \mathcal{L}^{\text{deph}}(\Gamma(B)) = -\text{tr}(\{B, F\}Q) + \sum_{i} \gamma_i \langle f_i, Bf_i \rangle \langle f_i, Qf_i \rangle. \tag{9.97}$$

Because $\hat{N} = \Gamma(1)$, (9.97) implies that $\omega \circ \mathcal{L}^{\text{deph}}(\hat{N}) = 0$. Due to the conservation of the total particle number, dephasing alone cannot induce a global particle current.²²

The complete dynamics, subject to dissipation, absorption, dephasing, and coherent dynamics, is, nevertheless, affected by the dephasing and so are the resulting stationary currents. Indeed, with (9.25, 9.96) the general dynamics (9.6) for a single-particle observable $\Gamma(B)$, $B \in \mathcal{T}(\mathcal{H})$, now reduces to

$$\frac{\mathrm{d}}{\mathrm{d}t}\Gamma(B) = i[\Gamma(H), \Gamma(B)] + \mathcal{L}^{d}(\Gamma(B)) + \mathcal{L}^{a}(\Gamma(B)) + \mathcal{L}^{\mathrm{deph}}(\Gamma(B))$$

$$= \Gamma\left(i[H, B] - \{A + D + F, B\} + \sum_{i} \gamma_{i} \langle f_{i}, Bf_{i} \rangle |f_{i} \rangle \langle f_{i}|\right) + \left(2\operatorname{tr} BA\right)\mathbf{1}.$$
(9.98)

These equations can be solved with the help of the methods described in Sect. 9.3.1, and we find that the mapping of any single-particle observable $\Gamma(B_0)$, $B_0 \in \mathcal{T}(\mathcal{H})$, is given by

$$\Lambda_t(\Gamma(B_0)) = \Gamma(B(t)) + z(t)\mathbf{1},\tag{9.99}$$

where B(t) and z(t) are solutions of the following set of equations:

²²Recall that, in Sect. 9.3.4, we introduced the global particle current as a flux of particles in and out of the system, induced by a generator. No such flux is induced by the dephasing generator.

$$\dot{B}(t) = i[H, B] - \{A + D + F, B\} + \sum_{i} \gamma_{i} \langle f_{i}, Bf_{i} \rangle |f_{i}\rangle \langle f_{i}|, \qquad (9.100)$$

$$z(t) = \int_0^t ds \, \text{tr} \{B(s)A\},\tag{9.101}$$

$$z(t=0) = 0, B(t=0) = B_0.$$
 (9.102)

We now formally define a super-operator \mathcal{D} , acting on $\mathcal{B}(\mathcal{H})$, such that

$$\mathcal{D}(B) := i[H, B] - \{A + D + F, B\} + \sum_{i} \gamma_{i} \langle f_{i}, B f_{i} \rangle |f_{i}\rangle \langle f_{i}|, \qquad (9.103)$$

which leads to the formal solution of (9.100):

$$B(t) = e^{t\mathcal{D}} B_0. \tag{9.104}$$

In the limit $t \to \infty$, we then generically²³ find that

$$\omega_{\text{NESS}}(\Gamma(B_0)) = \left(\omega \circ \lim_{t \to \infty} \Lambda_t\right) (\Gamma(B_0)) = 2 \int_0^\infty ds \, \text{tr} \left\{ A e^{s\mathcal{D}} B_0 \right\}
= 2 \text{tr} \left\{ B_0 \int_0^\infty ds \, e^{s\mathcal{D}^{\dagger}} A \right\}
:= \text{tr}(B_0 Q_{\text{NESS}}).$$
(9.105)

Let us now use the identity of (9.55) to rewrite

$$Q_{\text{NESS}} = \int_0^\infty ds \ e^{s\mathcal{D}^{\dagger}} 2A = -\mathcal{D}^{\dagger^{-1}}(2A).$$
 (9.106)

Hence, with (9.103), Q_{NESS} can be interpreted as a solution of the equation

$$\mathcal{D}^{\dagger}(Q_{\text{NESS}}) + 2A = 0, \tag{9.107}$$

which can be rewritten, with P = A + D from (9.25), as

$$-i[H, Q_{\text{NESS}}] - \{P + F, Q_{\text{NESS}}\} + \sum_{i} \gamma_i \langle f_i, Q_{\text{NESS}} f_i \rangle |f_i\rangle \langle f_i| + 2A = 0.$$
(9.108)

Because we are not directly aware of an explicit and general solution to this equation, we resort to numerics for any specific choice of Hamiltonian, and of the absorption-,

²³ Again, this is a mathematical statement, intended to indicate that the result does not hold for some pathological cases where decoherence-free subspaces are present. The set of systems for which the result does not hold is, however, mathematically negligible. In this sense we can say that this result holds for almost all systems.

dissipation- and dephasing channels. However, once we know $Q_{\rm NESS}$, we can use it to investigate the current. Indeed, we find that the continuity equation (9.40) still reads

$$\omega_{\text{NESS}} \circ \mathcal{L}(\Gamma(1)) = 0, \tag{9.109}$$

which, in combination with (9.25, 9.96), again leads to the equation

$$2\operatorname{tr} DQ_{\text{NESS}} = 2\operatorname{tr} \left(A - \operatorname{tr} AQ_{\text{NESS}} \right). \tag{9.110}$$

The latter expresses a balance between total incoming and total outgoing current. Therefore, we can again define

$$J = 2 \operatorname{tr} D Q_{\text{NESS}}, \tag{9.111}$$

where $Q_{\rm NESS}$ now obeys Eq. (9.108). Because we used the explicit form of $Q_{\rm NESS}$ in the proof of (9.66), it is not obvious that the obtained bound is still valid. We *conjecture* that the proof can be adjusted, with the redefinition

$$\mathcal{G}(X) := -i[H, X] + \{P + F, X\} - \sum_{i} \gamma_{i} \langle f_{i}, X f_{i} \rangle |f_{i}\rangle \langle f_{i}| \qquad (9.112)$$

in (9.52). However, we were unable to prove inequality (9.57) for (9.112).

To numerically assess the effect of dephasing, we consider the case where $\gamma_i = \gamma$ for all i. This gives rise to an overall dephasing which is the same for every mode in the specific dephasing basis.

9.6.2 Numerical Results

Our numerical data are again generated from random matrix ensembles. We sample H from the GOE (3.26), and A and D from the Wishart ensemble (9.69). With $\gamma_i = \gamma$, the dephasing operator (9.93) takes the form

$$F = \sum_{i} \frac{\gamma}{2} |f_i\rangle \langle f_i| = \frac{\gamma}{2} \mathbb{1}.$$
 (9.113)

Nevertheless, in (9.98) we find a second term which contributes to the specific dephasing dynamics:

$$\gamma \sum_{i} \langle f_i, Q_{\text{NESS}} f_i \rangle | f_i \rangle \langle f_i |$$
.

Therefore, even though F in (9.113) does not depend on the specific dephasing basis, the full generator (9.98) of the dynamics does. We must, thus, make a specific choice for the basis vectors $f_i \in \mathcal{H}$. Because we want to make an "unbiased" choice, we resort to the choice of a random basis. Inspired by Zyczkowski and Sommers (2001), we select random bases by sampling a unitary matrix from the *Haar measure*. We start with the standard basis $\{e_i\}$ of single-particle Hilbert space \mathcal{H} and act on it with the random U. The set $\{Ue_i\}$ now forms a new, orthonormal basis of \mathcal{H} . The basis $\{Ue_i\}$ naturally inherits statistical properties of the Haar measure. Recause $\{e_i\}$ is the standard basis, we can associate the vector $Ue_i := f_i$ with the ith column of U:

$$U = \begin{pmatrix} | & | & | \\ f_1 & f_2 & \dots & f_N \\ | & | & | \end{pmatrix}. \tag{9.114}$$

These $\{f_i\}$ will form a random dephasing basis in every realisation, such that we can rewrite (9.108) as

$$-i\lambda[H, Q_{\text{NESS}}] - \left\{P + \frac{\gamma}{2}\mathbb{1}, Q_{\text{NESS}}\right\} + \gamma \sum_{i} \langle f_i, Q_{\text{NESS}} f_i \rangle |f_i\rangle \langle f_i| + 2A = 0.$$

$$(9.115)$$

Equation (9.115) defines a linear system of equations, with the components of $Q_{\rm NESS}$ the unknowns, and can be solved numerically. The resulting $Q_{\rm NESS}$ are then inserted in the definition (9.111) of J, to produce the data shown in Figs. 9.6 and 9.7. Figure 9.6, is obtained for a uniform distribution of $\log_{10} \lambda \in [-5.5,]$ and shows the distribution of $J/J_{\rm max}$ as function of the dephasing strength. We observe that dephasing in a randomly selected basis enhances the current once the dephasing rate γ is sufficiently large. For the parameters in Fig. 9.6, the enhancement is pronounced from $\gamma \sim 100$ onwards, which suggests that $\gamma \gg m_A + m_D$ is a relevant limit, independently of the values of λ . We note that, based on these simulations, we cannot falsify the conjecture that the bound (9.66) still holds in the presence of dephasing.

When we include the information on λ in Fig. 9.7, we see that, mainly in the regime where λ , $\gamma \gg m_A + m_D$, the realisations really reach the bound J_{max} . Thus there is a benefit when combining coherent effects with a rather strong degree of dephasing noise. One would of course expect naively that the dephasing destroys all coherent effects on the long time scales which we consider. However, the presence of the absorptive channel can be understood as a type of driving. Particles are constantly being pumped into the system, which may counteract the destruction of coherence.

²⁴Note that we are not specifically interested in the statistical properties of the thus generated vectors. We here use random matrix ensembles as a tool to probe many different systems with no specific symmetries built in.

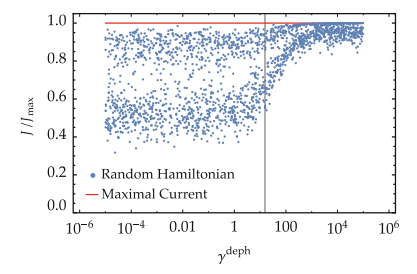


Fig. 9.6 Scatter plot which indicates the stationary current J (9.111, 9.115) relative to the maximal current J_{\max} (9.66). Data points are compared to the upper bound $J = J_{\max}$ (horizontal line). Every realisation corresponds to a randomly chosen dephasing rate γ , dephasing basis $\{f_i\}$, Hamiltonian H, channels A and D, and coherence strength λ : γ , λ in (9.115) are chosen randomly such that $\log_{10} \lambda$, $\log_{10} \gamma \in [-5, 5]$ are distributed uniformly. H in (9.115) is selected from the GOE (3.26) with typical interaction v/\sqrt{m} between modes, with v=1 and mode number m=10, and the channels (9.20) A and D in (9.111,9.115) are drawn from a Wishart ensemble (9.69), with $m_A=5$ and $m_D=10$. For each data point the dephasing takes place in a randomly chosen basis, generated via the Haar measure (9.114). J is obtained by numerically solving (9.115) to obtain $Q_{\rm NESS}$, which can be inserted in (9.111). The value $\gamma=m_A+m_D$ is indicated (vertical line) since it represents the typical incoherent rate associated with the channels as the mean eigenvalue of P=A+D (see discussion of (9.69))

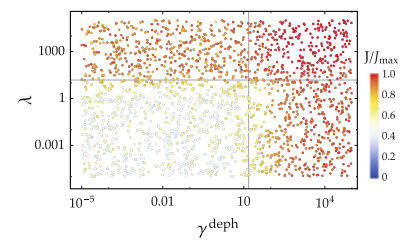


Fig. 9.7 Scatter plot which indicates the coherence strength λ (9.115), the dephasing rate γ (9.115), and the stationary current J (colour code; 9.111, 9.115) relative to the maximal current J_{max} (9.66). Variables λ , γ are randomly chosen such that $\log_{10} \lambda$ and $\log_{10} \gamma$ are uniformly distributed over the interval [-5, 5]. For each realisation, the Hamiltonian H in (9.115) is chosen from the GOE (3.26), with typical interaction v/\sqrt{m} between modes, with v=1 and mode number m=10, and the channels (9.20) A and D in (9.111,9.115) are drawn from a Wishart ensemble (9.69), with $m_A=5$ and $m_D=10$. The dephasing takes place in a random basis, generated via the Haar measure (9.114). J is obtained by numerically solving (9.115) to obtain Q_{NESS} , which can be inserted in (9.111). The value λ , $\gamma=m_A+m_D$ is indicated (grey lines) since it represents the typical incoherent rate associated with the channels as the mean eigenvalue of P=A+D (see discussion (9.69)). This figure was generated from the same data as Fig. 9.6

With the results of Figs. 9.6 and 9.7 we numerically demonstrated the mechanism of dephasing enhanced currents. However, the underlying physical principles responsible for this enhancement remain unclear to us.

9.6.3 Quasi-Free and Dephasing Maps*

We end our section on dephasing dynamics with an observation which was made during the development of our dephasing model. In what follows, we identify an open problem which is specifically interesting from the mathematical point of view.

First, we briefly introduce a result which proves that the dynamics induced by (9.21) and (9.22) maps quasi-free states (recall Sect. 7.7.1) into quasi-free states.

This result is a corollary of the characterisation (Dierckx et al. 2008) of general quasi-free channels $\mathcal{G}_{R,S}$, mapping $\mathcal{A}^{CAR}(\mathcal{H})$ on $\mathcal{A}^{CAR}(\mathcal{K})$ (defined in the Heisenberg picture, with \mathcal{K} another single-particle Hilbert space). It was proven (Dierckx et al. 2008) that such maps always have the following structure: The parameters R and S are linear operators such that

$$R: \mathcal{H} \to \mathcal{K},$$
 (9.116)

$$S: \mathcal{H} \to \mathcal{H},$$
 (9.117)

$$0 \leqslant S \leqslant \mathbb{1} - R^{\dagger} R. \tag{9.118}$$

The action of the map itself on normally ordered Wick monomials is given (Dierckx et al. 2008) by

$$\mathcal{G}_{R,S}\left(c^{*}(\phi_{1})\dots c^{*}(\phi_{n})c(\psi_{m})\dots c(\psi_{1})\right)
= \sum_{p_{1},p_{2}} \epsilon_{1}\epsilon_{2}\omega_{S}\left(c^{*}(\phi_{k_{1}})\dots c^{*}(\phi_{k_{r}})c(\psi_{l_{r}})\dots c(\psi_{l_{1}})\right)
\times c^{*}(R\phi_{i_{1}})\dots c^{*}(R\phi_{i_{n-r}})c(R\psi_{i_{n-r}})\dots c(R\psi_{i_{1}}),$$
(9.119)

where $p_1 = \{\{i_1, \ldots, i_{n-r}\}, \{k_1, \ldots, k_r\}\}$ is a partition of $\{1, \ldots, n\}$ and $p_2 = \{\{j_1, \ldots, j_{m-r}\}, \{l_1, \ldots, l_r\}\}$ is a partition of $\{1, \ldots, m\}$. Because we are dealing with fermions, sign-bookkeeping is necessary and therefore the factors ϵ_1 and ϵ_2 describe the signs of the permutations associated with p_1 and p_2 , respectively.

Whenever a mapping in the Heisenberg picture is given by (9.119), with conditions (9.116–9.118), the expectation value of $x \in \mathcal{A}^{CAR}(\mathcal{H})$, after transmision through the channel, in the quasi-free state $\omega_{\mathcal{Q}}(\mathcal{G}_{R,S}(x))$, can be written as $\omega_{\mathcal{Q}'}(x)$. The map is quasi-free because $\omega_{\mathcal{Q}'}$ is again a quasi-free state. Our dynamical map generated by (9.21) and (9.22) obeys these conditions and leads to

$$R = e^{t(iH - A - D)}$$
 and $S = 2 \int_0^t ds \ e^{s(iH - A - D)} A e^{s(-iH - A - D)},$ (9.120)

and, therefore, the channel is indeed quasi-free. ²⁵

²⁵A more extended discussion on the dynamics of quasi-free states in systems with absorption and dissipation was already provided in Davies 1977a.

The dephasing dynamics is interesting because it does not blow up the order in creation and annihilation operators, whereas, according to (9.119), it is *not* a quasifree map. The second term in (9.95), which prevents it from being cast in the form (9.119), destroys the quasi-free behaviour and makes sure that quasi-free states are not mapped into other quasi-free states. To the best of our knowledge these dephasing-type maps have not yet been characterised in a similar way as (9.119) characterises the quasi-free maps. However, the fact that the order of creation and annihilation operators remains conserved suggests intuitively that some analytical understanding of the properties of such maps may be within reach.

9.7 Bosonic Systems

In Davies (1977a), the author mentions that one can construct a similar model for the bosonic algebra of canonical commutation relations (CCR; recall Sect. 7.7.2). Even though this is formally correct, there are aspects that need to be taken into account.

A profound difference which we noted in Sect. 7.7.2 is that we cannot define bosonic creation and annihilation operators independently of the representation. Recall that for the CAR algebra such a procedure is possible as we explicitly showed in (7.211)–(7.213). This implies that we must construct our model in a specific representation, induced by any initial state ω . Nevertheless, in analogy to Sect. 9.3.3 we limit ourselves to states which are normal with respect to the bosonic Fock representation (Bratteli and Robinson 1997; Petz 1990), such that we avoid additional technical difficulties.

Let us start by recalling the Fock representation of the CCR algebra on a single-particle Hilbert space \mathcal{H} , as given by the GNS construction (7.295)

$$(\pi_{\Gamma}, \Omega_{\Gamma}, \Gamma(\mathcal{H})),$$
 (7.295)

and in this representation consider the creation and annihilation operators (7.296, 7.297):²⁶

$$[a(\phi), a^{\dagger}(\psi)] = \langle \phi, \psi \rangle \, \mathbb{1}, \quad [a(\phi), a(\psi)] = 0, \tag{7.296}$$

$$a(\psi)\Omega_{\Gamma} = 0. \tag{7.297}$$

With these creation and annihilation operators, we recall (7.92) in Sect. 7.5 and write a single-particle observable as

²⁶Because we always remain in the Fock representation, we denote the creation and annihilation operators as $a^{\#}(\psi)$ rather than $a_{\Gamma}^{\#}(\psi)$.

$$\Gamma(B) = \sum_{i,j} \langle \eta_i, B \eta_j \rangle a^{\dagger}(\eta_i) a(\eta_j), \qquad (9.121)$$

with $\{\eta_j\}$ an orthonormal basis of the single-particle Hilbert space \mathcal{H} . The normal states ω (with respect to the Fock representation) on the CCR can be represented as a density matrix ρ_{ω} which acts on the Fock space $\Gamma(\mathcal{H})$ and fulfils the condition:

$$\omega(\hat{N}) = \operatorname{tr}(\rho_{\omega} \Gamma(\mathbb{1})) < \infty. \tag{9.122}$$

We must note that the notation is not completely rigorous, since $\Gamma(1)$ is an unbounded operator.²⁷

For dynamics to be well-defined, we must make sure that we remain within the Fock representation. In terms of the dynamical map Λ_t which governs the dynamics, this implies the requirement

$$\operatorname{tr}\left(\rho_{\omega}\Lambda_{t}(\hat{N})\right) < \infty, \quad \text{for all } t > 0.$$
 (9.123)

In analogy to the fermionic case, let us describe our model in terms of the master equation²⁸

$$\frac{\mathrm{d}}{\mathrm{d}t}X = -i[\Gamma(H), X] + \mathcal{L}^{a}(X) + \mathcal{L}^{d}(X), \quad \text{for all } X \in \mathrm{Lin}(\Gamma(\mathcal{H})),$$
with
$$\mathcal{L}^{a/d}(X) = \sum_{i} L_{i}^{a/d^{\dagger}} X L_{i}^{a/d} - \frac{1}{2} \{ L_{i}^{a/d^{\dagger}} L_{i}^{a/d}, X \},$$
(9.124)

such that it remains to choose L_i under the constraint that the dynamics forms a completely positive map.

Assume that we again study dissipation and absorption mediated by $L_i^d = \sqrt{\gamma_i^d} a(\delta_i)$ and $L_i^a = \sqrt{\gamma_i^a} a^\dagger(\alpha_i)$, respectively. Let us note that, because the $L_i^{a,d}$ are unbounded, they are not captured by Lindblad's work (Lindblad 1976). Semigroups with unbounded operators have nevertheless been treated successfully in Davies (1977b) and this specific model, (9.124) with L_i^a and L_i^d as chosen here, was already studied in Alicki (1987, 1978). Alicki explicitly derives the model from hamiltonian principles and connects it to the framework of dynamical semigroups, hence we do not elaborate on these matters here. We will, however, reduce the generator to a simpler form for single-particle observables, in analogy to Sect. 9.3.1 and Alicki (1987, 1978). This allows us to obtain the specific constraint (9.144) for the generators, in order to satisfy (9.123).

 $^{^{27}}$ A slightly more formal statement would be that ρ_{ω} is contained within the domain of $\Gamma(1)$. A more elegant definition of a state on the CCR algebra which is normal with respect to the Fock representation is contained in Theorem 5.2.14 in Bratteli and Robinson (1997), although it also requires more mathematical background.

²⁸We define this equation for all linear operators on Fock space, a set which we denote $\text{Lin}(\Gamma(\mathcal{H}))$.

Considering the action of the generator \mathcal{L}^d (9.124) associated with one single L_i^d on $a^{\dagger}(\psi)a(\phi)$, we find that

$$\mathcal{L}^{d}\left(a^{\dagger}(\psi)a(\phi)\right) = \gamma^{d}\left(a^{\dagger}(\delta)a^{\dagger}(\psi)a(\phi)a(\delta) - \frac{1}{2}\left\{a^{\dagger}(\delta)a(\delta), a^{\dagger}(\psi)a(\phi)\right\}\right),\tag{9.125}$$

which we rewrite, term by term as

$$a^{\dagger}(\delta)a(\delta)a^{\dagger}(\psi)a(\phi) = \langle \delta, \psi \rangle a^{\dagger}(\delta)a(\phi) + a^{\dagger}(\delta)a^{\dagger}(\psi)a(\phi)a(\delta), \qquad (9.126)$$

$$a^{\dagger}(\psi)a(\phi)a^{\dagger}(\delta)a(\delta) = \langle \phi, \delta \rangle a^{\dagger}(\psi)a(\delta) + a^{\dagger}(\delta)a^{\dagger}(\psi)a(\phi)a(\delta). \tag{9.127}$$

These terms in (9.125) result in

$$\mathcal{L}^{d}(a^{\dagger}(\psi)a(\phi)) = -\frac{\gamma^{d}}{2} \langle \delta, \psi \rangle a^{\dagger}(\delta)a(\phi) - \langle \phi, \delta \rangle a^{\dagger}(\psi)a(\delta), \qquad (9.128)$$

which exactly reproduces expression (9.9), because we had there picked up an even number of extra minus signs as compared to (9.128). A very similar computation can be performed for the absorption part, acting on the element $a(\phi)a^{\dagger}(\psi)$, and leads to

$$\mathcal{L}^{a}(a(\phi)a^{\dagger}(\psi)) = \gamma^{a}(a(\alpha)a(\phi)a^{\dagger}(\psi)a^{\dagger}(\alpha) - \frac{1}{2}\{a(\alpha)a^{\dagger}(\alpha), a(\phi)a^{\dagger}(\psi)\}). \tag{9.129}$$

With

$$a(\alpha)a^{\dagger}(\alpha)a(\phi)a^{\dagger}(\psi) = -\langle \phi, \alpha \rangle a(\alpha)a^{\dagger}(\psi) + a(\alpha)a(\phi)a^{\dagger}(\psi)a^{\dagger}(\alpha), \quad (9.130)$$

$$a(\phi)a^{\dagger}(\psi)a(\alpha)a^{\dagger}(\alpha) = -\langle \alpha, \psi \rangle a(\phi)a^{\dagger}(\alpha) + a(\alpha)a(\phi)a^{\dagger}(\psi)a^{\dagger}(\alpha), \quad (9.131)$$

Equation (9.129) turns into

$$\mathcal{L}^{a}(a(\phi)a^{\dagger}(\psi)) = \frac{\gamma^{a}}{2} \langle \phi, \alpha \rangle a(\alpha)a^{\dagger}(\psi) + \frac{\gamma^{a}}{2} \langle \alpha, \psi \rangle a(\phi)a^{\dagger}(\alpha). \tag{9.132}$$

Again, to merge absorptive and dissipative parts in one generator, we need to derive the action of one generator \mathcal{L}^a on $a^{\dagger}(\psi)a(\phi)$ from (9.132). With (7.296), we obtain:

$$\mathcal{L}^{a}(a^{\dagger}(\psi)a(\phi)) = -\langle \phi, \psi \rangle \mathcal{L}^{a}(1) + \mathcal{L}^{a}(a(\phi)a^{\dagger}(\psi))$$

$$= \mathcal{L}^{a}(a(\phi)a^{\dagger}(\psi))$$

$$= \frac{\gamma^{a}}{2} \langle \phi, \alpha \rangle a(\alpha)a^{\dagger}(\psi) + \frac{\gamma^{a}}{2} \langle \alpha, \psi \rangle a(\phi)a^{\dagger}(\alpha)$$

$$= \frac{\gamma^{a}}{2} \langle \phi, \alpha \rangle a^{\dagger}(\psi)a(\alpha) + \frac{\gamma^{a}}{2} \langle \alpha, \psi \rangle a^{\dagger}(\alpha)a(\phi) + \gamma^{a} \langle \phi, \alpha \rangle \langle \alpha, \psi \rangle.$$

$$(9.133)$$

Notice that the expression of \mathcal{L}^a only minimally differs from the fermionic case (9.17): The first two terms in the final step of (9.133) are positive, whereas their

fermionic counterparts in (9.17) are negative. The full generator, with the identical A and D as earlier in (9.20), is thus given by

$$\mathcal{L}(a^{\dagger}(\phi)a(\psi)) = a^{\dagger}((iH - D + A\phi)a(\psi) + a^{\dagger}(\phi)a((iH - D + A)\psi) + 2\langle\phi, A\psi\rangle\mathbf{1}$$

$$= a^{\dagger}((iH - P\phi)a(\psi) + a^{\dagger}(\phi)a((iH - P)\psi) + 2\langle\phi, A\psi\rangle\mathbf{1},$$
(9.134)

where in the present bosonic case P is defined as

$$P := D - A. (9.135)$$

Apart from a difference in the definition of P (compare (9.25)), the bosonic dynamics is exactly the same as that of fermions. The different definition of P however has profound impact: We know that $A \ge 0$ and $D \ge 0$, but this no longer implies that P remains positive semi-definite, as was the case for fermions.

By virtue of (9.121, 9.134) the dynamics of a single-particle observable $\Gamma(B)$ for $B \in \mathcal{B}(\mathcal{H})$ is given by

$$\frac{\mathrm{d}}{\mathrm{d}t}\Gamma(B) = \Gamma\Big(i[H,B] - \{P,B\}\Big) + 2\mathrm{tr}(AB)\mathbf{1},\tag{9.136}$$

which can be solved using the same methods as in the fermionic case (recall Sect. 9.3.1 and (9.28)–(9.30)), to find

$$\dot{B}(t) = i[H, B(t)] + \{P, B(t)\}, \tag{9.137}$$

$$\dot{z}(t) = 2\operatorname{tr}(AB(t)),\tag{9.138}$$

$$z(t=0) = z_0$$
 and $B(t=0) = B_0$, (9.139)

with a final solution of the form

$$\Lambda_t(\Gamma(B_0)) = \Gamma\left(e^{t(iH-P)}B_0e^{t(-iH-P)}\right) + \text{tr}\left(\int_0^t ds \ 2Ae^{(iH-P)s}B_0e^{(-iH-P)s}\right)\mathbf{1}.$$
(9.140)

For any normal state ω (with respect to the Fock representation), we can consider the induced sesquilinear form on $\mathcal H$

$$\operatorname{tr}(\rho_{\omega}a^{\dagger}(\psi)a(\phi)) := \langle \psi, Q\phi \rangle \tag{9.141}$$

which defines $Q \in \mathcal{T}(\mathcal{H})$. The fact that ω is a normal state in the Fock representation directly implies that Q is trace-class, ergo tr $Q < \infty$. It now directly follows from (9.121) that

$$\operatorname{tr}(\rho_{\omega}\Gamma(B)) = \operatorname{tr}(QB),$$
 (9.142)

where we stress that the trace on the right hand side runs over the single-particle Hilbert space \mathcal{H} and the trace on the left hand side over the Fock space $\Gamma(\mathcal{H})$. We thus find

$$\left(\omega \circ \Lambda_{t}\right)(\Gamma(B_{0})) = \operatorname{tr}\left(Qe^{t(iH-P)}B_{0}e^{t(-iH-P)} + \int_{0}^{t} \operatorname{d}s \ 2Ae^{(iH-P)s}B_{0}e^{(-iH-P)s}\right). \tag{9.143}$$

In the fermionic case (see discussion on p. 382), we then used that generically P>0, such that the first term on the right hand side of (9.34) disappears and the second term is bounded. However, in absence of any further restrictions for the bosonic case, with P=D-A, the analogous expression (9.143) may diverge in the limit $t\to\infty$. In other words, the condition (9.123) is violated at $t\to\infty$. This does not necessarily mean that this corresponds to a physical problem, but it does defy the validity of the mathematical model. Fock space is simply too small to describe infinitely many particles in an accurate way. In other words, we need to dissipate at least as strongly as we pump particles in to keep the particle number from tending towards infinity. This is the only way to remain in the Fock space representation. Hence, for the dynamics to be well-defined we must impose the condition

$$P \geqslant 0 \iff D \geqslant A. \tag{9.144}$$

It is no surprise that we encounter the above type of problems: Bosons have the property that many particles can occupy the same mode and e.g. form a BEC (Anderson et al. 1995; Davis et al. 1995; Verbeure 2011). This problem is similar to the subtleties encountered for fermions in an infinitely large single-particle Hilbert space as discussed in Sect. 9.3.3. Nevertheless, a violation of (9.144) for bosons leads to more fundamental problems since the system will simply never reach a steady state. Moreover, in Sect. 9.3.3 we argued that infinitely large fermionic systems at least allow for local control. When we abandon restriction (9.144), it appears that even such local control of the system is unfeasible. Of course one may argue that in a BEC, there are also macroscopically occupied states and that a violation of (9.144) leads to a non-equilibrium BEC, comparable to Vorberg et al. (2013). However, upon studying Bose–Einstein condensation in a well-defined setting (Bratteli and Robinson 1997; Verbeure 2011), we encounter the condition that at least the density of particles in any mode must remain finite. Because a violation of (9.144) can lead to modes where the local particle number grows exponentially in time, ²⁹ we can argue

$$\left(\omega \circ \Lambda_t\right)(\hat{N}) = q e^{-2t(\gamma^d - \gamma^a)} + \int_0^t \mathrm{d}s \ 2\gamma^a e^{-2t(\gamma^d - \gamma^a)}, \tag{9.145}$$

where q is the initial particle number, and γ^d and γ^a the dissipation and absorption rates, respectively. We clearly see a problem for $\gamma^a > \gamma^d$ as time grows. It is not difficult to see that this problem

²⁹Let us briefly present the simplest example imaginable: We consider a harmonic oscillator, i.e. a one-mode bosonic system. Expression (9.143) for the number operator $\hat{N} = \Gamma(1)$ reduces to

that one must be extremely careful since the setup may even be unphysical. Let us proceed under the assumption that (9.144) is fulfilled.

We can again investigate the particle current by setting the single-particle observable $\Gamma(B_0) = \Gamma(\mathbb{1}) = \hat{N}$ in (9.143), such that we study the dynamics of the number operator. The current in the non-equilibrium steady state is determined by (recall (9.40) and our discussion in Sect. 9.3.4)

$$\lim_{t \to \infty} \omega \circ \mathcal{L}(\Gamma(1)) = 0, \tag{9.146}$$

which, with (9.136), leads to

$$-\operatorname{tr}(\{P, Q_{\text{NESS}}\}) + 2\operatorname{tr}(A) = 0, \tag{9.147}$$

which, with the definition (9.135) of P, can be rewritten as

$$2\operatorname{tr}(DQ_{\text{NESS}}) = 2\Big(\operatorname{tr}(A) + \operatorname{tr}(Q_{\text{NESS}}A)\Big). \tag{9.148}$$

Following the same logic as in the fermionic case (see Sect. 9.3.4), combined with the explicit requirement (9.144) $P \ge 0$, we find

$$Q_{\text{NESS}} = 2 \int_0^\infty ds \, e^{(-iH - P)s} A e^{(iH - P)s}, \qquad (9.149)$$

and, therefore,

$$J := 4 \int_0^\infty ds \, \text{tr} \Big\{ e^{(-iH - P)s} A e^{(iH - P)s} D \Big\}, \tag{9.150}$$

which is formally identical to the fermionic expression (9.50), though with a different definition (9.135) for P. Nevertheless, the main property of P, its positive semi-definiteness must be imposed by (9.144), and, therefore, the "fermionic" proof of Sect. 9.4 on the bound of J remains applicable, apart from the last step: We can still define the symmetrised Duhamel product (9.58), and we can still use (9.60). We still find that

$$\langle A, P \rangle_{\sim} = \text{tr}A, \tag{9.151}$$

$$\langle P, P \rangle_{\sim} = \text{tr} P, \tag{9.152}$$

$$\langle A, A \rangle_{\sim} = 2 \int_0^{\infty} ds \, \text{tr} \left(A \, e^{-s(P - iH)} \, A e^{-s(P + iH)} \right) = \text{tr}(A \, Q_{\text{NESS}}),$$
 (9.153)

but we can no longer use the very last step in (9.65), because the continuity equation (9.148) and the definition (9.135) of P are different compared to bosons! We now

also appears in larger systems when we consider (9.143) the particle number in a single mode, i.e. $a^{\dagger}(\psi)a(\psi) = \Gamma(|\psi\rangle\langle\psi|)$.

find that

$$(\operatorname{tr} A)^2 \le (J/2 - \operatorname{tr} A)\operatorname{tr} P,$$
 (9.154)

what implies

$$\operatorname{tr} A(\operatorname{tr} A + \operatorname{tr} P) \leqslant \frac{J}{2} \operatorname{tr} P, \tag{9.155}$$

and, therefore,

$$J \geqslant 2 \frac{\text{tr} A \text{tr} D}{\text{tr} (D - A)} =: J_{\min}.$$
(9.156)

While the modifications in the derivation of the present bosonic result with respect to the fermionic case may appear minor, they actually "invert" the final result: There is a *lower bound* (9.156) to the bosonic currents, whereas we found an upper bound (9.66) in the fermionic case. This also implies that by matching the absorption rates closely to the dissipation rates, we can get enormous currents.

In Sect. 9.5, we explained how to design the coherent dynamics to induce the optimal current. However, for bosons, there appears to be no optimal current, but rather a minimal current. Interestingly, this minimal current can be increased by manipulation of the incoherent coupling agents encoded in A and D.

We must stress that it is currently unclear whether this model is sufficiently realistic to be experimentally realisable, specifically in the regime where ${\rm tr}(D-A)$ is small and thus currents are large (9.156): This appears to be the regime where also the number of particles in the system is enormous, which may impose physical difficulties. The large currents which can be achieved in our model can be achieved because the bosons in the system do not experience, nor cause any resistivity due to interactions. Interactions (or nonlinearities) are, however, expected to become important once the density of particles in the system is sufficiently large. Examples are ubiquitous, ranging from cold atoms (Davis et al. 1995), over excitons (Magde and Mahr 1970) to even photons (Bulanov et al. 2010). Nevertheless, the fundamental difference between bosons and fermions, even in the non-equilibrium steady state for non-interacting particles, is striking.

We close this section by presenting numerical results on the currents, to verify that, indeed, the bosonic bound (9.156) holds, and to understand where it is sharp and where it is not. To gain better understanding of the influence of coherence on the currents, we again introduce the parameter λ to tune between dominantly coherent $(\lambda \to \infty)$ and dominantly incoherent dynamics $(\lambda \to 0)$:

$$J := 4 \int_0^\infty \mathrm{d}s \, \mathrm{tr} \Big\{ e^{(-i\lambda H - P)s} A e^{(i\lambda H - P)s} D \Big\}. \tag{9.157}$$

In Fig. 9.8, we show simulations with randomly generated Hamiltonians from the GOE (3.26), for an finite dimensional single-particle Hilbert space, with $m = \dim \mathcal{H} = 10$ modes. To certainly satisfy (9.144), we choose A and P from the Wishart ensemble (9.69), and set D = P + A such that (9.135) holds true. As an estimate for

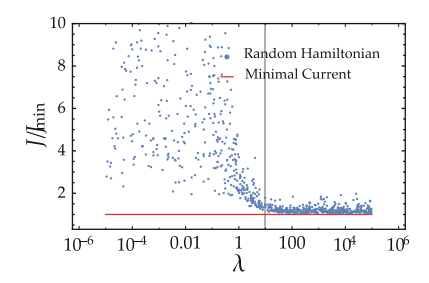


Fig. 9.8 Scatter plot which indicates the stationary current J (9.157) relative to the minimal current J_{\min} (9.156). Variable λ (9.157) controls the relative strength of the Hamiltonian and of incoherent contributions; for each data point, $\log_{10} \Lambda$ is randomly chosen from the interval [-5, 5]. Hamiltonians H in (9.157) are chosen from the GOE (3.26), with typical interaction v/\sqrt{m} between modes, with v=1 and mode number m=10. The channels P (9.135) and P (9.20) in (9.157) are drawn from a Wishart ensemble (9.69), with $m_A=5$ and $m_P=10$. D in (9.157) is directly obtained from (9.135). Data point s are compared to the lower bound P (9.135) are the value P is indicated (vertical line) since it represents the typical incoherent rate as the mean eigenvalue of P (see discussion (9.69))

the typical incoherent rate in the system, we can now use $\mathbb{E}(\operatorname{tr} P)/m = m_P$ (recall p. 390).

Based on Fig. 9.8 we cannot falsify the result (9.156), and, as was the case for the fermions, we find that most realisations approach the bound in the regime for dominantly coherent dynamics, i.e. $\lambda \gg m_P$. On the other hand, in the regime where the dynamics is mainly incoherent, we find a much larger spread and observe currents up to ten times as large as J_{\min} . This leads us to the conclusion that in random systems coherent dynamics tends to negatively influence the stationary bosonic currents. Note that from Sect. 4.3.2, a negative impact of coherent dynamics due to destructive interference may even be expected. This phenomenology is, however, in strong contrast to what we saw for random fermionic systems in Fig. 9.1, where strong coherent contributions to the dynamics are, in general, beneficial.

As a consequence of the many mathematical subtleties in our model (9.124) and in bosonic systems in general, our results, in particular (9.156), are difficult to interpret. Because the model is pushed to its mathematical limits (i.e. $\operatorname{tr}(D-A)$ small), it is not clear whether results should be interpreted as prediction of interesting physics or rather as mathematical artefacts. Hitherto we did not obtain an unambiguous physical interpretation for the behaviour of these bosonic currents and thus leave it as an open problem.

9.8 Summary and Outlook

In this chapter, we treated open systems, where identical particles are continuously entering and leaving, ultimately leading to a steady state with non-vanishing currents. We focussed our attention on the dynamics of single-particle observables and

specifically of the number operator. The latter was used to naturally define the current of particles that arises in the non-equilibrium steady state. As our main result, we have proven the existence of an upper bound (9.66) of this current for fermions, and of a lower bound (9.156) for bosons. For fermions, we learned that the system Hamiltonian can be specifically designed to saturate this bound, and that the necessary design principles rely on the same types of symmetries that were invoked in Sect. 4.4.1. This is in accordance with recent developments in literature, which have seen an increased interest in the role of symmetries to control quantum transport in the non-equilibrium steady state (Manzano and Hurtado 2017; Thingna et al. 2016). Furthermore, we set out to numerically understand the regime of dephasing enhanced currents, which exists, but remains difficult to understand analytically. Similar effects for bosons remain here unexplored.

In the numerical analyses presented in this chapter, we observed that, in randomly constructed systems, dominantly coherent contributions to the dynamics are beneficial for fermionic stationary currents (see Fig. 9.1). In contrast, they appear to be detrimental for bosonic stationary currents (see Fig. 9.8). In relation to Chap. 4, where we discussed that completely random systems are in general not optimal for efficient transport, the result for bosonic currents may appear more natural. Nevertheless, it may be both useful and feasible to understand in more detail how spectral properties of the Hamiltonian influence the behaviour of these stationary currents.

Throughout this chapter, we employed the algebraic framework of quantum statistical mechanics that was introduced in Sect. 7.7. Even though this approach is not strictly necessary to obtain the results that were discussed here, it comes with the advantage of being applicable to systems in the thermodynamic limit, i.e. systems with a infinite-dimensional single-particle Hilbert space. It must be stressed that such systems can generally not be described withint he common Hilbert space formalism of quantum mechanics. An illustration of the power of the methods is found in Walschaers et al. (2017), where the methods of this chapter are applied to an infinitely large translation invariant system, the so-called *quantum ribbon*.

A future objective, which imposes a very considerable complication, is the introduction of *interactions* between particles. In order to expand the model's potential realm of applicability, this is a necessary step. However, brute force approaches to this problem quickly become unfeasible, both from the analytical and numerical perspective. These problems can be understood in terms of the Bogoliubov-Born-Green-Kirkwood-Yvon (BBGKY) hierarchy (Bogoliubov 1946)³⁰: Even to understand the dynamics of a single-particle observable, one obtains enormous hierarchies of equations which couple sectors of different particle numbers. Modest first steps may focus on Hartree-Fock type models³¹ or the use of finitely correlated states (Fannes et al.

³⁰Originally the hierarchy was developed for classical systems by Yvon 1935. In connection to many-particle quantum physics this mathematical construction is also referred to as the Bogoliubov hierarchy, since Bogoliubov was the first to extend Yvon's hierarchy to quantum systems.

³¹This was also suggested in Alicki (1978) when discussing the addition of interactions to the specific model used in this chapter.

1992) or other tensor network methods (Haegeman and Verstraete 2017) to keep the computational complexity under control.

Let us finally consider the result in Dierckx et al. (2008) where quasi-free maps are formally characterised. These maps are defined by the fact that they send quasifree states onto quasi-free states when treated in the Schrödinger picture. Because a quasi-free state is a state for which the many-particle correlations factorise (as was extensively discussed in Sect. 7.7), we can interpret a quasi-free map³² as a transformation that does not induce correlations between particles. It was already known (Alicki 1987, 1978; Davies 1977a) that our model of Sect. 9.2 generates a dynamical map which is quasi-free. However, in Sect. 9.6.3 we observed that, with additional dephasing noise, our model no longer falls within this class. In other words, our dephasing model does not map a quasi-free state onto another quasifree state. Given that from a quantum statistical mechanics point of view (Verbeure 2011) quasi-free states are the most classical states which are known, this result is counter-intuitive; dephasing destroys phase coherence and is in that sense expected to make systems more classical. To our knowledge, this perspective of dephasing dynamics has never been studied in a structural way and therefore we identify it as an interesting open problem related to the mathematical physics of this chapter.

References

- N. Agraït, A.L. Yeyati, J.M. van Ruitenbeek, Quantum properties of atomic-sized conductors. Phys. Rep. 377, 81–279 (2003)
- M. Aizenman, E.H. Lieb, R. Seiringer, J.P. Solovej, J. Yngvason, Bose-Einstein quantum phase transition in an optical lattice model, in *Condensed Matter Physics and Exactly Soluble Models* ed. by P.B. Nachtergaele, P.J.P. Solovej, P.J. Yngvason (Springer, Berlin, 2004), pp. 337–349
- G. Akemann, J. Baik, P.D. Francesco (ed.), *The Oxford Handbook of Random Matrix Theory*. Oxford Handbooks in Mathematics (2011)
- R. Alicki, *Quantum Dynamical Semigroups and Applications*, 2nd edn. (Springer Science & Business Media, Berlin, 1987)
- R. Alicki, M. Fannes, *Quantum Dynamical Systems* (Oxford University Press, Oxford, 2001)
- R. Alicki, On the detailed balance condition for non-hamiltonian systems. Rep. Math. Phys. 10, 249–258 (1976)
- R. Alicki, The theory of open systems in application to unstable particles. Rep. Math. Phys. 14, 27–42 (1978)
- R. Alicki, The quantum open system as a model of the heat engine. J. Phys. A. Math. Gen. 12, L103–L107 (1979)
- M.H. Anderson, J.R. Ensher, M.R. Matthews, C.E. Wieman, E.A. Cornell, Observation of Bose-Einstein condensation in a dilute atomic vapor. Science **269**, 198–201 (1995)
- H. Araki, E.J. Woods, Representations of the canonical commutation relations describing a nonrelativistic infinite free Bose gas. J. Math. Phys. 4, 637–662 (1963)
- M. Arndt, A. Buchleitner, R.N. Mantegna, H. Walther, Experimental study of quantum and classical limits in microwave ionization of rubidium Rydberg atoms. Phys. Rev. Lett. 67, 2435–2438 (1991)
- A. Asadian, D. Manzano, M. Tiersch, H.J. Briegel, Heat transport through lattices of quantum harmonic oscillators in arbitrary dimensions. Phys. Rev. E 87, 012109 (2013)

³²These maps are also referred to as Gaussian or linear maps depending on the community.

References 417

- E. Balsley, A. Verbeure, States on clifford algebras. Commun. Math. Phys. 7, 55-76 (1968)
- R. Benzi, A. Sutera, A. Vulpiani, The mechanism of stochastic resonance. J. Phys. A. Math. Gen. 14, L453 (1981)
- R. Blümel, A. Buchleitner, R. Graham, L. Sirko, U. Smilansky, H. Walther, Dynamical localization in the microwave interaction of Rydberg atoms: the influence of noise. Phys. Rev. A **44**, 4521–4540 (1991)
- N.N. Bogoliubov, *Problems of the Dynamical Theory in Statistical Physics* (Gostechizdat, Moscow, 1946)
- O. Bratteli, D.W. Robinson, Operator Algebras and Quantum Statistical Mechanics 1 (Springer, Berlin, 1987)
- O. Bratteli, D.W. Robinson, Operator Algebras and Quantum Statistical Mechanics Equilibrium States (Models in Quantum Statistical Mechanics) (Springer, Berlin, 1997)
- H.-P. Breuer, F. Petruccione, *The Theory of Open Quantum Systems* (OUP Oxford, 2007)
- P.W. Brouwer, C.W.J. Beenakker, Voltage-probe and imaginary-potential models for dephasing in a chaotic quantum dot. Phys. Rev. B **55**, 4695–4702 (1997)
- S.S. Bulanov, T.Z. Esirkepov, A.G.R. Thomas, J.K. Koga, S.V. Bulanov, Schwinger limit attainability with extreme power lasers. Phys. Rev. Lett. **105**, 220407 (2010)
- G. Casati, T. Prosen, Anomalous heat conduction in a one-dimensional ideal gas. Phys. Rev. E 67, 015203 (2003)
- D. Cohen, Quantum chaos, dynamical correlations, and the effect of noise on localization. Phys. Rev. A 44, 2292–2313 (1991)
- D. Cohen, Y. Imry, Dephasing at low temperatures. Phys. Rev. B 59, 11143–11146 (1999)
- C. Cohen-Tannoudji, J. Dupont-Roc, G. Grynberg, Atom-Photon Interactions: Basic Processes and Applications (Wiley, USA, 1998)
- J.B. Conway, in *A Course in Functional Analysis*. Graduate Texts in Mathematics, vol. 96, 2nd edn. (Springer, New York, 1997)
- E.B. Davies, Irreversible dynamics of infinite fermion systems. Commun. Math. Phys. **55**, 231–258 (1977a)
- E.B. Davies, Quantum dynamical semigroups and the neutron diffusion equation. Rep. Math. Phys. 11, 169–188 (1977b)
- E.B. Davies, Generators of dynamical semigroups. J. Funct. Anal. 34, 421–432 (1979)
- K.B. Davis, M.O. Mewes, M.R. Andrews, N.J. van Druten, D.S. Durfee, D.M. Kurn, W. Ketterle, Bose-Einstein condensation in a gas of sodium atoms. Phys. Rev. Lett. **75**, 3969–3973 (1995)
- W. De Roeck, C. Maes, Steady state fluctuations of the dissipated heat for a quantum stochastic model. Rev. Math. Phys. 18, 619–653 (2006)
- B. Dierckx, M. Fannes, M. Pogorzelska, Fermionic quasifree states and maps in information theory. J. Math. Phys. **49**, 032109 (2008)
- G. Dufour, T. Brünner, C. Dittel, G. Weihs, R. Keil, A. Buchleitner, Many-particle interference in a two-component bosonic josephson junction: an all-optical simulation. New J. Phys. 19, 125015 (2017)
- F.J. Dyson, E.H. Lieb, B. Simon, Phase transitions in the quantum Heisenberg model. Phys. Rev. Lett. **37**, 120–123 (1976)
- F.J. Dyson, E.H. Lieb, B. Simon, Phase transitions in quantum spin systems with isotropic and nonisotropic interactions. J. Stat. Phys. 18, 335–383 (1978)
- M. Fannes, A. Verbeure, Correlation inequalities and equilibrium states. Commun. Math. Phys. **55**, 125–131 (1977a)
- M. Fannes, A. Verbeure, Correlation inequalities and equilibrium states II. Commun. Math. Phys. 57, 165–171 (1977b)
- M. Fannes, B. Nachtergaele, R.F. Werner, Finitely correlated states on quantum spin chains. Commun. Math. Phys. 144, 443–490 (1992)
- F.S. Fitzgerald, *The Great Gatsby* (Charles Scribner's Sons, 1925)
- Y.V. Fyodorov, D.V. Savin, Statistics of resonance width shifts as a signature of eigenfunction nonorthogonality. Phys. Rev. Lett. 108, 184101 (2012)

- L. Gammaitoni, P. Hänggi, P. Jung, F. Marchesoni, Stochastic resonance. Rev. Mod. Phys. 70, 223–287 (1998)
- R. Haag, The mathematical structure of the Bardeen–Cooper–Schrieffer model. Nuovo Cim. 25, 287–299 (1962)
- F. Haake, F. Izrailev, N. Lehmann, D. Saher, H.-J. Sommers, Statistics of complex levels of random matrices for decaying systems. Z. Phys. B. Condens. Matter 88, 359–370 (1992)
- J. Haegeman, F. Verstraete, Diagonalizing transfer matrices and matrix product operators: a medley of exact and computational methods. Annu. Rev. Condens. Matter Phys. 8, 355–406 (2017)
- P.C. Hohenberg, Existence of long-range order in one and two dimensions. Phys. Rev. **158**, 383–386 (1967)
- A.S. Holevo, *Statistical Structure of Quantum Theory* (Springer Science & Business Media, Berlin, 2001)
- S.F. Huelga, M.B. Plenio, Stochastic resonance phenomena in quantum many-body systems. Phys. Rev. Lett. 98, 170601 (2007)
- S. Jesenko, M. Žnidarič, Excitation energy transfer efficiency: Equivalence of transient and stationary setting and the absence of non-Markovian effects. J. Chem. Phys 138, 174103 (2013)
- G. Kordas, D. Witthaut, S. Wimberger, Non-equilibrium dynamics in dissipative Bose-Hubbard chains. Ann. Phys. (Berlin) **527**, 619–628 (2015)
- K. Kubo, T. Kishi, Rigorous bounds on the susceptibilities of the Hubbard model. Phys. Rev. B 41, 4866–4868 (1990)
- R. Landauer, Spatial variation of currents and fields due to localized scatterers in metallic conduction. IBM J. Res. Dev. 1, 223–231 (1957)
- D.A. Lidar, K.B. Whaley, Decoherence-Free Subspaces and Subsystems, in *Irreversible Quantum Dynamics*, ed. by F. Benatti, R. Floreanini. Lecture Notes in Physics, vol. 622 (Springer, Berlin, 2003), pp. 83–120. https://doi.org/10.1007/3-540-44874-8_5
- G. Lindblad, On the generators of quantum dynamical semigroups. Commun. Math. Phys. 48, 119–130 (1976)
- R. Loudon, *The Quantum Theory of Light*. Oxford Science Publications, 3rd edn. (Oxford University Press, Oxford, New York, 2000)
- D. Magde, H. Mahr, Exciton-exciton interaction in CdS, CdSe, and ZnO. Phys. Rev. Lett. 24, 890–893 (1970)
- D. Manzano, P.I. Hurtado, in Harnessing symmetry to control quantum transport (2017). arXiv:1707.07895
- D. Manzano, Quantum transport in networks and photosynthetic complexes at the steady state. PLoS ONE 8, e57041 (2013)
- D. Manzano, M. Tiersch, A. Asadian, H.J. Briegel, Quantum transport efficiency and Fourier's law. Phys. Rev. E 86, 061118 (2012)
- J. Naudts, A. Verbeure, Bounds on the admittance for KMS states. J. Math. Phys. 17, 419–423 (1976)
- J. Naudts, A. Verbeure, R. Weder, Linear response theory and the KMS condition. Commun. Math. Phys. 44, 87–99 (1975)
- A. Nitzan, M.A. Ratner, Electron transport in molecular wire junctions. Science **300**, 1384–1389 (2003)
- G.K. Pedersen, Analysis Now (Springer, New York, 1989)
- E.G. Petrov, Y.V. Shevchenko, V. May, P. Hänggi, Transient switch-on/off currents in molecular junctions. J. Chem. Phys. 134, 204701 (2011)
- D. Petz, An Invitation to the Algebra of Canonical Comutation Relations. Leuven Notes in Mathematical and Theoretical Physics Series A, vol. 2 (Leuven University Press, Leuven, 1990)
- D. Petz, G. Toth, The Bogoliubov inner product in quantum statistics. Lett. Math. Phys. 27, 205–216 (1993)
- M.B. Plenio, S.F. Huelga, Dephasing-assisted transport: quantum networks and biomolecules. New J. Phys. **10**, 113019 (2008)

References 419

A.V. Ponomarev, J. Madroñero, A.R. Kolovsky, A. Buchleitner, Atomic current across an optical lattice. Phys. Rev. Lett. **96**, 050404 (2006)

- T. Prosen, Third quantization: a general method to solve master equations for quadratic open Fermi systems. New J. Phys. 10, 043026 (2008)
- T. Prosen, M. Žnidarič, Matrix product simulations of non-equilibrium steady states of quantum spin chains. J. Stat. Mech. Theor. Exp. **2009**, P02035 (2009)
- D.W. Robinson, The ground state of the Bose gas. Commun. Math. Phys. 1, 159–174 (1965a)
- G. Roepstorff, A stronger version of Bogoliubov's inequality and the Heisenberg model. Commun. Math. Phys. 53, 143–150 (1977)
- D. Ruelle, Natural nonequilibrium states in quantum statistical mechanics. J. Stat. Phys. **98**, 57–75 (2000)
- T. Scholak, Transport and coherence in disordered networks. Ph.D. thesis, Albert-Ludwigs Universität Freiburg, Freiburg, 2011
- T. Scholak, F. Mintert, T. Wellens, A. Buchleitner, Transport and Entanglement, in *Biomolecular Systems*, ed. by E.R. Weber, M. Thorwart, U. Würfel. Quantum Efficiency in Complex Systems, 1st edn. (Elsevier, Oxford, 2010)
- M.O. Scully, M.S. Zubairy, *Quantum Optics* (Cambridge University Press, Cambridge, New York, 1997)
- D. Segal, A. Nitzan, Heating in current carrying molecular junctions. J. Chem. Phys. **117**, 3915–3927 (2002)
- D. Segal, A. Nitzan, P. Hänggi, Thermal conductance through molecular wires. J. Chem. Phys. 119, 6840–6855 (2003)
- D.A. Steck, V. Milner, W.H. Oskay, M.G. Raizen, Quantitative study of amplitude noise effects on dynamical localization. Phys. Rev. E 62, 3461–3475 (2000)
- T. Stegmann, O. Ujsághy, D.E. Wolf, Localization under the effect of randomly distributed decoherence. Eur. Phys. J. B **87**, 1–8 (2014)
- J. Thingna, D. Manzano, J. Cao, Dynamical signatures of molecular symmetries in nonequilibrium quantum transport. Sci. Rep. 6, 28027 EP (2016)
- K.A. Velizhanin, H. Wang, M. Thoss, Heat transport through model molecular junctions: a multilayer multiconfiguration time-dependent Hartree approach. Chem. Phys. Lett. 460, 325–330 (2008)
- A. Verbeure, Many-Body Boson Systems: Half a Century Later, Theoretical and Mathematical Physics (Springer, London, New York, 2011)
- D. Vorberg, W. Wustmann, R. Ketzmerick, A. Eckardt, Generalized Bose-Einstein condensation into multiple states in driven-dissipative systems. Phys. Rev. Lett. **111**, 240405 (2013)
- M. Walschaers, A. Buchleitner, M. Fannes, On optimal currents of indistinguishable particles. New J. Phys. 19, 023025 (2017)
- T. Wellens, A. Buchleitner, Stochastic resonance in the coherence of a quantum system. Phys. Rev. Lett. **84**, 5118–5121 (2000)
- T. Wellens, V. Shatokhin, A. Buchleitner, Stochastic resonance. Rep. Prog. Phys. 67, 45–105 (2004)
- J. Wishart, The generalised product moment distribution in samples from a normal multivariate population. Biometrika 20A, 32–52 (1928)
- B. Witt, F. Mintert, Stationary quantum coherence and transport in disordered networks. New J. Phys. 15, 093020 (2013)
- J. Yvon, La Théorie Statistique des Fluides et l'Equation d'Etat (Hermann, Paris, 1935)
- K. Zyczkowski, H.-J. Sommers, Induced measures in the space of mixed quantum states. J. Phys. A. Math. Gen. **34**, 7111 (2001)

Part IV General Conclusions and Prospects

Chapter 10 Conclusions and Outlook



The way I see it, every life is a pile of good things and bad things. The good things don't always soften the bad things, but vice versa the bad things don't always spoil the good things or make them unimportant. And we definitely added to his pile of good things

The Doctor in "Doctor Who" (Campbell 2010)

Conclusions

This dissertation focussed its attention on quantum transport phenomena in "complex" systems with a strong emphasis on the influence of quantum interference. In Part I we introduced heuristics of complex systems and reviewed several attempts to formally define what a complex system is. Complex systems presently are a highly fashionable topic in both classical and quantum physics, but also in a wide range of other fields ranging from economy to neuroscience. A formal definition of "a complex system" which fully captures the desired heuristics is still out of reach. In Sect. 3.1.3 we therefore focussed specifically on understanding complex *dynamical* quantum systems.

The dynamics of complex quantum systems can be a subtle topic; the skeptic is tempted to argue that one is "just solving the Schrödinger equation". Nevertheless, the mere act of determining and understanding dynamics is often very tedious. It typically requires effective descriptions and models, which can use a wide variety of tools: There are master equations (Alicki 1987; Breuer and Petruccione 2007; Davies 1979; Lindblad 1976), hierarchical equations (Bogoliubov 1946; Ishizaki and Tanimura 2005), semiclassical methods (de Almeida 1998; Doron and Smilansky 1992; Engl et al. 2014; Fischer and Buchleitner 2015; Gaspard 2014; Gutzwiller 1971; Heller 1981), Green's function methods (Kamenev 2011; Mahan 2000; Negele and Orland 1998), et cetera. It is regularly forgotten (particularly in the strongly reductionist

quantum optics and quantum information context) that one does not always need to model the system in a microscopically faithful manner; an alternative is to rather model the correct *statistical properties* of the system by using for example *random matrix theory* (Beenakker 1997; Haake 2010; Jalabert et al. 1994; Stöckmann 2007) (in analogy to the program of classical statistical mechanics and thermodynamics).

This provides us with a conceptual framework in which to embed the formalism of dynamical quantum systems as introduced in Chap. 2, and investigate "complex" dynamical quantum system. We argue that complexity must ultimately be encrypted in the spectral properties of the system Hamiltonian. In the context of statistical properties, the latter can be related to spectral graph theory and random matrix theory: We propose to connect typical spectral structures of the graphs which describe complex networks to spectral properties of Hamiltonians. In concreto, in Sect. 3.2 we identify power-law behaviour in the spectrum as a hallmark of complexity.

In Part II we considered complex systems where a single excitation (a quantum of energy, e.g. an exciton) is transported from an initial (input) state to a final (output) state, and in Chap. 5 we additionally allowed for these states to have external channels coupled to them. We challenged the common wisdom that quantum coherence in combination with disorder is detrimental for the directed transfer of energy. Our results, building on the work of Scholak (2011), Zech (2013), clearly show that this dogma does not hold for finite size systems. In Sect. 4.4 we presented a specific set of *design principles* that lead to fast and highly efficient excitation transfer, while still allowing a large degree of disorder.

These design principles, *centrosymmetry* (4.46) in the system Hamiltonian and a *dominant doublet* (4.68) of eigenstates that mainly carries the excitation, engineer a mechanism of statistical control in Sects. 4.5 and 5.5: Rather than determining one timescale and one efficiency, we control the shapes of the *distributions* of these quantities for an ensemble of many disorder realisations. We identified that these distributions can be controlled by typical spectral properties, such as the overall average level spacing in the vicinity of the dominant doublet's energy levels and the average coupling strength between the initial and final state to the intermediate states. Although we use random matrix ensembles in our derivations, these spectral properties can in principle be extracted for any type of systems, and therefore the model is applicable to a wide variety of settings, e.g. Rydberg gases (Scholak et al. 2014), photosynthetic biomolecular complexes (Walschaers et al. 2013), mesoscopic system (Brouwer 1997), et cetera.

One of these settings is that of molecular biology, as discussed in Chap. 6, where we studied the energy transport in the early stages of photosynthesis. In such systems, it is of crucial importance that excitons are swiftly and efficiently processed, to avoid that the harvested energy is lost (e.g. by recombination effects). In Sect. 6.3 we provided considerable indications that the design principles which we propose may be present in the FMO complex, a molecular complex which transfers excitons from the antenna complex to the reaction centre of green sulphur bacteria. Even though

¹One may argue that in genuine complex systems faithful microscopic modelling is even impossible.

our analysis is based on quantitative arguments, they do not yet approach the realistic in vivo setting.

Exploring quantum mechanics in the realm of complex systems is of crucial importance to gain insight beyond overly simplified toy models. Specifically the regime where these systems are genuinely complex, i.e. cannot be understood by microscopic models, but are too small to be treated in the thermodynamic limit, remains largely uncharted territory. On the one hand, the interplay between the system's complexity and quantum interference leads to interesting new insights in fundamental physics. Localisation phenomena (Anderson 1958) and conductance fluctuations (Jalabert et al. 1994) are striking examples of such typical quantum phenomena, but truly complex systems tend to combine disorder with pattern formation. In our work we use our design principles to induce these patterns and we do observe new transport properties (Walschaers et al. 2015).

On the other hand, there are many technologies which ultimately rely on quantum effects, with lasers (Schawlow and Townes 1958) and transistors (Bardeen and Brattain 1948) as most important representatives since they are key elements in most modern electronics devices. Even for these foundational examples, technological developments have led to the realm of complex quantum systems, see e.g. random lasers (Wiersma 2008) and the increasing importance of interference effects in microelectronics (Moors et al. 2015; Steinlesberger et al. 2002). Moreover, new technologies such as quantum cryptography (Bennett and Brassard 1984; Ekert 1991; Gisin et al. 2002) tend to exploit ever more intricate quantum effects. Overall, with increasing system sizes, these systems tend to become complex and it becomes relevant to understand how this influences the (often dynamical) quantum effects which they exploit. The main philosophy of the present dissertation is to *use* this complexity—and the unavoidable disorder—to our advantage, rather than fighting it. Therefore, the indications, in Sect. 6.3, that nature may also follows this philosophy (within one or several instances of light harvesting complexes) are fascinating.

In the above discussion, we focussed on complexity in quantum systems which is induced on the topological level, i.e. complexity contained in the single-particle Hamiltonian. Part III of this thesis focusses on a different type of complexity which also naturally appears in quantum systems: The complexity which arises due to many-particle effects. As explained in Chap. 7, quantum mechanics requires us to consider these particles as *fundamentally identical*, although they may differ in properties. Particles which do not differ in any degree of freedom, must be considered *indistinguishable*, hence it is impossible to tell which one is which. In Sect. 8.3, we explain how this indistinguishability, even when the particles are not physically interacting, can lead to highly non-trivial interference patterns, which are purely dynamical many-particle effects. Extensive amounts of work have been done on this topic, notably by Tichy et al. (Anger 2013; Mayer et al. 2011; Ra et al. 2013a, b;

²Also on the level of science politics there is interest in the development of such new "quantum technologies", as indicated by several funding efforts in the EU and the USA which are specifically intended to increase the research output in this direction. It is, however, noteworthy that there are currently many theoretical developments and proposal in contrast to reasonably few actual implementations.

Schlawin 2011; Schlawin et al. 2012a; Tichy 2011, 2014; Tichy et al. 2013, 2011, 2014, 2010, 2012), which forms the foundational basis for the work in this dissertation. Recently the topic gained increased attention due to the boson sampling debate.

In this thesis, we did not per se study many-particle interference itself, but rather the extent of its signatures. From the discussion in Sect. 8.3 it becomes clear that it is extremely difficult³ to understand these many-particle interference patterns, although they are also highly structured. In the light of Chap. 3, such a many-particle interferometer is a clear example of a complex system. This implies that it is to be expected that a *deterministic* assessment of the interference pattern is unfeasible. However, it also indicates that the problem may be suited for a *statistical* treatment, in line with how complex systems are treated in statistical mechanics. In Sects. 8.4 and 8.5 we introduced a fruitful method to unambiguously discover the statistical fingerprint of different types of many-particle interference by measuring correlation functions between different modes. We emphasised the role of these methods as a potential solution to the boson sampling certification problem. Furthermore, we indicate that these methods are useful diagnostic tools to characterise the degree of mutual distinguishability in a set of particles. More generally stated, statistical signatures, encrypted in correlation functions, may provide a toolbox to handle the very general problem of validation of quantum simulations.

Ultimately, in Chap. 9, we studied many-particle transport in the non-equilibrium stationary state of open systems. We limited ourselves to non-interacting particles and therefore could derive feasible expressions for the particle current that flows through such systems in their non-equilibrium steady states. Remarkably, we managed to prove that, for fermionic systems, there exists an overall upper bound for this current, which is independent of the details of the system, but is determined by its environment coupling agents. This setting is significantly different from Part II, because in Chap. 9 quantum statistical effects are included in the model. Nevertheless, centrosymmetry, again, serves as a *design principle*: It generates particle currents which saturate the bound and are in this sense optimal. Another intriguing result is the profound difference between fermionic and bosonic steady state currents: We found that for bosonic systems there is no upper bound for the particle current, but, remarkably, a lower bound appears.

Outlook

We close this dissertation by briefly summarising what, from the author's perspective, are the most profound and intriguing challenges for related future research.

Let us start by considering the open problems related to the topics treated in Part II:

• Obviously, the design principles presented in Sect. 4.4 are not the only possible scenarios. We believe that there lies a lot of potential in the more general scheme of using back-bone structures (such as our dominant doublet) in combination with additional constituents that never carry significant amounts of "population", but

³And according to the results in Aaronson and Arkhipov (2013) also computationally hard.

nevertheless influence the energetics and hence the time scales of the system. We may extend this scheme by also considering environment-related effects, which can be Markovian noise, but also—and probably more interestingly—there is the possibility of strongly coupled degrees of freedom that influence the system in a coherent fashion (sometimes also dealt with in "non-Markovian" approaches). Currently we are attempting to use Floquet theory to explore such scenario (Brugger 2015).

- When we turn to quantum effects in biological systems (as discussed in Chap. 6), there are several grand open problems. At first, there is a need to learn more about the initial and final states of the transfer process. This implies both a deeper understanding of the light-matter interaction, and of the interaction between different light harvesting complexes. A specific, long lasting debate which is still open, is whether at all incoherent light can generate coherence in such photosynthetic complexes. There are strong, skeptic views on this matter (Brumer and Shapiro 2012; Dodin et al. 2016; Pachón et al. 2017), but we feel that most arguments remain too vague to be conclusive. When one models complex molecular systems, one is bound to making several assumptions in order to gain an understanding, it appears that the validity of such assumptions is not always clear. Many models of light-harvesting complexes consider an effective Hamiltonian to describe the interactions between molecules and ignore the fact that these interactions are themselves mediated by the electromagnetic field. To study light-matter interactions which create the excitons in such coupled molecules, it appears to be relevant to also consider the (often ignored) collective interactions between the molecules and the electromagnetic field (Shatokhin et al. 2016). Ignoring such interactions implies ignoring an energy current which persists in the long-time limit and therefore (see Chap. 9) a non-vanishing coherence. On transient timescales, the effect of the initial state is also important. In our opinion, posing the question whether the absorption of a photon from an incoherent bath can generate coherence, implies that these events are resolved in time (Shatokhin et al. 2016). When one considers the initial state to be a non-equilibrium steady state, one clearly studies a different type of problem where individual photon absorption events are not registered.
- The previous point leads us towards another challenge which one must sooner or later dare to address. Currently, the models that offer physical insight, including our own, are still what one might mockingly call "toy models": They do not quantitatively predict outcomes of experiments. Therefore, we must find a smoking gun to determine the direction in which to proceed. Especially it is important to find a probe that may allow to identify unambiguously whether the transport of energy is coherent or not. Additionally, one should be ambitious enough to attempt to calculate useful quantities such as quantum efficiencies. During the final phase of our research, it became clear that the "holy grail" for the future is ultimately the quantitive prediction of these quantum efficiencies, based on tractable physical models, where one can understand how the coherence impacts the functional level of light harvesting.
- A final outlook on the matter of designed quantum transport, mainly in relation to Chap. 9, is related to many-particle effects. It is currently completely unclear how

our models behave when more particles enter the system. Also in the context of photosynthesis this is a relevant question, which is usually cast aside (Cheng and Fleming 2009; Renger et al. 2001; Scholak 2011) in the study of energy transfer where generally only the the single-exciton manifold is considered. It is well-known that two-exciton effects are of relevance in 2D spectroscopy (Abramavicius et al. 2008), but their potential role in the context of quantum transport remains unclear. However, relevant progress on the level of spectroscopic tools to study such questions is being made (Dorfman et al. 2016; Schlawin et al. 2012b, 2013).

Also in Part III several open problems and future prospects were identified. We include a list of those which we consider most interesting:

- The most straightforward direction in future research lies in experimental realisations. There has been a considerable amount of progress in many-particle interferometry experiments, partially boosted by the debate on boson sampling and work on quantum walks. Our proposed certification methods of Sect. 8.5, which use truncated correlation functions, are directly implementable in such settings (Giordani et al. 2018). With realistic applications in mind, we also included a study of particle distinguishability in Sect. 8.5.3. However, it is reasonable to assume that there are several other obstacles to be overcome in experiments, such as the limited accuracy of detectors.
- In Sect. 8.5.3, partial distinguishability of particles also raised a more fundamental question. We have shown several concrete instances of setups with partially distinguishable particles and we found a very similar behaviour of the statistical properties of truncated correlation functions as a function of the degree of distinguishability. It is a very interesting question to which degree such an approach can be generalised. Specifically it is interesting to investigate whether or not there can be an unambiguous measure of the degree of distinguishability for which the random matrix prediction for the truncated correlation functions describe a monotonic transition from fully distinguishable to genuinely indistinguishable behaviour. If such a measure exists, it implies that the measurements of C-datasets of Sect. 8.5 could serve as diagnostic tool in a similar way as the Hong-Ou-Mandel effect is used to benchmark the indistinguishability of two particles (recall Sect. 8.3.4).
- In Sect. 8.4, we devoted attention to the actual measurement operators for sampling setups and used these as starting point for our analysis of the statistical fingerprints of many-particle interference in Sect. 8.5. An interesting, and potentially important question is what happens when the measurement procedure changes. In a quantum optics setup, one can also use homodyne detectors to do measurements in the continuous variable regime (Chabaud et al. 2017; Chakhmakhchyan and Cerf 2017), which is of particular interest for bosonic states which differ from the number states considered throughout this dissertation. On the other hand, one may also explore whether the methods of Sect. 8.5 are fruitful to certify Gaussian boson sampling (Hamilton et al. 2017).
- Apart from the methods we described in Sect. 8.5 to obtain information about many-particle interference patterns, one could opt for completely different routes. We have shown that C-datasets can be distinguished from each other via machine

learning algorithms (Giordani et al. 2018). In general, one might wonder whether such algorithms may be able to find (bosonic) patterns in sample data. A very intriguing question is whether such an algorithm could be trained with simulated data for few particles and applied for large particle numbers. Recently, one has started to explore this direction of research (Agresti et al. 2017).

- In the realm of many-particle systems, we encountered several possibilities to go beyond the typical Gaussian or number states. In Sect. 9.6.3, we discussed that a simple dephasing dynamics is sufficient to generate states which are no longer Gaussian and we also mentioned experimentally available methods such as photon addition and subtraction. These classes of new many-body states are still poorly understood and not sufficiently characterised. We see a long and exciting road ahead of us in this direction (Walschaers et al. 2017).
- Finally, also this part of the dissertation allows us to identify a direction which is both a "holy grail" and a horrific prospect: Interacting particles. Interaction in many-boson and many-fermion systems is usually extremely difficult to deal with, hence the existence of methods such as Hartree-Fock and density functional theory, or the development of finitely-correlated (e.g. matrix product) states. It is important to know how such interactions influence both many-particle interference effects, and particle currents in the non-equilibrium steady state. In the debate of manyparticle dynamics, many-particle interference effects have rarely been explicitly taken into consideration in combination with interactions between particles (see Dufour et al. 2017; Geiger et al. 2012 for notable exceptions). It is a big open question how these effects jointly contribute to many-particle dynamics and how these contributions can be identified and, possibly, disentangled. In Sect. 8.5, we showed that many-particle interference has signatures in the system's correlation functions. The same holds for interactions which even tend to induce more correlations in the system, as can be seen in the BBGKY hierarchy (Bogoliubov 1946). Therefore a starting point is to identify the effect of interaction on the C-datasets of Sect. 8.5.

With this set of inspiring problems which are open for future research, we conclude this thesis.

References

- D. Abramavicius, D.V. Voronine, S. Mukamel, Double-quantum resonances and exciton-scattering in coherent 2D spectroscopy of photosynthetic complexes. PNAS **105**, 8525–8530 (2008)
- I. Agresti, N. Viggianiello, F. Flamini, N. Spagnolo, A. Crespi, R. Osellame, N. Wiebe, F. Sciarrino, Pattern recognition techniques for boson sampling validation (2017). arXiv:1712.06863
- R. Alicki, *Quantum Dynamical Semigroups and Applications*, 2nd edn. (Springer Science & Business Media, Berlin, 1987)
- P.W. Anderson, Absence of diffusion in certain random lattices. Phys. Rev. 109, 1492–1505 (1958)
 F.R. Anger, Disorder effects on interference: from one to many particles. Master thesis, Ludwig-Maximilians-Universität München, München, 2013

- S. Aaronson, A. Arkhipov, The computational complexity of linear optics. Theory Comput. 9, 143–252 (2013)
- J. Bardeen, W.H. Brattain, The transistor, a semi-conductor triode. Phys. Rev. 74, 230–231 (1948)
 C.W.J. Beenakker, Random-matrix theory of quantum transport. Rev. Mod. Phys. 69, 731–808 (1997)
- C.H. Bennett, G. Brassard, Quantum cryptography: public key distribution and coin tossing. Theor. Comput. Sci. Part-1 560, 7–11 (1984)
- N.N. Bogoliubov, *Problems of the Dynamical Theory in Statistical Physics* (Gostechizdat, Moscow, 1946)
- H.-P. Breuer, F. Petruccione, *The Theory of Open Quantum Systems* (Oxford University Press, Oxford, 2007)
- P.W. Brouwer, On the random-matrix theory of quantum transport. Ph.D. thesis, Leiden University, Leiden, 1997
- J. Brugger, Phononen-assistierter Quantentransport auf endlichen Netzwerken. Bachelor thesis, Albert-Ludwigs-Universität Freiburg, Freiburg, 2015
- P. Brumer, M. Shapiro, Molecular response in one-photon absorption via natural thermal light versus pulsed laser excitation. PNAS **109**, 19575–19578 (2012)
- J. Campbell, Vincent and the Doctor (2010)
- U. Chabaud, T. Douce, D. Markham, P. van Loock, E. Kashefi, G. Ferrini, Continuous-variable sampling from photon-added or photon-subtracted squeezed states. Phys. Rev. A 96, 062307 (2017)
- L. Chakhmakhchyan, N.J. Cerf, Boson sampling with Gaussian measurements. Phys. Rev. A 96, 032326 (2017)
- Y.-C. Cheng, G.R. Fleming, Dynamics of light harvesting in photosynthesis. Annu. Rev. Phys. Chem. 60, 241–262 (2009)
- E.B. Davies, Generators of dynamical semigroups. J. Funct. Anal. 34, 421–432 (1979)
- A.M.O. de Almeida, The Weyl representation in classical and quantum mechanics. Phys. Rep. **295**, 265–342 (1998)
- A. Dodin, T.V. Tscherbul, P. Brumer, Coherent dynamics of v-type systems driven by time-dependent incoherent radiation. J. Chem. Phys. **145**, 244313 (2016)
- K.E. Dorfman, F. Schlawin, S. Mukamel, Nonlinear optical signals and spectroscopy with quantum light. Rev. Mod. Phys. **88**, 045008 (2016)
- E. Doron, U. Smilansky, Semiclassical quantization of chaotic billiards: a scattering theory approach. Nonlinearity 5, 1055 (1992)
- G. Dufour, T. Brünner, C. Dittel, G. Weihs, R. Keil, A. Buchleitner, Many-particle interference in a two-component bosonic Josephson junction: an all-optical simulation. New J. Phys. 19, 125015 (2017)
- A.K. Ekert, Quantum cryptography based on Bell's theorem. Phys. Rev. Lett. 67, 661–663 (1991)
- T. Engl, J. Dujardin, A. Argüelles, P. Schlagheck, K. Richter, J.D. Urbina, Coherent backscattering in fock space: a signature of quantum many-body interference in interacting bosonic systems. Phys. Rev. Lett. **112**, 140403 (2014)
- S.G. Fischer, A. Buchleitner, On the derivation of the semiclassical approximation to the quantum propagator. J. Math. Phys. **56**, 072105 (2015)
- P. Gaspard, Quantum chaotic scattering. Scholarpedia 9, 9806 (2014)
- T. Geiger, T. Wellens, A. Buchleitner, Inelastic multiple scattering of interacting bosons in weak random potentials. Phys. Rev. Lett. **109**, 030601 (2012)
- T. Giordani, F. Flamini, M. Pompili, N. Viggianiello, N. Spagnolo, A. Crespi, R. Osellame, N. Wiebe, M. Walschaers, A. Buchleitner, F. Sciarrino, Experimental statistical signature of many-body quantum interference. Nat. Photonics 12, 173–178 (2018)
- N. Gisin, G. Ribordy, W. Tittel, H. Zbinden, Quantum cryptography. Rev. Mod. Phys. **74**, 145–195 (2002)
- M.C. Gutzwiller, Periodic orbits and classical quantization conditions. J. Math. Phys. 12, 343–358 (1971)

References 431

- F. Haake, Quantum Signatures of Chaos, vol. 54 (Springer Science & Business Media, Berlin, 2010)
- C.S. Hamilton, R. Kruse, L. Sansoni, S. Barkhofen, C. Silberhorn, I. Jex, Gaussian Boson sampling. Phys. Rev. Lett. **119**, 170501 (2017)
- E.J. Heller, Frozen Gaussians: a very simple semiclassical approximation. J. Chem. Phys. 75, 2923–2931 (1981)
- A. Ishizaki, Y. Tanimura, Quantum dynamics of system strongly coupled to low-temperature colored noise bath: reduced hierarchy equations approach. J. Phys. Soc. Jpn. **74**, 3131–3134 (2005)
- R.A. Jalabert, J.-L. Pichard, C.W.J. Beenakker, Universal quantum signatures of chaos in ballistic transport. EPL **27**, 255 (1994)
- A. Kamenev, *Field Theory of Non-Equilibrium Systems* (Cambridge University Press, Cambridge, 2011)
- G. Lindblad, On the generators of quantum dynamical semigroups. Commun. Math. Phys. 48, 119–130 (1976)
- G.D. Mahan, Many-Particle Physics (Springer, Boston, 2000)
- K. Mayer, M.C. Tichy, F. Mintert, T. Konrad, A. Buchleitner, Counting statistics of many-particle quantum walks. Phys. Rev. A 83, 062307 (2011)
- K. Moors, B. Sorée, W. Magnus, Modeling surface roughness scattering in metallic nanowires. J. Appl. Phys. 118, 124307 (2015)
- J.W. Negele, H. Orland, *Quantum Many-Particle Systems* (Perseus Books, Reading, 1998)
- L.A. Pachón, J.D. Botero, P. Brumer, Open system perspective on incoherent excitation of light-harvesting systems. J. Phys. B: At. Mol. Opt. Phys. 50, 184003 (2017)
- Y.-S. Ra, M.C. Tichy, H.-T. Lim, O. Kwon, F. Mintert, A. Buchleitner, Y.-H. Kim, Nonmonotonic quantum-to-classical transition in multiparticle interference. PNAS 110, 1227–1231 (2013a)
- Y.-S. Ra, M.C. Tichy, H.-T. Lim, O. Kwon, F. Mintert, A. Buchleitner, Y.-H. Kim, Observation of detection-dependent multi-photon coherence times. Nat. Commun. 4 (2013b)
- T. Renger, V. May, O. Kühn, Ultrafast excitation energy transfer dynamics in photosynthetic pigment-protein complexes. Phys. Rep. 343, 137–254 (2001)
- A.L. Schawlow, C.H. Townes, Infrared and optical masers. Phys. Rev. 112, 1940–1949 (1958)
- F. Schlawin, Propagation of quantum particles in disordered media. Diploma thesis, Albert-Ludwigs-Universität Freiburg, Freiburg, 2011
- F. Schlawin, N. Cherroret, A. Buchleitner, Bunching and anti-bunching of localised particles in disordered media. EPL (Europhysics Letters) **99**, 14001 (2012a)
- F. Schlawin, K.E. Dorfman, B.P. Fingerhut, S. Mukamel, Manipulation of two-photon-induced fluorescence spectra of chromophore aggregates with entangled photons: a simulation study. Phys. Rev. A **86**, 023851 (2012b)
- F. Schlawin, K.E. Dorfman, B.P. Fingerhut, S. Mukamel, Suppression of population transport and control of exciton distributions by entangled photons. Nat. Commun. **4**, 1782 (2013)
- T. Scholak, Transport and coherence in disordered networks. Ph.D. thesis, Albert-Ludwigs Universität Freiburg, Freiburg, 2011
- T. Scholak, T. Wellens, A. Buchleitner, Spectral backbone of excitation transport in ultracold Rydberg gases. Phys. Rev. A 90, 063415 (2014)
- V. Shatokhin, M. Walschaers, F. Schlawin, A. Buchleitner, Coherence turned on by incoherent light (2016). arXiv:1602.07878
- G. Steinlesberger, M. Engelhardt, G. Schindler, W. Steinhögl, A. von Glasow, K. Mosig, E. Bertagnolli, Electrical assessment of copper damascene interconnects down to sub-50 nm feature sizes. Microelectron. Eng. 64, 409–416 (2002)
- H.-J. Stöckmann, Quantum Chaos: An Introduction (Cambridge University Press, Cambridge, 2007)
 M.C. Tichy, Entanglement and interference of identical particles. Ph.D. thesis, Albert-Ludwigs Universität Freiburg, Freiburg, 2011
- M.C. Tichy, Interference of identical particles from entanglement to boson-sampling. J. Phys. B: At. Mol. Opt. Phys. 47, 103001 (2014)
- M.C. Tichy, F. de Melo, M. Kuś, F. Mintert, A. Buchleitner, Entanglement of identical particles and the detection process. Fortschr. Phys. **61**, 225–237 (2013)

- M.C. Tichy, H.-T. Lim, Y.-S. Ra, F. Mintert, Y.-H. Kim, A. Buchleitner, Four-photon indistinguishability transition. Phys. Rev. A 83, 062111 (2011)
- M.C. Tichy, K. Mayer, A. Buchleitner, K. Mølmer, Stringent and efficient assessment of Boson-sampling devices. Phys. Rev. Lett. 113, 020502 (2014)
- M.C. Tichy, M. Tiersch, F. de Melo, F. Mintert, A. Buchleitner, Zero-transmission law for multiport beam splitters. Phys. Rev. Lett. **104**, 220405 (2010)
- M.C. Tichy, M. Tiersch, F. Mintert, A. Buchleitner, Many-particle interference beyond many-boson and many-fermion statistics. New J. Phys. 14, 093015 (2012)
- M. Walschaers, JF-d-C Diaz, R. Mulet, A. Buchleitner, Optimally designed quantum transport across disordered networks. Phys. Rev. Lett. 111, 180601 (2013)
- M. Walschaers, C. Fabre, V. Parigi, N. Treps, Entanglement and wigner function negativity of multimode non-Gaussian states. Phys. Rev. Lett. 119, 183601 (2017)
- M. Walschaers, R. Mulet, T. Wellens, A. Buchleitner, Statistical theory of designed quantum transport across disordered networks. Phys. Rev. E 91, 042137 (2015)
- D.S. Wiersma, The physics and applications of random lasers. Nat. Phys. 4, 359–367 (2008)
- T. Zech, Hidden symmetries of quantum transport in photosynthesis. Diploma thesis, Albert-Ludwigs Universität Freiburg, Freiburg, 2013

Appendix A

Basic Definitions of Mathematical Algebras

This appendix is partially based on the lecture notes of the course *spectral theory* and operator algebras taught at the KU Leuven by Johan Quaegebeur and hence follows the notation used there.

A.1 Algebras on \mathbb{C}

The goal of the Appendix is to provide formal definitions of abstract algebras used throughout this thesis.

It turns out that an associative algebra as such is already a highly structured object. At its core lie three mathematical operations: *the addition* "+", *the multiplication* "·" and the *scalar product*. In principle, one can consider R-algebras, where the scalar product is defined for a general *commutative ring* R, but we only consider \mathbb{C} -algebras throughout this dissertation. Let us start by introducing the these operations and the structure they generate.

A first demand is that the algebra \mathcal{A} form a group for the addition

$$+: \mathcal{A} \times \mathcal{A} \to \mathcal{A},$$
 (A.1)

as determined by Definition 1.

Definition 1 A group is a set A equipped with an operation + with the following properties

- **Closure**: For all $a, b \in \mathcal{A}$, also $a + b \in \mathcal{A}$.
- Associativity: For all $a, b, c \in A$ the identity (a + b) + c = a + (b + c) holds.
- The existence of an identity element: There exists a $0 \in A$ such that for all $a \in A$ we find that 0 + a = a + 0 = a.
- Invertibility: For every $a \in \mathcal{A}$ there exists an element $b \in \mathcal{A}$ such that a + b = b + a = 0.

The group is called **Abelian** or **commutative** when for all $a, b \in A$ the identity a + b = b + a holds.

Assuming that the set \mathcal{A} equipped with + forms an abelian group, when we additionally equip \mathcal{A} with a multiplication

$$\cdot: \mathcal{A} \times \mathcal{A} \to \mathcal{A},\tag{A.2}$$

it can acquire the structure of a ring as defined by Definition 4.

Definition 2 A **ring** is an abelian group (A, +) equipped with an additional operation \cdot with the following properties

- Closure: For all $a, b \in \mathcal{A}$, also $a \cdot b \in \mathcal{A}$.
- Associativity: For all $a, b, c \in A$ the identity $(a \cdot b) \cdot c = a \cdot (b \cdot c)$ holds.
- **Distributivity**: For all $a, b, c \in A$ the identities $(a + b) \cdot c = a \cdot c + b \cdot c$ and $a \cdot (b + c) = a \cdot b + a \cdot c$ hold.

The ring is called **unital** if there exists an element $1 \in A$ such that for all $a \in A$ $1 \cdot a = a \cdot 1 = a$.

Alternatively, an abelian group can acquire additional structure by equipping it with a scalar multiplication, which turns it into a vector space as defined in Definition 3.

Definition 3 A (complex) vector space is an abelian group (A, +) equipped with an additional scalar multiplication with elements from \mathbb{C} , with the following properties

- Closure: For all $a \in A$ and $z \in \mathbb{C}$, also $za \in A$.
- Compatibility: For all $a \in \mathcal{A}$ and $y, z \in \mathbb{C}$ the identity y(za) = (yz)a holds.
- **Distributivity for the group addition**: For all $a, b \in \mathcal{A}$ and $z \in \mathbb{C}$ the identity z(a+b) = za + zb holds.
- **Distributivity for the addition of complex number**: For all $a \in \mathcal{A}$ and $y, z \in \mathbb{C}$ the identity (y + z)a = ya + za holds.

All the above structures now allow us to define the algebras that are considered throughout this thesis:

Definition 4 An **associative complex unital algebra** (from now on simply referred to as "unital algebra") is a *ring* $(A, +, \cdot)$ which also forms a *vector space* under scalar multiplication with elements of \mathbb{C} .

Throughout the dissertation, we commit the explicit mention of the operations and simply talk about the unital algebra A.

A.2 Including Topological Structure

For most applications in physics, the algebraic structure is insufficient, since it is not rich enough to do mathematical analysis. Analysis requires a notion of distance, which implies the existence of a topological structure. The the most direct way of adding such a structure to an algebra, is equipping it with a norm $\|.\|$, thus converting it to a Banach algebra as defined in Definition 5.

Definition 5 A **unital Banach algebra** is a *unital algebra* \mathcal{A} which is equipped with a norm $\|.\|: \mathcal{A} \to \mathbb{R}^+$ such that \mathcal{A} is a Banach space (Definition 6) and

$$||ab|| \le ||a|| ||b||$$
 for all $a, b \in \mathcal{A}$. (A.3)

Definition 6 A **Banach space** is a complex¹ vector space X equipped with a norm $\|.\|: \mathcal{A} \to \mathbb{R}^+$, which is **complete** with respect to that norm. In other words, for any Cauchy sequence $\{x_n\}$ in X, there is an $x \in X$ such that $\lim_{n \to \infty} \|x_n - x\| = 0$.

Such Banach algebras are the basic structures on which much of spectral theory is constructed (Conway 1997). However, for application in physics, we require an addition layer of structure which is required to get a consistent notion of positivity.

A.3 Involutions

Algebras that are relevant in quantum physics are equipped with an involution, usually often referred to as the *-operation, as defined in Definition 7

Definition 7 An algebra \mathcal{A} can be equipped with an additional operation, which is called an **involution**

$$^*: \mathcal{A} \to \mathcal{A}: a \mapsto a^*.$$
 (A.4)

with properties

- For all $a \in \mathcal{A}$, $a^{**} = a$.
- For all $a, b \in \mathcal{A}$, we find that $(a + b)^* = a^* + b^*$.
- For all $z \in \mathbb{C}$ and $a \in \mathcal{A}$, $(za)^* = \overline{z}a^*$.
- For all $a, b \in \mathcal{A}$, $(a \cdot b)^* = b^* \cdot a^*$.

A unital algebra, equipped with an involution is called a *unital* *-algebra.

It is no coincidence that the *-operation shares its properties with the adjoint operation (or hermitian conjugation) defined for linear operators on a Hilbert space. The goal of this algebraic formulation is to make an abstraction of the basic mathematical

¹Complexity is demanded because it fits the scope of our work. In is also possible to consider Banach spaces on the real numbers.

structure that is generated by such operators. Several types of elements in *-algebras share terminology with linear operators in Hilbert spaces: $a \in \mathcal{A}$ is called

- Hermitian or self-adjoint if $a^* = a$,
- *unitary* if $a^*a = aa^* = 1$,
- normal if $a^*a = aa^*$,
- a projection if $a^* = a$ and $a \cdot a = a$.

An important terminology which appear several times throughout the dissertation discusses mappings between algebras. Therefore, we formally define a *-homomorphism here in Definition 8.

Definition 8 A mapping $\phi : \mathcal{A} \to \mathcal{B}$, where both \mathcal{A} and \mathcal{B} as *-algebras, is called a *-homomorphism if for $a, b \in \mathcal{A}$ and $z \in \mathbb{C}$, we find that

- $\phi(a+b) = \phi(a) + \phi(b),$
- $\phi(a \cdot b) = \phi(a) \cdot \phi(b)$,

If the mapping has the above properties and maps \mathcal{A} onto itself, such that $\phi: \mathcal{A} \to \mathcal{A}$, it is referred to as a *-automorphism.

The final step towards the structures that are relevant in physics contains the combination of this involution with the topological structure.

A.4 C*-algebras

In the previous section we defined *-algebras via the introduction of an abstract adjoint operation. Generally, this structure can become quite wild and therefore needs to be tamed by the correct introduction of topological constraint. This leads us to the definition of Banach *-algebras and C^* -algebras

Definition 9 A unital Banach algebra, which is equipped with the involution of Definition 7 such that $||a^*|| = ||a||$ for all $a \in A$ is called a **Banach *-algebra**.

A unital Banach algebra, which is equipped with the involution of Definition 7, such that it fulfils the stronger demand that $||a^*a|| = ||a||^2$ for all $a \in \mathcal{A}$ is called a **C*-algebra**.

The demand that $\|a^*a\| = \|a\|^2$ for all $a \in \mathcal{A}$ is known as the C^* -property. This demand implies that $\|a^*\| = \|a\|$ and therefore one can say that any C^* -algebra is also a Banach *-algebra, which on its turn is always a Banach algebra. This is fundamental because it implies that there is a well defined notion of a spectrum for a C^* -algebra. It turns out that there are several crucial results in spectral theory that specifically apply to C^* -algebras, such as the fact that self-adjoint elements of a C^* -algebra always give rise to spectra that are contained in \mathbb{R} (Conway 1997).

A final fundamental aspect of of formal algebra is *representation theory*. In general, the main idea of representation theory is to consider an abstract algebraic framework and embed it in a concrete space which makes it possible to do explicitly computations. Because this is done both implicitly and explicitly throughout the dissertation, we provide a formal definition for a representation of a C^* -algebra in Definition 10.

Definition 10 A **representation** π of a C^* -algebra \mathcal{A} on a Hilbert space \mathcal{H} is a *-homomorphism $\pi: \mathcal{A} \to \mathcal{B}(\mathcal{H})$.

A representation is called **faithful** if it is injective. It is **non-degenerate** if the space

$$\pi(\mathcal{A})\mathcal{H} := \left\{ \sum_{j=1}^{n} \pi(a_j)\psi_j \mid n \in \mathbb{N}_0; a_1, \dots a_n \in \mathcal{A}; \psi_1, \dots, \psi_n \in \mathcal{H} \right\}$$
(A.5)

is dense in \mathcal{H} .

When there exists a vector $\Omega \in \mathcal{H}$ such that $\pi(\mathcal{A})\Omega$ is dense in \mathcal{H} , we call the representation **cyclic** and the vector Ω is called the **cyclic vector**.

A subspace \mathcal{K} of \mathcal{H} is called **invariant** if $\pi(\mathcal{A})\mathcal{K} \subset \mathcal{K}$. A representation π is called **irreducible** if the only closed invariant subspaces are $\{0\}$ and \mathcal{H} itself.

The GNS construction discussed in Chaps. 2 and 7 connects representations to states on the C^* -algebra and more specifically, it shows that each state fixes a unique cyclic representation.

Reference

J.B. Conway, *A Course in Functional Analysis*. Graduate Texts in Mathematics, vol. 96, 2nd edn. (Springer, New York, 1997)

Appendix B

Averaging over Random Unitary Matrices

Man! You guys should build a company and kick some ass
Juan-Diego Urbina — during e-mail exchange about this topic.

In this additional appendix chapter, we present a more technical introduction to the methods used to average over the unitary group with respect to the Haar measure. This outline is mainly based on the notes and work of Jack Kuipers.

To make the connection to more common random matrix language, we must stress that the random matrix ensemble which we here consider, generated by the unitary group with the Haar measure imposed on it, is also known as the *circular unitary ensemble* (CUE). In a physical context, one might say that it describes the propagators that are obtained from random Hamiltonians from the GUE (Akemann et al. 2011; Mehta 2004).

Integration over the unitary group can be performed using methods of (Brouwer and Beenakker 1996) or the slightly more general and rigorous frameworks of Collins and Śniady (2006), which was for example also used in Gessner and Breuer (2013). At the heart of these methods lies the identity

$$\mathbb{E}_{U}(U_{a_{1},b_{1}}\dots U_{a_{n},b_{n}}\overline{U}_{\alpha_{1},\beta_{1}}\dots\overline{U}_{\alpha_{n},\beta_{n}}) = \sum_{\sigma,\pi\in\mathcal{S}_{n}} V_{m}(\sigma^{-1}\pi) \prod_{k=1}^{n} \delta(a_{k} - \alpha_{\sigma(k)})\delta(b_{k} - \beta_{\pi(k)}).$$
(B.1)

The Weingarten functions (Weingarten 1978) which we denote V_m (where m denotes the number of modes and therefore the dimension of the matrix) can be evaluated using the explicit expression of Collins and Śniady (2006) or with help of the tables provided in Brouwer and Beenakker (1996). What remains is to consider permutations and count the terms in the sum, on the righthand side of (B.1), which give non-zero contributions.

Straightforward as the approach might seem, it is often highly impractical to go over all permutations once the product gets longer. In practice, we used Maple scripts to evaluate the functions of longer products of such components, but it is also possible to employ semiclassical techniques (Kuipers and Sieber 2008). The aim of this appendix is to give a slight taste of how such an algorithm works, by studying rather

simple examples and gradually considering slightly more complicated instances to indicate where the difficulties lie.

Let us consider the bosonic correlator

$$C_{rs}^{b} = \sum_{\substack{k,l=1\\k \neq l}}^{n} U_{ri_k} U_{si_l} \overline{U}_{ri_l} \overline{U}_{si_k} - \sum_{k=1}^{n} U_{ri_k} U_{si_k} \overline{U}_{ri_k} \overline{U}_{si_k}, \tag{B.2}$$

where we must treat each term separately. For the first term, note that

$$\mathbb{E}_{U}\left(\sum_{\substack{k,l=1\\k\neq l}}^{n} U_{ri_{k}} U_{si_{l}} \overline{U}_{ri_{l}} \overline{U}_{si_{k}}\right) = \sum_{\substack{k,l=1\\k\neq l}}^{n} \mathbb{E}_{U}\left(U_{ri_{k}} U_{si_{l}} \overline{U}_{ri_{l}} \overline{U}_{si_{k}}\right), \tag{B.3}$$

which means that we can focus on the computation of

$$\mathbb{E}_{U}\left(U_{ri_{k}}U_{si_{l}}\overline{U}_{ri_{l}}\overline{U}_{si_{k}}\right). \tag{B.4}$$

Now, we must exploit that $k \neq l$ and $r \neq s$. The permutations over which we sum in (B.1) are those in S_2 , since we only consider two terms. This implies that there are only two operation on the indices: either we exchange (e) them or we do nothing (which is the identity map id). More formally, one might write $e:(1,2)\mapsto(2,1)$ and $id:(1,2)\mapsto(1,2)$. Let us first of all see which of the operations lead to non-zero terms in (B.1). Because the first index of the components is ordered and $r \neq s$, we can safely drop the sum over these indices, since only the id permutation will give non-zero contributions. We find that

$$\mathbb{E}_{U}\left(U_{ri_{k}}U_{si_{l}}\overline{U}_{ri_{l}}\overline{U}_{si_{k}}\right) = V_{m}(id)\delta(i_{k} - i_{l})\delta(i_{l} - i_{k}) + V_{m}(e)\delta(i_{k} - i_{k})\delta(i_{l} - i_{l})$$

$$= V_{m}(2).$$
(B.5)

We used explicitly that $i_k \neq i_l$ and in the last step, we adopt the notation of Brouwer and Beenakker (1996), where it is emphasised that the value of the Weingarten function only depends on the lengths of the cycles that build the permutation. In this case, the cycle for e has length 2.

The second term is given by

$$\mathbb{E}_{U}\left(\sum_{k=1}^{n} U_{ri_{k}} U_{si_{k}} \overline{U}_{ri_{k}} \overline{U}_{si_{k}}\right) = \sum_{k=1}^{n} \mathbb{E}_{U}\left(U_{ri_{k}} U_{si_{k}} \overline{U}_{ri_{k}} \overline{U}_{si_{k}}\right)$$
(B.6)

In this case, there is only one index, so we find that

$$\mathbb{E}_{U}\left(U_{ri_{k}}U_{si_{k}}\overline{U}_{ri_{k}}\overline{U}_{si_{k}}\right) = V_{m}(id)\delta(i_{k} - i_{k})\delta(i_{k} - i_{k}) + V_{m}(e)\delta(i_{k} - i_{k})\delta(i_{k} - i_{k})$$

$$= V_{m}(1, 1) + V_{m}(2).$$
(B.7)

We can combine (B.5) and (B.7) to obtain that

$$\mathbb{E}_{U}(C_{rs}^{b}) = \sum_{\substack{k,l=1\\k\neq l}}^{n} V_{m}(2) - \sum_{k=1}^{n} \left(V_{m}(1,1) + V_{m}(2)\right)$$

$$= -\frac{n(m+n-2)}{m(m^{2}-1)},$$
(B.8)

where the final equality follows by using the tabulated values for the Weingarten function as given in Brouwer and Beenakker (1996).

The random matrix results for the first moments for fermions, distinguishable particles and the mean-field sampler are all obtained in a similar fashion. The first moment of the three point correlator is also not too difficult: Once we have all the structured expressions, separating terms where indices are repeated, we can simply run over all permutation. For the three-point correlator, it should not come as a surprise that these permutations are contained in S_3 .

Coming back to the two-point truncated correlation function, we also showed results for the second and the third moment. These quickly become much more difficult and here we only consider the second moment, which directly indicates where the difficulties originate. We must calculate

$$\mathbb{E}_{U}\left(\left(\sum_{\substack{k_{1},l_{1}=1\\k_{1}\neq l_{1}}}^{n}U_{ri_{k_{1}}}U_{si_{l_{1}}}\overline{U}_{ri_{l_{1}}}\overline{U}_{si_{k_{1}}} - \sum_{k_{1}=1}^{n}U_{ri_{k_{1}}}U_{si_{k_{1}}}\overline{U}_{ri_{k_{1}}}\overline{U}_{si_{k_{1}}}\right) \times \left(\sum_{\substack{k_{2},l_{2}=1\\k_{2}\neq l_{2}}}^{n}U_{ri_{k_{2}}}U_{si_{l_{2}}}\overline{U}_{ri_{l_{2}}}\overline{U}_{si_{k_{2}}} - \sum_{k_{2}=1}^{n}U_{ri_{k_{2}}}U_{si_{k_{2}}}\overline{U}_{ri_{k_{2}}}\overline{U}_{si_{k_{2}}}\right)\right),$$
(B.9)

where we know that $k_1 \neq l_1$ and $k_2 \neq l_2$, but we do not know anything about how the indices with and index "1" compare to those with an index "2". This implies that we must consider a serious amount of different options. Just to make it more feasible to keep the overview, we go over all these options by assuming that the indices all come from the set (1, 2, 3, 4), this is the smallest possible set that offers enough diversity to go over all options. Notice that now also the other index has changed, comparing (B.1)–(B.9), we see that $\mathbf{a} = \alpha = (r, s, r, s)$, which implies that there are also more permutations that contribute here.

There are a total of four terms in C_{rs}^b that need to be considered, the first one being the longest:

$$\mathbb{E}_{U}\left(\sum_{\substack{k_{1},l_{1}=1\\k_{1}\neq l_{1}}}^{n}\sum_{\substack{k_{2},l_{2}=1\\k_{2}\neq l_{2}}}^{n}U_{ri_{k_{1}}}U_{si_{l_{1}}}U_{ri_{k_{2}}}U_{si_{l_{2}}}\overline{U}_{ri_{l_{1}}}\overline{U}_{si_{k_{1}}}\overline{U}_{ri_{l_{2}}}\overline{U}_{si_{k_{2}}}\right). \tag{B.10}$$

Now, since we know that $k_1 \neq l_1$, we can start our index bookkeeping by setting $i_{k_1} = 1$ and $i_{l_1} = 2$, which leads to the following different options and number of terms per option

$$\begin{cases} i_{k_1} = 1 & \begin{cases} i_{l_2} = 2 & n(n-1) \\ i_{l_2} = 3 & n(n-1)(n-2) \end{cases} \\ i_{k_2} = 2 & \begin{cases} i_{l_2} = 2 & n(n-1) \\ i_{l_2} = 3 & n(n-1)(n-2) \end{cases} \\ i_{l_2} = 1 & n(n-1) \\ i_{l_2} = 3 & n(n-1)(n-2) \end{cases} \\ i_{l_2} = 1 & n(n-1)(n-2) \\ i_{l_2} = 2 & n(n-1)(n-2) \\ i_{l_2} = 4 & n(n-1)(n-2)(n-3) \end{cases}$$

$$(B.11)$$

Each of these options needs to be considered separately and on each one we have to evaluate (B.1), afterward all these contribution have to be added up, with the correct multiplicity (which is given on the far right side of (B.11)).

The following two terms can be considered jointly, since they are equivalent:

$$\mathbb{E}_{U}\left(\sum_{\substack{k_{1},l_{1}=1\\k_{1}\neq l_{1}}}^{n}\sum_{k_{2}=1}^{n}U_{ri_{k_{1}}}U_{si_{l_{1}}}U_{ri_{k_{2}}}U_{si_{k_{2}}}\overline{U}_{ri_{l_{1}}}\overline{U}_{si_{k_{1}}}\overline{U}_{ri_{k_{2}}}\overline{U}_{si_{k_{2}}}\right),\tag{B.12}$$

where we can apply similar logic as for the previous terms. We again obtain a list of options, each occurring with its own multiplicity:

$$\begin{cases} i_{k_1} = 1 & \begin{cases} i_{l_1} = 2 \end{cases} & \begin{cases} i_{k_2} = 1 & n(n-1) \\ i_{k_2} = 2 & n(n-1) \\ i_{k_2} = 3 & n(n-1)(n-2) \end{cases}$$
 (B.13)

Yet again, we have to let identity (B.1) act on each to these terms. Even though it might seem that this is less work, since there are fewer options, each of these different options typically forces us to consider more permutations given that there are more non-vanishing contributions for these terms due to the repetition of indices. Again, after evaluation (B.1) for each options, the results have to be summed with the correct multiplicity, this joint result now needs to be considered twice, since two of the four terms in $(C_{rs}^b)^2$ contribute in this fashion. The final term which we must consider is of the form

$$\mathbb{E}_{U}\left(\sum_{k_{1}=1}^{n}\sum_{k_{2}=1}^{n}U_{ri_{k_{1}}}U_{si_{k_{1}}}U_{ri_{k_{2}}}U_{si_{k_{2}}}\overline{U}_{ri_{k_{1}}}\overline{U}_{si_{k_{1}}}\overline{U}_{ri_{k_{2}}}\overline{U}_{si_{k_{2}}}\right),\tag{B.14}$$

and the different option can be listed as follows

$$\begin{cases} i_{k_1} = 1 & \begin{cases} i_{k_2} = 1 & n \\ i_{k_2} = 2 & n(n-1) \end{cases}$$
 (B.15)

This also needs to be added to the other two results.

The difference between the different particle types lies mainly in how these terms are added up. Some terms vanish for distinguishable particles and some signs are different for bosons and fermions. It is clear that the situation becomes even more complicated when higher moments are considered, which leads to ever more tedious combinatorics. What needs to be done is nevertheless very straightforward, hence it can be done by an algorithm, although the scaling of such algorithm is very unpleasant, implying that such a method is only fruitful for lower moments. In our case, the evaluations and combination of all these different terms were worked out by Jack Kuipers, using his own script, written in Maple. The program essentially executes all the steps such as they are described here and automatically runs over all possible permutations. This ultimately leads to the RMT results as described in Sect. 8.5.

Once we are considering partial distinguishability, the multiplicities have to be replaced with weighted sums that consider the distinguishability of the different particles. With these remarks, we conclude this technical appendix on the evaluations of RMT averages over the unitary group. The interested reader is referred to Berkolaiko and Kuipers (2010), (2011), Brouwer and Beenakker (1996), Collins and Śniady (2006) for more background.

References

- G. Akemann, J. Baik, P.D. Francesco (eds.), *The Oxford Handbook of Random Matrix Theory*. Oxford Handbooks in Mathematics (Oxford University Press, Oxford, 2011)
- G. Berkolaiko, J. Kuipers, Moments of the Wigner delay times. J. Phys. A: Math. Theor. 43, 035101 (2010)
- G. Berkolaiko, J. Kuipers, Transport moments beyond the leading order. New J. Phys. 13, 063020 (2011)
- P.W. Brouwer, C.W.J. Beenakker, Diagrammatic method of integration over the unitary group, with applications to quantum transport in mesoscopic systems. J. Math. Phys. **37**, 4904–4934 (1996)
- B. Collins, P. Śniady, Integration with respect to the Haar measure on unitary, orthogonal and symplectic group. Commun. Math. Phys. **264**, 773–795 (2006)
- M. Gessner, H.-P. Breuer, Generic features of the dynamics of complex open quantum systems: statistical approach based on averages over the unitary group. Phys. Rev. E 87, 042128 (2013)

- J. Kuipers, M. Sieber, Semiclassical relation between open trajectories and periodic orbits for the Wigner time delay. Phys. Rev. E 77, 046219 (2008)
- M.L. Mehta, Random Matrices (Elsevier/Academic Press, Amsterdam, 2004)
- D. Weingarten, Asymptotic behavior of group integrals in the limit of infinite rank. J. Math. Phys. **19**, 999–1001 (1978)

Appendix C

Higher-Order Many-Particle Interference

In this appendix, we present some brief comments on many-particle interference, which extend the result of Sect. 8.3 to more general number states. For simplicity, we limit this discussion to bosons, but the extension to fermions can be done in a trivial manner.

Our discussions on many-particle interference in Chap. 8 were all based on "elementary tensors", i.e. wave functions of the form

$$\Psi' = \frac{1}{\sqrt{\text{perm } G}} a^{\dagger}(\psi_1) \dots a^{\dagger}(\psi_n) \Omega. \tag{C.1}$$

However, in Sect. 7.6.1 we explicitly stressed that these vectors only form a basis of a much broader class of number states, which is often overlooked in literature. Indeed, a *general* number state is rather of the form

$$\Psi := \sum_{i} c_i \Psi_i, \tag{C.2}$$

where $\sum_{i} |c_{i}|^{2} = 1$ and

$$\Psi_i := \frac{1}{\sqrt{\operatorname{perm} G^{(i)}}} a^{\dagger}(\psi_1^{(i)}) \dots a^{\dagger}(\psi_n^{(i)}) \Omega. \tag{C.3}$$

Although this may seem like a pathological case which is only relevant to mathematical purists, it most certainly is not. The most well-known example of such a structure is probably a "N00N-state" (Kok et al. 2002). We can generate a two-particle N00N-state with a Hong-Ou-Mandel setup, but for higher particle numbers, this is no longer possible.

In general, states of the type (C.2) cannot be obtained via the propagation of (C.1) through a single-particle unitary channel E(U), $U \in \mathcal{B}(\mathcal{H})$. Hence, this is not a completely trivial generalisation of the phenomenology studied in Chap. 8. In this

appendix, we briefly show what happens when we transmit Ψ in (C.2) trough such a single-particle unitary channel and measure its transition probability to the state

$$\Xi = \frac{1}{\sqrt{\text{perm }G'}} a^{\dagger}(\xi_1) \dots a^{\dagger}(\xi_n) \Omega. \tag{C.4}$$

The action of the unitary channel on (C.2) is simply obtained via

$$\sum_{i} c_{i} \Psi_{i} \mapsto \sum_{i} c_{i} E(U) \Psi_{i} = \sum_{i} c_{i} \frac{1}{\sqrt{\operatorname{perm} G^{(i)}}} a^{\dagger} (U \psi_{1}^{(i)}) \dots a^{\dagger} (U \psi_{n}^{(i)}) \Omega.$$
(C.5)

Of more interest is the detection probability

$$p_{\Psi \to \Xi} = |\langle \Xi, E(U)\Psi \rangle|^{2}$$

$$= \left| \sum_{i} c_{i} \langle \Xi, E(U)\Psi_{i} \rangle \right|^{2}$$

$$= \sum_{i} |c_{i}|^{2} |\langle \Xi, E(U)\Psi_{i} \rangle|^{2} + \sum_{i \neq j} c_{i} \overline{c}_{j} \langle \Psi_{j}, E(U^{\dagger})\Xi \rangle \langle \Xi, E(U)\Psi_{i} \rangle.$$
(C.6)

Note that *all* many-particle interference effects discussed in Chap. 8 are of the form $|\langle \Xi, E(U)\Psi_i \rangle|^2$. This implies that in the final step of (C.6), we have an incoherent mixture of many-particle interference patterns as obtained for elementary tensors, and *in addition* a whole set of completely new "higher-order" interference terms. The latter is really an interference effect between the interference patterns induced by the different terms Ψ_i (C.3). One may say that the terms

$$\sum_{i\neq j} c_i \overline{c}_j \left\langle \Psi_j, E(U^{\dagger}) \Xi \right\rangle \left\langle \Xi, E(U) \Psi_i \right\rangle$$

are to many-particle interference what many-particle interference itself is to single-particle interference.

It is needless to say that the interference patterns of as described in (C.6) are most probably even harder to understand than the interference effects in Chap. 8 and, thus, they clearly fall out of the scope of our present work.

Reference

P. Kok, H. Lee, J.P. Dowling, Creation of large-photon-number path entanglement conditioned on photodetection. Phys. Rev. A **65**, 052104 (2002)

Appendix D

Fermionic Correlation Functions

In this appendix, we provide the derivation of Eq. (8.159).

Let us start from the general expression

$$c_W^f := \langle a^{\dagger}(U^{\dagger}\xi_1) \dots a^{\dagger}(U^{\dagger}\xi_q) a(U^{\dagger}\xi_q) \dots a(U^{\dagger}\xi_1) \rangle. \tag{D.1}$$

The state $\langle . \rangle$ is a fermionic number state, generated by a wave function with particles prepared in a set of modes $V = \{\psi_1, ..., \psi_n\}, \psi_j \in \mathcal{H}$, such that the wave function $\Psi \in \Gamma^f(\mathcal{H})$ is given by

$$\Psi = \frac{1}{\sqrt{\det G^{V,V}}} a^{\dagger}(\psi_1) \dots a^{\dagger}(\psi_n) \Omega. \tag{D.2}$$

We insert this wave function into (D.1) and obtain

$$c_W^f = \frac{\left\langle a(U^{\dagger}\xi_q) \dots a(U^{\dagger}\xi_1)a^{\dagger}(\psi_1) \dots a^{\dagger}(\psi_n)\Omega, a(U^{\dagger}\xi_q) \dots a(U^{\dagger}\xi_1)a^{\dagger}(\psi_1) \dots a^{\dagger}(\psi_n)\Omega \right\rangle}{\det G^{V,V}}.$$
(D.3)

To evaluate this expression, we must again re-express the Wick monomial in the numerator of (D.3) in normal order. By means of the fermionic identity

$$a(U^{\dagger}f_i)a^{\dagger}(e_j) = \langle U^{\dagger}f_i, e_j \rangle - a^{\dagger}(e_j)a(U^{\dagger}f_i), \tag{D.4}$$

we find

$$a(U^{\dagger}\xi_{q})\dots a(U^{\dagger}\xi_{1})a^{\dagger}(\psi_{1})\dots a^{\dagger}(\psi_{n})\Omega$$

$$= \sum_{\substack{j_{1},\dots,j_{q}=1\\j_{1}>j_{2}>\dots>j_{q}}}^{n} \sum_{\pi\in S_{q}} \operatorname{sign}(\pi) \left\langle \xi_{1}, U\psi_{j_{\pi(1)}} \right\rangle \dots \left\langle \xi_{q}, U\psi_{j_{\pi(q)}} \right\rangle \prod_{k\notin \{j_{1},\dots,j_{n}\}} a^{\dagger}(\psi_{k})\Omega.$$
(D.5)

© Springer International Publishing AG, part of Springer Nature 2018 M. Walschaers, *Statistical Benchmarks for Quantum Transport in Complex Systems*, Springer Theses, https://doi.org/10.1007/978-3-319-93151-7

Expression (D.5) can be inserted in (D.3) to obtain

$$c_{W}^{f} = \frac{1}{\det G^{V,V}} \sum_{\substack{j_{1},j'_{1},\ldots,j_{q},j'_{q}=1\\j_{1}>j_{2}>\cdots>j_{q}\\j'_{1}>j'_{2}>\cdots>j'_{q}}} \left(\sum_{\pi,\sigma\in S_{q}} \operatorname{sign}(\pi)\operatorname{sign}(\sigma) \left\langle \psi_{j'_{\sigma(1)}},U^{\dagger}\xi_{1} \right\rangle \left\langle \xi_{1},U\psi_{j_{\pi(1)}} \right\rangle \right. \\ \left. \ldots \left\langle \psi_{j'_{\sigma(q)}},U^{\dagger}\xi_{q} \right\rangle \left\langle \xi_{q},U\psi_{j_{\pi(q)}} \right\rangle \right) \\ \times \left\langle \prod_{l\notin\{j'_{1},\ldots,j''_{n}\}} a^{\dagger}(\psi_{l})\Omega, \prod_{k\notin\{j_{1},\ldots,j_{n}\}} a^{\dagger}(\psi_{k})\Omega \right\rangle. \tag{D.6}$$

We can now use (7.31) to obtain

$$\left\langle \prod_{l \notin \{j'_1, \dots, j'_n\}} a^{\dagger}(\psi_l) \Omega, \prod_{k \notin \{j_1, \dots, j_n\}} a^{\dagger}(\psi_k) \Omega \right\rangle = \det G^{V \setminus \{\psi_{j'_1}, \dots, \psi_{j'_q}\}, V \setminus \{\psi_{j_1}, \dots, \psi_{j_q}\}}, \quad (D.7)$$

which can be inserted in (D.6) and the final result for the fermionic correlation function directly follows:

$$c_{W}^{f} = \sum_{\substack{j_{1}, j'_{1}, \dots, j_{q}, j'_{q} = 1 \\ j_{1} > j_{2} > \dots > j_{q} \\ j'_{1} > j'_{2} > \dots > j'_{q}}} \left(\sum_{\pi, \sigma \in S_{q}} \operatorname{sign}(\pi) \operatorname{sign}(\sigma) \left\langle \psi_{j'_{\sigma(1)}}, U^{\dagger} \xi_{1} \right\rangle \left\langle \xi_{1}, U \psi_{j_{\pi(1)}} \right\rangle \right. \\ \left. \dots \left\langle \psi_{j'_{\sigma(q)}}, U^{\dagger} \xi_{q} \right\rangle \left\langle \xi_{q}, U \psi_{j_{\pi(q)}} \right\rangle \right) \\ \times \frac{\det G^{V \setminus \{\psi_{j'_{1}}, \dots, \psi_{j'_{q}}\}, V \setminus \{\psi_{j_{1}}, \dots, \psi_{j_{q}}\}}}{\det G^{V, V}}.$$

$$(8.159)$$

Glossary

Because of the reasonably broad topical range of this dissertation, some terminology may be slightly ambiguous. Hence, some brief remarks on jargon are in order:

- Wave functions— It is the habit throughout this text to refer to any normalised element of a Hilbert space, e.g. $\psi \in \mathcal{H}$, as a wave function. This stands in contrast to some fields where it is commonplace to only use the term wave function in the context of specific representations in position or momentum basis. Note that the elements of Hilbert space are also referred to as vectors, and when they are normalised to characterise a quantum state we also refer to them as state vectors. Ergo, the terms wave function and state vector are used interchangeably throughout this dissertation.
- **Quantum states** When referring to a *quantum state* we consider a positive, normalised functional on the algebra of observables (see Sect. 2.3.2). This is in contrast to the habit of many physicists to use the term *state* for a density matrix or a wave function.
- Quasi-Free vs. Gaussian—Throughout this work, we regularly refer to quasi-free and Gaussian states (and channels). These terms are very closely related, but we intend to make a slight difference: In the bosonic case, a *Gaussian* state is a state with a quantum characteristic function (7.199) that is Gaussian (see Sect. 7.6.4). The more general definition, which also holds for fermions, states that a state is Gaussian when its truncated correlation functions of order higher than two vanish (see Sect. 7.7). Both for bosons and fermions, a *quasi-free* state is in this sense a special type of Gaussian state, where also the truncated correlation function of order one vanishes and thus only the second order truncated correlation function is non-zero. This implies that all quasi-free states are Gaussian states, but, for example, Glauber coherent states (see Sect. 7.6.2) are Gaussian states which are not quasi-free (see also Sect. 7.6.2). Note that in the fermionic case it is uncommon to consider Gaussian states which are not quasi-free, mainly because they are still very poorly understood.

Gaussian (quasi-free) *channels* are channels which map Gaussian (quasi-free) states onto other Gaussian (quasi-free) states. In some literature, one also encoun-

450 Glossary

ters the term *linear channels* instead of Gaussian channels (which is derived from "linear optics").

In physical terms, one may consider Gaussian states as states for which correlations between different particles become negligible. They naturally arise as the thermal states for many-particle systems of without interactions. As a consequence, they are typically successful to describe dilute quantum gases and are also employed in mean-field models. Gaussian channels are therefore operations or dynamical maps which do not induce additional correlations in the system.